



HAL
open science

Using SXRF and LA-ICP-TOFMS to Explore Evidence of Treatment and Physiological Responses to Leprosy in Medieval Denmark

Anastasia Brozou, Marcello A Mannino, Stijn J M van Malderen, Jan Garrevoet, Eric Pubert, Benjamin T Fuller, M. Christopher Dean, Thomas Colard, Frédéric Santos, Niels Lynnerup, et al.

► To cite this version:

Anastasia Brozou, Marcello A Mannino, Stijn J M van Malderen, Jan Garrevoet, Eric Pubert, et al.. Using SXRF and LA-ICP-TOFMS to Explore Evidence of Treatment and Physiological Responses to Leprosy in Medieval Denmark. *Biology*, 2023, 12 (2), pp.184. 10.3390/biology12020184 . hal-03990232

HAL Id: hal-03990232

<https://hal.science/hal-03990232>

Submitted on 15 Feb 2023

HAL is a multi-disciplinary open access archive for the deposit and dissemination of scientific research documents, whether they are published or not. The documents may come from teaching and research institutions in France or abroad, or from public or private research centers.

L'archive ouverte pluridisciplinaire **HAL**, est destinée au dépôt et à la diffusion de documents scientifiques de niveau recherche, publiés ou non, émanant des établissements d'enseignement et de recherche français ou étrangers, des laboratoires publics ou privés.



Distributed under a Creative Commons Attribution 4.0 International License



biology

IMPACT
FACTOR
5.168

Indexed in:
PubMed

Article

Using SXRF and LA-ICP-TOFMS to Explore Evidence of Treatment and Physiological Responses to Leprosy in Medieval Denmark

Anastasia Brozou, Marcello A. Mannino, Stijn J. M. Van Malderen, Jan Garrevoet, Eric Pubert, Benjamin T. Fuller, M. Christopher Dean, Thomas Colard, Frédéric Santos, Niels Lynnerup et al.

Special Issue

Evolutionary Insights into Life History

Edited by


Prof. Dr. Thomas Colard and Dr. Adeline Le Cabec



<https://doi.org/10.3390/biology12020184>

Article

Using SXRF and LA-ICP-TOFMS to Explore Evidence of Treatment and Physiological Responses to Leprosy in Medieval Denmark

Anastasia Brozou ^{1,2}, Marcello A. Mannino ¹, Stijn J. M. Van Malderen ^{3,4}, Jan Garrevoet ³, Eric Pubert ⁵, Benjamin T. Fuller ^{1,6}, M. Christopher Dean ^{7,8}, Thomas Colard ^{5,9}, Frédéric Santos ⁵, Niels Lynnerup ¹⁰, Jesper L. Boldsen ¹¹, Marie Louise Jørkov ¹⁰, Andrei Dorian Soficaru ¹², Laszlo Vincze ¹³ and Adeline Le Cabec ^{5,14,*}

- ¹ Department of Archaeology and Heritage Studies, Aarhus University, Moesgård Allé 20, 8270 Højbjerg, Denmark
 - ² Department of Biology, University of Rome “Tor Vergata”, Via della Ricerca Scientifica 1, 00133 Rome, Italy
 - ³ Deutsches Elektronen-Synchrotron DESY, Notkestraße 85, D-22607 Hamburg, Germany
 - ⁴ Department of Chemistry, Ghent University, Campus Sterre, Krijgslaan 281-S12, 9000 Gent, Belgium
 - ⁵ Univ. Bordeaux, CNRS, MCC, PACEA, UMR 5199, F-33600 Pessac, France
 - ⁶ Géosciences Environnement Toulouse, UMR 5563, CNRS, Observatoire Midi-Pyrénées, 31400 Toulouse, France
 - ⁷ Department of Earth Sciences, Centre for Human Evolution Research, Natural History Museum, Cromwell Road, London SW7 5BD, UK
 - ⁸ Department of Cell and Developmental Biology, University College London, Gower Street, London WC1E 6BT, UK
 - ⁹ Department of Oral and Maxillofacial Radiology, University of Lille, Lille University Hospital, F-59000 Lille, France
 - ¹⁰ Department of Forensic Medicine, University of Copenhagen, Frederik V's Vej 11, 2100 Copenhagen, Denmark
 - ¹¹ Department of Forensic Medicine, University of Southern Denmark, Campusvej 55, 5230 Odense, Denmark
 - ¹² ‘Francisc I. Rainer’ Institute of Anthropology, Romanian Academy, 050474 Bucharest, Romania
 - ¹³ Department of Chemistry, X-ray Microspectroscopy and Imaging Research Group (XMI), Ghent University, Krijgslaan 281 S12, 9000 Ghent, Belgium
 - ¹⁴ Department of Human Evolution, Max Planck Institute for Evolutionary Anthropology, Deutscher Platz 6, D-04103 Leipzig, Germany
- * Correspondence: adeline.le-cabec@u-bordeaux.fr



Citation: Brozou, A.; Mannino, M.A.; Van Malderen, S.J.M.; Garrevoet, J.; Pubert, E.; Fuller, B.T.; Dean, M.C.; Colard, T.; Santos, F.; Lynnerup, N.; et al. Using SXRF and LA-ICP-TOFMS to Explore Evidence of Treatment and Physiological Responses to Leprosy in Medieval Denmark. *Biology* **2023**, *12*, 184. <https://doi.org/10.3390/biology12020184>

Academic Editor: Eugénia Cunha

Received: 9 December 2022

Revised: 19 January 2023

Accepted: 20 January 2023

Published: 25 January 2023



Copyright: © 2023 by the authors. Licensee MDPI, Basel, Switzerland. This article is an open access article distributed under the terms and conditions of the Creative Commons Attribution (CC BY) license (<https://creativecommons.org/licenses/by/4.0/>).

Simple Summary: Leprosy, a chronic infectious disease, leads to blood mineral imbalances: low levels of zinc, calcium, magnesium, and iron and high levels of copper. Interestingly, in late medieval Europe, minerals were used to treat leprosy. We investigated physiological responses to leprosy and possible evidence of treatment in dental tissues of leprosy sufferers from medieval Denmark and early 20th century Romania when multidrug therapy was not then yet invented. Using Synchrotron Fluorescence (SXRF) and laser ablation (LA-ICP-TOFMS), we show marked covariations in the zinc, calcium, and magnesium distributions, which are compatible with clinical studies but cannot be directly attributed to leprosy. Minerals used historically as a treatment for leprosy show no detectable intake (arsenic, mercury) or a diffuse distribution (lead) related to the daily consumption of contaminated water and food. Intense lead enrichments indicate acute incorporations, potentially through the administration of lead-enriched medication or the mobilization of lead from bone stores to the bloodstream during intense physiological stress related to leprosy. However, comparisons with a healthy control group are needed to ascertain these interpretations. The positive correlations and the patterns observed between lead and essential elements may indicate underlying pathophysiological conditions, demonstrating the potential of the two techniques for investigating diseases in past populations.

Abstract: Leprosy can lead to blood depletion in Zn, Ca, Mg, and Fe and blood enrichment in Cu. In late medieval Europe, minerals were used to treat leprosy. Here, physiological responses to leprosy and possible evidence of treatment are investigated in enamel, dentine, and cementum of leprosy sufferers from medieval Denmark (n = 12) and early 20th century Romania (n = 2). Using

SXRF and LA-ICP-TOFMS, 12 elements were mapped in 15 tooth thin sections, and the statistical covariation of paired elements was computed to assess their biological relevance. The results show marked covariations in the Zn, Ca, and Mg distributions, which are compatible with clinical studies but cannot be directly attributed to leprosy. Minerals used historically as a treatment for leprosy show no detectable intake (As, Hg) or a diffuse distribution (Pb) related to daily ingestion. Intense Pb enrichments indicate acute incorporations of Pb, potentially through the administration of Pb-enriched medication or the mobilization of Pb from bone stores to the bloodstream during intense physiological stress related to leprosy. However, comparisons with a healthy control group are needed to ascertain these interpretations. The positive correlations and the patterns observed between Pb and essential elements may indicate underlying pathophysiological conditions, demonstrating the potential of SXRF and LA-ICP-TOFMS for paleopathological investigations.

Keywords: dental tissues; mineral imbalances; zinc; calcium; leprosy treatment; lead

1. Introduction

Leprosy (a.k.a. Hansen's disease) is a chronic infectious disease that is mainly encountered today in South-East Asia, Africa, and Latin America [1]. However, during the medieval period, the disease was highly prevalent in Europe. Caused by two bacteria (*Mycobacterium leprae* and *Mycobacterium lepromatosis*) [2,3], leprosy is expressed through a range of clinical manifestations, with tuberculoid leprosy and lepromatous leprosy being the two extremes of the spectrum. They usually represent, respectively, a paucibacillary (low bacterial load) and a multibacillary (high bacterial load) form [4]. The expression of leprosy depends on the immune status of each infected individual [5], and several factors that affect the immune system's performance, such as poor living conditions, inadequate diets, and food shortages [6–10], have been considered in relation to the manifestation of the disease. There is a vicious cycle between malnutrition and infection [11,12]. On the one hand, nutritional deficiencies of vitamins and minerals lower the immune status, which increases the susceptibility to infections. On the other hand, however, the micronutrients are further depleted during infections by the invading pathogens, while the requirements are increased [13]. Several studies have reported mineral deficiencies or excesses in the blood serum of individuals suffering from leprosy (e.g., [14–18]).

Using Synchrotron X-ray Fluorescence (SXRF) and Laser Ablation-Inductively Coupled Plasma-Time of Flight Mass Spectrometry (LA-ICP-TOFMS), the present study investigates whether mineral imbalances of calcium (Ca), zinc (Zn), copper (Cu), iron (Fe), and magnesium (Mg) are recorded in dental hard tissues (enamel, dentine, and cementum) of leprosy sufferers from medieval Denmark and early 20th century Romania; an observation that could provide an insight into the physiological responses of leprosy sufferers from past populations. Due to repeated leprosy reactions, which are "acute exacerbations of the signs and symptoms of leprosy occurring during the natural course of the disease" and are the result of the body's immune response to the bacteria [19], periodicity and variation in strength (depletions and enrichments) in the elemental distributions could be expected. Additional elements of interest are lead (Pb), mercury (Hg), and arsenic (As) since historical records attest to the use of these heavy metals to treat skin diseases, including leprosy, in late medieval and early 20th century Europe [20–22].

Unlike bone, dental tissues do not remodel once formed, constituting a record of life and health, as well as age at death [23–28]. Having different mineralization processes [29,30], enamel and primary dentine complete their formation during infancy and adolescence, while (cellular and acellular) cementum and secondary dentine develop throughout an individual's life [29]. Consequently, when combined, enamel, dentine (primary and secondary), and cementum may provide information from as early as the first few months of life until the death of the individual under study. SXRF and synchrotron X-ray absorption spectroscopy have been widely employed to explore the normal and

pathological distributions of trace elements in human tissues of modern populations (for a review, see [31]). By visualizing biochemical variations in thin-sectioned dental hard tissues, the present study is the first to explore the potential of SXRF and LA-ICP-TOFMS for the study of pathophysiological changes in past populations.

Mineral Imbalances in Leprosy

Mineral elements are inorganic substances that are essential in living organisms for a variety of functions, such as the formation and maintenance of bone tissue [32]. They are classified as major (e.g., calcium, potassium, and phosphorus) or trace (e.g., manganese and copper) elements based on the required amounts, which are greater and lesser than 100 mg per day, respectively [33]. Mineral deficiencies or excesses, as well as interrelationships between different mineral elements (i.e., covariations with similar or opposite behaviors) related to diet or disease, lead to disturbances in normal metabolism and tissue structure [34–36].

By comparing blood serum levels between leprosy sufferers and a healthy control group, Rao et al. [37] reported depleted levels of Zn, Ca and Mg but elevated levels of Cu in the leprosy group. Such mineral imbalances in leprosy sufferers were also reported by several other studies (e.g., [14,16,38–44]). The depleted Zn levels correlate with an increased bacterial load [45] and not with the presence or absence of leprosy-related skin lesions [46]. Comparisons of serum levels between leprosy and non-leprosy patients with the same diet revealed that depleted Zn and Ca levels are associated with the disease and not with dietary depletions [47,48]. Moreover, by examining the serum Cu and Zn concentrations of leprosy patients before and during multidrug therapy, Sethi et al. [13] demonstrated a correlation between low Zn and high Cu serum levels with the severity and type of leprosy. Specifically, over the course of the treatment, the levels of both trace elements shifted toward the values of the control group [13].

The progressively depleted blood serum mineral levels in patients suffering from low to high bacterial loads could indicate the redistribution of the minerals from the blood to various tissues (e.g., liver), which is induced by the liberation of endogenous leukocyte mediators caused by the bacilli [49]. However, this has been reported in relation to acute, and not chronic, infections [50]. An alternative explanation could be the low absorption of the elements from the intestine; however, Kumar et al. [51] examined the small bowel in lepromatous leprosy patients and reported a normal absorptive function. Bhattacharya et al. [52] suggest that high blood levels of Cu in leprosy sufferers result from low levels of ascorbic acid (Vitamin C) that facilitate an increased absorption of Cu by the gut. Additionally, depleted serum levels of iron (Fe) in leprosy patients seem to result not from a failure to deliver Fe from Fe stores in the bone marrow but from an impaired circulation of Fe [53–55]. The accumulation of mineral elements in leprosy bacilli suggests that the bacteria retain elements originating from the host to cover their metabolic needs [13,56]. Furthermore, the values of oxidative stress in leprosy patients, which are potentially associated with the utilization of mineral elements by leprosy bacilli, are related to the duration of the infection, the bacterial load as well as the type of leprosy [57]. The imbalance of elemental levels in leprosy sufferers may also be related to the defense mechanisms of the hosts. This may either involve withholding nutrient metals from invading bacteria (known as “nutritional immunity”; [58,59]) and/or using the toxic properties of the mineral elements against the bacilli [60–62].

2. Materials and Methods

Material included in this study derives from the cemeteries of two medieval leprosy hospitals, which were located outside of Næstved and Odense in Denmark (Figure 1). Both hospitals functioned from around 1260 CE (Næstved [63,64]) and 1270 CE (Odense [65,66]) until their dissolution in 1542 CE [67]. The leprosy hospitals at Næstved and Odense are historically documented institutions that have been archaeologically investigated [68–72].

Hundreds of skeletons found in their associated cemeteries have been previously studied [73–75].



Figure 1. Map of Denmark depicting the location of Odense and Næstved (CC0 1.0 Universal; edited). Graphic programs used: Adobe Photoshop CS5.1 and Adobe Illustrator CS5.1.

Six individuals with osteological evidence of leprosy were selected from each site (Table S1). A permanent canine (C) and a permanent first molar (M1) was chosen from each individual (a total of 24 teeth) based on minimal wear and the absence of obvious pathologies, including carious lesions. These two tooth types were preferred as permanent first molars record information from as early as the perinatal period, while permanent canines from the first 4–5 months after birth [76]. Additionally, permanent teeth from two modern (beginning of the 20th century) Romanian individuals with documented evidence of a leprosy infection and who predate the advent of multidrug therapy were included for comparative purposes: the upper right canine and the lower right M1 of individual A1651; and the upper right canine and the lower right M2 of individual R1386. Authorization to work on these teeth was provided by the curating institutions (i.e., Odense Bys Museer, Medicinsk Museion, and the “Francisc I. Rainer” Institute of Anthropology, Romanian Academy).

Teeth were thin-sectioned using a Buehler Linear Precision Saw Isomet 5000 in the Histology Laboratory at PACEA (University of Bordeaux, France). Transmitted light micrographs (TLM) were used to assess the quality of dental tissue microstructure and select the best teeth for SXRF scanning. The visibility of growth increments was screened in both acellular and cellular cementum. Additional selection criteria were also considered, such as minimal visible taphonomic damages, including cracks, as well as tracks left by fungi. In total, 15 teeth from 10 different individuals (eight medieval—four from each site and two modern) were selected to undergo SXRF scanning (Table 1). Sex and age estimations, as well as radiocarbon dates for the eight medieval individuals, are presented in Table S2.

Table 1. Medieval and modern tooth samples for SXRF and LA-ICP-TOFMS multiscale imaging.

Site	Gr. Nr.	Teeth	SXRF Overview Scan		SXRF High-Resolution Scan			LA-ICP-TOFMS
			Spot Size (μm)	Exposure Time (ms)	Tissue	Spot Size (μm)	Exposure Time (ms)	
Odense	533	LLM1	10	3	AC	—	—	2 μm
					CC	1	1	1 μm
					SD	1	3	2 μm
Odense	896	LLC	10	3	—	—	—	—
		LLM1	10	2.5	TC	1.5	3	—
Odense	914	ULM1	10	3	CC	1	3	—
Odense	1149	URC	10	4	AC	1	10	—
		ULM1	10	4	CMSC?	1	3	—
Næstved	6	ULC	10	4	AC	1	10	—
Næstved	211	URC	10	3	CC	1	—	20 μm overview + 2 μm
		LRM1	10	2.5	AC	1.5	3	—
Næstved	268	LLM1	10	4	CC	1.5	3	—
Næstved	305	LLC	10	3	—	—	—	—
		LRM1	10	2.5	CC	1.5	3	—
Romania	A1651	URC	10	3	CC	1	3	—
		LRM1	10	2.5	TC	1.5	3	—
Romania	R1386	LRM2	10	2.5	CC	1.5	3	—

“Gr. Nr.” stands for “Grave Number.” “AC” stands for “acellular cementum” (on the cervical half of the root), “CC” for “cellular cementum” (apical half of the root), and “SD” stands for “secondary dentine.” “T” stands for “transition,” depicting a zone between acellular and cellular cementum, and “CMSC” for “cellular mixed stratified cementum.” Abbreviations of teeth are designed as follows: “L” or “U” for “lower” or “upper”; “L” or “R” for “left” or “right”; “C” or “M” for “canine” or “molar”; and finally, the tooth position in Arabic numerals. For instance, “LLM1” represents “lower left first molar.”

SXRF experiments were performed on the P06 Beamline [77,78], Petra III, at DESY (Deutsches Elektronen-Synchrotron, Hamburg, Germany). The scanning strategy followed a multiscale approach for each tooth (Table 1). First, a fast overview scan with a step size of 200 or 100 μm (dwell time: 10 ms) was acquired to check that the tooth section was well-centered in the field of view and to assess the overall signal-to-noise ratio of the elemental signature. Second, a higher resolution overview scan (10 μm ; integration time: 2.5–4 ms) was used to visualize the elemental variation within the entire tooth section (i.e., enamel, dentine, pulp cavity, and cementum). Finally, based on prior observations of the tooth sections under the microscope and on the SXRF signal quality in the 10 μm scans, a small region of interest was selected in the cementum of 14 teeth and the secondary dentine of one tooth (Odense 533M) for scanning at 1–1.5 μm (integration time of 3 ms or 10 ms).

All dental tissues of permanent canines and first molars were targeted with the aim of acquiring elemental values reflecting the entire life period of the individuals under study. Indeed, while enamel and primary dentine start developing shortly before birth in permanent first molars or within the first 4–5 months of postnatal life in permanent canines, both tissues complete their formation between 7 and 10 years of age [79]. Secondary dentine and (cellular and acellular) cementum start forming incrementally once the root dentine area is completed and continue slowly developing until the death of the individual [29,30].

Two teeth that showed the best SXRF signal in cellular cementum (especially regarding the Zn pattern) were selected for comparative LA-ICP-TOFMS. LA-ICP-TOFMS offers high-speed multiplexed nuclide imaging [80,81] and quantitatively reliable images of the distribution of elements that were not quantifiable or reliably detectable with the SXRF setup (notably Pb). LA-ICP-TOFMS imaging was performed at the Department of Chemistry, Ghent University (Belgium) with an Iridia 193 nm ArF* excimer-based laser ablation system

(Teledyne Photon Machines, Bozeman, MT, U.S.A.) coupled to an icpTOF 2R (TOFWERK AG, Thun, Switzerland) TOF-based ICP-MS instrument. During the calibration of the LA-ICP-TOFMS data, limits of detection (LOD) and quantitation (LOQ) were calculated, both in ppm, for each captured isotope (see [82]). LOD and LOQ values are reported in Table S3 for the isotopes selected to represent the chemical element it belongs to, based on their natural abundance, ionization potential, and lack of spectral interferences, which can induce some bias in the data. In summary, the isotope providing the cleanest signal was selected to represent each element of interest. Note that, compared to SXRF, LA-ICP-TOFMS shows better detection power in the higher-mass range, since detection power for SXRF is poor in the high-mass range. These are used as a guide for interpreting the results and for comparison with previously published studies. Note the LA-ICP-TOFMS scans left only a barely visible mark (a slight rectangular shadow) on the tooth section as a result of laser ablation. This was corrected with a fine polishing at 1 μm to recover an artefact-free thin section. Visualization and analysis of the SXRF and LA-ICP-TOFMS data were performed in HDIP v-1.3.3.1073 (Teledyne CETAC Technologies, Bozeman, MT, USA). With the aim to denoise the images, a 2D Gauss filter was applied, the kernel size of which is indicated in the Supplementary Information (Files S2 and S3).

To assess whether pairs of elements vary together or in opposition within statistical significance, Pearson's r and Spearman's ρ correlation coefficients were calculated on the concentration data measured along a transect on the high-resolution LA-ICP-TOFMS scans. The raw data for the transect of each LA-ICP-TOFMS scan are reported in Tables S4–S7. Note that Spearman's " ρ " is henceforth spelled "rho" to avoid confusion with p -values. Statistical tests and graphs were performed in RStudio (version 1.3.1093 [83]) and Excel; p -values were computed with a significance level of $\alpha = 0.05$. An extensive description of the statistical analysis, as well as of the tooth thin section preparation, the SXRF data acquisition and processing, and the LA-ICP-TOFMS imaging, is provided in the Supplementary Information (File S1).

3. Results

3.1. Copper (Cu) and Iron (Fe)

No distinct pattern was observed in the Cu and Fe distributions in the SXRF overview maps of the modern and archaeological teeth. In overview and high-resolution SXRF maps (Figures 2 and 3, File S2), Cu shows a uniform distribution within all tooth tissues, with baseline levels at ~ 100 ppm. In all teeth, the enamel is depleted in Fe, and dentine and cementum show values similar to the epoxy bond of the thin section, presumably reflecting a negligible Fe content close to ~ 0 ppm. Fe enrichment on the root surface and within dental cracks and the pulp chamber indicates exogenous contamination from the burial environment. High-resolution LA-ICP-TOFMS scans (File S3) reveal that in Odense 533M, Fe is at ~ 0 ppm in the acellular cementum, probably also in the cellular cementum, where the concentration is at ~ 600 – 700 ppm, which is similar to the epoxy of the thin section. Copper is <5 ppm in acellular cementum and probably at ~ 0 ppm in cellular cementum (concentrations similar to epoxy: ~ 10 – 20 ppm). The cellular cementum of Næstved 211C shows a considerable Fe enrichment of the surface (1400 ppm) and Fe and Cu enrichment of the sub-surface (Figure 4), respectively, of 200 ppm and ~ 15 ppm. The secondary dentine of Odense 533M has Cu levels close to ~ 2 – 4 ppm, while Fe reaches ~ 220 ppm, although this could be contamination as the epoxy shows similar values.

3.2. Calcium (Ca) and Magnesium (Mg)

The SXRF overview maps of the medieval Danish and modern Romanian teeth show the well-established pattern of Ca-rich enamel (Figure 2, File S2). The enriched Ca levels in enamel (ranging from $\sim 370,000$ – $400,000$ ppm) reflect its higher calcification levels compared to dentine (ranging from $\sim 300,000$ – $\sim 380,000$ ppm). Dentine has a homogenous Ca distribution with slightly depleted Ca levels around the pulp cavity due to the presence of secondary dentine, as well as within the cementum and at the junction between cemen-

tum and primary dentine. Some teeth, among which the modern Romanian A1651C and R1386M2, and the archaeological teeth Næstved 6C, 305M and C and Odense 533M, present accentuated lines reflecting variations in the Ca levels, often located (and best visible) in the dentine above the roof of the pulp chamber. The higher resolution Ca maps reveal subtle alternating enrichments and depletions in the cementum of three teeth (Næstved 211M, Odense 533M, and R1386M; see also Figure 4 showing calibrated LA-ICP-TOFMS high-resolution maps in the cellular cementum of Næstved 211C).

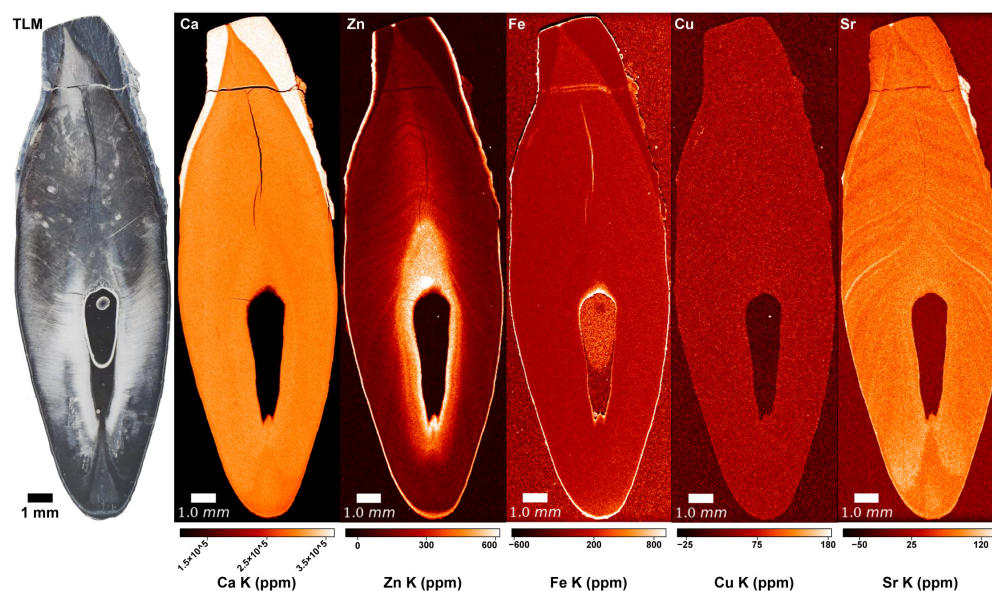


Figure 2. SXRf overview maps of Næstved 305C depicting the distributions of elements potentially impacted in leprosy, i.e., Ca, Zn, Fe, and Cu. The Sr map is shown for comparison with the Zn map since it also shows a pattern of alternating enrichments and depletions visible in the primary dentine. Ca, Fe, and Cu present uniform distributions. Contamination of Fe is visible on the surfaces of the tooth and within cracks. The Zn map reveals a rich pattern of enrichments and depletions in the primary dentine and a substantial enrichment at the outer enamel surface, the secondary dentine, and the cementum. Graphic programs used: Adobe Photoshop CS6 and Adobe Illustrator CS6.

The uncalibrated LA-ICP-TOFMS overview map of Mg acquired in Næstved 211C reveals that cementum is strongly Mg-depleted in comparison to dentine (File S3). At high-resolution (calibrated LA-ICP-TOFMS data), the Mg content in primary dentine ranges from 2000–2200 ppm, while the cellular cementum shows values fluctuating between 1000–1800 ppm (Figure 4). Interestingly, the Mg distribution generally follows the Ca and Zn distributions ($\rho = 0.45$ and 0.19 , respectively, $p < 0.05$, File S1). In Odense 533M, the cellular cementum contains Mg between ~1000–~1400 ppm, and these covary positively with Ca ($\rho = 0.47$, $p < 0.05$; File S1) and Zn ($\rho = 0.50$, $p < 0.05$). The secondary dentine is at ~1000 ppm Mg content, with no visible pattern of fluctuations. Ca and Zn show a moderate positive correlation with Mg in secondary dentine ($\rho = 0.79$ and 0.55 , respectively, $p < 0.05$; File S1). On the LA-ICP-TOFMS scan for acellular cementum of Odense 533M, the primary dentine contains 1000–1300 ppm, while the acellular cementum is Mg-enriched at 1800–2200 ppm. Note that this area of acellular cementum is affected by cracks, which, however, do not affect the reported concentrations, as they contain no Mg, thus, attesting to an endogenous origin of the Mg detected in the tooth tissues.

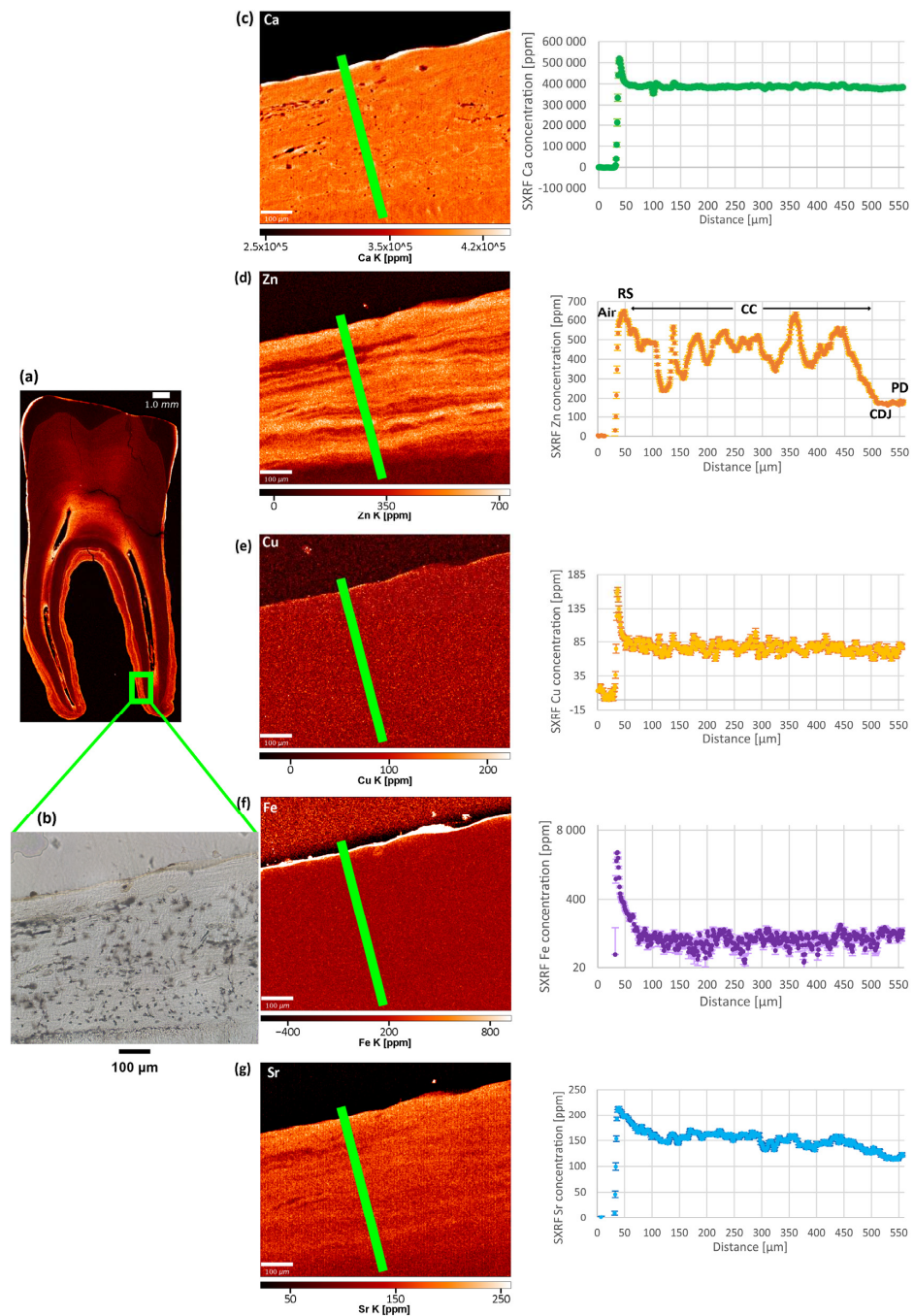


Figure 3. Distributions of elements potentially affected in leprosy (Ca, Zn, Cu, Fe) and Sr in Næstved 268M. The region of interest in the cellular cementum (green frame on the Zn overview map (a)) shows few identifiable increments in TLM (b). The SXRF data were collected on a scan at 1 μm, for each element of interest, along the green path (c–g). Elemental concentrations (in ppm) were then plotted against distance along the path in μm. As depicted on the Zn map, the path starts in the air (“Air”), reaches the root surface (RS), the cellular cementum (CC), the cementum-dentine junction (CDJ), and ends in the primary dentine (PD). Calcium (c) shows little variation, although a slight regular pattern may be visible on the Ca map. The Zn map (d) displays the clearest pattern of alternating enrichments and depletions, while Cu (e) and Fe (f) show uniform levels throughout the cementum. A subtle pattern recalling that of the Zn map can be observed in the Sr map (g). Note that a logarithmic scale was used to plot Fe, as the root surface enrichment at ~3000 ppm obscured the visibility of the pattern within the cementum at ~40–100 ppm. Graphic programs used: Adobe Photoshop CS6 and Adobe Illustrator CS6.

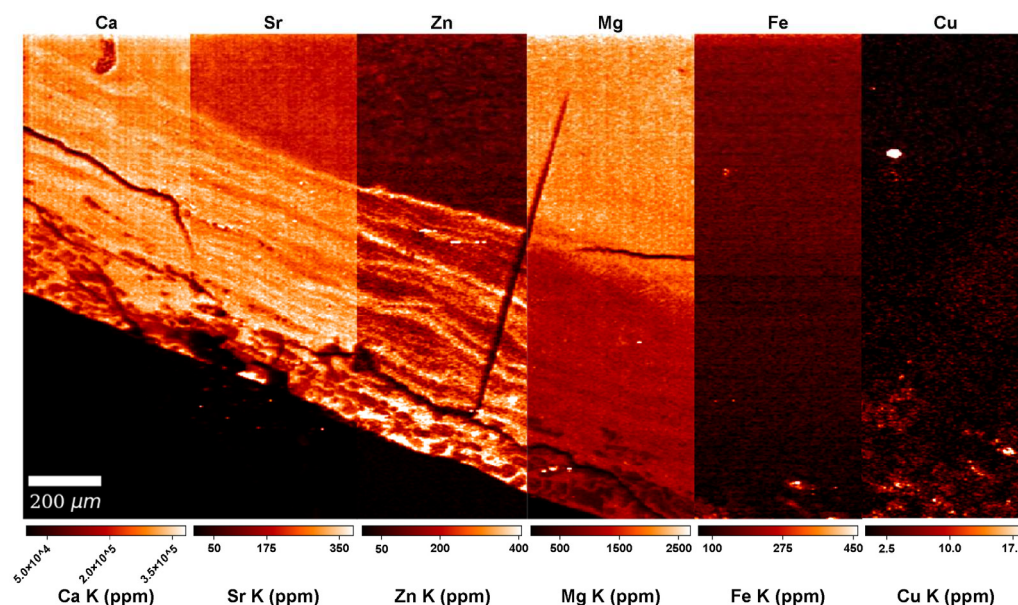


Figure 4. Calibrated LA-ICP-TOFMS high-resolution (2 μm) maps of the cellular cementum of Næstved 211C (See File S3) depicting the distributions of elements potentially impacted in leprosy, i.e., Ca, Zn, Mg, Fe, and Cu, as well as Sr. Note the weak signal in the Mg map, showing the same enrichment and depletion events as in the Ca, Zn, and Sr maps, with a positive, although weak, correlation to the Mg variations ($\rho = 0.45$ for Ca, $\rho = 0.19$ for Zn, and $\rho = 0.27$ for Sr). Graphic programs used: Adobe Photoshop CS6 and Adobe Illustrator CS6.

3.3. Zinc (Zn)

In all teeth, Zn content follows a similar distribution, with an enriched layer at the outer enamel surface and an accumulation in cementum and secondary dentine (Figure 2, see overview SXRF maps in File S2). In enamel, Zn is ~ 100 ppm with an enriched layer at ~ 650 ppm within the first tens of microns of the enamel surface, which has been interpreted in light of the process of enamel mineralization and maturation [84–86]. In dentine, the Zn baseline fluctuates between ~ 150 – 350 ppm, with marked alternating enrichments and depletions following the direction of the long-period growth increments. At higher resolution, a clear banding pattern is seen in the SXRF and LA-ICP-TOFMS Zn maps of cellular cementum (Figures 3 and 4, Files S2 and S3). The secondary dentine seems to record this pattern slightly less clearly (range: ~ 200 – 600 ppm; File S2). In TLM, the border between secondary and primary dentine is visible due to the difference in orientation of the long-period growth lines in both tissues (Figure 2). However, due to their similar chemical composition, this border is difficult to identify in elemental mapping when looking at the Ca, P, and Sr maps (File S2). As seen by the Zn map in the secondary dentine of Odense 533M, Zn is the only element that allows this border to be identified with confidence (Figure 2, Files S2 and S3). No differences in the Zn (as well as Cu, Fe, Ca, and Mg) content and distribution are observed between sex and age groups or across chronological periods (Table S2).

3.4. Strontium (Sr)

Another observation concerns Sr (Figures 2–4), which appears to covary positively with Ca, Mg, and Zn, although Sr is not an element known to bear any significance regarding leprosy. The strongest positive correlations are between Sr and Ca (in the cellular cementum of Næstved 211C, $\rho = 0.88$, while in Odense 533M $\rho = 0.57$, $p < 0.05$ for both; File S1) as well as Sr and Zn (cellular cementum: $\rho = 0.77$ for Næstved 211C and $\rho = 0.78$ for Odense 533M, $p < 0.05$ for both). Sr is slightly less strongly correlated with Mg ($\rho = 0.69$ for Odense 533M and $\rho = 0.27$ for Næstved 211C in the cellular cementum, $\rho = 0.86$ and $\rho = -0.34$ for the secondary dentine and the acellular cementum of Odense 533M).

The correlations of Sr with these elements (also for all other pairs of elements concerned) are weak (although significant) in the acellular cementum since the growth increments and accentuated markings are harder to resolve and much more tightly packed in this tissue (File S1). In general, Sr shows a clear pattern of variation, mostly in the primary dentine and in the cellular cementum (Figure 3), which is attested to be an authentic biological signal since these Sr variations follow the direction of the growth increments.

3.5. Arsenic (As) and Mercury (Hg)

In the SXRF data, the fitting of the As signal was not good enough to provide reliable data (the second emission peak was missing to safely identify the elemental signature). In the uncalibrated high-resolution LA-ICP-TOFMS map of the cellular cementum of Næstved 211C (File S3), the As level in cementum and primary dentine is close to ~1 ppm with noisy values at ~2–4 ppm. Similarly, in Odense 533M, high-resolution maps (File S3) in the acellular cementum and secondary dentine show a background noise in the tooth tissues at 3–5 ppm (as opposed to ~0 ppm in epoxy), while As is not detected in the cellular cementum. However, with a LOD \approx of 380 ppm and a LOQ \approx of 1250 ppm (Table S3), this cannot be considered a reliable biological signal. Additionally, neither the SXRF nor LA-ICP-TOFMS setups were sensitive enough to detect Hg concentrations.

3.6. Lead (Pb)

The SXRF datasets for Pb are uncalibrated and, thus, no quantitative values can be provided; instead, “arbitrary units” (“a.u.”) give an idea about the relative Pb distribution across specimens. Qualitative values are hereafter reported from direct measurements in the software HDIP, while the contrast has been adjusted in the Pb maps (File S2) to better reveal the Pb banding pattern. Overview SXRF maps (Figure 5, File S2) show that primary dentine (50–60 a.u.) is slightly enriched in Pb compared to enamel (~30–40 a.u.), while secondary dentine and cementum reach, overall, higher levels (60–70 a.u.). In Næstved 211C and 6C, the primary dentine contains 40–50 a.u. of Pb, while cementum and secondary dentine reach ~80 a.u.. Lead accumulation increases between dental tissues in Odense 914M (40–50 a.u. in enamel, ~60 a.u. in primary dentine, > 60–80 a.u. in cementum, and 120–140 a.u. in secondary dentine). The modern Romanian teeth show the greatest Pb accumulation with ~40–60 a.u. in enamel, 50–60 a.u. and 80 a.u. in the primary dentine of A1651M and R1386M, respectively, 80–100 a.u. in the secondary dentine of A1651M, while in R1386M it reaches 300 a.u. R1386M seems to concentrate Pb in cementum (Figure 5) with values of ~300 a.u. and peaks at 400 a.u., while in A1651M, the cementum is at ~100 a.u. with peaks at 120 a.u. An alternation of Pb enrichments and depletions is visible within the cementum and secondary dentine of R1386M (Figure 5, File S2). A consistent enrichment of Pb, probably linked to post-eruptive remineralization processes [87], is observed within the first 10 μ m of the outer enamel surface in some of the teeth, reaching maximum amounts from ~500–700 a.u. in the M2 of R1386 and weaker values in the archaeological specimens (~80–100 a.u.). No obvious pattern could be observed between sexes or chronological periods in the specimens (Table S2) besides the strong enrichment seen in the modern teeth. The data do not reveal an accumulation of Pb in older individuals, as was suggested by Bercovitz and Laufer [88].

Using LA-ICP-TOFMS, quantitative Pb concentrations were measured in areas of interest in the cellular cementum of Næstved 211C (Figure 5), in the acellular and cellular cementum, and in the secondary dentine of Odense 533M (Table 1). The limits of the current instrumentation are 5 ppm (LOD) and 16 ppm (LOQ) (Table S3). Both teeth show a substantial Pb enrichment at the surface of the cellular cementum, at ~10 ppm in Næstved 211C and at 40–100 ppm in Odense 533M (File S3). No cracks are visible on the surface of the scanned area for Odense 533M, while the three cracks seen in the cementum of Næstved 211C do not show any diffusion of Pb in the inner layers, suggesting that these surface enrichments are biogenic and not taphonomic. Further Pb surface enrichment in Odense 533M involves the surface of the acellular cementum at ~60–80 ppm and the surface of

secondary dentine (facing pulp cavity) at $\sim 2\text{--}7$ ppm (File S3). In Odense 533M, average background Pb levels range from $\sim 0.1\text{--}0.3$ ppm in primary dentine, $\sim 0.2\text{--}0.4$ ppm (with peaks at $\sim 2\text{--}4$ ppm) within the secondary dentine, to $\sim 1.1\text{--}1.5$ ppm (with a peak at ~ 8 ppm) in acellular cementum and ~ 1 ppm (peaks at ~ 2 ppm and a maximum at ~ 7 ppm) in cellular cementum.

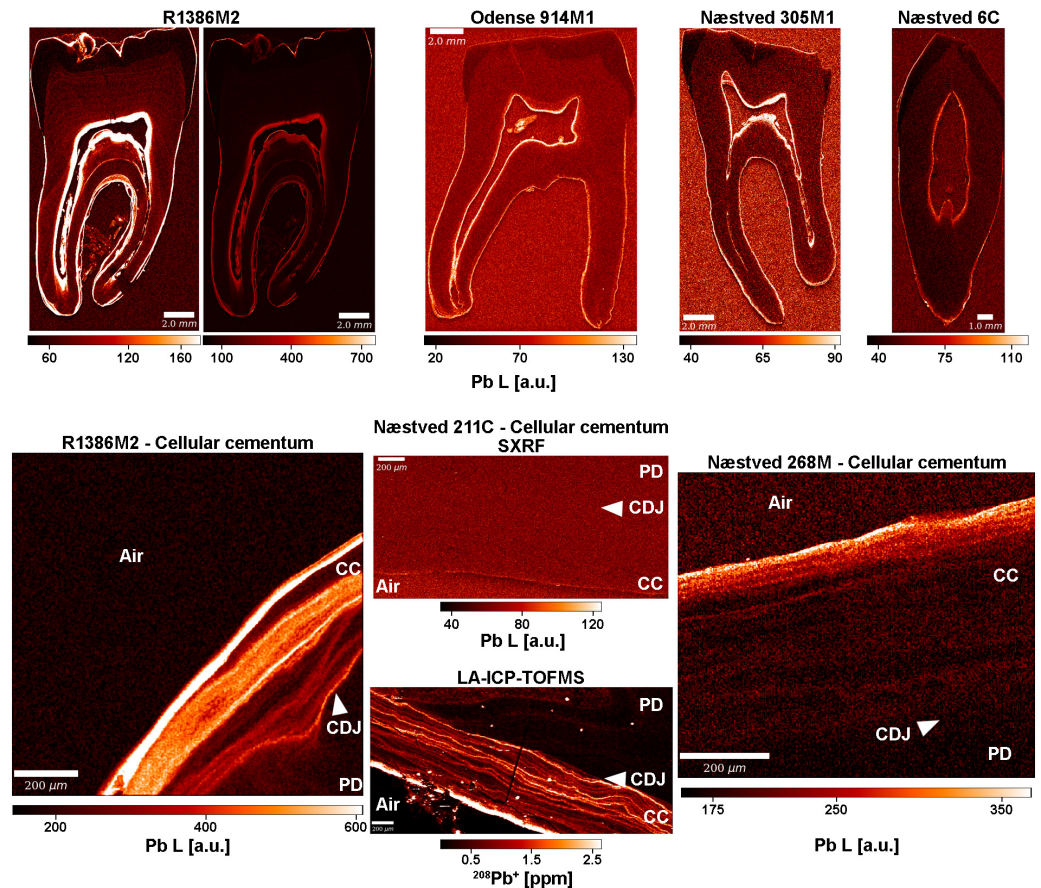


Figure 5. Uncalibrated XRF Pb maps (detection of the Pb L lines) for the modern R1386M, Odense 914M, Næstved 305M, and 6C showing a preferential accumulation of Pb in the slow-forming secondary dentine and cementum (**top row**). Relative XRF Pb enrichments and depletions are expressed in arbitrary units (“a.u.”). A very light alternation pattern of Pb is visible in the primary dentine of R1386M. This is confirmed at high-resolution (**bottom row**), where the cellular cementum of R1386M2 scanned in XRF reveals a well-defined Pb pattern. In Næstved 268M, the surface of the cellular cementum is enriched in Pb, with a decreasing gradient involving an alternation of enrichments and depletions within the sub-surface. This Pb content fades away within the cellular cementum. Note that XRF is not sensitive enough to resolve the Pb variation in the cellular cementum of Næstved 211C, while LA-ICP-TOFMS can quantify these variations with a high level of detail. “CC” stands for “cellular cementum,” “CDJ” for “cementodentine junction,” and “PD” for “primary dentine.” Graphic programs used: Adobe Photoshop CS6 and Adobe Illustrator CS6.

4. Discussion

4.1. Exploring Leprosy-Induced Mineral Imbalances in Dental Tissues

Studies conducted on blood samples of modern leprosy patients revealed depleted levels of Zn, Ca, Mg and Fe and elevated levels of Cu compared to healthy control groups [37,39,41,44,55]. These mineral imbalances appeared to be correlated with the severity and type of leprosy but returned to the normal values of the control groups during multidrug leprosy therapy [13]. Here, XRF and LA-ICP-TOFMS elemental mapping was used to determine if mineral imbalances in leprosy sufferers are imprinted within dental hard tissues. Whether induced by the invading bacteria and/or by the defending

host [13,58,62], detected mineral imbalances in blood samples of leprosy sufferers may be associated with recurrent leprosy reactions since, in clinical studies, oral zinc therapy has been shown to reduce the frequency, duration, and severity of reactions [89]. Leprosy reactions may occur as type 1 (or reversal reactions) in borderline leprosy and type 2 (or erythema nodosum leprosum) in lepromatous leprosy, the latter of which may lead to “widespread and recurrent lesions which continue to appear for months or even years” [90]. Due to repeated leprosy reactions, therefore, periodicity and variation in strength of elemental depletions and enrichments may be expected in dental tissues.

Using SXRF, distributions of elements potentially affected by the disease (i.e., Cu, Fe, Zn and Ca) were mapped on the whole teeth, while high-resolution scans were also taken in areas of cementum (Figures 2 and 3, File S2). The observed Ca-enriched levels in enamel and homogenous Ca distributions in dentine were also reported as a normal pattern in human teeth by Cool et al. [91], Dean et al. [84], and Martin et al. [92,93]. Moreover, the alternating Ca enrichments and depletions seen in the higher resolution Ca maps of some teeth (e.g., Næstved 211M, Odense 533M and R1386M) have also been observed by Dean et al. [94] in the acellular cementum of a *Pongo* incisor and in the cellular cementum of a *Pan* incisor. Besides the normal physiological Ca distribution and the slight fluctuations within the tissues of the scanned teeth, no significant Ca variations were observed that could be related to the leprosy infection of these medieval and early 20th-century individuals. Alternating enriched and depleted concentrations are also present in the Zn maps (Figures 2–4). The dentine of Næstved 305M and Odense 896M and 914M, for example, shows some marked accentuated bands with strong and broad Zn depletions. A very clear banding pattern of Zn is also visible in the cementum of both medieval and early 20th-century leprosy sufferers (File S2).

Using synchrotron X-ray fluorescence and X-ray diffraction mapping, Stock et al. [95] investigated the Zn intensities in cementum annual growth bands of Beluga whale teeth and reported that Zn is a sensitive indicator of mineralization, with higher and lower levels corresponding, respectively, to the light and dark bands that are visible in TLM. Dean et al. [94] also reported an alignment between high Zn concentrations with light cementum bands, and vice versa, in great ape and fossil hominin teeth and suggested that cementum layers rich in Zn are either indicative of a proliferation in apposition and/or mineralization, or of a decrease in the mineralization rate, which could result in more Zn exchanging with calcium over time. Indeed, the presence of high zinc levels in areas with mineralization activity, such as peritubular dentine, suggests that zinc is involved in the mineralization process [96]. The role of Zn in mineralization was also suggested in relation to high Zn concentrations observed in outer enamel areas [85]. An accumulation of Zn is observed at the outer enamel surface as well as in the cementum and the secondary dentine of all scanned teeth (File S2). The Zn enrichment of the latter two tissues may result from their slow growth rate and prolonged direct contact with tissue fluid during formation [84,94]. Similar results were previously documented in modern and fossil primate teeth [84,92–94,97–99].

Overall, no distinctive pattern in elemental distributions can be clearly attributed to the leprosy infection. Although enamel and primary dentine develop during childhood, the slow and annual growth of cementum and secondary dentine during adulthood, when these individuals were not only infected by the mycobacterium but had also manifested the disease, could potentially capture the blood mineral imbalances experienced by the leprosy sufferers. However, no significant variation in Fe and Cu is seen in the medieval or 20th-century teeth that could be interpreted as resulting from leprosy. Although studies have reported Fe and Cu concentrations in human teeth (e.g., [97,99,100]), dental hard tissues may not imprint the Fe and Cu variations documented in blood due to the naturally low content of these two elements in teeth. The alternating pattern of Zn (and, to a lesser extent, Ca) enrichments and depletions observed in the cellular cementum is presumably natural and a physiological marker of tooth tissue incremental growth. Although, one cannot exclude that these patterns may also be related to recurrent leprosy reactions

and the associated mineral imbalances documented in blood serum. For example, the homeostatic control of Ca by vitamin D [101] may indicate that blood Ca levels would need to drop significantly for a depleted Ca concentration to be imprinted in dental tissues. However, it is noteworthy that in the cellular cementum of Næstved 211C, as well as in the cellular cementum and the secondary dentine of Odense 533M, Zn and Ca have a positive correlation (File S1), also with Mg (see File S1). These trends are in agreement with clinical studies on the blood serum elemental levels of modern leprosy sufferers (e.g., [37,39,41]). Nonetheless, the correlations in dental hard tissues between Cu and Fe with the other elements (Zn, Ca, Mg) do not show the expected strength, direction, or significance compared to blood (e.g., [37,44,55]).

Considering the different homeostatic and metabolic factors that may influence the absorption and distribution of different elements from blood to body tissues, such as intestinal absorption [102,103], age [104], and pregnancy [105], it becomes evident that a direct and proportional link between blood and dental tissue elemental levels may not be applicable.

4.2. Exploring Evidence of Leprosy Treatment by Heavy Metals in Dental Tissues

Being influenced by the Hippocratic theory of humourism, medieval physicians believed that good health depended on a humoral balance in the body of the four principal substances (i.e., black bile, yellow bile, phlegm, blood), and, thus, the different types of treatment employed to cure an individual aimed at restoring the lost humoral equilibrium [106]. For example, bloodletting, which enabled the removal of excessive humours from the body [107], occurred four times every year at the leprosy hospital of Salle-aux-Puelles in Normandy, France, and was accompanied by a period of rest and special provisions [108]. Diet was also considered important for maintaining and restoring the humoral balance in the body. In medieval England, for example, mild and moist foods, such as poultry, eggs, and fresh fish, were considered appropriate for restoring the balance of the digestive system of leprosy sufferers [22], while in Spain, a special diet of chicken, mutton, sugar, dried fruits, and nuts preceded the consultation by a physician [109].

The few historical sources that provide information about the treatment of leprosy in medieval Denmark date to the 16th century and mention mainly the use of different plants and animals [110–112]. An exception was the following recipe, mentioned in Christian Pedersen's book *En nøttelig legebog* [110], specifically for wealthy individuals, which included gold as an ingredient. Nevertheless, medicinal preparations that included minerals were used in other areas (e.g., England) as a treatment for leprosy (as well as other diseases) towards the end of the medieval period when the Odense and Næstved leprosy hospitals were still in operation [22,113–116]. For instance, mercury and lead were mixed with animal products and plants and administered epidermally [114,117,118]. The use of minerals in medicinal preparations during that time is also attested to archaeologically, as mineral residues were discovered in an infirmary at the medieval priory and hospital of St Mary Spital in London [119]. Mineral preparations of mercury as well as arsenic were still used for the treatment of leprosy during the 19th and early 20th centuries; now administered also by fumigation, as well as orally and intravenously [20,21,120].

Previous work conducted by Rasmussen et al. [121] on bone samples of individuals from three medieval monastic sites in Denmark (Øm Kloster, Franciscan friaries in Odense and Svendborg) demonstrated a fourfold Hg increase in individuals with leprosy lesions (~200 ppb) compared to the control group (34 ± 15 ppb), suggesting that mercury-containing medicine was administered in 79% (11 out of 14) of the cases. Moreover, in medieval Danish rural populations, Rasmussen et al. [122] showed Hg background exposure levels at 80 and 300 ppb in cortical and trabecular bone, respectively. Regarding As concentrations, there are no published values measured in the bones or teeth of leprosy sufferers. Rasmussen [123] reports the range of the arsenic content in the enamel of individuals from medieval Denmark as being <0.001 – 0.239 ppm, while Hg ranges from 0.046 – 1.88 ppm. Moreover, Rasmussen et al. [124] interpret the 0.4 – 120 ppm As content

of bones from medieval and post-medieval individuals from Denmark as resulting from diagenesis, while the 7–78,730 ppb Hg concentration is interpreted as reflecting medicinal treatments. Here, neither the SXRF nor LA-ICP-TOFMS setups were sensitive enough to detect Hg concentrations, while the low As concentrations visualized by LA-ICP-TOFMS in the cellular cementum of Næstved 211C as well as in the secondary dentine and in the cellular and acellular cementum of Odense 533M is not considered a reliable biological signal. If any Hg and/or As intake, therefore, was intentionally occurring for medicinal purposes by our scanned individuals, this remains well below the detection limit of the two techniques used here.

Lead concentrations, on the other hand, are well detected, with SXRF overview maps showing an accumulation of Pb in the slow-forming secondary dentine and cementum and high-resolution maps (SXRF and LA-ICP-TOFMS) depicting a well-defined pattern of alternating enriched and depleted Pb concentrations (Figure 5). Exposure to lead (Pb) was common during the medieval period [125–128], also in relation to medical treatment [115,129,130]. In medieval rural populations from Denmark, Rasmussen et al. [122] measured a Pb background level of 5 and 7 ppm in cortical and trabecular bone, respectively. Nielsen et al. [131], however, document much higher Pb concentrations in bones from two early medieval Danish sites (means of 30 and 105 ppm). In another study, Rasmussen et al. [124] interpreted the Pb content in human bone (range: 0.8–426 ppm) as being related to the increased use in Denmark, from 1400–1700 CE, of Pb-glazed ceramics for the storage of food. The skeleton is known to accumulate Pb due to the low solubility of lead phosphate; teeth and bones contain 94% of the total Pb body burden [87,131]. Because Pb^{2+} has the same chemical affinities as Ca^{2+} , Zn^{2+} , and Sr^{2+} , Pb is expected to substitute for Ca and P in the hydroxyapatite crystalline structure since it has a small enough ionic radius [132–134]. The storage and release of Pb involve the same molecular mechanisms and hormones as Ca metabolism [134].

Under constant exposure, Pb incorporation in permanent teeth increases with age until reaching a plateau [135,136]. There is substantial variation of Pb levels in modern urban human teeth (e.g., [97,137]), with the element being preferentially deposited in cementum [92,99], especially at the root apex, where the presence of cellular cementum and the larger surface area may favor Pb exchange from blood to tooth tissues [138]. Secondary dentine was also identified as the dental tissue storing most of the Pb [139,140] due to the proximity of blood in the pulp chamber [137,141]. This tissue, therefore, may provide direct insight into Pb exposure, Pb plasma levels, and Pb intake until the death of an individual or the cessation of tooth function [142,143]. This Pb enrichment may be favored by the slow growth or crystal size in secondary dentine [143].

Here, the overview SXRF maps show consistently higher Pb levels in both the secondary dentine and cementum of all scanned teeth. However, the greatest accumulation of Pb is seen in the modern Romanian teeth. According to the records of the “Francisc I. Rainer” Institute of Anthropology, individual R1386 was male and died in 1926 at 36 years of age at the Colentina Hospital (Bucharest, Romania). This individual was a blacksmith and, thus, experienced daily exposure to metals during his adult life (Pb is accumulated in cementum and secondary dentine) and probably as early as his adolescence (Pb increases from the mid-root of his M2; see Figure 5 and File S2). Pascu [144] reports that in the 1920s, industrial production was flourishing in Romania and was especially focused on exploiting Pb, among other metals. Although concentrations in Pb cannot be calculated from the SXRF data for R1386M, his Pb content is clearly higher than that of the other modern Romanian individual and well above that of all the Danish archaeological teeth.

Quantitative Pb concentrations were measured by LA-ICP-TOFMS for two medieval teeth (Næstved 211C and Odense 533M). The results found a moderate to strong correlation between Pb and Zn (as well as Ca and Mg) variations within tooth tissues formed during adult life (File S1). In Odense 533M, a single strong Pb enrichment occurs close to the CDJ (at ~10 years of age; estimation from root formation stage in [79]). This Pb peak is preceded by two long and strong Zn depletions (Figure 6), also seen in Ca, P, Sr, Mg, and

Na (File S3). These depletions in essential elements may have favored Pb incorporation and, thus, increased its toxicity. In Næstved 211C, a major Pb peak occurs at the CDJ at the time of formation of the first cellular cementum layers (~12 years of age; estimation from root formation stage in [79]) and is followed by two strong peaks registered a little later during adult life (~17 years and early 20s, rough estimation based on Zn map). These Pb enrichments seem to be systematically followed by Zn-depleted bands (Figure 6), which could result from a reduced Zn absorption due to the increased load and toxicity of Pb in the body.

Previous studies have also observed a positive correlation between Pb and Zn. This covariation has been suggested to represent a biological signal reflecting the bloodstream in the pulp cavity and the metabolism of dentine-forming cells [92,145,146]. Talpur et al. [147] showed that compared to well-nourished children, the blood and hair of malnourished children have Pb levels that are two times higher and levels of essential elements (e.g., Ca, Fe, and Zn) that are one to twofold lower. When the diet is of insufficient quality, therefore, the correlation between Pb and Ca, Fe, or Zn becomes negative [147]. This may be explained by the increased urinary Zn excretion according to the duration and level of Pb exposure [148]. Bartón [149] also reported a strong negative correlation between hair Pb and Zn levels in preschool children. The incorporation of Zn and Pb in dental tissues may depend on formation rates and permeability [150]. Experiments found that Pb is incorporated almost instantaneously in forming dentine [151,152]. In modern humans, root formation (dentine) slows down towards completion [153]; this leaves a longer time period for incorporating Pb at the root apex, more specifically into the mineralizing matrix of the forming cementum [138].

The overall Pb background level measured in the cementum of the scanned medieval leprosy sufferers from Denmark may be related to daily Pb exposure through the consumption of contaminated water and food (lead-tiled roofs and glazed ceramics [124,154]). The few strong Pb enrichments, however, correspond to a marked exposure to the element. A possible explanation for the Pb peaks could potentially be the administration of Pb in the form of medication. Although no historical record survives that attests to the treatment of leprosy using Pb in medieval Denmark, this element was used in medicinal preparations during the later Middle Ages (cf., [22]). The administration of Pb-containing medicine would indicate that the mineral was used for medical purposes in Denmark already from the late 12th to mid-13th centuries, according to the radiocarbon dates of the two leprosy patients from Næstved (211) and Odense (533) (Table S2).

Nevertheless, during physiological events, such as pregnancy (e.g., [155,156]) or pathological events, such as severe illness [157], Pb (along with other major and trace elements) is mobilized from the bone matrix into the bloodstream due to disruptions in skeletal homeostasis. The elevated blood Pb levels are then incorporated into the mineralizing dental tissues and are recorded as Pb-enriched bands [157]. Consequently, the Pb enrichments imprinted in the dental tissues of the leprosy sufferers could indicate a period of intense physiological stress, possibly a period of exacerbated leprosy reactions. This could also be true for the cementum root surface Pb enrichment of Næstved 211C and Odense 533M, which is surprising by its intensity and duration, and which lasted until the death of both leprosy sufferers. Although it would be tempting to interpret this high Pb intoxication as being related to the occurrence of death, more research needs to be done to confirm this hypothesis. Nonetheless, the maximum Pb concentration that is found at the root surface of Odense 533M is ~100 ppm. Several public health studies report a positive correlation between Pb content in blood and teeth and further document a Pb blood concentration of 6 µg/dL for a Pb content in teeth of ~100 ppm [149,158,159]. The incorporation of Pb from the blood into dental tissues is a complex matter, yet one may speculate that following these clinical data, the degree of impairment induced by this Pb intoxication could have reached a level affecting development and health [160,161].

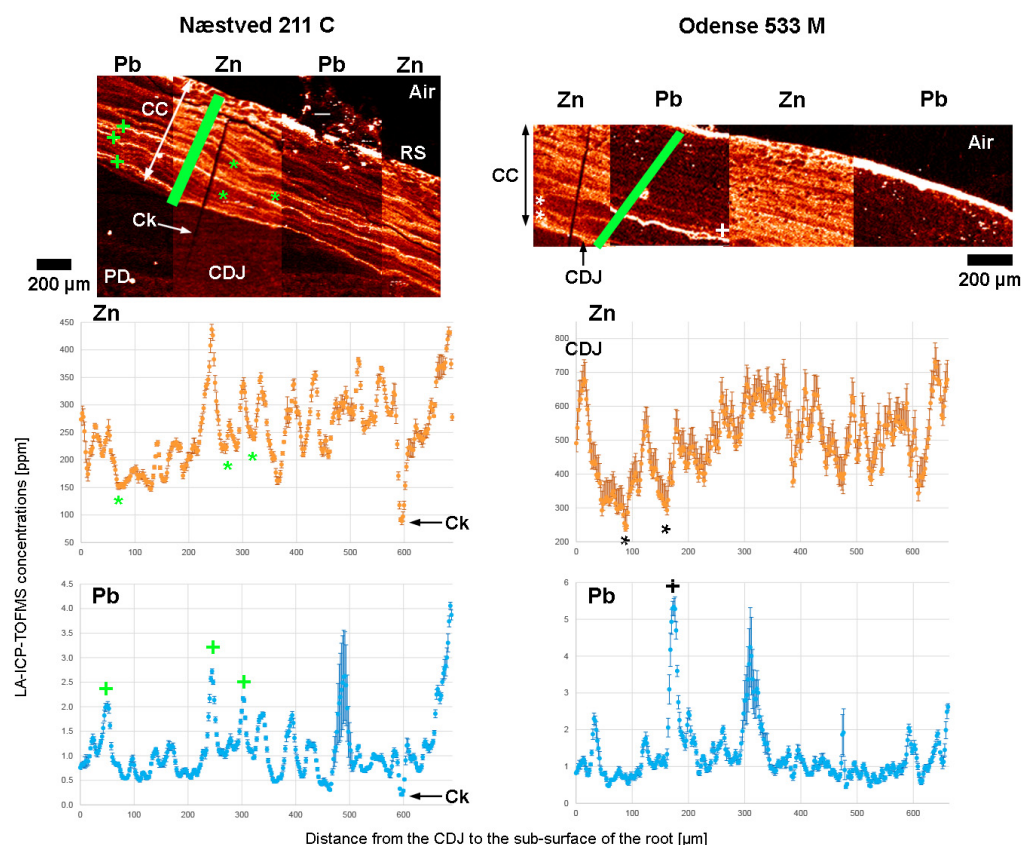


Figure 6. Covariation of Pb and Zn in the cellular cementum of Næstved 211C (left) and Odense 533M (right) (LA-ICP-TOFMS data used for the correlation tests, File S1). Note that two Zn depletions (black star on the graph, white star on the map) are followed by a Pb enrichment (black cross on the graph, white cross on the map) in Odense 533M, while three Pb enrichments (green cross) are followed by Zn depletions (green star) in Næstved 211C. The range of the *y*-axes has been adapted to best present the fluctuations of Zn and Pb in the two teeth. The root surface is enriched in Pb over the first ~30µm, which were avoided here to best represent the elemental covariations. Error bars represent 1 SD on either side. “CC” stands for “cellular cementum,” “CDJ” for “cementodentine junction,” “PD” for “primary dentine,” “RS” for “root surface,” “Ck” for “crack” in the cellular cementum of Næstved 211C. Graphic programs used: Adobe Photoshop CS6 and Adobe Illustrator CS6.

5. Conclusions

This study investigated markers of elemental blood fluctuations in the archaeological teeth of leprosy sufferers. The moderate to strong positive correlation between Zn, Ca, and Mg distributions seen in the dental tissues of Næstved 211C and Odense 533M corresponds to the results of clinical studies on blood samples of modern individuals suffering from leprosy. However, no distinctive pattern is observed in the concentration distributions of the elements that could be directly linked to the leprosy infection. Future studies on teeth and blood samples of modern leprosy sufferers with a recorded medical history could elucidate whether elemental blood imbalances related to leprosy are imprinted in dental tissues or if the elemental concentration and correlation patterns seen here indicate natural and physiological markers of tooth tissue incremental growth.

This is the first study using laser ablation to perform continuous mapping without having to extrapolate data from line scans, thus providing a true and reliable elemental mapping of the dental tissues. LA-ICP-TOFMS results reveal a constant exposure to Pb, which most likely reflects the ingestion of contaminated water and food. Although the administration of Pb in the form of medication cannot be excluded, the few strong Pb enrichments may be related to periods of intense physiological stress and to the enrichment of blood with Pb from bone stores. This is perhaps supported by the Pb enrichment seen

in the last deposited cementum growth layers of Næstved 211C and Odense 533M. The positive correlation that is observed between Pb and Zn concentrations, as well as the patterns that emerge when there is relatively high incorporation of Pb in the dental tissues, may indicate underlying pathophysiological conditions that promote or are induced by an increased Pb incorporation. A similar study on a larger sample size as well as on a non-leprosy control group from the same geographical regions and time period, however, is needed in order to ascertain these interpretations.

This study is the first to investigate mineral element distributions in dental tissues of leprosy sufferers, demonstrating the potential of SXRF and LA-ICP-TOFMS for paleopathological investigations. By targeting all dental tissues and by employing a methodology that allows different degrees of resolution, we have explored elemental distributions spanning the entire life of the individuals under study.

Supplementary Materials: The following supporting information can be downloaded at: <https://www.mdpi.com/article/10.3390/biology12020184/s1>, Table S1: List of individuals and teeth included in the study from the two medieval Danish leprosy sites (Odense and Næstved); Table S2: Age and sex determination and ^{14}C dates of the individuals of interest for SXRF and LA-ICP-TOFMS scanning (^{14}C dates reported by Brozou et al. 2021, American Journal of Physical Anthropology); Table S3: Limits of detection (LOD) and of quantitation (LOQ) of the calibrated LA-ICP-TOFMS data; Table S4: LA-ICP-TOFMS concentrations (in ppm) along a transect (in μm ; See page 5 of File S1) in the cellular cementum of the Næstved 211 C; Table S5: LA-ICP-TOFMS concentrations (in ppm) along a transect (in μm ; See page 55 of File S1) in the cellular cementum of the Odense 533 M1; Table S6: LA-ICP-TOFMS concentrations (in ppm) along a transect (in μm ; See page 30 of File S1) in the acellular cementum of the Odense 533 M1; Table S7: LA-ICP-TOFMS concentrations (in ppm) along a transect (in μm ; See page 77 of File S1) in the secondary dentine of the Odense 533 M1). File S1. Methods and Statistical results. File S2. Synchrotron Fluorescence (SXRF) results. File S3. Laser Ablation (LA-ICP-TOFMS) results.

Author Contributions: Conceptualization: A.B., A.L.C., B.T.F., T.C. and M.A.M.; Methodology: A.B., A.L.C., M.C.D., S.J.M.V.M., J.G. and L.V.; Formal analysis and investigation: A.B., S.J.M.V.M. and A.L.C.; Writing—original draft preparation: A.B. and A.L.C.; Writing—review and editing: all authors; Funding acquisition: A.B., A.L.C. and M.A.M.; Resources: N.L., J.L.B., M.L.J. and A.D.S.; Statistical Analysis: A.L.C. and F.S.; Sample Preparation: E.P.; Supervision: A.L.C. and M.A.M. All authors have read and agreed to the published version of the manuscript.

Funding: The SXRF data were acquired on the PETRA III P06 beamline at the Deutsches Elektronen-Synchrotron (DESY, Hamburg, Germany), a member of the Helmholtz Association HGF. The experiment was performed using beamtime granted by Proposal I-20190203 and supported partly through Maxwell computational resources operated at DESY. A. Brozou acknowledges the funding provided by the Faculty of Arts (Aarhus University) to finance her Ph.D. position. M.C. Dean is supported by the Calleva Foundation at CHER, Natural History Museum, London. M.A. Mannino is indebted to the Aarhus University Research Foundation, which funded the analyses that initiated the project and enabled the sample selection (project: “Danish & European Diets in Time”; AUFF-E-2015-FLS-8-2).

Institutional Review Board Statement: The study was conducted in accordance with the laboratories (PACEA, University of Bordeaux, France, and the Department of Archaeology and Heritage Studies, Aarhus University, Denmark) steering committee.

Informed Consent Statement: Patient consent was waived due to the archaeological/historical age of the specimens.

Data Availability Statement: The data used in this study are contained within the Supplementary Material or referenced within the text.

Acknowledgments: Odense Bys Museer, Medicinsk Museion, and the “Francisc I. Rainer” Institute of Anthropology, Romanian Academy are thanked for authorizing and encouraging this work. A. Brozou acknowledges ADBOU (University of Southern Denmark) and the Institute of Forensic Medicine (University of Copenhagen) for facilitating access to the skeletal collections. Thanks go to Gerald Falkenberg and those who have developed techniques employed in this study, to the DESY User Office, to Mihaela Culea for extracting the modern teeth, to Gundula Müldner, Janet

Montgomery, Simon Roffey and Magdalena Ewa Naum for insightful discussions on the results of this research and to Klervia Jaouen for discussions about Zn and Pb incorporation into dental tissues. M. Christopher Dean is grateful to the Calleva Foundation at CHER, Natural History Museum, London. This research benefited from the scientific framework of the University of Bordeaux's IdEx "Investments for the Future" program/GPR "Human Past".

Conflicts of Interest: The authors declare no conflict of interest.

References

- World Health Organization. Global leprosy update, 2018: Moving towards a leprosy-free world—Situation de la lèpre dans le monde, 2018: Parvenir à un monde exempt de lèpre. *Wkly. Epidemiol. Rec. Relev. Épidémiologique Hebd.* **2019**, *94*, 389–412.
- Han, X.Y.; Sizer, K.C.; Thompson, E.J.; Kabanja, J.; Li, J.; Hu, P.; Gómez-Valero, L.; Silva, F.J. Comparative Sequence Analysis of *Mycobacterium leprae* and the New Leprosy-Causing *Mycobacterium lepromatosis*. *J. Bacteriol.* **2009**, *191*, 6067–6074. [[CrossRef](#)] [[PubMed](#)]
- Han, X.Y.; Seo, Y.-H.; Sizer, K.C.; Schoberle, T.; May, G.S.; Spencer, J.S.; Li, W.; Nair, R.G. A New *Mycobacterium* Species Causing Diffuse Lepromatous Leprosy. *Am. J. Clin. Pathol.* **2008**, *130*, 856–864. [[CrossRef](#)] [[PubMed](#)]
- Lynnerup, N.; Boldsen, J.L. Leprosy (Hansen's Disease). In *A Companion to Paleopathology*; Grauer, A.L., Ed.; Wiley-Blackwell: Chichester, UK, 2012; pp. 458–471.
- Ridley, D.; Jopling, W. Classification of Leprosy According to Immunity. A Five-Group System. *Int. J. Lepr. Other Mycobact. Dis.* **1966**, *34*, 255–273. [[PubMed](#)]
- Dwivedi, V.P.; Banerjee, A.; Das, I.; Saha, A.; Dutta, M.; Bhardwaj, B.; Biswas, S.; Chattopadhyay, D. Diet and Nutrition: An Important Risk Factor in Leprosy. *Microb. Pathog.* **2019**, *137*, 103714. [[CrossRef](#)] [[PubMed](#)]
- Feenstra, S.G.; Nahar, Q.; Pahan, D.; Oskam, L.; Richardus, J.H. Recent Food Shortage Is Associated with Leprosy Disease in Bangladesh: A Case-Control Study. *PLoS Negl. Trop. Dis.* **2011**, *5*, e1029. [[CrossRef](#)] [[PubMed](#)]
- Kerr-Pontes, L.R.; Barreto, M.L.; Evangelista, C.M.; Rodrigues, L.C.; Heukelbach, J.; Feldmeier, H. Socioeconomic, Environmental, and Behavioural Risk Factors for Leprosy in North-East Brazil: Results of a Case-Control Study. *Int. J. Epidemiol.* **2006**, *35*, 994–1000. [[CrossRef](#)]
- Oktaria, S.; Hurif, N.S.; Naim, W.; Thio, H.B.; Nijsten, T.; Richardus, J. Dietary Diversity and Poverty as Risk Factors for Leprosy in Indonesia: A Case-Control Study. *PLoS Negl. Trop. Dis.* **2018**, *12*, e0006317. [[CrossRef](#)]
- Wagenaar, I.; van Muiden, L.; Alam, K.; Bowers, R.; Hossain, M.A.; Kispotta, K.; Richardus, J.H. Diet-Related Risk Factors for Leprosy: A Case-Control Study. *PLoS Negl. Trop. Dis.* **2015**, *9*, e0003766. [[CrossRef](#)]
- Katona, P.; Katona-Apte, J. The Interaction between Nutrition and Infection. *Clin. Infect. Dis.* **2008**, *46*, 1582–1588. [[CrossRef](#)]
- Oz, H. Nutrients, Infectious and Inflammatory Diseases. *Nutrients* **2017**, *9*, 1085. [[CrossRef](#)] [[PubMed](#)]
- Sethi, N.; Madadi, A.J.; Bhandari, S. Serum Zinc, Copper, Magnesium, Proteins and Superoxide Dismutase in Leprosy Patients on Multidrug Therapy—a Follow-up Study. *Indian J. Lepr.* **1996**, *68*, 325–333. [[PubMed](#)]
- Fatimah, S.; Rahfiludin, M.Z. The Difference of BMI and Micronutrient Intake Between Multibacillary Leprosy and Non Leprosy (A Study in District Brondong, Lamongan 2013). *Adv. Sci. Lett.* **2017**, *23*, 3421–3423. [[CrossRef](#)]
- Foster, R.; Sanchez, A.; Foulkes, J.; Cameron, L.J. Profile of Blood Elements in Leprosy Patients. *Indian J. Lepr.* **1991**, *63*, 12–33. [[PubMed](#)]
- Khalid, H.N.; Mostafa, M.I.; Attia, N.S.; Bazid, H.A.S.E. Serum Level of Selenium, Zinc, and Vitamin C and Their Relation to the Clinical Spectrum of Leprosy. *J. Infect. Dev. Ctries* **2022**, *16*, 491–499. [[CrossRef](#)]
- Nigam, P.; Dayal, S.; Sriwastava, P.; Joshi, L. Serum Calcium and Magnesium in Leprosy. *Asian J. Infect. Dis.* **1979**, *3*, 81–83.
- Venkatesan, K.; Kannan, K.B.; Bharadwaj, V.P.; Sritharan, V.; Katoch, K.; Usha, R.; Ramu, G. Serum Copper & Zinc in Leprosy & Effect of Oral Zinc Therapy. *Indian J. Med. Res.* **1983**, *78*, 37–41.
- World Health Organization. Leprosy/Hansen Disease: Management of Reactions and Prevention of Disabilities. In *Technical Guidance*; World Health Organization, Regional Office for South-East Asia: New Delhi, India, 2020.
- MacLeod, J.M.H. Sections of Tropical Diseases and Parasitology, Dermatology, and Therapeutics and Pharmacology. *Proc. R. Soc. Med.* **1927**, *6*, 987–1025.
- Muir, E. Treatment of Leprosy. A Review. *Int. J. Lepr.* **1933**, *1*, 407–458.
- Rawcliffe, C. *Leprosy in Medieval England*; The Boydell Press: Woodbridge, UK, 2006.
- Beaumont, J.; Montgomery, J. The Great Irish Famine: Identifying Starvation in the Tissues of Victims Using Stable Isotope Analysis of Bone and Incremental Dentine Collagen. *PLoS ONE* **2016**, *11*, e0160065. [[CrossRef](#)]
- Cerrito, P.; Bailey, S.E.; Hu, B.; Bromage, T.G. Parturitions, Menopause and Other Physiological Stressors Are Recorded in Dental Cementum Microstructure. *Sci. Rep.* **2020**, *10*, 5381. [[CrossRef](#)] [[PubMed](#)]
- Colard, T.; Bertrand, B.; Naji, S.; Delannoy, Y.; Bécart, A. Toward the Adoption of Cementochronology in Forensic Context. *Int. J. Legal Med.* **2018**, *132*, 1117–1124. [[CrossRef](#)] [[PubMed](#)]
- Dean, M.C. Retrieving Chronological Age from Dental Remains of Early Fossil Hominins to Reconstruct Human Growth in the Past. *Phil. Trans. R. Soc. B* **2010**, *365*, 3397–3410. [[CrossRef](#)] [[PubMed](#)]

27. Schwartz, G.T.; Reid, D.J.; Dean, M.C.; Zihlman, A.L. A Faithful Record of Stressful Life Events Recorded in the Dental Developmental Record of a Juvenile Gorilla. *Int. J. Primatol.* **2006**, *27*, 1201–1219. [[CrossRef](#)]
28. Skinner, M.; Byra, C. Signatures of Stress: Pilot Study of Accentuated Laminations in Porcine Enamel. *Am. J. Phys. Anthropol.* **2019**, *169*, 619–631. [[CrossRef](#)] [[PubMed](#)]
29. Fehrenbach, M.J.; Popowics, T. *Dental Embryology, Histology and Anatomy*; Elsevier: St. Louis, MI, USA, 2020; ISBN 978-0-323-63990-3.
30. Nanci, A. *Ten Cate's Oral Histology. Development, Structure and Function*; Elsevier: St. Louis, MI, USA, 2018.
31. Gherase, M.R.; Fleming, D.E.B. Probing Trace Elements in Human Tissues with Synchrotron Radiation. *Crystals* **2019**, *10*, 12. [[CrossRef](#)] [[PubMed](#)]
32. National Research Council. *Diet and Health: Implications for Reducing Chronic Disease Risk*; National Academies Press: Washington, DC, USA, 1989.
33. Prashanth, L.; Kattapagari, K.; Chitturi, R.T.; Baddam, V.R.R.; Prasad, L.K. A Review on Role of Essential Trace Elements in Health and Disease. *J. NTR Univ. Health Sci.* **2015**, *4*, 75–85. [[CrossRef](#)]
34. Fairweather-Tait, S.; Hurrell, R.F. Bioavailability of Minerals and Trace Elements: Members of EC Flair Concerted Action No. 10: Measurements of Micronutrient Absorption and Status. *Nutr. Res. Rev.* **1996**, *9*, 295–324. [[CrossRef](#)]
35. Soetan, K.; Olaiya, C.O.; Oyewole, O. The Importance of Mineral Elements for Humans, Domestic Animals and Plants: A Review. *Afr. J. Food Sci.* **2010**, *4*, 200–222.
36. Wada, O. What Are Trace Elements? Their Deficiency and Excess States. *JMAJ* **2004**, *47*, 351–358.
37. Rao, K.; Gupta, J.D.; Sehgal, V.; Chakrabarti, A.; Saha, K. Trace Elements in the Sera of Leprosy Spectrum. *Indian J. Lepr.* **1985**, *57*, 556–561. [[PubMed](#)]
38. Arora, P.; Dhillon, K.; Rajan, S.; Sayal, S.; Das, A. Serum Zinc Levels in Cutaneous Disorders. *MJAFI* **2002**, *58*, 304–306. [[CrossRef](#)] [[PubMed](#)]
39. George, J.; Bhatia, V.N.; Balakrishnan, S.; Ramu, G. Serum Zinc/Copper Ratio in Subtypes of Leprosy and Effect of Oral Zinc Therapy on Reactional States. *Int. J. Lepr. Other Mycobact. Dis.* **1991**, *59*, 20–24. [[PubMed](#)]
40. Mathur, N.K.; Sharma, M.L.; Mangal, H.N.; Rai, S.M. Serum Zinc Levels in Subtypes of Leprosy. *Int. J. Lepr. Other Mycobact. Dis.* **1984**, *52*, 327–330. [[PubMed](#)]
41. Pradhan, T.; Kumari, S. Evaluation of Oxidative Status and Zinc Level in Leprosy Patients after Zinc Supplementation. *Int. Biol. Med. Res.* **2015**, *6*, 4984–4987.
42. Saxena, N.; Sharma, R.; Singh, V.S. Study of Serum Zinc Level in Leprosy. *Indian J. Lepr.* **1988**, *60*, 556–561. [[PubMed](#)]
43. Saxena, N.; Sharma, R.; Singh, V.S. Serum Iron and Total Iron Binding Capacity in Leprosy Patients. *Indian J. Lepr.* **1990**, *62*, 219–222. [[PubMed](#)]
44. Bhattacharya, R.N.; Goswami, K.; Bandyopadhyay, A. Copper and Ascorbic Acid Status in Children Suffering from Leprosy. *EJBPS* **2020**, *7*, 421–423.
45. Jain, P.; Khare, V.; Koshti, A.; Malik, R.; Bhimte, B. Serum Zinc Level Estimation- Comparison between Normal Control and in Leprosy Patients. *Int. J. Biol. Med. Res.* **2014**, *5*, 3847–3849.
46. Oon, B.B.; Khong, K.Y.; Greaves, M.W.; Plummer, V.M. Trophic Skin Ulceration of Leprosy: Skin and Serum Zinc Concentrations. *BMJ* **1974**, *2*, 531–533. [[CrossRef](#)]
47. Mennen, U.; Howells, C.; Wiese, A. Serum Zinc, Sodium, Calcium, Magnesium and Potassium Levels and Standard Diet in Leprosy Patients. *Indian J. Lepr.* **1993**, *65*, 415–421. [[PubMed](#)]
48. Rao, K.N.; Saha, K. Undernutrition in Lepromatous Leprosy, Part II. Altered Levels of Serum Elements. Their Association with the Disease and Not with Food Deprivation. *Lepr. Rev.* **1986**, *57*, 311–316. [[CrossRef](#)] [[PubMed](#)]
49. Sher, R.; Shulman, G.; Baily, P.; Politzer, W.M. Serum Trace Elements and Vitamin A in Leprosy Subtypes. *Am. J. Clin. Nutr.* **1981**, *34*, 1918–1924. [[CrossRef](#)] [[PubMed](#)]
50. Wannemacher, R.W.; Pekarek, R.S.; Klainer, A.S.; Bartelloni, P.J.; Dupont, H.L.; Hornick, R.B.; Beisel, W.R. Detection of a Leukocytic Endogenous Mediator-like Mediator of Serum Amino Acid and Zinc Depression during Various Infectious Illnesses. *Infect. Immun.* **1975**, *11*, 873–875. [[CrossRef](#)] [[PubMed](#)]
51. Kumar, N.; Malhotra, V.; Singh, R.; Vij, J.; Anand, B. Structure and Function of the Small Bowel in Lepromatous Leprosy. *Int. J. Lepr. Other Mycobact. Dis.* **1982**, *50*, 148–151. [[PubMed](#)]
52. Bhattacharya, R.N.; Goswami, K.; Bandyopadhyay, A. Plasma Copper and Ascorbic Acid Status in Leprosy. *EJBPS* **2020**, *7*, 248–252.
53. Bharadwaj, V.P.; Venkatesan, K.; Ramu, G.; Desikan, K.V. Serum Iron and Total Iron Binding Capacity in Leprosy Patients. *Leprosy in India* **1978**, *50*, 11–17. [[PubMed](#)]
54. Shwe, T.; Than-Toe; Tu, A.T.B. Serum Iron and Total Iron Binding Capacity in Burmese Patients with Leprosy. *Lepr. Rev.* **1976**, *47*, 190–287. [[CrossRef](#)]
55. Tamara, R.; Muchtar, S.V.; Amin, S.; Seweng, A.; Sjahril, R.; Adam, A.M. Serum Iron, Total Iron Binding Capacity and Transferrin Saturation Levels in Leprosy Patients before Multi Drug Therapy - World Health Organization (MDT-WHO) Compared with Healthy Control Group. *Int. J. Med. Rev. Case Rep.* **2018**, *2*, 105–108.

56. Jain, A.; Mukherjee, A.; Chattopadhyaya, D.; Saha, K. Biometals in Skin and Sera of Leprosy Patients and Their Correlation to Trace Element Contents of M. Leprae and Histological Types of the Disease, a Comparative Study with Cutaneous Tuberculosis. *Int. J. Lepr. Other Mycobact. Dis.* **1995**, *63*, 249.
57. Swathi, M.; Tagore, R. Study of Oxidative Stress in Different Forms of Leprosy. *Indian J. Dermatol.* **2015**, *60*, 321. [[CrossRef](#)] [[PubMed](#)]
58. Skaar, E.P.; Raffatellu, M. Metals in Infectious Diseases and Nutritional Immunity. *Metallomics* **2015**, *7*, 926–928. [[CrossRef](#)] [[PubMed](#)]
59. Weinberg, E.D. Nutritional Immunity: Host's Attempt to Withhold Iron from Microbial Invaders. *JAMA* **1975**, *231*, 39–41. [[CrossRef](#)] [[PubMed](#)]
60. Botella, H.; Stadthagen, G.; Lugo-Villarino, G.; de Chastellier, C.; Neyrolles, O. Metallobiology of Host–Pathogen Interactions: An Intoxicating New Insight. *Trends Microbiol.* **2012**, *20*, 106–112. [[CrossRef](#)] [[PubMed](#)]
61. Hood, M.I.; Skaar, E.P. Nutritional Immunity: Transition Metals at the Pathogen–Host Interface. *Nat. Rev. Microbiol.* **2012**, *10*, 525–537. [[CrossRef](#)] [[PubMed](#)]
62. Neyrolles, O.; Mintz, E.; Catty, P. Zinc and Copper Toxicity in Host Defense against Pathogens: Mycobacterium Tuberculosis as a Model Example of an Emerging Paradigm. *Front. Cell. Infect. Microbiol.* **2013**, *3*, 89. [[CrossRef](#)] [[PubMed](#)]
63. Møller-Christensen, V. Hvad de Døde Fortalte. *Historisk Samfund for Præstø Amt* **1954**, *4*, 86–101.
64. Madsen, K. *Spedalskhed Og Sct. Jørgensgård*; Næstved Museum: Næstved, Denmark, 1990.
65. Arentoft, E. *De spedalskes hospital: Udgravning af Sankt Jørgensgården i Odense*; Odense Bys Museer: Odense, Denmark, 1999; ISBN 87-7838-500-8.
66. Nielsen, E. *Beretning for Udgravningen 1980-81 Af Sct. Jørgensgården, Odense*. 1981.
67. Michelsen, F. St. Jørgensgården i Aaderup Ved Næstved. *Årbog Hist. Samf. Præstø* **1954**, *4*, 72–85.
68. Ehlers, E. *Danske St. Jørgensgaard i Middelalderen.*; FR. Bagges Bogtrykkeri: Copenhagen, Denmark, 1898.
69. Erslev, K. *Testamenter fra Danmarks Middelalder indtil 1450*; Den Gyldendalske Boghandel: Copenhagen, Denmark, 1901.
70. Møller-Christensen, V. Location and Excavation of the First Danish Leper Graveyard from the Middle Ages – St. Jørgen's Farm, Næstved. *Bull. Hist. Med.* **1953**, *27*, 112–123. [[PubMed](#)]
71. Nielsen, E. Sct. Jørgensgården i Odense. *Fynske Minder 1982* **1983**, 61–74.
72. Richards, P. *The Medieval Leper and His Northern Heirs*; Butler & Tanner Ltd.: Cambridge, UK, 1977.
73. Boldsen, J.L.; Møllerup, L. Outside St. Jørgen: Leprosy in the Medieval Danish City of Odense. *Am. J. Phys. Anthropol.* **2006**, *130*, 344–351. [[CrossRef](#)]
74. Møller-Christensen, V. *Bone Changes in Leprosy*; Munksgaard: Copenhagen, Denmark, 1961.
75. Møller-Christensen, V. *Ten Lepers from Næstved in Denmark. A Study of Skeletons from a Medieval Danish Leper Hospital*; Danish Science Press: Copenhagen, Denmark, 1953.
76. Schuur, A. *Pathology of the Hard Dental Tissues*; John Wiley & Sons: Chichester, UK, 2013.
77. Boesenberg, U.; Ryan, C.G.; Kirkham, R.; Siddons, D.P.; Alfeld, M.; Garrevoet, J.; Núñez, T.; Claussen, T.; Kracht, T.; Falkenberg, G. Fast X-Ray Microfluorescence Imaging with Submicrometer-Resolution Integrating a Maia Detector at Beamline P06 at PETRA III. *J. Synchrotron Rad.* **2016**, *23*, 1550–1560. [[CrossRef](#)] [[PubMed](#)]
78. Schroer, C.; Boye, P.; Feldkamp, J.; Patommel, J.; Samberg, D.; Schropp, A.; Schwab, A.; Stephan, S.; Falkenberg, G.; Wellenreuther, G.; et al. Hard X-Ray Nanoprobe at Beamline P06 at PETRA III. *Nucl. Instrum. Meth. A* **2010**, *616*, 93–97. [[CrossRef](#)]
79. AlQahtani, S.J.; Hector, M.P.; Liversidge, H.M. Brief Communication: The London Atlas of Human Tooth Development and Eruption. *Am. J. Phys. Anthropol.* **2010**, *142*, 481–490. [[CrossRef](#)] [[PubMed](#)]
80. Burger, M.; Gundlach-Graham, A.; Allner, S.; Schwarz, G.; Wang, H.A.O.; Gyr, L.; Burgener, S.; Hattendorf, B.; Grolimund, D.; Günther, D. High-Speed, High-Resolution, Multielemental LA-ICP-TOFMS Imaging: Part II. Critical Evaluation of Quantitative Three-Dimensional Imaging of Major, Minor, and Trace Elements in Geological Samples. *Anal. Chem.* **2015**, *87*, 8259–8267. [[CrossRef](#)] [[PubMed](#)]
81. Gundlach-Graham, A.; Günther, D. Toward Faster and Higher Resolution LA-ICPMS Imaging: On the Co-Evolution of LA Cell Design and ICPMS Instrumentation. *Anal. Bioanal. Chem.* **2016**, *408*, 2687–2695. [[CrossRef](#)] [[PubMed](#)]
82. Armbruster, D.A.; Pry, T. Limit of Blank, Limit of Detection and Limit of Quantitation. *Clin. Biochem. Rev.* **2008**, *29*, S49–S52.
83. RStudio Team. *RStudio: Integrated Development Environment for R*; RStudio, PBC: Boston, MA, USA, 2020.
84. Dean, M.C.; Spiers, K.M.; Garrevoet, J.; Le Cabec, A. Synchrotron X-Ray Fluorescence Mapping of Ca, Sr and Zn at the Neonatal Line in Human Deciduous Teeth Reflects Changing Perinatal Physiology. *Arch. Oral Biol.* **2019**, *104*, 90–102. [[CrossRef](#)]
85. Humphrey, L.T.; Jeffries, T.E.; Dean, M.C. Micro Spatial Distributions of Lead and Zinc in Human Deciduous Tooth Enamel. In *Technique and application in Dental Anthropology*; Irish, J.D., Nelson, G.C., Eds.; Cambridge University Press: Cambridge, UK, 2008; pp. 87–110.
86. Müller, W.; Nava, A.; Evans, D.; Rossi, P.F.; Alt, K.W.; Bondioli, L. Enamel Mineralization and Compositional Time-Resolution in Human Teeth Evaluated via Histologically-Defined LA-ICPMS Profiles. *Geochim. Cosmochim. Acta* **2019**, *255*, 105–126. [[CrossRef](#)]
87. Barbosa, F.; Tanus-Santos, J.E.; Gerlach, R.F.; Parsons, P.J. A Critical Review of Biomarkers Used for Monitoring Human Exposure to Lead: Advantages, Limitations, and Future Needs. *Environ. Health Perspect.* **2005**, *113*, 1669–1674. [[CrossRef](#)]
88. Bercovitz, K.; Laufer, D. Age and Gender Influence on Lead Accumulation in Root Dentine of Human Permanent Teeth. *Arch. Oral Biol.* **1991**, *36*, 671–673. [[CrossRef](#)]

89. Mahajan, P.; Jadhav, V.; Patki, A.H.; Jogaikar, D.G.; Mehta, J. Oral Zinc Therapy in Recurrent Erythema Nodosum Leprosum: A Clinical Study. *Indian J. Lepr.* **1994**, *66*, 51–57. [[PubMed](#)]
90. Naafs, B.; Noto, S. Reactions in Leprosy. In *Leprosy. A Practical Guide.*; Nunzi, E., Massone, C., Eds.; Springer-Verlag: Milan, Italy, 2012; pp. 219–240.
91. Cool, S.M.; Forwood, M.R.; Campbell, P.; Bennett, M.B. Comparisons between Bone and Cementum Compositions and the Possible Basis for Their Layered Appearances. *Bone* **2002**, *30*, 386–392. [[CrossRef](#)] [[PubMed](#)]
92. Martin, R.R.; Naftel, S.J.; Nelson, A.J.; Feilen, A.B.; Narvaez, A. Metal Distributions in the Cementum Rings of Human Teeth: Possible Depositional Chronologies and Diagenesis. *J. Archaeol. Sci.* **2007**, *34*, 936–945. [[CrossRef](#)]
93. Martin, R.R.; Naftel, S.J.; Nelson, A.J.; Feilen, A.B.; Narvaez, A. Synchrotron X-Ray Fluorescence and Trace Metals in the Cementum Rings of Human Teeth. *J. Environ. Monit.* **2004**, *6*, 783–786. [[CrossRef](#)] [[PubMed](#)]
94. Dean, C.; Le Cabec, A.; Spiers, K.; Zhang, Y.; Garrevoet, J. Incremental Distribution of Strontium and Zinc in Great Ape and Fossil Hominin Cementum Using Synchrotron X-Ray Fluorescence Mapping. *J. R. Soc. Interface.* **2018**, *15*, 20170626. [[CrossRef](#)] [[PubMed](#)]
95. Stock, S.R.; Finney, L.A.; Telser, A.; Maxey, E.; Vogt, S.; Okasinski, J.S. Cementum Structure in Beluga Whale Teeth. *Acta Biomater.* **2017**, *48*, 289–299. [[CrossRef](#)] [[PubMed](#)]
96. Stock, S.R.; Deymier-Black, A.C.; Veis, A.; Telser, A.; Lux, E.; Cai, Z. Bovine and Equine Peritubular and Intertubular Dentin. *Acta Biomater.* **2014**, *10*, 3969–3977. [[CrossRef](#)] [[PubMed](#)]
97. Cohen, D.D.; Clayton, E.; Ainsworth, T. Preliminary Investigations of Trace Element Concentrations in Human Teeth. *Nucl. Instrum. Methods Phys. Res., B* **1981**, *188*, 203–209. [[CrossRef](#)]
98. Dean, C.; Le Cabec, A.; Van Malderen, S.J.M.; Garrevoet, J. Synchrotron X-Ray Fluorescence Imaging of Strontium Incorporated into the Enamel and Dentine of Wild-Shot Orangutan Canine Teeth. *Arch. Oral Biol.* **2020**, 104879. [[CrossRef](#)]
99. Rautray, T.R.; Das, S.; Rautray, A.C. *In Situ* Analysis of Human Teeth by External PIXE. *Nucl. Instrum. Methods Phys. Res., B* **2010**, *268*, 2371–2374. [[CrossRef](#)]
100. Carvalho, M.L.; Casaca, C.; Marques, J.P.; Pinheiro, T.; Cunha, A.S. Human Teeth Elemental Profiles Measured by Synchrotron X-Ray Fluorescence: Dietary Habits and Environmental Influence. *X-Ray Spectrom.* **2001**, *30*, 190–193. [[CrossRef](#)]
101. Bouillon, R.; Suda, T. Vitamin D: Calcium and Bone Homeostasis during Evolution. *BoneKey Reports* **2014**, 1–10. [[CrossRef](#)] [[PubMed](#)]
102. King, J.C.; Shames, D.M.; Woodhouse, L.R. Zinc Homeostasis in Humans. *J. Nutr.* **2000**, *130*, 1360S–1366S. [[CrossRef](#)] [[PubMed](#)]
103. Walczyk, T.; von Blanckenburg, F. Natural Iron Isotope Variations in Human Blood. *Science* **2002**, *295*, 2065–2066. [[CrossRef](#)] [[PubMed](#)]
104. Veldurthy, V.; Wei, R.; Oz, L.; Dhawan, P.; Jeon, Y.H.; Christakos, S. Vitamin D, Calcium Homeostasis and Aging. *Bone Research* **2016**, *4*, 1–7. [[CrossRef](#)] [[PubMed](#)]
105. Kovacs, C.S. Calcium and Bone Metabolism during Pregnancy and Lactation. *J. Mammary Gland Biol. Neoplasia* **2015**, *10*. [[CrossRef](#)]
106. Rawcliffe, C. *Medicine and Society in Later Medieval England*, 2nd ed.; Sandpiper Books Ltd.: London, UK, 1999.
107. Demaitre, L. *Leprosy in Premodern Medicine. A Malady of the Whole Body*; The Johns Hopkins University Press: Baltimore, MD, USA, 2007.
108. Brenner, E. *Leprosy and Charity in Medieval Rouen*; The Boydell Press: Woodbridge, VA, USA, 2015.
109. Jáuregui, C. Inside the Leprosarium: Illness in the Daily Life of 14th Century Rouen. In *New Approaches to Disease, Disability, and Medicine in Medieval Europe*; Connolly, E., Künzel, S., Eds.; The Holywell Press: Oxford, UK, 2018.
110. Pedersen, C. *En Nøttelig Legebog*; Pedersen: Malmø, Sweden, 1533.
111. Smit, H. *En Skøn Nyttelig Lægebog Ind Hollendis Atskillige Mange Skøne Forfarne Lægedommer Huilcke Som Tiæne Barts Kerrerne, Oc Dem Som Ville Læge Ferske Oc Gamle Saar. Desligiste Oc Om Bad Aare Ladelse Oc Koppe Settelse, Och Om de Lagedomme Som Findis i Apotecken Fale.*; Vingaard, Hans: Malmø, Sweden, 1557.
112. Norse Medical and Herbal Healing. *A Medical Book from Medieval Iceland*; Troth Publications: New Haven, CT, USA, 2011.
113. Arrizabalaga, J.; Henderson, J.; French, R. *The Great Pox. The French Disease in Renaissance Europe*; Yale University Press: New Haven, CT, USA, 1997.
114. Goldwater, L.J. *Mercury. A History of Quicksilver*; York Press: Baltimore, MD, USA, 1972.
115. Lev, E. Drugs Held and Sold by Pharmacists of the Jewish Community of Medieval (11–14th Centuries) Cairo According to Lists of Materia Medica Found at the Taylor–Schechter Genizah Collection, Cambridge. *J. Ethnopharmacol.* **2007**, *110*, 275–293. [[CrossRef](#)]
116. Nriagu, J.O. Saturnine Drugs and Medicinal Exposure to Lead: An Historical Outline. In *Human Lead Exposure*; Needleman, H.L., Ed.; CRC Press: Boca Raton, FL, USA, 1992; pp. 3–22.
117. Dawson, W.R. *A Leechbook or Collection of Medical Recipes of the Fifteenth Century*; MacMillan and Co., Limited: London, UK, 1934.
118. Ogden, M.S. *The Liber de Diversis Medicinis*; Oxford University Press: London, UK, 1969.
119. Harward, C.; Holder, N.; Phillipotts, C.; Thomas, C. *The Medieval Priory and Hospital of St Mary Spital and the Bishopsgate Suburb. Excavations at Spitalfields Market, London E1, 1991–2007*; MOLA Monograph 59; MOLA: London, UK, 2019.
120. Buckingham, J. *Leprosy in Colonial South India: Medicine and Confinement.*; Palgrave Macmillan: New York, NY, USA, 2002; ISBN 1-349-42530-3.

121. Rasmussen, K.L.; Boldsen, J.L.; Kristensen, H.K.; Skytte, L.; Hansen, K.L.; Mølholm, L.; Grootes, P.M.; Nadeau, M.-J.; Eriksen, K.M.F. Mercury Levels in Danish Medieval Human Bones. *J. Archaeol. Sci.* **2008**, *35*, 2295–2306. [[CrossRef](#)]
122. Rasmussen, K.L.; Skytte, L.; Jensen, A.J.; Boldsen, J.L. Comparison of Mercury and Lead Levels in the Bones of Rural and Urban Populations in Southern Denmark and Northern Germany during the Middle Ages. *J. Archaeol. Sci. Rep.* **2015**, *3*, 358–370. [[CrossRef](#)]
123. Rasmussen, E.G. Antimony, Arsenic, Bromine and Mercury in Enamel from Human Teeth. *Eur. J. Oral Sci.* **1974**, *82*, 562–565. [[CrossRef](#)] [[PubMed](#)]
124. Rasmussen, L.K.; Skytte, L.; D'Imporzano, P.; Thomsen, O.P.; Søvsø, M.; Lier Boldsen, J. On the Distribution of Trace Element Concentrations in Multiple Bone Elements in 10 Danish Medieval and Post-Medieval Individuals. *Am. J. Phys. Anthropol.* **2016**, *162*, 90–102. [[CrossRef](#)] [[PubMed](#)]
125. Budd, P.; Millard, A.; Chenery, C.; Lucy, S.; Roberts, C. Investigating Population Movement by Stable Isotope Analysis: A Report from Britain. *Antiquity* **2004**, *78*, 127–141. [[CrossRef](#)]
126. Le Roux, G.; Weiss, D.; Grattan, J.; Givélet, N.; Krachler, M.; Cheburkin, A.; Rausch, N.; Kober, B.; Shotyk, W. Identifying the Sources and Timing of Ancient and Medieval Atmospheric Lead Pollution in England Using a Peat Profile from Lindow Bog, Manchester. *J. Environ. Monit.* **2004**, *6*, 502–510. [[CrossRef](#)] [[PubMed](#)]
127. Lessler, M.A. Lead and Lead Poisoning from Antiquity to Modern Times. *Ohio J. Sci.* **1988**, *88*, 78–84.
128. Rasmussen, K.L.; Delbey, T.; d'Imporzano, P.; Skytte, L.; Schiavone, S.; Torino, M.; Tarp, P.; Thomsen, P.O. Comparison of Trace Element Chemistry in Human Bones Interred in Two Private Chapels Attached to Franciscan Friaries in Italy and Denmark: An Investigation of Social Stratification in Two Medieval and Post-Medieval Societies. *Herit. Sci.* **2020**, *8*, 65. [[CrossRef](#)]
129. Alexandrovskaya, E.I.; Panova, T. History of the Soil, Cultural Layer, and People in Medieval Moscow. *Rev. Mex. Cienc.* **2003**, *20*, 289–294. [[CrossRef](#)]
130. *Critical Approaches to the History of Western Herbal Medicine: From Classical Antiquity to the Early Modern Period*; Francia, S.; Stobart, A. (Eds.) Bloomsbury: London, UK, 2014; ISBN 978-1-4411-8418-4.
131. Nielsen, O.V.; Grandjean, P.; Bennike, P. Chemical Analyses of Archaeological Bone-Samples: Evidence for High Lead Exposure on the Faroe Islands. *J. Dan. Archaeol.* **1982**, *1*, 145–148. [[CrossRef](#)]
132. Bigi, A.; Gandolfi, M.; Gazzano, M.; Ripamonti, A.; Roveri, N.; Thomas, S.A. Structural Modifications of Hydroxyapatite Induced by Lead Substitution for Calcium. *J. Chem. Soc., Dalton Trans.* **1991**, 2883–2886. [[CrossRef](#)]
133. Carvalho, M.L.; Casaca, C.; Pinheiro, T.; Marques, J.P.; Chevallerier, P.; Cunha, A.S. Analysis of Human Teeth and Bones from the Chalcolithic Period by X-Ray Spectrometry. *Nucl. Instrum. Methods Phys. Res. B* **2000**, *168*, 559–565. [[CrossRef](#)]
134. Pounds, G.J.; Long, G.J.; Rosen, J.F. Cellular and Molecular Toxicity of Lead in Bone. *Environ. Health Perspect.* **1991**, *91*, 17–32. [[CrossRef](#)] [[PubMed](#)]
135. Rabinowitz, M.B.; Leviton, A.; Bellinger, D. Relationships between Serial Blood Lead Levels and Exfoliated Tooth Dentin Lead Levels: Models of Tooth Lead Kinetics. *Calcif. Tissue Int.* **1993**, *53*, 338–341. [[CrossRef](#)]
136. Steenhout, A. Kinetics of Lead Storage in Teeth and Bones: An Epidemiologic Approach. *Arch. Environ. Health* **1982**, *37*, 224–231. [[CrossRef](#)] [[PubMed](#)]
137. Gulson, B.L.; Gillings, B.R. Lead Exchange in Teeth and Bone—A Pilot Study Using Stable Lead Isotopes. *Environ. Health Perspect.* **1997**, *105*, 820–824. [[CrossRef](#)] [[PubMed](#)]
138. Arora, M.Y.; Chan, S.W.; Kennedy, B.J.; Sharma, A.; Crisante, D.; Murray Walker, D. Spatial Distribution of Lead in the Roots of Human Primary Teeth. *J. Trace Elem. Med. Biol.* **2004**, *18*, 135–139. [[CrossRef](#)] [[PubMed](#)]
139. Cox, A.; Keenan, F.; Cooke, M.; Appleton, J. Trace Element Profiling of Dental Tissues Using Laser Ablation-Inductively Coupled Plasma-Mass Spectrometry. *Fresen. J. Anal. Chem.* **1996**, *354*, 254–258. [[CrossRef](#)]
140. Gulson, B.L. Tooth Analyses of Sources and Intensity of Lead Exposure in Children. *Environ. Health Perspect.* **1996**, *104*, 306–312. [[CrossRef](#)] [[PubMed](#)]
141. Steenhout, A.; Pourtois, M. Lead Accumulation in Teeth as a Function of Age with Different Exposures. *Br. J. Ind. Med.* **1981**, *38*, 297. [[CrossRef](#)]
142. Shapiro, I.M.; Mitchell, G.; Davidson, I.; Katz, S.H. The Lead Content of Teeth. *Arch. Environ. Health* **1975**, *30*, 483–486. [[CrossRef](#)]
143. Shepherd, T.J.; Dirks, W.; Manmee, C.; Hodgson, S.; Banks, D.A.; Averley, P.; Pless-Mulloli, T. Reconstructing the Life-Time Lead Exposure in Children Using Dentine in Deciduous Teeth. *Sci. Total Environ.* **2012**, *425*, 214–222. [[CrossRef](#)]
144. Pascu, G. Le Patrimoine Industriel-Minier Facteur de Développement Territorial: Complexité et Enjeux en Roumanie, en Comparaison Avec la France et la Grande-Bretagne. Master thesis, Université Jean Monnet (Saint-Etienne, France) and Universitatea Politehnica (Timisoara, Romania), Timisoara, Romania, 2015.
145. Ide-Ektessabi, A.; Shirasawa, K.; Koizumi, A.; Azechi, M. Application of Synchrotron Radiation Microbeams to Environmental Monitoring. *Nucl. Instrum. Methods Phys. Res. B* **2004**, *213*, 761–765. [[CrossRef](#)]
146. Wang, Y.; Specht, A.; Liu, Y.; Finney, L.; Maxey, E.; Vogt, S.; Zheng, W.; Weisskopf, M.; Nie, L.H. Microdistribution of Lead in Human Teeth Using Microbeam Synchrotron Radiation X-Ray Fluorescence (μ -SRXRF): Microdistribution of Lead in Human Teeth Using μ -SRXRF. *X-Ray Spectrom.* **2016**, *46*, 19–26. [[CrossRef](#)] [[PubMed](#)]
147. Talpur, S.; Afridi, H.I.; Kazi, T.G.; Talpur, F.N. Interaction of Lead with Calcium, Iron, and Zinc in the Biological Samples of Malnourished Children. *Biol. Trace Elem. Res.* **2018**, *183*, 209–217. [[CrossRef](#)]

148. Miller, G.D.; Massaro, T.; Massaro, E.J. Interactions between Lead and Essential Elements: A Review. *Neurotoxicology* **1990**, *11*, 99–119.
149. Bartoń, H. Advantages of the Use of Deciduous Teeth, Hair, and Blood Analysis for Lead and Cadmium Bio-Monitoring in Children. A Study of 6-Year-Old Children from Krakow (Poland). *Biol. Trace Elem. Res.* **2011**, *143*, 637–658. [[CrossRef](#)]
150. Brudevold, F.; Steadman, L.T.; Smith, F.A. Inorganic and Organic Components of Tooth Structure. *Ann. N. Y. Acad. Sci.* **1960**, *85*, 110–132. [[CrossRef](#)] [[PubMed](#)]
151. Okada, M. Hard Tissues of Animal Body: Highly Interesting Details of Nippon Studies in Periodic Patterns of Hard Tissues Are Described. *Shanghai Evening Post* **1943**, *recreation and medical progress.*, 15–31.
152. Papakyrikos, A.M.; Arora, M.; Austin, C.; Boughner, J.C.; Capellini, T.D.; Dingwall, H.L.; Greba, Q.; Howland, J.G.; Kato, A.; Wang, X.-P.; et al. Biological Clocks and Incremental Growth Line Formation in Dentine. *J. Anat.* **2020**, *237*, 367–378. [[CrossRef](#)]
153. Macchiarelli, R.; Bondioli, L.; Debénath, A.; Mazurier, A.; Tournepiche, J.-F.; Birch, W.; Dean, M.C. How Neanderthal Molar Teeth Grew. *Nature* **2006**, *444*, 748–751. [[CrossRef](#)]
154. Grandjean, P. Lead in Danes. In *Lead*; Griffin, T.B., Knelson, J.H., Eds.; Georg Thieme Publishers: Stuttgart, Germany, 1975; pp. 6–75.
155. Franklin, C.A.; Inskip, M.J.; Bacchanale, C.L.; Edwards, C.M.; Manton, W.I.; Edwards, E.; O’Flaherty, E.J. Use of Sequentially Administered Stable Lead Isotopes to Investigate Changes in Blood Lead during Pregnancy in a Nonhuman Primate (*Macaca Fascicularis*). *Fundam. Appl. Toxicol.* **1997**, *39*, 109–119. [[CrossRef](#)]
156. Gulson, B.; Mizon, K.; Korsch, M.; Taylor, A. Revisiting Mobilisation of Skeletal Lead during Pregnancy Based on Monthly Sampling and Cord/Maternal Blood Lead Relationships Confirm Placental Transfer of Lead. *Arch. Toxicol.* **2016**, *90*, 805–816. [[CrossRef](#)]
157. Austin, C.; Smith, T.M.; Farahani, R.M.Z.; Hinde, K.; Carter, E.A.; Lee, J.; Lay, P.A.; Kennedy, B.J.; Sarrafpour, B.; Wright, R.J.; et al. Uncovering System-Specific Stress Signatures in Primate Teeth with Multimodal Imaging. *Sci. Rep.* **2016**, *6*, 18802. [[CrossRef](#)]
158. Cleymaet, R.; Collys, K.; Retief, D.H.; Michotte, Y.; Slop, D.; Taghon, E.; Maex, W.; Coomans, D. Relation between Lead in Surface Tooth Enamel, Blood, and Saliva from Children Residing in the Vicinity of a Non-Ferrous Metal Plant in Belgium. *Br. J. Ind. Med.* **1991**, *48*, 702. [[CrossRef](#)]
159. Habercam, J.W.; Keil, J.E.; Routt Reigart, J.; Croft, H.W. Lead Content of Human Blood, Hair, and Deciduous Teeth: Correlation with Environmental Factors and Growth. *J. Dent. Res.* **1974**, *53*, 1160–1163. [[CrossRef](#)]
160. Fewtrell, L.; Kaufmann, R.; Prüss-Üstün, A. *Lead: Assessing the Environmental Burden of Disease at National and Local Levels*; WHO Environmental Burden of Disease Series, No. 2; World Health Organization: Geneva, Switzerland, 2003.
161. *World Health Organization Childhood Lead Poisoning*; WHO Document Production Services: Geneva, Switzerland, 2010.

Disclaimer/Publisher’s Note: The statements, opinions and data contained in all publications are solely those of the individual author(s) and contributor(s) and not of MDPI and/or the editor(s). MDPI and/or the editor(s) disclaim responsibility for any injury to people or property resulting from any ideas, methods, instructions or products referred to in the content.

File S1

Methods and Statistical results

Using SXRF and LA-ICP-TOFMS to explore evidence of treatment and physiological responses to leprosy in medieval Denmark

Biology

Anastasia Brozou, Marcello A. Mannino, Stijn J.M. Van Malderen, Jan Garrevoet, Eric Pubert, Benjamin T. Fuller, M. Christopher Dean, Thomas Colard, Frédéric Santos, Niels Lynnerup, Jesper L. Boldsen, Marie Louise Jørkov, Andrei Dorian Soficaru, Laszlo Vincze, Adeline Le Cabec

Corresponding author:

Adeline Le Cabec

E-mail: adeline.le-cabec@u-bordeaux.fr

Content

1. Methods

Tooth thin section preparation	2
SXRF data acquisition and processing	2
LA-ICP-TOFMS imaging of Odense 533M and Næstved 211C	3
Statistical analysis	3
References	4

2. Results

Næstved 211C – Cellular Cementum	5
Odense 533M1 – Acellular Cementum	18
Odense 533M1 – Cellular Cementum	31
Odense 533M1 – Secondary Dentine	42

1. Methods

Tooth thin section preparation

To optimise the chances of visualising an area of cementum not affected by taphonomic damages (e.g., cracks, remineralisation, fungi), and avoid restricting the field of view to acellular cementum where increments are tightly packed, the tooth root was sectioned longitudinally through the root apices. Single-rooted teeth (i.e., canines) were sectioned labio-lingually. For lower molars, a mesio-distal section enables to involve both root apices, while for three-rooted maxillary molars, the plane of section passed through the apices of the lingual root and the mesio-buccal root. Note that for molars, the plane of section was oriented to pass through the cusp tips as much as possible, in order to access the earliest information recorded during tooth growth.

Prior to sectioning, the teeth were embedded in epoxy resin for a minimum of 12 hours. A Buehler Linear Precision Saw Isomet 5000 was used in the cementochronology laboratory at *PACEA* (University of Bordeaux, France) to slice the tooth a bit off the desired plane of section. Subsequently, the tooth surface of the thicker half was first briefly polished using an abrasive disk P240 (NAC, Presi) with 58 μm particles size and resin disks (Imax-R, Presi) with 54 μm or 18 μm diamond particles embedded, and then glued on a glass slide (30 x 45 mm or 45 x 60 mm based on the size of each tooth) using epoxy resin at 65°C, under pressure for one hour. A further sectioning followed to produce tooth slices of ~300-400 μm , which were ground and lapped down to between 80-100 μm , first as described above and then using a fine diamond abrasive suspension at 9 μm , 3 μm and 1 μm (LDP polycrystalline diamond suspension, Presi) deposited on polishing clothes (PAD MAG, Presi).

SXRF data acquisition and processing

Experiments were performed on the P06 Beamline (Boesenberg et al., 2016; Schroer et al., 2010), Petra III, at DESY (Deutsches Elektronen-Synchrotron, Hamburg, Germany). The storage ring was operated in 480-bunch mode using top-up filling mode with a current of 120 mA \pm 0.5 mA, and an undulator gap of 11.07 mm. The primary X-ray beam was monochromatised to 16.6 keV using a double crystal Si111 monochromator and focused using a Kirkpatrick-Baez (KB) mirror system (JTEC, Japan) to 500 \times 500 nm². The experimental configuration consisted of two Vortex EM silicon drift detectors, Hitachi High-Tech Science America, Inc., the second of which was collimated. Both detectors were positioned symmetrically at scattering angles of 135 degrees at a distance of 9 mm from the focal point. The use of dual-detector “backscatter” geometry enables maximising the solid angle during analysis of thin polished samples (~100 μm -thick in this study), and imaging large area SXRF with micrometric resolution using millisecond dwell times (Falkenberg et al., 2017). This setup allowed capturing the K α emission lines from Si to Sr and the L α emission lines of Hg and Pb. The Mg signal, however, is drastically lowered by absorption through the sample itself and the air path. Furthermore, the Mg K α emission line is at 1.254 keV, which is not well-suited for the primary energy (16.6 keV). To note that some interferences within the spectrum may affect the sensitivity for detecting elements, such as Pb or Hg.

Spectral peak deconvolution and integration was performed using the core of PyMca 5.5.0 (Solé et al., 2007), whilst calibration was performed by an in-house script. Image analysis was performed in HDIP v-1.3.3.1073 (Teledyne CETAC Technologies, Bozeman, MT, USA). The X-ray yield calculations were performed assuming a hydroxyapatite matrix (Ca₁₀(PO₄)₆(OH)₂) with density of 2.85 g.cm⁻³ for the enamel phase and of 1.6 g.cm⁻³ for the dentine phase (Djomehri et al., 2015). Elemental mass fractions were determined by calculating an areal density sensitivity from measurements of standard Ti, Fe, and Cu foils with areal density of 59.0, 55.0, and 47.9 $\mu\text{g.cm}^{-2}$, respectively (Micromatter Technologies Inc. Canada), and measured thickness of the samples. Tooth section thickness was measured throughout the whole surface of the specimen in five positions for canines and eight positions for molars. The average tooth section thickness was also taken into account in the x-ray mass attenuation coefficients of the hydroxyapatite phase during attenuation correction

(Szczerbowska-Boruchowska, 2012). Glass slides substrates were included in the overall sample model as appropriate (i.e., background subtraction). Normalisation to the incoming X-ray flux was applied. In the calibrated data, SXRF concentrations are reported by mass fraction ($\mu\text{g}\cdot\text{g}^{-1}$, i.e., ppm), and/or areal density ($\text{g}\cdot\text{cm}^{-3}$). Pb images contain no quantitative data (i.e., relative Pb content is expressed in arbitrary units 'a.u.'), as L-lines were not modelled.

LA-ICP-TOFMS imaging of Odense 533M and Næstved 211C

LA-ICP-TOFMS imaging was performed at the Department of Chemistry, Ghent University (Belgium) with a setup consisting of an Iridia 193 nm ArF* excimer-based laser ablation system (Teledyne Photon Machines, Bozeman, MT, U.S.A.) coupled to an icpTOF 2R (TOFWERK AG, Thun, Switzerland) TOF-based ICP-MS instrument. The laser ablation system was equipped with the Cobalt Long-Pulse ablation cell and the aerosol rapid introduction system (ARIS), which introduced an Ar make-up gas flow ($\sim 1.05\text{ L}\cdot\text{min}^{-1}$) into an optimised He carrier gas flow of $0.60\text{ L}\cdot\text{min}^{-1}$ before entering the plasma. The LA-ICP-MS system was optimised via ablation of NIST SRM612 (National Institute for Standards and Technology, Gaithersburg, MD, U.S.A.), with tuning for the highest intensities for $^{24}\text{Mg}^+$, $^{115}\text{In}^+$ and $^{238}\text{U}^+$, whilst maintaining low oxide formation ($<1\% \text{ }^{238}\text{U}^{16}\text{O}^+ / ^{238}\text{U}^+$) and a ratio of $^{238}\text{U}^+ / ^{232}\text{Th}^+$ ratio ~ 1 . Imaging was performed in fixed dosage mode 1 and with an energy density of $3\text{ J}\cdot\text{cm}^{-2}$, at a repetition rate of 250 Hz, using a circular spot size of 4 or 2 μm , with a vertical interspacing between the lines between 20 and 2 μm . The images were recorded using bracketing with NIST SRM612. The icpTOF 2R ICP-TOFMS was operated in standard operation mode with a mass coverage range of 14-254 m/q. The read-out frames of 3.8 ms were synchronised with the laser ablation repetition rate, with a transfer delay of 53.7 ms. The iCAP Q was equipped with the LA injector of 2.5 mm inner diameter and nickel sample and skimmer cones with a skimmer cone insert of 2.8 mm in diameter. The RF power was set to 1500 W, and an auxiliary Ar gas flow rate of $\sim 0.90\text{ L}\cdot\text{min}^{-1}$ and a plasma Ar gas flow rate of $15\text{ L}\cdot\text{min}^{-1}$ were used.

Statistical analysis

The classical correlation tests involving Pearson's r and Spearman ρ (rho), (with $\alpha=0.05$) were computed in RStudio using the function `cor.test()`, and adjusting the method to "pearson" or "spearman". However, the Pearson correlation is sensitive to outliers, which may weaken the strength and the significance of the results. A more robust correlation test involving the Minimum Covariance Determinant (MCD) was calculated using the `corr.plot()` function. The MCD is a highly robust estimator of multivariate location and scatter (Hubert et al., 2018; Rousseeuw and Driessen, 1999; Santos, 2020). This procedure runs the correlation test on a user-defined percentage of the data (here `quan= 0.8`, meaning 80% of the data are kept) representing the "good part" of the data, thus removing values detected as outliers. Some elements such as Fe, Mn or Pb showed a substantial root surface enrichment, which may considerably disturb the computation of the tests. However, the MCD procedure may not remove all of the datapoints related to the root surface, but also exclude hotspots or high concentrations occurring within the cementum thickness, which could be related to a biological signal and, thus, be meaningful. Therefore, the classical and robust tests were also run by excluding the datapoints of the root surface and sub-surface defined by a peak in Pb, Mn or Fe, to assess if the significance of the correlation tests would be affected and change. All detailed results are reported below, and the classical Pearson results are plotted in blue while the MCD correlation is plotted in red. Correlation coefficient matrices were computed using the Spearman method, and plotted using 'corr.plot', which enables displaying the rho values following a colour code, and crossing out rho values when p-values are not significant.

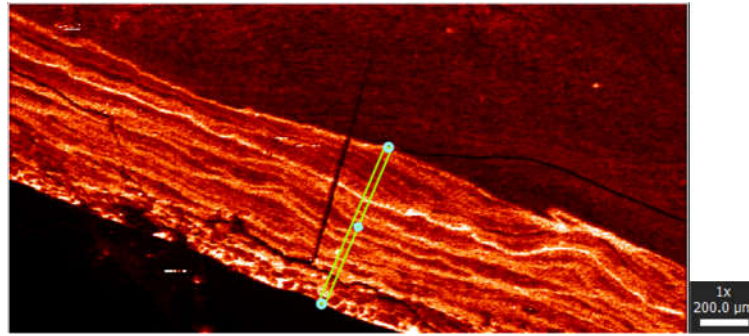
References

- Boesenberg, U., Ryan, C.G., Kirkham, R., Siddons, D.P., Alfeld, M., Garrevoet, J., Núñez, T., Claussen, T., Kracht, T., Falkenberg, G., 2016. Fast X-ray microfluorescence imaging with submicrometer-resolution integrating a Maia detector at beamline P06 at PETRA III. *J Synchrotron Rad* 23, 1550–1560. <https://doi.org/10.1107/S1600577516015289>
- Djomehri, S.I., Candell, S., Case, T., Browning, A., Marshall, G.W., Yun, W., Lau, S.H., Webb, S., Ho, S.P., 2015. Mineral density volume gradients in normal and diseased human tissues. *PLoS ONE* 10, e0121611. <https://doi.org/10.1371/journal.pone.0121611>
- Falkenberg, G., Fleissner, Gerta, Fleissner, Guenther, Alraun, P., Boesenberg, U., Spiers, K., 2017. Large-scale high-resolution micro-XRF analysis of histological structures in the skin of the pigeon beak. *X-Ray Spectrom.* 46, 467–473. <https://doi.org/10.1002/xrs.2769>
- Hubert, M., Debruyne, M., Rousseeuw, P.J., 2018. Minimum covariance determinant and extensions. *WIREs Computational Statistics* 10, e1421. <https://doi.org/10.1002/wics.1421>
- Rousseeuw, P.J., Driessen, K.V., 1999. A fast algorithm for the minimum covariance determinant estimator. *Technometrics* 41, 212–223. <https://doi.org/10.1080/00401706.1999.10485670>
- Santos, F., 2020. Modern methods for old data: An overview of some robust methods for outliers detection with applications in osteology. *J. Archaeol. Sci. Rep.* 32, 102423. <https://doi.org/10.1016/j.jasrep.2020.102423>
- Schroer, C., Boye, P., Feldkamp, J., Patommel, J., Samberg, D., Schropp, A., Schwab, A., Stephan, S., Falkenberg, G., Wellenreuther, G., Reimers, N., 2010. Hard X-ray nanoprobe at beamline P06 at PETRA III. *Nucl. Instrum. Meth. A* 616, 93–97. <https://doi.org/10.1063/1.4952830>
- Solé, V.A., Papillon, E., Cotte, M., Walter, P., Susini, J., 2007. A multiplatform code for the analysis of energy-dispersive X-ray fluorescence spectra. *Spectrochim. Acta Part B* 62, 63–68. <https://doi.org/10.1016/j.sab.2006.12.002>
- Szczerbowska-Boruchowska, M., 2012. Sample thickness considerations for quantitative X-ray fluorescence analysis of the soft and skeletal tissues of the human body - theoretical evaluation and experimental validation. *X-Ray Spectrom.* 41, 328–337. <https://doi.org/10.1002/xrs.2407>

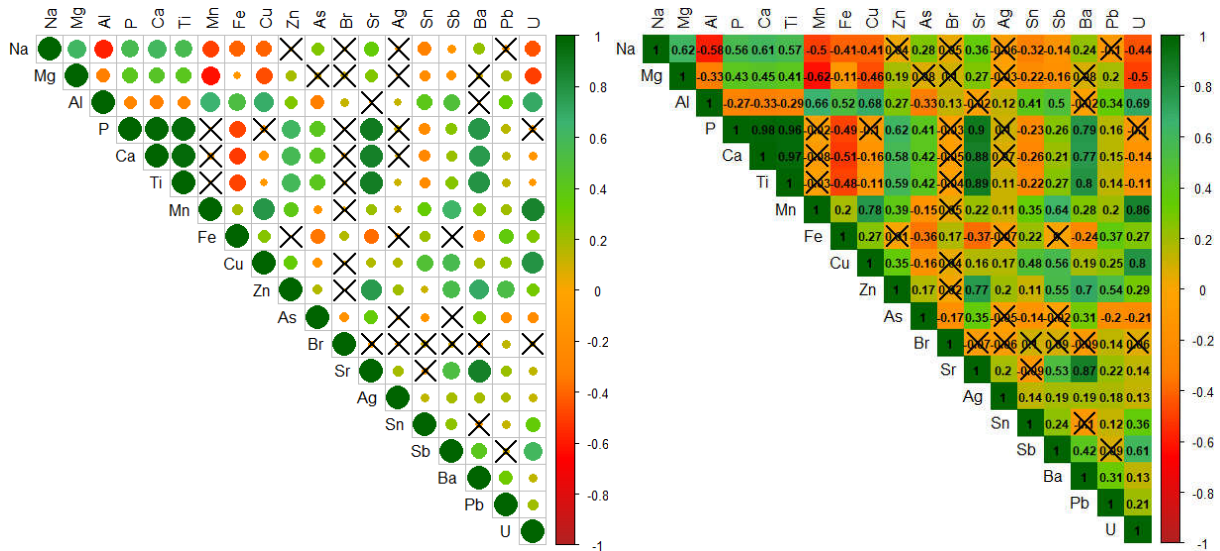
2. Results

Statistical analysis

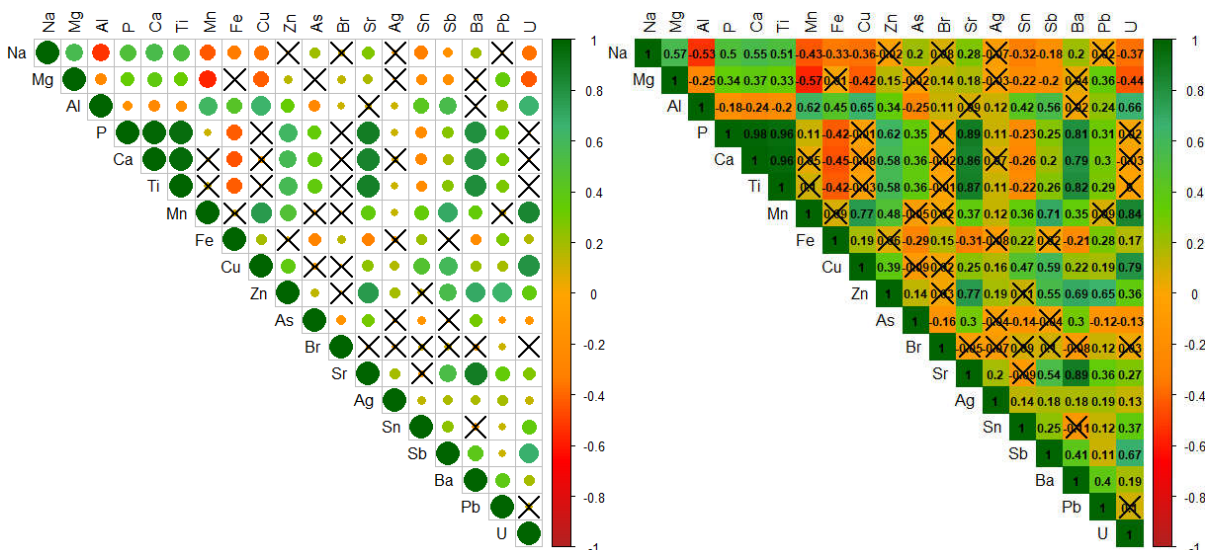
Næstved 211C – Cellular Cementum (total thickness=721 μm) Correlations between pairs of elements



Zn map (yellow path indicates where the measurements are taken)
Summary: whole cementum thickness, Spearman correlations.



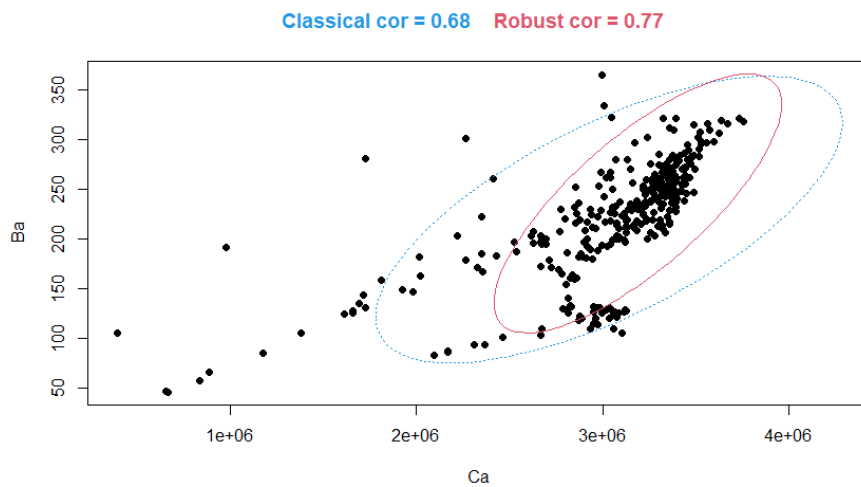
Summary: removing the first 30 μm of root surface, Spearman correlations.



wRS: without Root surface [Pb = $\sim 27 \mu\text{m}$; Fe = $\sim 15 \mu\text{m}$; Mn = $\sim 200 \mu\text{m}$; Al = $\sim 17 \mu\text{m}$]

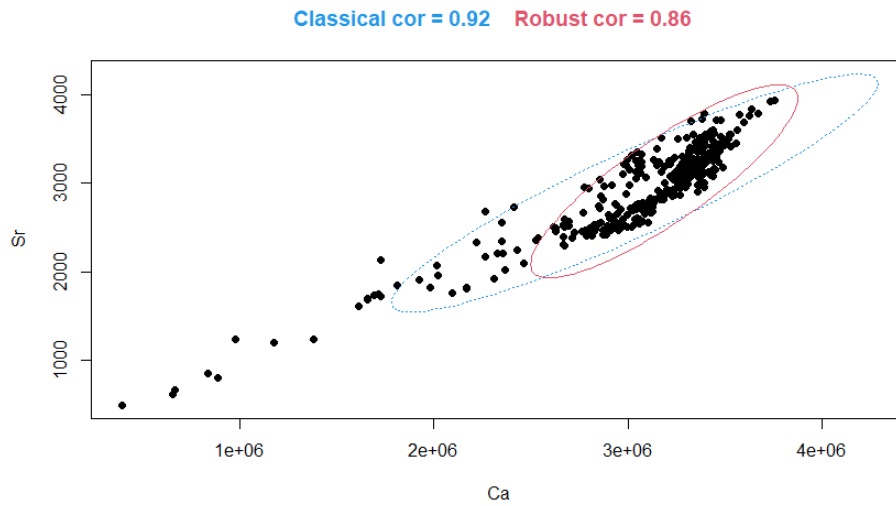
• **Ca vs Ba**

Classical test	<p>Pearson's product-moment correlation</p> <p>data: Aa211C_CC\$Ca and Aa211C_CC\$Ba $t = 16.927$, $df = 338$, p-value < 2.2e-16 alternative hypothesis: true correlation is not equal to 0 95 percent confidence interval: 0.6153113 0.7310395 sample estimates: cor 0.6773442</p>	<p>Spearman's rank correlation rho</p> <p>data: Aa211C_CC\$Ca and Aa211C_CC\$Ba $S = 1527564$, p-value < 2.2e-16 alternative hypothesis: true rho is not equal to 0 sample estimates: rho 0.7668058</p>
	<p>MCD ($\alpha=0.05$; quant=0.8)</p>	<p>\$cor.rob 0.7691947</p>



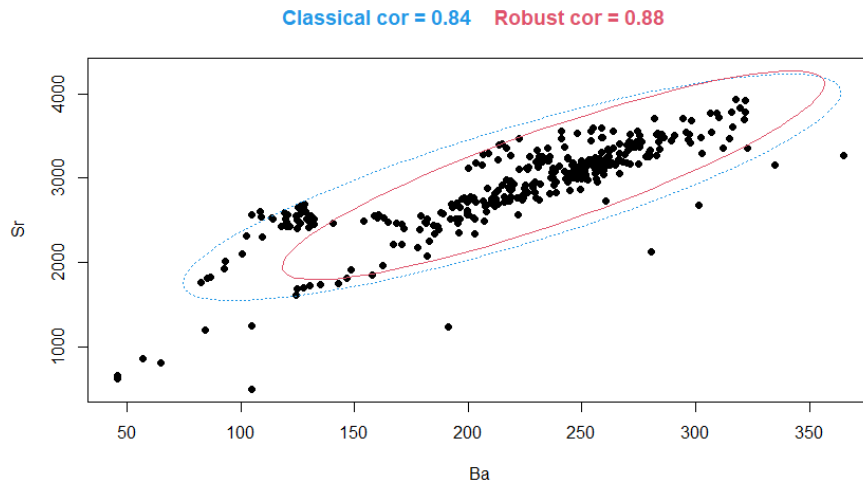
• **Ca vs Sr**

Classical test	<p>Pearson's product-moment correlation</p> <p>data: Aa211C_CC\$Ca and Aa211C_CC\$Sr $t = 43.337$, $df = 338$, p-value < 2.2e-16 alternative hypothesis: true correlation is not equal to 0 95 percent confidence interval: 0.9026035 0.9353623 sample estimates: cor 0.9205867</p>	<p>Spearman's rank correlation rho</p> <p>data: Aa211C_CC\$Ca and Aa211C_CC\$Sr $S = 815088$, p-value < 2.2e-16 alternative hypothesis: true rho is not equal to 0 sample estimates: rho 0.8755707</p>
	<p>MCD ($\alpha=0.05$; quant=0.8)</p>	<p>\$cor.rob [1] 0.8612135</p>



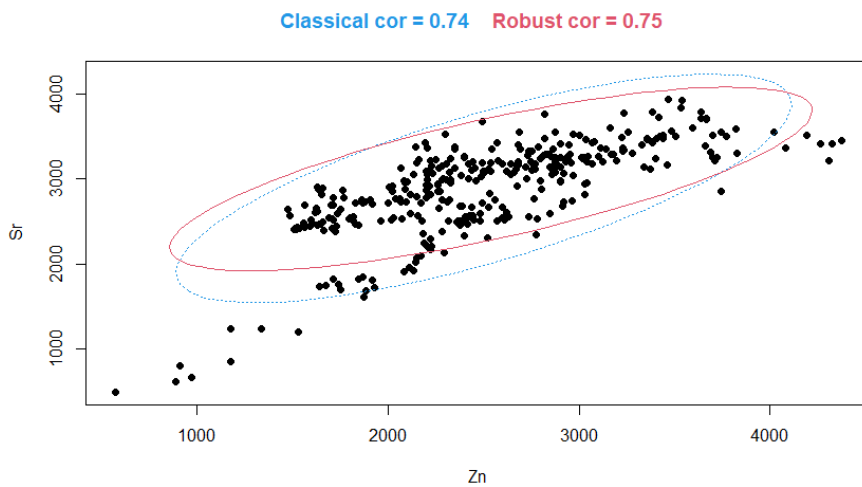
• Ba vs Sr

Classical test	<p>Pearson's product-moment correlation</p> <p>data: Aa211C_CC\$Ba and Aa211C_CC\$Sr $t = 29$, $df = 338$, p-value < 2.2e-16 alternative hypothesis: true correlation is not equal to 0 95 percent confidence interval: 0.8110749 0.8725568 sample estimates:</p> <p style="text-align: center;">cor 0.8445774</p>	<p>Spearman's rank correlation rho</p> <p>data: Aa211C_CC\$Ba and Aa211C_CC\$Sr $S = 844406$, p-value < 2.2e-16 alternative hypothesis: true rho is not equal to 0 sample estimates:</p> <p style="text-align: center;">rho 0.8710951</p>
	<p>MCD $(\alpha=0.05;$ $quant=0.8)$</p>	<p>$\\$cor.rob$ [1] 0.8781067</p>



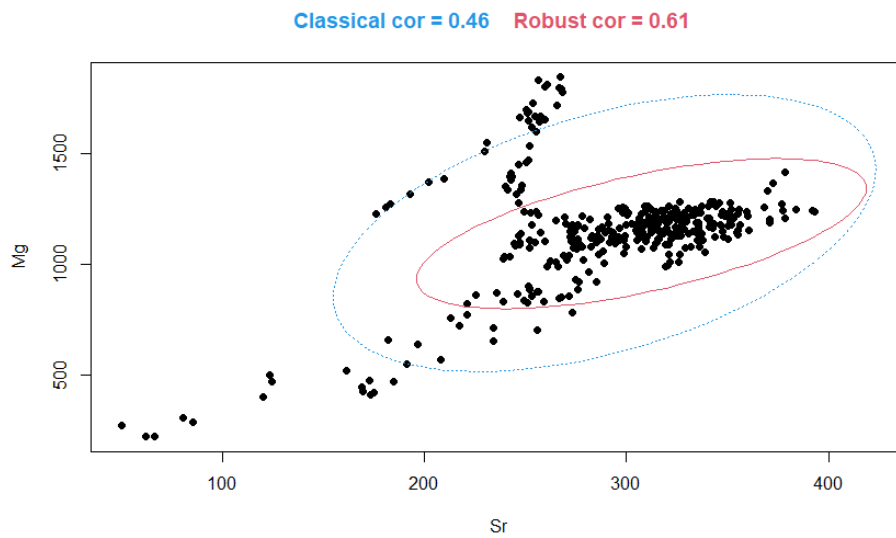
• Zn vs Sr

Classical test	<p>Pearson's product-moment correlation</p> <p>data: Aa211C_CC\$Zn and Aa211C_CC\$Sr $t = 20.166$, $df = 338$, p-value < 2.2e-16 alternative hypothesis: true correlation is not equal to 0 95 percent confidence interval: 0.6865859 0.7837428 sample estimates: cor 0.7389826</p>	<p>Spearman's rank correlation rho</p> <p>data: Aa211C_CC\$Zn and Aa211C_CC\$Sr $S = 1506568$, p-value < 2.2e-16 alternative hypothesis: true rho is not equal to 0 sample estimates: rho 0.770011</p>
MCD ($\alpha=0.05$; quant=0.8)	<p>\$cor.rob [1] 0.7459763</p>	



• Mg vs Sr

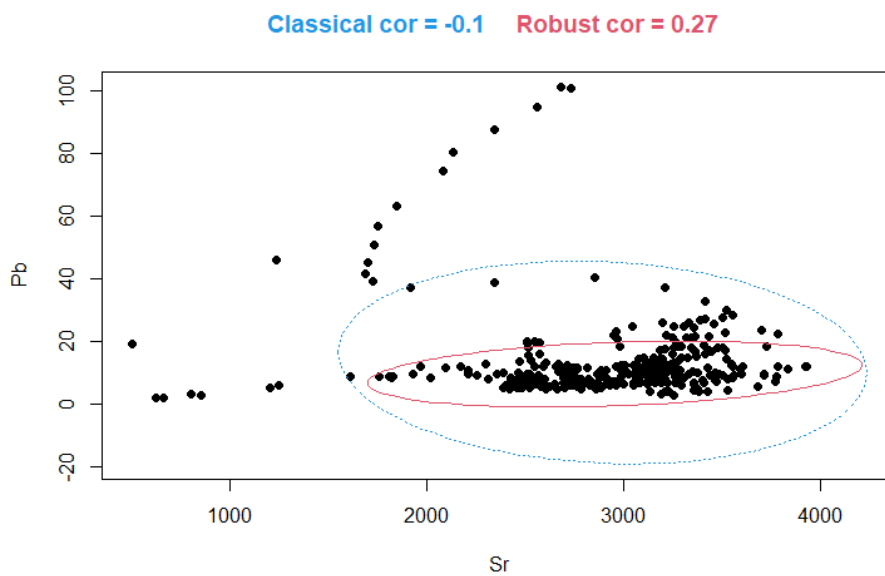
Classical test	<p>Pearson's product-moment correlation</p> <p>data: Aa211C_CC\$Mg and Aa211C_CC\$Sr $t = 9.5244$, $df = 338$, p-value < 2.2e-16 alternative hypothesis: true correlation is not equal to 0 95 percent confidence interval: 0.3718262 0.5399413 sample estimates: cor 0.4599964</p>	<p>Spearman's rank correlation rho</p> <p>data: Aa211C_CC\$Mg and Aa211C_CC\$Sr $S = 4795796$, p-value = 5.916e-07 alternative hypothesis: true rho is not equal to 0 sample estimates: rho 0.2678856</p>
MCD ($\alpha=0.05$; quant=0.8)	<p>\$cor.rob [1] 0.607433</p>	



• **Pb vs Sr**

Whole cementum thickness:

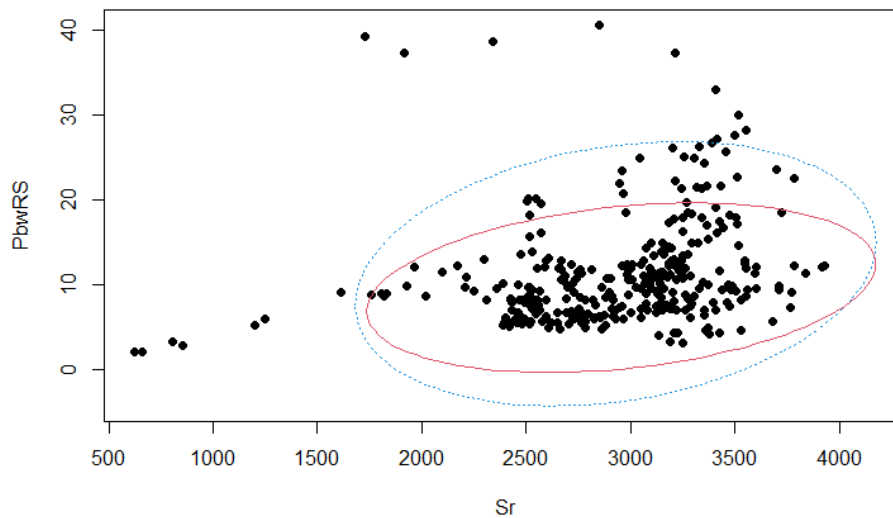
Classical test	<p style="color: blue;">Pearson's product-moment correlation</p> <p>data: Aa211C_CC\$Sr and Aa211C_CC\$Pb $t = -1.9403$, $df = 338$, p-value = 0.05318 alternative hypothesis: true correlation is not equal to 0 95 percent confidence interval: -0.20898408 0.00142329 sample estimates: cor -0.1049548</p>	<p>Spearman's rank correlation rho</p> <p>data: Aa211C_CC\$Sr and Aa211C_CC\$Pb $S = 5138998$, p-value = 6.42e-05 alternative hypothesis: true rho is not equal to 0 sample estimates: rho 0.2154932</p>
	<p style="color: red;">MCD $(\alpha=0.05;$ $quant=0.8)$</p>	<p style="color: red;">\$cor.rob $[1] 0.2704948$</p>



Removing 27 μm of Pb-enriched root surface:

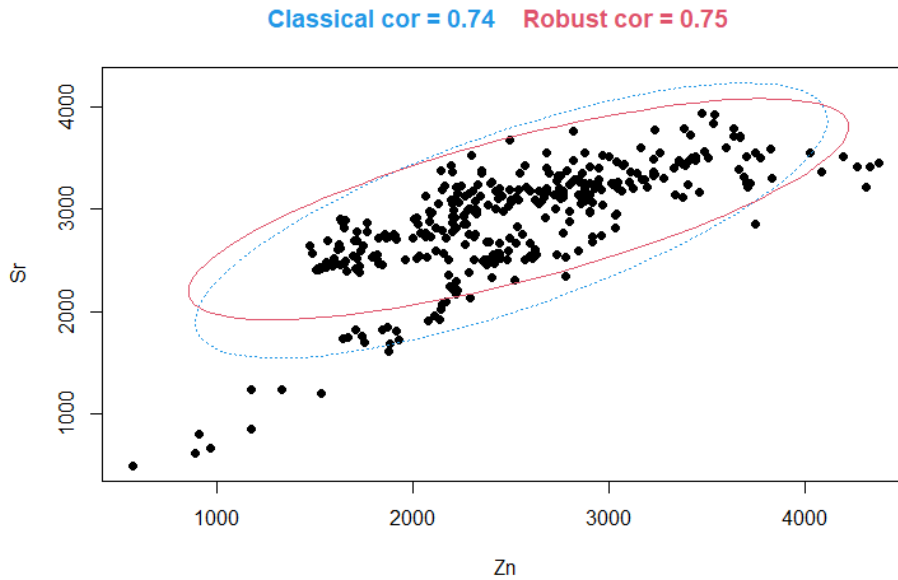
Classical test	<p>Pearson's product-moment correlation</p> <p>data: Aa211C_CC_wRS\$Sr and Aa211C_CC_wRS\$Pb $t = 4.4666$, $df = 325$, p-value = 1.098e-05 alternative hypothesis: true correlation is not equal to 0 95 percent confidence interval: 0.1355669 0.3400778 sample estimates: cor 0.2404895</p>	<p>Spearman's rank correlation rho</p> <p>data: Aa211C_CC_wRS\$Zn and Aa211C_CC_wRS\$Pb $S = 2159708$, p-value < 2.2e-16 alternative hypothesis: true rho is not equal to 0 sample estimates: rho 0.6293986</p>
	<p>MCD $(\alpha=0.05;$ $quant=0.8)$</p>	<p>\$cor.rob [1] 0.2800147</p>

Classical cor = 0.24 Robust cor = 0.28



• Sr vs Zn

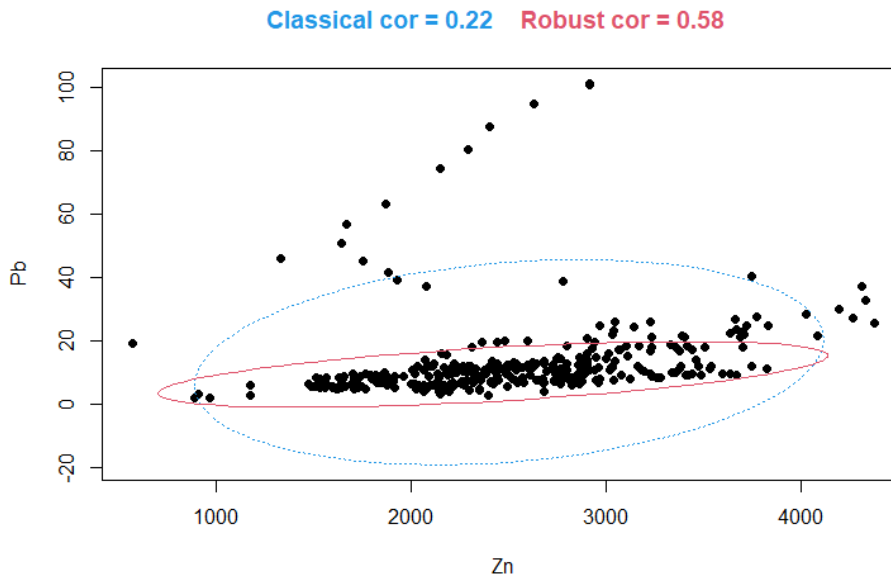
Classical test	<p>Pearson's product-moment correlation</p> <p>data: Aa211C_CC\$Zn and Aa211C_CC\$Sr $t = 20.166$, $df = 338$, p-value < 2.2e-16 alternative hypothesis: true correlation is not equal to 0 95 percent confidence interval: 0.6865859 0.7837428 sample estimates: cor 0.7389826</p>	<p>Spearman's rank correlation rho</p> <p>data: Aa211C_CC\$Zn and Aa211C_CC\$Sr $S = 1506568$, p-value < 2.2e-16 alternative hypothesis: true rho is not equal to 0 sample estimates: rho 0.770011</p>
	<p>MCD $(\alpha=0.05;$ $quant=0.8)$</p>	<p>\$cor.rob [1] 0.7459763</p>



• **Pb vs Zn**

Whole cementum thickness:

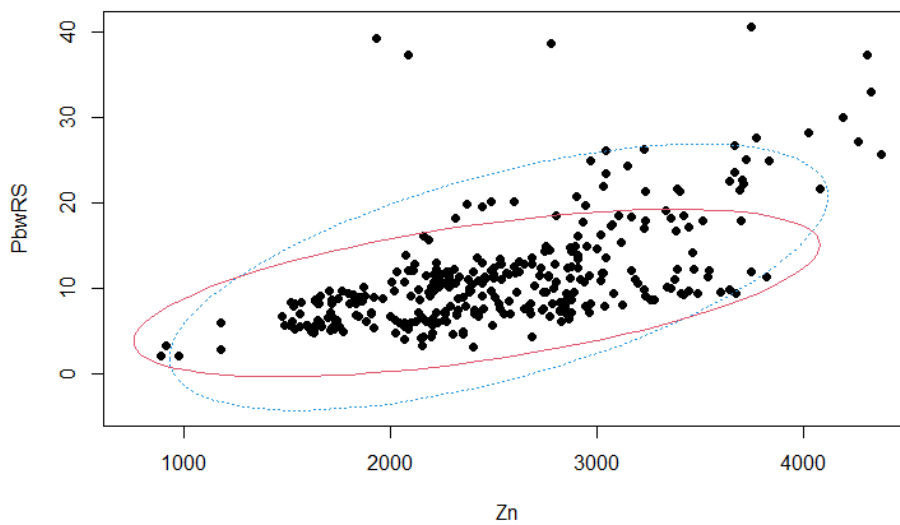
Classical test	<p>Pearson's product-moment correlation</p> <p>data: Aa211C_CC\$Zn and Aa211C_CC\$Pb $t = 4.2406$, $df = 338$, p-value = 2.88e-05 alternative hypothesis: true correlation is not equal to 0 95 percent confidence interval: 0.1212964 0.3233902 sample estimates: cor 0.2247589</p>	<p>Spearman's rank correlation rho</p> <p>data: Aa211C_CC\$Zn and Aa211C_CC\$Pb $S = 3010790$, p-value < 2.2e-16 alternative hypothesis: true rho is not equal to 0 sample estimates: rho 0.5403802</p>
	<p>MCD $(\alpha=0.05;$ $quant=0.8)$</p>	<p>\$cor.rob [1] 0.5789923</p>



Removing 27 μm of Pb-enriched root surface:

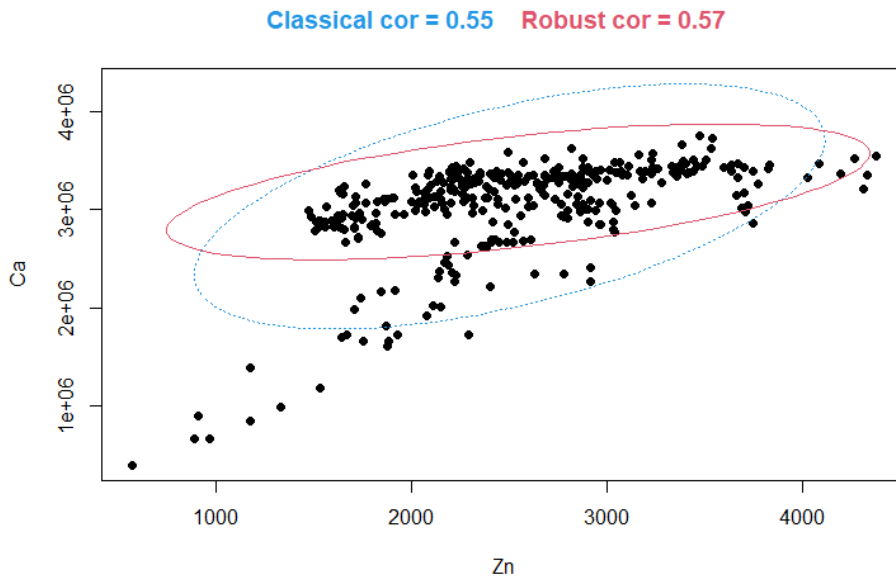
Classical test	<p>Pearson's product-moment correlation</p> <p>data: Aa211C_CC_wRS\$Zn and Aa211C_CC_wRS\$Pb $t = 13.887$, $df = 325$, p-value < 2.2e-16 alternative hypothesis: true correlation is not equal to 0 95 percent confidence interval: 0.5373619 0.6740960 sample estimates: cor 0.610254</p>	<p>Spearman's rank correlation rho</p> <p>data: Aa211C_CC_wRS\$Zn and Aa211C_CC_wRS\$Pb $S = 2159708$, p-value < 2.2e-16 alternative hypothesis: true rho is not equal to 0 sample estimates: rho 0.6293986</p>
	<p>MCD $(\alpha=0.05;$ $\text{quant}=0.8)$</p>	<p>\$cor.rob [1] 0.5752824</p>

Classical cor = 0.61 Robust cor = 0.58



• Zn vs Ca

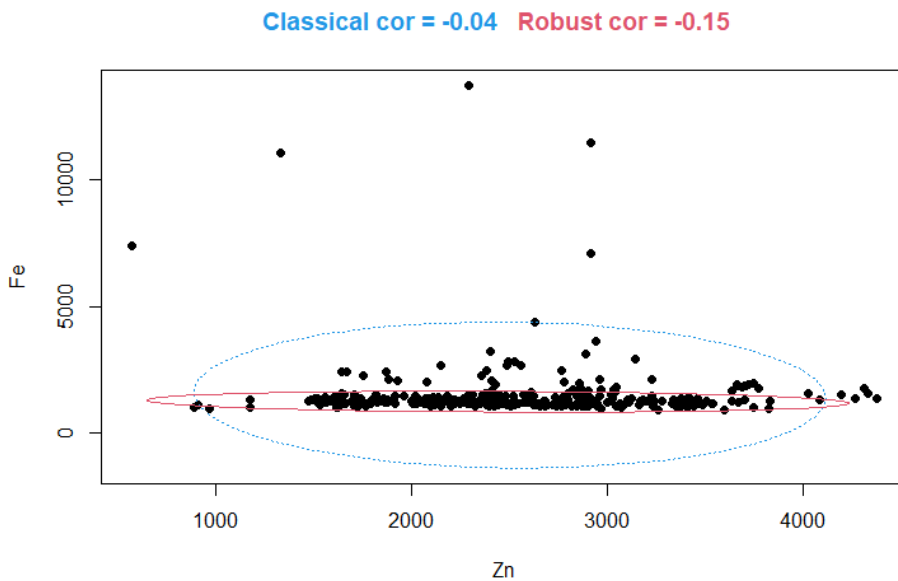
Classical test	<p>Pearson's product-moment correlation</p> <p>data: Aa211C_CC\$Zn and Aa211C_CC\$Ca $t = 12.248$, $df = 338$, p-value < 2.2e-16 alternative hypothesis: true correlation is not equal to 0 95 percent confidence interval: 0.4761334 0.6239848 sample estimates: cor 0.5544184</p>	<p>Spearman's rank correlation rho</p> <p>data: Aa211C_CC\$Zn and Aa211C_CC\$Ca $S = 2718964$, p-value < 2.2e-16 alternative hypothesis: true rho is not equal to 0 sample estimates: rho 0.5849296</p>
	<p>MCD $(\alpha=0.05;$ $\text{quant}=0.8)$</p>	<p>\$cor.rob [1] 0.5666424</p>



- Zn vs Fe**

Whole cementum thickness:

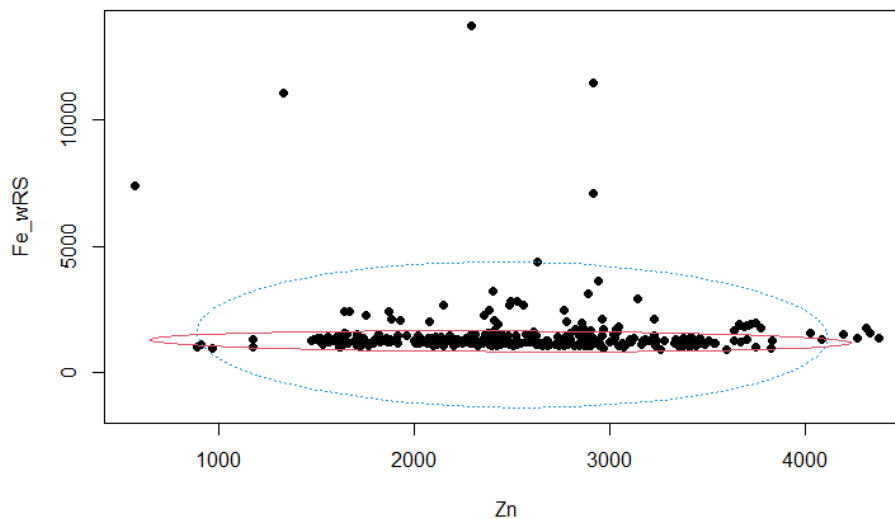
Classical test	<p>Pearson's product-moment correlation</p> <p>data: Aa211C_CC\$Zn and Aa211C_CC\$Fe $t = -0.79887$, $df = 338$, p-value = 0.4249 alternative hypothesis: true correlation is not equal to 0 95 percent confidence interval: -0.14908558 0.06324246 sample estimates: cor -0.04341176</p>	<p>Spearman's rank correlation rho</p> <p>data: Aa211C_CC\$Zn and Aa211C_CC\$Fe $S = 6501830$, p-value = 0.8911 alternative hypothesis: true rho is not equal to 0 sample estimates: rho 0.007446635</p>
	<p>MCD ($\alpha=0.05$; quant=0.8)</p>	<p>\$cor.rob [1] -0.1496604</p>



Removing 15 μm of Fe-enriched root surface:

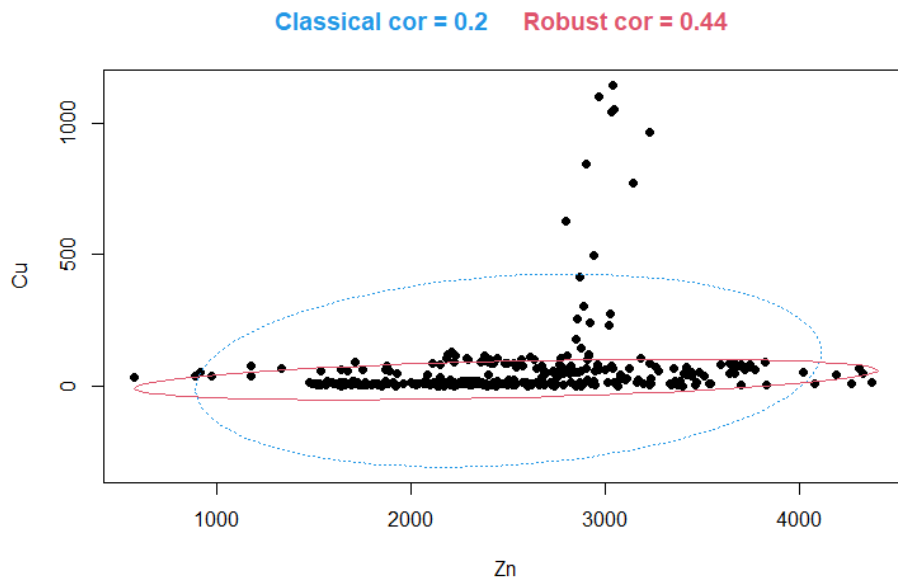
Classical test	<p>Pearson's product-moment correlation</p> <p>data: Aa211C_CC\$Zn and Aa211C_CC\$Fe $t = -0.79887$, $df = 338$, p-value = 0.4249 alternative hypothesis: true correlation is not equal to 0 95 percent confidence interval: -0.14908558 0.06324246 sample estimates: cor -0.04341176</p>	<p>Spearman's rank correlation rho</p> <p>data: Aa211C_CC\$Zn and Aa211C_CC\$Fe $S = 6501830$, p-value = 0.8911 alternative hypothesis: true rho is not equal to 0 sample estimates: rho 0.007446635</p>
	<p>MCD $(\alpha=0.05;$ $\text{quant}=0.8)$</p>	<p>\$cor.rob [1] -0.1496604</p>

Classical cor = -0.04 Robust cor = -0.15



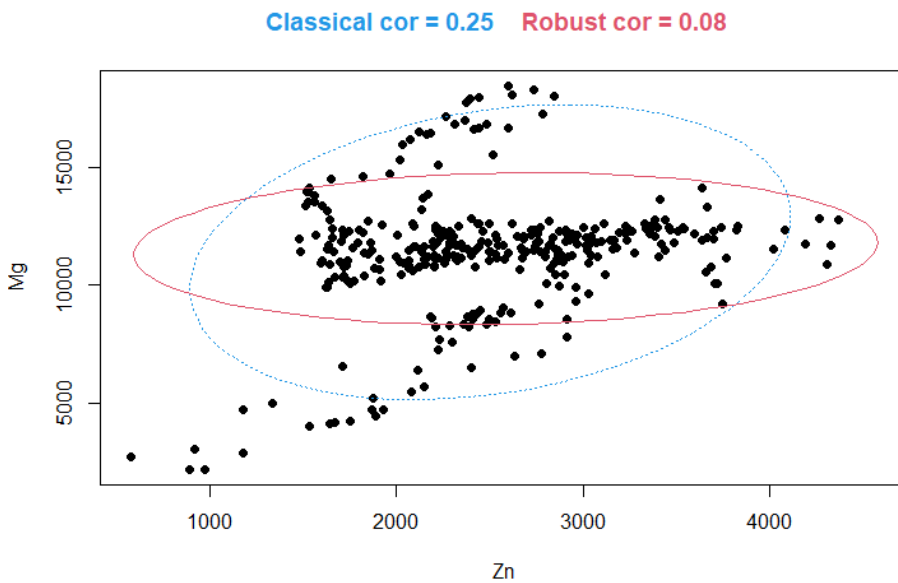
• Zn vs Cu

Classical test	<p>Pearson's product-moment correlation</p> <p>data: Aa211C_CC\$Zn and Aa211C_CC\$Cu $t = 3.6814$, $df = 338$, p-value = 0.0002699 alternative hypothesis: true correlation is not equal to 0 95 percent confidence interval: 0.09190018 0.29651317 sample estimates: cor 0.1963432</p>	<p>Spearman's rank correlation rho</p> <p>data: Aa211C_CC\$Zn and Aa211C_CC\$Cu $S = 4278960$, p-value = 6.446e-11 alternative hypothesis: true rho is not equal to 0 sample estimates: rho 0.3467845</p>
	<p>MCD $(\alpha=0.05;$ $\text{quant}=0.8)$</p>	<p>\$cor.rob [1] 0.4401857</p>



• Zn vs Mg

Classical test	<p>Pearson's product-moment correlation</p> <p>data: Aa211C_CC\$Zn and Aa211C_CC\$Mg $t = 4.7487$, $df = 338$, p-value = 3.03e-06 alternative hypothesis: true correlation is not equal to 0 95 percent confidence interval: 0.1476523 0.3472134 sample estimates: cor 0.250087</p>	<p>Spearman's rank correlation rho</p> <p>data: Aa211C_CC\$Zn and Aa211C_CC\$Mg $S = 5277330$, p-value = 0.0003195 alternative hypothesis: true rho is not equal to 0 sample estimates: rho 0.1943758</p>
	<p>MCD $(\alpha=0.05;$ $quant=0.8)$</p>	<p>$\\$cor.rob$ [1] 0.08211205</p>

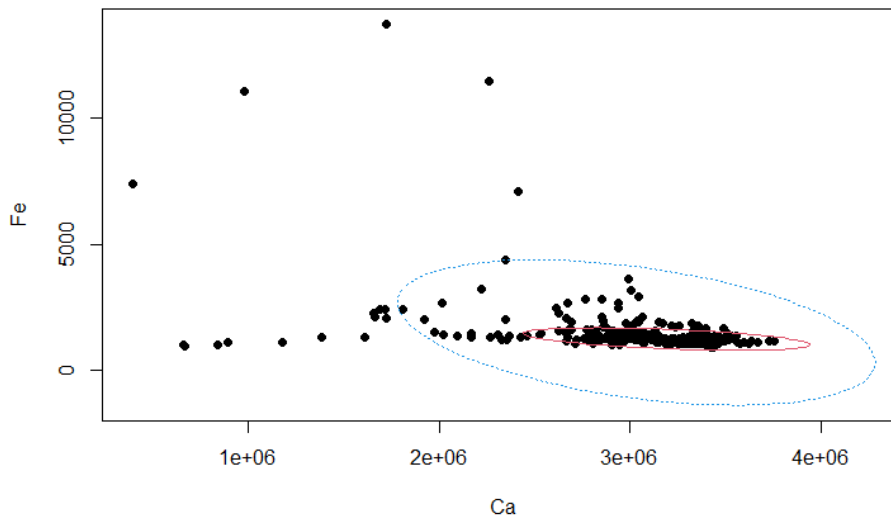


- **Ca vs Fe**

Whole cementum thickness:

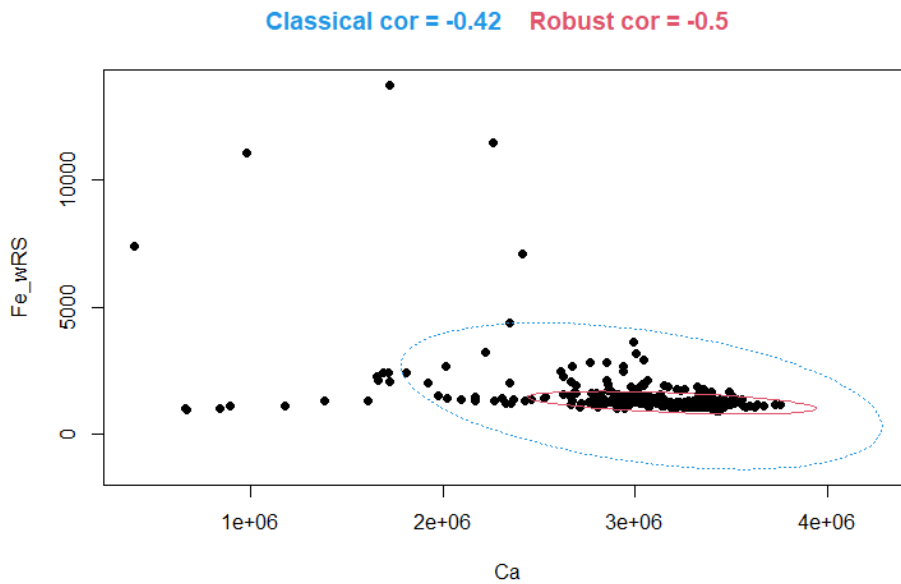
Classical test	<p>Pearson's product-moment correlation</p> <p>data: Aa211C_CC\$Ca and Aa211C_CC\$Fe $t = -8.4272$, $df = 338$, p-value = 1.033e-15 alternative hypothesis: true correlation is not equal to 0 95 percent confidence interval: -0.5008532 -0.3247181 sample estimates: cor -0.4166888</p>	<p>Spearman's rank correlation rho</p> <p>data: Aa211C_CC\$Ca and Aa211C_CC\$Fe $S = 9906092$, p-value < 2.2e-16 alternative hypothesis: true rho is not equal to 0 sample estimates: rho -0.5122396</p>
	<p>MCD $(\alpha=0.05;$ $quant=0.8)$</p>	<p>\$cor.rob [1] -0.4999543</p>

Classical cor = -0.42 Robust cor = -0.5



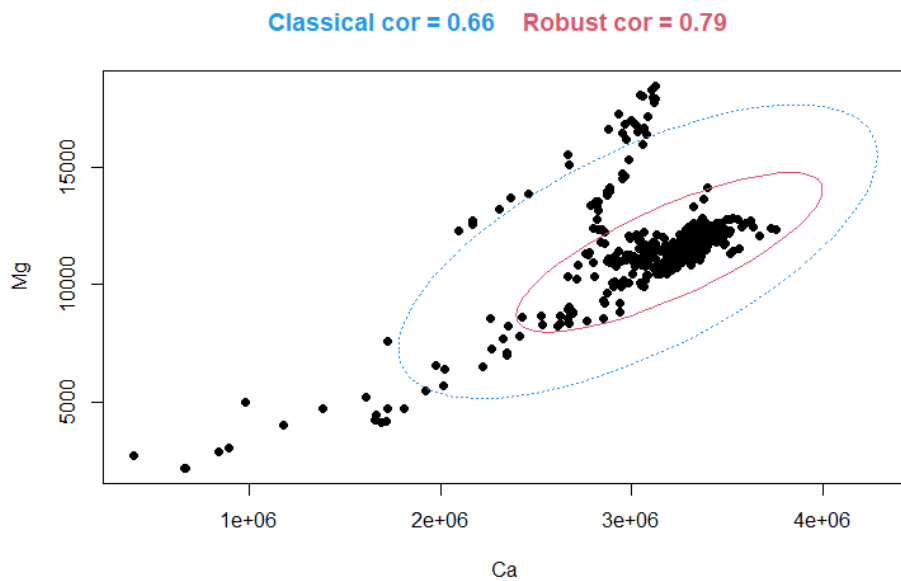
Removing 15 μm of Fe-enriched root surface:

Classical test	<p>Pearson's product-moment correlation</p> <p>data: Aa211C_CC\$Ca and Aa211C_CC\$Fe $t = -8.4272$, $df = 338$, p-value = 1.033e-15 alternative hypothesis: true correlation is not equal to 0 95 percent confidence interval: -0.5008532 -0.3247181 sample estimates: cor -0.4166888</p>	<p>Spearman's rank correlation rho</p> <p>data: Aa211C_CC\$Ca and Aa211C_CC\$Fe $S = 9906092$, p-value < 2.2e-16 alternative hypothesis: true rho is not equal to 0 sample estimates: rho -0.5122396</p>
	<p>MCD $(\alpha=0.05;$ $quant=0.8)$</p>	<p>\$cor.rob [1] -0.4999543</p>



• Ca vs Mg

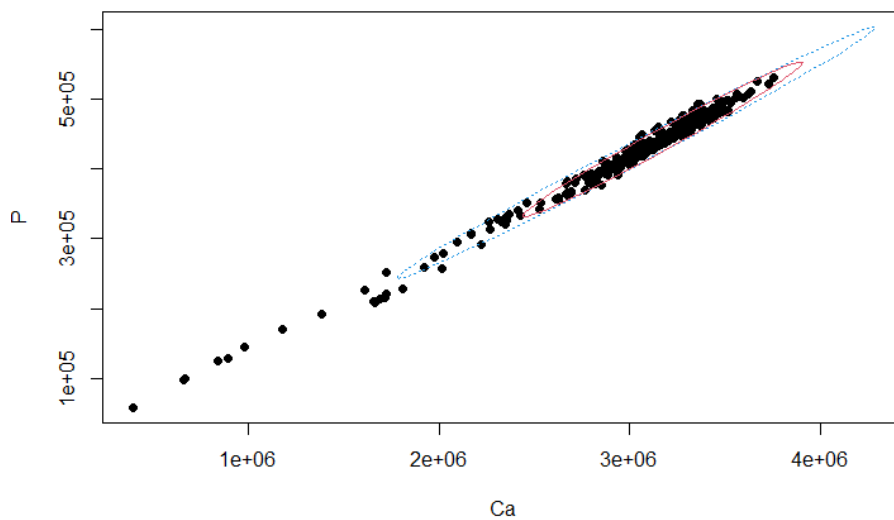
Classical test	<p>Pearson's product-moment correlation</p> <p>data: Aa211C_CC\$Ca and Aa211C_CC\$Mg $t = 16.104$, $df = 338$, p-value < 2.2e-16 alternative hypothesis: true correlation is not equal to 0 95 percent confidence interval: 0.5941831 0.7151465 sample estimates: cor 0.6589035</p>	<p>Spearman's rank correlation rho</p> <p>data: Aa211C_CC\$Ca and Aa211C_CC\$Mg $S = 3592892$, p-value < 2.2e-16 alternative hypothesis: true rho is not equal to 0 sample estimates: rho 0.451518</p>
	<p>MCD $(\alpha=0.05;$ $quant=0.8)$</p>	<p>$\\$cor.rob$ [1] 0.7879131</p>



• **Ca vs P**

Classical test	<p>Pearson's product-moment correlation</p> <p>data: Aa211C_CC\$Ca and Aa211C_CC\$P $t = 175.03$, $df = 338$, p-value < 2.2e-16 alternative hypothesis: true correlation is not equal to 0 95 percent confidence interval: 0.9932310 0.9955785 sample estimates: cor 0.9945289</p>	<p>Spearman's rank correlation rho</p> <p>data: Aa211C_CC\$Ca and Aa211C_CC\$P $S = 112302$, p-value < 2.2e-16 alternative hypothesis: true rho is not equal to 0 sample estimates: rho 0.9828563</p>
	<p>MCD $(\alpha=0.05;$ $quant=0.8)$</p>	<p>\$cor.rob [1] 0.9880191</p>

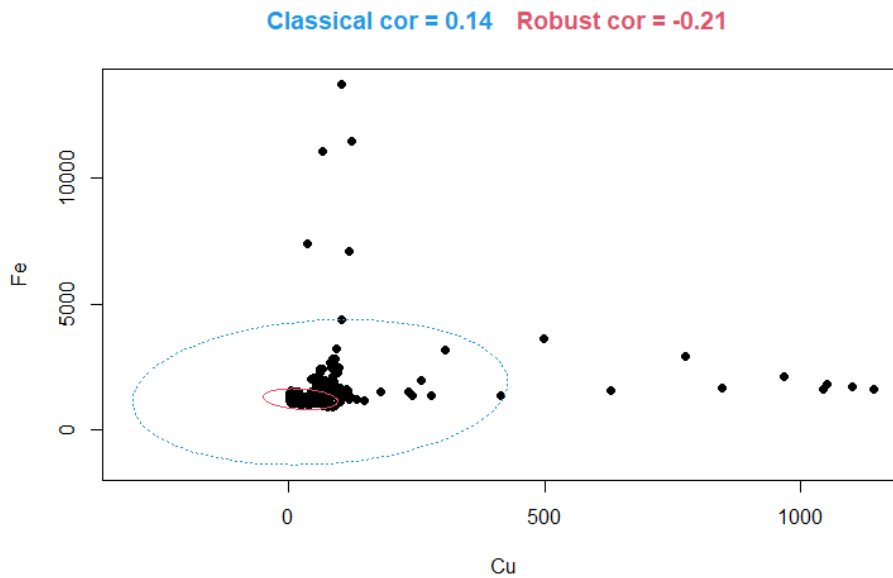
Classical cor = 0.99 Robust cor = 0.99



• **Cu vs Fe**

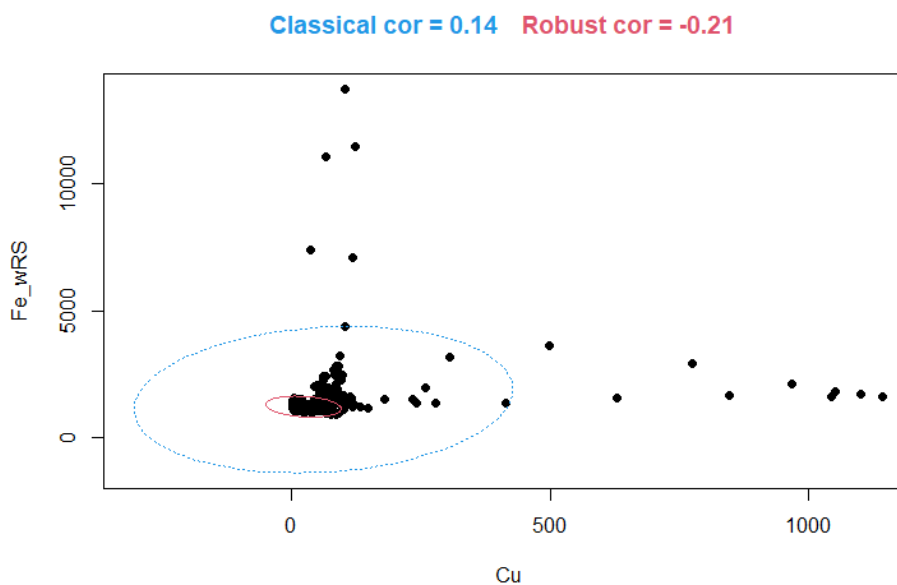
Whole cementum thickness:

Classical test	<p>Pearson's product-moment correlation</p> <p>data: Aa211C_CC\$Cu and Aa211C_CC\$Fe $t = 2.5683$, $df = 338$, p-value = 0.01065 alternative hypothesis: true correlation is not equal to 0 95 percent confidence interval: 0.03246759 0.24116538 sample estimates: cor 0.138352</p>	<p>Spearman's rank correlation rho</p> <p>data: Aa211C_CC\$Cu and Aa211C_CC\$Fe $S = 4806092$, p-value = 6.913e-07 alternative hypothesis: true rho is not equal to 0 sample estimates: rho 0.2663138</p>
	<p>MCD $(\alpha=0.05;$ $quant=0.8)$</p>	<p>\$cor.rob [1] -0.2079025</p>



Removing 15 μm of Fe-enriched root surface:

Classical test	<p>Pearson's product-moment correlation</p> <p>data: Aa211C_CC\$Cu and Aa211C_CC\$Fe $t = 2.5683$, $df = 338$, p-value = 0.01065 alternative hypothesis: true correlation is not equal to 0 95 percent confidence interval: 0.03246759 0.24116538 sample estimates: cor 0.138352</p>	<p>Spearman's rank correlation rho</p> <p>data: Aa211C_CC\$Cu and Aa211C_CC\$Fe $S = 4806092$, p-value = 6.913e-07 alternative hypothesis: true rho is not equal to 0 sample estimates: rho 0.2663138</p>
	<p>MCD $(\alpha=0.05;$ $quant=0.8)$</p>	<p>$\\$cor.rob$ [1] -0.2079025</p>

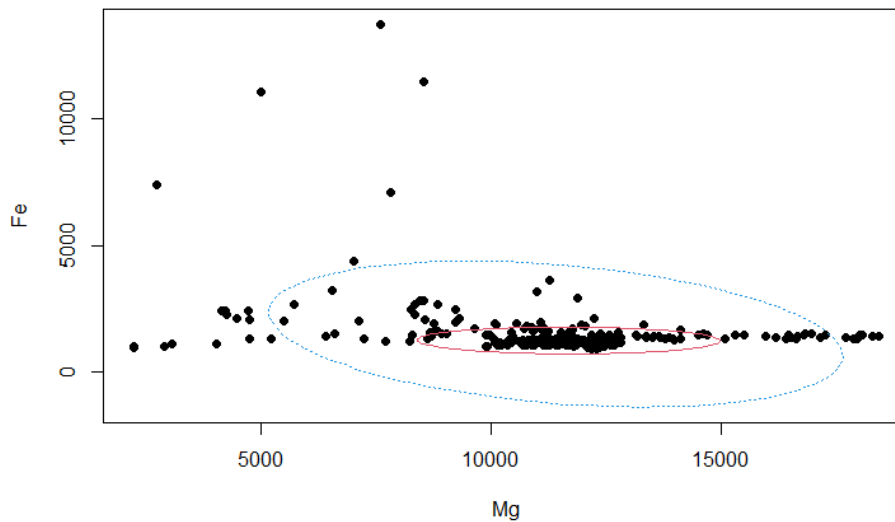


- **Mg vs Fe**

Whole cementum thickness:

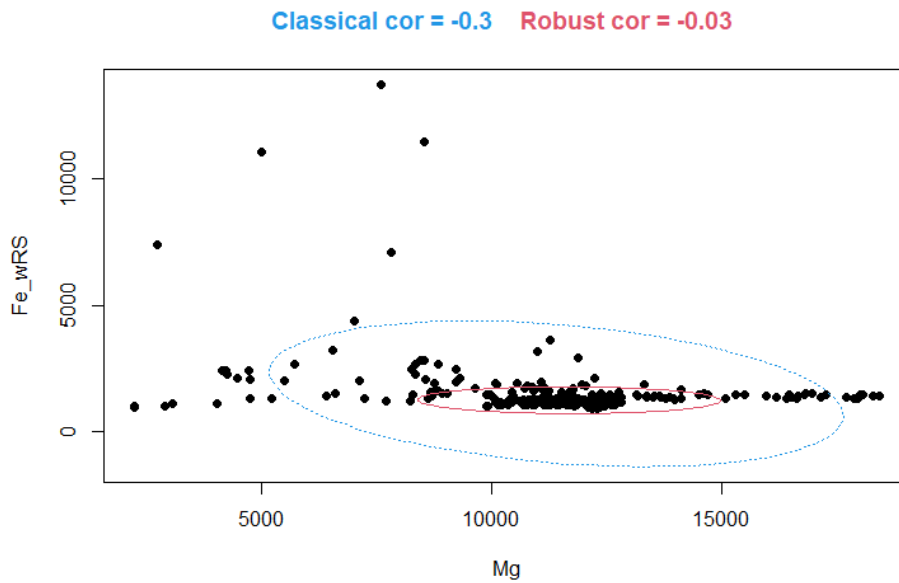
Classical test	<p>Pearson's product-moment correlation</p> <p>data: Aa211C_CC\$Mg and Aa211C_CC\$Fe $t = -5.8506$, $df = 338$, p-value = 1.157e-08 alternative hypothesis: true correlation is not equal to 0 95 percent confidence interval: -0.3968103 -0.2034466 sample estimates: cor -0.3032469</p>	<p>Spearman's rank correlation rho</p> <p>data: Aa211C_CC\$Mg and Aa211C_CC\$Fe $S = 7273132$, p-value = 0.04214 alternative hypothesis: true rho is not equal to 0 sample estimates: rho -0.1102984</p>
	<p>MCD $(\alpha=0.05;$ $quant=0.8)$</p>	<p>\$cor.rob $[1] -0.02840057$</p>

Classical cor = -0.3 Robust cor = -0.03



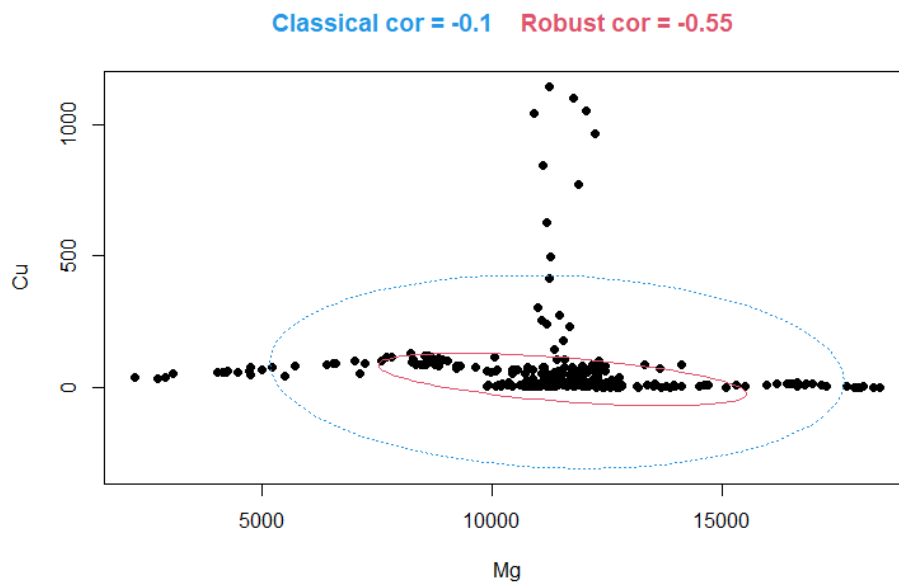
Removing 15 μm of Fe-enriched root surface:

Classical test	<p>Pearson's product-moment correlation</p> <p>data: Aa211C_CC\$Mg and Aa211C_CC\$Fe $t = -5.8506$, $df = 338$, p-value = 1.157e-08 alternative hypothesis: true correlation is not equal to 0 95 percent confidence interval: -0.3968103 -0.2034466 sample estimates: cor -0.3032469</p>	<p>Spearman's rank correlation rho</p> <p>data: Aa211C_CC\$Mg and Aa211C_CC\$Fe $S = 7273132$, p-value = 0.04214 alternative hypothesis: true rho is not equal to 0 sample estimates: rho -0.1102984</p>
	<p>MCD $(\alpha=0.05;$ $quant=0.8)$</p>	<p>\$cor.rob $[1] -0.02840057$</p>



• Cu vs Mg

Classical test	<p>Pearson's product-moment correlation</p> <p>data: Aa211C_CC\$Mg and Aa211C_CC\$Cu $t = -1.8016$, $df = 338$, p-value = 0.0725 alternative hypothesis: true correlation is not equal to 0 95 percent confidence interval: -0.201796969 0.008926746 sample estimates: cor -0.09752806</p>	<p>Spearman's rank correlation rho</p> <p>data: Aa211C_CC\$Mg and Aa211C_CC\$Cu $S = 9576908$, p-value < 2.2e-16 alternative hypothesis: true rho is not equal to 0 sample estimates: rho -0.4619872</p>
	<p>MCD $(\alpha=0.05;$ $quant=0.8)$</p>	<p>$\\$cor.rob$ [1] -0.5469069</p>



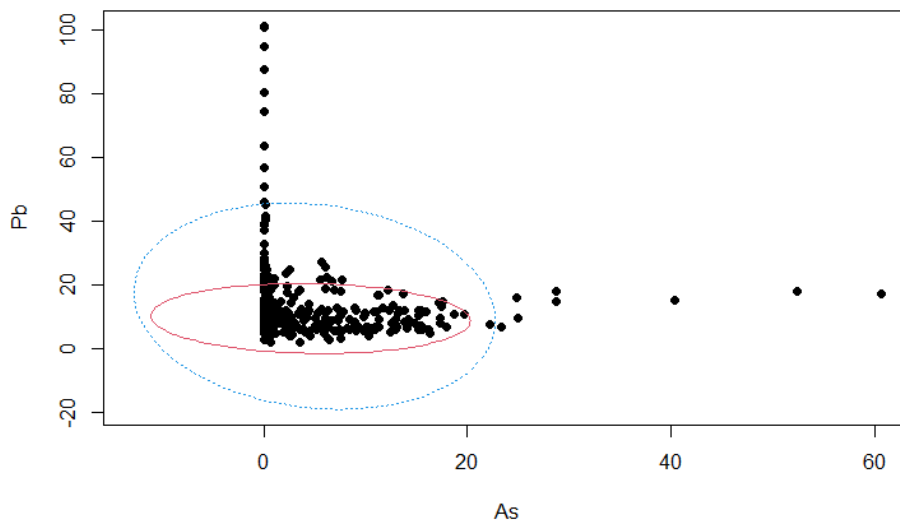
- As vs Hg, Pb vs Hg (no Hg at all). => Not Applicable.

- Pb vs As

Whole cementum thickness:

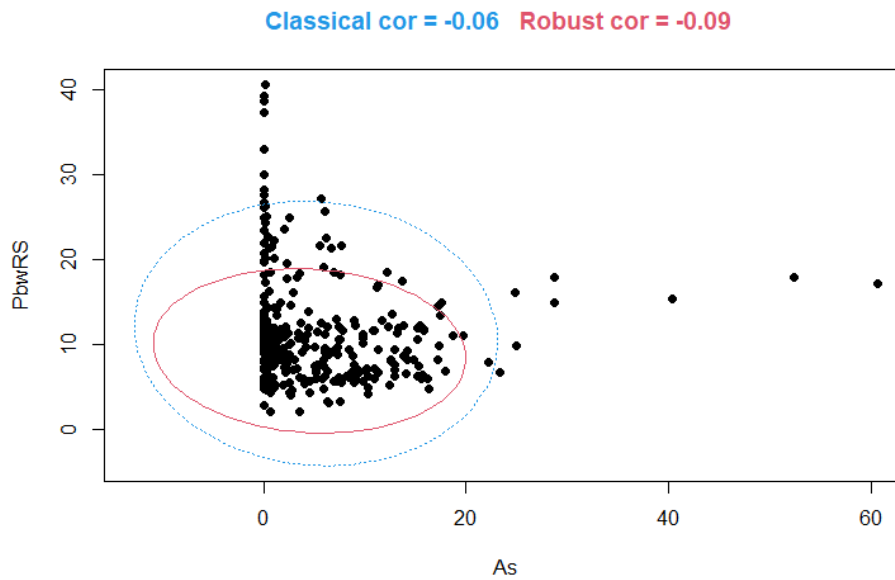
Classical test	<p>Pearson's product-moment correlation</p> <p>data: Aa211C_CC\$As and Aa211C_CC\$Pb $t = -2.565$, $df = 338$, p-value = 0.01075 alternative hypothesis: true correlation is not equal to 0 95 percent confidence interval: -0.24099712 -0.03228913 sample estimates: cor -0.1381768</p>	<p>Spearman's rank correlation rho</p> <p>data: Aa211C_CC\$As and Aa211C_CC\$Pb $S = 7893065$, p-value = 0.0001416 alternative hypothesis: true rho is not equal to 0 sample estimates: rho -0.2049359 <i>Impossible to calculate the exact p-value with ex-aequos</i></p>
	<p>MCD $(\alpha=0.05;$ $quant=0.8)$</p>	<p>\$cor.rob [1] -0.07379289</p>

Classical cor = -0.14 Robust cor = -0.07



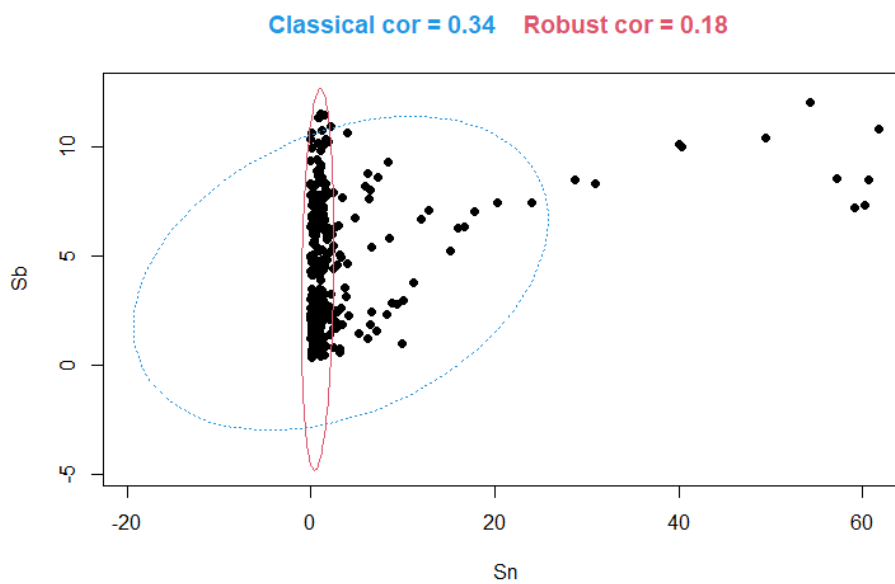
Removing 27 μm of Pb-enriched root surface:

Classical test	<p>Pearson's product-moment correlation</p> <p>data: Aa211C_CC_wRS\$As and Aa211C_CC_wRS\$Pb $t = -1.1211$, $df = 325$, p-value = 0.2631 alternative hypothesis: true correlation is not equal to 0 95 percent confidence interval: -0.16938326 0.04670812 sample estimates: cor -0.06206488</p>	<p>Spearman's rank correlation rho</p> <p>data: Aa211C_CC_wRS\$As and Aa211C_CC_wRS\$Pb $S = 6591902$, p-value = 0.01765 alternative hypothesis: true rho is not equal to 0 sample estimates: rho -0.1311567 <i>Impossible to calculate the exact p-value with ex-aequos</i></p>
	<p>MCD $(\alpha=0.05;$ $quant=0.8)$</p>	<p>\$cor.rob [1] -0.08793329</p>



• **Sb vs Sn**

Classical test	<p>Pearson's product-moment correlation</p> <p>data: Aa211C_CC\$Sn and Aa211C_CC\$Sb $t = 6.6484$, $df = 338$, p-value = $1.191e-10$ alternative hypothesis: true correlation is not equal to 0 95 percent confidence interval: 0.2424784 0.4308482 sample estimates: cor 0.34007</p>	<p>Spearman's rank correlation rho</p> <p>data: Aa211C_CC\$Sn and Aa211C_CC\$Sb $S = 4952632$, p-value = $5.724e-06$ alternative hypothesis: true rho is not equal to 0 sample estimates: rho 0.2439434</p>
	<p>MCD $(\alpha=0.05;$ $quant=0.8)$</p>	<p>$\\$cor.rob$ $[1] \mathbf{0.1804737}$</p>

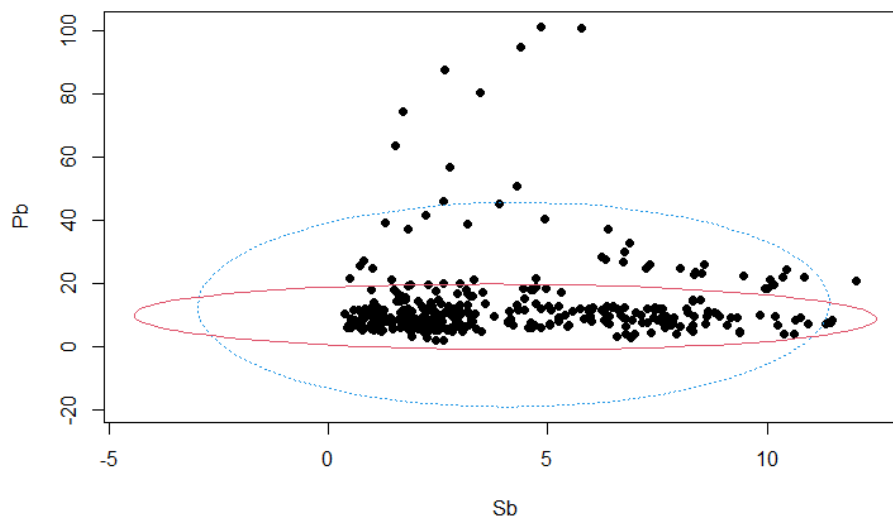


- **Pb vs Sb**

Whole cementum thickness:

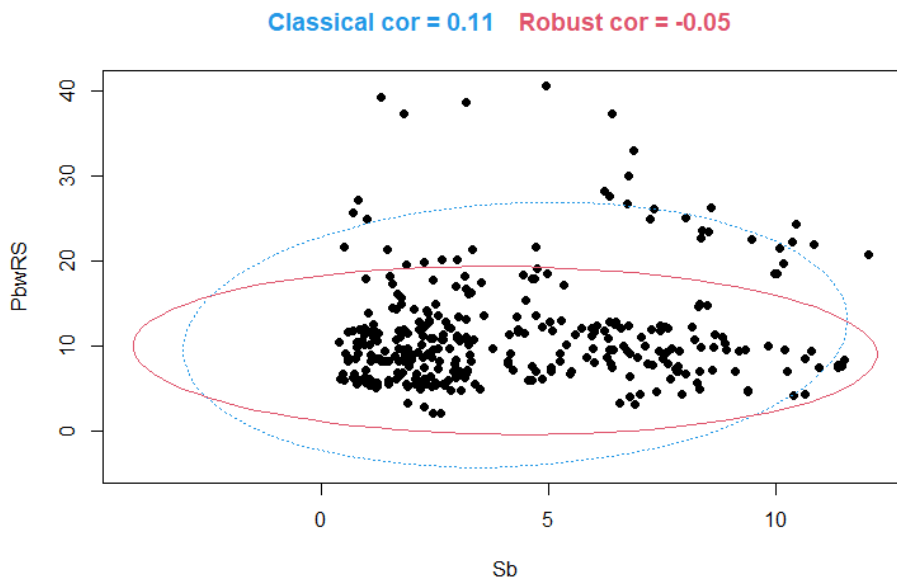
Classical test	<p>Pearson's product-moment correlation</p> <p>data: Aa211C_CC\$Sb and Aa211C_CC\$Pb $t = 0.31289$, $df = 338$, p-value = 0.7546 alternative hypothesis: true correlation is not equal to 0 95 percent confidence interval: -0.08950772 0.12315580 sample estimates: cor 0.01701649</p>	<p>Spearman's rank correlation rho</p> <p>data: Aa211C_CC\$Sb and Aa211C_CC\$Pb $S = 5975776$, p-value = 0.1062 alternative hypothesis: true rho is not equal to 0 sample estimates: rho 0.08775274</p>
	<p>MCD $(\alpha=0.05;$ $quant=0.8)$</p>	<p>\$cor.rob $[1] -0.05452402$</p>

Classical cor = 0.02 Robust cor = -0.05



Removing 27 μm of Pb-enriched root surface:

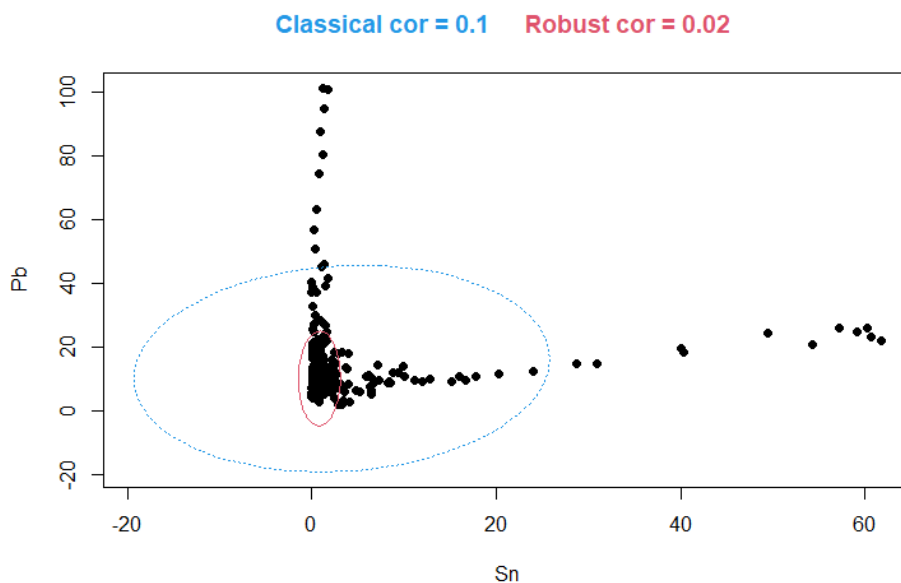
Classical test	<p>Pearson's product-moment correlation</p> <p>data: Aa211C_CC_wRS\$Sb and Aa211C_CC_wRS\$Pb $t = 2.0427$, $df = 325$, p-value = 0.04189 alternative hypothesis: true correlation is not equal to 0 95 percent confidence interval: 0.004181806 0.218381198 sample estimates: cor 0.1125893</p>	<p>Spearman's rank correlation rho</p> <p>data: Aa211C_CC_wRS\$Sb and Aa211C_CC_wRS\$Pb $S = 5227674$, p-value = 0.063 alternative hypothesis: true rho is not equal to 0 sample estimates: rho 0.1029419</p>
	<p>MCD $(\alpha=0.05;$ $quant=0.8)$</p>	<p>\$cor.rob $[1] -0.04749927$</p>



• **Pb vs Sn**

Whole cementum thickness:

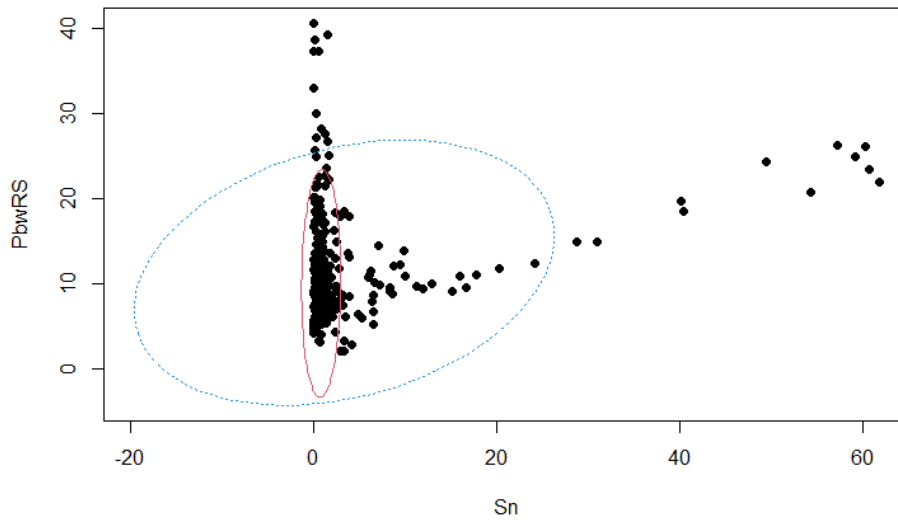
Classical test	<p style="text-align: center; color: blue;">Pearson's product-moment correlation</p> <p>data: Aa211C_CC\$Sn and Aa211C_CC\$Pb $t = 1.7675$, $df = 338$, p-value = 0.07805 alternative hypothesis: true correlation is not equal to 0 95 percent confidence interval: -0.01077634 0.20002186 sample estimates: cor 0.09569555</p>	<p style="text-align: center;">Spearman's rank correlation rho</p> <p>data: Aa211C_CC\$Sn and Aa211C_CC\$Pb $S = 5741980$, p-value = 0.02287 alternative hypothesis: true rho is not equal to 0 sample estimates: rho 0.1234435</p>
	<p style="text-align: center; color: red;">MCD ($\alpha=0.05$; quant=0.8)</p>	<p style="color: red;">$\\$cor.rob$ [1] 0.02039293</p>



Removing 27 μm of Pb-enriched root surface:

Classical test	<p>Pearson's product-moment correlation</p> <p>data: Aa211C_CC_wRS\$Sn and Aa211C_CC_wRS\$Pb $t = 5.3054$, $df = 325$, p-value = 2.084e-07 alternative hypothesis: true correlation is not equal to 0 95 percent confidence interval: 0.1793539 0.3791690 sample estimates: cor 0.2823206</p>	<p>Spearman's rank correlation rho</p> <p>data: Aa211C_CC_wRS\$Sn and Aa211C_CC_wRS\$Pb $S = 5124926$, p-value = 0.02931 alternative hypothesis: true rho is not equal to 0 sample estimates: rho 0.1205733</p>
	<p>MCD $(\alpha=0.05;$ $\text{quant}=0.8)$</p>	<p>\$cor.rob [1] 0.05272294</p>

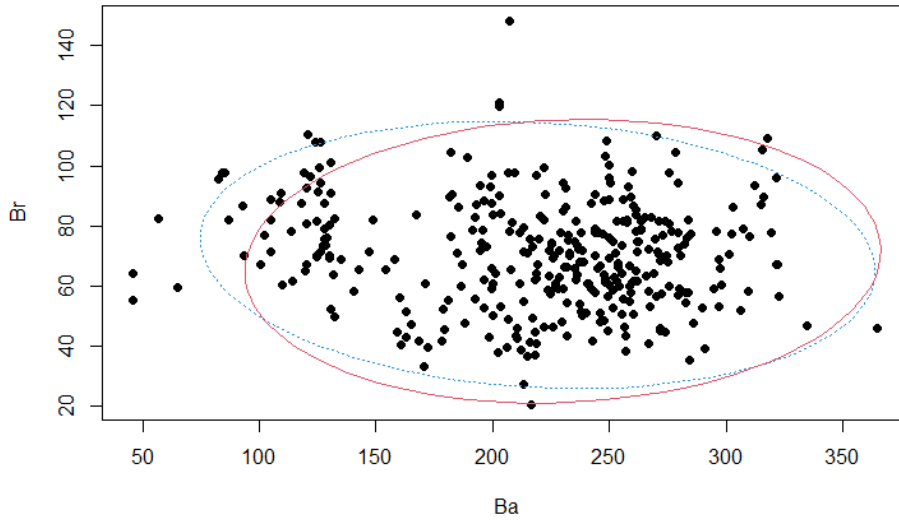
Classical cor = 0.28 Robust cor = 0.05



• Br vs Ba

Classical test	<p>Pearson's product-moment correlation</p> <p>data: Aa211C_CC\$Ba and Aa211C_CC\$Br $t = -2.2626$, $df = 338$, p-value = 0.0243 alternative hypothesis: true correlation is not equal to 0 95 percent confidence interval: -0.22557786 -0.01599186 sample estimates: cor -0.1221463</p>	<p>Spearman's rank correlation rho</p> <p>data: Aa211C_CC\$Ba and Aa211C_CC\$Br $S = 7161164$, p-value = 0.08615 alternative hypothesis: true rho is not equal to 0 sample estimates: rho -0.09320567</p>
	<p>MCD $(\alpha=0.05;$ $\text{quant}=0.8)$</p>	<p>\$cor.rob [1] 0.0757424</p>

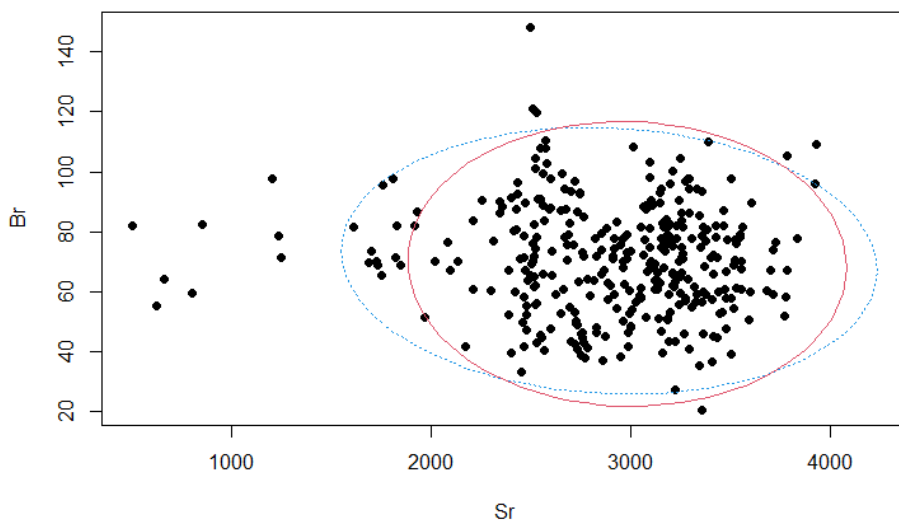
Classical cor = -0.12 Robust cor = 0.08



• Br vs Sr

Classical test	<p>Pearson's product-moment correlation</p> <p>data: Aa211C_CC\$Sr and Aa211C_CC\$Br $t = -1.3668$, $df = 338$, p-value = 0.1726 alternative hypothesis: true correlation is not equal to 0 95 percent confidence interval: -0.17908762 0.03248073 sample estimates: cor -0.0741376</p>	<p>Spearman's rank correlation rho</p> <p>data: Aa211C_CC\$Sr and Aa211C_CC\$Br $S = 7018806$, p-value = 0.1885 alternative hypothesis: true rho is not equal to 0 sample estimates: rho -0.07147365</p>
	<p>MCD $(\alpha=0.05;$ $quant=0.8)$</p>	<p>\$cor.rob [1] -0.02307787</p>

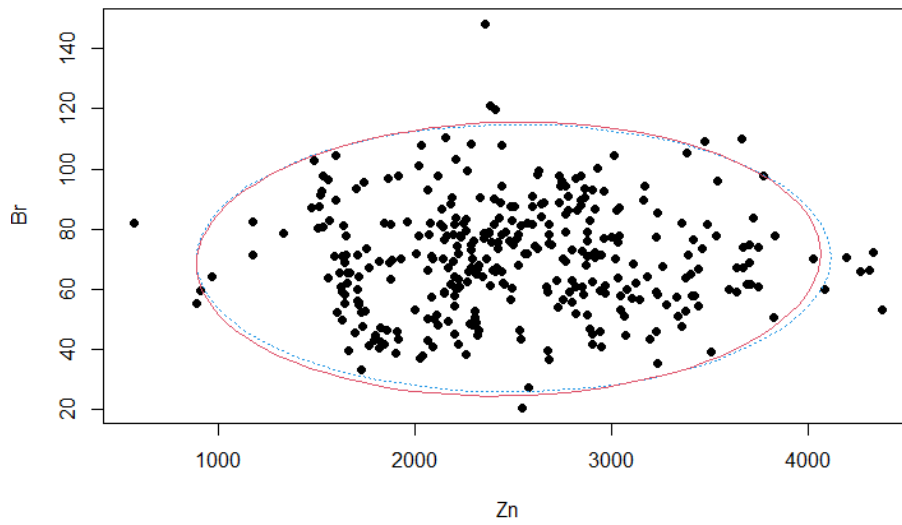
Classical cor = -0.07 Robust cor = -0.02



• Br vs Zn

Classical test	<p>Pearson's product-moment correlation</p> <p>data: Aa211C_CC\$Zn and Aa211C_CC\$Br $t = 0.19553$, $df = 338$, p-value = 0.8451 alternative hypothesis: true correlation is not equal to 0 95 percent confidence interval: -0.09583573 0.11686490 sample estimates: cor 0.01063488</p>	<p>Spearman's rank correlation rho</p> <p>data: Aa211C_CC\$Zn and Aa211C_CC\$Br $S = 6435608$, p-value = 0.7469 alternative hypothesis: true rho is not equal to 0 sample estimates: rho 0.01755592</p>
	<p>MCD $(\alpha=0.05;$ $quant=0.8)$</p>	<p>\$cor.rob [1] 0.03940319</p>

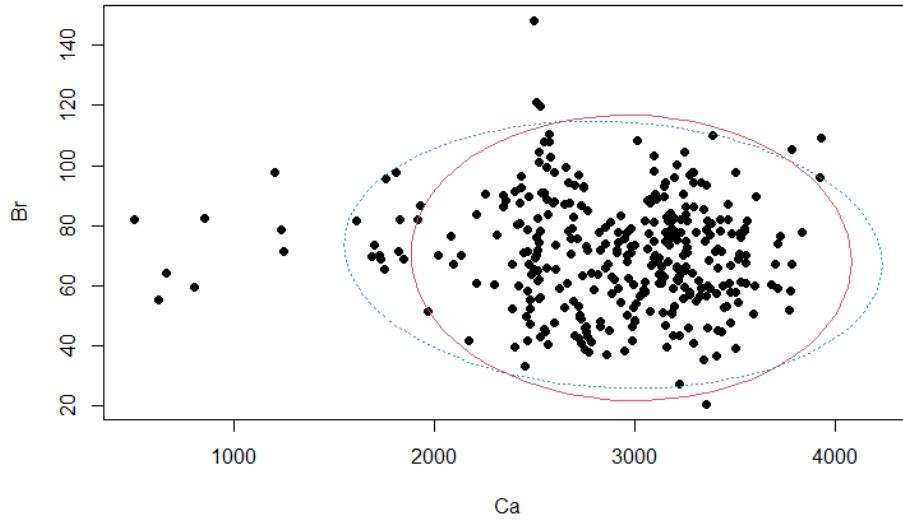
Classical cor = 0.01 Robust cor = 0.04



• Br vs Ca

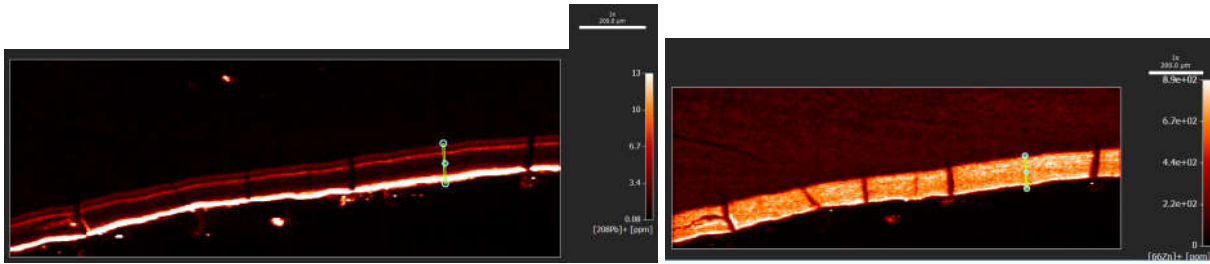
Classical test	<p>Pearson's product-moment correlation</p> <p>data: Aa211C_CC\$Ca and Aa211C_CC\$Br $t = -1.3833$, $df = 338$, p-value = 0.1675 alternative hypothesis: true correlation is not equal to 0 95 percent confidence interval: -0.17995719 0.03158313 sample estimates: cor -0.07503112</p>	<p>Spearman's rank correlation rho</p> <p>data: Aa211C_CC\$Ca and Aa211C_CC\$Br $S = 6896554$, p-value = 0.3314 alternative hypothesis: true rho is not equal to 0 sample estimates: rho -0.05281096</p>
	<p>MCD $(\alpha=0.05;$ $quant=0.8)$</p>	<p>\$cor.rob [1] -0.02307787</p>

Classical cor = -0.07 Robust cor = -0.02



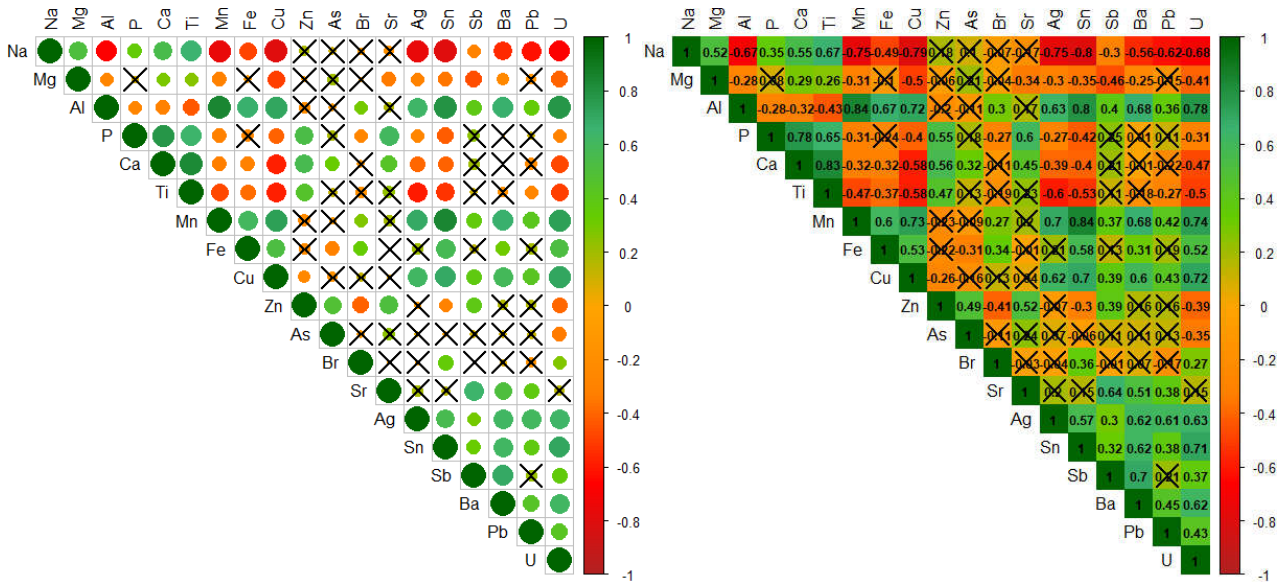
Odense 533M1 – Acellular Cementum (total thickness=122 μm)

Correlations between pairs of elements

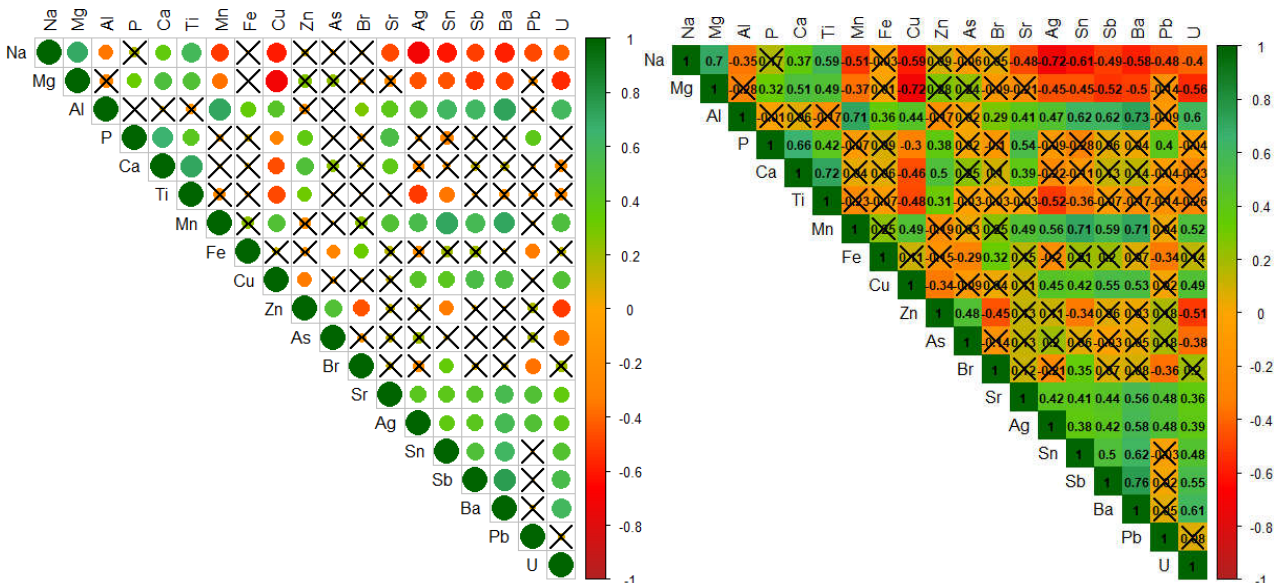


Pb (left) and Zn (right) maps (green path indicates where the measurements are taken)

Summary: whole cementum thickness, Spearman correlations.



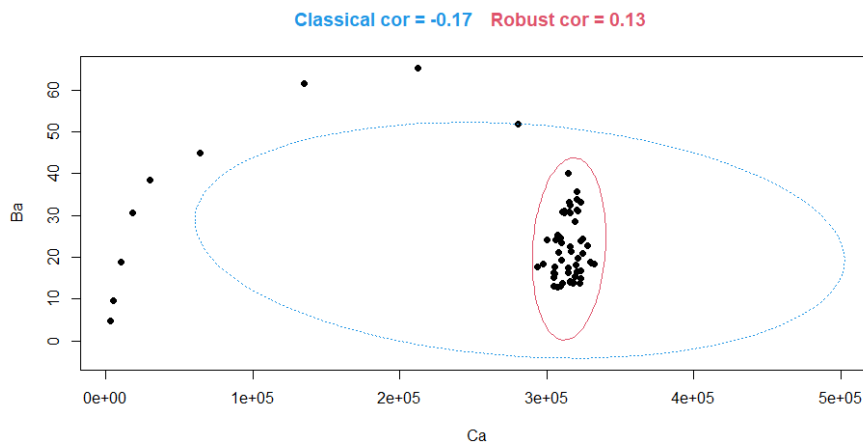
Summary: removing the first 25 μm of root surface, Spearman correlations.



wRS: without Root surface [Pb = $\sim 25 \mu\text{m}$; Fe = $\sim 20 \mu\text{m}$; Mn = $\sim 25 \mu\text{m}$; Al = $\sim 18 \mu\text{m}$]

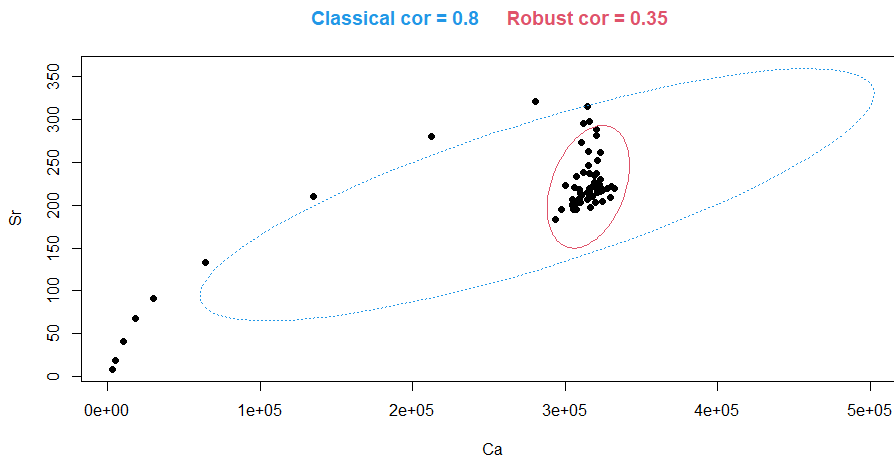
• **Ca vs Ba**

Classical test	<p>Pearson's product-moment correlation</p> <p>data: Od533M_AC\$Ca and Od533M_AC\$Ba $t = -1.3231$, $df = 60$, p-value = 0.1908 alternative hypothesis: true correlation is not equal to 0 95 percent confidence interval: -0.40126689 0.08496775 sample estimates: cor -0.1683737</p>	<p>Spearman's rank correlation rho</p> <p>data: Od533M_AC\$Ca and Od533M_AC\$Ba $S = 40122$, p-value = 0.9363 alternative hypothesis: true rho is not equal to 0 sample estimates: rho -0.01034978</p>
	<p>MCD ($\alpha=0.05$; quant=0.8)</p> <p style="text-align: center;">\$cor.rob [1] 0.1322351</p>	



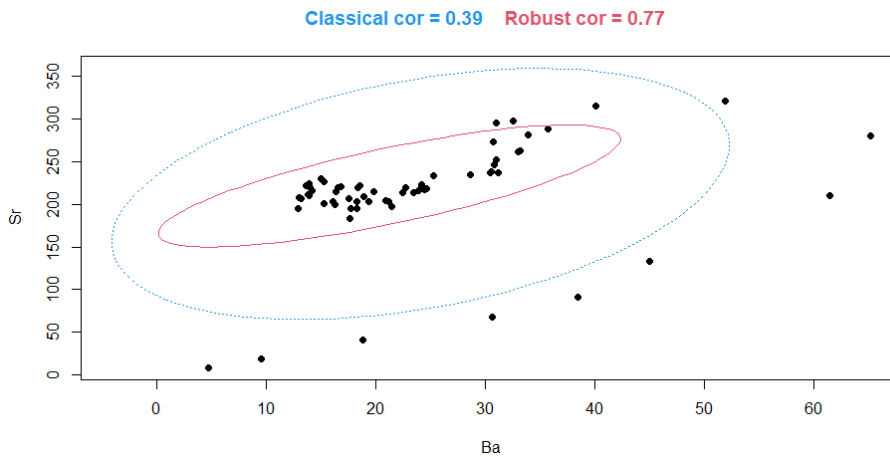
• **Ca vs Sr**

Classical test	<p>Pearson's product-moment correlation</p> <p>data: Od533M_AC\$Ca and Od533M_AC\$Sr $t = 10.43$, $df = 60$, p-value = 4.231e-15 alternative hypothesis: true correlation is not equal to 0 95 percent confidence interval: 0.6917803 0.8767852 sample estimates: cor 0.8028315</p>	<p>Spearman's rank correlation rho</p> <p>data: Od533M_AC\$Ca and Od533M_AC\$Sr $S = 21722$, p-value = 0.0002536 alternative hypothesis: true rho is not equal to 0 sample estimates: rho 0.4529979</p>
	<p>MCD ($\alpha=0.05$; quant=0.8)</p> <p style="text-align: center;">\$cor.rob [1] 0.3525441</p>	



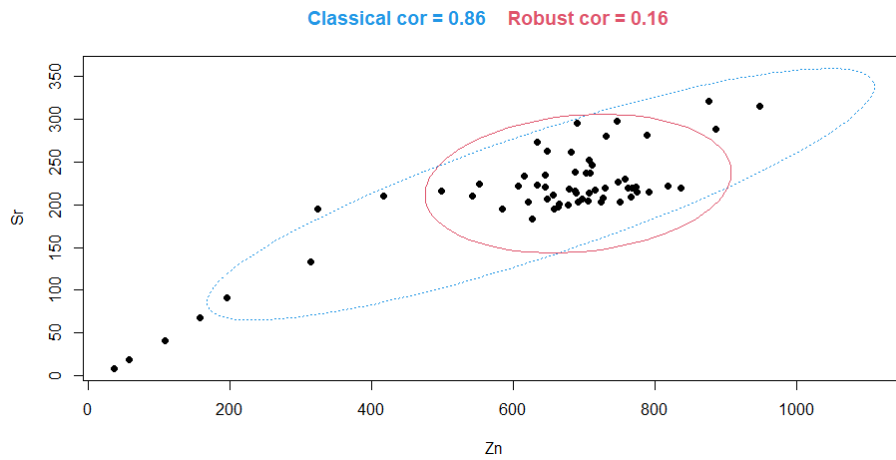
• **Ba vs Sr**

Classical test	<p>Pearson's product-moment correlation</p> <p>data: Od533M_AC\$Ba and Od533M_AC\$Sr $t = 3.2487$, $df = 60$, p-value = 0.001901 alternative hypothesis: true correlation is not equal to 0 95 percent confidence interval: 0.1516530 0.5804646 sample estimates: cor 0.3867711</p>	<p>Spearman's rank correlation rho</p> <p>data: Od533M_AC\$Ba and Od533M_AC\$Sr $S = 19484$, p-value = 3.066e-05 alternative hypothesis: true rho is not equal to 0 sample estimates: rho 0.5093551</p>
	<p>MCD $(\alpha=0.05;$ $quant=0.8)$</p>	<p>\$cor.rob [1] 0.773796</p>



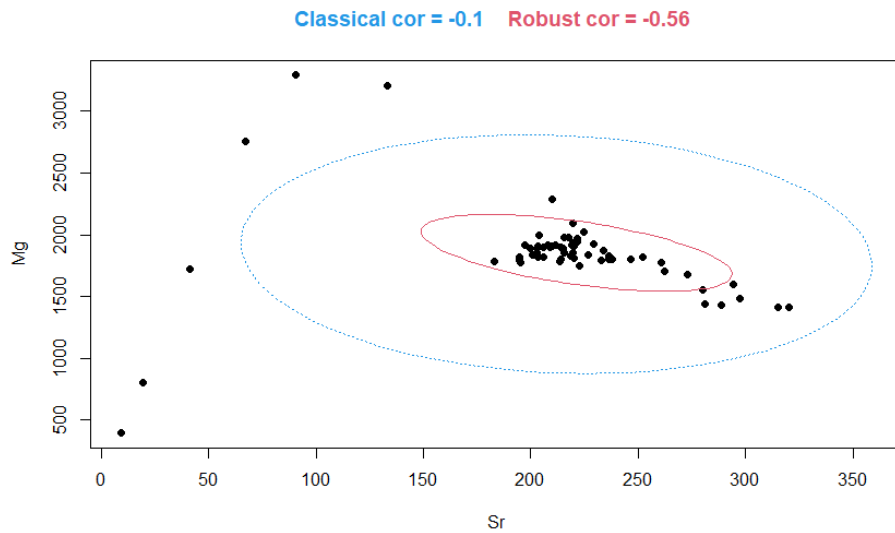
• Zn vs Sr

Classical test	<p>Pearson's product-moment correlation</p> <p>data: Od533M_AC\$Zn and Od533M_AC\$Sr $t = 12.962$, $df = 60$, p-value < 2.2e-16 alternative hypothesis: true correlation is not equal to 0 95 percent confidence interval: 0.7747542 0.9125301 sample estimates: cor 0.858412</p>	<p>Spearman's rank correlation rho</p> <p>data: Od533M_AC\$Zn and Od533M_AC\$Sr $S = 19190$, p-value = 2.263e-05 alternative hypothesis: true rho is not equal to 0 sample estimates: rho 0.5167586</p>
MCD ($\alpha=0.05$; quant=0.8)	<p>\$cor.rob [1] 0.1622059</p>	



• Mg vs Sr

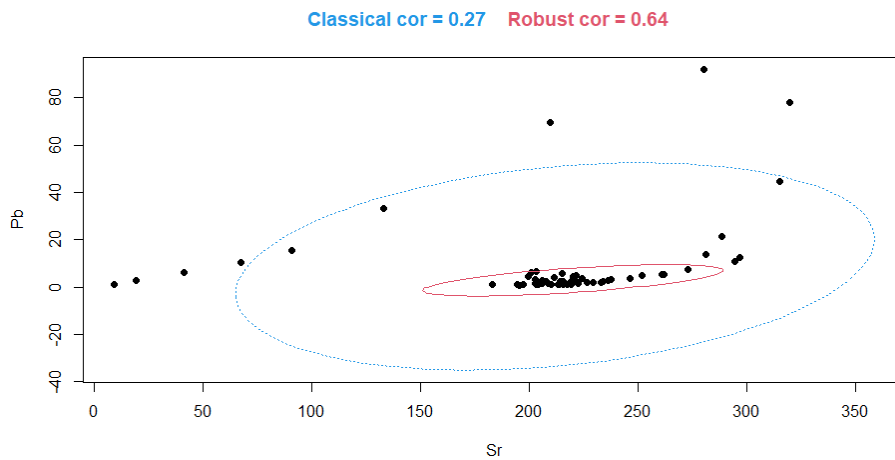
Classical test	<p>Pearson's product-moment correlation</p> <p>data: Od533M_AC\$Sr and Od533M_AC\$Mg $t = -0.74167$, $df = 60$, p-value = 0.4612 alternative hypothesis: true correlation is not equal to 0 95 percent confidence interval: -0.3370577 0.1582213 sample estimates: cor -0.09531356</p>	<p>Spearman's rank correlation rho</p> <p>data: Od533M_AC\$Sr and Od533M_AC\$Mg $S = 53034$, p-value = 0.00795 alternative hypothesis: true rho is not equal to 0 sample estimates: rho 0</p>
MCD ($\alpha=0.05$; quant=0.8)	<p>\$cor.rob [1] -0.5588916</p>	



- **Pb vs Sr**

Whole cementum thickness:

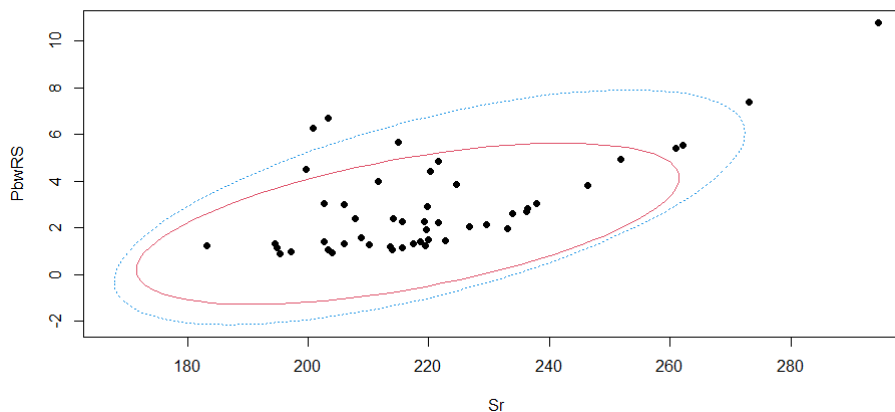
Classical test	<p>Pearson's product-moment correlation</p> <p>data: Od533M_AC\$Sr and Od533M_AC\$Pb $t = 2.1467$, $df = 60$, p-value = 0.03587 alternative hypothesis: true correlation is not equal to 0 95 percent confidence interval: 0.0185453 0.4845234 sample estimates: cor 0.2670764</p>	<p>Spearman's rank correlation rho</p> <p>data: Od533M_AC\$Sr and Od533M_AC\$Pb $S = 24506$, p-value = 0.002278 alternative hypothesis: true rho is not equal to 0 sample estimates: rho 0.3828914</p>
	<p>MCD ($\alpha=0.05$; quant=0.8)</p> <p>$\\$cor.rob$ [1] 0.6354589</p>	



Removing 25 μm of Pb-enriched root surface:

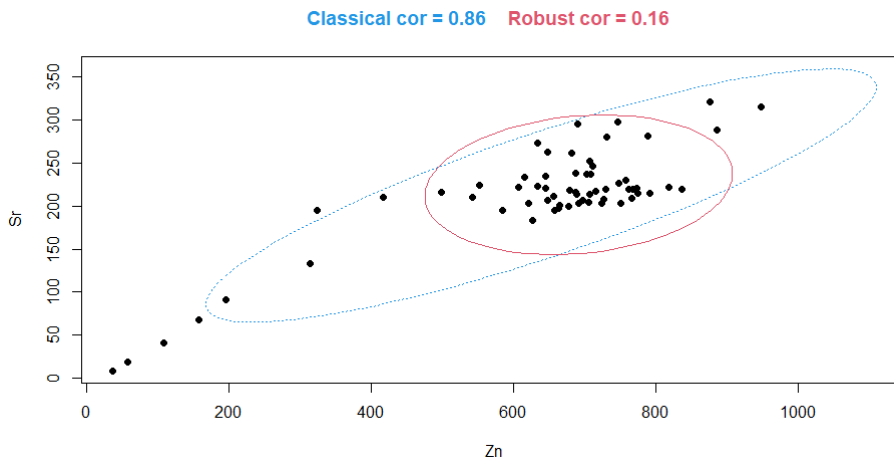
Classical test	<p>Pearson's product-moment correlation</p> <p>data: Od533M_AC_wRS\$Sr and Od533M_AC_wRS\$Pb $t = 5.6421$, $df = 47$, p-value = 9.329e-07 alternative hypothesis: true correlation is not equal to 0 95 percent confidence interval: 0.4313376 0.7776908 sample estimates: cor 0.6354589</p>	<p>Spearman's rank correlation rho</p> <p>data: Od533M_AC_wRS\$Zn and Od533M_AC_wRS\$Pb $S = 16154$, p-value = 0.2262 alternative hypothesis: true rho is not equal to 0 sample estimates: rho 0.1758163</p>
	<p>MCD $(\alpha=0.05;$ $\text{quant}=0.8)$</p>	<p>\$cor.rob [1] 0.5718473</p>

Classical cor = 0.64 Robust cor = 0.57



• Sr vs Zn

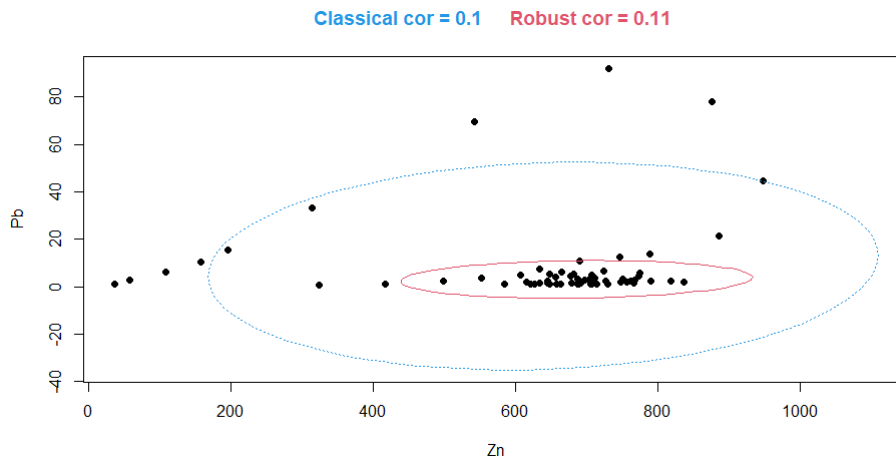
Classical test	<p>Pearson's product-moment correlation</p> <p>data: Od533M_AC\$Zn and Od533M_AC\$Sr $t = 12.962$, $df = 60$, p-value < 2.2e-16 alternative hypothesis: true correlation is not equal to 0 95 percent confidence interval: 0.7747542 0.9125301 sample estimates: cor 0.858412</p>	<p>Spearman's rank correlation rho</p> <p>data: Od533M_AC\$Zn and Od533M_AC\$Sr $S = 19190$, p-value = 2.263e-05 alternative hypothesis: true rho is not equal to 0 sample estimates: rho 0.5167586</p>
	<p>MCD $(\alpha=0.05;$ $\text{quant}=0.8)$</p>	<p>\$cor.rob [1] 0.1622059</p>



• **Pb vs Zn**

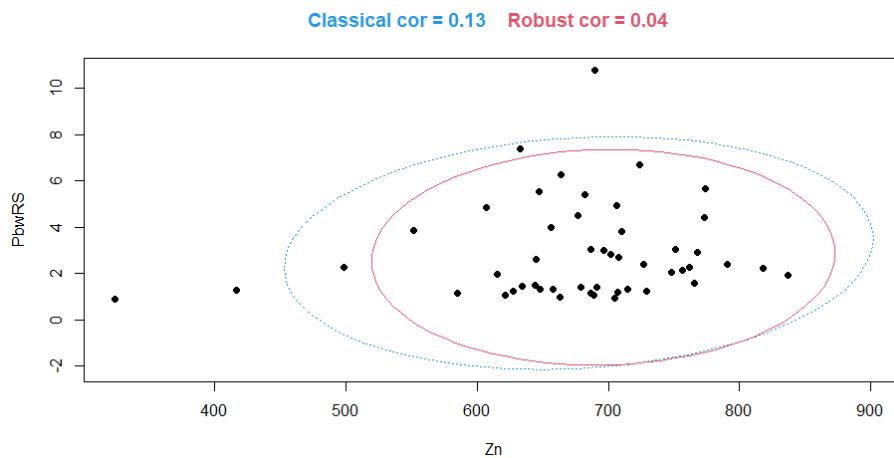
Whole cementum thickness:

Classical test	<p>Pearson's product-moment correlation</p> <p>data: Od533M_AC\$Zn and Od533M_AC\$Pb $t = 0.78748$, $df = 60$, p-value = 0.4341 alternative hypothesis: true correlation is not equal to 0 95 percent confidence interval: -0.1524783 0.3422638 sample estimates: cor 0.1011418</p>	<p>Spearman's rank correlation rho</p> <p>data: Od533M_AC\$Zn and Od533M_AC\$Pb $S = 33264$, p-value = 0.2069 alternative hypothesis: true rho is not equal to 0 sample estimates: rho 0.162348</p>
	<p>MCD $(\alpha=0.05;$ $quant=0.8)$</p>	<p>\$cor.rob [1] 0.1101698</p>



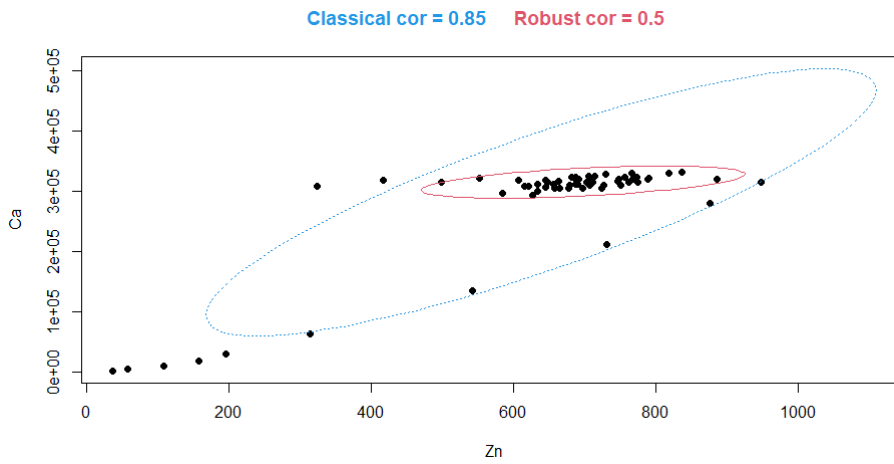
Removing 25 μm of Pb-enriched root surface:

Classical test	<p>Pearson's product-moment correlation</p> <p>data: Od533M_AC_wRS\$Zn and Od533M_AC_wRS\$Pb $t = 0.8646$, $df = 47$, p-value = 0.3916 alternative hypothesis: true correlation is not equal to 0 95 percent confidence interval: -0.1617640 0.3925105 sample estimates: cor 0.1251242</p>	<p>Spearman's rank correlation rho</p> <p>data: Od533M_AC_wRS\$Zn and Od533M_AC_wRS\$Pb $S = 16154$, p-value = 0.2262 alternative hypothesis: true rho is not equal to 0 sample estimates: rho 0.1758163</p>
	<p>MCD $(\alpha=0.05;$ $\text{quant}=0.8)$</p>	<p>\$cor.rob [1] 0.03672209</p>



• Zn vs Ca

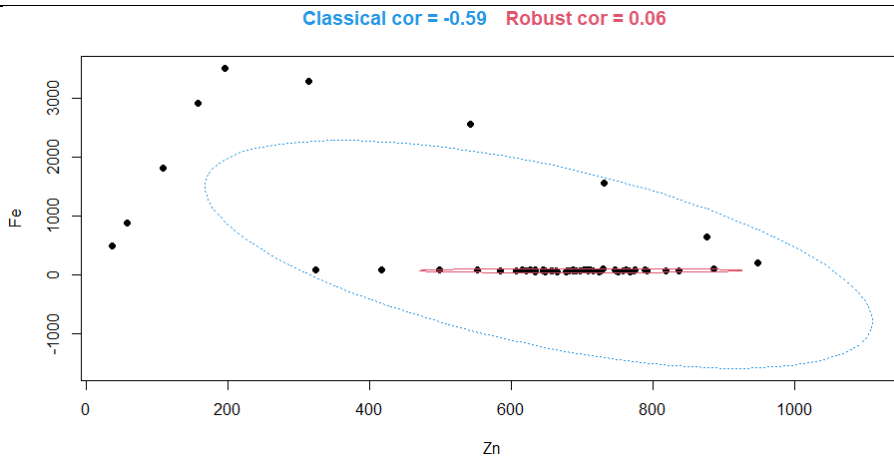
Classical test	<p>Pearson's product-moment correlation</p> <p>data: Od533M_AC\$Zn and Od533M_AC\$Ca $t = 12.292$, $df = 60$, p-value < 2.2e-16 alternative hypothesis: true correlation is not equal to 0 95 percent confidence interval: 0.7560046 0.9046328 sample estimates: cor 0.846022</p>	<p>Spearman's rank correlation rho</p> <p>data: Od533M_AC\$Zn and Od533M_AC\$Ca $S = 17394$, p-value = 3.074e-06 alternative hypothesis: true rho is not equal to 0 sample estimates: rho 0.5619853</p>
	<p>MCD $(\alpha=0.05;$ $\text{quant}=0.8)$</p>	<p>\$cor.rob [1] 0.495149</p>



- **Zn vs Fe**

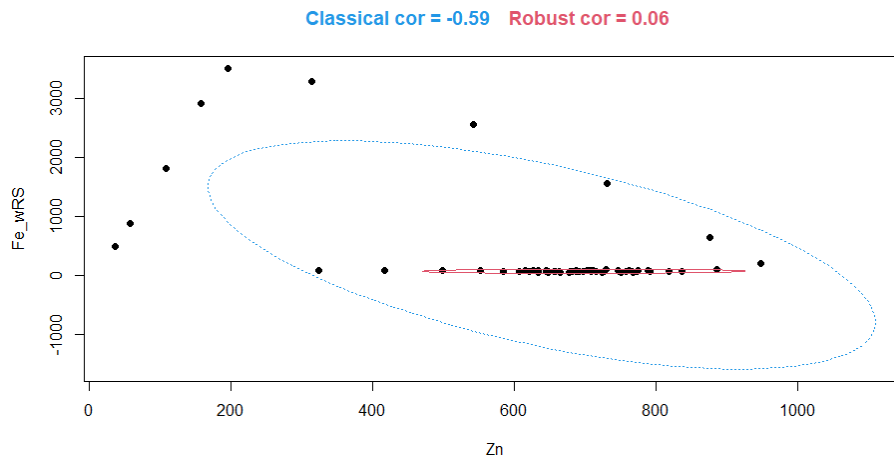
Whole cementum thickness:

Classical test	<p>Pearson's product-moment correlation</p> <p>data: Od533M_AC\$Zn and Od533M_AC\$Fe $t = -5.7009$, $df = 60$, p-value = 3.858e-07 alternative hypothesis: true correlation is not equal to 0 95 percent confidence interval: -0.7338670 -0.4025811 sample estimates: cor -0.5927474</p>	<p>Spearman's rank correlation rho</p> <p>data: Od533M_AC\$Zn and Od533M_AC\$Fe $S = 48500$, p-value = 0.08392 alternative hypothesis: true rho is not equal to 0 sample estimates: rho -0.2213241</p>
	<p>MCD $(\alpha=0.05;$ $quant=0.8)$</p> <p>\$cor.rob [1] 0.05539145</p>	



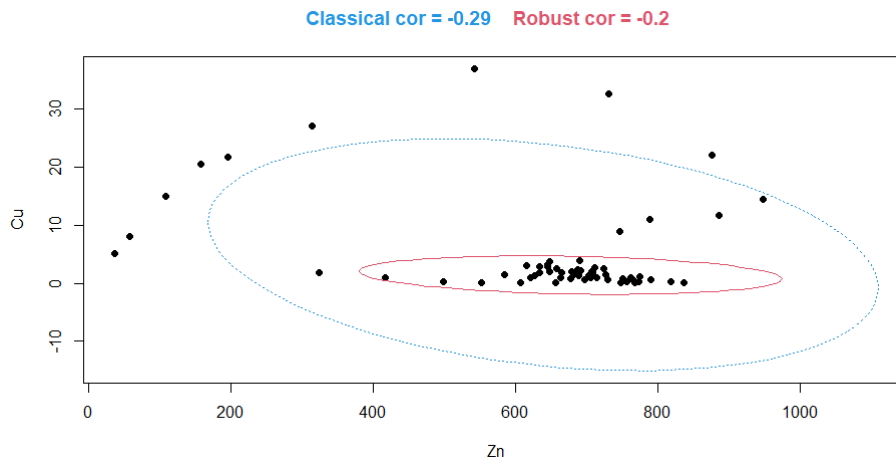
Removing 20 μm of Fe-enriched root surface:

Classical test	<p>Pearson's product-moment correlation</p> <p>data: Od533M_AC\$Zn and Od533M_AC\$Fe $t = -5.7009$, $df = 60$, p-value = 3.858e-07 alternative hypothesis: true correlation is not equal to 0 95 percent confidence interval: -0.7338670 -0.4025811 sample estimates: cor -0.5927474</p>	<p>Spearman's rank correlation rho</p> <p>data: Od533M_AC\$Zn and Od533M_AC\$Fe $S = 48500$, p-value = 0.08392 alternative hypothesis: true rho is not equal to 0 sample estimates: rho -0.2213241</p>
	<p>MCD $(\alpha=0.05;$ $\text{quant}=0.8)$</p>	<p>\$cor.rob [1] 0.05539145</p>



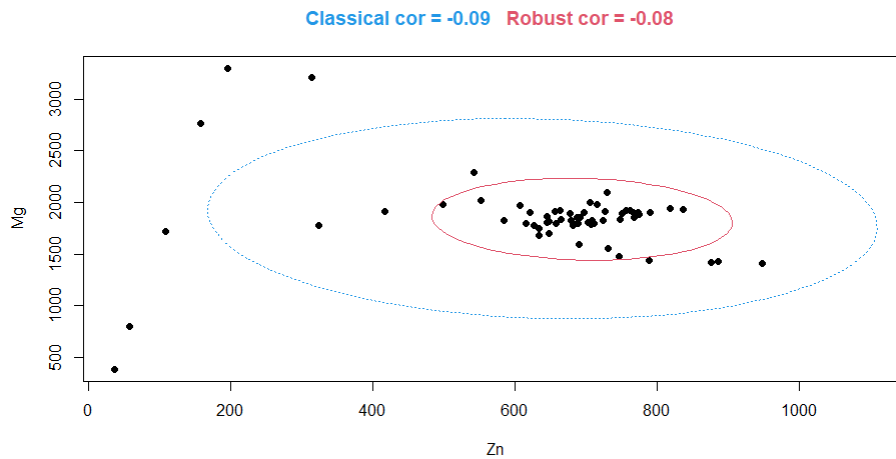
• Zn vs Cu

Classical test	<p>Pearson's product-moment correlation</p> <p>data: Od533M_AC\$Zn and Od533M_AC\$Cu $t = -2.3242$, $df = 60$, p-value = 0.02352 alternative hypothesis: true correlation is not equal to 0 95 percent confidence interval: -0.5011898 -0.0405404 sample estimates: cor -0.2873985</p>	<p>Spearman's rank correlation rho</p> <p>data: Od533M_AC\$Zn and Od533M_AC\$Cu $S = 50118$, p-value = 0.03992 alternative hypothesis: true rho is not equal to 0 sample estimates: rho -0.2620684</p>
	<p>MCD $(\alpha=0.05;$ $\text{quant}=0.8)$</p>	<p>\$cor.rob [1] -0.199509</p>



• Zn vs Mg

Classical test	<p>Pearson's product-moment correlation</p> <p>data: Od533M_AC\$Zn and Od533M_AC\$Mg $t = -0.67332$, $df = 60$, p-value = 0.5033 alternative hypothesis: true correlation is not equal to 0 95 percent confidence interval: -0.3292453 0.1667769 sample estimates: cor -0.08659857</p>	<p>Spearman's rank correlation rho</p> <p>data: Od533M_AC\$Zn and Od533M_AC\$Mg $S = 42232$, p-value = 0.6232 alternative hypothesis: true rho is not equal to 0 sample estimates: rho -0.06348367</p>
	<p>MCD $(\alpha=0.05;$ $quant=0.8)$</p>	<p>$\\$cor.rob$ $[1] -0.08098037$</p>

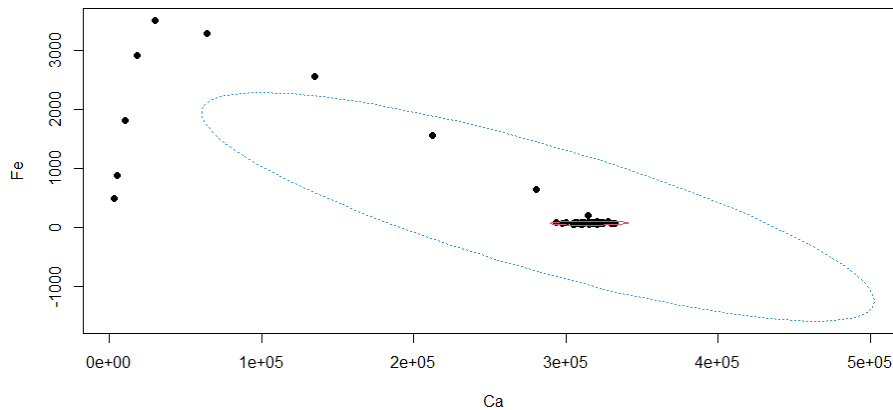


- **Ca vs Fe**

Whole cementum thickness:

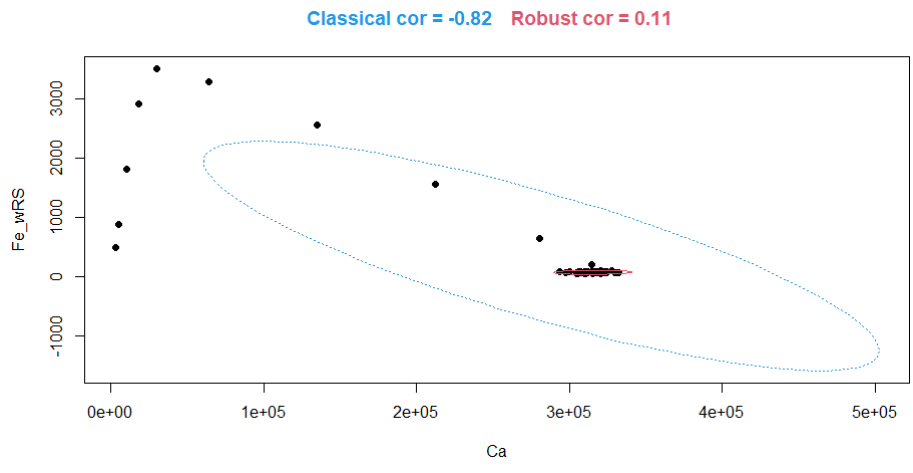
Classical test	<p>Pearson's product-moment correlation</p> <p>data: Od533M_AC\$Ca and Od533M_AC\$Fe $t = -11.254$, $df = 60$, p-value < 2.2e-16 alternative hypothesis: true correlation is not equal to 0 95 percent confidence interval: -0.8903300 -0.7226572 sample estimates: cor -0.8237425</p>	<p>Spearman's rank correlation rho</p> <p>data: Od533M_AC\$Ca and Od533M_AC\$Fe $S = 52262$, p-value = 0.01264 alternative hypothesis: true rho is not equal to 0 sample estimates: rho -0.3160585</p>
	<p>MCD ($\alpha=0.05$; quant=0.8)</p>	<p>\$cor.rob [1] 0.1122484</p>

Classical cor = -0.82 Robust cor = 0.11



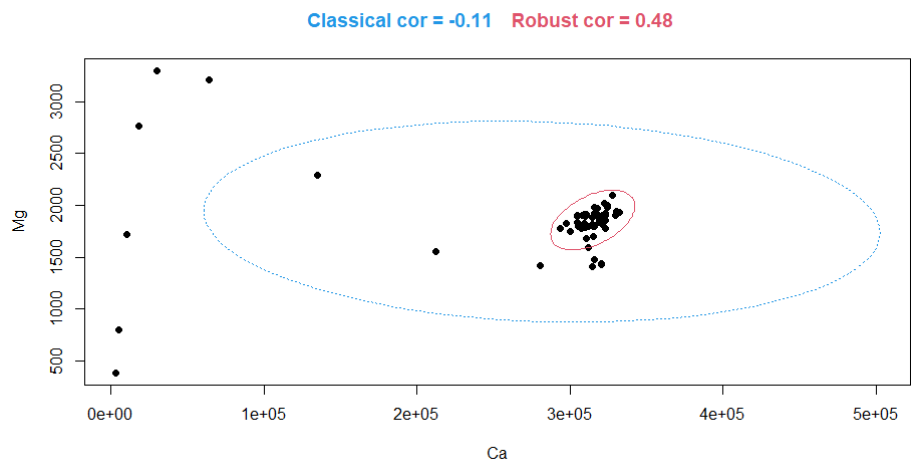
Removing 20 μm of Fe-enriched root surface:

Classical test	<p>Pearson's product-moment correlation</p> <p>data: Od533M_AC\$Ca and Od533M_AC\$Fe $t = -11.254$, $df = 60$, p-value < 2.2e-16 alternative hypothesis: true correlation is not equal to 0 95 percent confidence interval: -0.8903300 -0.7226572 sample estimates: cor -0.8237425</p>	<p>Spearman's rank correlation rho</p> <p>data: Od533M_AC\$Ca and Od533M_AC\$Fe $S = 52262$, p-value = 0.01264 alternative hypothesis: true rho is not equal to 0 sample estimates: rho -0.3160585</p>
	<p>MCD ($\alpha=0.05$; quant=0.8)</p>	<p>\$cor.rob [1] 0.1122484</p>



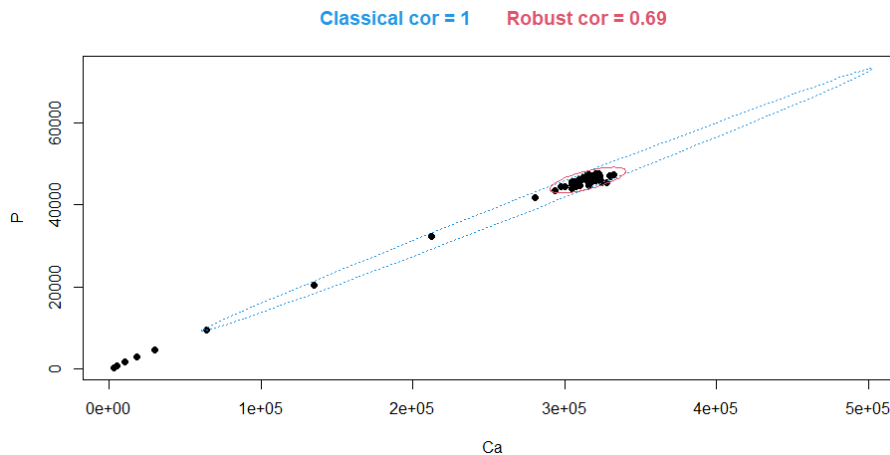
• Ca vs Mg

Classical test	<p>Pearson's product-moment correlation</p> <p>data: Od533M_AC\$Ca and Od533M_AC\$Mg $t = -0.84899$, $df = 60$, p-value = 0.3993 alternative hypothesis: true correlation is not equal to 0 95 percent confidence interval: -0.3492168 0.1447556 sample estimates: cor -0.1089518</p>	<p>Spearman's rank correlation rho</p> <p>data: Od533M_AC\$Ca and Od533M_AC\$Mg $S = 28360$, p-value = 0.02465 alternative hypothesis: true rho is not equal to 0 sample estimates: rho 0.2858402</p>
	<p>MCD $(\alpha=0.05;$ $quant=0.8)$</p>	<p>$\\$cor.rob$ [1] 0.4769753</p>



• **Ca vs P**

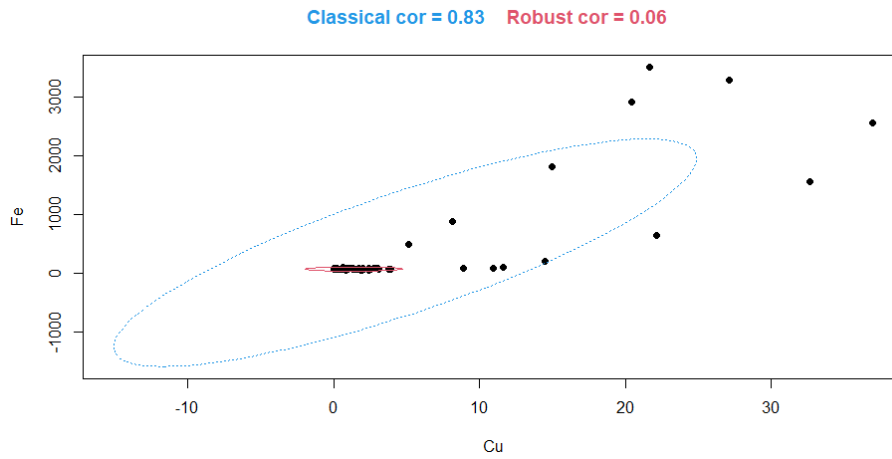
Classical test	Pearson's product-moment correlation data: Od533M_AC\$Ca and Od533M_AC\$P $t = 119.66$, $df = 60$, p-value < 2.2e-16 alternative hypothesis: true correlation is not equal to 0 95 percent confidence interval: 0.9965231 0.9987457 sample estimates: cor 0.9979114	Spearman's rank correlation rho data: Od533M_AC\$Ca and Od533M_AC\$P $S = 8874$, p-value < 2.2e-16 alternative hypothesis: true rho is not equal to 0 sample estimates: rho 0.7765355
	MCD ($\alpha=0.05$; quant=0.8)	\$cor.rob [1] 0.6936723



• **Cu vs Fe**

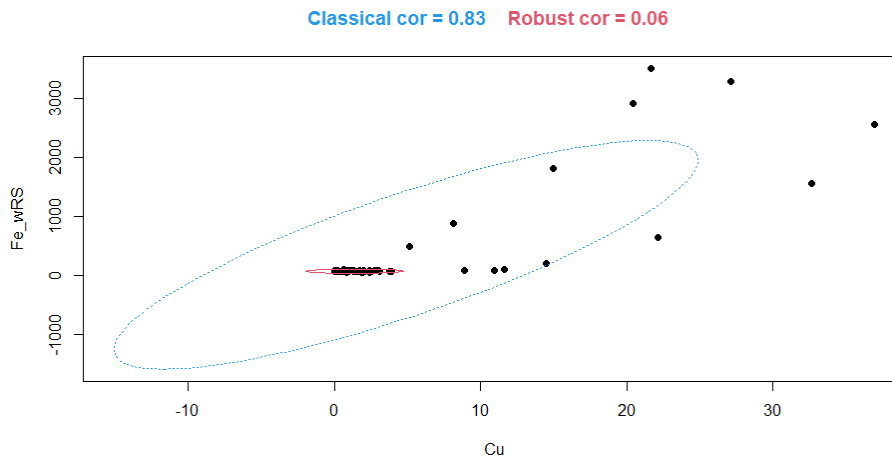
Whole cementum thickness:

Classical test	Pearson's product-moment correlation data: Od533M_AC\$Cu and Od533M_AC\$Fe $t = 11.496$, $df = 60$, p-value < 2.2e-16 alternative hypothesis: true correlation is not equal to 0 95 percent confidence interval: 0.7309596 0.8939221 sample estimates: cor 0.8293187	Spearman's rank correlation rho data: Od533M_AC\$Cu and Od533M_AC\$Fe $S = 18542$, p-value = 1.133e-05 alternative hypothesis: true rho is not equal to 0 sample estimates: rho 0.5330765
	MCD ($\alpha=0.05$; quant=0.8)	\$cor.rob [1] 0.05517098



Removing 15 μm of Fe-enriched root surface:

Classical test	<p>Pearson's product-moment correlation</p> <p>data: Od533M_AC\$Cu and Od533M_AC\$Fe $t = 11.496$, $df = 60$, p-value < 2.2e-16 alternative hypothesis: true correlation is not equal to 0 95 percent confidence interval: 0.7309596 0.8939221 sample estimates: cor 0.8293187</p>	<p>Spearman's rank correlation rho</p> <p>data: Od533M_AC\$Cu and Od533M_AC\$Fe $S = 18542$, p-value = 1.133e-05 alternative hypothesis: true rho is not equal to 0 sample estimates: rho 0.5330765</p>
	<p>MCD $(\alpha=0.05;$ $quant=0.8)$</p>	<p>$\\$cor.rob$ [1] 0.05517098</p>

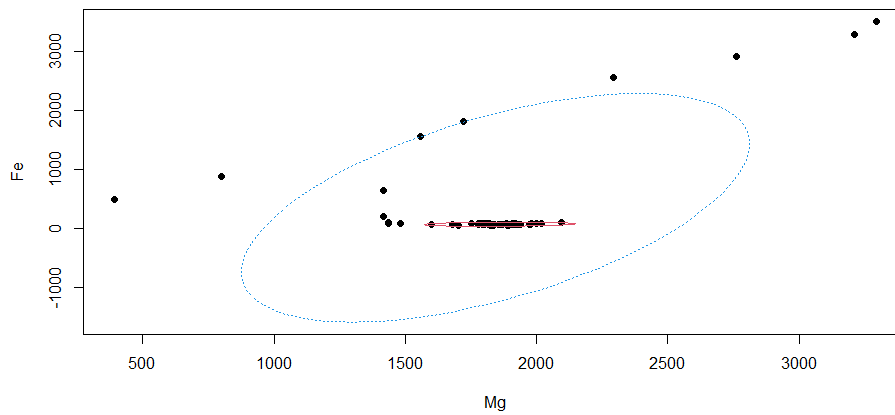


- **Mg vs Fe**

Whole cementum thickness:

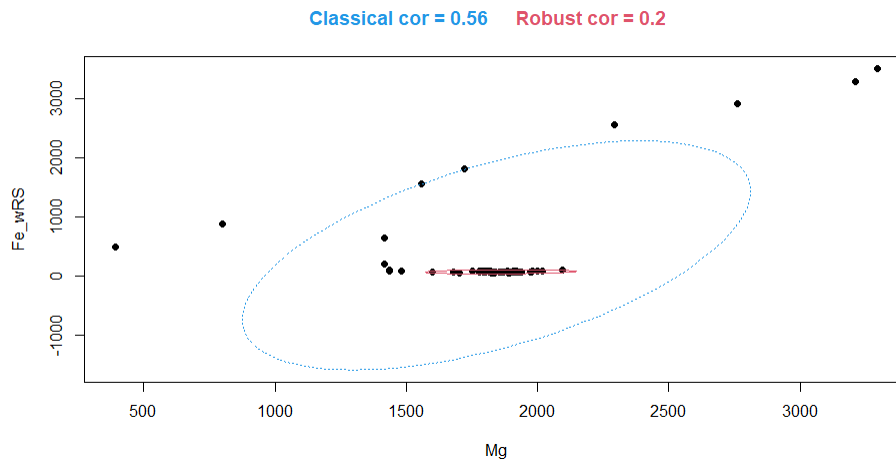
Classical test	<p>Pearson's product-moment correlation</p> <p>data: Od533M_AC\$Mg and Od533M_AC\$Fe $t = 5.2596$, $df = 60$, p-value = 2.03e-06 alternative hypothesis: true correlation is not equal to 0 95 percent confidence interval: 0.3628988 0.7116660 sample estimates: cor 0.5617497</p>	<p>Spearman's rank correlation rho</p> <p>data: Od533M_AC\$Mg and Od533M_AC\$Fe $S = 43784$, p-value = 0.4266 alternative hypothesis: true rho is not equal to 0 sample estimates: rho -0.102566</p>
	<p>MCD $(\alpha=0.05;$ $quant=0.8)$</p>	<p>\$cor.rob $[1] 0.1951158$</p>

Classical cor = 0.56 Robust cor = 0.2



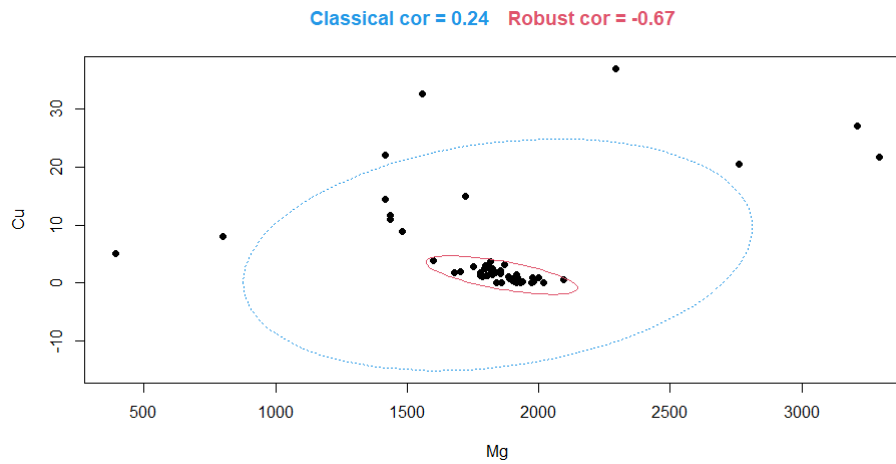
Removing 20 μm of Fe-enriched root surface:

Classical test	<p>Pearson's product-moment correlation</p> <p>data: Od533M_AC\$Mg and Od533M_AC\$Fe $t = 5.2596$, $df = 60$, p-value = 2.03e-06 alternative hypothesis: true correlation is not equal to 0 95 percent confidence interval: 0.3628988 0.7116660 sample estimates: cor 0.5617497</p>	<p>Spearman's rank correlation rho</p> <p>data: Od533M_AC\$Mg and Od533M_AC\$Fe $S = 43784$, p-value = 0.4266 alternative hypothesis: true rho is not equal to 0 sample estimates: rho -0.102566</p>
	<p>MCD $(\alpha=0.05;$ $quant=0.8)$</p>	<p>\$cor.rob $[1] 0.1951158$</p>



• Cu vs Mg

Classical test	<p>Pearson's product-moment correlation</p> <p>data: Od533M_AC\$Mg and Od533M_AC\$Cu $t = 1.8879$, $df = 60$, p-value = 0.06388 alternative hypothesis: true correlation is not equal to 0 95 percent confidence interval: -0.01379117 0.45939099 sample estimates: cor 0.2367927</p>	<p>Spearman's rank correlation rho</p> <p>data: Od533M_AC\$Mg and Od533M_AC\$Cu $S = 59714$, p-value = 3.847e-05 alternative hypothesis: true rho is not equal to 0 sample estimates: rho -0.5037143</p>
	<p>MCD $(\alpha=0.05;$ $quant=0.8)$</p>	<p>\$cor.rob [1] -0.6742311</p>

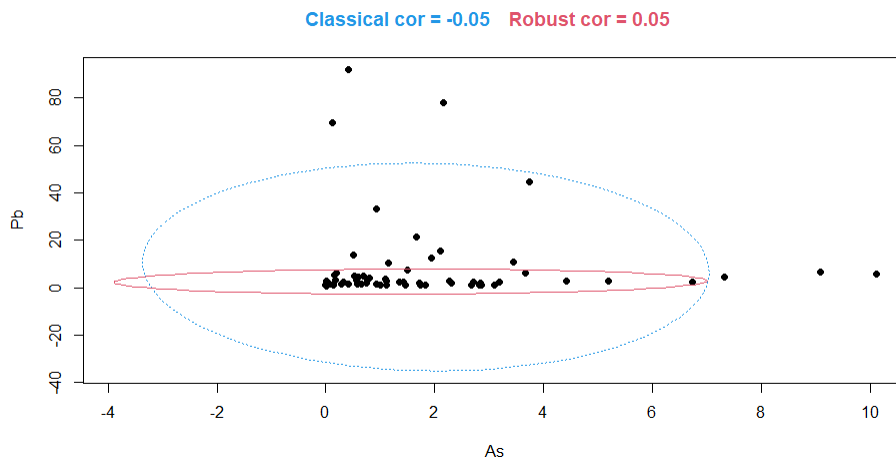


• As vs Hg, Pb vs Hg (no Hg at all). => Not Applicable.

- **Pb vs As**

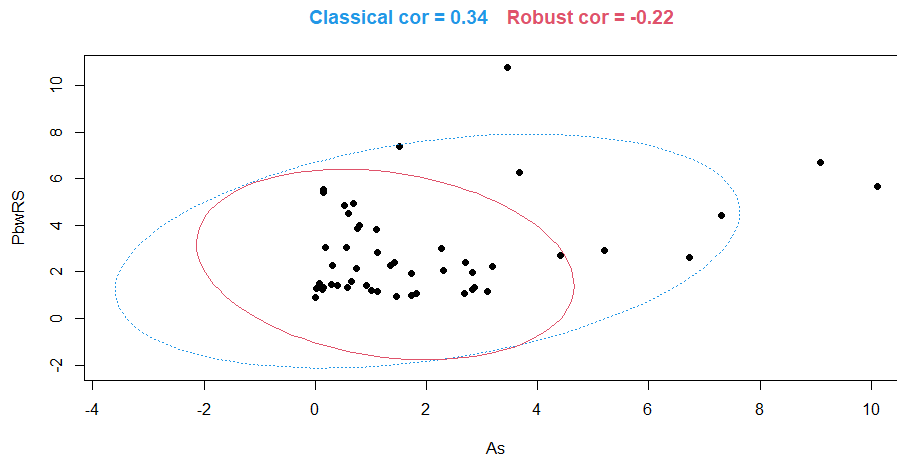
Whole cementum thickness:

Classical test	<p>Pearson's product-moment correlation</p> <p>data: Od533M_AC\$As and Od533M_AC\$Pb $t = -0.36151$, $df = 60$, p-value = 0.719 alternative hypothesis: true correlation is not equal to 0 95 percent confidence interval: -0.2929768 0.2055414 sample estimates: cor -0.04662013</p>	<p>Spearman's rank correlation rho</p> <p>data: Od533M_AC\$As and Od533M_AC\$Pb $S = 34662$, p-value = 0.3239 alternative hypothesis: true rho is not equal to 0 sample estimates: rho 0.1271436</p>
	<p>MCD $(\alpha=0.05;$ $quant=0.8)$</p>	<p>\$cor.rob [1] 0.05151116</p>



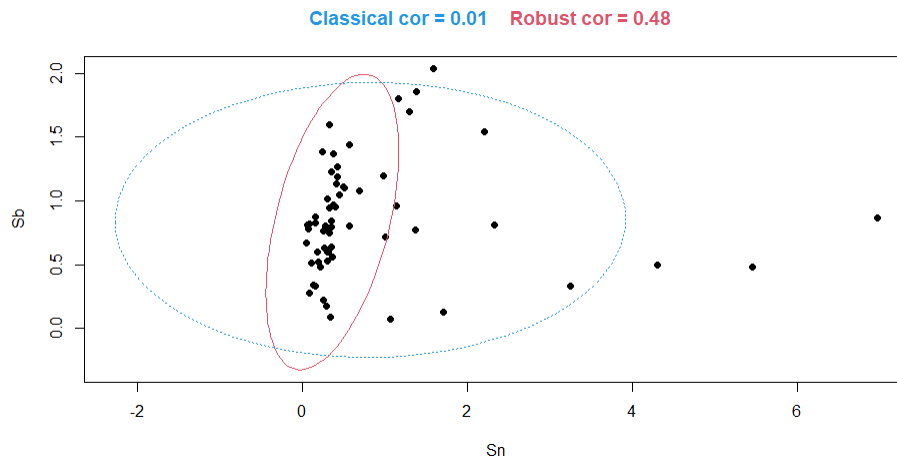
Removing 25 μm of Pb-enriched root surface:

Classical test	<p>Pearson's product-moment correlation</p> <p>data: Od533M_AC_wRS\$As and Od533M_AC_wRS\$Pb $t = 2.4433$, $df = 47$, p-value = 0.01836 alternative hypothesis: true correlation is not equal to 0 95 percent confidence interval: 0.06020137 0.56369734 sample estimates: cor 0.3357148</p>	<p>Spearman's rank correlation rho</p> <p>data: Od533M_AC_wRS\$As and Od533M_AC_wRS\$Pb $S = 15974$, p-value = 0.2025 alternative hypothesis: true rho is not equal to 0 sample estimates: rho 0.185</p>
	<p>MCD $(\alpha=0.05;$ $quant=0.8)$</p>	<p>\$cor.rob [1] -0.2204023</p>



• **Sb vs Sn**

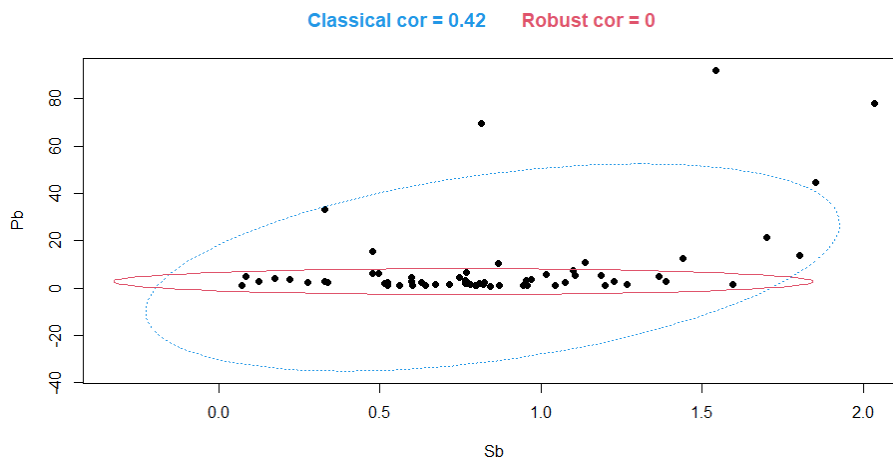
Classical test	<p>Pearson's product-moment correlation</p> <p>data: Od533M_AC\$Sn and Od533M_AC\$Sb $t = 0.082198$, $df = 60$, p-value = 0.9348 alternative hypothesis: true correlation is not equal to 0 95 percent confidence interval: -0.2397926 0.2596911 sample estimates: cor 0.01061118</p>	<p>Spearman's rank correlation rho</p> <p>data: Od533M_AC\$Sn and Od533M_AC\$Sb $S = 26930$, p-value = 0.01104 alternative hypothesis: true rho is not equal to 0 sample estimates: rho 0.3218504</p>
	<p>MCD $(\alpha=0.05;$ $quant=0.8)$</p>	<p>$\\$cor.rob$ $[1] 0.4795098$</p>



- Pb vs Sb**

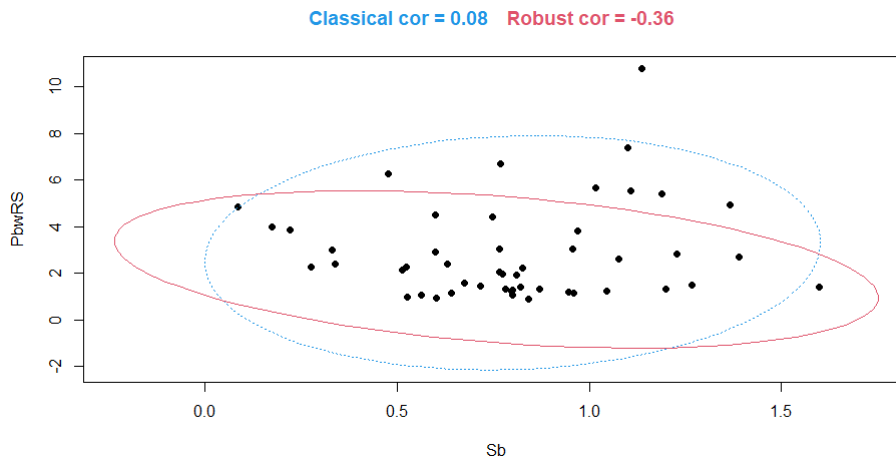
Whole cementum thickness:

Classical test	<p>Pearson's product-moment correlation</p> <p>data: Od533M_AC\$Sb and Od533M_AC\$Pb $t = 3.6301$, $df = 60$, p-value = 0.0005873 alternative hypothesis: true correlation is not equal to 0 95 percent confidence interval: 0.1952898 0.6095230 sample estimates: cor 0.424359</p>	<p>Spearman's rank correlation rho</p> <p>data: Od533M_AC\$Sb and Od533M_AC\$Pb $S = 31236$, p-value = 0.09582 alternative hypothesis: true rho is not equal to 0 sample estimates: rho 0.2134169</p>
	<p>MCD $(\alpha=0.05;$ $quant=0.8)$</p>	<p>\$cor.rob $[1] -0.002296206$</p>



Removing 25 μ m of Pb-enriched root surface:

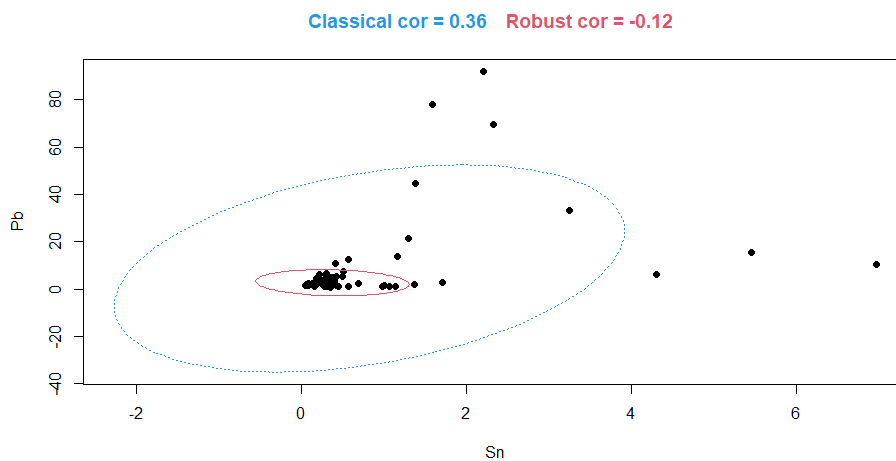
Classical test	<p>Pearson's product-moment correlation</p> <p>data: Od533M_AC_wRS\$Sb and Od533M_AC_wRS\$Pb $t = 0.5351$, $df = 47$, p-value = 0.5951 alternative hypothesis: true correlation is not equal to 0 95 percent confidence interval: -0.2079310 0.3513245 sample estimates: cor 0.07781542</p>	<p>Spearman's rank correlation rho</p> <p>data: Od533M_AC_wRS\$Sb and Od533M_AC_wRS\$Pb $S = 19266$, p-value = 0.9074 alternative hypothesis: true rho is not equal to 0 sample estimates: rho 0.01704082</p>
	<p>MCD $(\alpha=0.05;$ $quant=0.8)$</p>	<p>\$cor.rob $[1] -0.3605865$</p>



- Pb vs Sn**

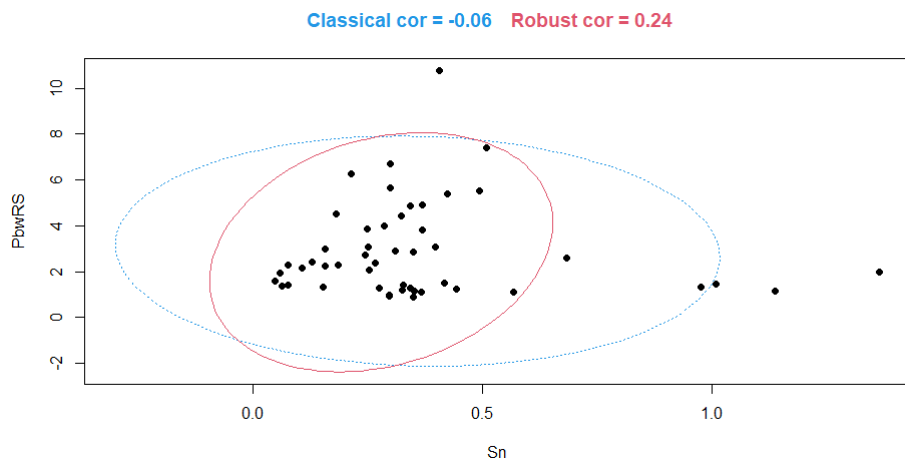
Whole cementum thickness:

Classical test	<p>Pearson's product-moment correlation</p> <p>data: Od533M_AC\$Sn and Od533M_AC\$Pb $t = 3.0305$, $df = 60$, p-value = 0.0036 alternative hypothesis: true correlation is not equal to 0 95 percent confidence interval: 0.1260418 0.5628855 sample estimates: cor 0.3643402</p>	<p>Spearman's rank correlation rho</p> <p>data: Od533M_AC\$Sn and Od533M_AC\$Pb $S = 24746$, p-value = 0.002698 alternative hypothesis: true rho is not equal to 0 sample estimates: rho 0.3768477</p>
	<p>MCD $(\alpha=0.05;$ $quant=0.8)$</p>	<p>\$cor.rob [1] -0.1243023</p>



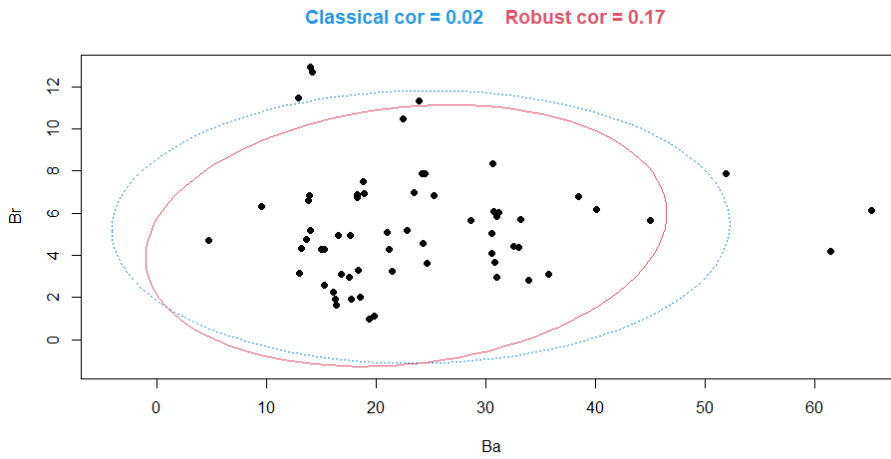
Removing 25 μm of Pb-enriched root surface:

Classical test	<p>Pearson's product-moment correlation</p> <p>data: Od533M_AC_wRS\$Sn and Od533M_AC_wRS\$Pb $t = -0.3783$, $df = 47$, p-value = 0.7069 alternative hypothesis: true correlation is not equal to 0 95 percent confidence interval: -0.3311624 0.2296582 sample estimates: cor -0.05509644</p>	<p>Spearman's rank correlation rho</p> <p>data: Od533M_AC_wRS\$Sn and Od533M_AC_wRS\$Pb $S = 20154$, p-value = 0.8468 alternative hypothesis: true rho is not equal to 0 sample estimates: rho -0.02826531</p>
	<p>MCD $(\alpha=0.05;$ $quant=0.8)$</p>	<p>\$cor.rob [1] 0.2403129</p>



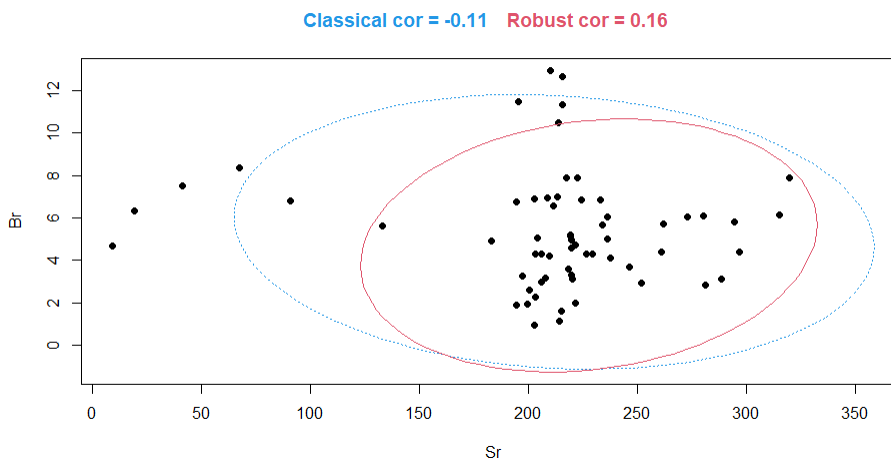
• **Br vs Ba**

Classical test	<p>Pearson's product-moment correlation</p> <p>data: Od533M_AC\$Ba and Od533M_AC\$Br $t = 0.18099$, $df = 60$, p-value = 0.857 alternative hypothesis: true correlation is not equal to 0 95 percent confidence interval: -0.2277374 0.2715435 sample estimates: cor 0.02335957</p>	<p>Spearman's rank correlation rho</p> <p>data: Od533M_AC\$Ba and Od533M_AC\$Br $S = 36878$, p-value = 0.5807 alternative hypothesis: true rho is not equal to 0 sample estimates: rho 0.07134043</p>
	<p>MCD $(\alpha=0.05;$ $quant=0.8)$</p>	<p>\$cor.rob [1] 0.1710217</p>



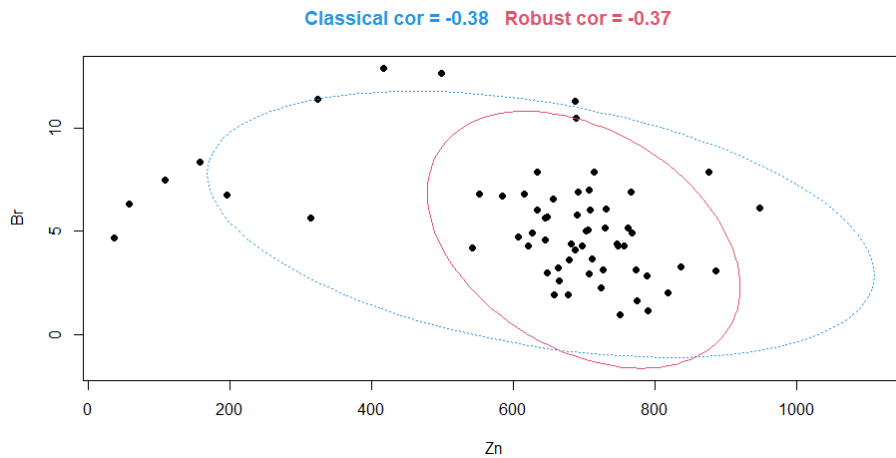
• Br vs Sr

Classical test	<p>Pearson's product-moment correlation</p> <p>data: Od533M_AC\$Sr and Od533M_AC\$Br $t = -0.85807$, $df = 60$, p-value = 0.3943 alternative hypothesis: true correlation is not equal to 0 95 percent confidence interval: -0.3502397 0.1436145 sample estimates: cor -0.1101032</p>	<p>Spearman's rank correlation rho</p> <p>data: Od533M_AC\$Sr and Od533M_AC\$Br $S = 41026$, p-value = 0.7979 alternative hypothesis: true rho is not equal to 0 sample estimates: rho -0.03311425</p>
	<p>MCD ($\alpha=0.05$; quant=0.8)</p> <p>\$cor.rob [1] 0.1626547</p>	



• **Br vs Zn**

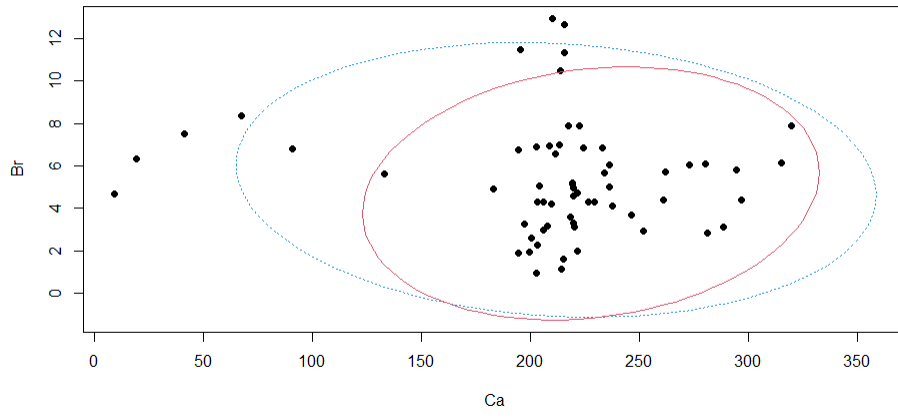
Classical test	<p>Pearson's product-moment correlation</p> <p>data: Od533M_AC\$Zn and Od533M_AC\$Br $t = -3.1715$, $df = 60$, p-value = 0.00239 alternative hypothesis: true correlation is not equal to 0 95 percent confidence interval: -0.5743247 -0.1426418 sample estimates: cor -0.3789104</p>	<p>Spearman's rank correlation rho</p> <p>data: Od533M_AC\$Zn and Od533M_AC\$Br $S = 55904$, p-value = 0.001099 alternative hypothesis: true rho is not equal to 0 sample estimates: rho -0.4077711</p>
	<p>MCD ($\alpha=0.05$; quant=0.8)</p>	<p>\$cor.rob [1] -0.3694156</p>



• **Br vs Ca**

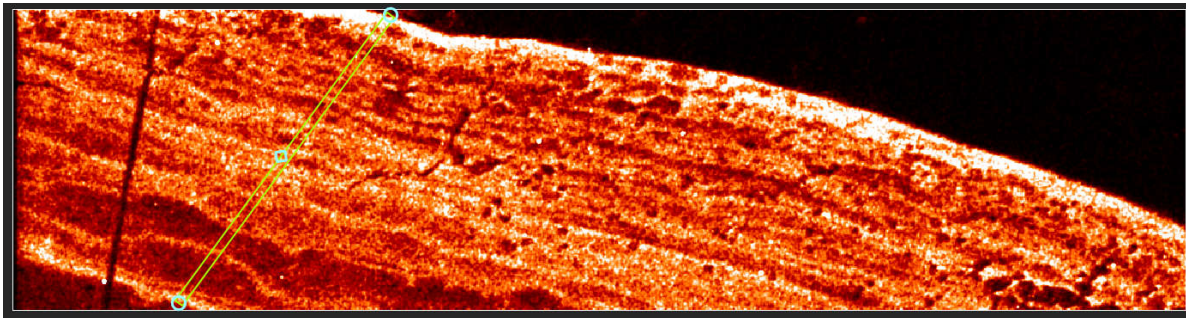
Classical test	<p>Pearson's product-moment correlation</p> <p>data: Od533M_AC\$Ca and Od533M_AC\$Br $t = -1.1183$, $df = 60$, p-value = 0.2679 alternative hypothesis: true correlation is not equal to 0 95 percent confidence interval: -0.3791260 0.1108354 sample estimates: cor -0.1428884</p>	<p>Spearman's rank correlation rho</p> <p>data: Od533M_AC\$Ca and Od533M_AC\$Br $S = 44066$, p-value = 0.3952 alternative hypothesis: true rho is not equal to 0 sample estimates: rho -0.1096673</p>
	<p>MCD ($\alpha=0.05$; quant=0.8)</p>	<p>\$cor.rob [1] 0.1626547</p>

Classical cor = -0.11 Robust cor = 0.16



Odense 533M1 – Cellular Cementum (total thickness=694 μm)

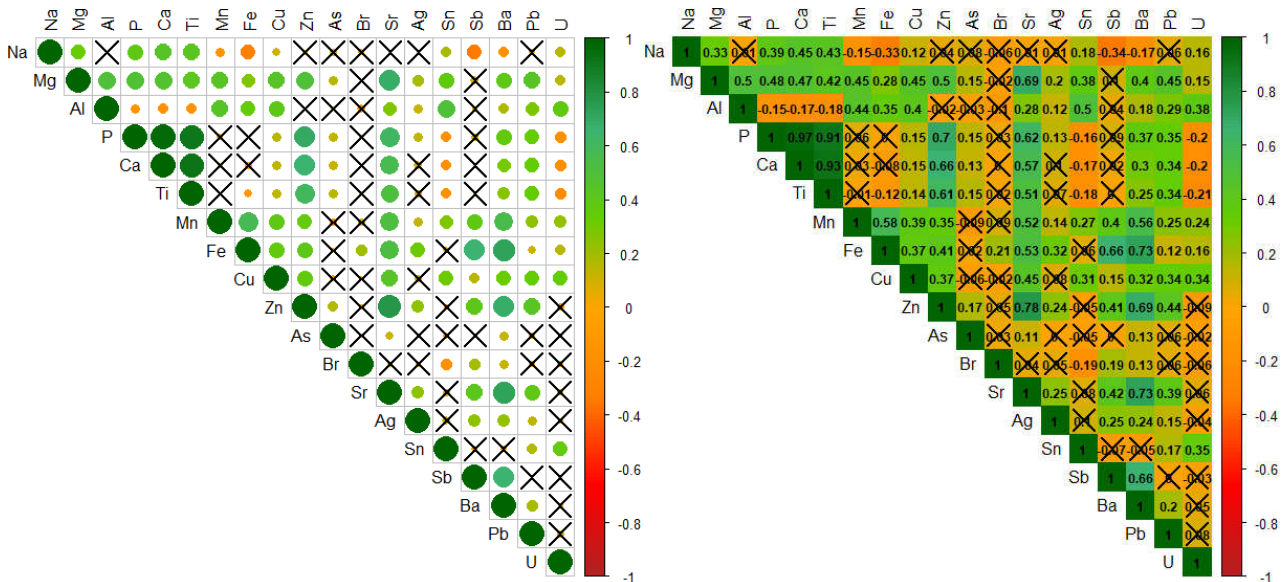
Correlations between pairs of elements



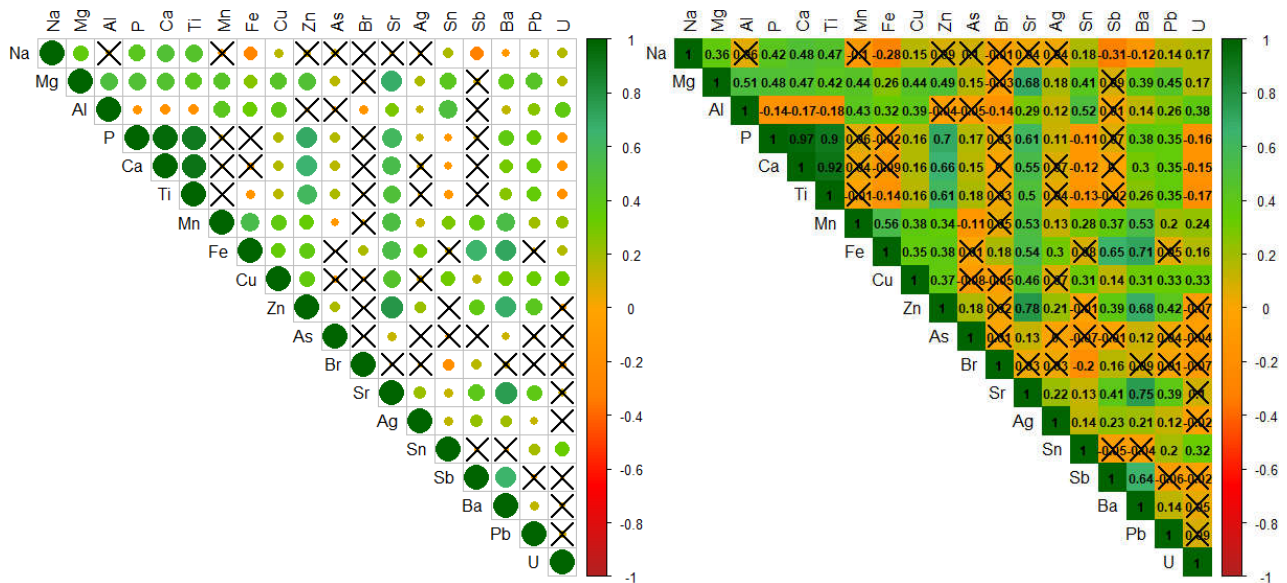
1x
200.0 μm

Zn maps (green path indicates where the measurements are taken)

Summary : whole cementum thickness, Spearman correlations.



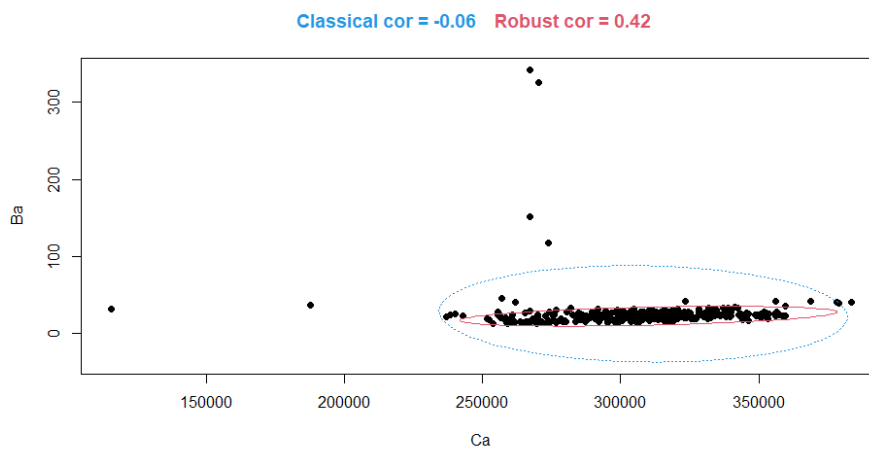
Summary : removing the first 15 μm of root surface, Spearman correlations.



wRS: without Root surface [Pb = ~15 μm ; Fe, Mn, Al not included in the path]

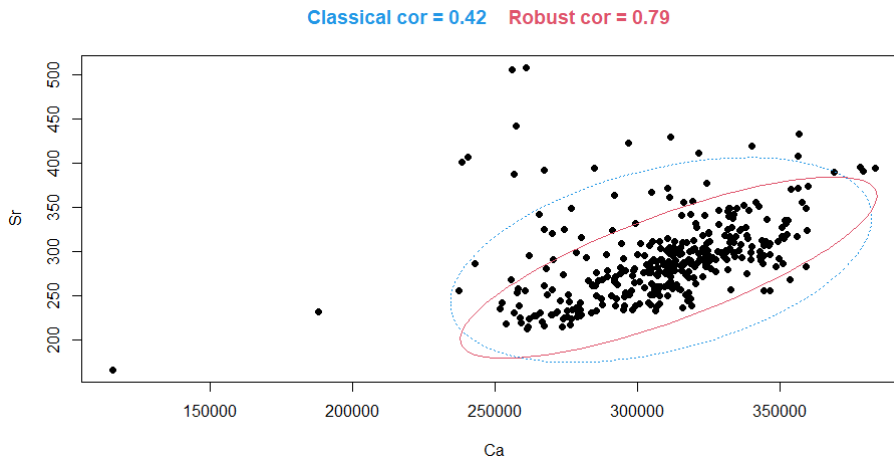
• **Ca vs Ba**

Classical test	<p>Pearson's product-moment correlation</p> <p>data: Od533M_CC\$Ca and Od533M_CC\$Ba $t = -1.192$, $df = 346$, p-value = 0.2341 alternative hypothesis: true correlation is not equal to 0 95 percent confidence interval: -0.16795239 0.04145918 sample estimates: cor -0.06395056</p>	<p>Spearman's rank correlation rho</p> <p>data: Od533M_CC\$Ca and Od533M_CC\$Ba $S = 4937240$, p-value = 1.881e-08 alternative hypothesis: true rho is not equal to 0 sample estimates: rho 0.2970874</p>
	<p>MCD $(\alpha=0.05;$ $quant=0.8)$</p>	<p>\$cor.rob [1] 0.4222214</p>



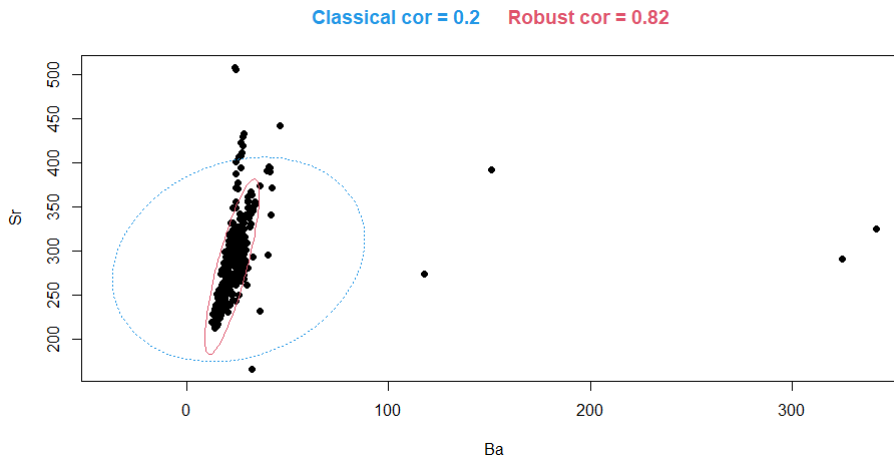
• **Ca vs Sr**

Classical test	<p>Pearson's product-moment correlation</p> <p>data: Od533M_CC\$Ca and Od533M_CC\$Sr $t = 8.5503$, $df = 346$, p-value = 4.012e-16 alternative hypothesis: true correlation is not equal to 0 95 percent confidence interval: 0.3268786 0.5007984 sample estimates: cor 0.4176568</p>	<p>Spearman's rank correlation rho</p> <p>data: Od533M_CC\$Ca and Od533M_CC\$Sr $S = 3051902$, p-value < 2.2e-16 alternative hypothesis: true rho is not equal to 0 sample estimates: rho 0.5655021</p>
	<p>MCD $(\alpha=0.05;$ $quant=0.8)$</p>	<p>\$cor.rob [1] 0.7877556</p>



• Ba vs Sr

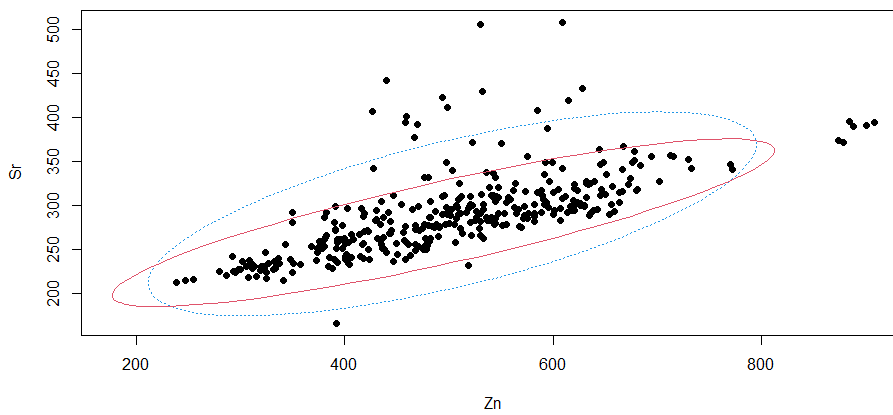
Classical test	<p>Pearson's product-moment correlation</p> <p>data: Od533M_CC\$Ba and Od533M_CC\$Sr $t = 3.768$, $df = 346$, p-value = 0.0001934 alternative hypothesis: true correlation is not equal to 0 95 percent confidence interval: 0.09539602 0.29745827 sample estimates: cor 0.1985359</p>	<p>Spearman's rank correlation rho</p> <p>data: Od533M_CC\$Ba and Od533M_CC\$Sr $S = 1899564$, p-value < 2.2e-16 alternative hypothesis: true rho is not equal to 0 sample estimates: rho 0.7295599</p>
	<p>MCD $(\alpha=0.05;$ $quant=0.8)$</p>	<p>\$cor.rob [1] 0.8230075</p>



• Zn vs Sr

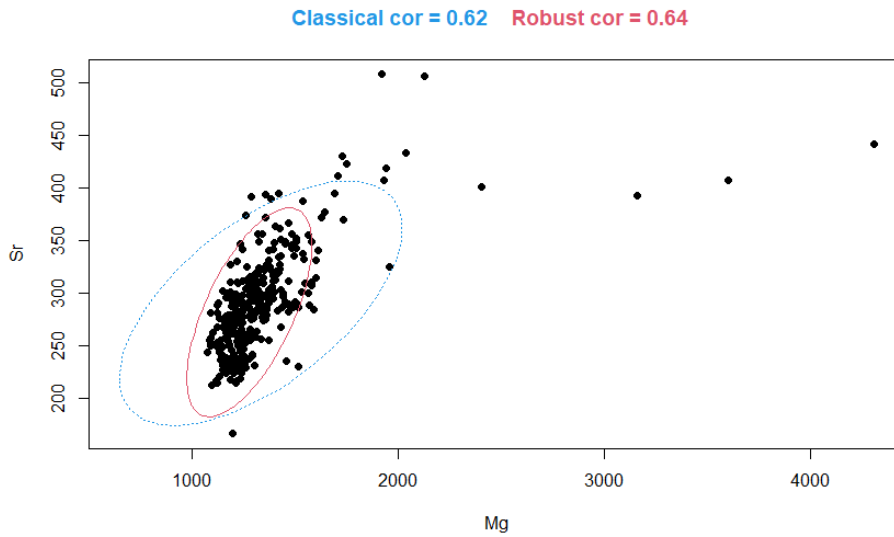
Classical test	<p>Pearson's product-moment correlation</p> <p>data: Od533M_CC\$Zn and Od533M_CC\$Sr $t = 17.291$, $df = 346$, p-value < 2.2e-16 alternative hypothesis: true correlation is not equal to 0 95 percent confidence interval: 0.6201049 0.7334794 sample estimates: cor 0.6808497</p>	<p>Spearman's rank correlation rho</p> <p>data: Od533M_CC\$Zn and Od533M_CC\$Sr $S = 1538210$, p-value < 2.2e-16 alternative hypothesis: true rho is not equal to 0 sample estimates: rho 0.7810057</p>
	<p>MCD $(\alpha=0.05;$ $quant=0.8)$</p>	<p>\$cor.rob [1] 0.8659534</p>

Classical cor = 0.68 Robust cor = 0.87



• Mg vs Sr

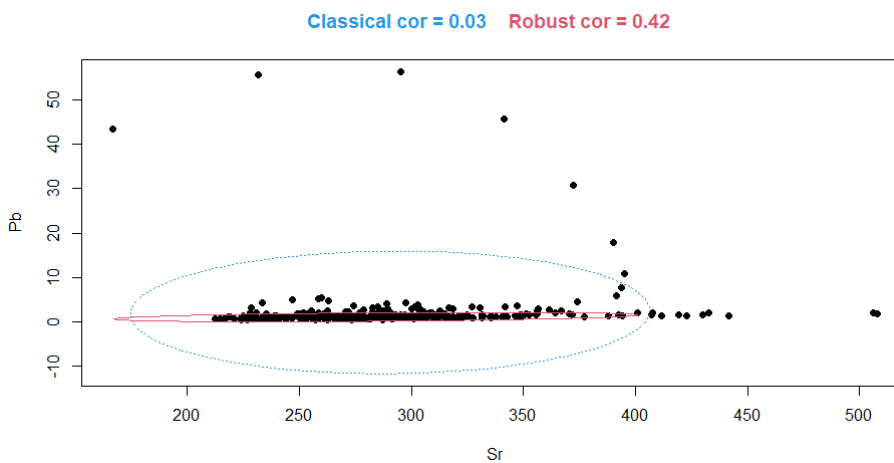
Classical test	<p>Pearson's product-moment correlation</p> <p>data: Od533M_CC\$Mg and Od533M_CC\$Sr $t = 14.517$, $df = 346$, p-value < 2.2e-16 alternative hypothesis: true correlation is not equal to 0 95 percent confidence interval: 0.5453866 0.6766088 sample estimates: cor 0.6152415</p>	<p>Spearman's rank correlation rho</p> <p>data: Od533M_CC\$Mg and Od533M_CC\$Sr $S = 2212532$, p-value < 2.2e-16 alternative hypothesis: true rho is not equal to 0 sample estimates: rho 0.6850028</p>
	<p>MCD $(\alpha=0.05;$ $quant=0.8)$</p>	<p>\$cor.rob [1] 0.6402011</p>



• **Pb vs Sr**

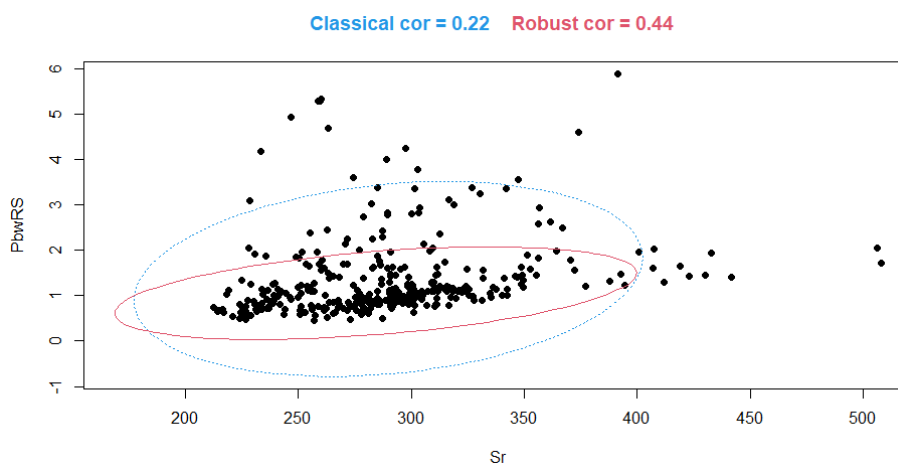
Whole cementum thickness:

Classical test	<p>Pearson's product-moment correlation</p> <p>data: Od533M_CC\$Sr and Od533M_CC\$Pb $t = 0.55828$, $df = 346$, p-value = 0.577 alternative hypothesis: true correlation is not equal to 0 95 percent confidence interval: -0.07536916 0.13470571 sample estimates: cor 0.02999955</p>	<p>Spearman's rank correlation rho</p> <p>data: Od533M_CC\$Sr and Od533M_CC\$Pb $S = 4282912$, p-value = 4.798e-14 alternative hypothesis: true rho is not equal to 0 sample estimates: rho 0.3902438</p>
	<p>MCD $(\alpha=0.05;$ $quant=0.8)$</p>	<p>$\\$cor.rob$ [1] 0.4150683</p>



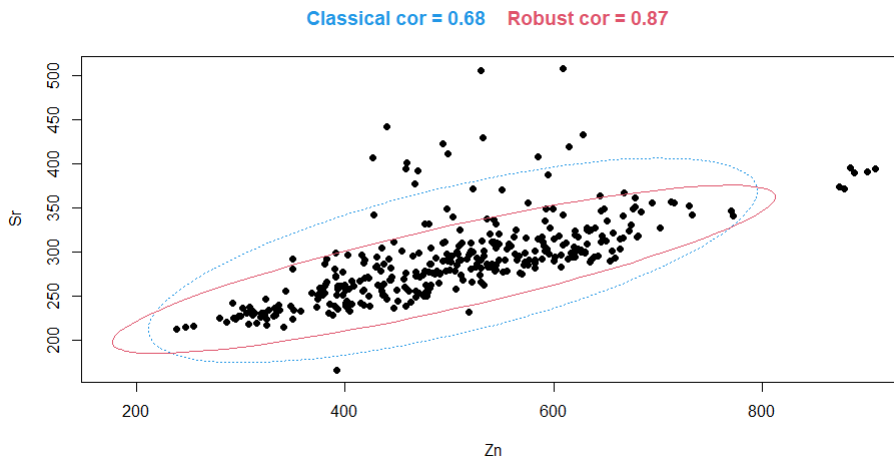
Removing 15 μm of Pb-enriched root surface:

Classical test	<p>Pearson's product-moment correlation</p> <p>data: Od533M_CC_wRS\$Sr and Od533M_CC_wRS\$Pb $t = 4.1906$, $df = 338$, p-value = $3.556e-05$ alternative hypothesis: true correlation is not equal to 0 95 percent confidence interval: 0.1186810 0.3210121 sample estimates: cor 0.2222379</p>	<p>Spearman's rank correlation rho</p> <p>data: Od533M_CC_wRS\$Zn and Od533M_CC_wRS\$Pb $S = 3812334$, p-value < $2.2e-16$ alternative hypothesis: true rho is not equal to 0 sample estimates: rho 0.4180185</p>
	<p>MCD $(\alpha=0.05;$ $quant=0.8)$</p>	<p>\$cor.rob [1] 0.435669</p>



• **Sr vs Zn**

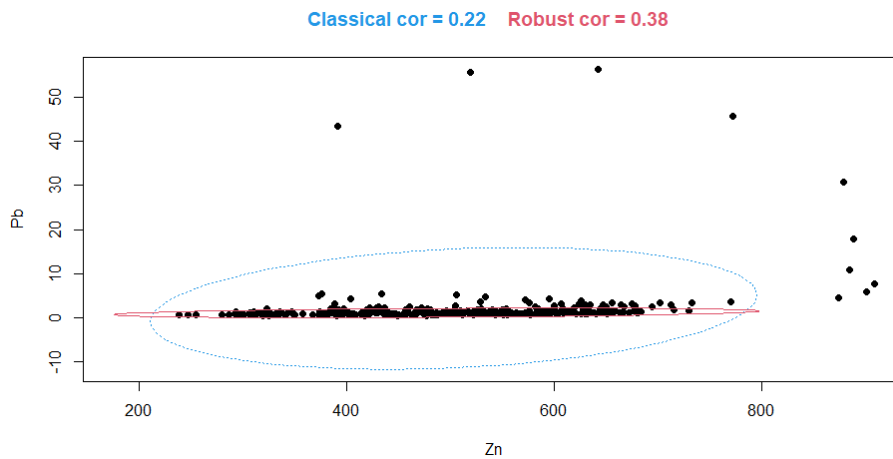
Classical test	<p>Pearson's product-moment correlation</p> <p>data: Od533M_CC\$Zn and Od533M_CC\$Sr $t = 17.291$, $df = 346$, p-value < $2.2e-16$ alternative hypothesis: true correlation is not equal to 0 95 percent confidence interval: 0.6201049 0.7334794 sample estimates: cor 0.6808497</p>	<p>Spearman's rank correlation rho</p> <p>data: Od533M_CC\$Zn and Od533M_CC\$Sr $S = 1538210$, p-value < $2.2e-16$ alternative hypothesis: true rho is not equal to 0 sample estimates: rho 0.7810057</p>
	<p>MCD $(\alpha=0.05;$ $quant=0.8)$</p>	<p>\$cor.rob [1] 0.8659534</p>



• **Pb vs Zn**

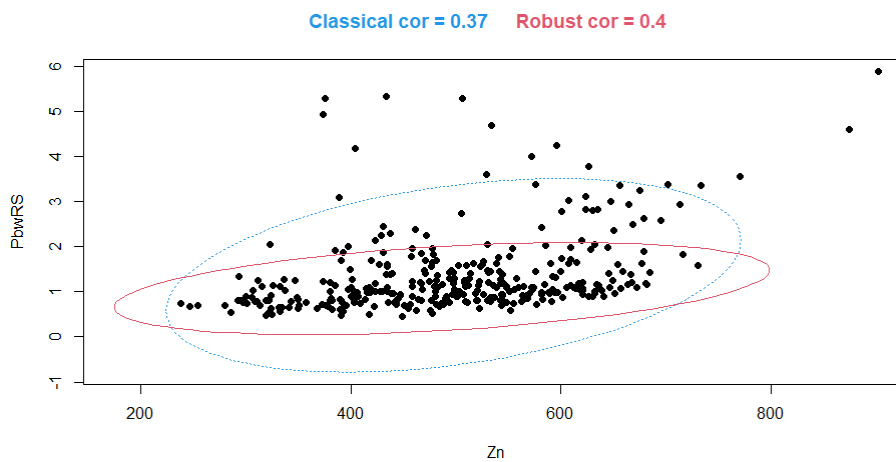
Whole cementum thickness:

Classical test	<p>Pearson's product-moment correlation</p> <p>data: Od533M_CC\$Zn and Od533M_CC\$Pb $t = 4.2036$, $df = 346$, p-value = 3.348e-05 alternative hypothesis: true correlation is not equal to 0 95 percent confidence interval: 0.1180325 0.3181857 sample estimates: cor 0.2204283</p>	<p>Spearman's rank correlation rho</p> <p>data: Od533M_CC\$Zn and Od533M_CC\$Pb $S = 3949120$, p-value < 2.2e-16 alternative hypothesis: true rho is not equal to 0 sample estimates: rho 0.4377656</p>
	<p>MCD $(\alpha=0.05;$ $quant=0.8)$</p>	<p>$\\$cor.rob$ [1] 0.3801596</p>



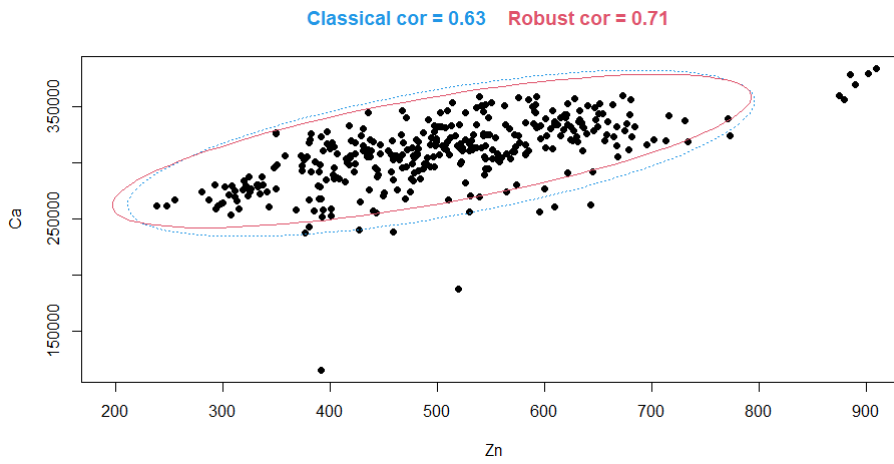
Removing 15 μm of Pb-enriched root surface:

<p>Classical test</p>	<p>Pearson's product-moment correlation</p> <p>data: Od533M_CC_wRS\$Zn and Od533M_CC_wRS\$Pb $t = 7.2751$, $df = 338$, p-value = $2.435e-12$ alternative hypothesis: true correlation is not equal to 0 95 percent confidence interval: 0.2722422 0.4564486 sample estimates: cor 0.3679499</p>	<p>Spearman's rank correlation rho</p> <p>data: Od533M_CC_wRS\$Zn and Od533M_CC_wRS\$Pb $S = 3812334$, p-value < $2.2e-16$ alternative hypothesis: true rho is not equal to 0 sample estimates: rho 0.4180185</p>
<p>MCD $(\alpha=0.05;$ $quant=0.8)$</p>	<p>\$cor.rob [1] 0.4035045</p>	



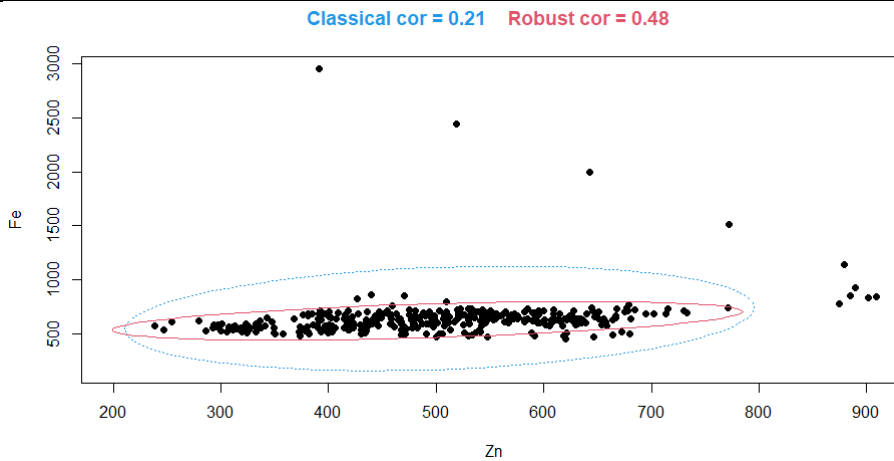
• Zn vs Ca

<p>Classical test</p>	<p>Pearson's product-moment correlation</p> <p>data: Od533M_CC\$Zn and Od533M_CC\$Ca $t = 15.055$, $df = 346$, p-value < $2.2e-16$ alternative hypothesis: true correlation is not equal to 0 95 percent confidence interval: 0.5611166 0.6887129 sample estimates: cor 0.6291345</p>	<p>Spearman's rank correlation rho</p> <p>data: Od533M_CC\$Zn and Od533M_CC\$Ca $S = 2381548$, p-value < $2.2e-16$ alternative hypothesis: true rho is not equal to 0 sample estimates: rho 0.6609401</p>
<p>MCD $(\alpha=0.05;$ $quant=0.8)$</p>	<p>\$cor.rob [1] 0.710546</p>	



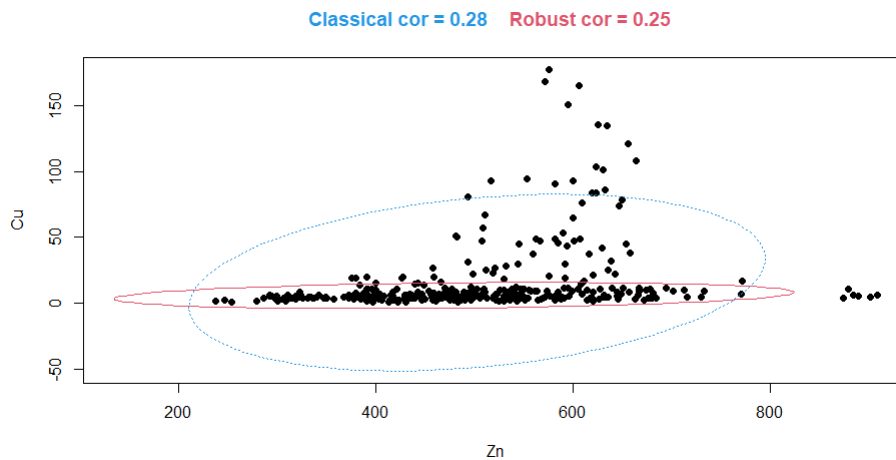
• Zn vs Fe

Classical test	<p>Pearson's product-moment correlation</p> <p>data: Od533M_CC\$Zn and Od533M_CC\$Fe $t = 4.0683$, $df = 346$, p-value = 5.869e-05 alternative hypothesis: true correlation is not equal to 0 95 percent confidence interval: 0.1110267 0.3117911 sample estimates: cor 0.2136638</p>	<p>Spearman's rank correlation rho</p> <p>data: Od533M_CC\$Zn and Od533M_CC\$Fe $S = 4179194$, p-value = 1.234e-15 alternative hypothesis: true rho is not equal to 0 sample estimates: rho 0.40501</p>
	<p>MCD $(\alpha=0.05;$ $quant=0.8)$</p>	<p>\$cor.rob [1] 0.4823483</p>



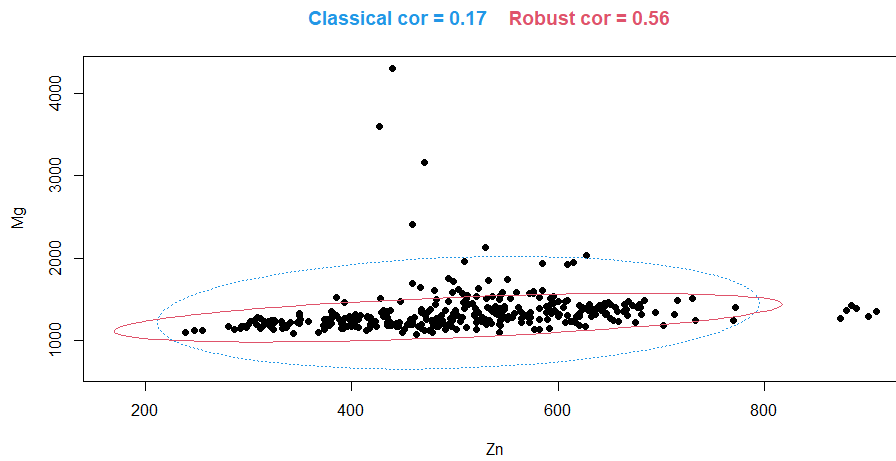
• Zn vs Cu

Classical test	<p>Pearson's product-moment correlation</p> <p>data: Od533M_CC\$Zn and Od533M_CC\$Cu $t = 5.3372$, $df = 346$, p-value = 1.712e-07 alternative hypothesis: true correlation is not equal to 0 95 percent confidence interval: 0.1757652 0.3701970 sample estimates: cor 0.2757999</p>	<p>Spearman's rank correlation rho</p> <p>data: Od533M_CC\$Zn and Od533M_CC\$Cu $S = 4437736$, p-value = 1.792e-12 alternative hypothesis: true rho is not equal to 0 sample estimates: rho 0.3682015</p>
MCD ($\alpha=0.05$; quant=0.8)	<p>\$cor.rob [1] 0.2541785</p>	



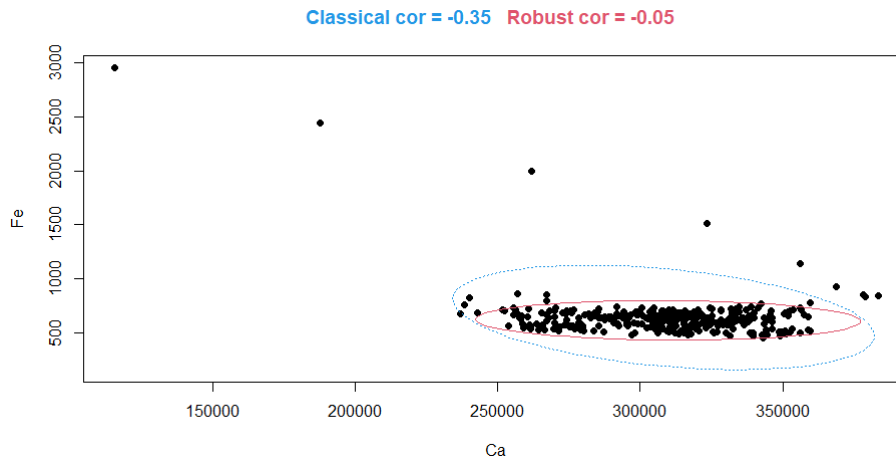
• Zn vs Mg

Classical test	<p>Pearson's product-moment correlation</p> <p>data: Od533M_CC\$Zn and Od533M_CC\$Mg $t = 3.2595$, $df = 346$, p-value = 0.001227 alternative hypothesis: true correlation is not equal to 0 95 percent confidence interval: 0.06871983 0.27278489 sample estimates: cor 0.1726038</p>	<p>Spearman's rank correlation rho</p> <p>data: Od533M_CC\$Zn and Od533M_CC\$Mg $S = 3506054$, p-value < 2.2e-16 alternative hypothesis: true rho is not equal to 0 sample estimates: rho 0.5008447</p>
MCD ($\alpha=0.05$; quant=0.8)	<p>\$cor.rob [1] 0.5550434</p>	



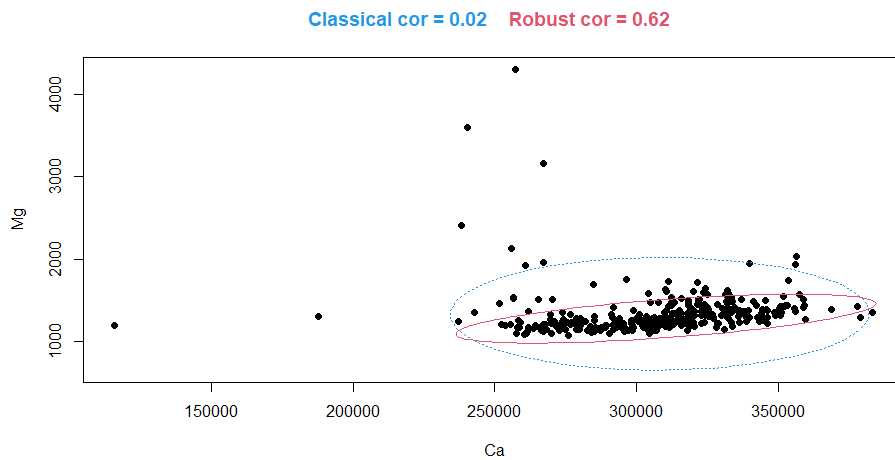
• Ca vs Fe

Classical test	<p>Pearson's product-moment correlation</p> <p>data: Od533M_CC\$Ca and Od533M_CC\$Fe $t = -6.9981$, $df = 346$, p-value = 1.352e-11 alternative hypothesis: true correlation is not equal to 0 95 percent confidence interval: -0.4409332 -0.2564893 sample estimates: cor -0.3521252</p>	<p>Spearman's rank correlation rho</p> <p>data: Od533M_CC\$Ca and Od533M_CC\$Fe $S = 7553372$, p-value = 0.1606 alternative hypothesis: true rho is not equal to 0 sample estimates: rho -0.07537015</p>
	<p>MCD $(\alpha=0.05;$ $quant=0.8)$</p>	<p>$\\$cor.rob$ $[1] -0.04928535$</p>



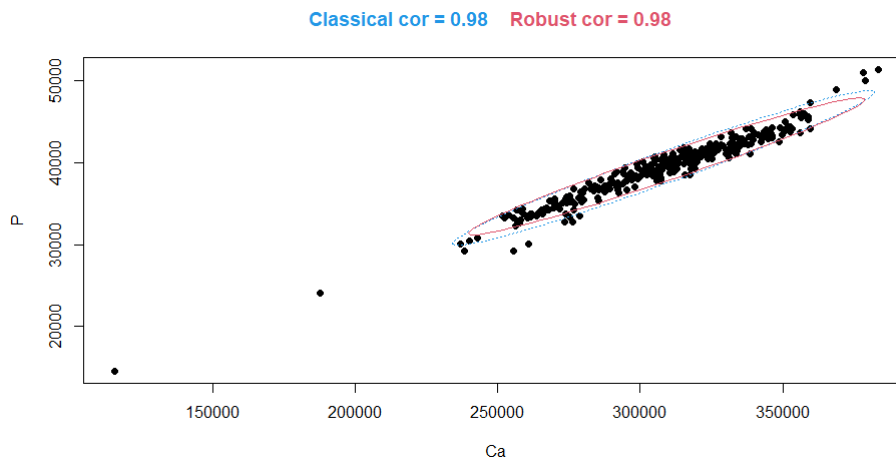
• Ca vs Mg

Classical test	<p>Pearson's product-moment correlation</p> <p>data: Od533M_CC\$Ca and Od533M_CC\$Mg $t = 0.28031$, $df = 346$, p-value = 0.7794 alternative hypothesis: true correlation is not equal to 0 95 percent confidence interval: -0.09020595 0.12000885 sample estimates: cor 0.01506795</p>	<p>Spearman's rank correlation rho</p> <p>data: Od533M_CC\$Ca and Od533M_CC\$Mg $S = 3704688$, p-value < 2.2e-16 alternative hypothesis: true rho is not equal to 0 sample estimates: rho 0.4725652</p>
	<p>MCD $(\alpha=0.05;$ $quant=0.8)$</p>	<p>\$cor.rob [1] 0.6241344</p>



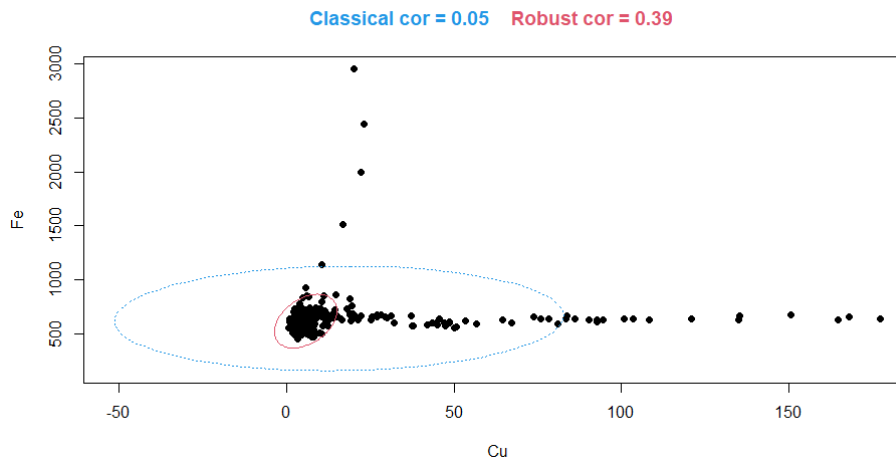
• Ca vs P

Classical test	<p>Pearson's product-moment correlation</p> <p>data: Od533M_CC\$Ca and Od533M_CC\$P $t = 83.901$, $df = 346$, p-value < 2.2e-16 alternative hypothesis: true correlation is not equal to 0 95 percent confidence interval: 0.9708054 0.9807610 sample estimates: cor 0.9762941</p>	<p>Spearman's rank correlation rho</p> <p>data: Od533M_CC\$Ca and Od533M_CC\$P $S = 200644$, p-value < 2.2e-16 alternative hypothesis: true rho is not equal to 0 sample estimates: rho 0.9714344</p>
	<p>MCD $(\alpha=0.05;$ $quant=0.8)$</p>	<p>\$cor.rob [1] 0.9763796</p>



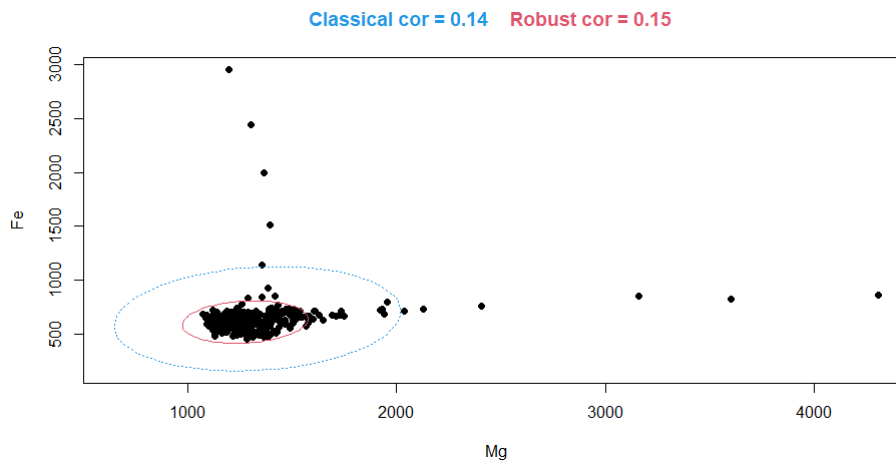
• **Cu vs Fe**

Classical test	<p>Pearson's product-moment correlation</p> <p>data: Od533M_CC\$Cu and Od533M_CC\$Fe $t = 0.9357$, $df = 346$, p-value = 0.3501 alternative hypothesis: true correlation is not equal to 0 95 percent confidence interval: -0.05518252 0.15455463 sample estimates: cor 0.05023995</p>	<p>Spearman's rank correlation rho</p> <p>data: Od533M_CC\$Cu and Od533M_CC\$Fe $S = 4457044$, p-value = 2.702e-12 alternative hypothesis: true rho is not equal to 0 sample estimates: rho 0.3654527</p>
	<p>MCD $(\alpha=0.05;$ $quant=0.8)$</p>	<p>\$cor.rob $[1] 0.3913524$</p>



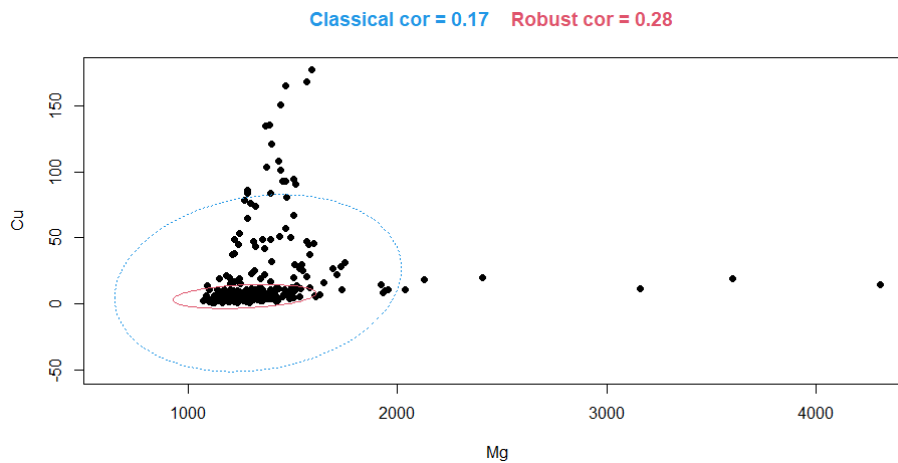
• **Mg vs Fe**

Classical test	<p>Pearson's product-moment correlation</p> <p>data: Od533M_CC\$Mg and Od533M_CC\$Fe $t = 2.6355$, $df = 346$, p-value = 0.00878 alternative hypothesis: true correlation is not equal to 0 95 percent confidence interval: 0.03567788 0.24184694 sample estimates: cor 0.1402827</p>	<p>Spearman's rank correlation rho</p> <p>data: Od533M_CC\$Mg and Od533M_CC\$Fe $S = 5072070$, p-value = 1.543e-07 alternative hypothesis: true rho is not equal to 0 sample estimates: rho 0.2778917</p>
	<p>MCD $(\alpha=0.05;$ $quant=0.8)$</p>	<p>\$cor.rob [1] 0.1465132</p>



• **Cu vs Mg**

Classical test	<p>Pearson's product-moment correlation</p> <p>data: Od533M_CC\$Mg and Od533M_CC\$Cu $t = 3.1556$, $df = 346$, p-value = 0.001742 alternative hypothesis: true correlation is not equal to 0 95 percent confidence interval: 0.06323774 0.26768091 sample estimates: cor 0.1672568</p>	<p>Spearman's rank correlation rho</p> <p>data: Od533M_CC\$Mg and Od533M_CC\$Cu $S = 3894676$, p-value < 2.2e-16 alternative hypothesis: true rho is not equal to 0 sample estimates: rho 0.4455167</p>
	<p>MCD $(\alpha=0.05;$ $quant=0.8)$</p>	<p>\$cor.rob [1] 0.2762911</p>

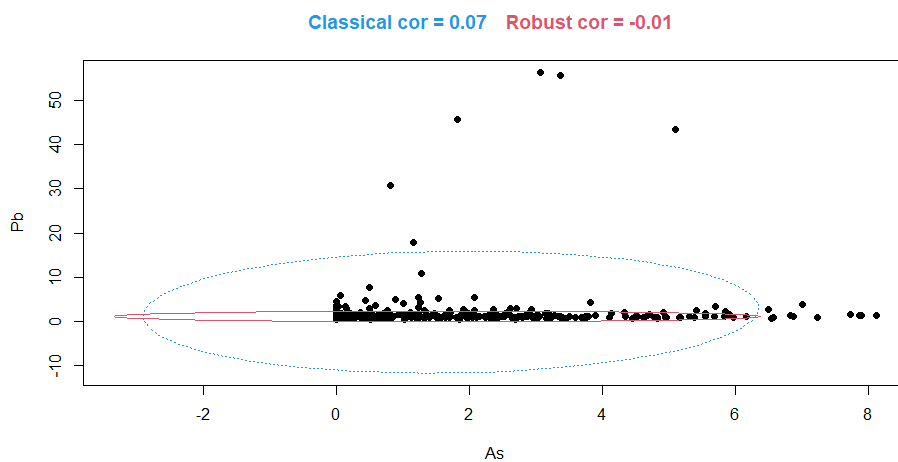


- As vs Hg, Pb vs Hg (no Hg at all). => Not Applicable.

- Pb vs As

Whole cementum thickness:

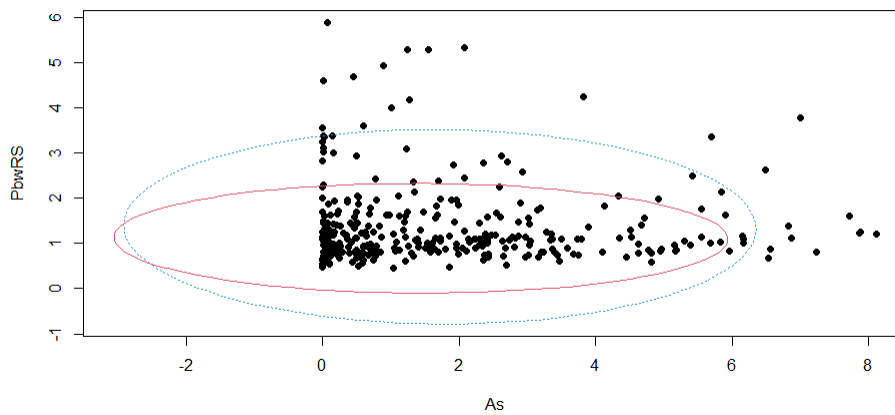
Classical test	<p>Pearson's product-moment correlation</p> <p>data: Od533M_CC\$As and Od533M_CC\$Pb $t = 1.2663$, $df = 346$, p-value = 0.2063 alternative hypothesis: true correlation is not equal to 0 95 percent confidence interval: -0.03747891 0.17182381 sample estimates: cor 0.06791971</p>	<p>Spearman's rank correlation rho</p> <p>data: Od533M_CC\$As and Od533M_CC\$Pb $S = 6636242$, p-value = 0.3045 alternative hypothesis: true rho is not equal to 0 sample estimates: rho 0.05520125 <i>Impossible to calculate the exact p-value with ex-aequos</i></p>
	<p>MCD $(\alpha=0.05;$ $quant=0.8)$</p>	<p>$\\$cor.rob$ $[1] -0.01183972$</p>



Removing 15 μm of Pb-enriched root surface:

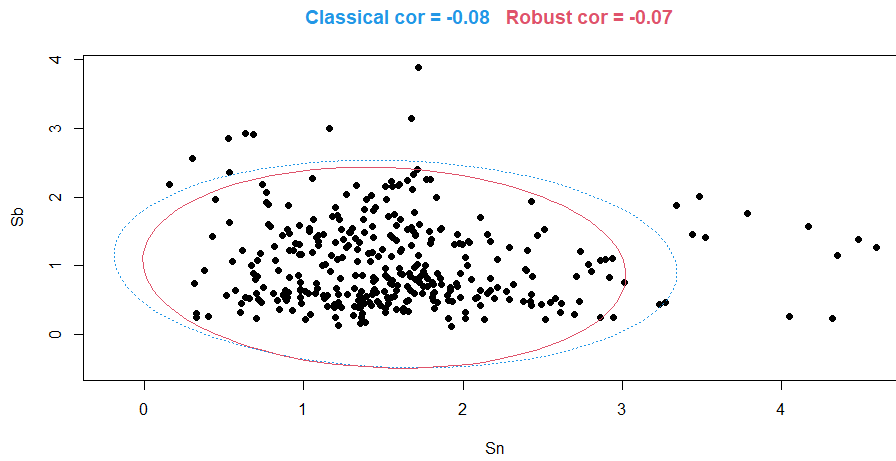
Classical test	<p>Pearson's product-moment correlation</p> <p>data: Od533M_CC_wRS\$As and Od533M_CC_wRS\$Pb $t = -0.33905$, $df = 338$, p-value = 0.7348 alternative hypothesis: true correlation is not equal to 0 95 percent confidence interval: -0.12455677 0.08809614 sample estimates: cor -0.01843885</p>	<p>Spearman's rank correlation rho</p> <p>data: Od533M_CC_wRS\$As and Od533M_CC_wRS\$Pb $S = 6300312$, p-value = 0.4825 alternative hypothesis: true rho is not equal to 0 sample estimates: rho 0.03820989 <i>Impossible to calculate the exact p-value with ex-aequos</i></p>
	<p>MCD $(\alpha=0.05;$ $\text{quant}=0.8)$</p>	<p>\$cor.rob [1] -0.01645062</p>

Classical cor = -0.02 Robust cor = -0.02



• **Sb vs Sn**

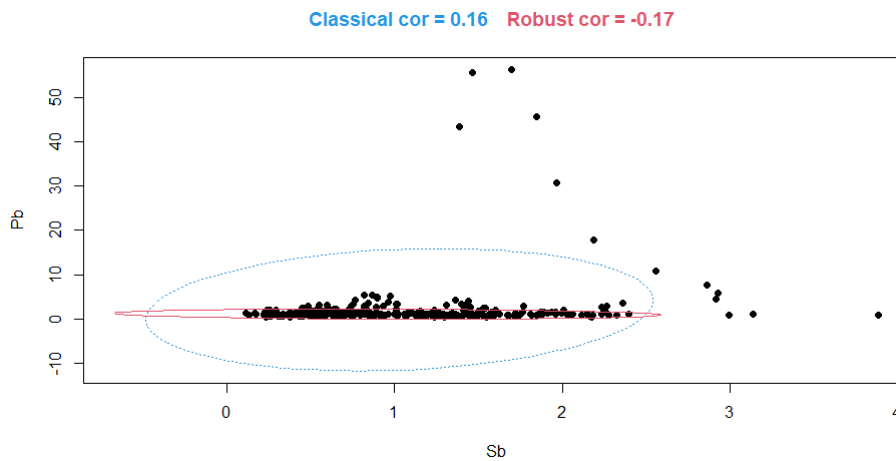
Classical test	<p>Pearson's product-moment correlation</p> <p>data: Od533M_CC\$Sn and Od533M_CC\$Sb $t = -1.5008$, $df = 346$, p-value = 0.1343 alternative hypothesis: true correlation is not equal to 0 95 percent confidence interval: -0.18399834 0.02491866 sample estimates: cor -0.08042303</p>	<p>Spearman's rank correlation rho</p> <p>data: Od533M_CC\$Sn and Od533M_CC\$Sb $S = 7514274$, p-value = 0.1938 alternative hypothesis: true rho is not equal to 0 sample estimates: rho -0.06980379</p>
	<p>MCD $(\alpha=0.05;$ $\text{quant}=0.8)$</p>	<p>\$cor.rob [1] -0.07359742</p>



• **Pb vs Sb**

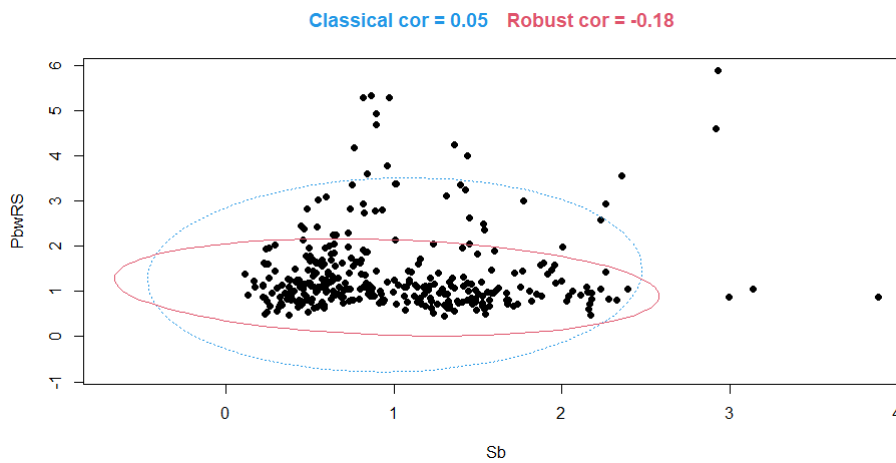
Whole cementum thickness:

Classical test	<p>Pearson's product-moment correlation</p> <p>data: Od533M_CC\$Sb and Od533M_CC\$Pb $t = 3.0237$, $df = 346$, p-value = 0.002684 alternative hypothesis: true correlation is not equal to 0 95 percent confidence interval: 0.05626567 0.26117312 sample estimates: cor 0.1604476</p>	<p>Spearman's rank correlation rho</p> <p>data: Od533M_CC\$Sb and Od533M_CC\$Pb $S = 7033012$, p-value = 0.9809 alternative hypothesis: true rho is not equal to 0 sample estimates: rho -0.001286736</p>
	<p>MCD $(\alpha=0.05;$ $quant=0.8)$</p>	<p>$\\$cor.rob$ [1] -0.1667674</p>



Removing 15 μm of Pb-enriched root surface:

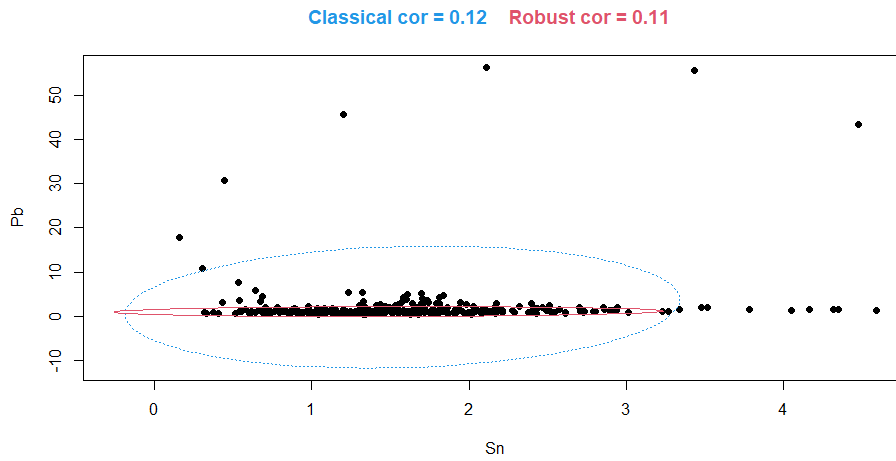
Classical test	<p>Pearson's product-moment correlation</p> <p>data: Od533M_CC_wRS\$Sb and Od533M_CC_wRS\$Pb $t = 0.99995$, $df = 338$, p-value = 0.3181 alternative hypothesis: true correlation is not equal to 0 95 percent confidence interval: -0.05235506 0.15974899 sample estimates: cor 0.05430957</p>	<p>Spearman's rank correlation rho</p> <p>data: Od533M_CC_wRS\$Sb and Od533M_CC_wRS\$Pb $S = 6929224$, p-value = 0.2878 alternative hypothesis: true rho is not equal to 0 sample estimates: rho -0.05779828</p>
	<p>MCD $(\alpha=0.05;$ $\text{quant}=0.8)$</p>	<p>\$cor.rob [1] -0.1805594</p>



• **Pb vs Sn**

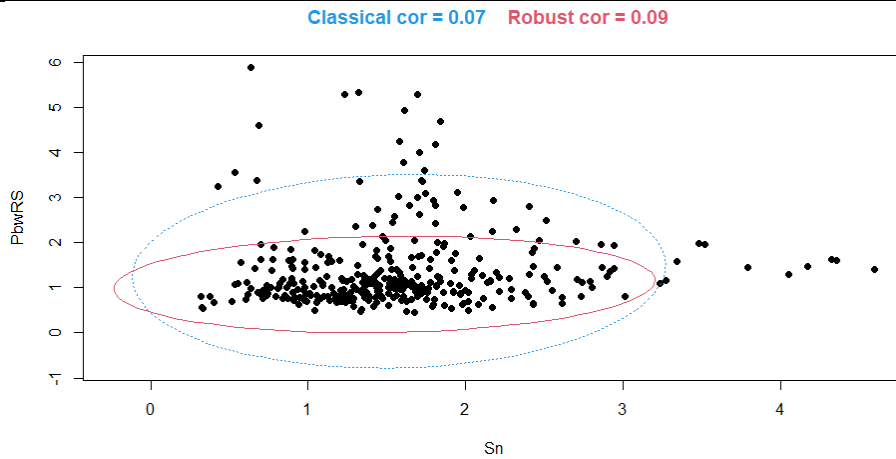
Whole cementum thickness:

Classical test	<p>Pearson's product-moment correlation</p> <p>data: Od533M_CC\$Sn and Od533M_CC\$Pb $t = 2.3224$, $df = 346$, p-value = 0.02079 alternative hypothesis: true correlation is not equal to 0 95 percent confidence interval: 0.01900917 0.22607892 sample estimates: cor 0.1238926</p>	<p>Spearman's rank correlation rho</p> <p>data: Od533M_CC\$Sn and Od533M_CC\$Pb $S = 5821180$, p-value = 0.001362 alternative hypothesis: true rho is not equal to 0 sample estimates: rho 0.1712412</p>
	<p>MCD $(\alpha=0.05;$ $\text{quant}=0.8)$</p>	<p>\$cor.rob [1] 0.1078794</p>



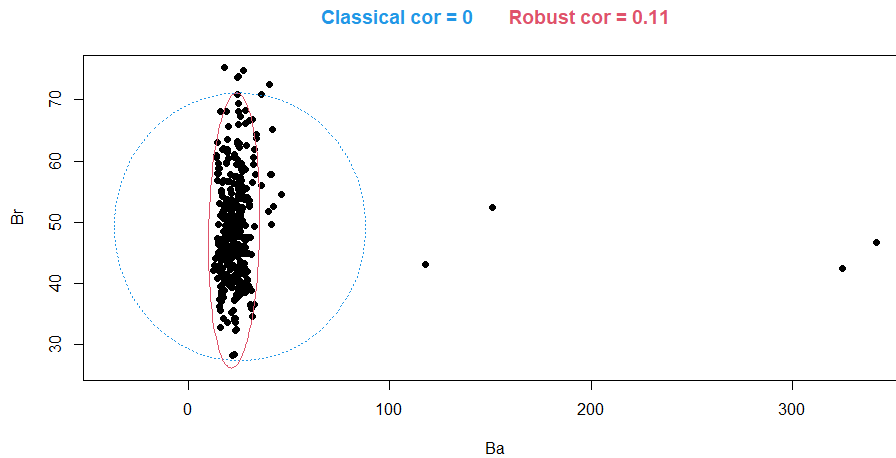
Removing 15 μm of Pb-enriched root surface:

Classical test	<p style="text-align: center; color: blue;">Pearson's product-moment correlation</p> <p style="text-align: center;">data: Od533M_CC_wRS\$Sn and Od533M_CC_wRS\$Pb $t = 1.2308$, $df = 338$, p-value = 0.2192 alternative hypothesis: true correlation is not equal to 0 95 percent confidence interval: -0.03984622 0.17193969 sample estimates: cor 0.0667991</p>	<p style="text-align: center;">Spearman's rank correlation rho</p> <p style="text-align: center;">data: Od533M_CC_wRS\$Sn and Od533M_CC_wRS\$Pb $S = 5262186$, p-value = 0.0002701 alternative hypothesis: true rho is not equal to 0 sample estimates: rho 0.1966876</p>
	<p style="text-align: center; color: red;">MCD $(\alpha=0.05;$ quant=0.8)</p>	<p style="text-align: center; color: red;">\$cor.rob [1] 0.08510237</p>



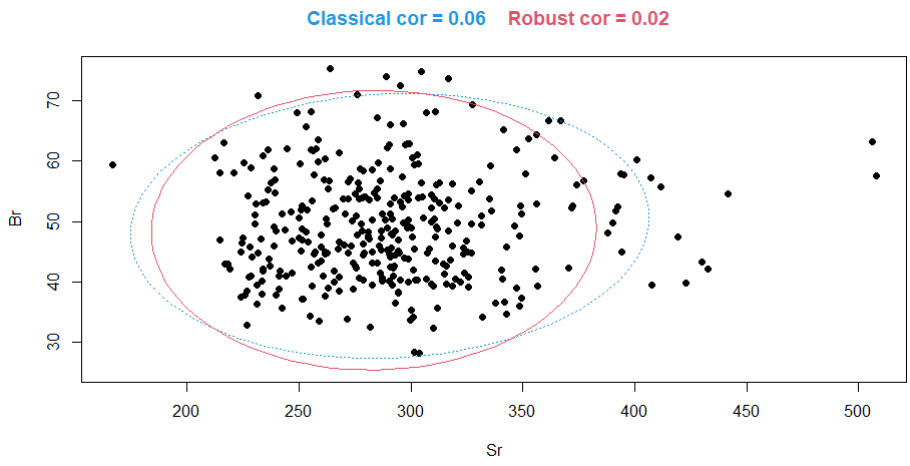
• **Br vs Ba**

Classical test	<p>Pearson's product-moment correlation</p> <p>data: Od533M_CC\$Ba and Od533M_CC\$Br $t = -0.030879$, $df = 346$, p-value = 0.9754 alternative hypothesis: true correlation is not equal to 0 95 percent confidence interval: -0.1067725 0.1034890 sample estimates: cor -0.001660083</p>	<p>Spearman's rank correlation rho</p> <p>data: Od533M_CC\$Ba and Od533M_CC\$Br $S = 6124820$, p-value = 0.01693 alternative hypothesis: true rho is not equal to 0 sample estimates: rho 0.1280121</p>
	<p>MCD $(\alpha=0.05;$ $quant=0.8)$</p>	<p>\$cor.rob [1] 0.107534</p>



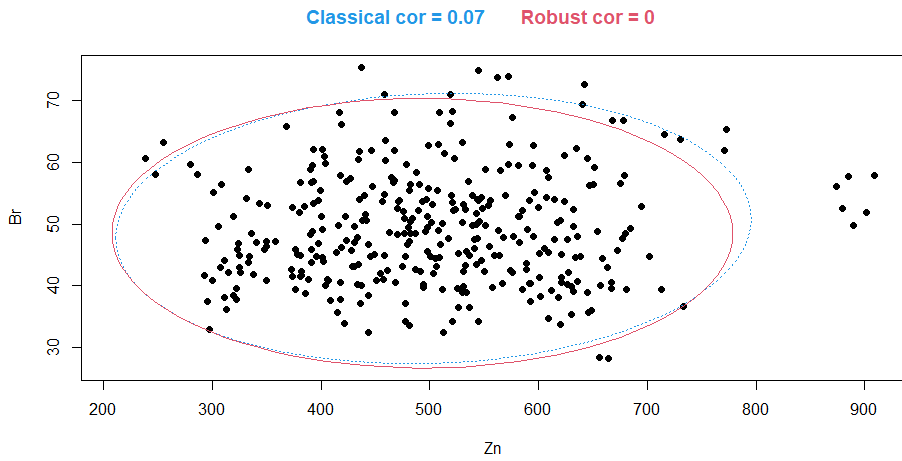
• **Br vs Sr**

Classical test	<p>Pearson's product-moment correlation</p> <p>data: Od533M_CC\$Sr and Od533M_CC\$Br $t = 1.1968$, $df = 346$, p-value = 0.2322 alternative hypothesis: true correlation is not equal to 0 95 percent confidence interval: -0.04120406 0.16820073 sample estimates: cor 0.06420507</p>	<p>Spearman's rank correlation rho</p> <p>data: Od533M_CC\$Sr and Od533M_CC\$Br $S = 6739054$, p-value = 0.4505 alternative hypothesis: true rho is not equal to 0 sample estimates: rho 0.04056393</p>
	<p>MCD $(\alpha=0.05;$ $quant=0.8)$</p>	<p>\$cor.rob [1] 0.01599081</p>



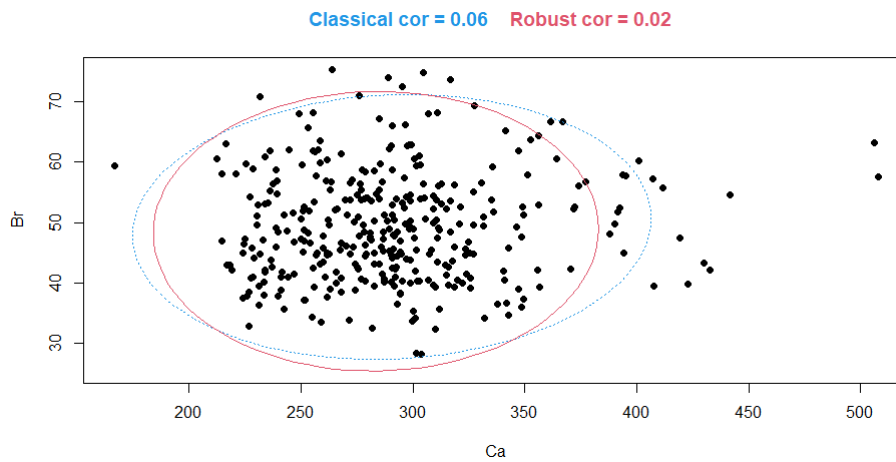
• Br vs Zn

Classical test	<p>Pearson's product-moment correlation</p> <p>data: Od533M_CC\$Zn and Od533M_CC\$Br $t = 1.2881$, $df = 346$, p-value = 0.1986 alternative hypothesis: true correlation is not equal to 0 95 percent confidence interval: -0.03631413 0.17295552 sample estimates: cor 0.06908061</p>	<p>Spearman's rank correlation rho</p> <p>data: Od533M_CC\$Zn and Od533M_CC\$Br $S = 6704876$, p-value = 0.398 alternative hypothesis: true rho is not equal to 0 sample estimates: rho 0.04542984</p>
	<p>MCD $(\alpha=0.05;$ $quant=0.8)$</p>	<p>\$cor.rob [1] -0.001427677</p>



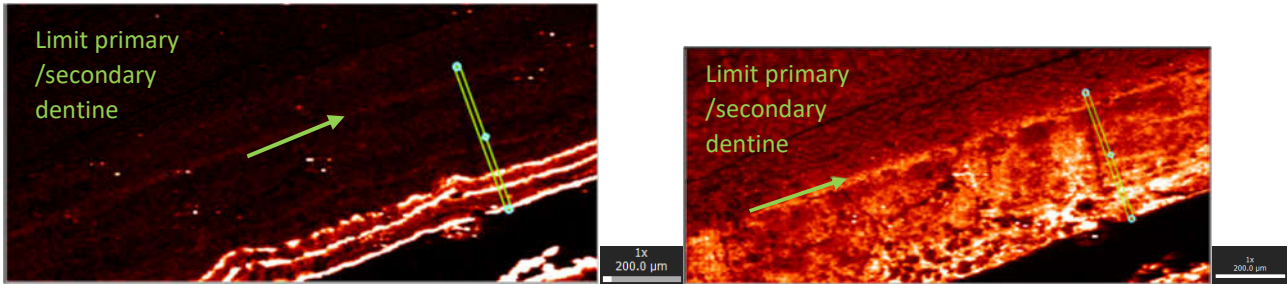
• Br vs Ca

Classical test	<p>Pearson's product-moment correlation</p> <p>data: Od533M_CC\$Ca and Od533M_CC\$Br $t = -0.45575$, $df = 346$, p-value = 0.6489 alternative hypothesis: true correlation is not equal to 0 95 percent confidence interval: -0.12929178 0.08084547 sample estimates: cor -0.02449371</p>	<p>Spearman's rank correlation rho</p> <p>data: Od533M_CC\$Ca and Od533M_CC\$Br $S = 7026418$, p-value = 0.9948 alternative hypothesis: true rho is not equal to 0 sample estimates: rho -0.0003479512</p>
	<p>MCD $(\alpha=0.05;$ $quant=0.8)$</p>	<p>\$cor.rob [1] 0.01599081</p>



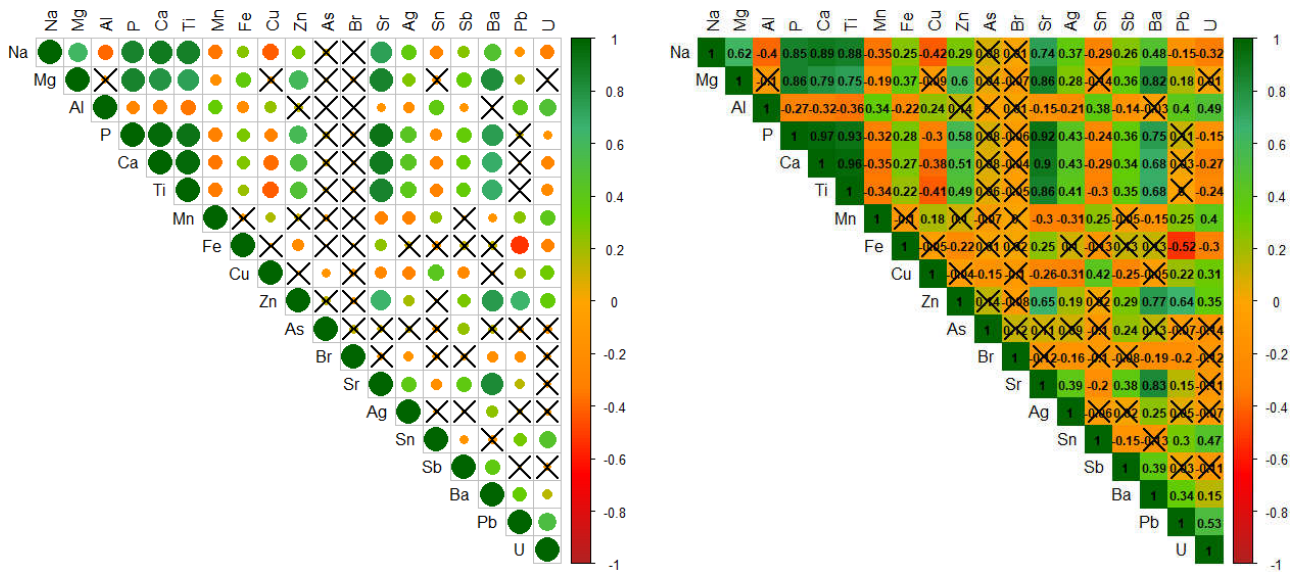
Odense 533M1 – Secondary Dentine (total thickness=396 μm)

Correlations between pairs of elements

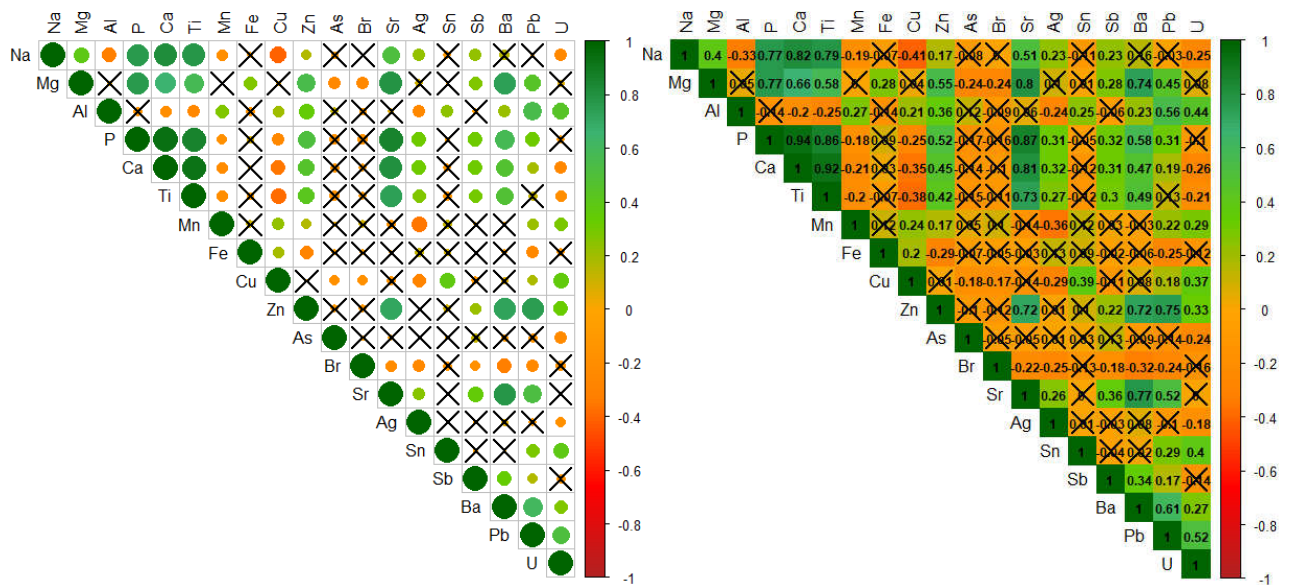


Pb (left) and Zn (right) maps (green path indicates where the measurements are taken)

Summary: whole secondary dentine thickness, Spearman correlations.



Summary: removing the first 110 μm of secondary dentine surface, Spearman correlations.

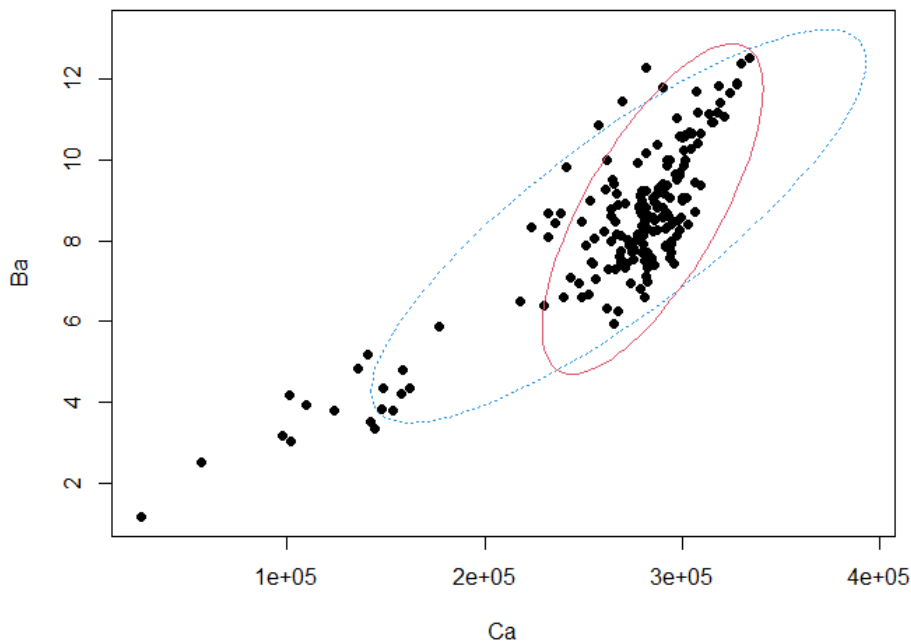


wSDS: without Secondary Dentine surface [Pb = ~109 μm containing 3 strong (biological) accentuated lines; no significant surface enrichment for Fe, Mn, Cu, Al]

• **Ca vs Ba**

Classical test	<p>Pearson's product-moment correlation</p> <p>data: Od533M_SD\$Ca and Od533M_SD\$Ba $t = 21.276$, $df = 188$, p-value < 2.2e-16 alternative hypothesis: true correlation is not equal to 0 95 percent confidence interval: 0.7931194 0.8778780 sample estimates: cor 0.8405697</p>	<p>Spearman's rank correlation rho</p> <p>data: Od533M_SD\$Ca and Od533M_SD\$Ba $S = 361716$, p-value < 2.2e-16 alternative hypothesis: true rho is not equal to 0 sample estimates: rho 0.6835754</p>
	<p>MCD $(\alpha=0.05;$ $quant=0.8)$</p>	<p>\$cor.rob [1] 0.7271962</p>

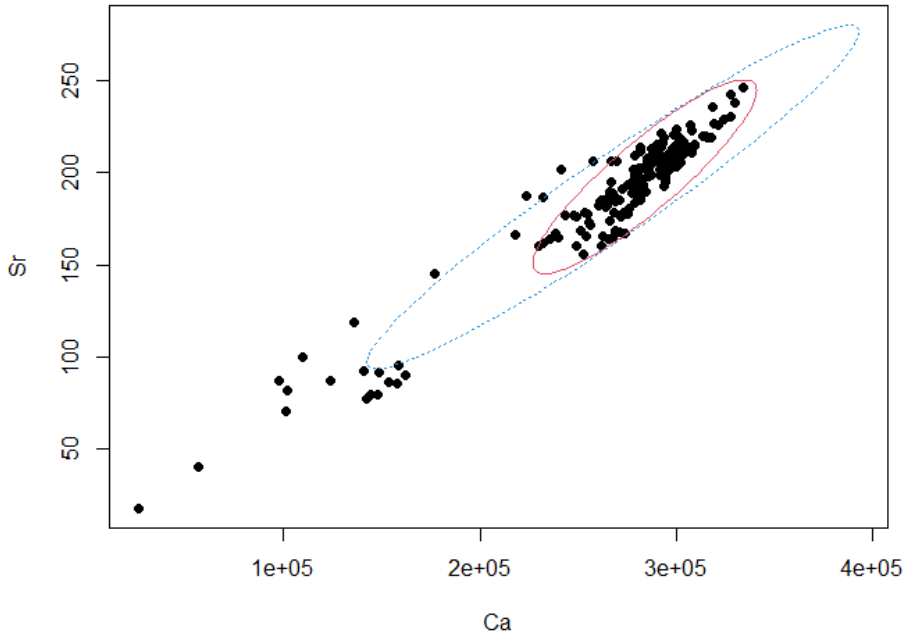
Classical cor = 0.84 Robust cor = 0.73



• **Ca vs Sr**

Classical test	<p>Pearson's product-moment correlation</p> <p>data: Od533M_SD\$Ca and Od533M_SD\$Sr $t = 47.692$, $df = 188$, p-value < 2.2e-16 alternative hypothesis: true correlation is not equal to 0 95 percent confidence interval: 0.9484792 0.9706298 sample estimates: cor 0.9610697</p>	<p>Spearman's rank correlation rho</p> <p>data: Od533M_SD\$Ca and Od533M_SD\$Sr $S = 111092$, p-value < 2.2e-16 alternative hypothesis: true rho is not equal to 0 sample estimates: rho 0.9028181</p>
	<p>MCD $(\alpha=0.05;$ $quant=0.8)$</p>	<p>\$cor.rob [1] 0.8939784</p>

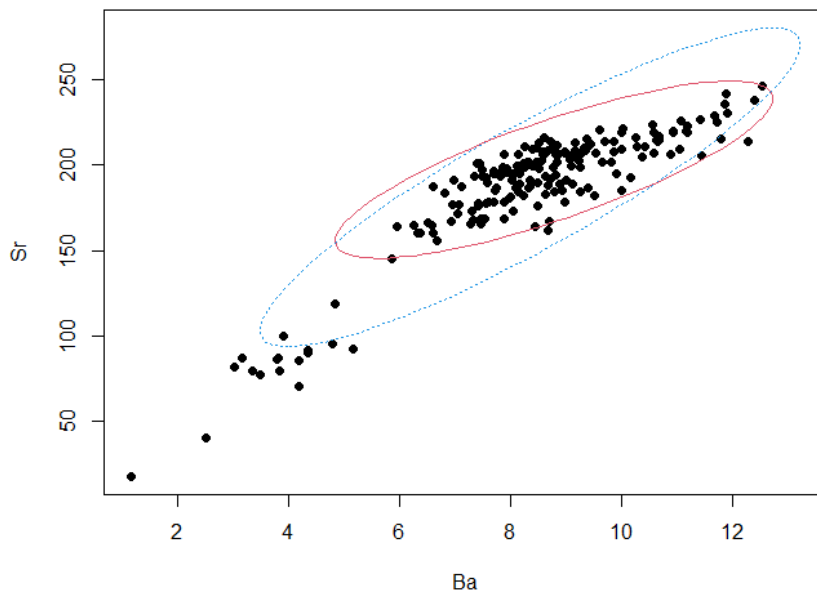
Classical cor = 0.96 Robust cor = 0.89



• Ba vs Sr

Classical test	<p>Pearson's product-moment correlation</p> <p>data: Od533M_SD\$Ba and Od533M_SD\$Sr $t = 28.16$, $df = 188$, p-value < 2.2e-16 alternative hypothesis: true correlation is not equal to 0 95 percent confidence interval: 0.8678047 0.9232742 sample estimates: cor 0.8990891</p>	<p>Spearman's rank correlation rho</p> <p>data: Od533M_SD\$Ba and Od533M_SD\$Sr $S = 197406$, p-value < 2.2e-16 alternative hypothesis: true rho is not equal to 0 sample estimates: rho 0.8273117</p>
	<p>MCD ($\alpha=0.05$; quant=0.8)</p> <p>$\\$cor.rob$ [1] 0.8067172</p>	

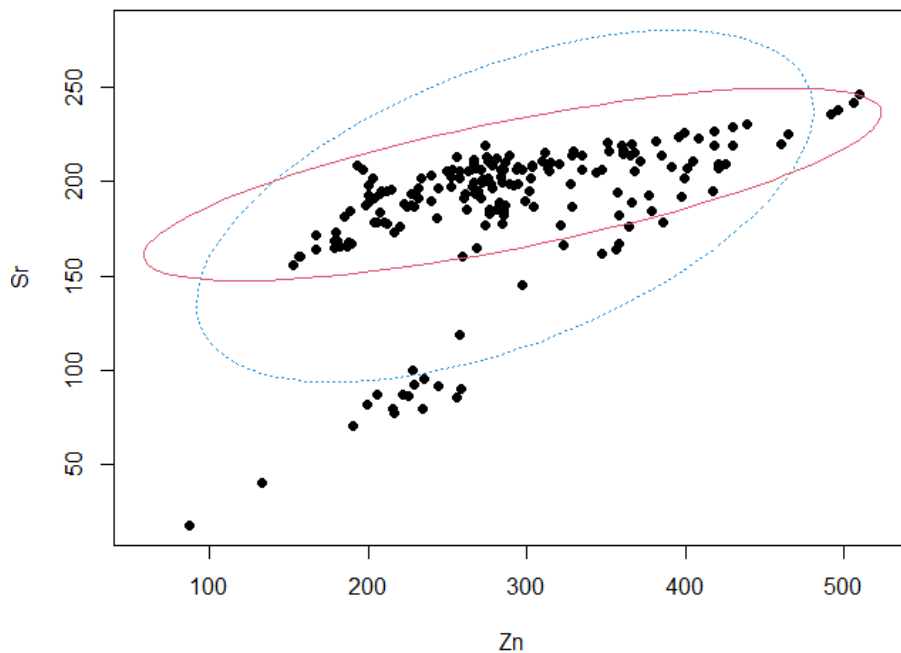
Classical cor = 0.9 Robust cor = 0.81



• Zn vs Sr

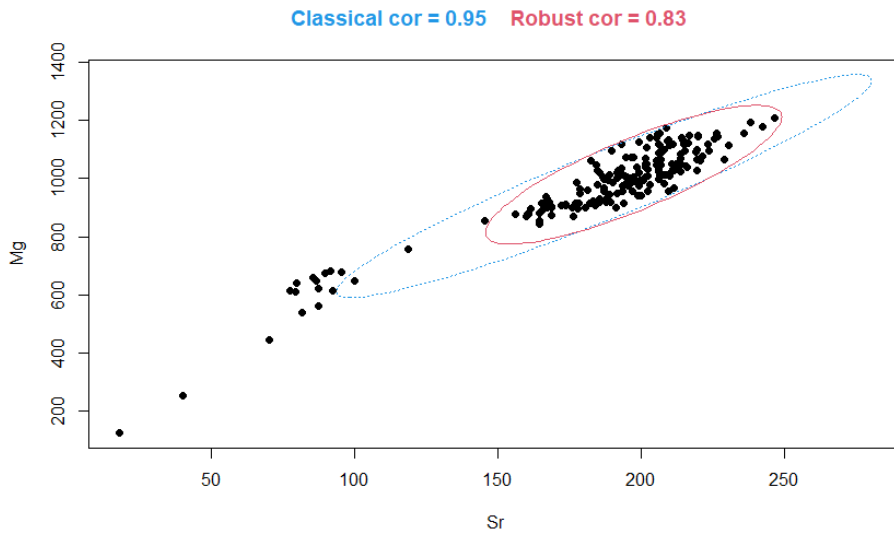
Classical test	<p>Pearson's product-moment correlation</p> <p>data: Od533M_SD\$Zn and Od533M_SD\$Sr $t = 9.0389$, $df = 188$, p-value < 2.2e-16 alternative hypothesis: true correlation is not equal to 0 95 percent confidence interval: 0.4427294 0.6424145 sample estimates: cor 0.5503947</p>	<p>Spearman's rank correlation rho</p> <p>data: Od533M_SD\$Zn and Od533M_SD\$Sr $S = 405396$, p-value < 2.2e-16 alternative hypothesis: true rho is not equal to 0 sample estimates: rho 0.6453647</p>
	<p>MCD $(\alpha=0.05;$ $quant=0.8)$</p>	<p>\$cor.rob [1] 0.7399384</p>

Classical cor = 0.55 Robust cor = 0.74



• Mg vs Sr

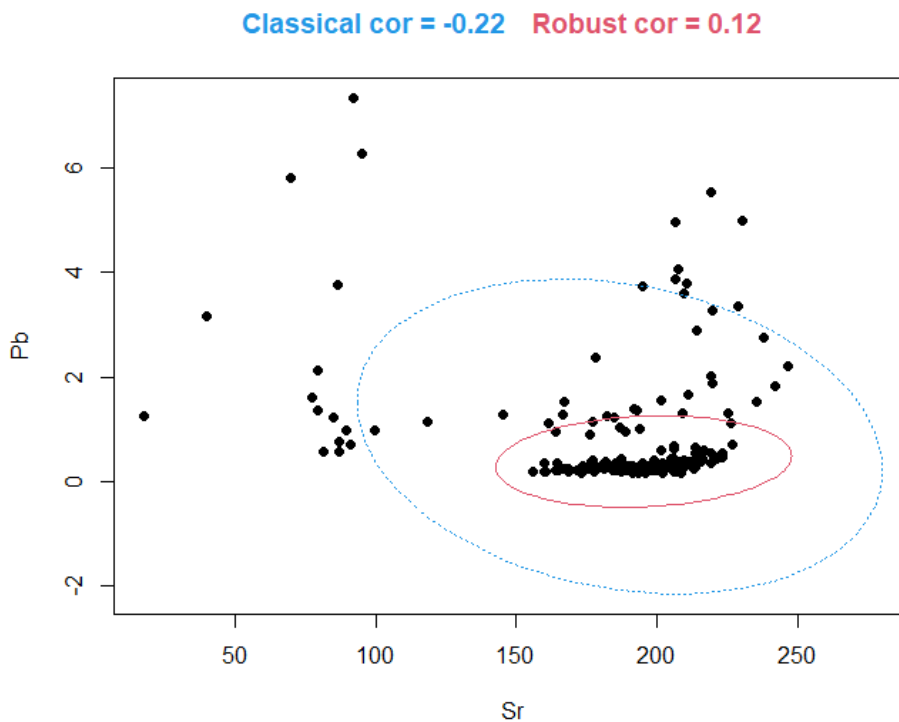
Classical test	<p>Pearson's product-moment correlation</p> <p>data: Od533M_SD\$Mg and Od533M_SD\$Sr $t = 39.904$, $df = 188$, p-value < 2.2e-16 alternative hypothesis: true correlation is not equal to 0 95 percent confidence interval: 0.9283560 0.9589761 sample estimates: cor 0.9457272</p>	<p>Spearman's rank correlation rho</p> <p>data: Od533M_SD\$Mg and Od533M_SD\$Sr $S = 160422$, p-value < 2.2e-16 alternative hypothesis: true rho is not equal to 0 sample estimates: rho 0.8596649</p>
	<p>MCD $(\alpha=0.05;$ $quant=0.8)$</p>	<p>\$cor.rob [1] 0.8330961</p>



- **Pb vs Sr**

Whole secondary dentine thickness:

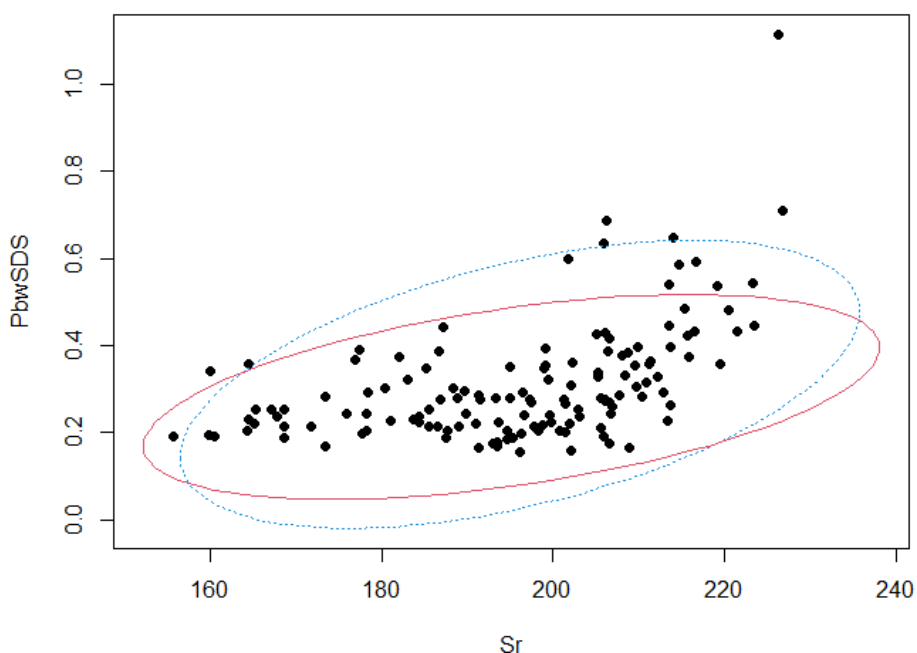
Classical test	<p>Pearson's product-moment correlation</p> <p>data: Od533M_SD\$Sr and Od533M_SD\$Pb $t = -3.0443$, $df = 188$, p-value = 0.002666 alternative hypothesis: true correlation is not equal to 0 95 percent confidence interval: -0.34835595 -0.07676657 sample estimates: cor -0.2167512</p>	<p>Spearman's rank correlation rho</p> <p>data: Od533M_SD\$Sr and Od533M_SD\$Pb $S = 967754$, p-value = 0.03466 alternative hypothesis: true rho is not equal to 0 sample estimates: rho 0.1534211</p>
	<p>MCD $(\alpha=0.05;$ $quant=0.8)$</p>	<p>$\\$cor.rob$ $[1] 0.1233295$</p>



Removing 110 μm of Pb-enriched secondary dentine surface:

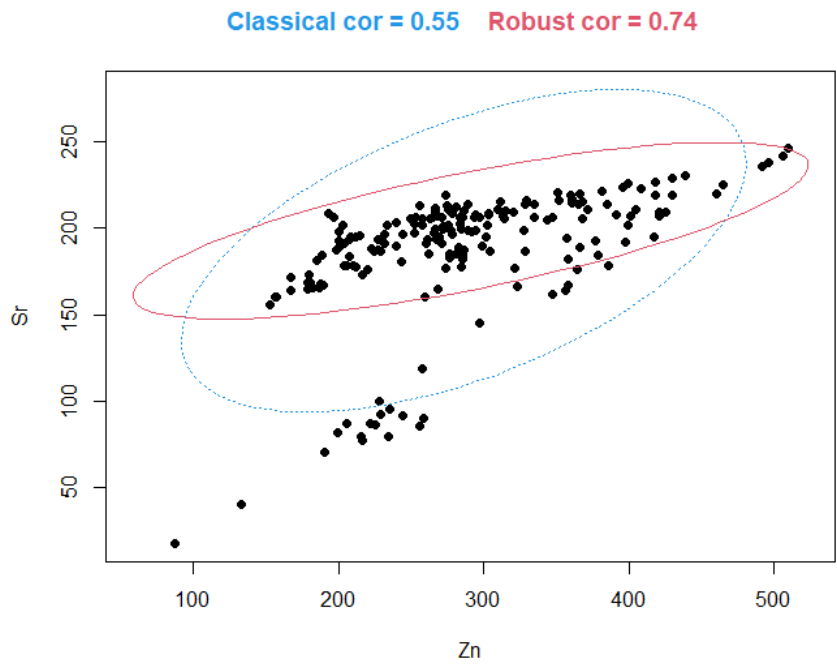
Classical test	<p>Pearson's product-moment correlation</p> <p>data: Od533M_SD_wSDS\$Sr and Od533M_SD_wSDS\$Pb</p> <p>t = 6.8029, df = 135, p-value = 3.039e-10</p> <p>alternative hypothesis: true correlation is not equal to 0</p> <p>95 percent confidence interval: 0.3688022 0.6204068</p> <p>sample estimates: cor 0.5052651</p>	<p>Spearman's rank correlation rho</p> <p>data: Od533M_SD_wSDS\$Zn and Od533M_SD_wSDS\$Pb</p> <p>S = 106274, p-value < 2.2e-16</p> <p>alternative hypothesis: true rho is not equal to 0</p> <p>sample estimates: rho 0.7520068</p>
	<p>MCD ($\alpha=0.05$; quant=0.8)</p>	<p>\$cor.rob [1] 0.4864732</p>

Classical cor = 0.51 Robust cor = 0.49



• Sr vs Zn

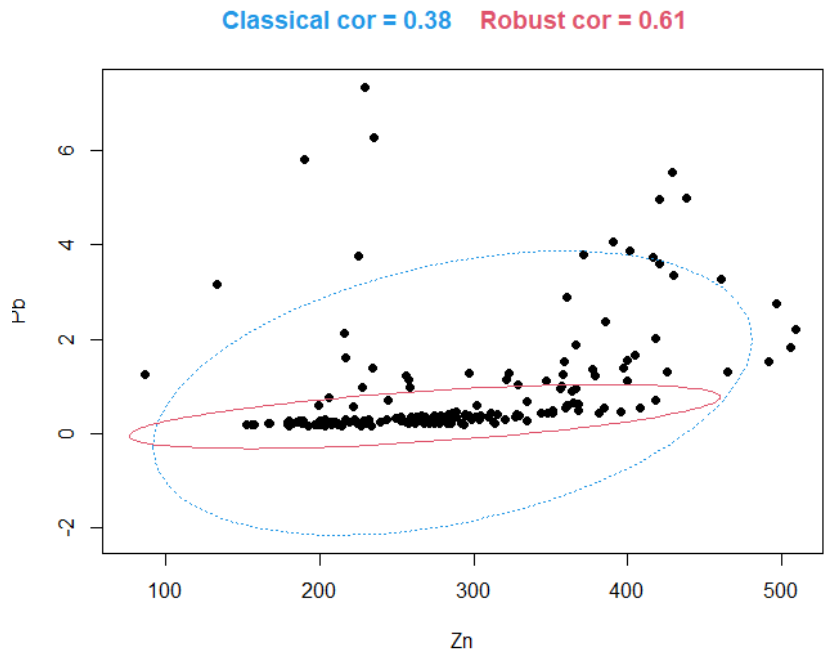
Classical test	<p>Pearson's product-moment correlation</p> <p>data: Od533M_SD\$Zn and Od533M_SD\$Sr</p> <p>t = 9.0389, df = 188, p-value < 2.2e-16</p> <p>alternative hypothesis: true correlation is not equal to 0</p> <p>95 percent confidence interval: 0.4427294 0.6424145</p> <p>sample estimates: cor 0.5503947</p>	<p>Spearman's rank correlation rho</p> <p>data: Od533M_SD\$Zn and Od533M_SD\$Sr</p> <p>S = 405396, p-value < 2.2e-16</p> <p>alternative hypothesis: true rho is not equal to 0</p> <p>sample estimates: rho 0.6453647</p>
	<p>MCD ($\alpha=0.05$; quant=0.8)</p>	<p>\$cor.rob [1] 0.7399384</p>



• **Pb vs Zn**

Whole secondary dentine thickness:

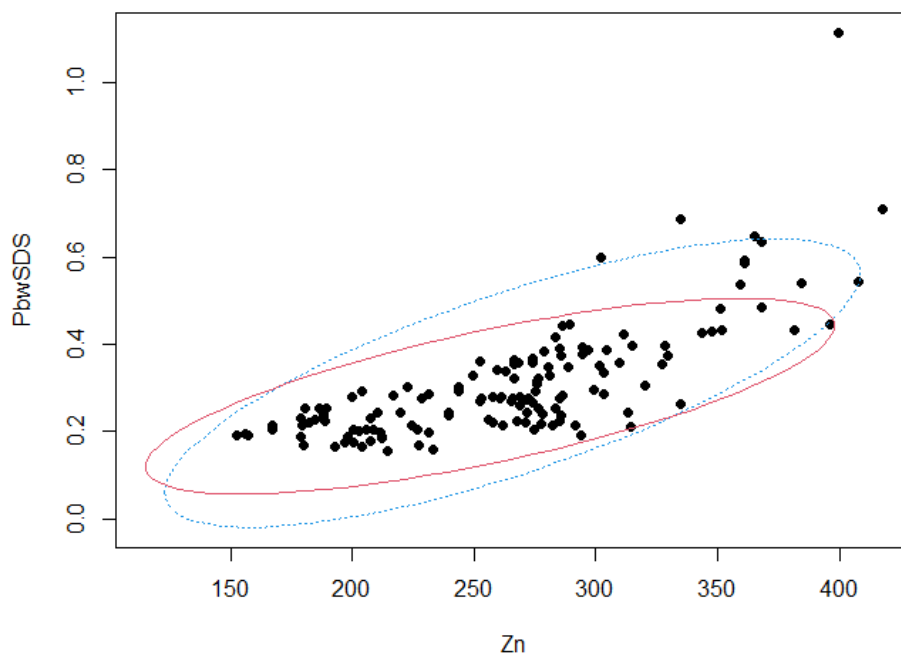
Classical test	<p>Pearson's product-moment correlation</p> <p>data: Od533M_SD\$Zn and Od533M_SD\$Pb $t = 5.5906$, $df = 188$, p-value = 7.874e-08 alternative hypothesis: true correlation is not equal to 0 95 percent confidence interval: 0.2485614 0.4933909 sample estimates: cor 0.3775555</p>	<p>Spearman's rank correlation rho</p> <p>data: Od533M_SD\$Zn and Od533M_SD\$Pb $S = 411004$, p-value < 2.2e-16 alternative hypothesis: true rho is not equal to 0 sample estimates: rho 0.6404589</p>
	<p>MCD ($\alpha=0.05$; quant=0.8)</p> <p>$\\$cor.rob$ [1] 0.6087622</p>	



Removing 110 μm of Pb-enriched secondary dentine surface:

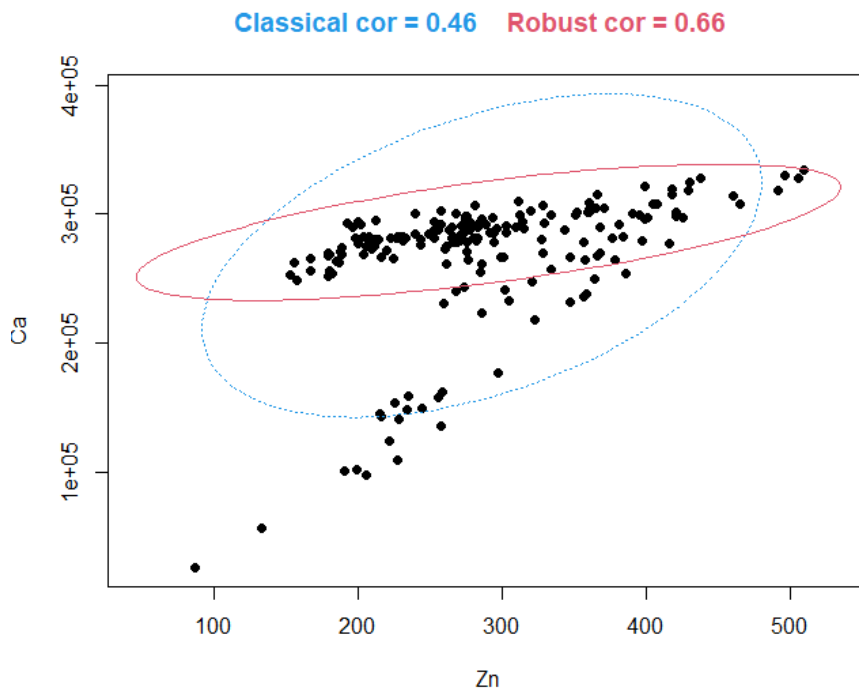
Classical test	<p>Pearson's product-moment correlation</p> <p>data: Od533M_SD_wSDS\$Zn and Od533M_SD_wSDS\$Pb $t = 13.47$, $df = 135$, p-value < 2.2e-16 alternative hypothesis: true correlation is not equal to 0 95 percent confidence interval: 0.6752670 0.8207112 sample estimates: cor 0.7572247</p>	<p>Spearman's rank correlation rho</p> <p>data: Od533M_SD_wSDS\$Zn and Od533M_SD_wSDS\$Pb $S = 106274$, p-value < 2.2e-16 alternative hypothesis: true rho is not equal to 0 sample estimates: rho 0.7520068</p>
MCD ($\alpha=0.05$; quant=0.8)	<p>\$cor.rob [1] 0.7244165</p>	

Classical cor = 0.76 Robust cor = 0.72



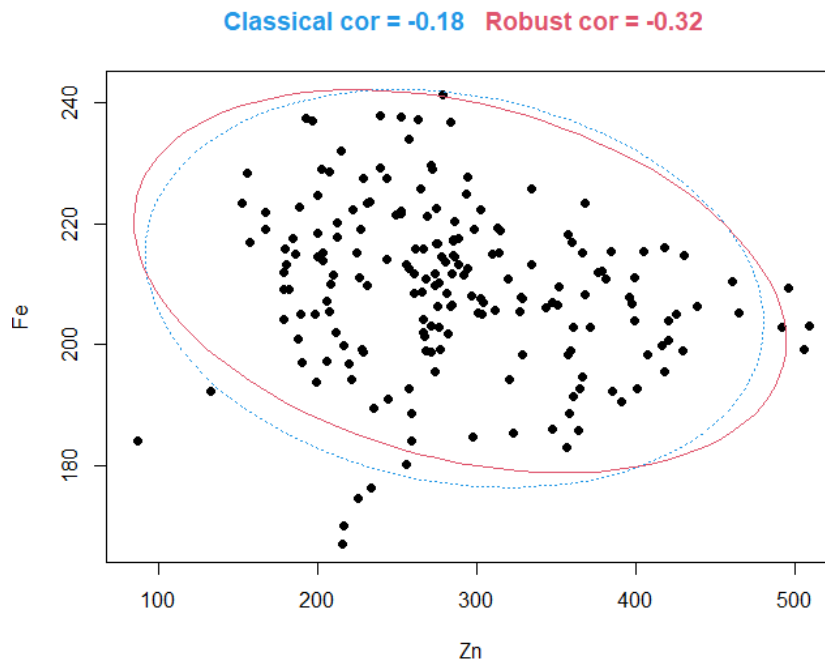
• Zn vs Ca

Classical test	<p>Pearson's product-moment correlation</p> <p>data: Od533M_SD\$Zn and Od533M_SD\$Ca $t = 7.0081$, $df = 188$, p-value = 4.196e-11 alternative hypothesis: true correlation is not equal to 0 95 percent confidence interval: 0.3344273 0.5611145 sample estimates: cor 0.4551141</p>	<p>Spearman's rank correlation rho</p> <p>data: Od533M_SD\$Zn and Od533M_SD\$Ca $S = 560218$, p-value < 2.2e-16 alternative hypothesis: true rho is not equal to 0 sample estimates: rho 0.5099284</p>
MCD ($\alpha=0.05$; quant=0.8)	<p>\$cor.rob [1] 0.6601464</p>	



• Zn vs Fe

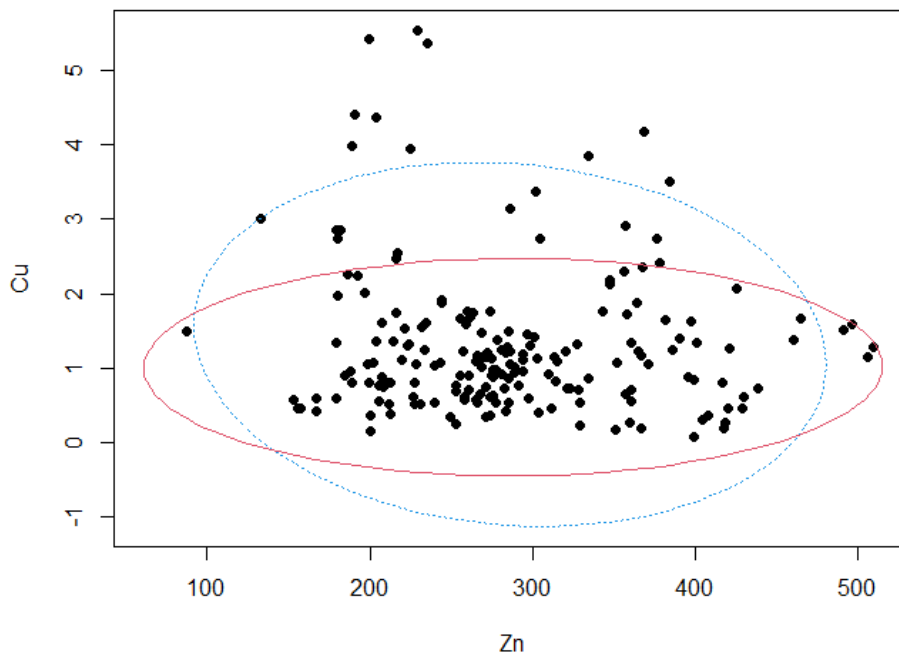
Classical test	<p>Pearson's product-moment correlation</p> <p>data: Od533M_SD\$Zn and Od533M_SD\$Fe $t = -2.455$, $df = 188$, p-value = 0.015 alternative hypothesis: true correlation is not equal to 0 95 percent confidence interval: -0.31080458 -0.03476824 sample estimates: cor -0.1762492</p>	<p>Spearman's rank correlation rho</p> <p>data: Od533M_SD\$Zn and Od533M_SD\$Fe $S = 1399172$, p-value = 0.001936 alternative hypothesis: true rho is not equal to 0 sample estimates: rho -0.2239779</p>
	<p>MCD $(\alpha=0.05;$ $quant=0.8)$</p>	<p>$\\$cor.rob$ [1] -0.3170197</p>



• Zn vs Cu

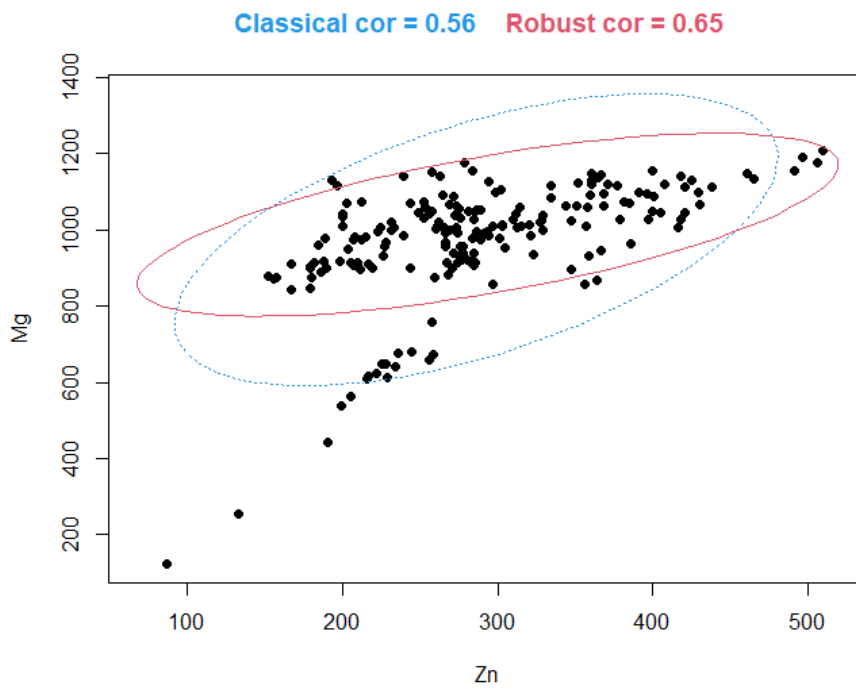
Classical test	<p>Pearson's product-moment correlation</p> <p>data: Od533M_SD\$Zn and Od533M_SD\$Cu $t = -1.4594$, $df = 188$, p-value = 0.1461 alternative hypothesis: true correlation is not equal to 0 95 percent confidence interval: -0.24450631 0.03707514 sample estimates: cor -0.1058368</p>	<p>Spearman's rank correlation rho</p> <p>data: Od533M_SD\$Zn and Od533M_SD\$Cu $S = 1193286$, p-value = 0.5475 alternative hypothesis: true rho is not equal to 0 sample estimates: rho -0.04387146</p>
	<p>MCD $(\alpha=0.05;$ $quant=0.8)$</p>	<p>\$cor.rob [1] 0.009811241</p>

Classical cor = -0.11 Robust cor = 0.01



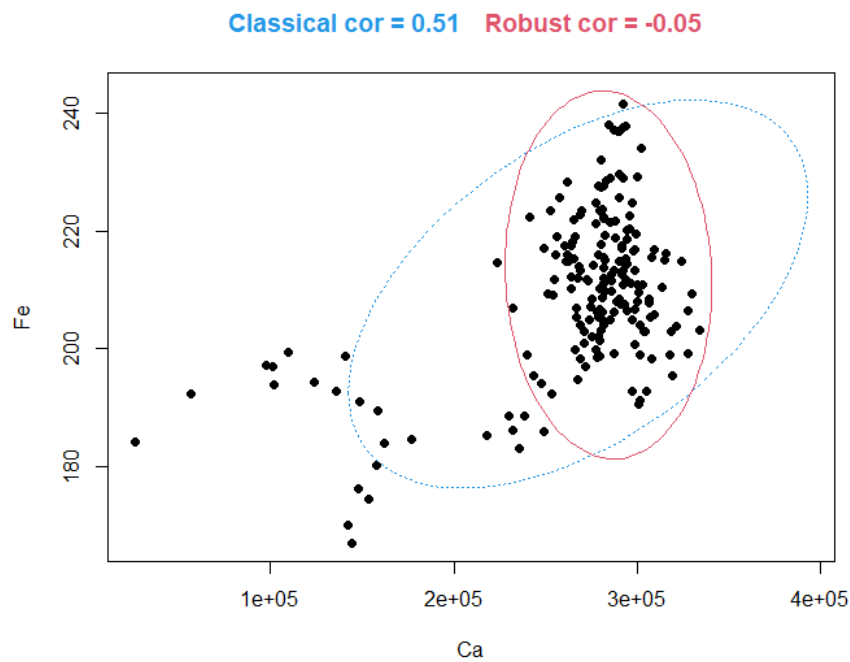
• Zn vs Mg

Classical test	<p>Pearson's product-moment correlation</p> <p>data: Od533M_SD\$Zn and Od533M_SD\$Mg $t = 9.3848$, $df = 188$, p-value < 2.2e-16 alternative hypothesis: true correlation is not equal to 0 95 percent confidence interval: 0.4594057 0.6545460 sample estimates: cor 0.5648209</p>	<p>Spearman's rank correlation rho</p> <p>data: Od533M_SD\$Zn and Od533M_SD\$Mg $S = 457680$, p-value < 2.2e-16 alternative hypothesis: true rho is not equal to 0 sample estimates: rho 0.5996273</p>
	<p>MCD $(\alpha=0.05;$ $quant=0.8)$</p>	<p>\$cor.rob [1] 0.6538013</p>



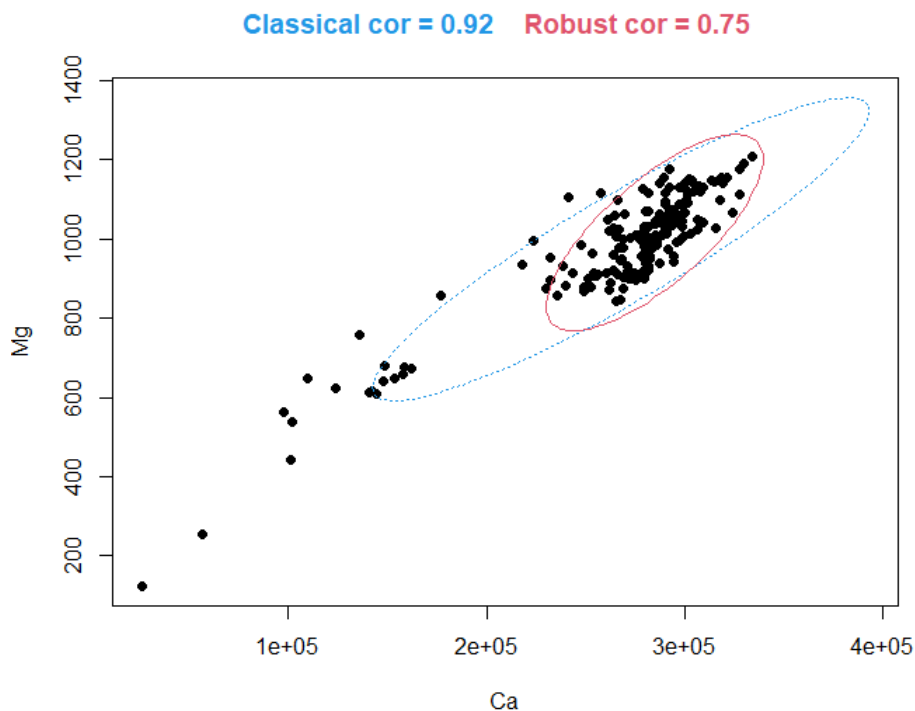
• Ca vs Fe

Classical test	<p>Pearson's product-moment correlation</p> <p>data: Od533M_SD\$Ca and Od533M_SD\$Fe $t = 8.0258$, $df = 188$, p-value = $1.063e-13$ alternative hypothesis: true correlation is not equal to 0 95 percent confidence interval: 0.3909232 0.6040775 sample estimates: cor 0.5051645</p>	<p>Spearman's rank correlation rho</p> <p>data: Od533M_SD\$Ca and Od533M_SD\$Fe $S = 832466$, p-value = 0.0001572 alternative hypothesis: true rho is not equal to 0 sample estimates: rho 0.2717693</p>
	<p>MCD $(\alpha=0.05;$ $quant=0.8)$</p>	<p>$\\$cor.rob$ $[1] -0.05379779$</p>



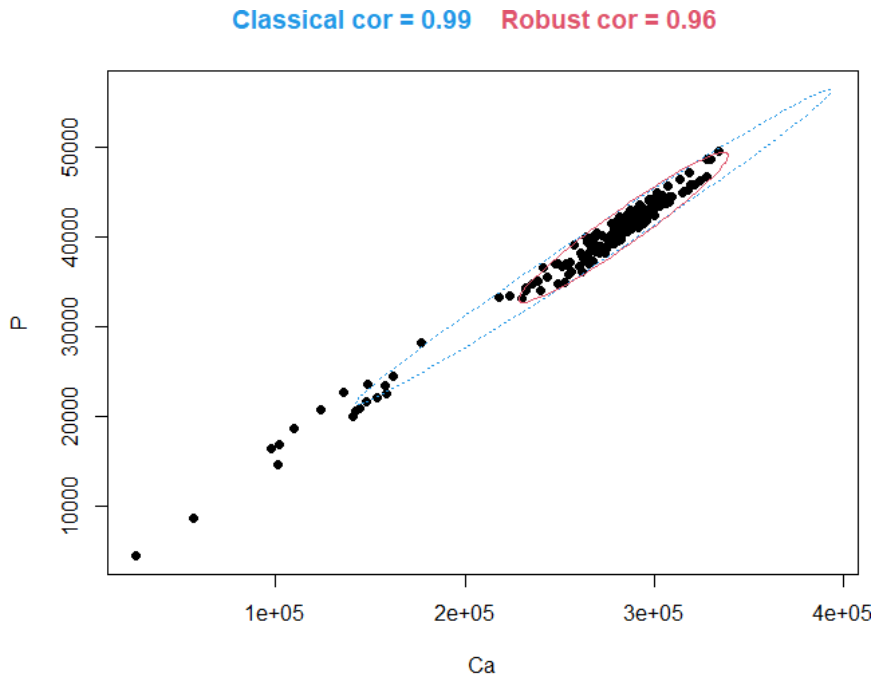
• Ca vs Mg

Classical test	<p>Pearson's product-moment correlation</p> <p>data: Od533M_SD\$Ca and Od533M_SD\$Mg $t = 31.118$, $df = 188$, p-value < 2.2e-16 alternative hypothesis: true correlation is not equal to 0 95 percent confidence interval: 0.8884944 0.9355818 sample estimates: cor 0.9151051</p>	<p>Spearman's rank correlation rho</p> <p>data: Od533M_SD\$Ca and Od533M_SD\$Mg $S = 236192$, p-value < 2.2e-16 alternative hypothesis: true rho is not equal to 0 sample estimates: rho 0.7933822</p>
	<p>MCD $(\alpha=0.05;$ $quant=0.8)$</p>	<p>\$cor.rob [1] 0.7510065</p>



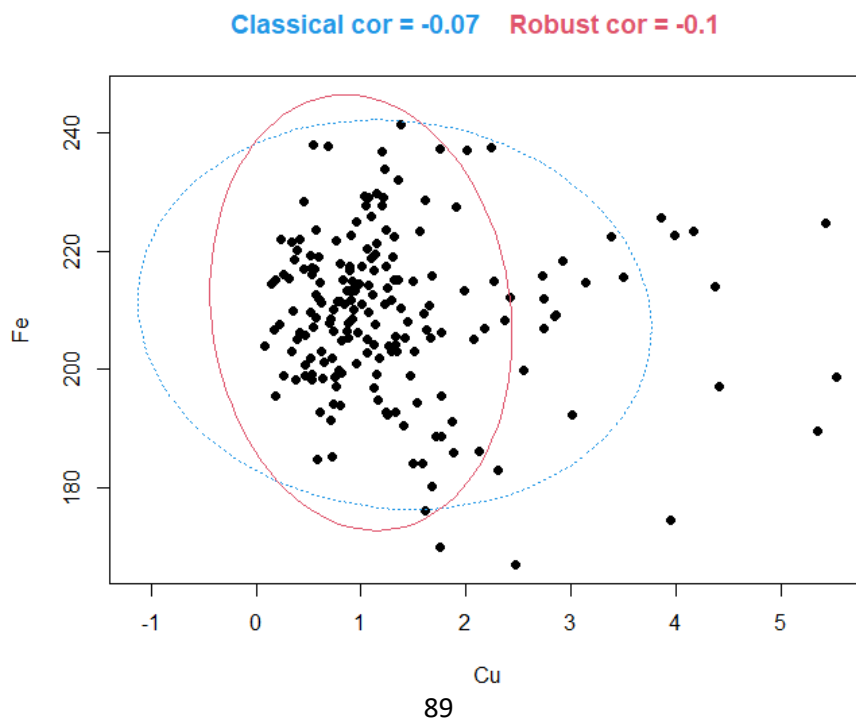
• Ca vs P

Classical test	<p>Pearson's product-moment correlation</p> <p>data: Od533M_SD\$Ca and Od533M_SD\$P $t = 113.46$, $df = 188$, p-value < 2.2e-16 alternative hypothesis: true correlation is not equal to 0 95 percent confidence interval: 0.9903906 0.9945722 sample estimates: cor 0.9927769</p>	<p>Spearman's rank correlation rho</p> <p>data: Od533M_SD\$Ca and Od533M_SD\$P $S = 36556$, p-value < 2.2e-16 alternative hypothesis: true rho is not equal to 0 sample estimates: rho 0.9680213</p>
	<p>MCD $(\alpha=0.05;$ $quant=0.8)$</p>	<p>\$cor.rob [1] 0.9609519</p>



• **Cu vs Fe**

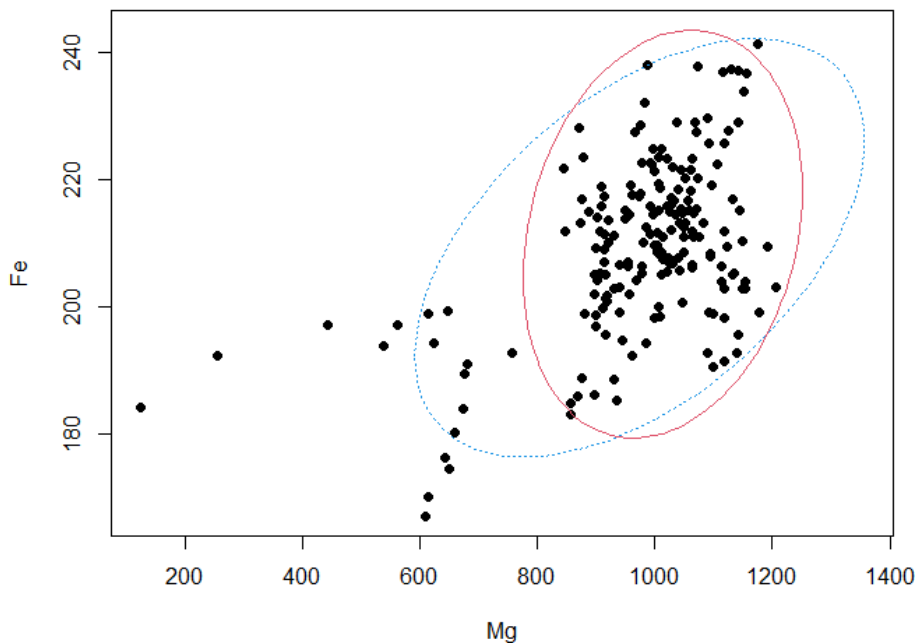
Classical test	<p>Pearson's product-moment correlation</p> <p>data: Od533M_SD\$Cu and Od533M_SD\$Fe $t = -0.99885$, $df = 188$, p-value = 0.3192 alternative hypothesis: true correlation is not equal to 0 95 percent confidence interval: -0.21280835 0.07042566 sample estimates: cor -0.07265607</p>	<p>Spearman's rank correlation rho</p> <p>data: Od533M_SD\$Cu and Od533M_SD\$Fe $S = 1199798$, p-value = 0.4967 alternative hypothesis: true rho is not equal to 0 sample estimates: rho -0.04956807</p>
	<p>MCD $(\alpha=0.05;$ $quant=0.8)$</p>	<p>$\\$cor.rob$ $[1] -0.1037514$</p>



• **Mg vs Fe**

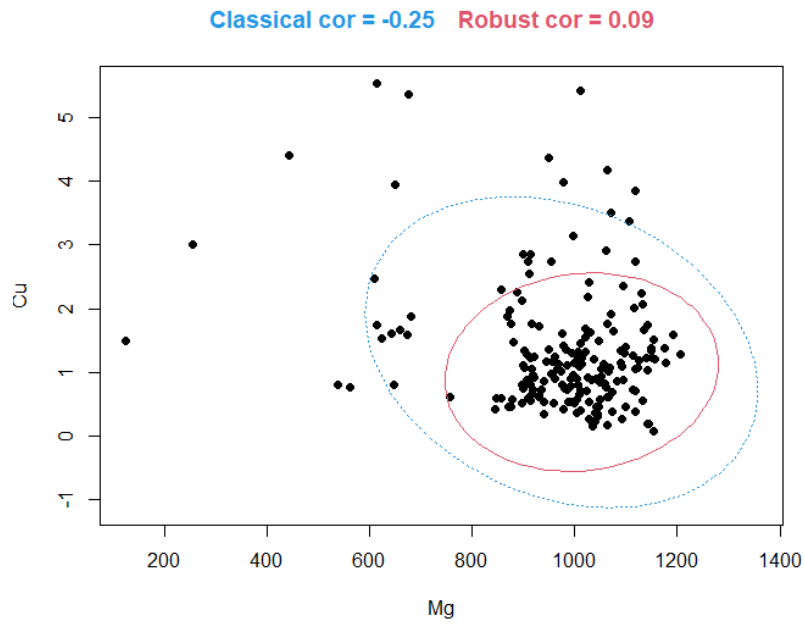
Classical test	Pearson's product-moment correlation data: Od533M_SD\$Mg and Od533M_SD\$Fe t = 8.243, df = 188, p-value = 2.823e-14 alternative hypothesis: true correlation is not equal to 0 95 percent confidence interval: 0.4024041 0.6126594 sample estimates: cor 0.5152425	Spearman's rank correlation rho data: Od533M_SD\$Mg and Od533M_SD\$Fe S = 717378, p-value = 1.513e-07 alternative hypothesis: true rho is not equal to 0 sample estimates: rho 0.3724468
	MCD ($\alpha=0.05$; quant=0.8)	\$cor.rob [1] 0.2092387

Classical cor = 0.52 Robust cor = 0.21



• **Cu vs Mg**

Classical test	Pearson's product-moment correlation data: Od533M_SD\$Mg and Od533M_SD\$Cu t = -3.5432, df = 188, p-value = 0.0004986 alternative hypothesis: true correlation is not equal to 0 95 percent confidence interval: -0.3790493 -0.1118258 sample estimates: cor -0.2501963	Spearman's rank correlation rho data: Od533M_SD\$Mg and Od533M_SD\$Cu S = 1249146, p-value = 0.203 alternative hypothesis: true rho is not equal to 0 sample estimates: rho -0.09273708
	MCD ($\alpha=0.05$; quant=0.8)	\$cor.rob [1] 0.08609909

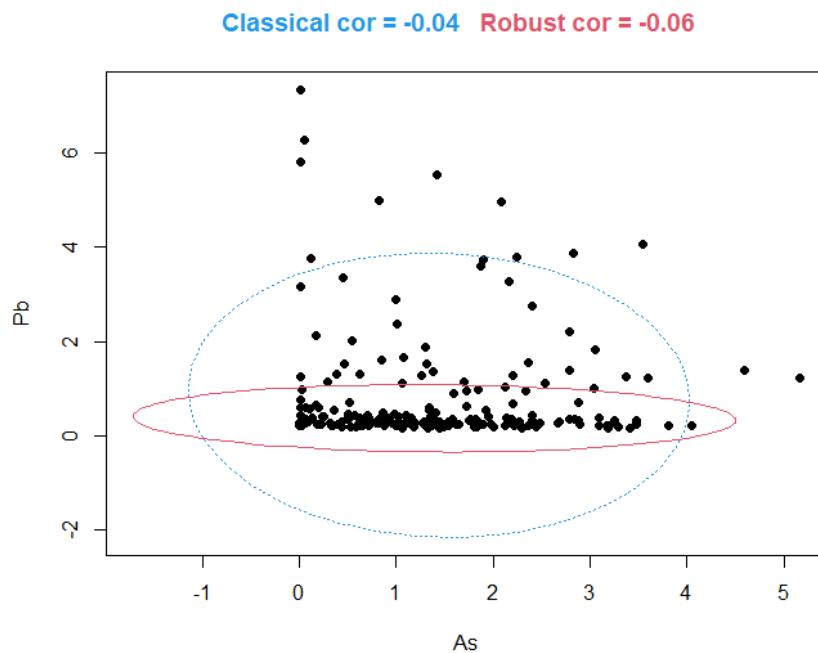


- As vs Hg, Pb vs Hg (no Hg at all). => Not Applicable.

- Pb vs As

Whole secondary dentine thickness:

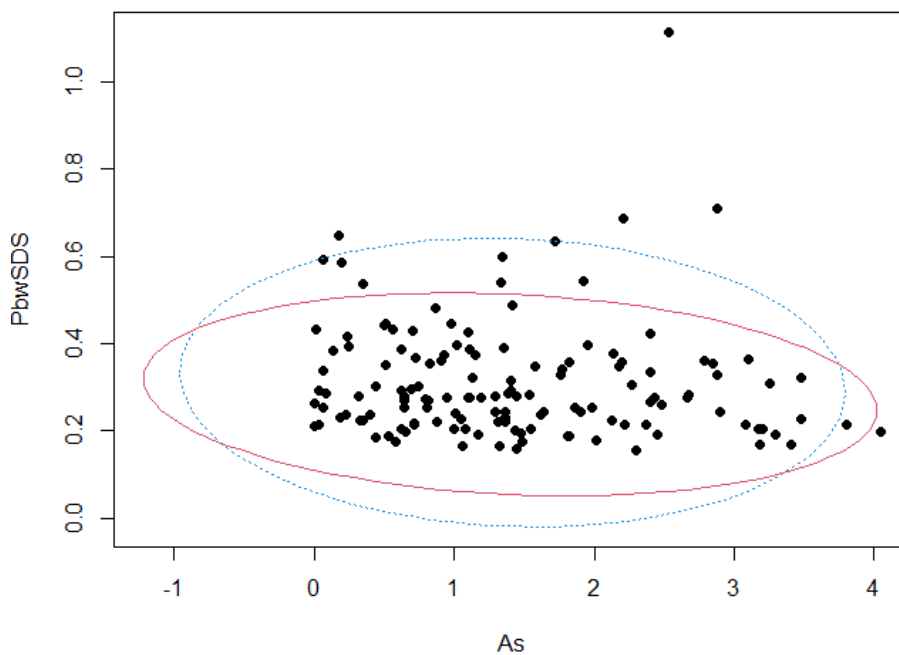
Classical test	<p>Pearson's product-moment correlation</p> <p>data: Od533M_SD\$As and Od533M_SD\$Pb $t = -0.57847$, $df = 188$, p-value = 0.5636 alternative hypothesis: true correlation is not equal to 0 95 percent confidence interval: -0.1834048 0.1008063 sample estimates: cor -0.04215196</p>	<p>Spearman's rank correlation rho</p> <p>data: Od533M_SD\$As and Od533M_SD\$Pb $S = 1228634$, p-value = 0.3048 alternative hypothesis: true rho is not equal to 0 sample estimates: rho -0.07479344</p>
	<p>MCD $(\alpha=0.05;$ $quant=0.8)$</p>	<p>$\\$cor.rob$ $[1] -0.05585069$</p>



Removing 110 μm of Pb-enriched secondary dentine surface:

Classical test	<p>Pearson's product-moment correlation</p> <p>data: Od533M_SD_wSDS\$As and Od533M_SD_wSDS\$Pb $t = -0.79052$, $df = 135$, p-value = 0.4306 alternative hypothesis: true correlation is not equal to 0 95 percent confidence interval: -0.2329440 0.1009847 sample estimates: cor -0.0678805</p>	<p>Spearman's rank correlation rho</p> <p>data: Od533M_SD_wSDS\$As and Od533M_SD_wSDS\$Pb $S = 490286$, p-value = 0.09296 alternative hypothesis: true rho is not equal to 0 sample estimates: rho -0.1440952</p>
	<p>MCD $(\alpha=0.05;$ $\text{quant}=0.8)$</p>	<p>$\\$cor.rob$ [1] -0.1582813</p>

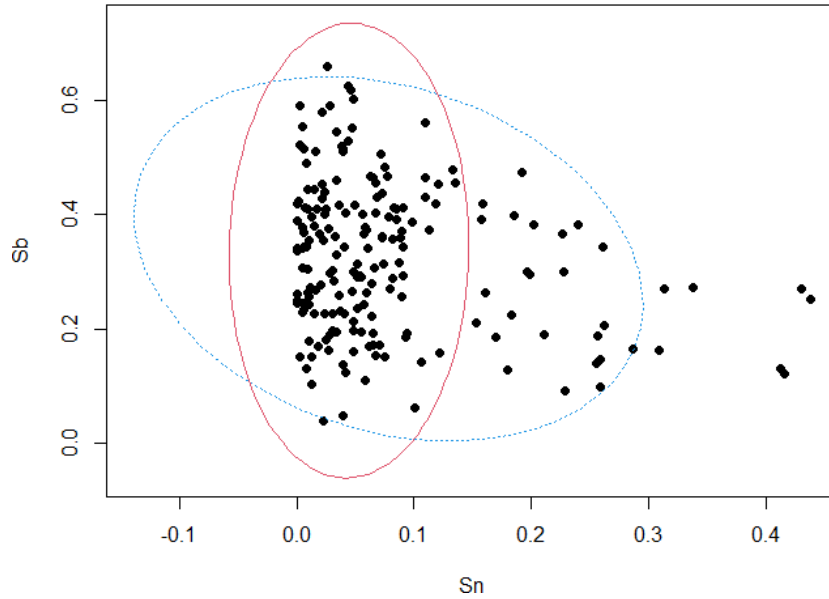
Classical cor = -0.07 Robust cor = -0.16



• Sb vs Sn

Classical test	<p>Pearson's product-moment correlation</p> <p>data: Od533M_SD\$Sn and Od533M_SD\$Sb $t = -3.4518$, $df = 188$, p-value = 0.0006878 alternative hypothesis: true correlation is not equal to 0 95 percent confidence interval: -0.3735037 -0.1054417 sample estimates: cor -0.2441307</p>	<p>Spearman's rank correlation rho</p> <p>data: Od533M_SD\$Sn and Od533M_SD\$Sb $S = 1315916$, p-value = 0.03746 alternative hypothesis: true rho is not equal to 0 sample estimates: rho -0.1511466</p>
	<p>MCD $(\alpha=0.05;$ $\text{quant}=0.8)$</p>	<p>$\\$cor.rob$ [1] 0.023168</p>

Classical cor = -0.24 Robust cor = 0.02

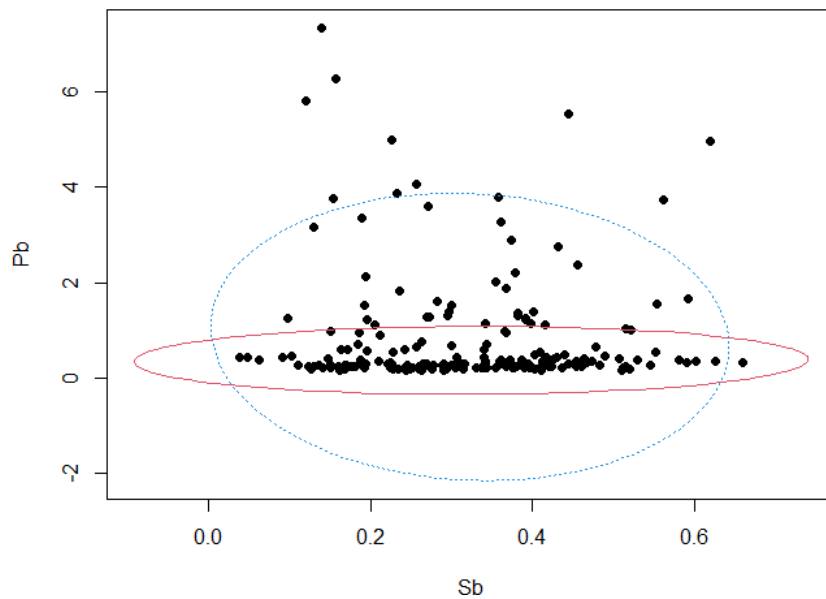


• Pb vs Sb

Whole secondary dentine thickness:

Classical test	<p>Pearson's product-moment correlation</p> <p>data: Od533M_SD\$Sb and Od533M_SD\$Pb $t = -0.93918$, $df = 188$, p-value = 0.3488 alternative hypothesis: true correlation is not equal to 0 95 percent confidence interval: -0.20866014 0.07474378 sample estimates: cor -0.06833665</p>	<p>Spearman's rank correlation rho</p> <p>data: Od533M_SD\$Sb and Od533M_SD\$Pb $S = 1110492$, p-value = 0.6955 alternative hypothesis: true rho is not equal to 0 sample estimates: rho 0.02855568</p>
	<p>MCD ($\alpha=0.05$; quant=0.8)</p> <p>$\\$cor.rob$ [1] 0.03371059</p>	

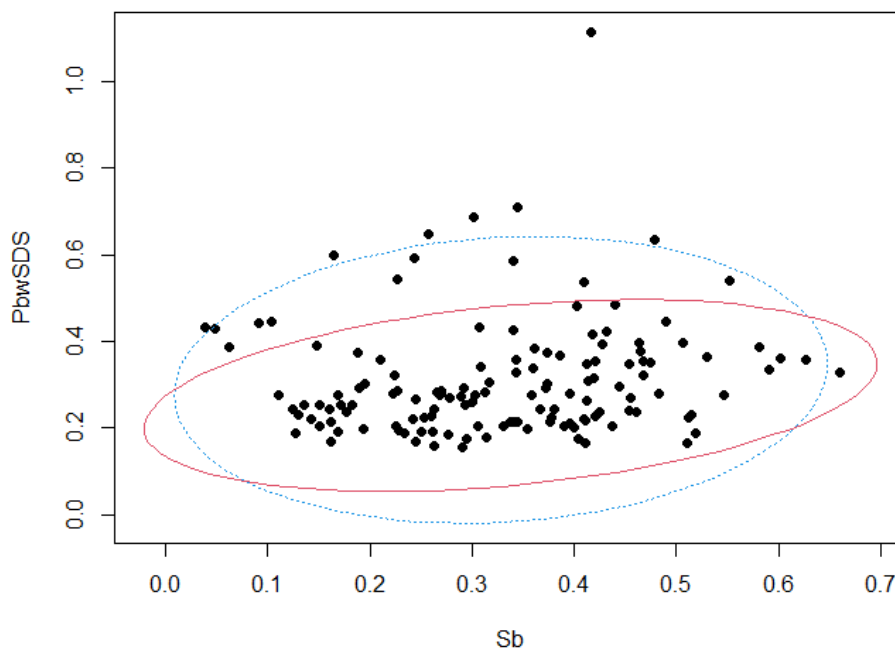
Classical cor = -0.07 Robust cor = 0.03



Removing 110 μm of Pb-enriched secondary dentinee surface:

Classical test	<p>Pearson's product-moment correlation</p> <p>data: Od533M_SD_wSDS\$Sb and Od533M_SD_wSDS\$Pb $t = 1.284$, $df = 135$, p-value = 0.2013 alternative hypothesis: true correlation is not equal to 0 95 percent confidence interval: -0.05896091 0.27253560 sample estimates: cor 0.1098408</p>	<p>Spearman's rank correlation rho</p> <p>data: Od533M_SD_wSDS\$Sb and Od533M_SD_wSDS\$Pb $S = 356020$, p-value = 0.04817 alternative hypothesis: true rho is not equal to 0 sample estimates: rho 0.169218</p>
MCD ($\alpha=0.05$; quant=0.8)	<p>\$cor.rob [1] 0.340878</p>	

Classical cor = 0.11 Robust cor = 0.34

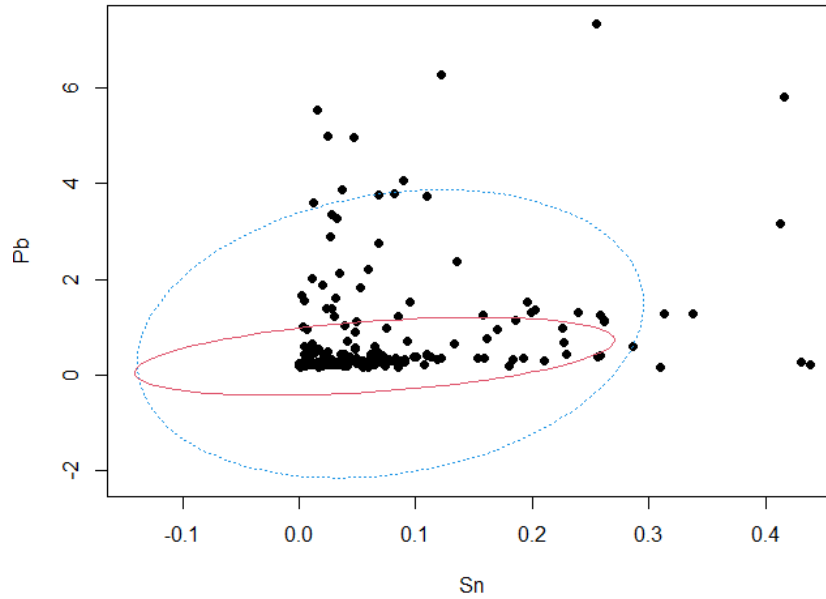


• Pb vs Sn

Whole secondary dentinee thickness:

Classical test	<p>Pearson's product-moment correlation</p> <p>data: Od533M_SD\$Sn and Od533M_SD\$Pb $t = 2.8353$, $df = 188$, p-value = 0.005079 alternative hypothesis: true correlation is not equal to 0 95 percent confidence interval: 0.06193476 0.33519342 sample estimates: cor 0.2025027</p>	<p>Spearman's rank correlation rho</p> <p>data: Od533M_SD\$Sn and Od533M_SD\$Pb $S = 805144$, p-value = 3.737e-05 alternative hypothesis: true rho is not equal to 0 sample estimates: rho 0.2956702</p>
MCD ($\alpha=0.05$; quant=0.8)	<p>\$cor.rob [1] 0.424453</p>	

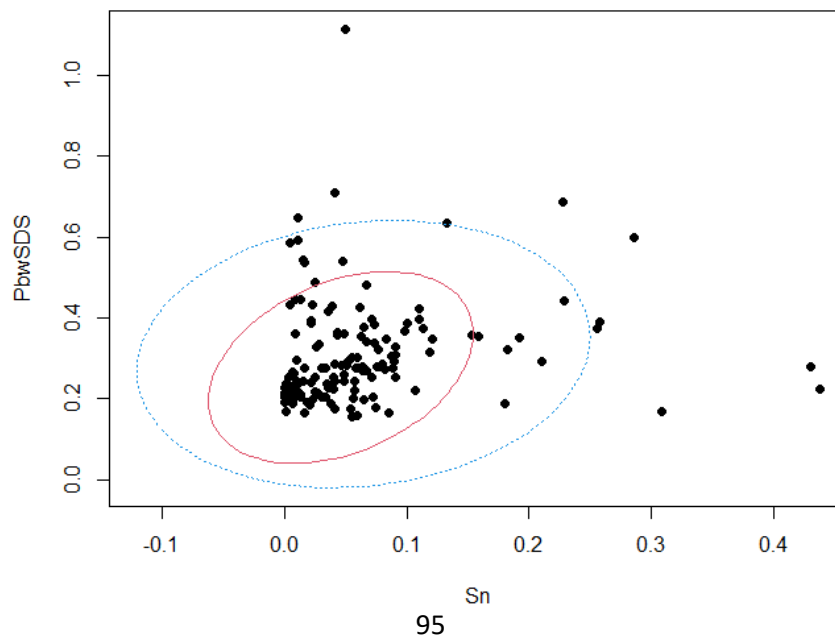
Classical cor = 0.2 Robust cor = 0.42



Removing 110 μ m of Pb-enriched secondary dentine surface:

Classical test	<p>Pearson's product-moment correlation</p> <p>data: Od533M_SD_wSDS\$Sn and Od533M_SD_wSDS\$Pb</p> <p>t = 1.5529, df = 135, p-value = 0.1228</p> <p>alternative hypothesis: true correlation is not equal to 0</p> <p>95 percent confidence interval: -0.0360418 0.2936653</p> <p>sample estimates: cor 0.1324745</p>	<p>Spearman's rank correlation rho</p> <p>data: Od533M_SD_wSDS\$Sn and Od533M_SD_wSDS\$Pb</p> <p>S = 304920, p-value = 0.0006611</p> <p>alternative hypothesis: true rho is not equal to 0</p> <p>sample estimates: rho 0.2884612</p>
	<p>MCD ($\alpha=0.05$; quant=0.8)</p>	<p>\$cor.rob [1] 0.3515933</p>

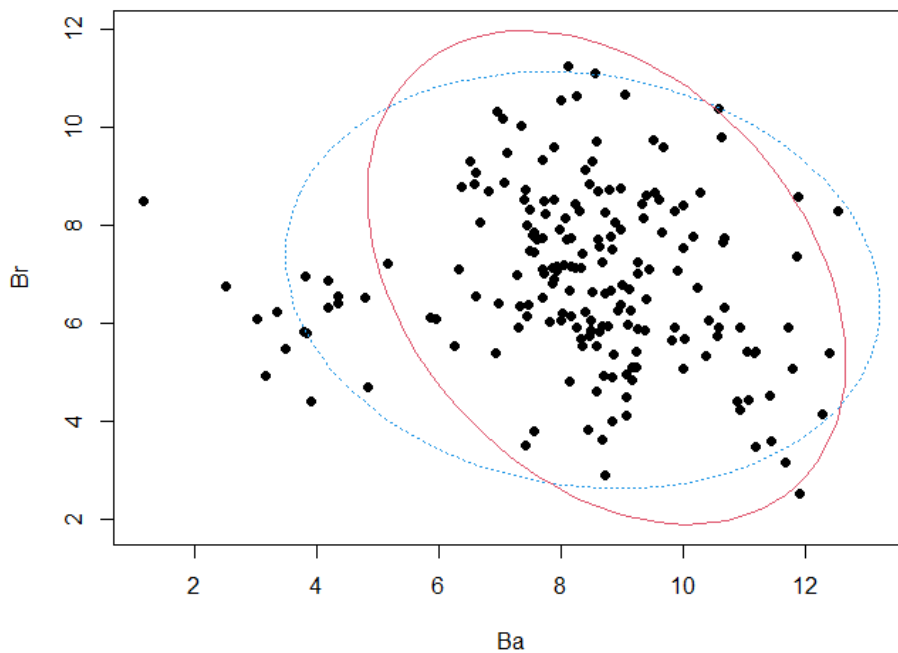
Classical cor = 0.13 Robust cor = 0.35



• Br vs Ba

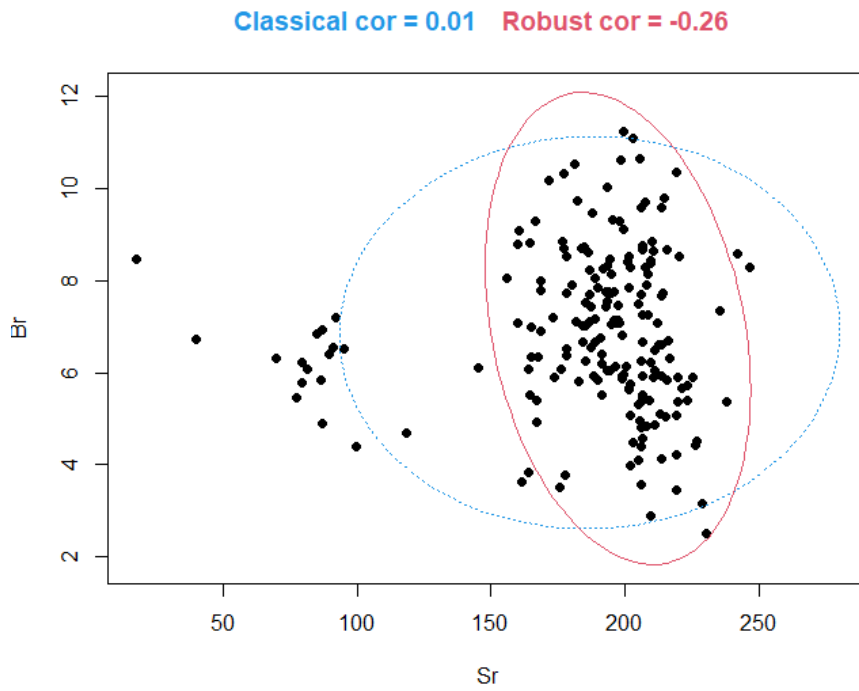
Classical test	<p>Pearson's product-moment correlation</p> <p>data: Od533M_SD\$Ba and Od533M_SD\$Br $t = -1.6732$, $df = 188$, p-value = 0.09595 alternative hypothesis: true correlation is not equal to 0 95 percent confidence interval: -0.2590202 0.0215923 sample estimates: cor -0.1211334</p>	<p>Spearman's rank correlation rho</p> <p>data: Od533M_SD\$Ba and Od533M_SD\$Br $S = 1364608$, p-value = 0.007479 alternative hypothesis: true rho is not equal to 0 sample estimates: rho -0.1937418</p>
	<p>MCD $(\alpha=0.05;$ $quant=0.8)$</p>	<p>\$cor.rob [1] -0.3389472</p>

Classical cor = -0.12 Robust cor = -0.34



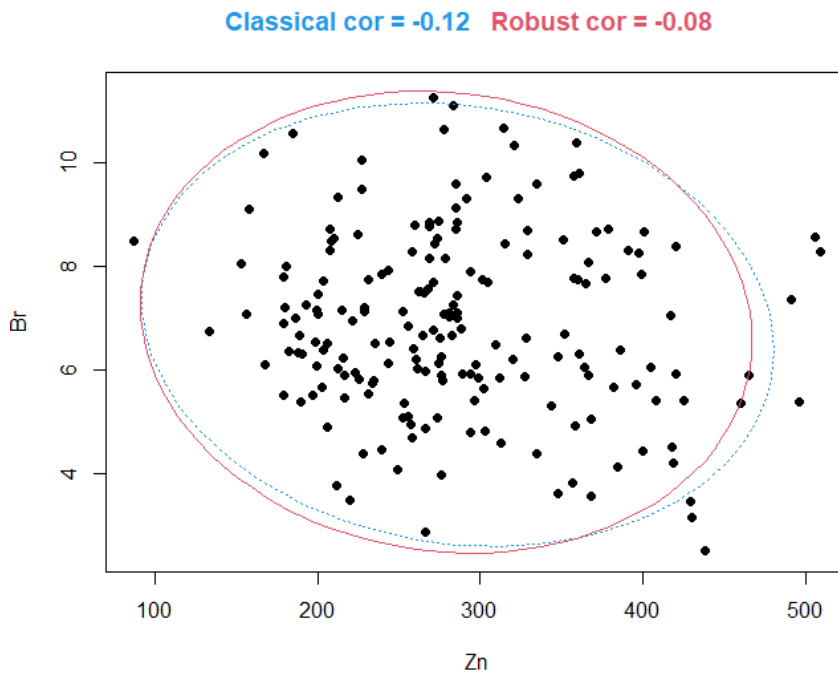
• Br vs Sr

Classical test	<p>Pearson's product-moment correlation</p> <p>data: Od533M_SD\$Sr and Od533M_SD\$Br $t = 0.19459$, $df = 188$, p-value = 0.8459 alternative hypothesis: true correlation is not equal to 0 95 percent confidence interval: -0.1284221 0.1562284 sample estimates: cor 0.01419062</p>	<p>Spearman's rank correlation rho</p> <p>data: Od533M_SD\$Sr and Od533M_SD\$Br $S = 1275574$, p-value = 0.1114 alternative hypothesis: true rho is not equal to 0 sample estimates: rho -0.115856</p>
	<p>MCD $(\alpha=0.05;$ $quant=0.8)$</p>	<p>\$cor.rob [1] -0.2620026</p>



• Br vs Zn

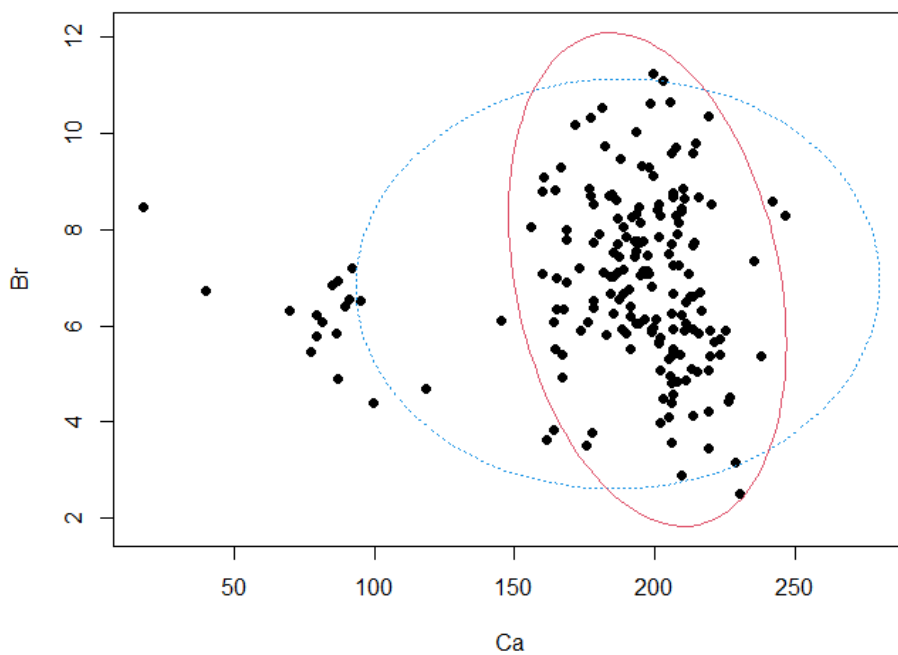
Classical test	<p>Pearson's product-moment correlation</p> <p>data: Od533M_SD\$Zn and Od533M_SD\$Br $t = -1.6138$, $df = 188$, p-value = 0.1083 alternative hypothesis: true correlation is not equal to 0 95 percent confidence interval: -0.25499849 0.02589603 sample estimates: cor -0.1168882</p>	<p>Spearman's rank correlation rho</p> <p>data: Od533M_SD\$Zn and Od533M_SD\$Br $S = 1232840$, p-value = 0.2816 alternative hypothesis: true rho is not equal to 0 sample estimates: rho -0.0784728</p>
	<p>MCD $(\alpha=0.05;$ $quant=0.8)$</p>	<p>$\\$cor.rob$ $[1] -0.08039107$</p>



- Br vs Ca

Classical test	<p>Pearson's product-moment correlation</p> <p>data: Od533M_SD\$Ca and Od533M_SD\$Br $t = 0.59652$, $df = 188$, p-value = 0.5515 alternative hypothesis: true correlation is not equal to 0 95 percent confidence interval: -0.09950427 0.18467540 sample estimates: cor 0.04346472</p>	<p>Spearman's rank correlation rho</p> <p>data: Od533M_SD\$Ca and Od533M_SD\$Br $S = 1193966$, p-value = 0.5421 alternative hypothesis: true rho is not equal to 0 sample estimates: rho -0.04446631</p>
	<p>MCD $(\alpha=0.05;$ $quant=0.8)$</p>	<p>\$cor.rob [1] -0.2620026</p>

Classical cor = 0.01 Robust cor = -0.26



File S2

Synchrotron Fluorescence (SXRF) results

Using SXRF and LA-ICP-TOFMS to explore evidence of treatment and physiological responses to leprosy in medieval Denmark

Biology

Anastasia Brozou, Marcello A. Mannino, Stijn J.M. Van Malderen, Jan Garrevoet, Eric Pubert, Benjamin T. Fuller, M. Christopher Dean, Thomas Colard, Frédéric Santos, Niels Lynnerup, Jesper L. Boldsen, Marie Louise Jørkov, Andrei Dorian Soficaru, Laszlo Vincze, Adeline Le Cabec

Corresponding author:

Adeline Le Cabec

E-mail: adeline.le-cabec@u-bordeaux.fr

Data reconstruction

- Raw data were fitted and calibrated.
- The calculation takes into account the **average thickness of the tooth section** measured by subtracting the thickness of the glass slide from {tooth section + epoxy bond ~negligible thickness + glass slide}.
- The **background noise has been subtracted** from the sample for each element.

In the next slides:

- “*Scanning*”: actual areas scanned.
- Images reported in this ppt are “Mass diffraction”, in mg.kg^{-1} (ppm).
- It is also possible to report “areal density”, in g.cm^{-3}
- To save space, the elemental maps of some teeth may have been rotated by 90° .
- Maps are displayed using the “Gistheat” colormap.
- To enhance the banding/stress pattern while reducing overall noise, a 2D Gaussian filter was applied to the datasets. The kernel size (=strength of the filter) used is indicated for x and y. This will induce a slight smoothing of any curve generated from a transect. The curve may be saved from the same transect on the unfiltered dataset.
- To improve the visibility of distribution patterns, the contrast is adjusted on the maps, thus not displaying the full range of concentrations recorded in the scan. Numbers cited in the text have been directly measured on the scans, with the full range of concentrations.

K emission lines.

- For elements which $K\alpha < 17$ keV, the detectors capture the K emission lines within the remitted fluorescent light: Ca, Zn, Sr, Cu, Fe, Mn.
- Data are fitted and calibrated, and were processed (open .nxs, colormap, 2D Gauss filter) in HDIP.

L emission lines.

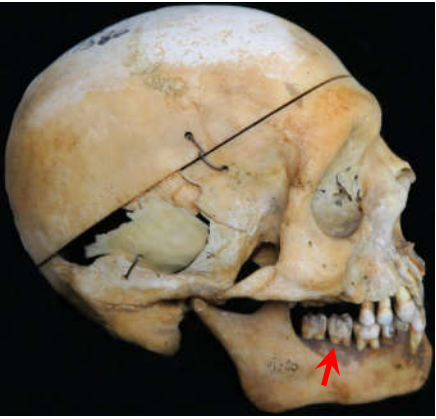
- For elements which $K\alpha > 17$ keV, the detectors only capture the L emission lines within the remitted fluorescent light: Pb and Ba.
- For these elements, data were NOT calibrated.
- For each element, the 32 bit images from Detector 0 and Detector 2 were added in Image J (Process> Image Calculator), and then filtered using a Gaussian blur (Process> Filters> Gaussian blur) with a kernel size of 0.7-0.9.

Romania – R1386 LRM2

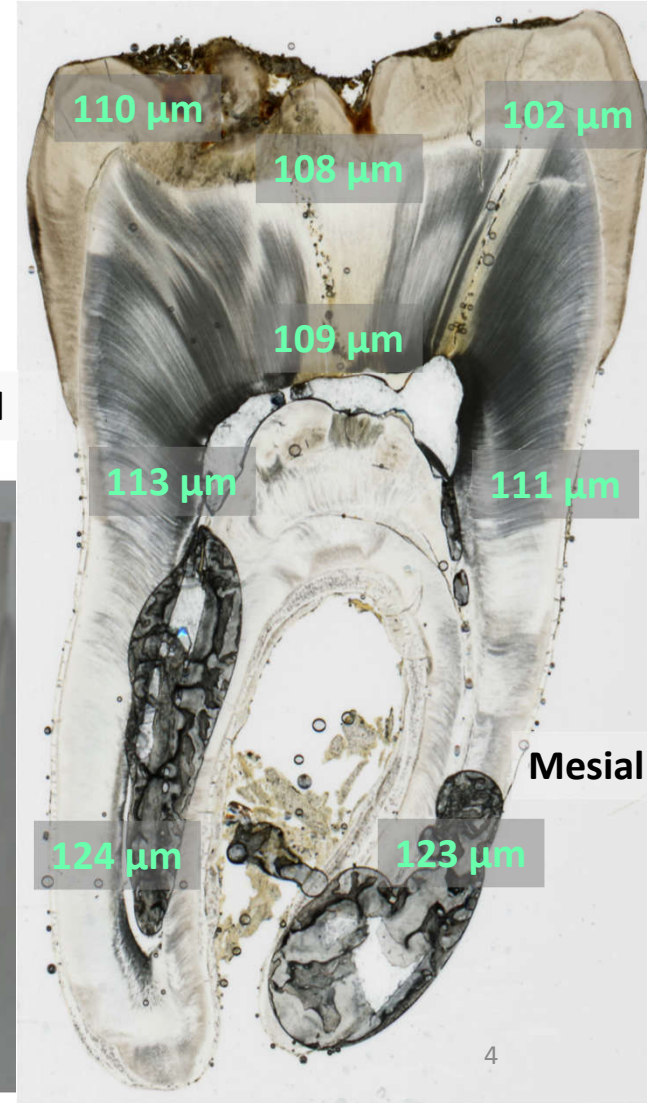


36 yrs. 1890 – 1926 CE

Blacksmith deceased in Colentina Hospital (Bucharest)

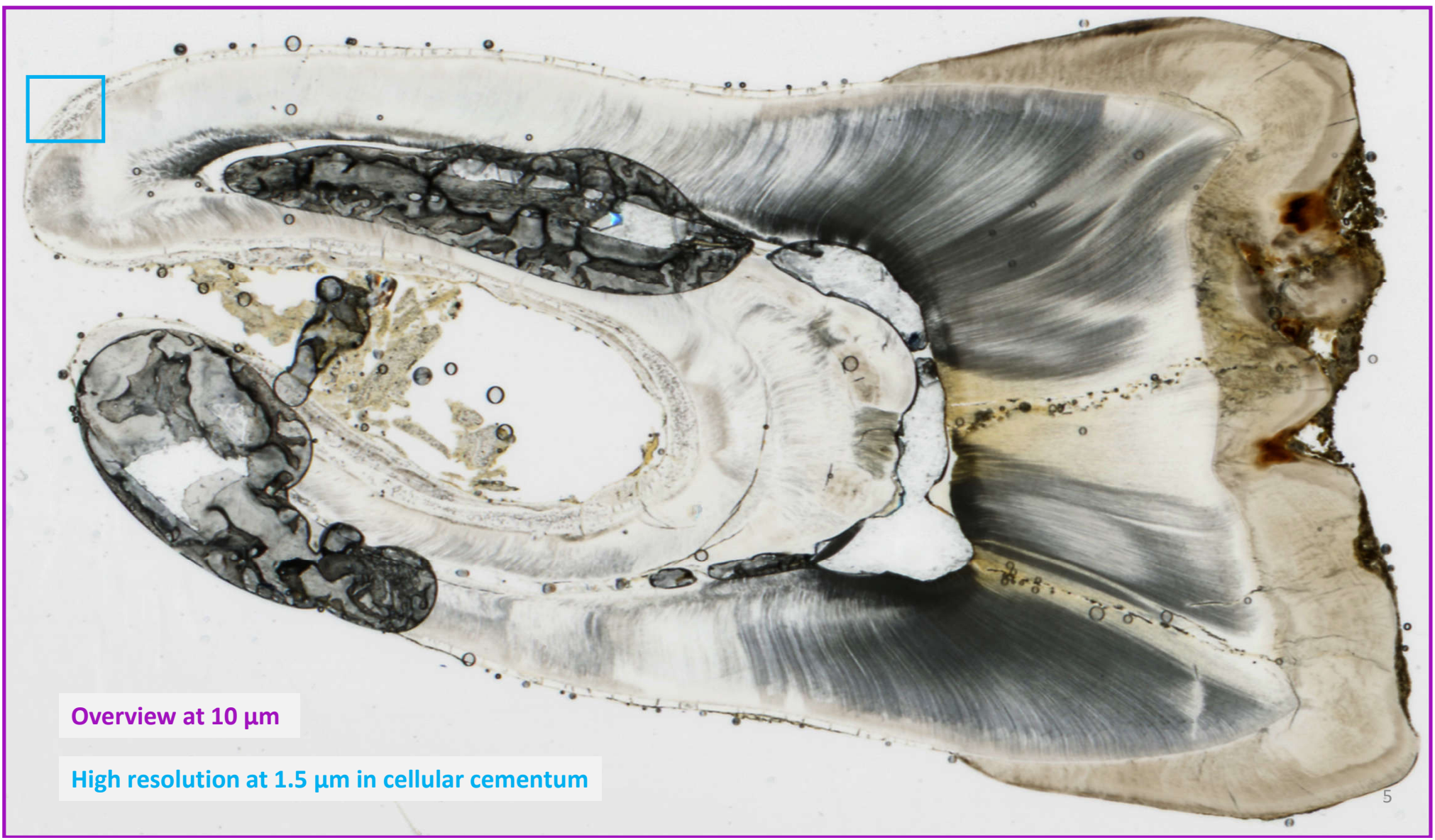


Average tooth section thickness (μm): 112.5



R1386 LRM2

Scanning



Overview at 10 μm

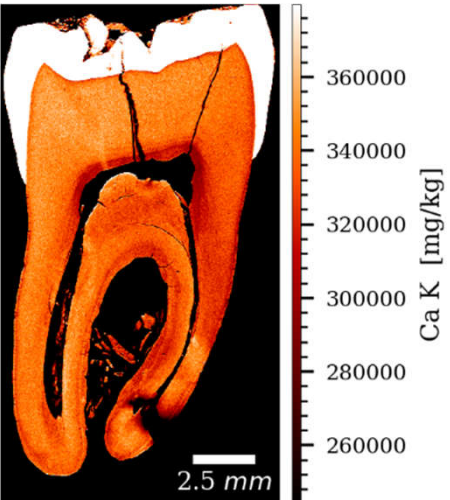
High resolution at 1.5 μm in cellular cementum

R1386 LRM2

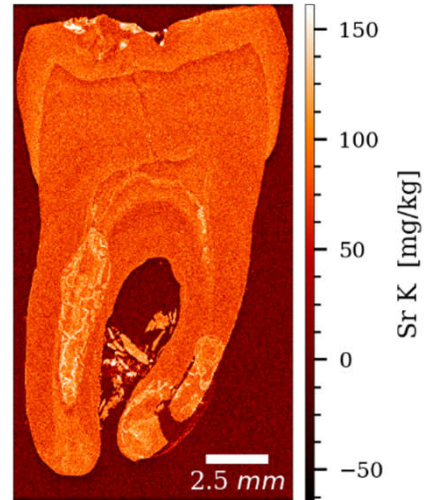
Overview at 10 μ m

Gauss (1x1)

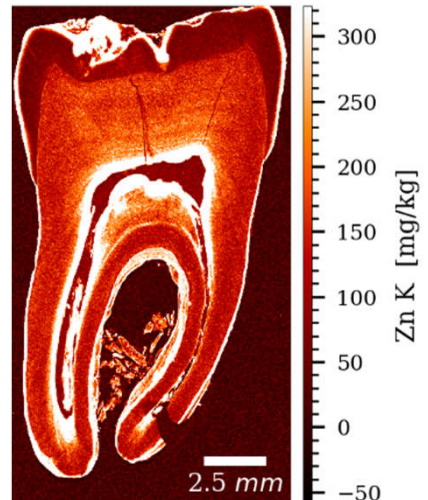
Ca K (Optimised for dentine)



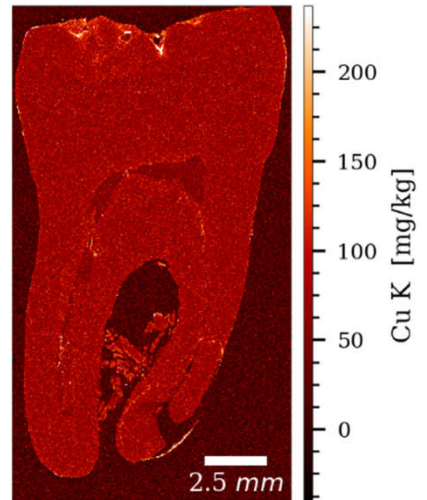
Sr K



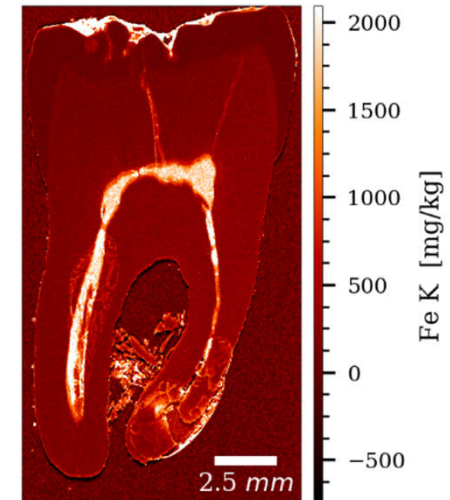
Zn K



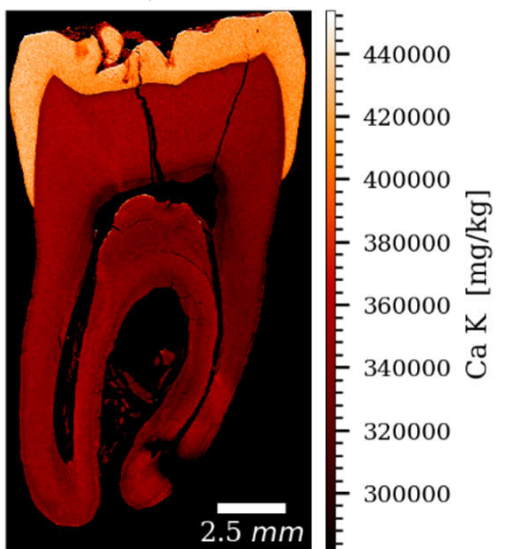
Cu K



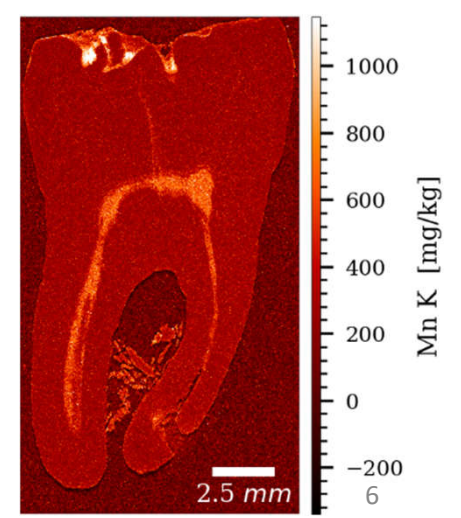
Fe K



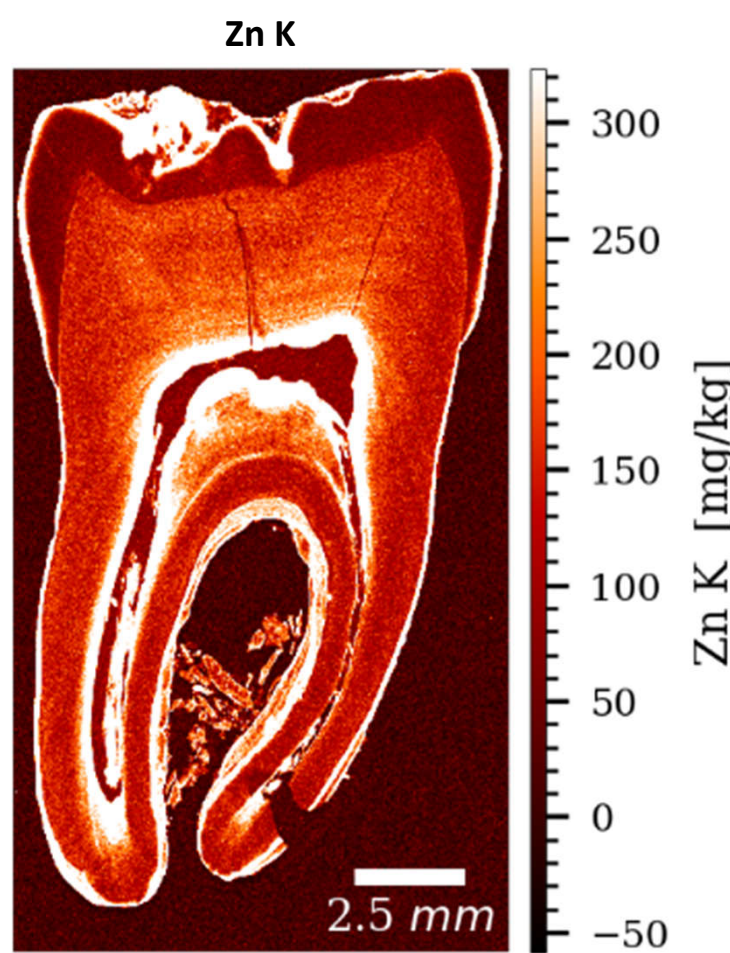
Ca K (Optimised for enamel)



Mn K

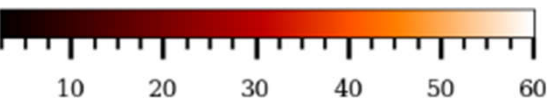
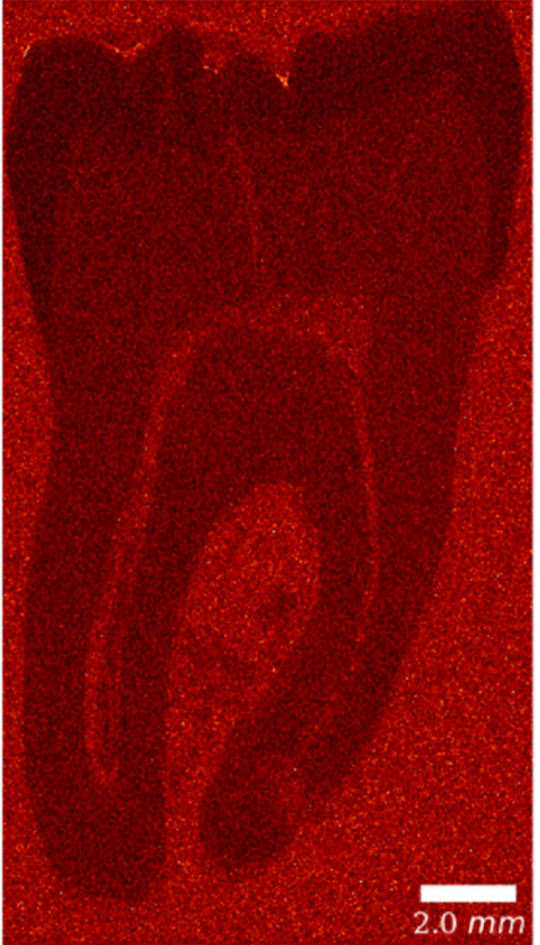


Close-ups for elemental variations in the dentine



R1386 LRM2

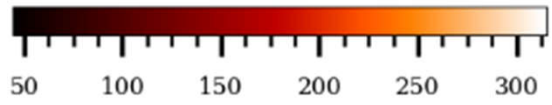
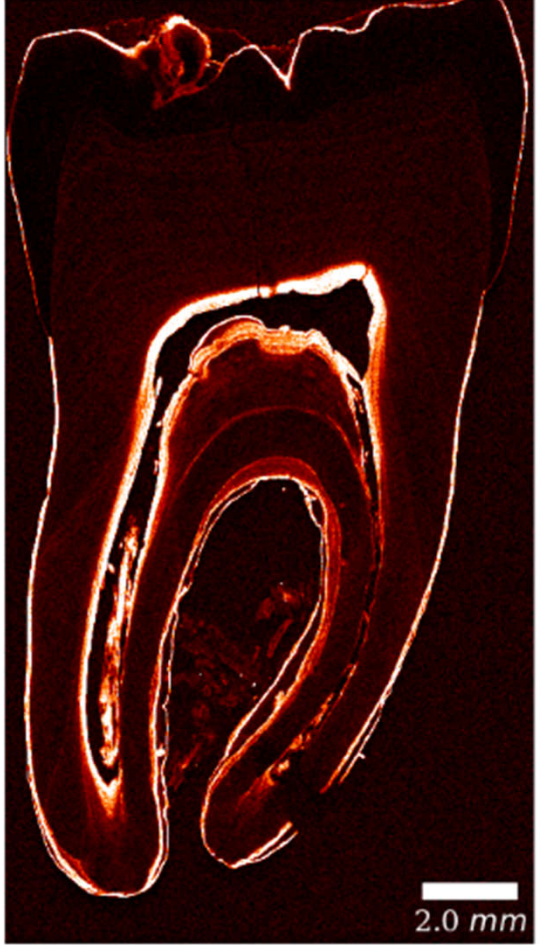
Br K



Br K [a.u.]

Overview at 10 μ m

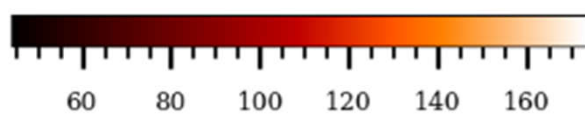
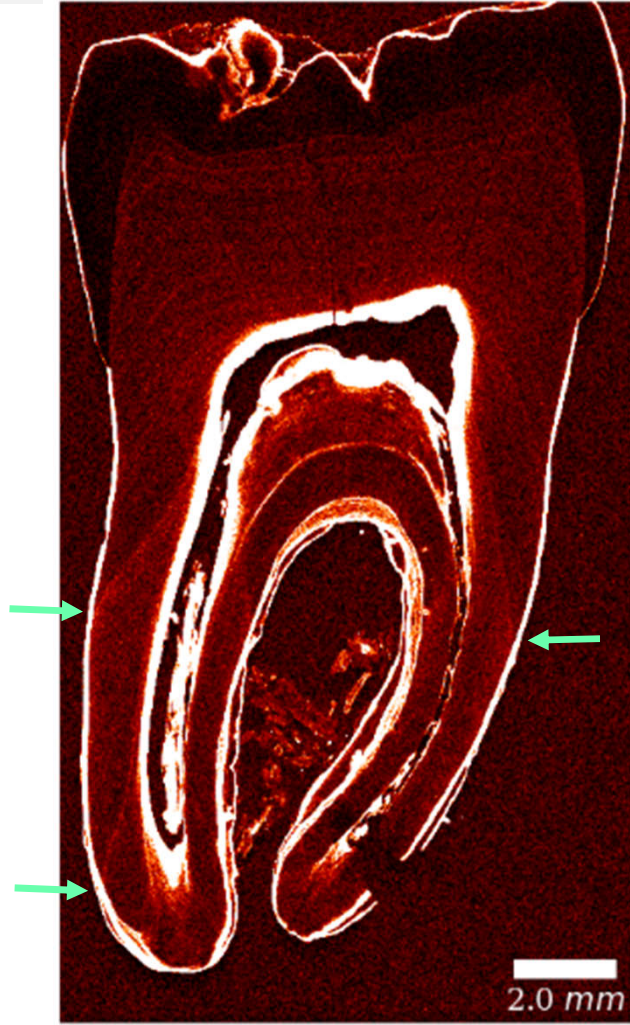
Pb L



Pb L [a.u.]

Optimised for cementum and secondary dentine

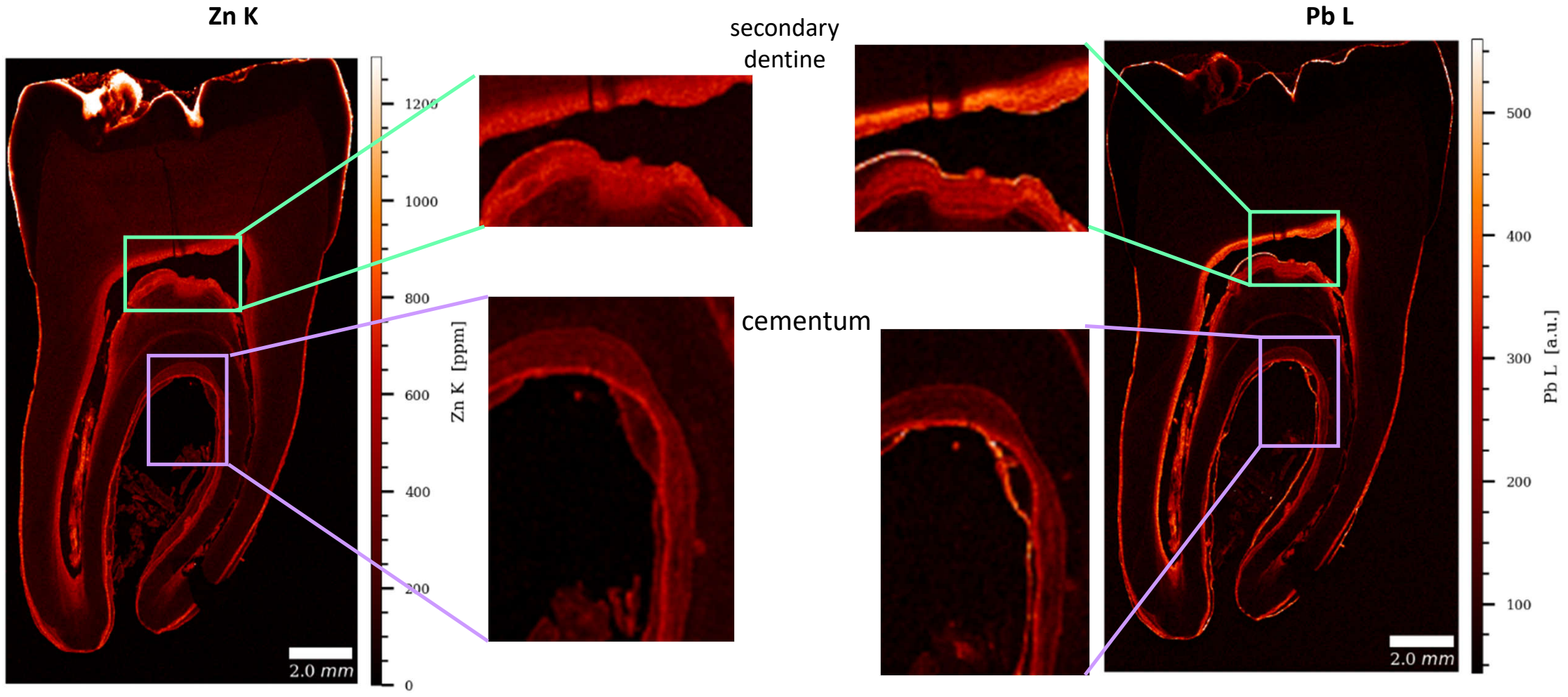
Uncalibrated data (arbitrary units) Gauss (1x1)



Pb L [a.u.]

- Optimised for primary dentine
- Significant increase in Pb at mid-root (~adolescence)

Close-ups for elemental variations in the cementum and secondary dentine

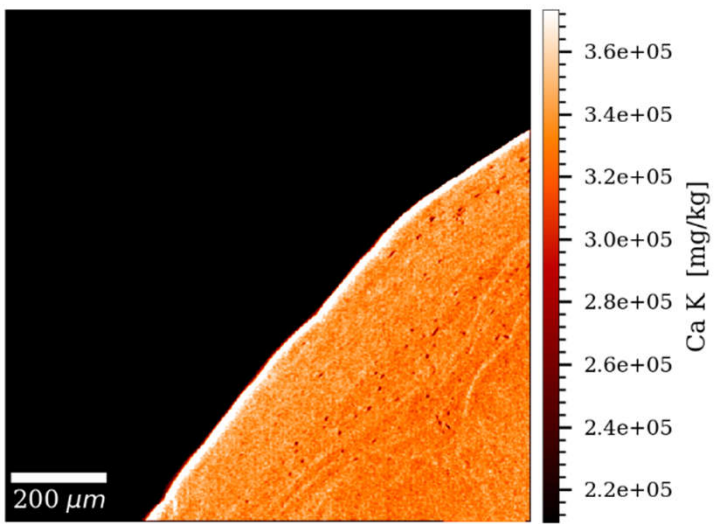


R1386 LRM2

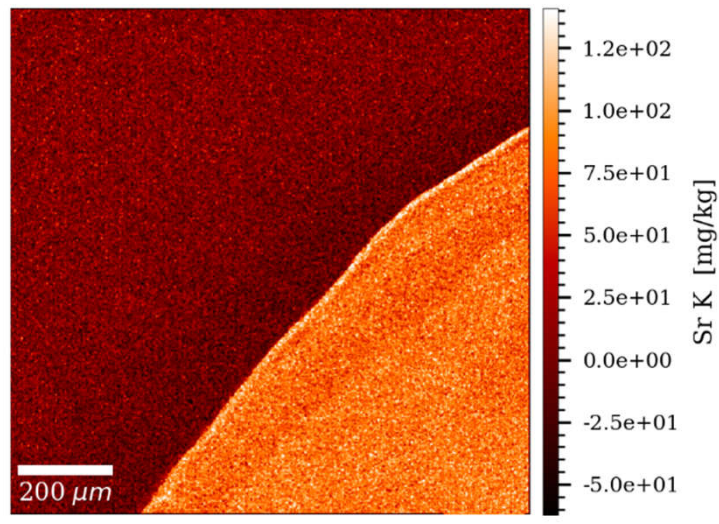
High resolution at 1.5 μm

Gauss (0.8x0.8)

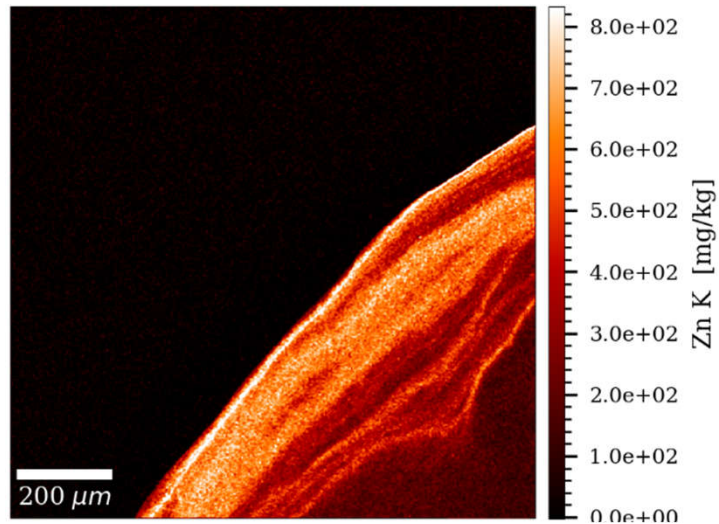
Ca K



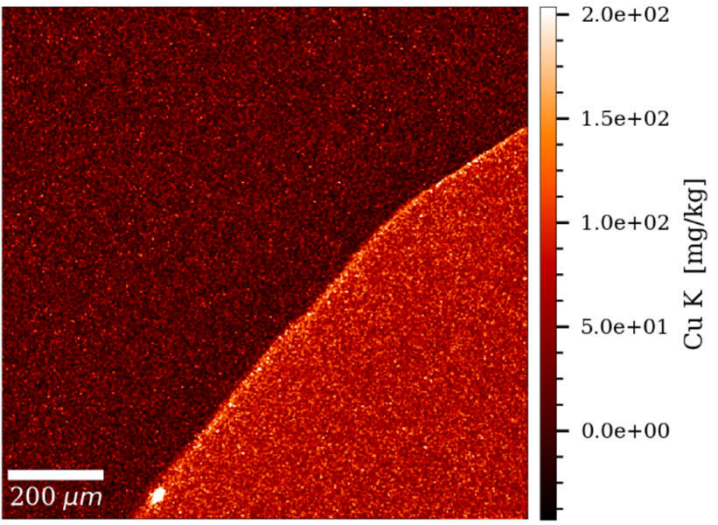
Sr K



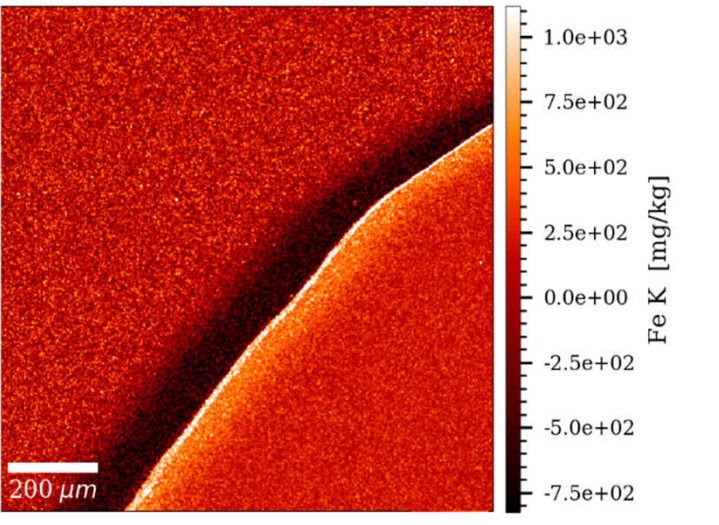
Zn K



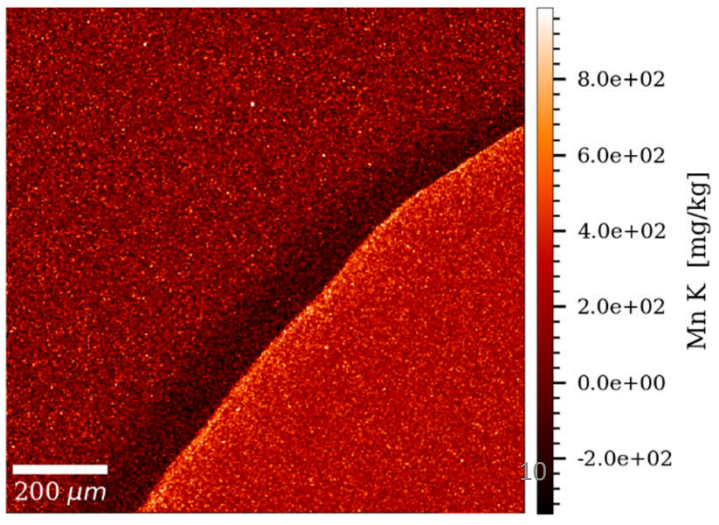
Cu K

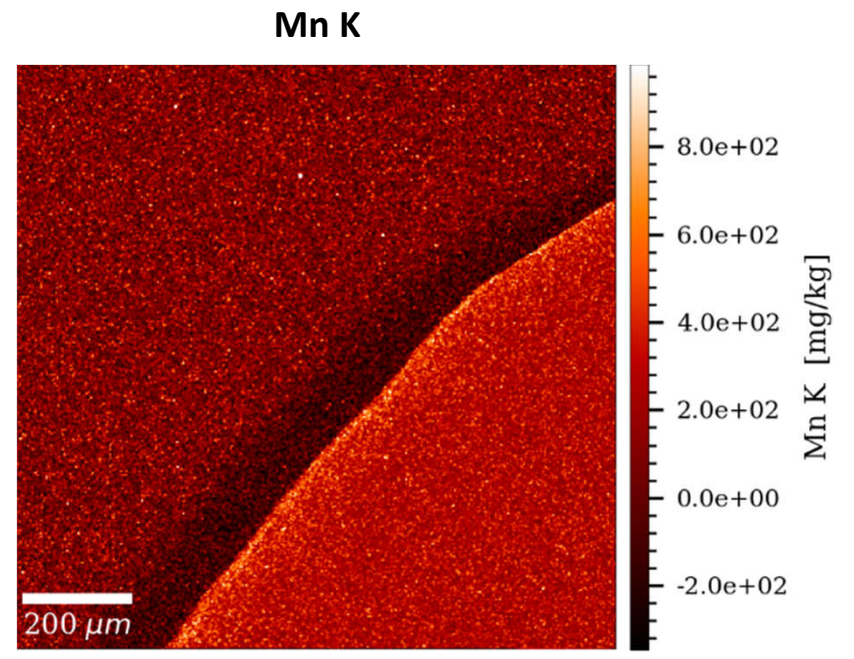
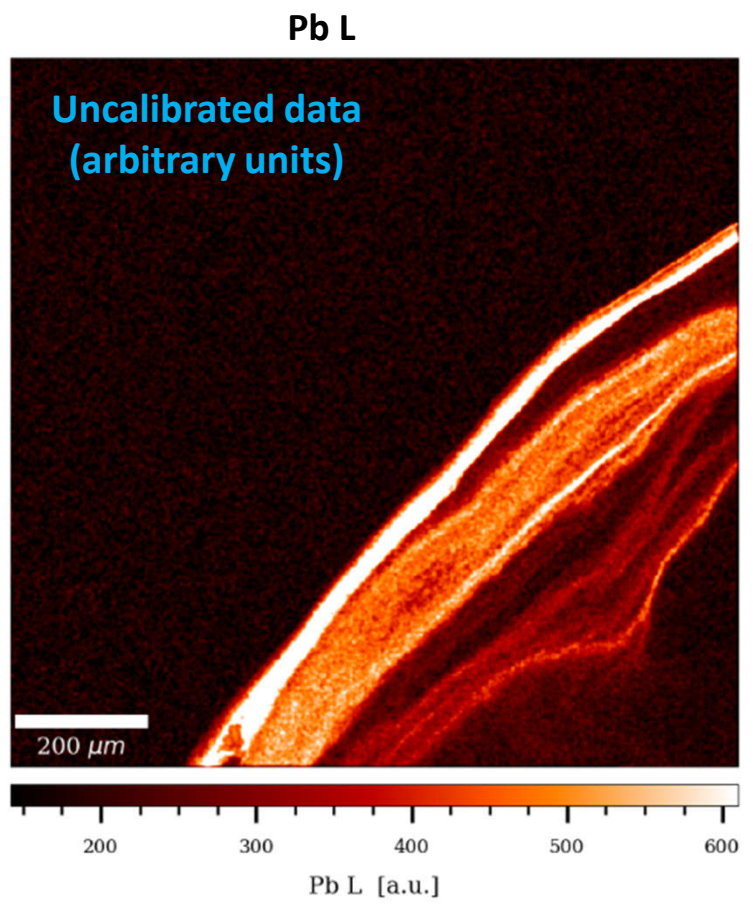


Fe K



Mn K





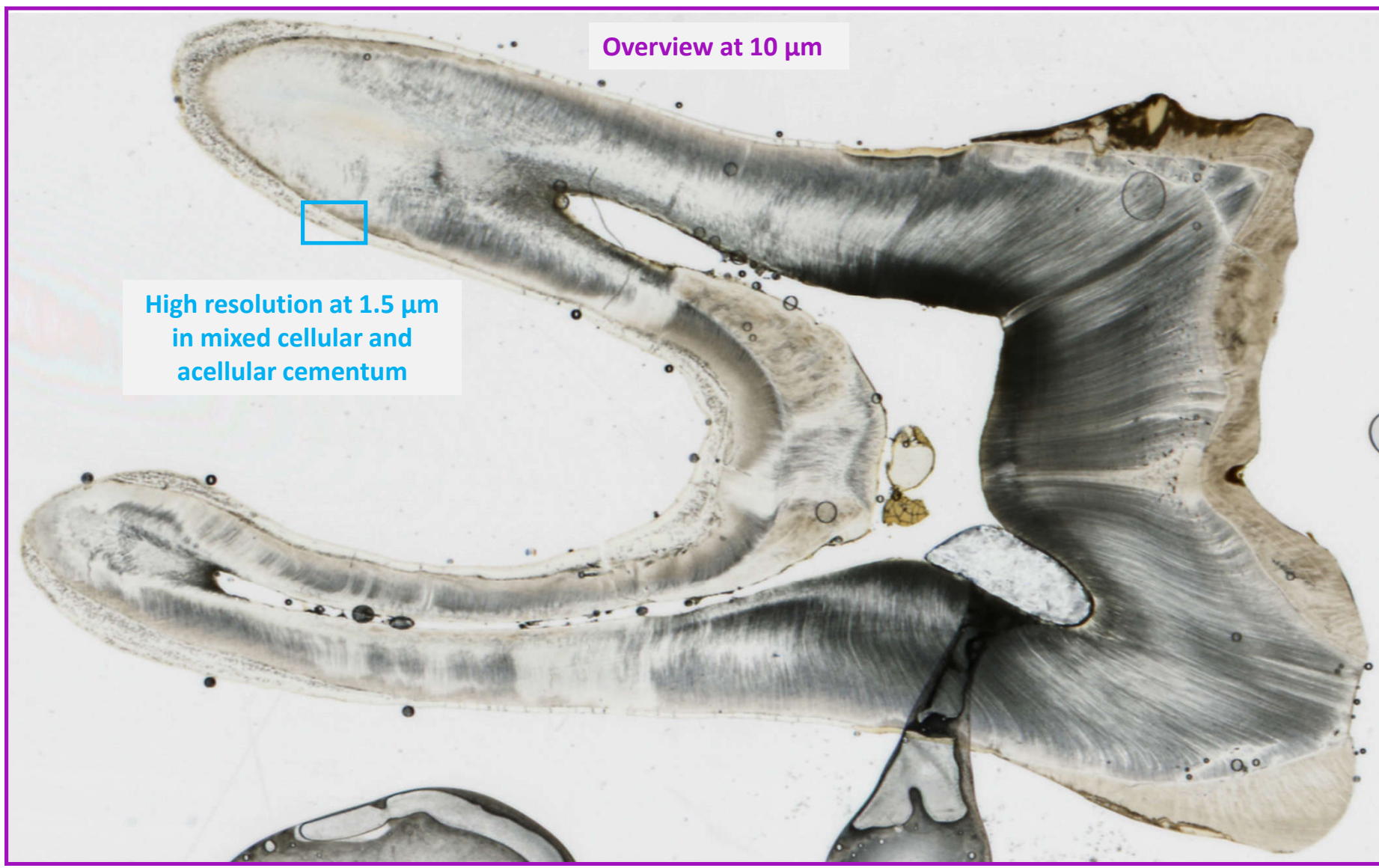
Romania – A1651 LRM1

♂ Beginning of 20th c.

Average tooth section thickness (μm): 121.75



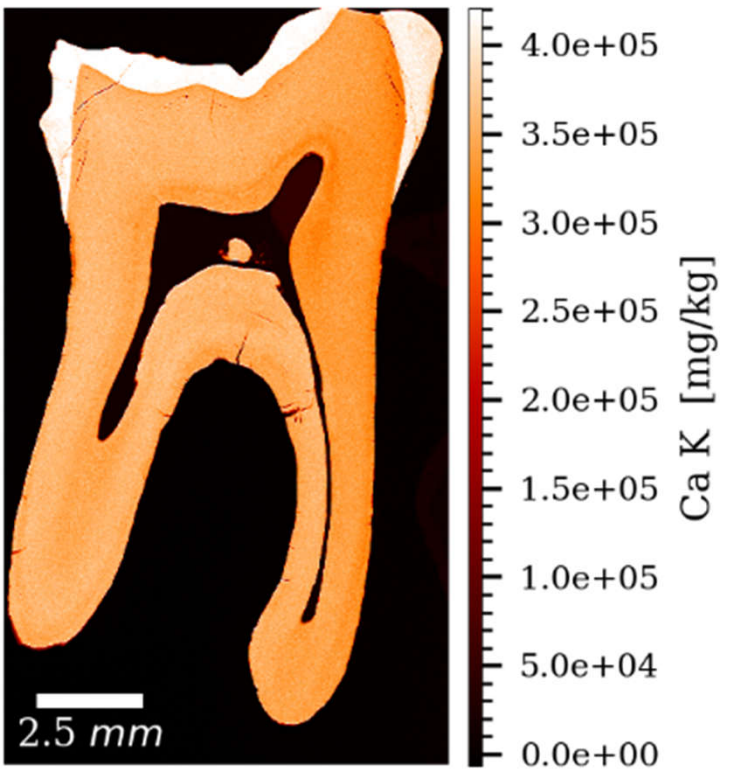
Scanning



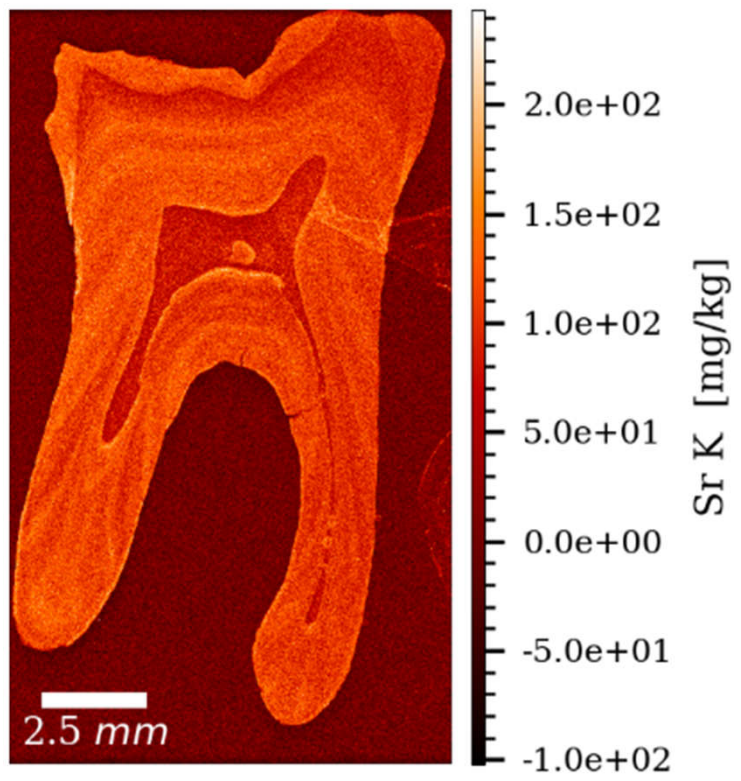
Overview at 10 μm

High resolution at 1.5 μm
in mixed cellular and
acellular cementum

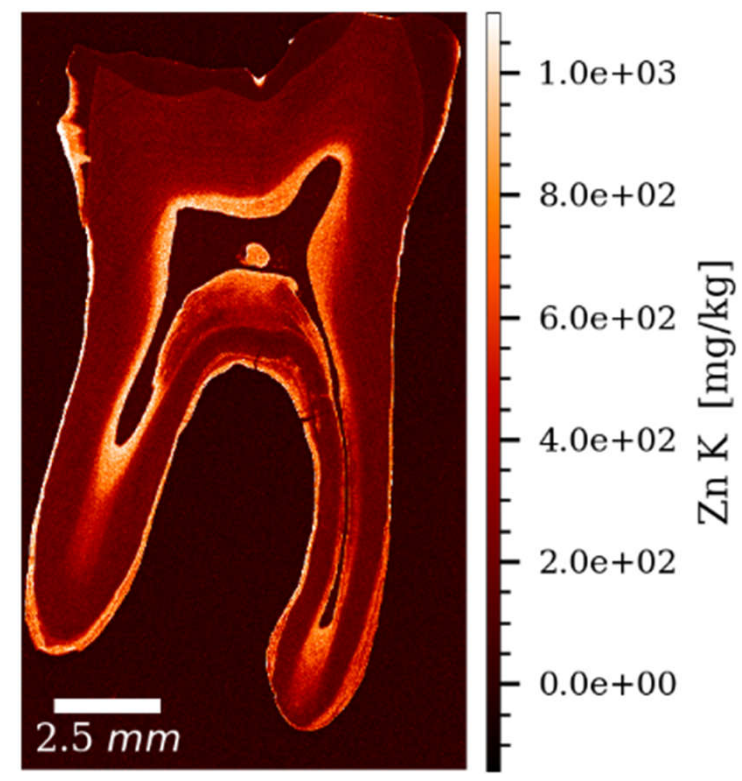
Ca K

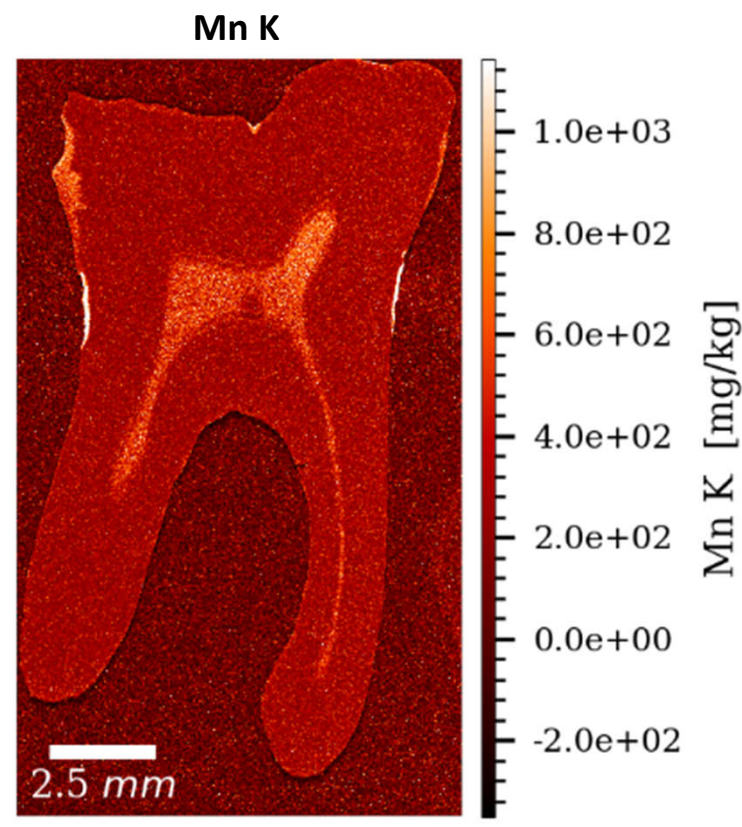
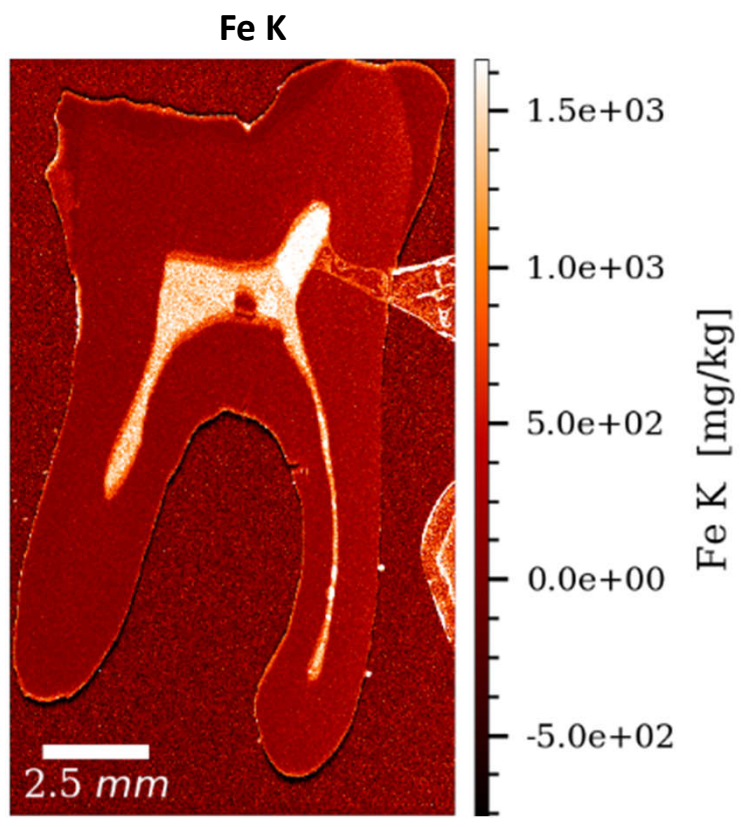
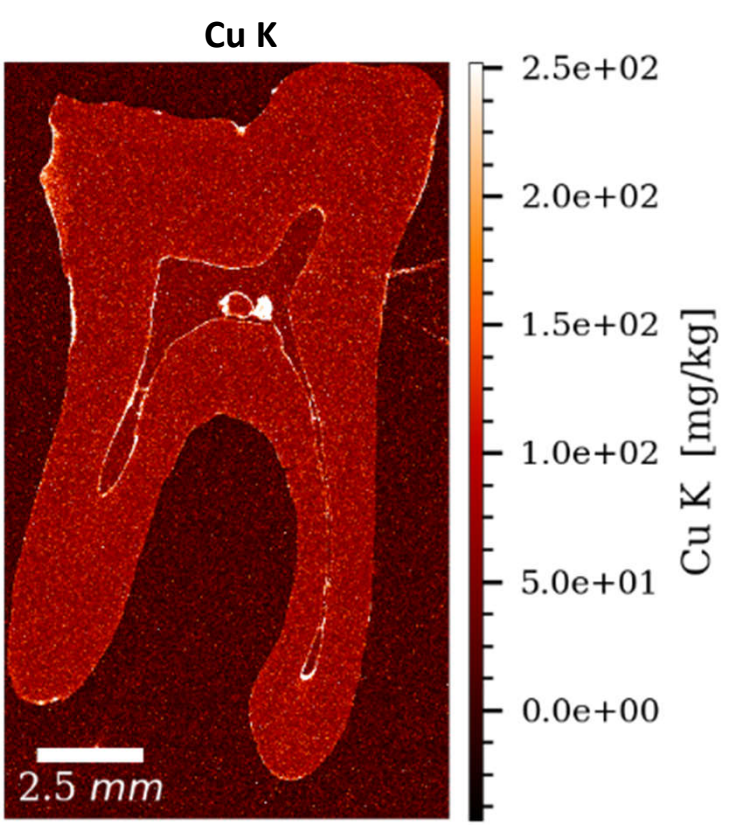


Sr K



Zn K





A1651 LRM1

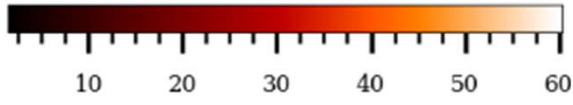
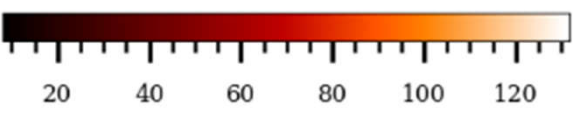
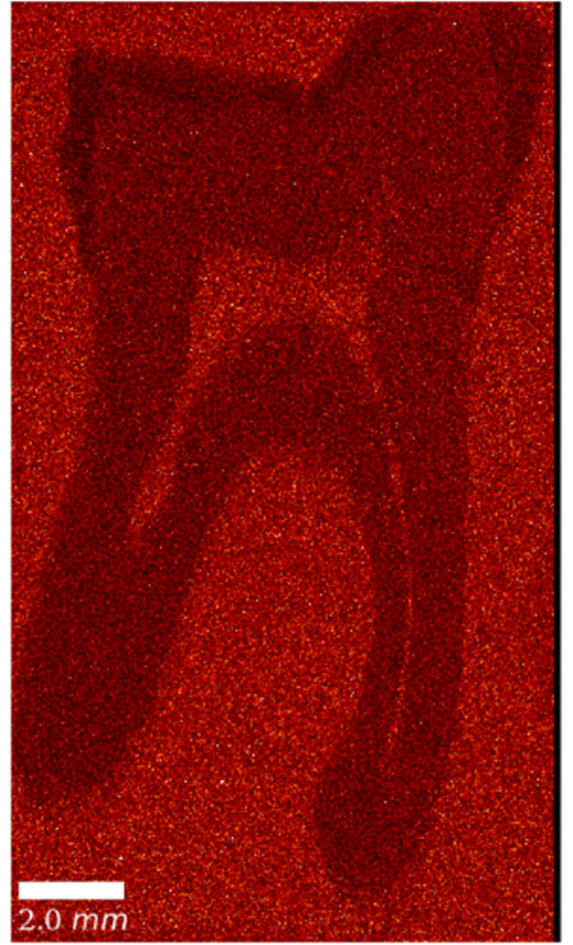
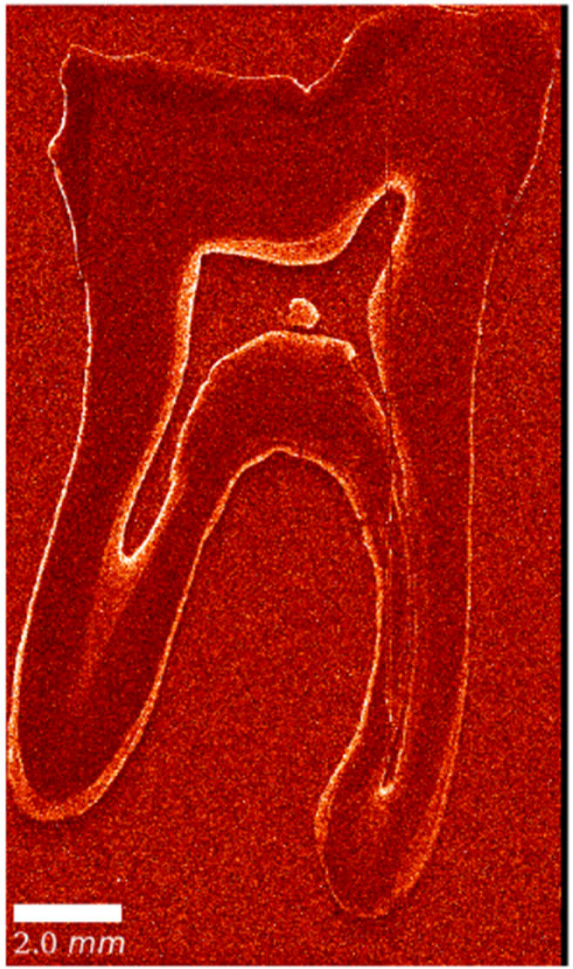
Overview at 10 μ m

Uncalibrated data
(arbitrary units)

Gauss (0.7x0.7)

Pb L

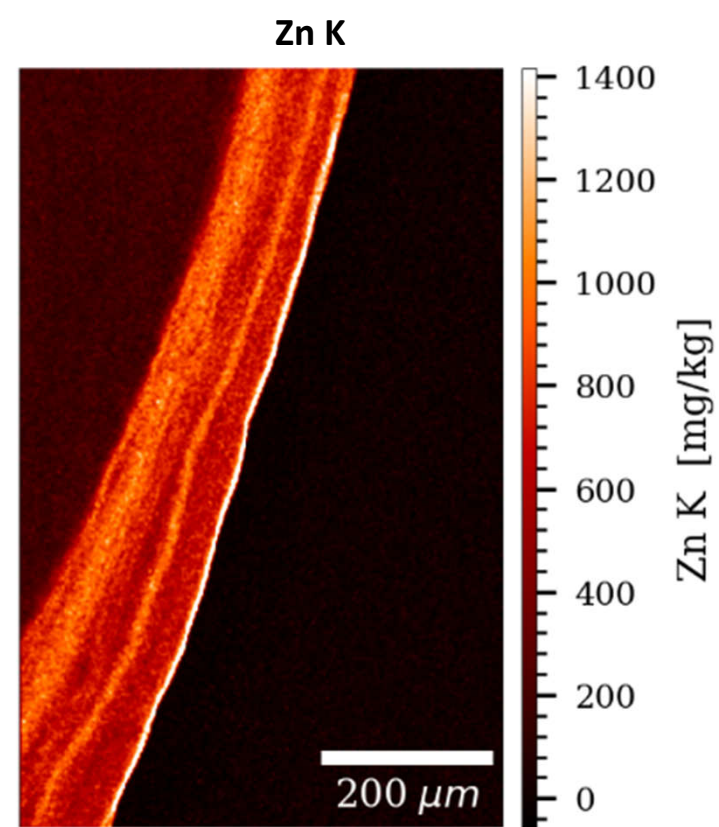
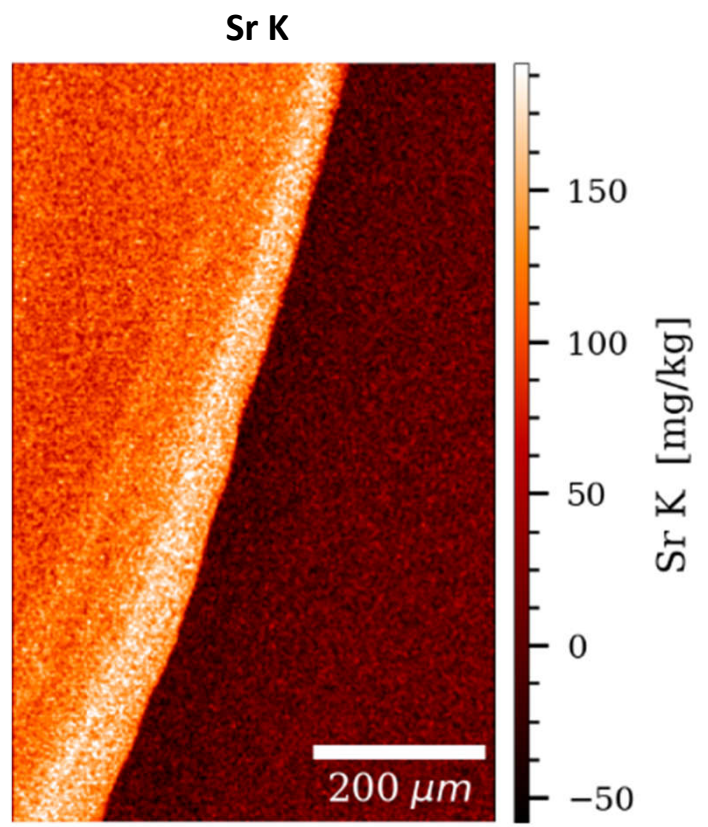
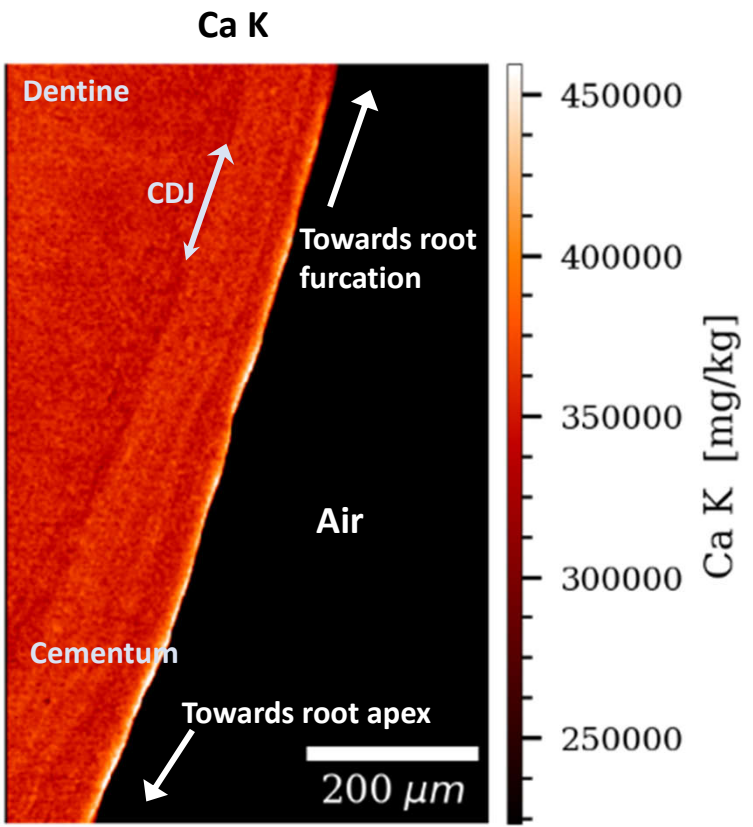
Br K

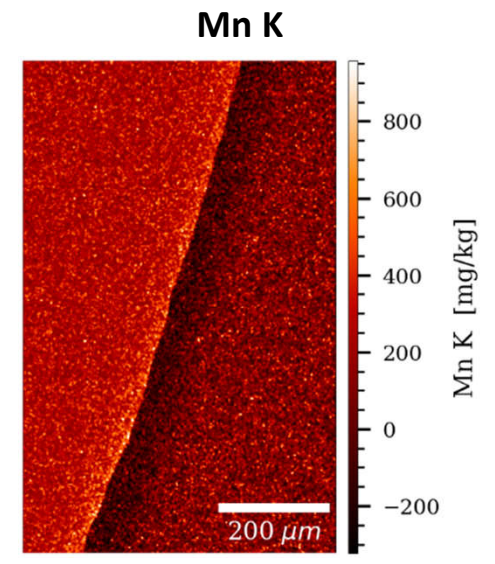
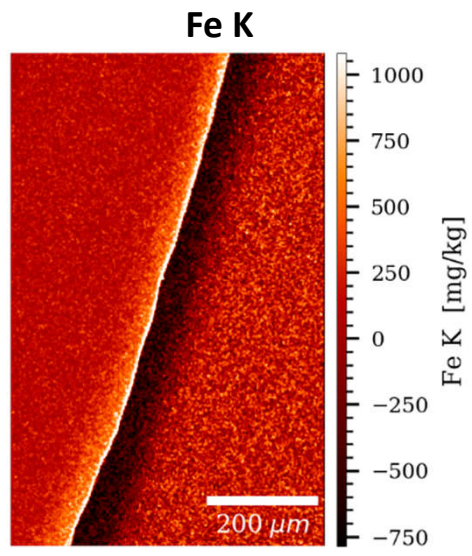
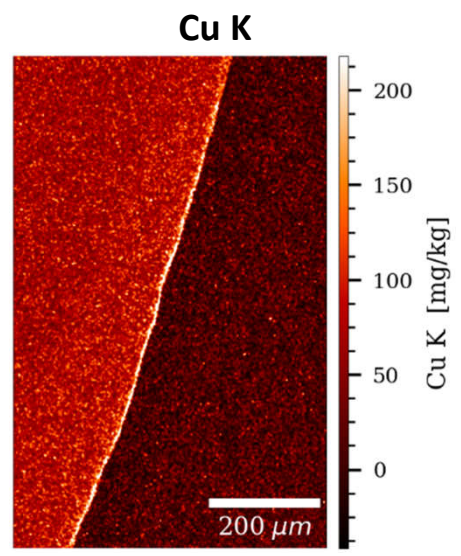


A1651 LRM1

High resolution at 1.5 μ m

Gauss (0.85 x 0.85)





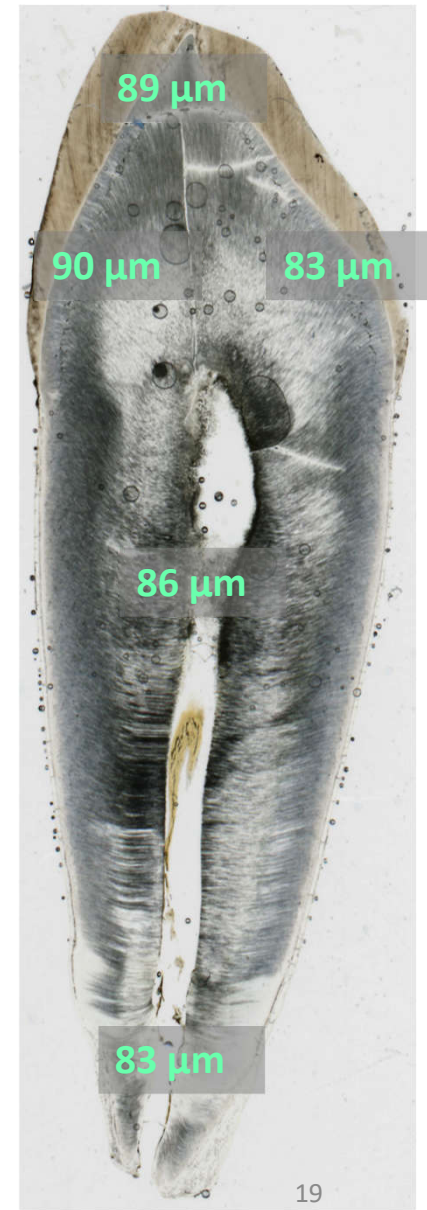


Romania – A1651 URC

♂ Beginning of 20th c.



Average tooth section thickness (μm): 86.2



A1651 URC

Scanning

Overview at 10 μm

High resolution at 1 μm in cellular cementum

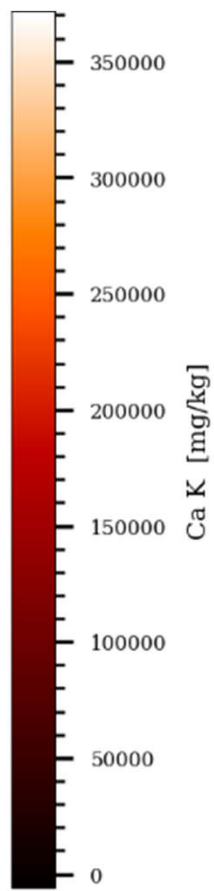


A1651 URC

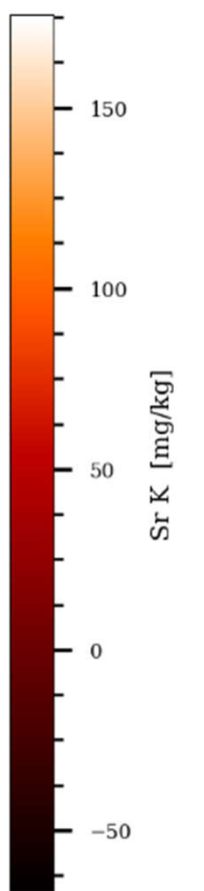
Overview at 10 μ m

Gauss (0.9x0.9)

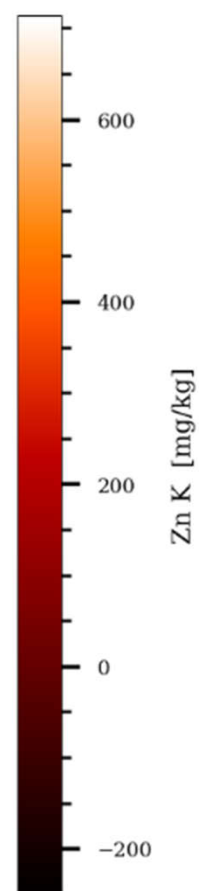
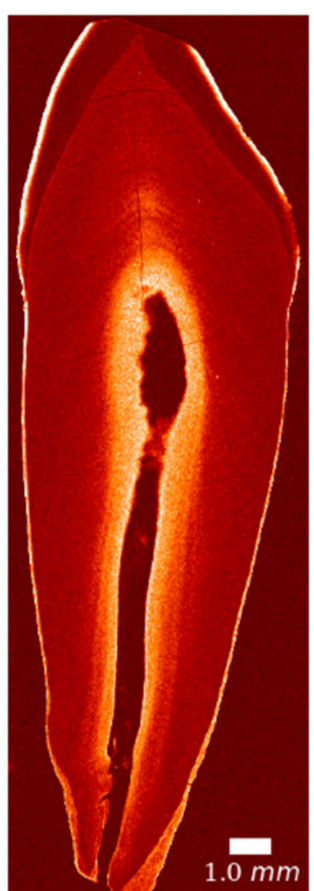
Ca K



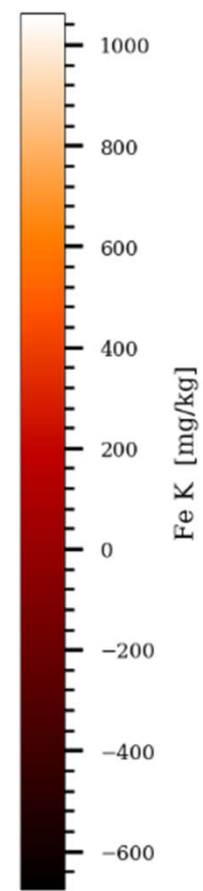
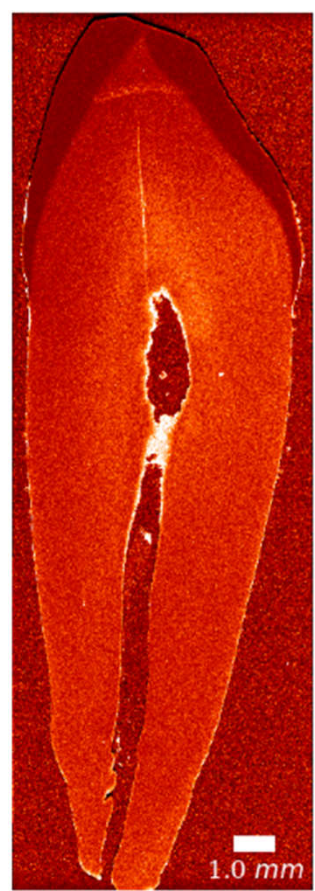
Sr K



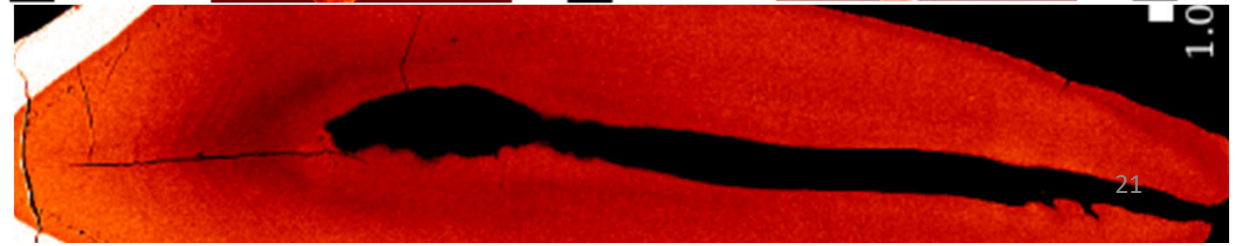
Zn K

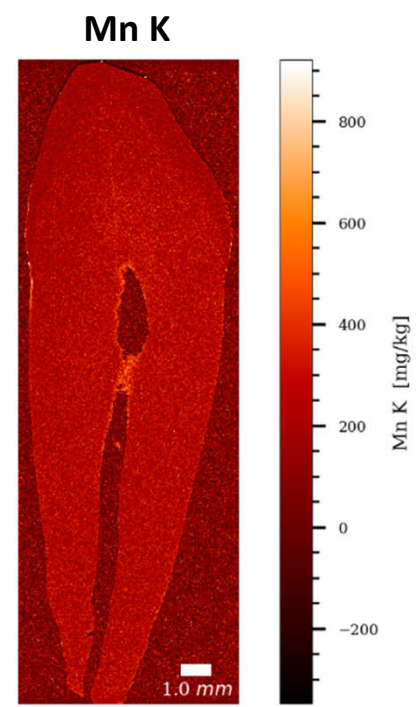
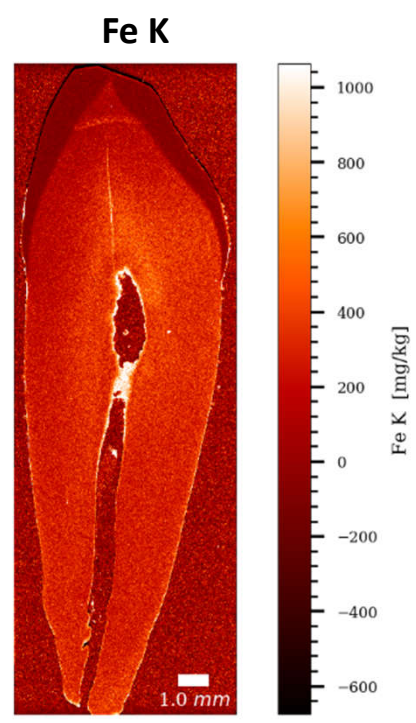
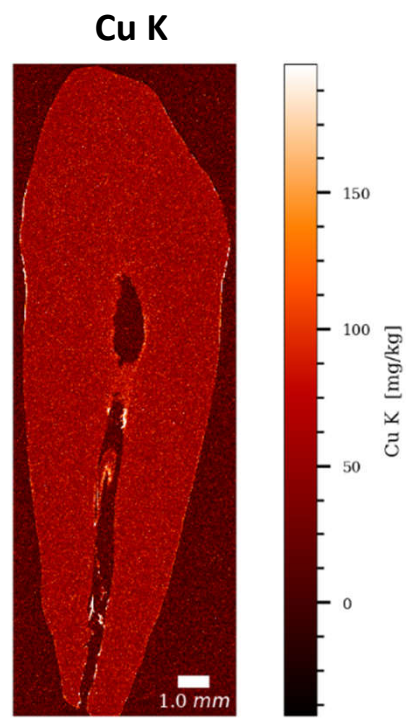


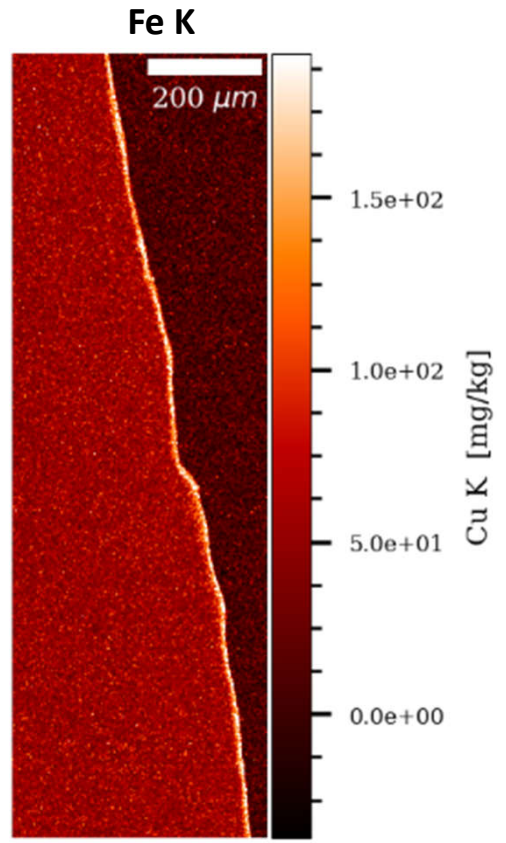
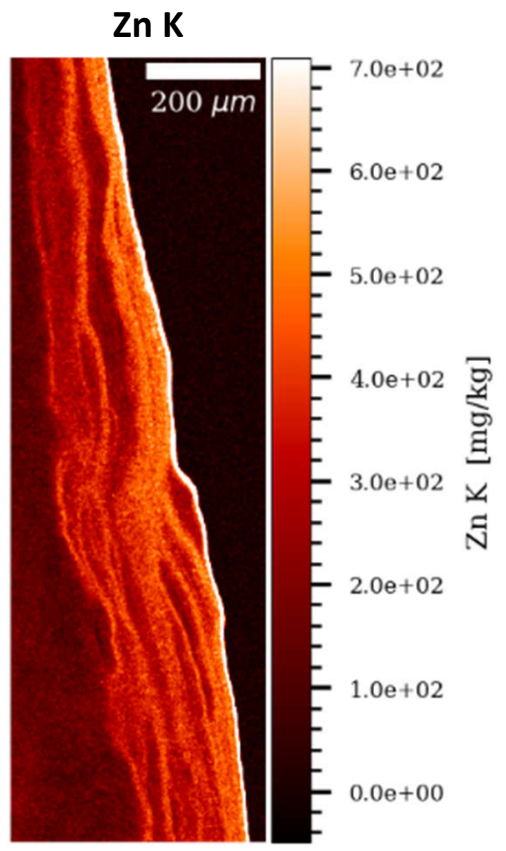
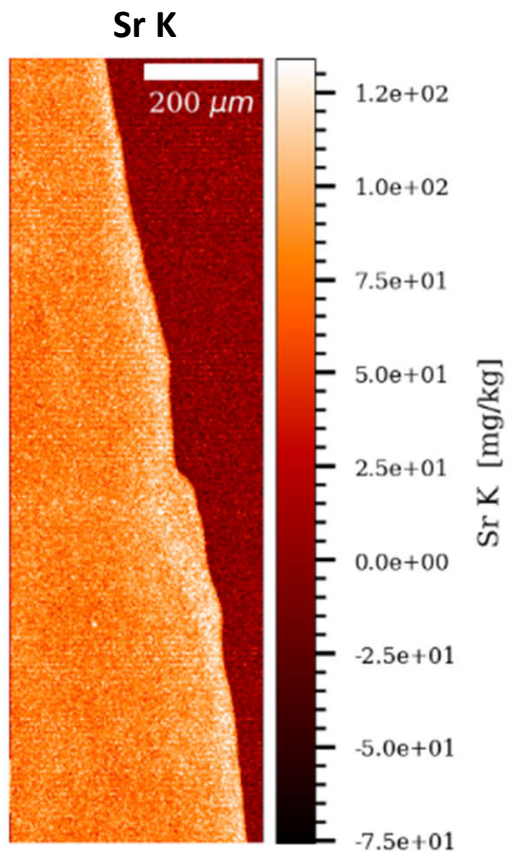
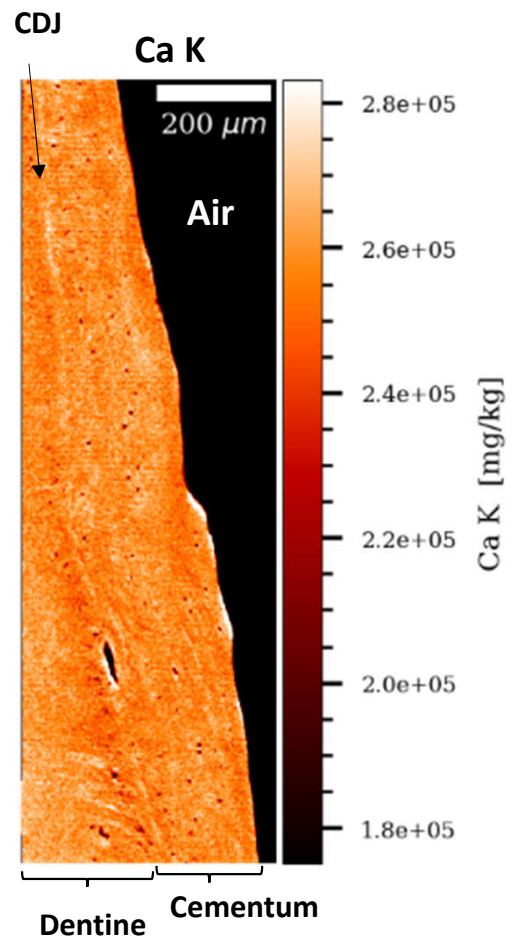
Fe K

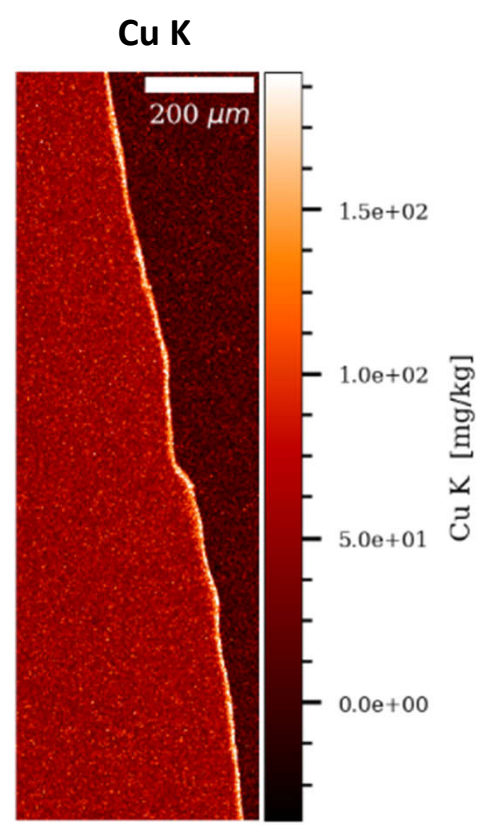
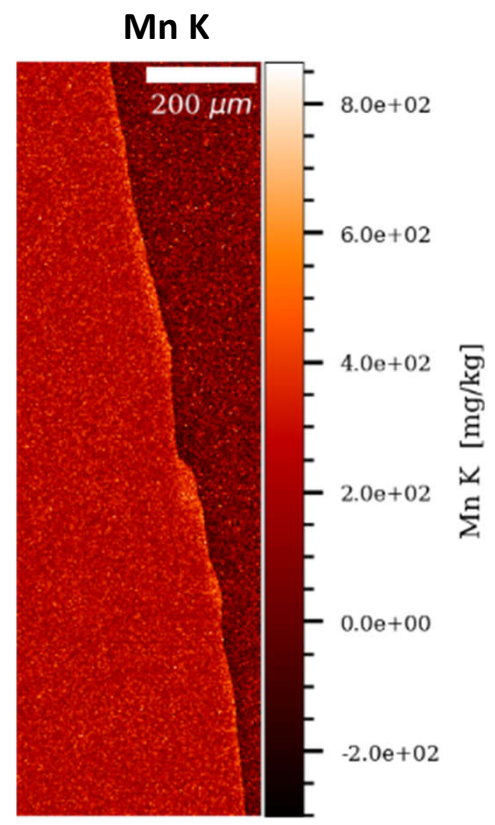


Ca K (optimised for dentine for elemental variations)





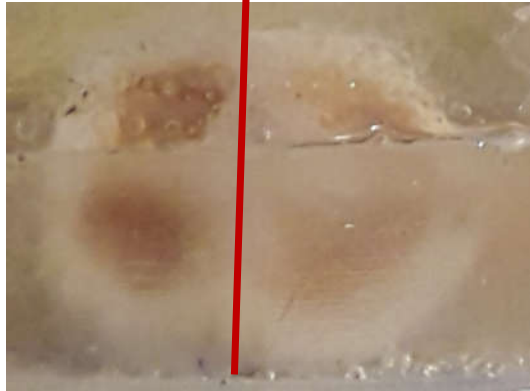




Odense – 533 LLM1

♀ 25-35 yrs. 1191 – 1269 cal. CE

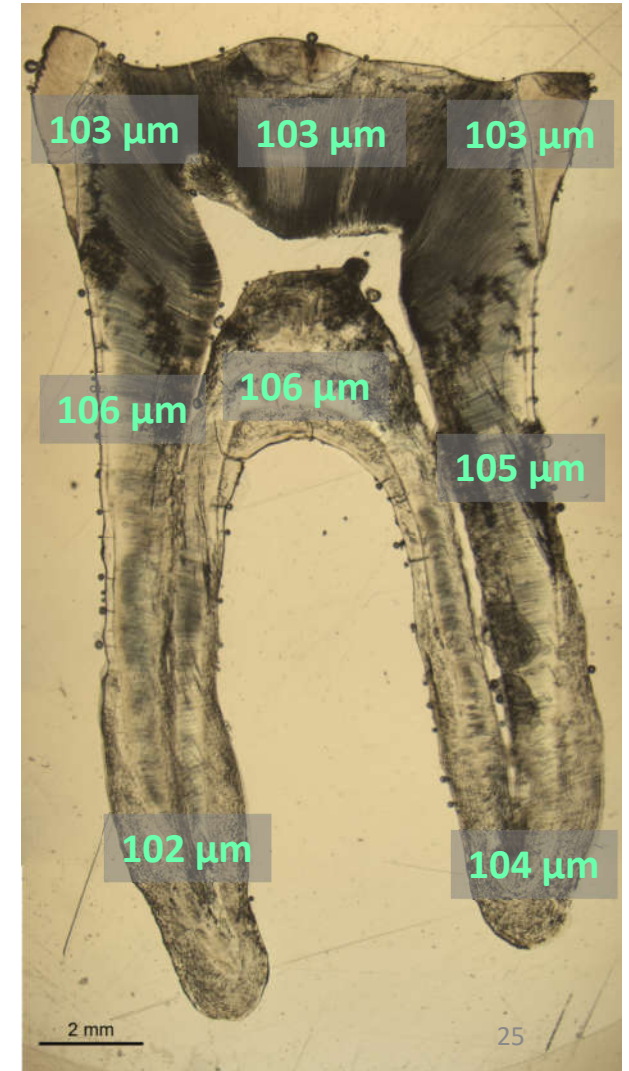
mesial



distal

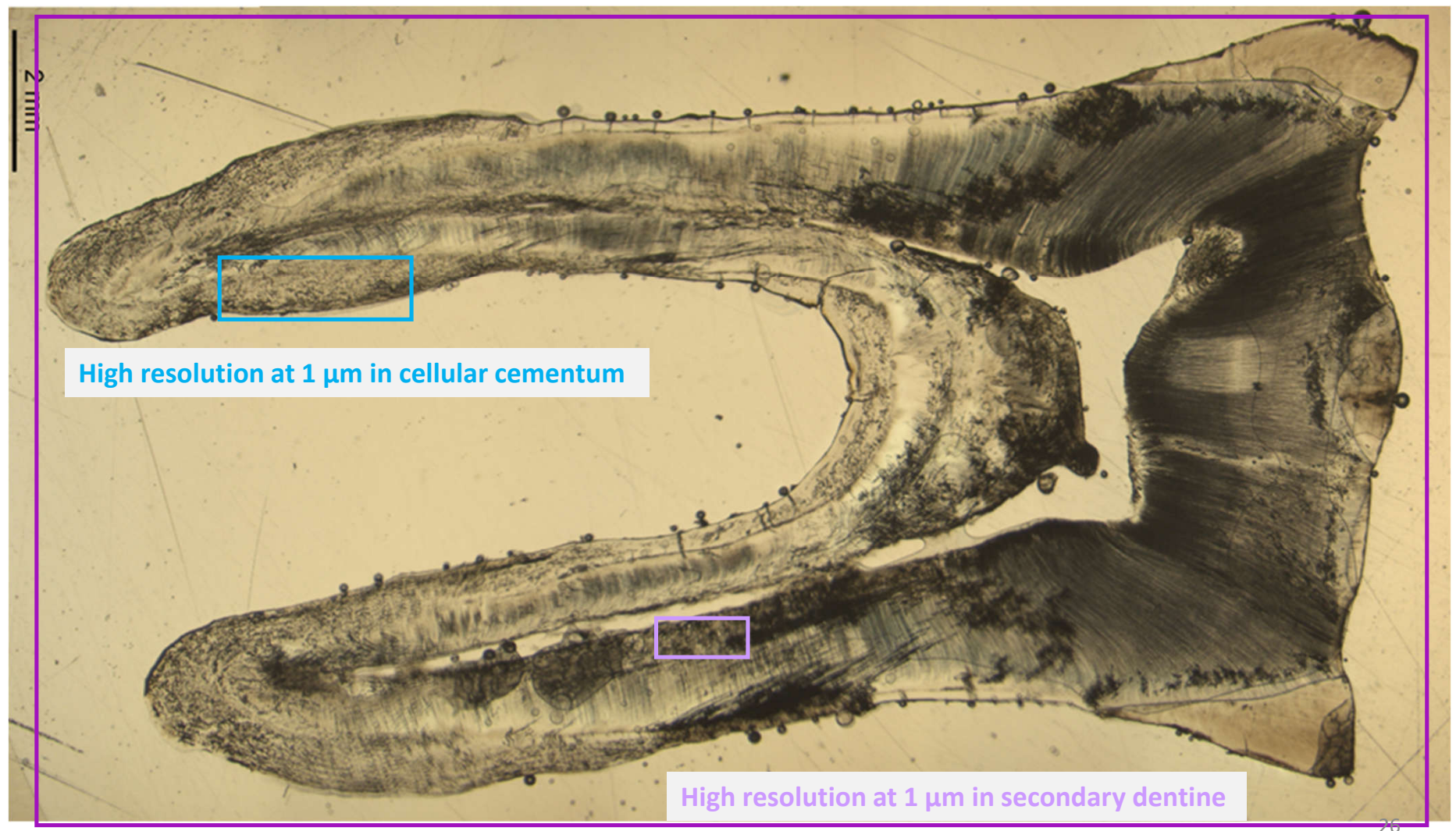


Average tooth section thickness (μm): 104.0



Scanning

Overview at 10 μ m



High resolution at 1 μ m in cellular cementum

High resolution at 1 μ m in secondary dentine

Odense 533 LLM1

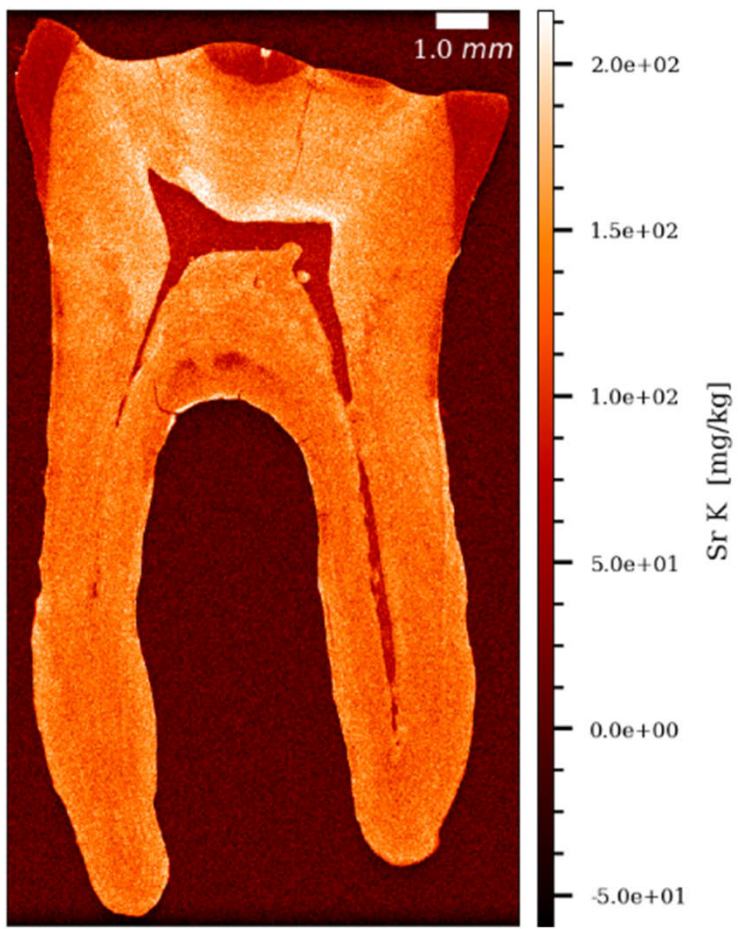
Overview at 10 μ m

Gauss (0.9x0.9)

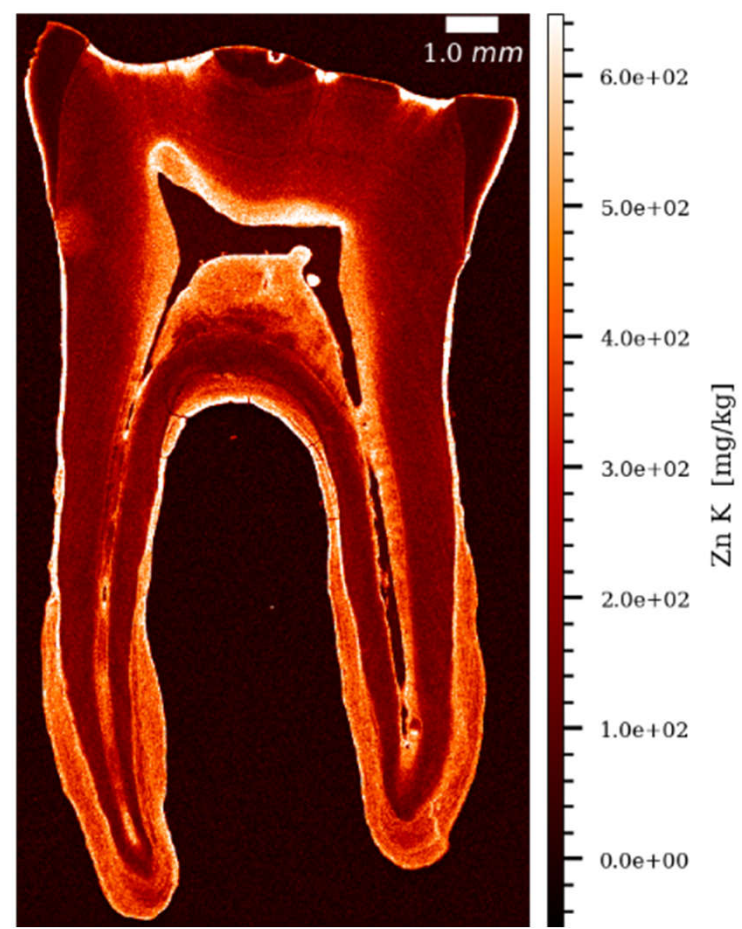
Ca K

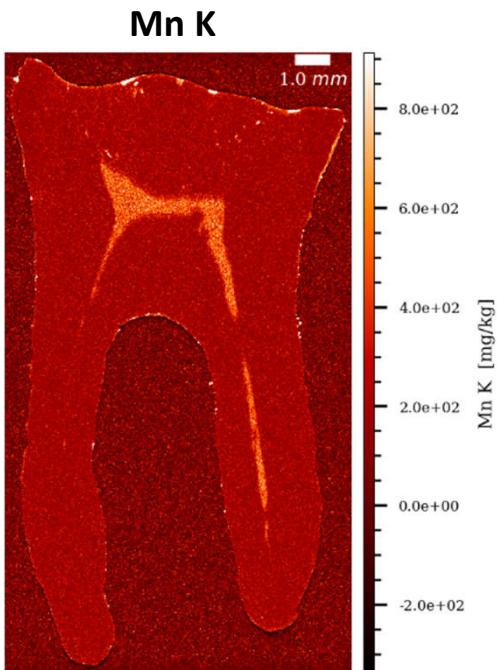
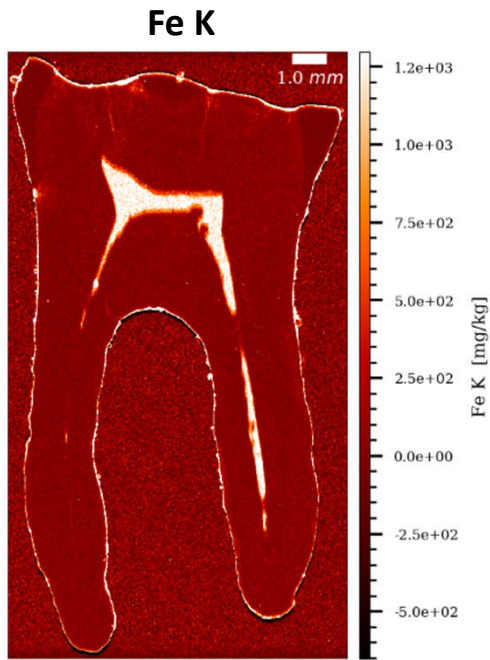
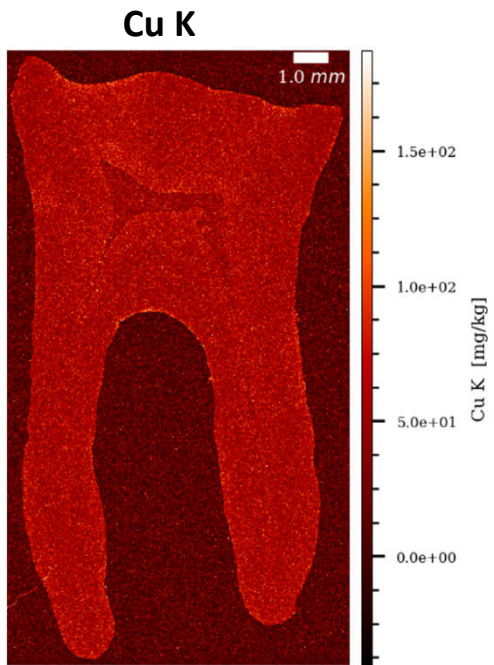


Sr K



Zn K

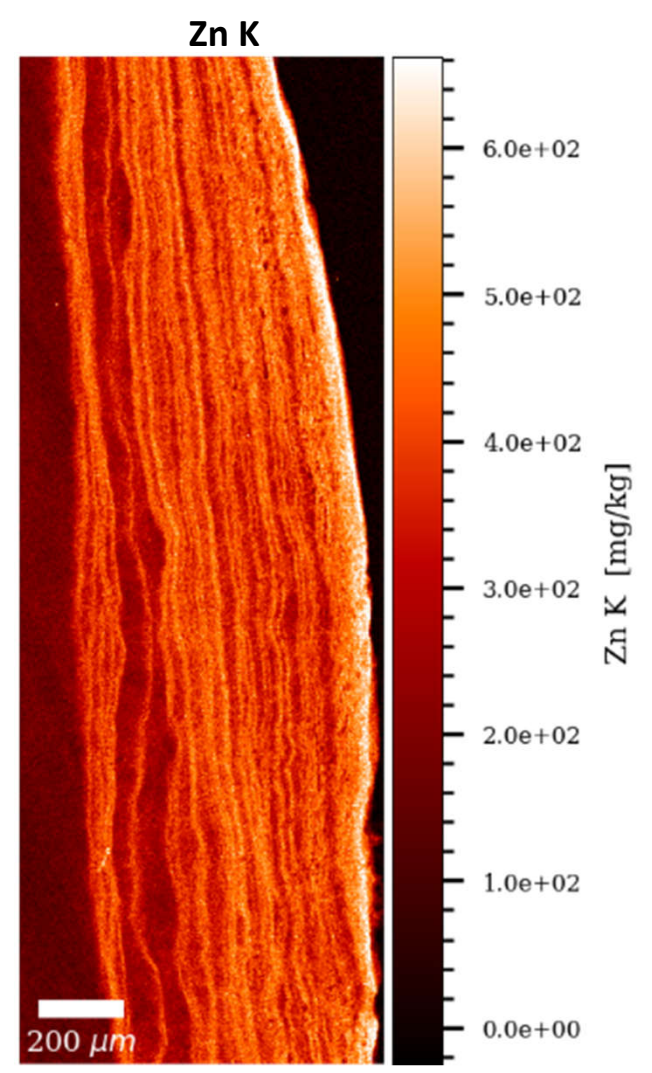
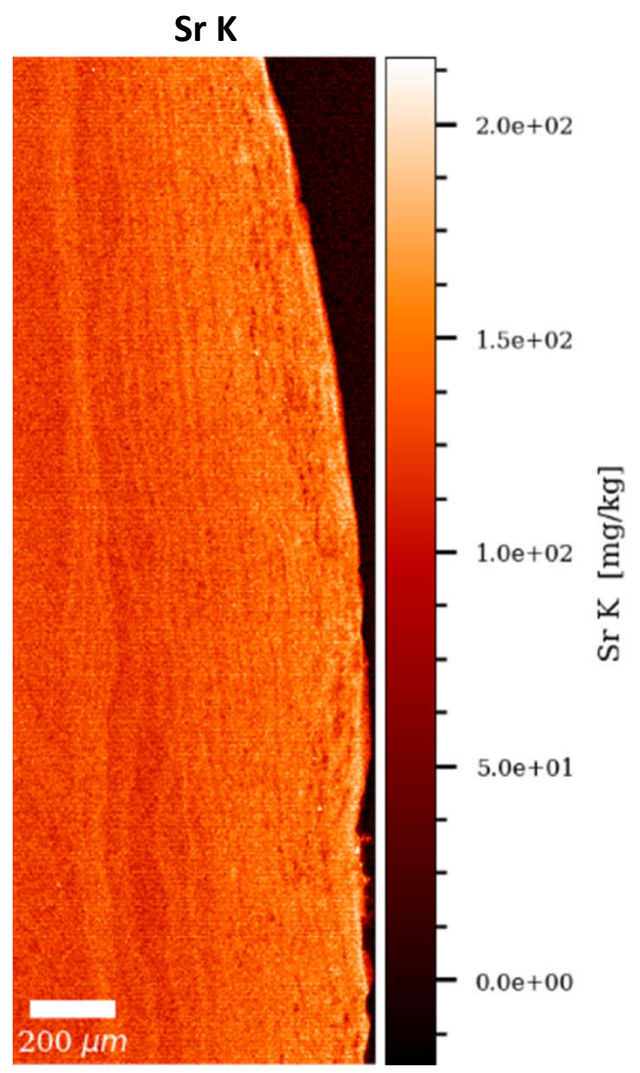
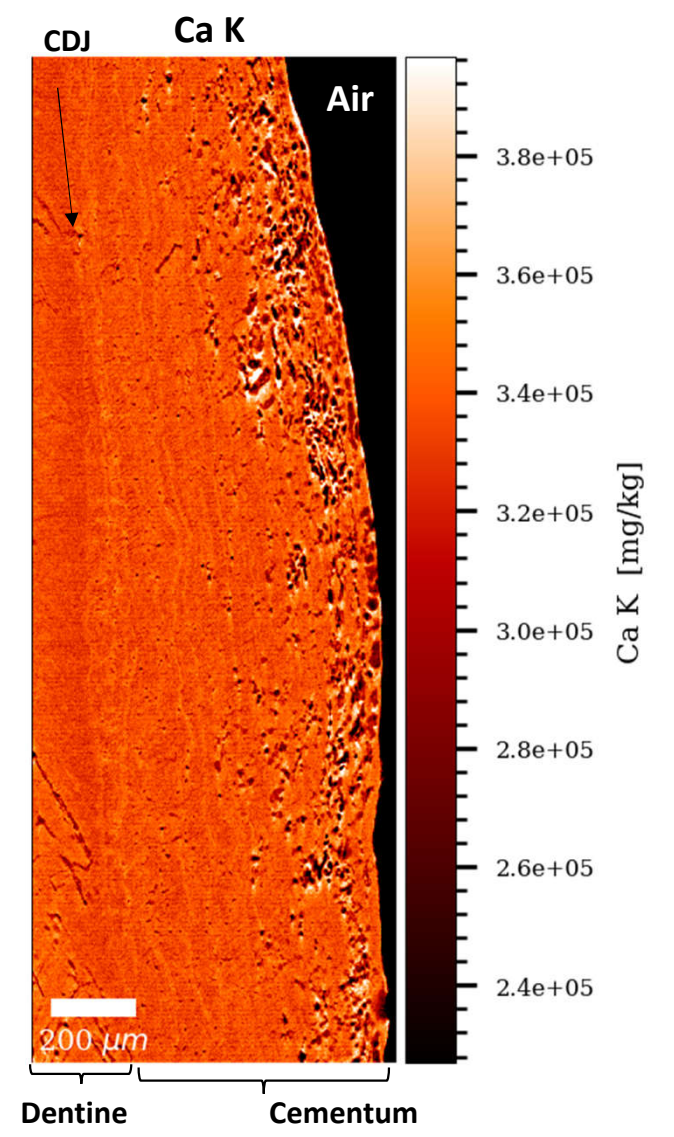


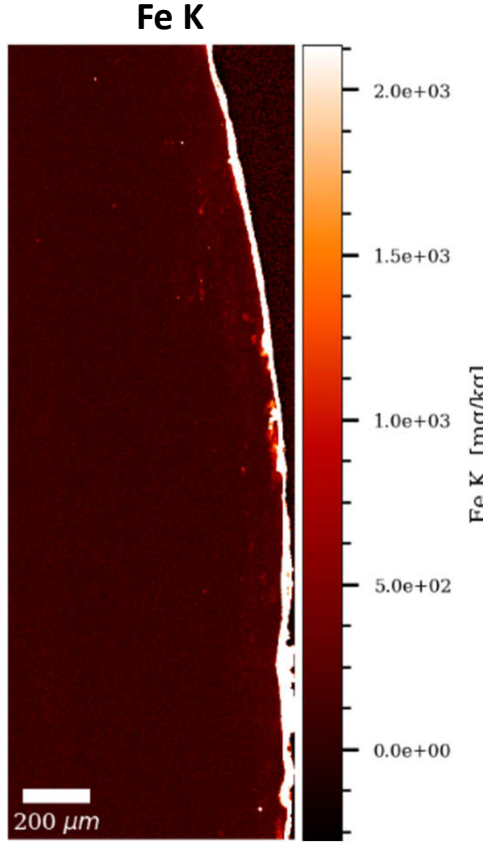
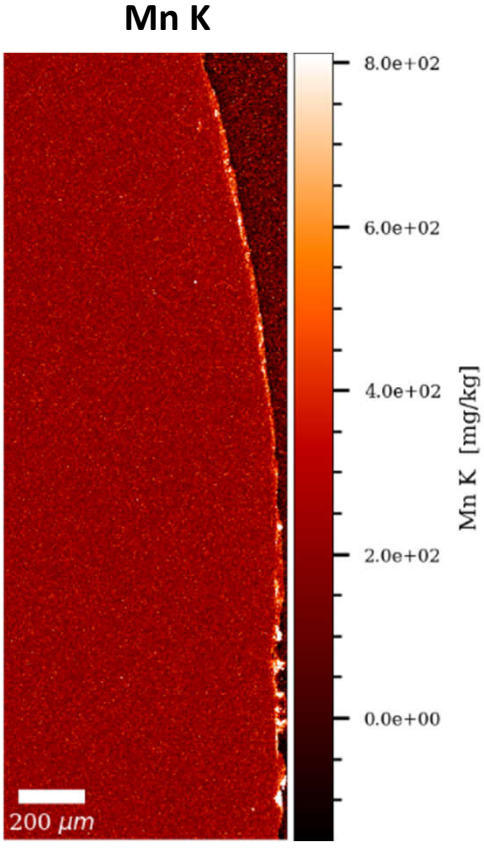
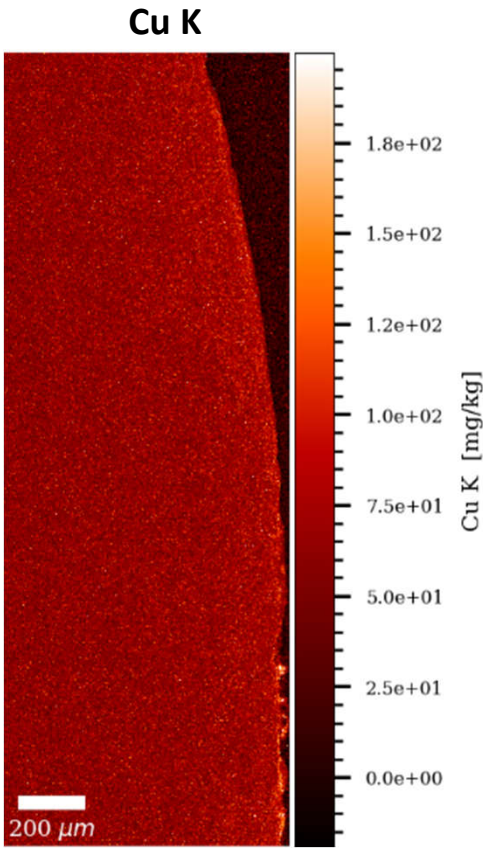


Odense 533 LLM1

High resolution at 1 μm in cellular cementum

Gauss (1x1)

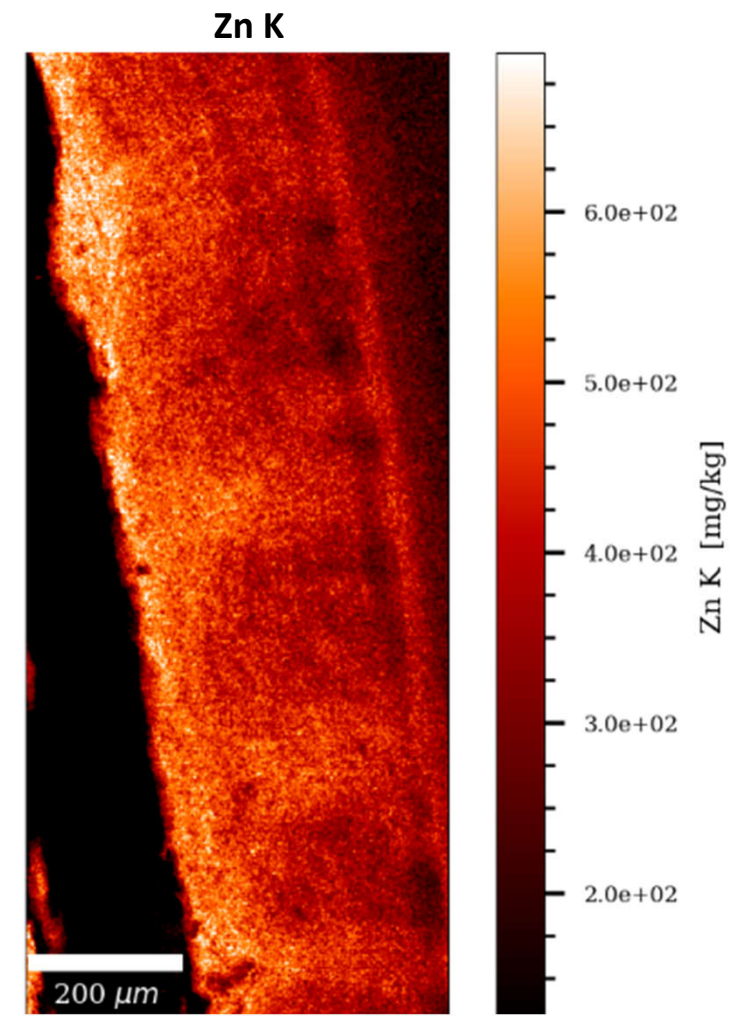
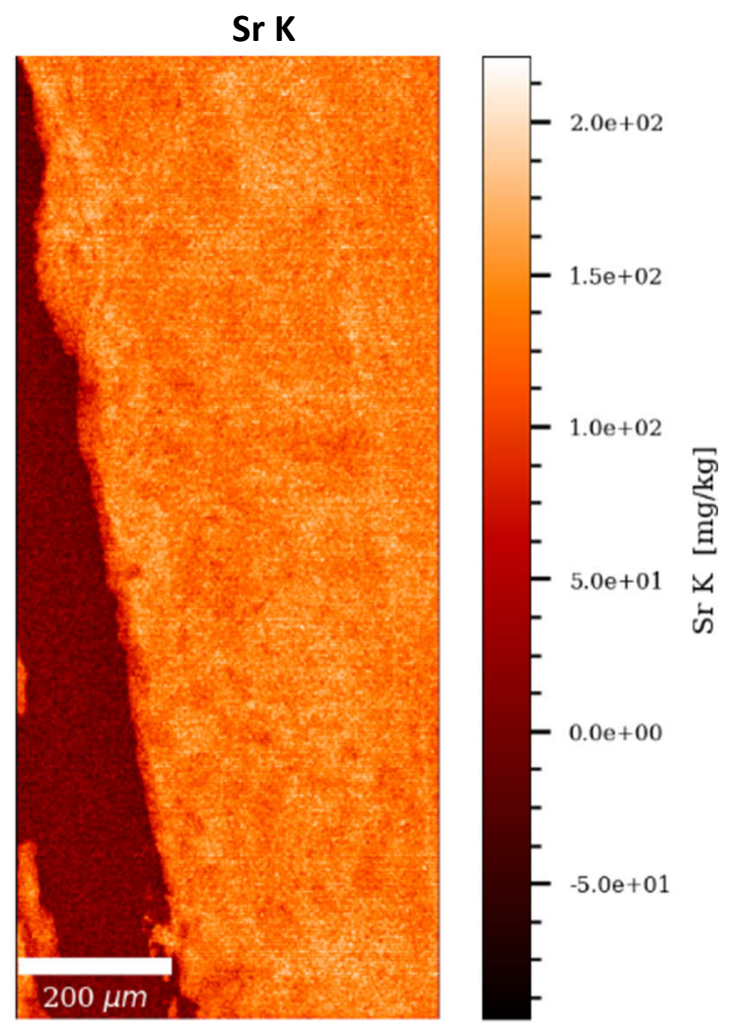
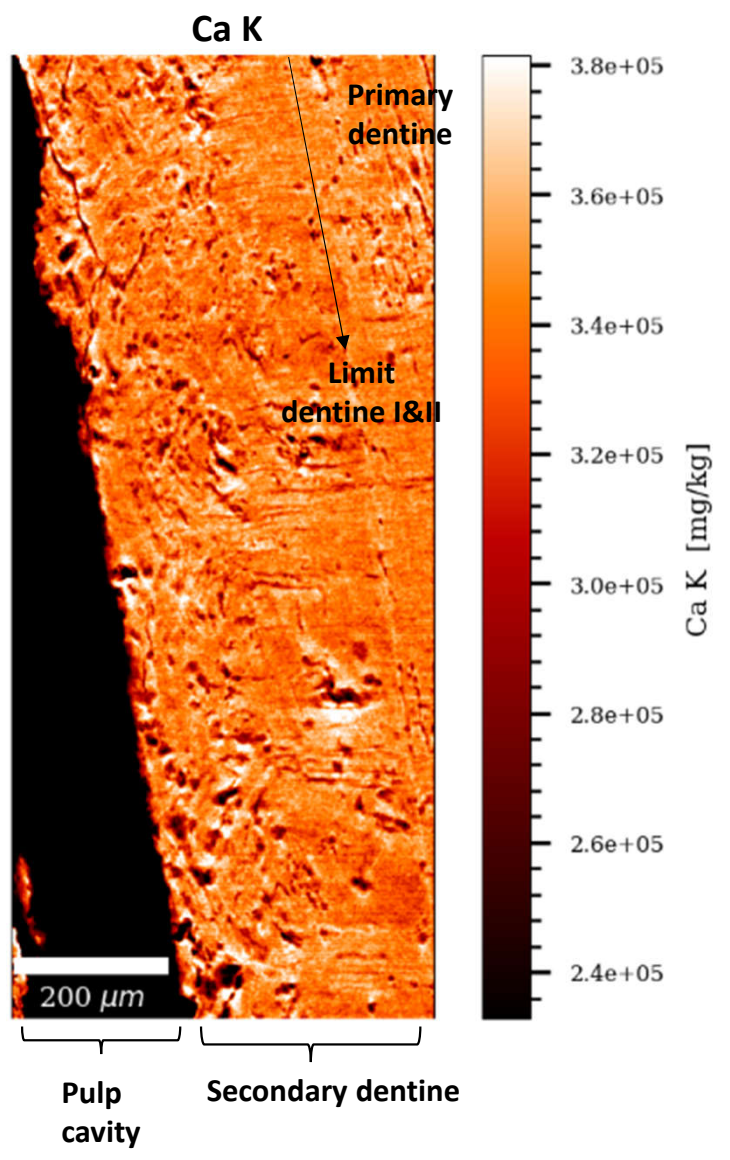


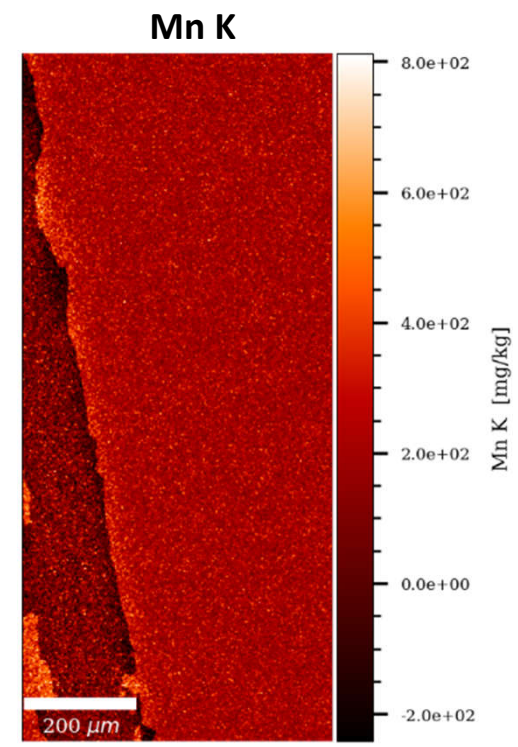
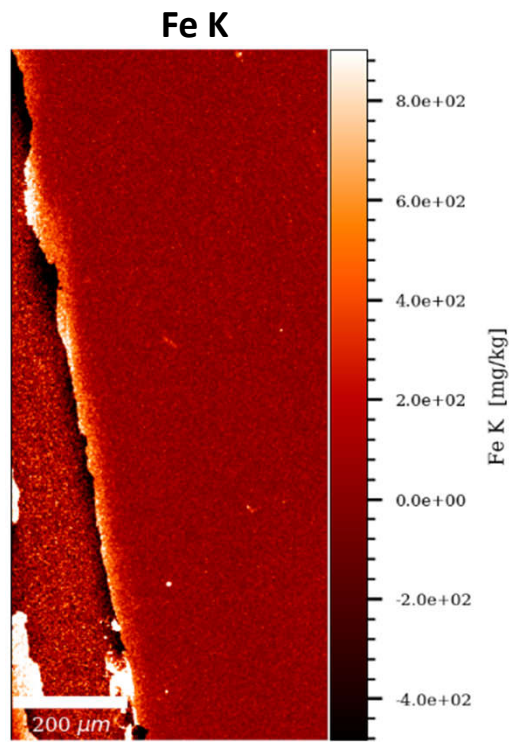
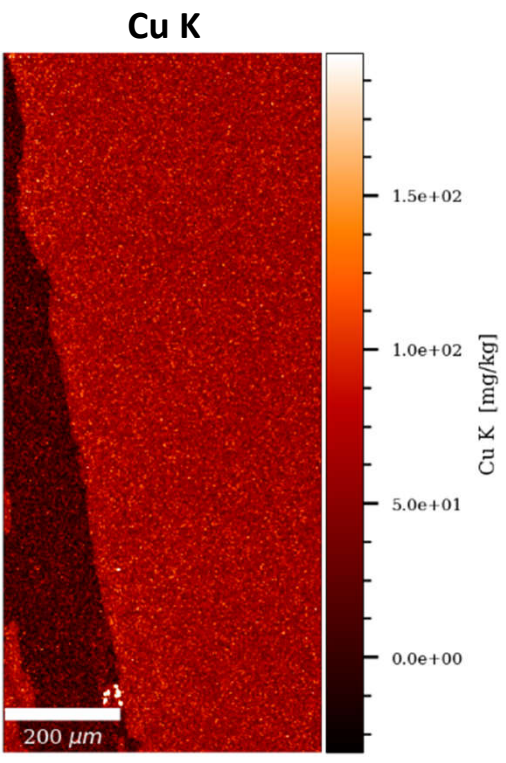


Odense 533 LLM1

High resolution at 1 μm in secondary dentine

Gauss (1x1)



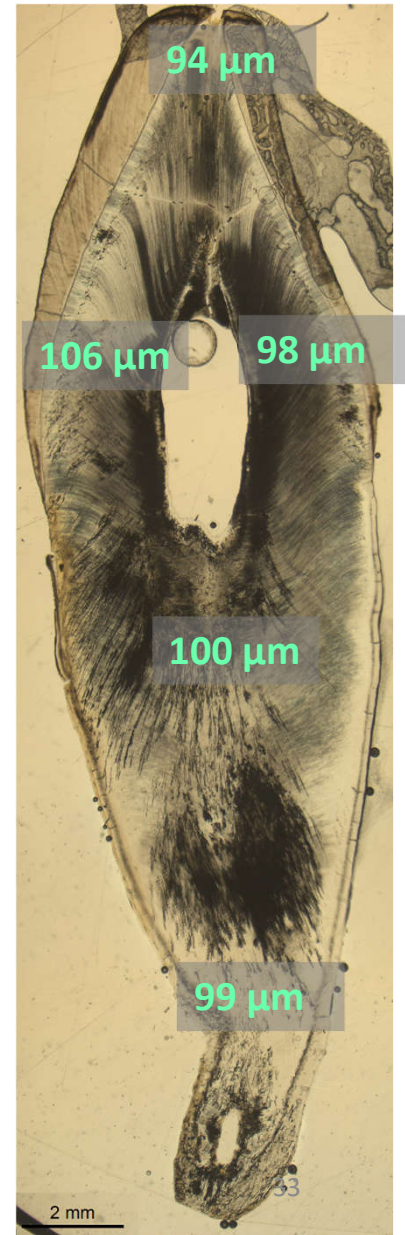




Odense – 896 LLC

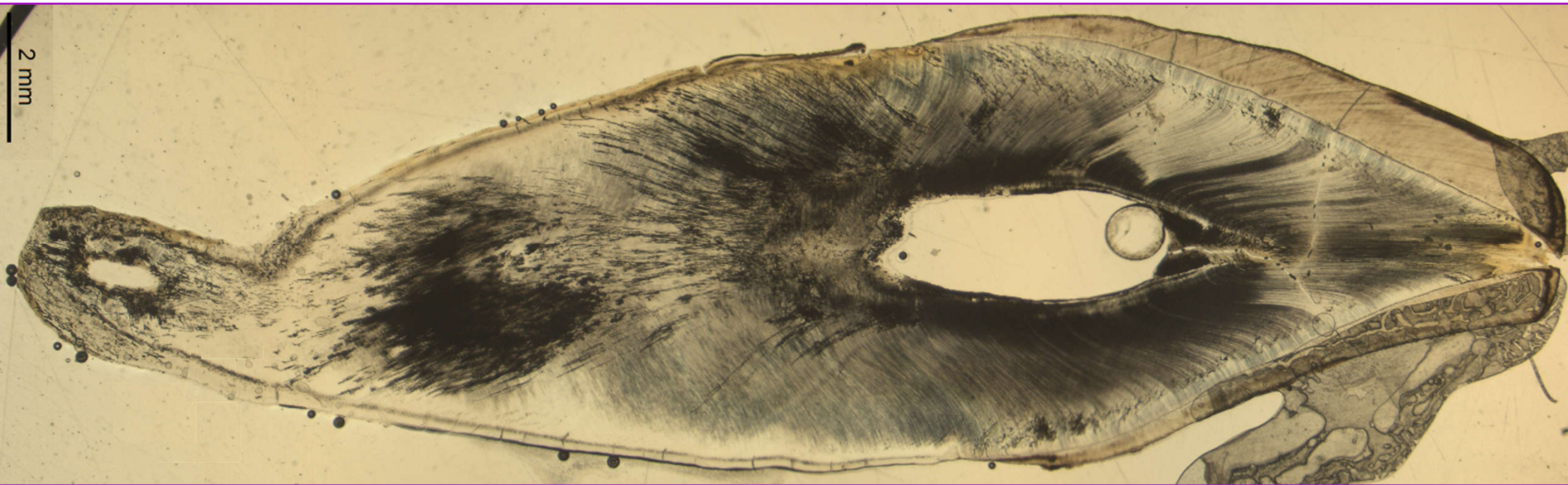


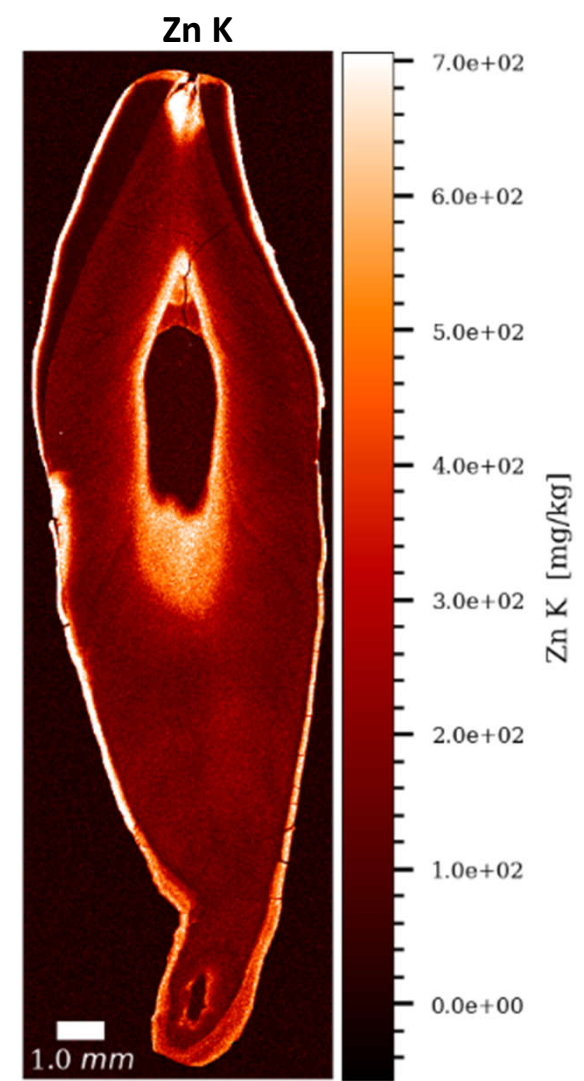
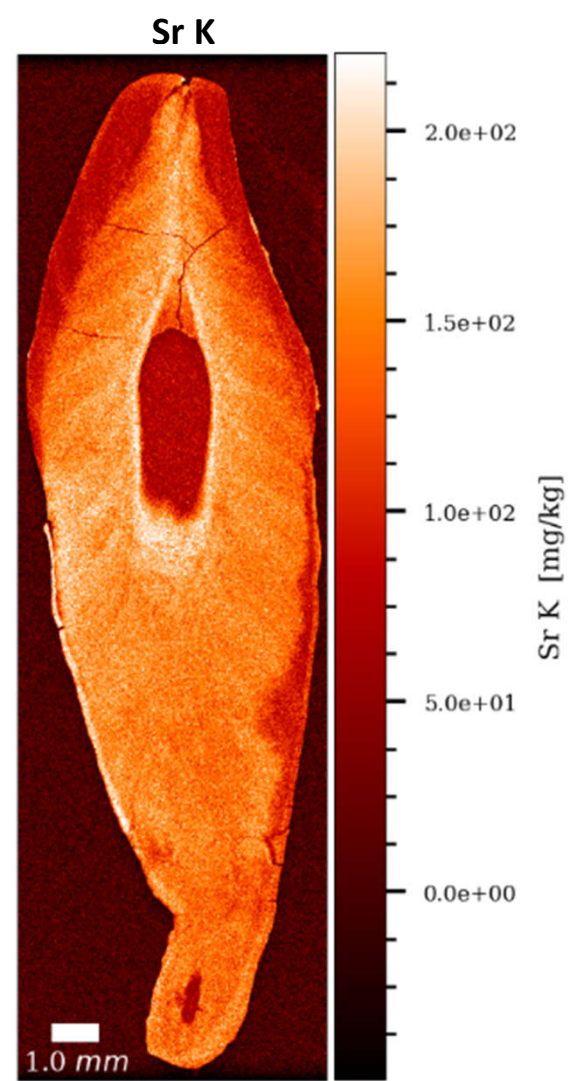
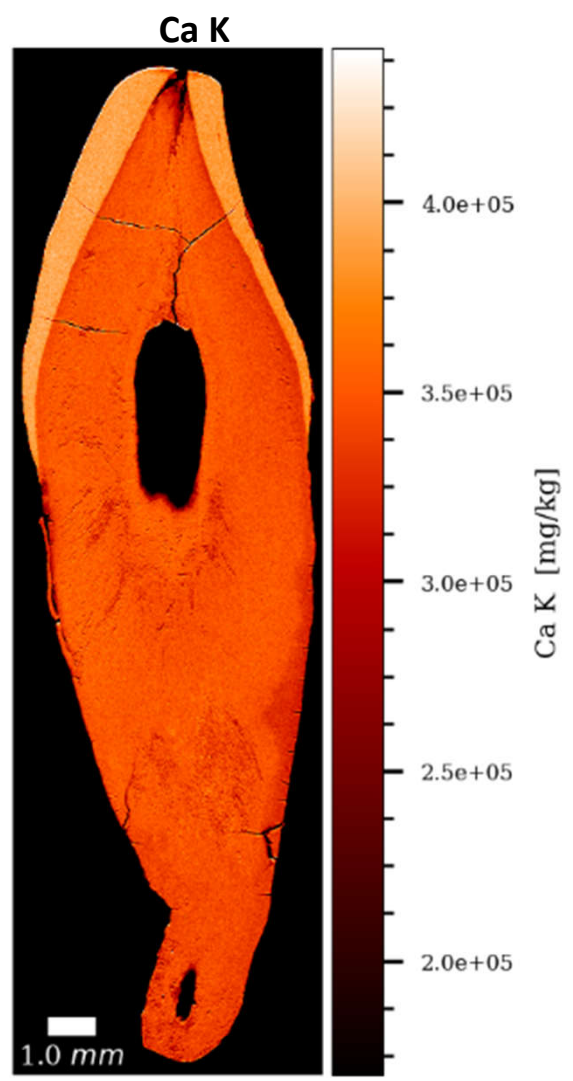
35-45 yrs. 1183 – 1265 cal. CE

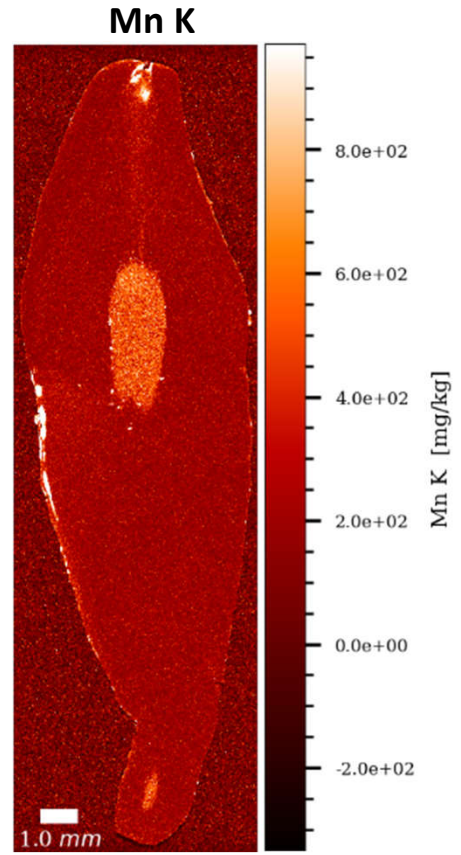
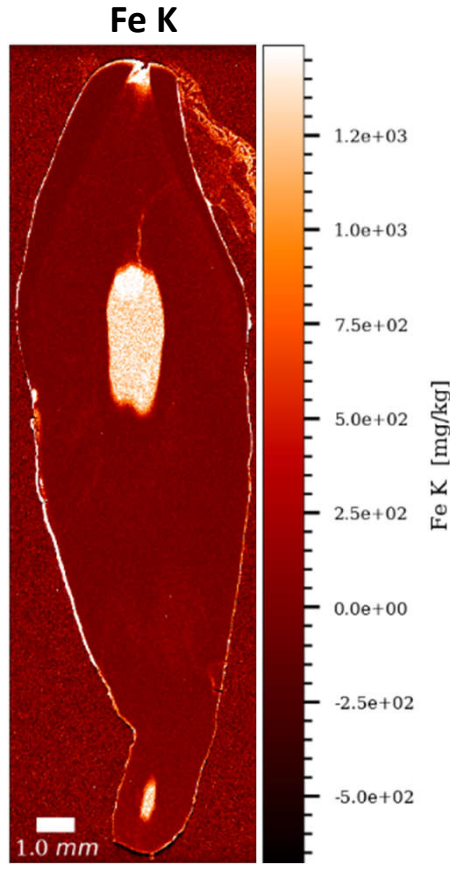
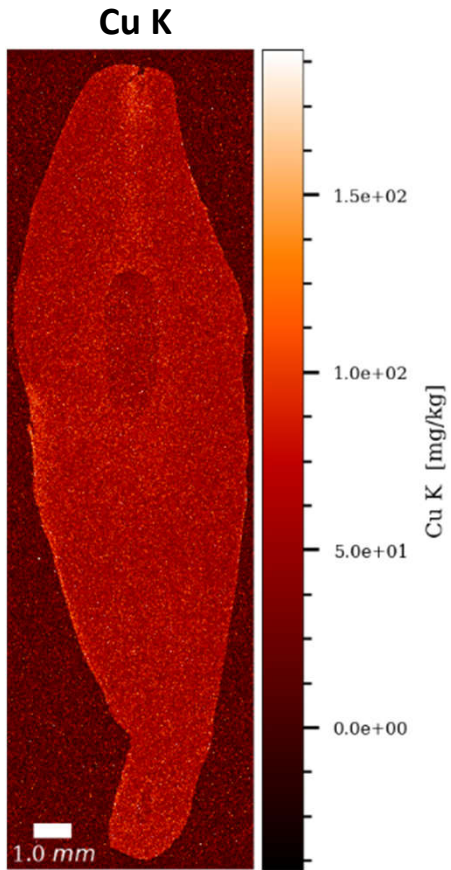


Average tooth section
thickness (μm): 99.4

Overview at 10 μ m

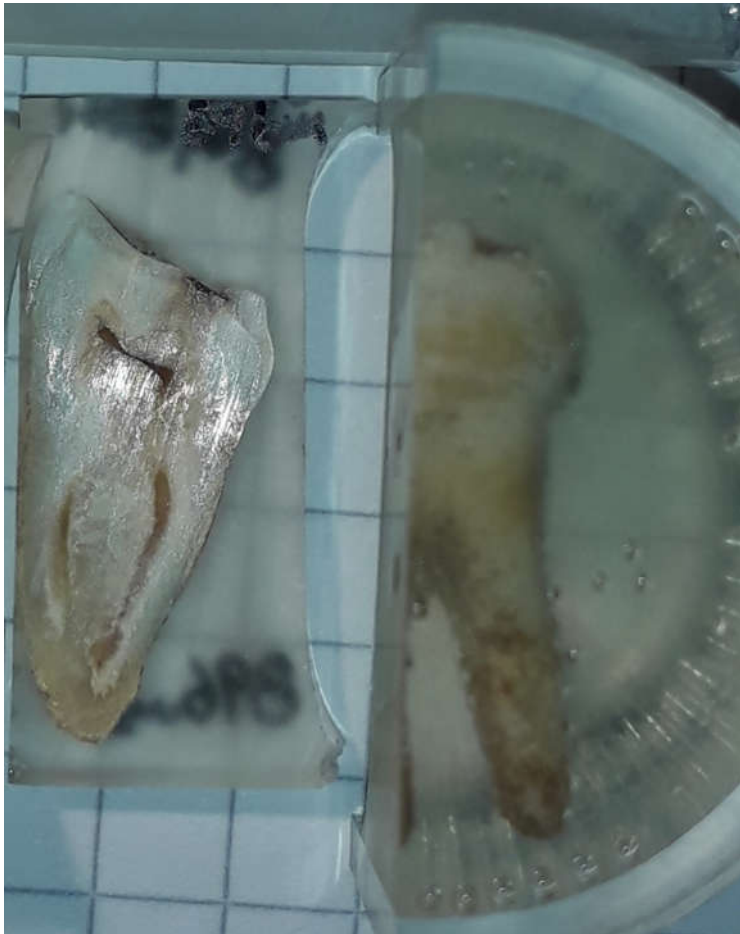






Odense – 896 LLM1

♂ 35-45 yrs. 1183 – 1265 cal. CE

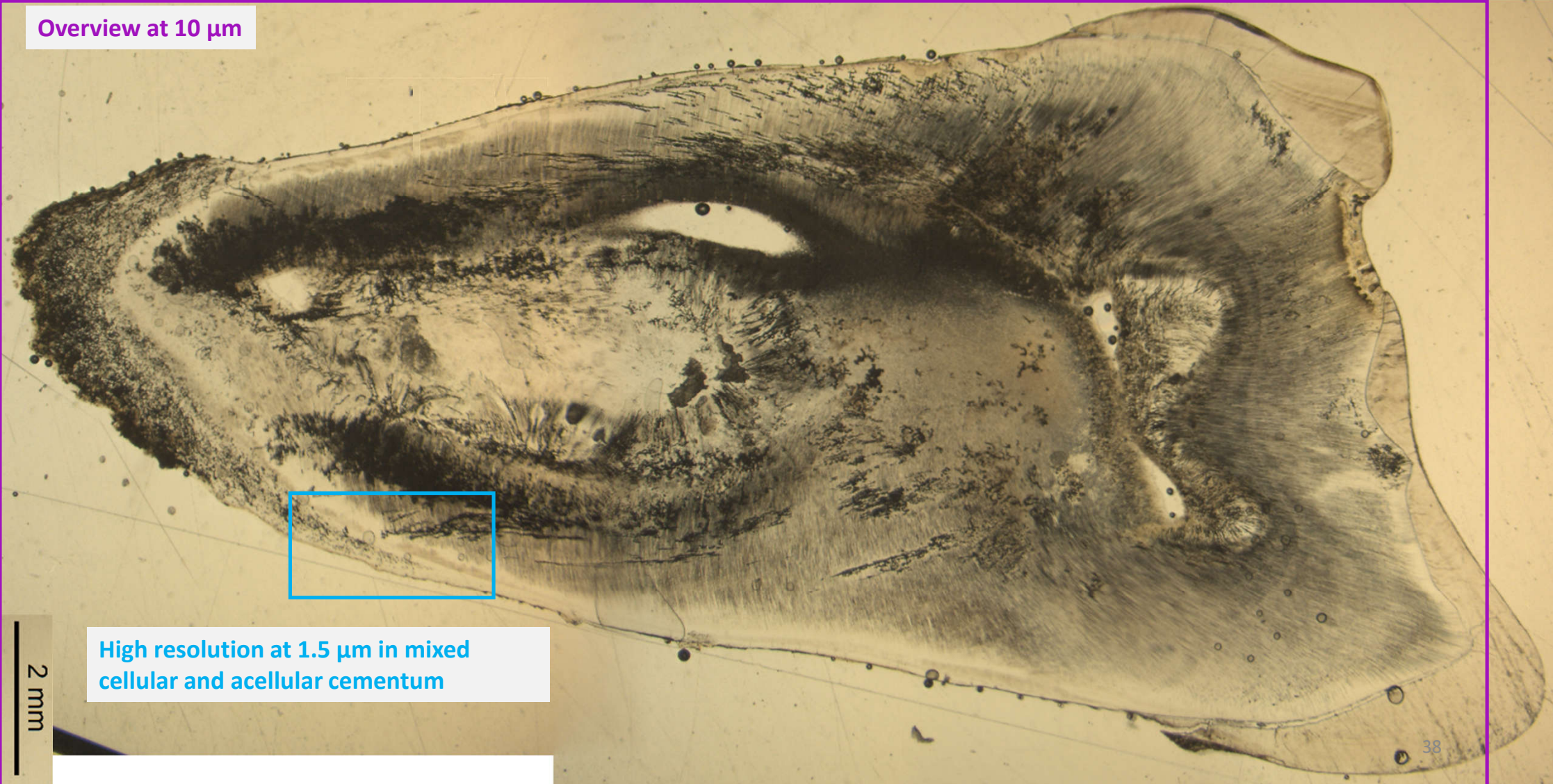


Average tooth section thickness (μm): 99.4

Odense 896 LLM1

Scanning

Overview at 10 μm



High resolution at 1.5 μm in mixed cellular and acellular cementum

2 mm

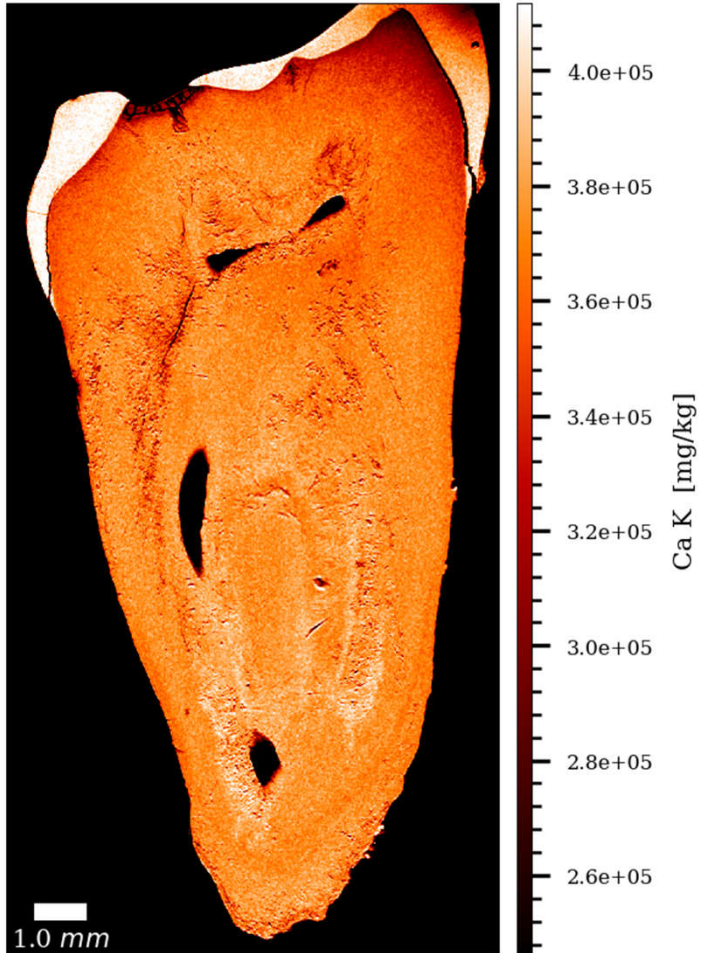
38

Odense 896 LLM1

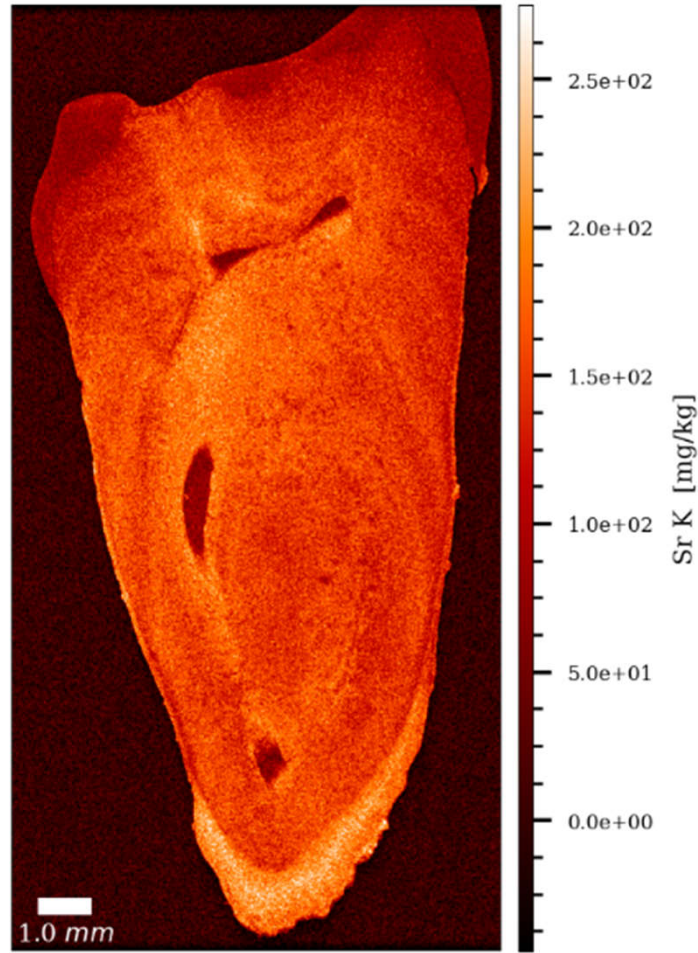
Overview at 10 μ m

Gauss (1x1)

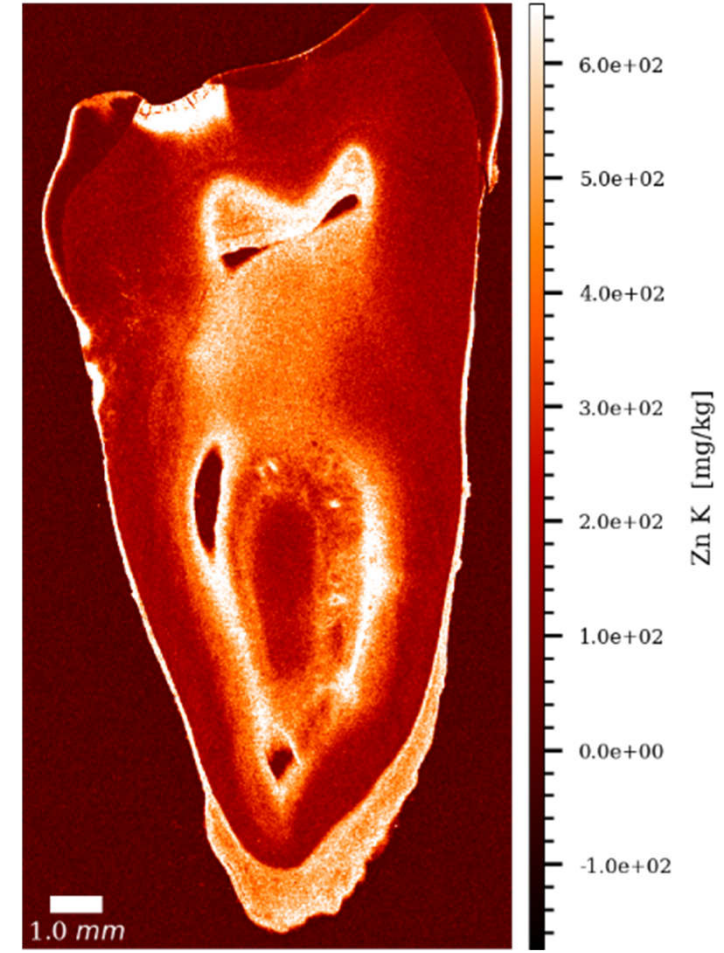
Ca K

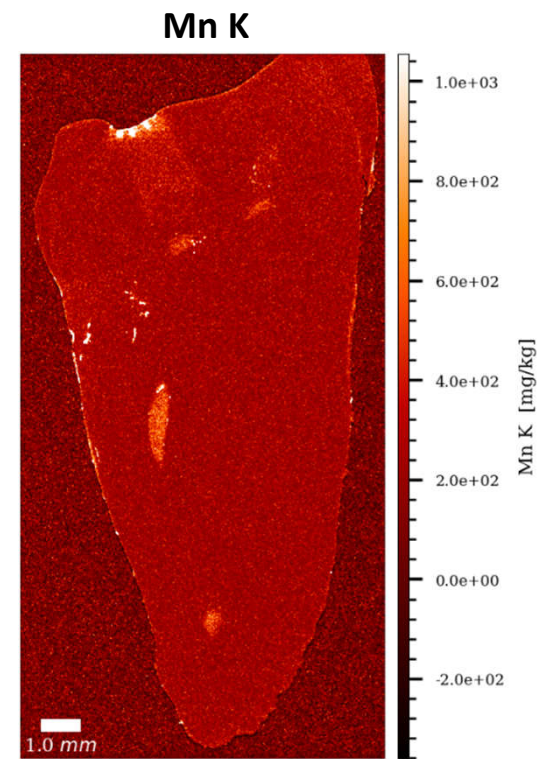
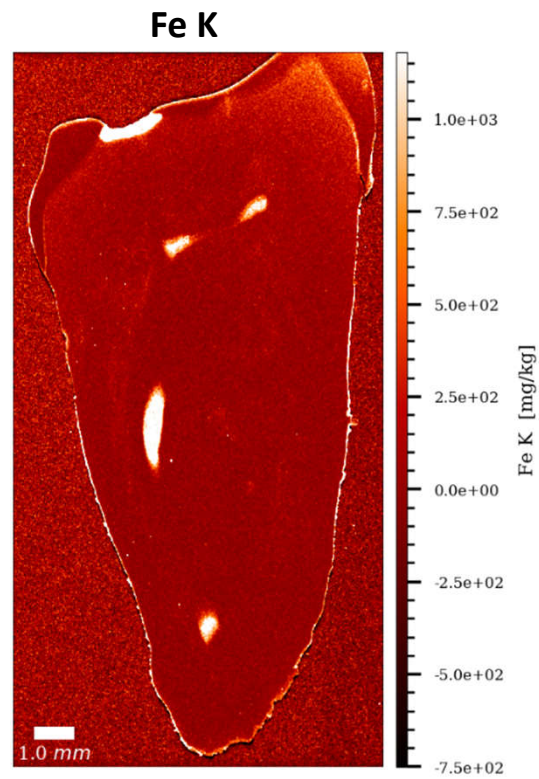
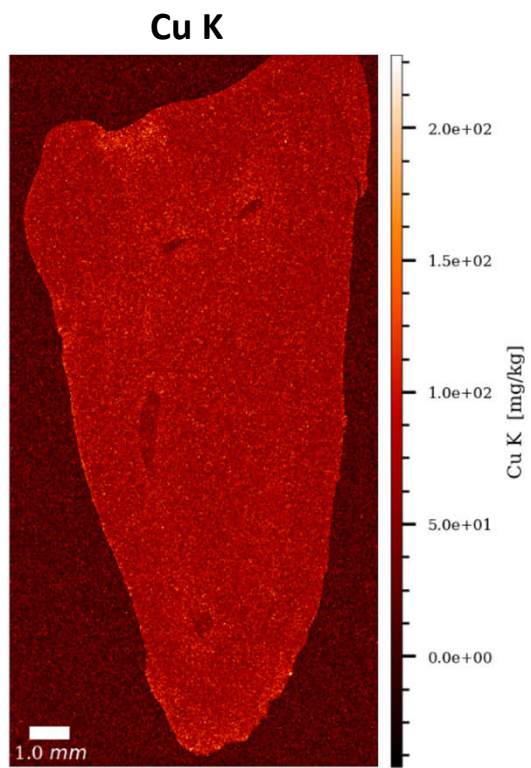


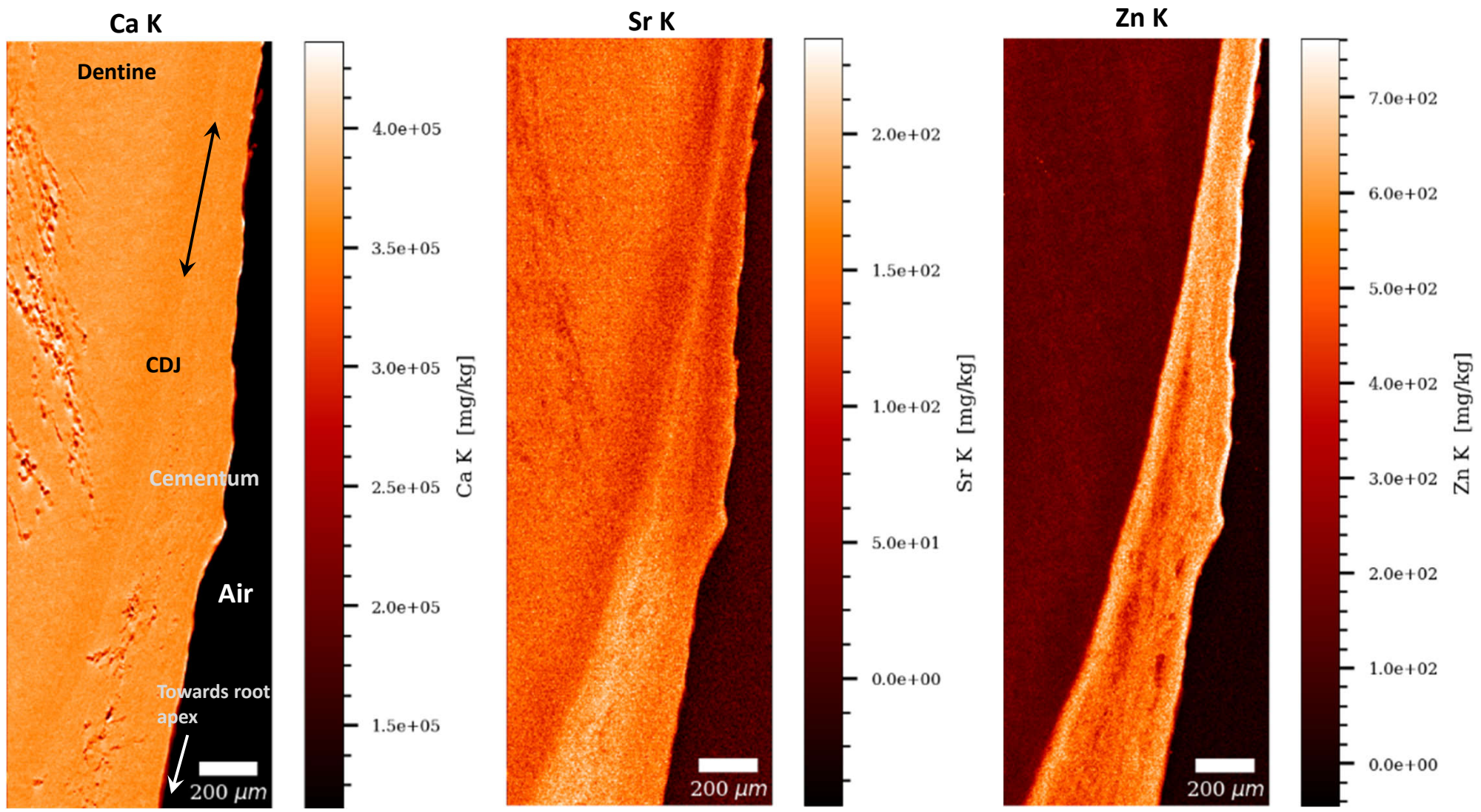
Sr K

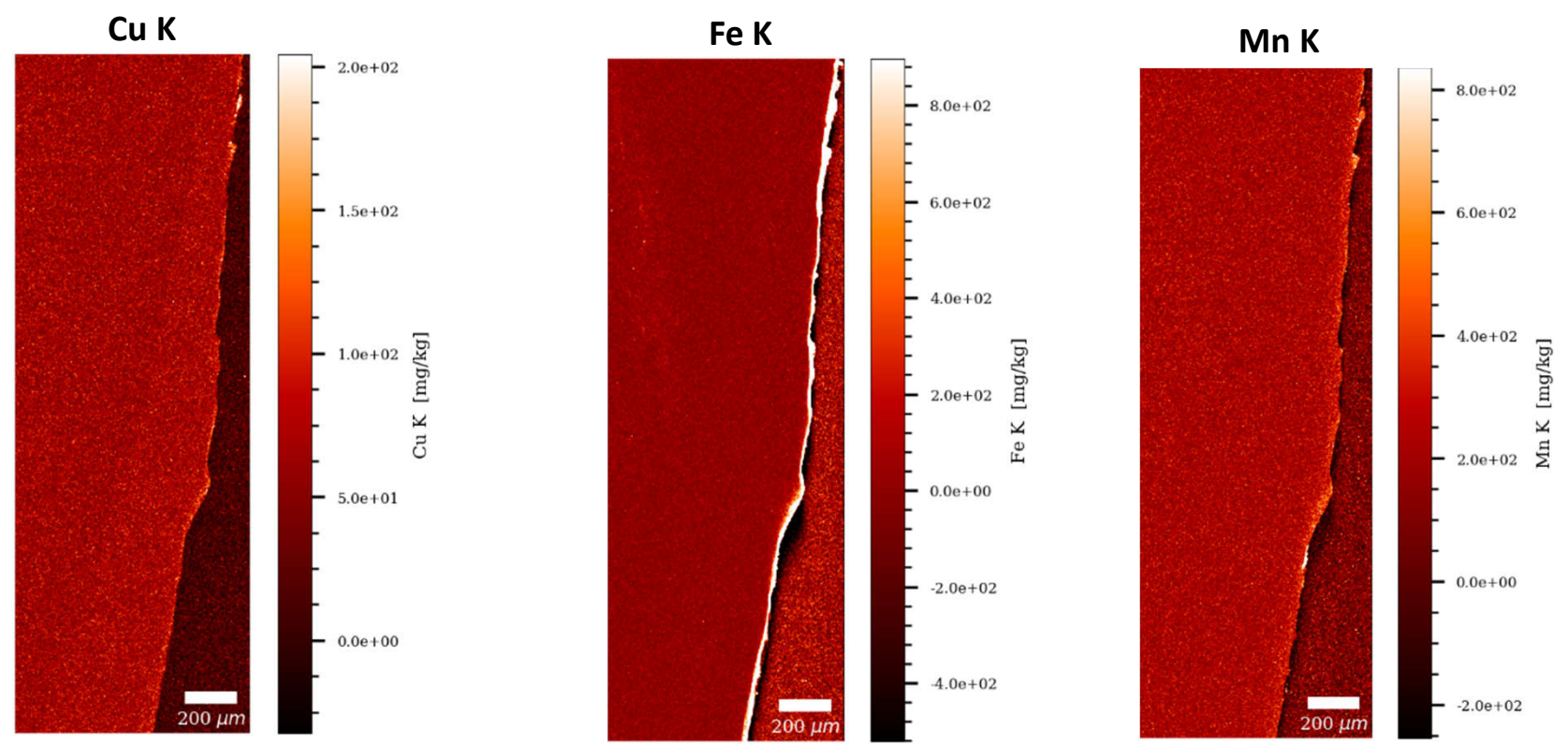


Zn K









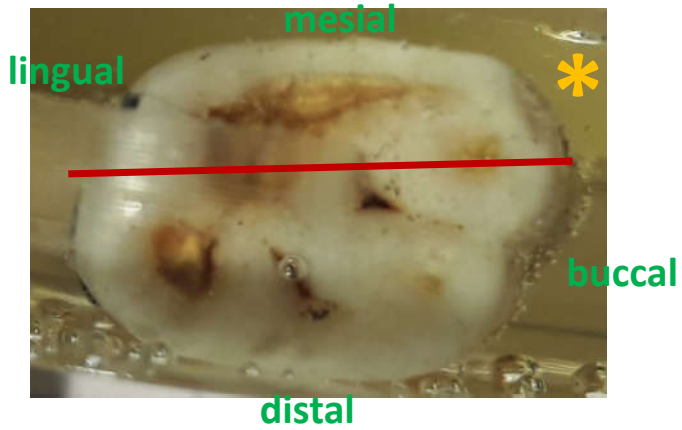
Odense – 914 ULM1

♀ 25-35 yrs. 1459 – 1566 cal. CE

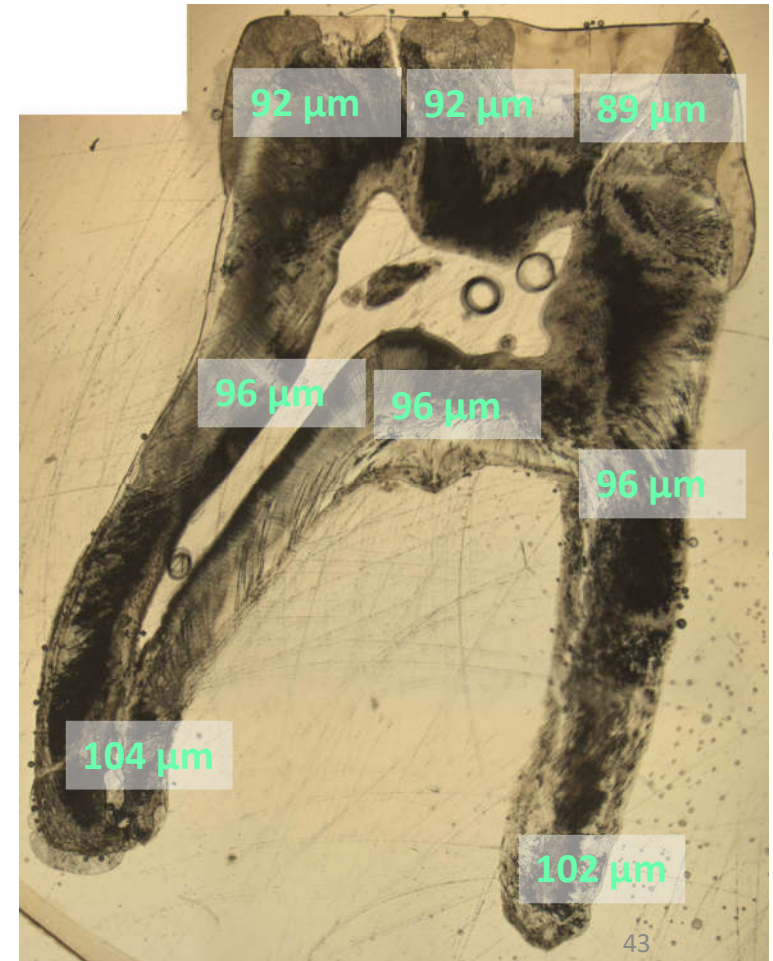
Average tooth section thickness (µm): 95.9



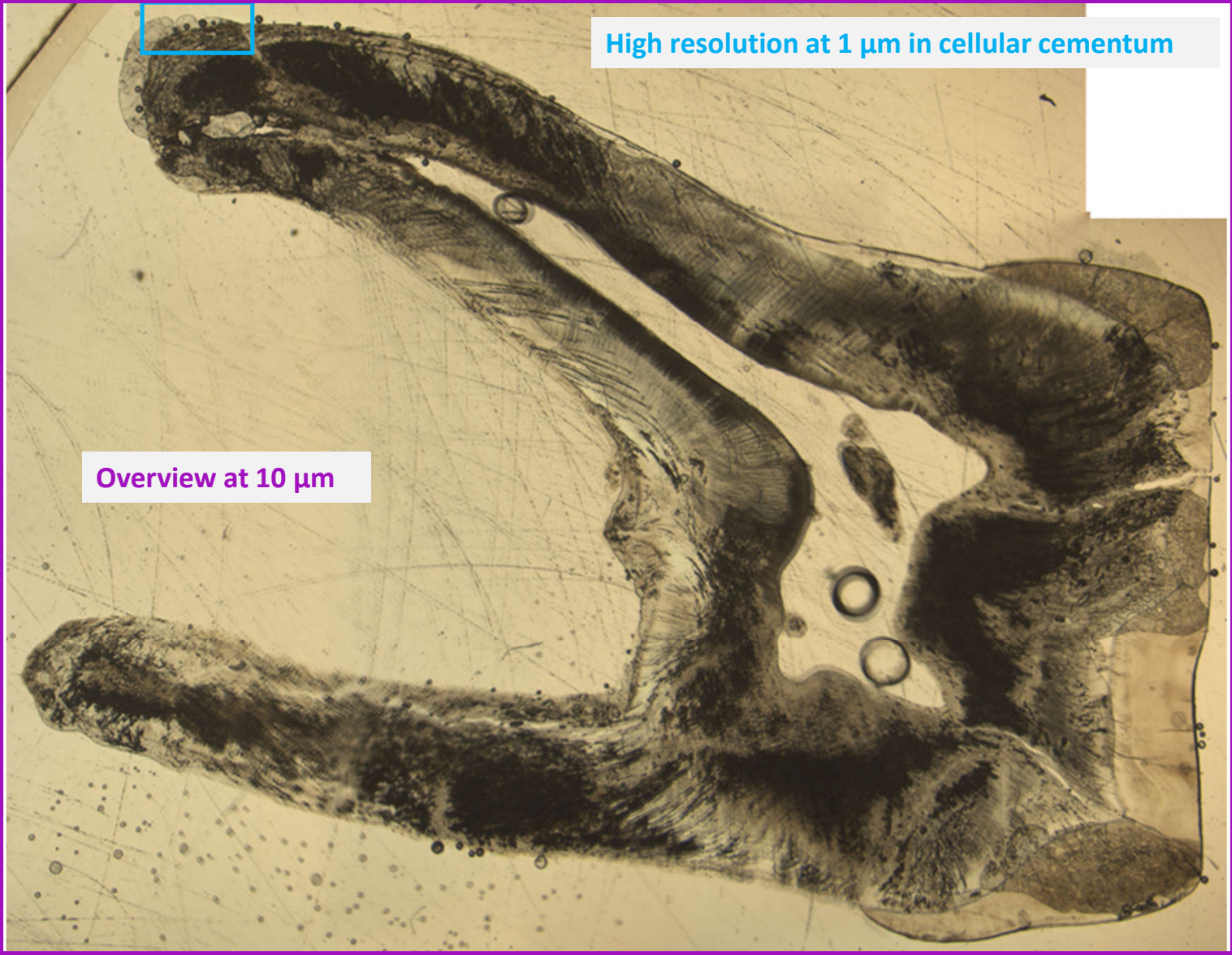
2 buccal roots



2 buccal roots



Scanning

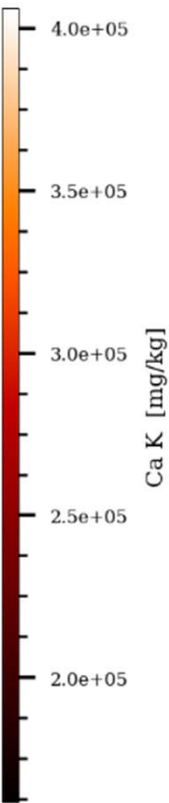
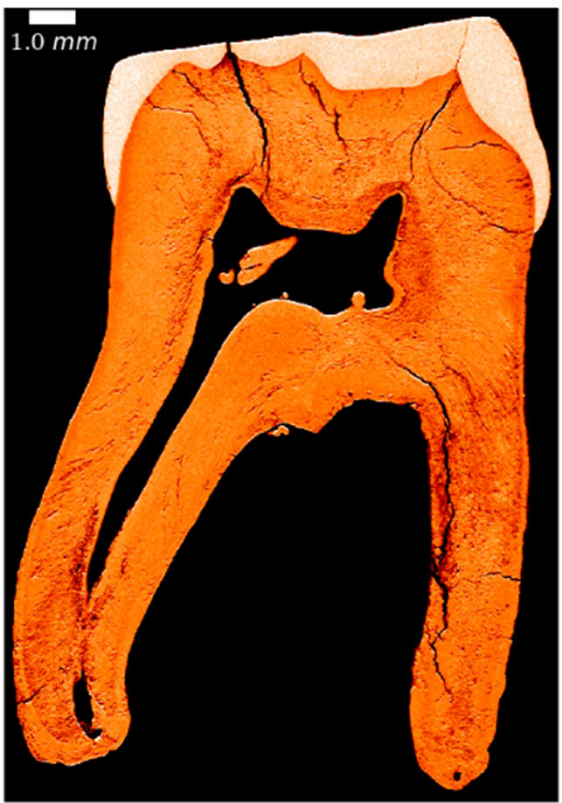


Odense 914 ULM1

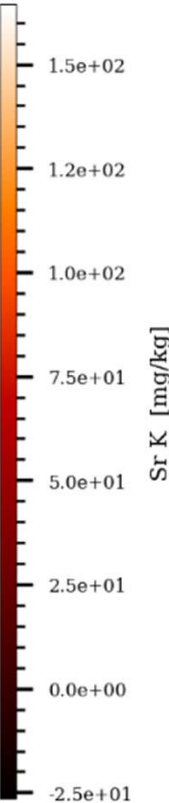
Overview at 10 μ m

Gauss (1x1)

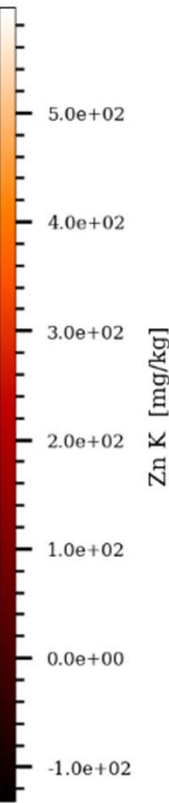
Ca K

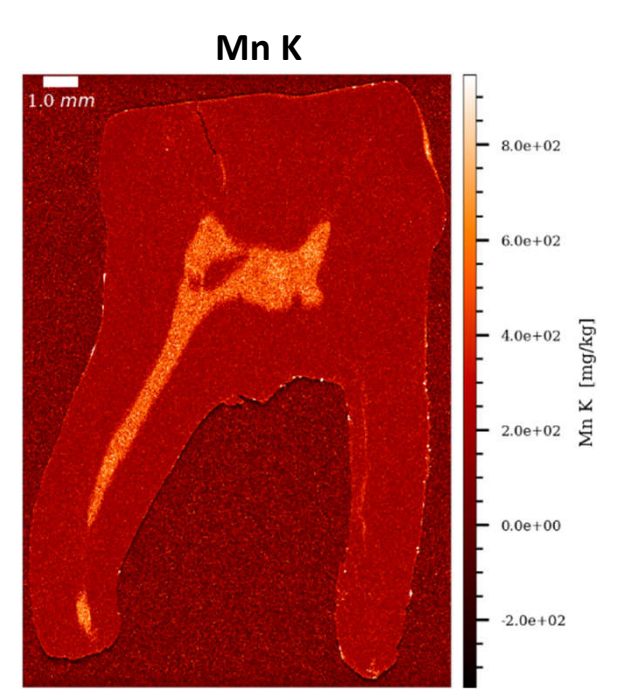
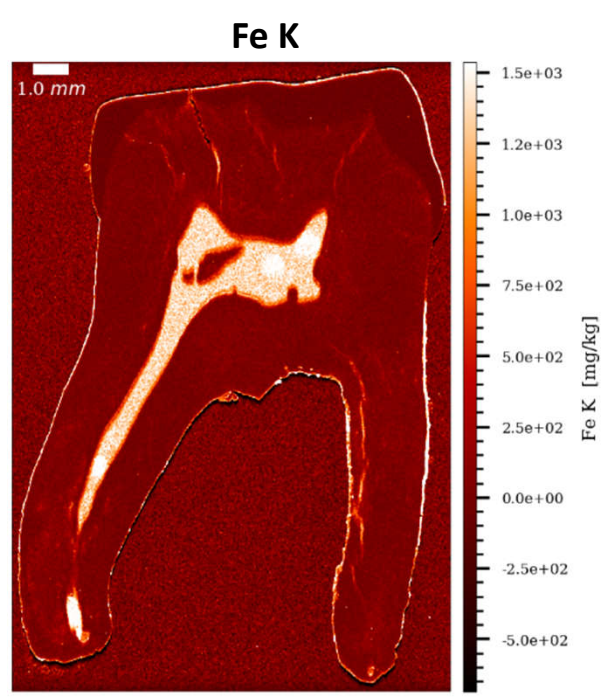
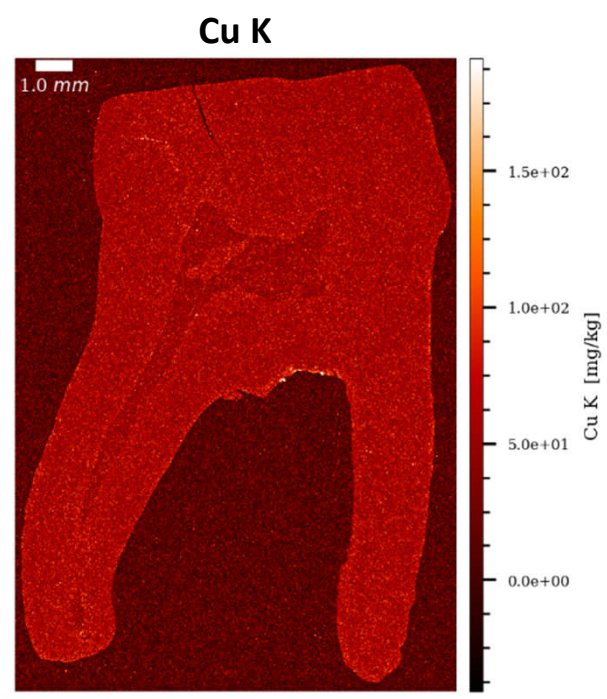


Sr K



Zn K





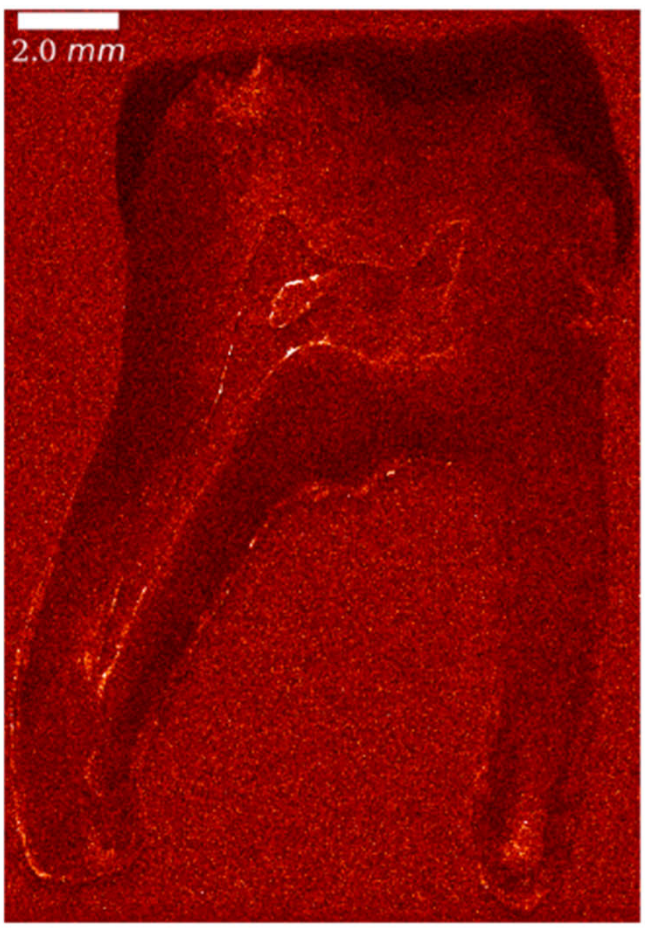
Odense 914 ULM1

Overview at 10 μm

Uncalibrated data
(arbitrary units)

Gauss (1x1)

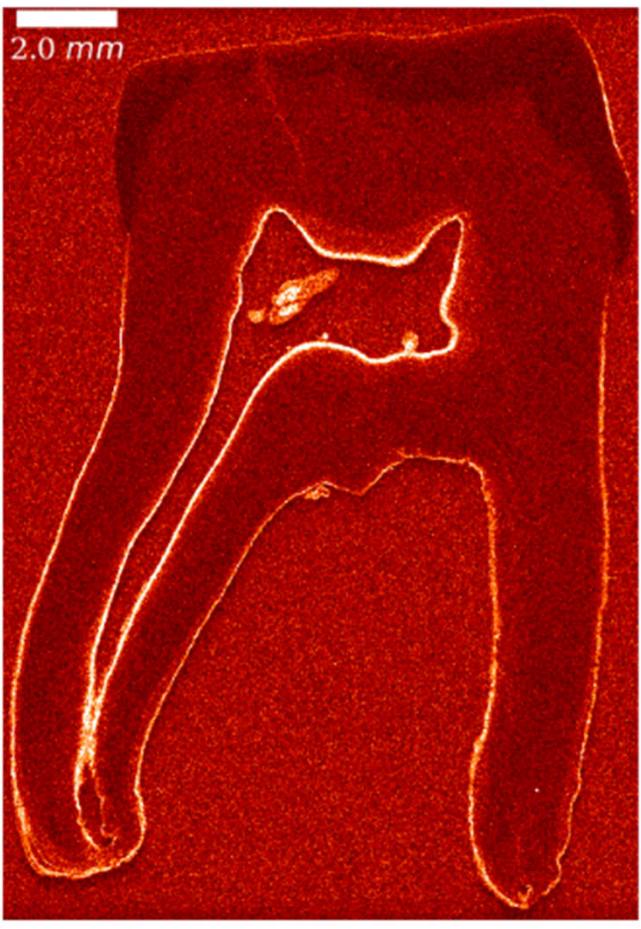
Br K



10 20 30 40 50 60

Br K [a.u.]

Pb L



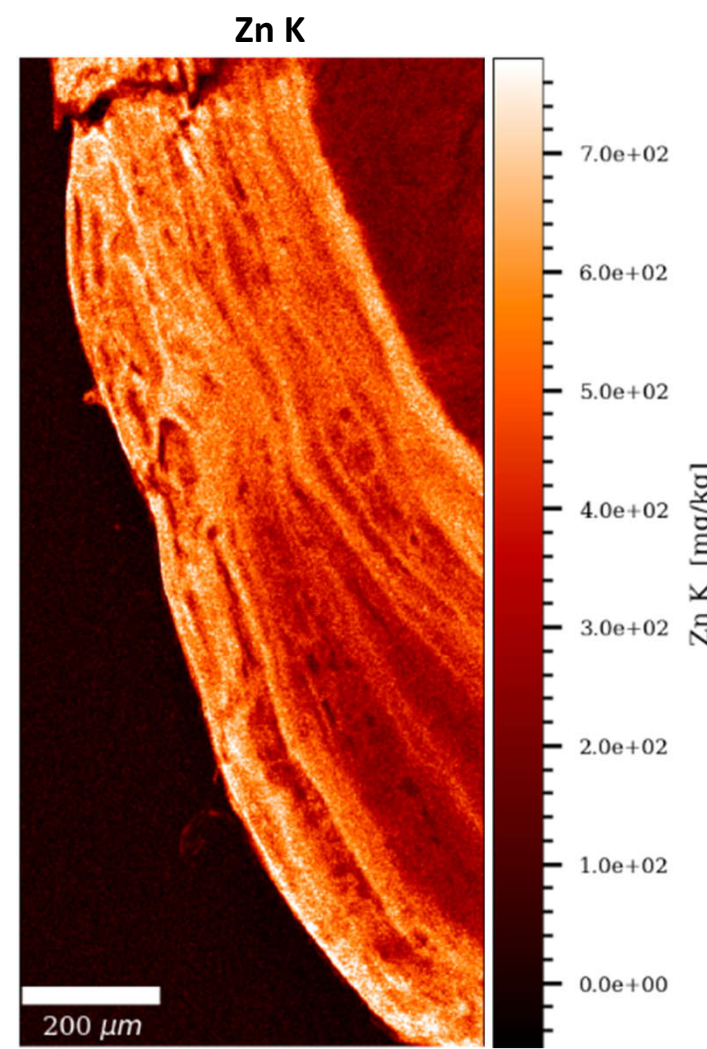
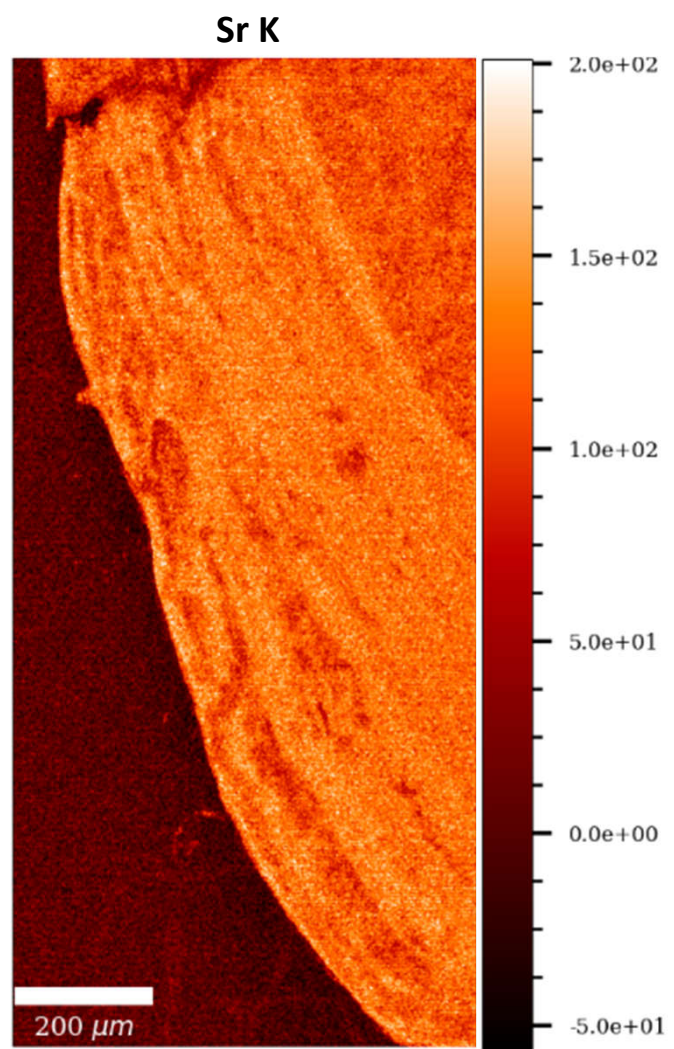
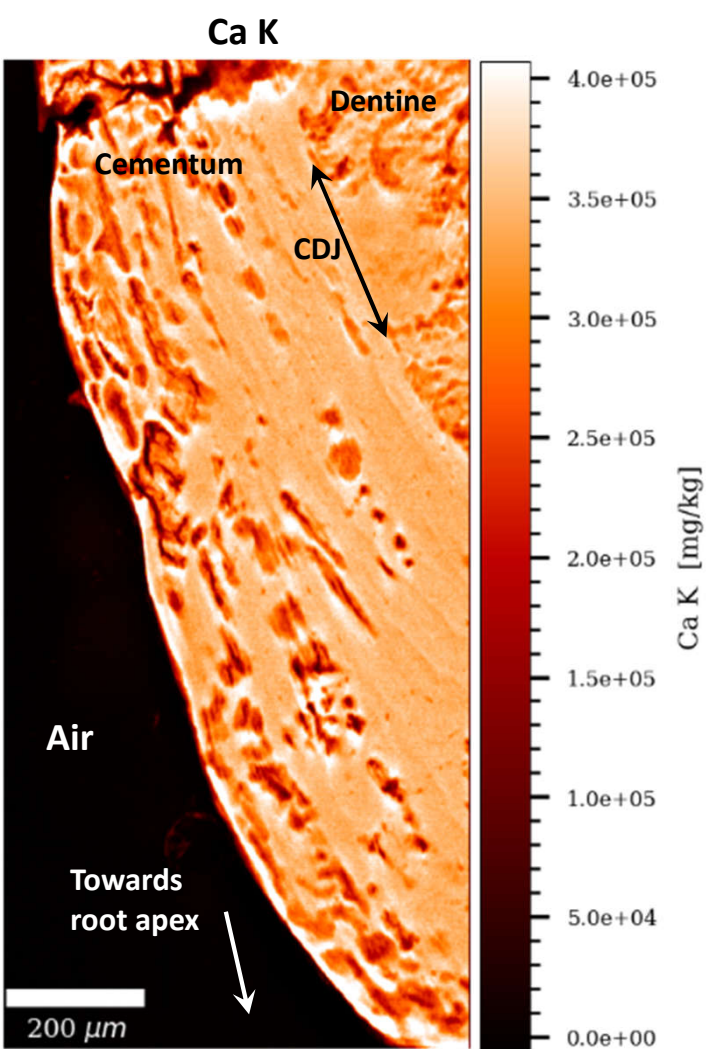
20 40 60 80 100 120

Pb L [a.u.]

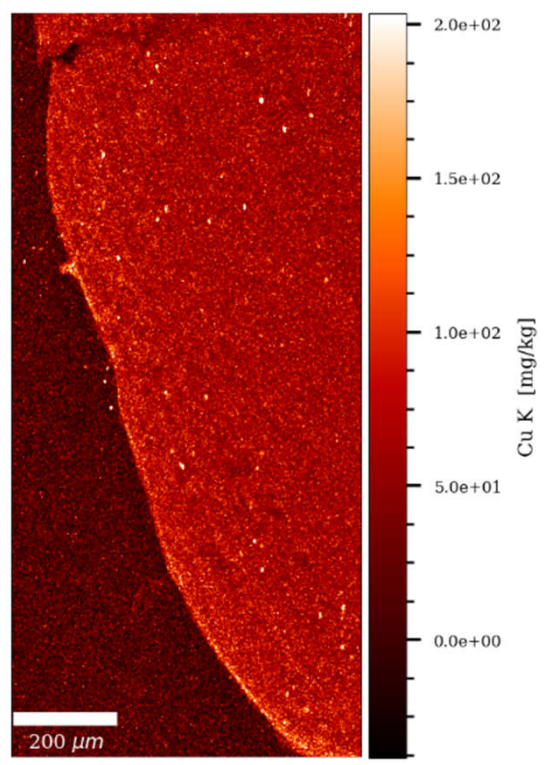
Odense 914 ULM1

High resolution at 1 μ m

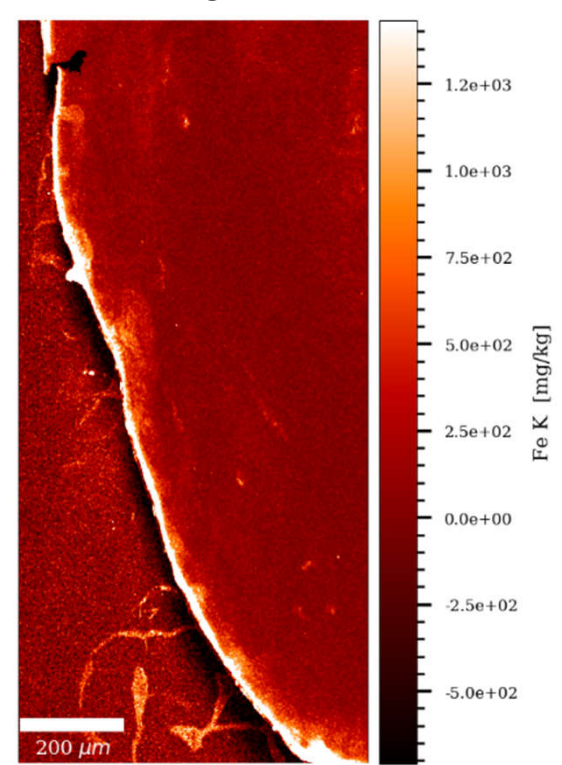
Gauss (0.9x0.9)



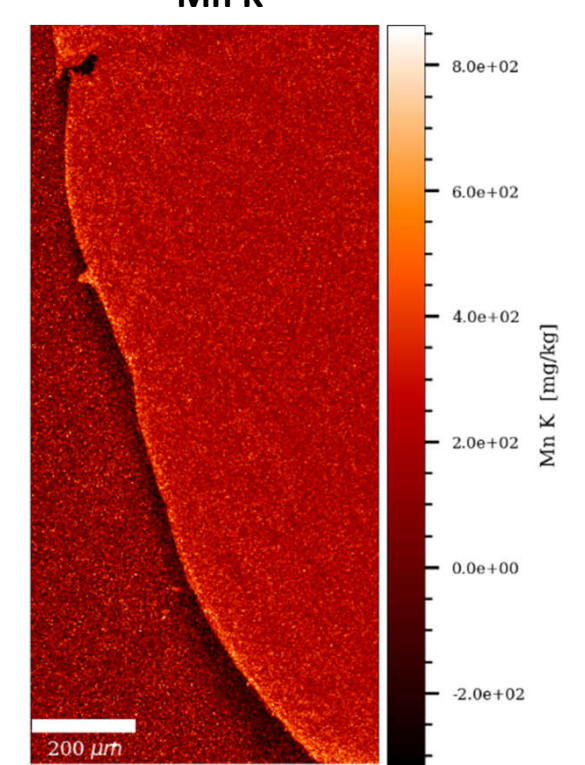
Cu K



Fe K

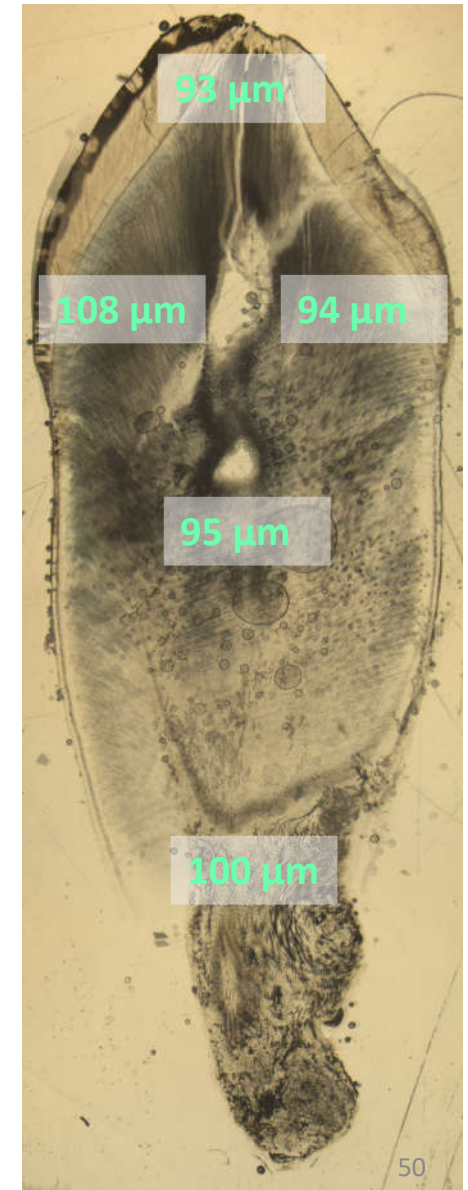


Mn K



Odense – 1149 URC

♀ 20-30 yrs. 1301 – 1415 cal. CE

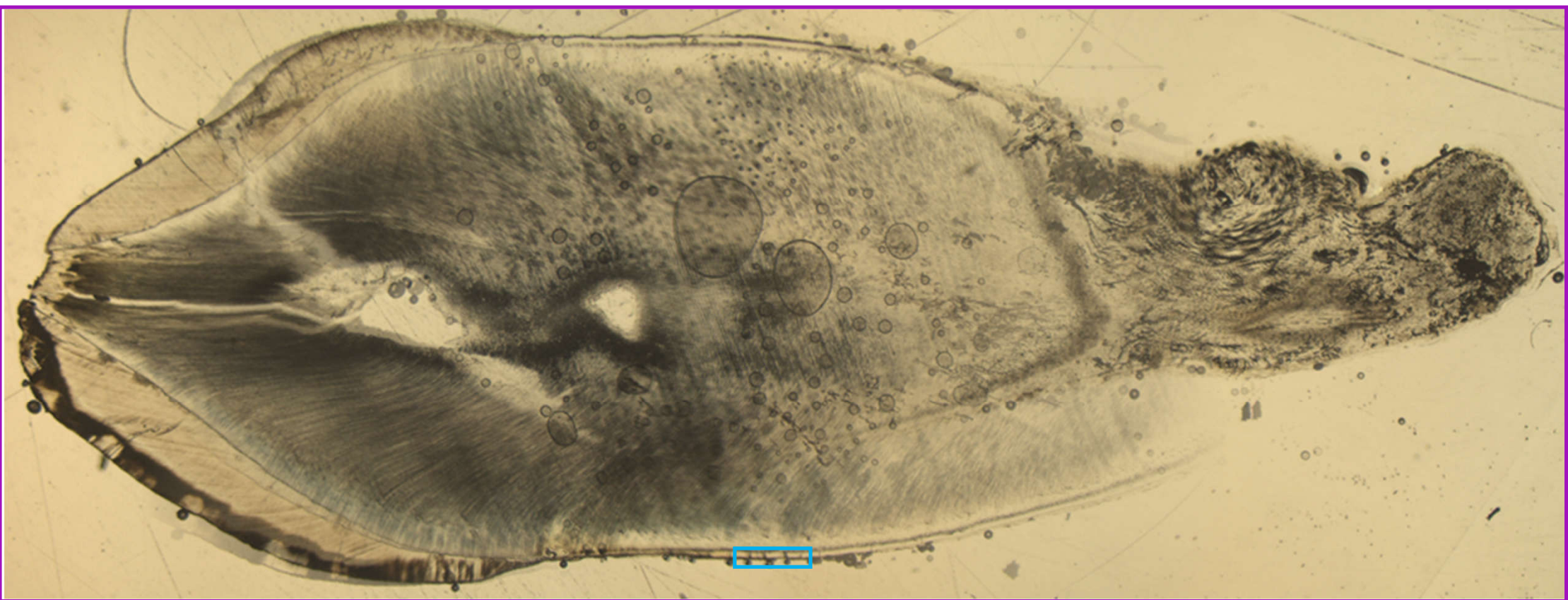


Average tooth section
thickness (μm): 98.0

Odense 1149 URC

Scanning

Overview at 10 μm

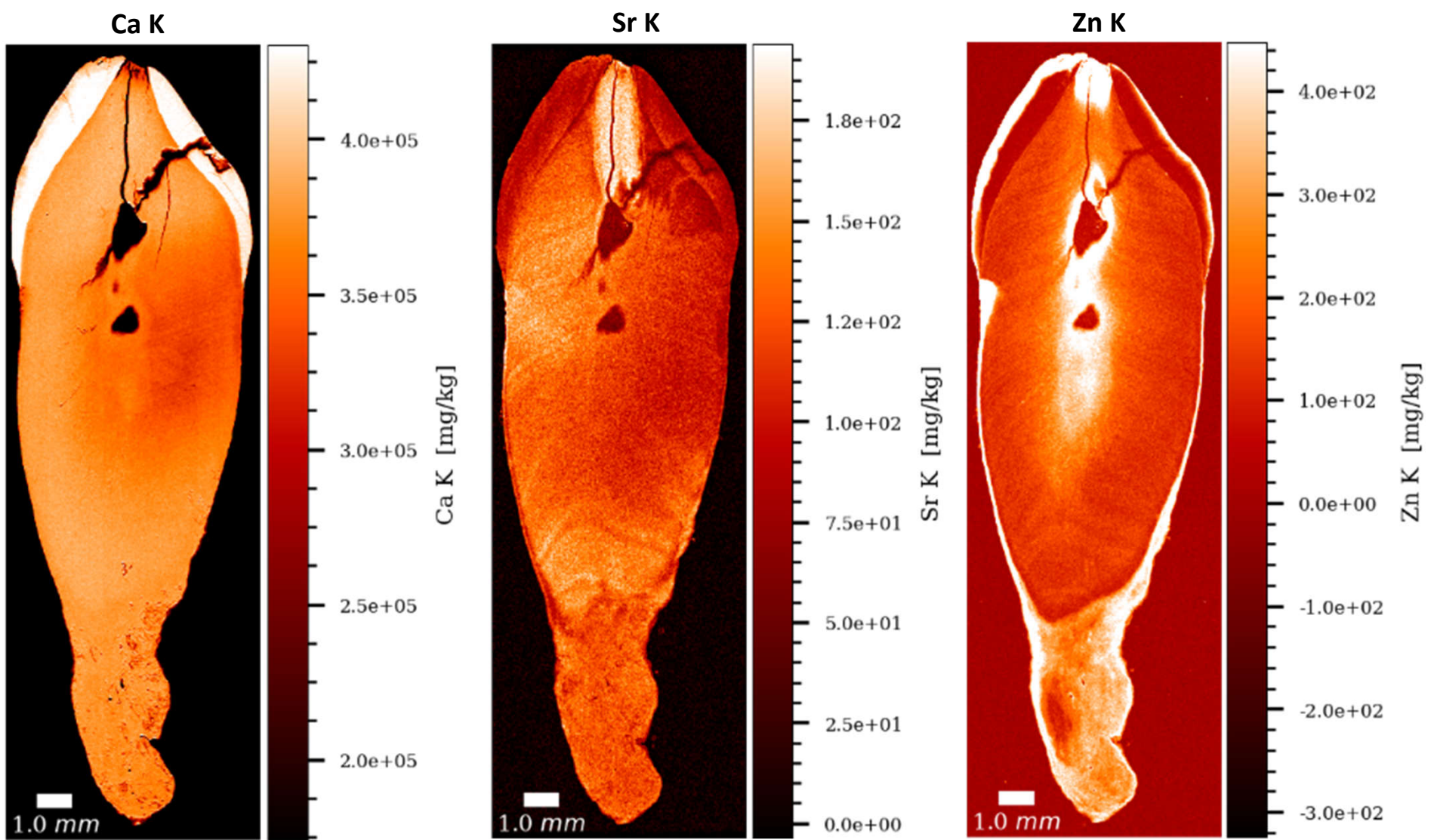


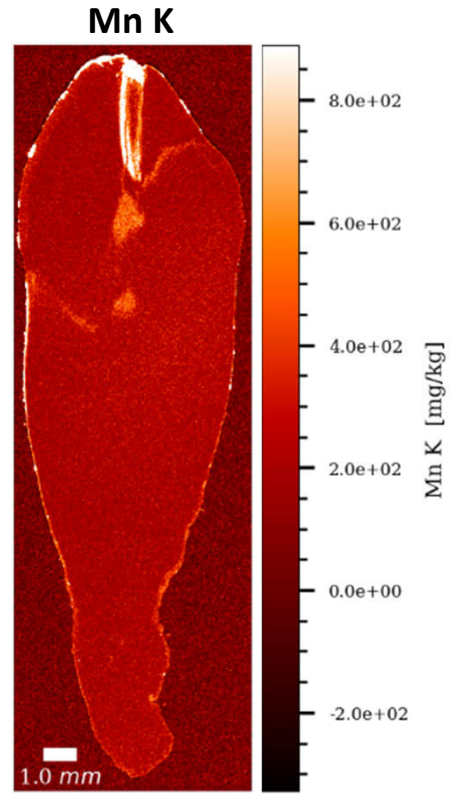
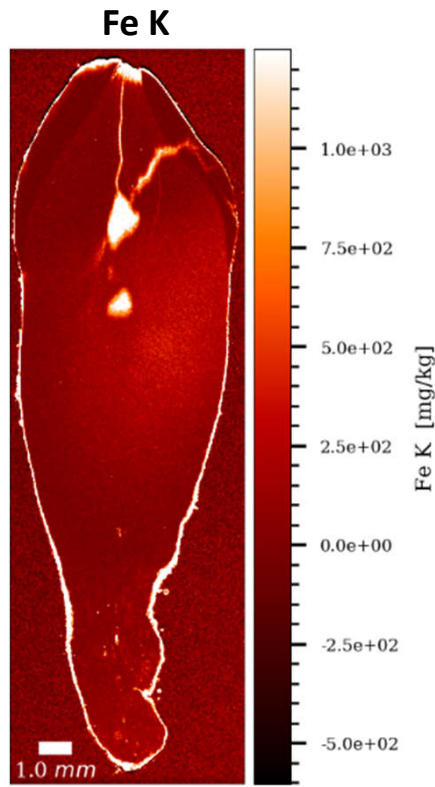
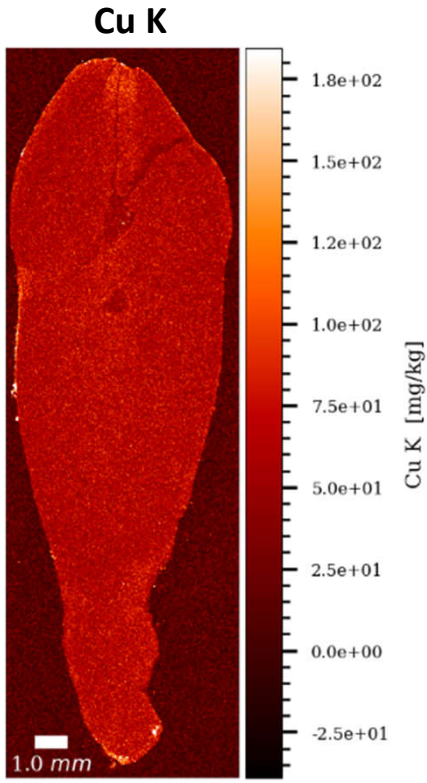
High resolution at 1 μm in acellular cementum

Odense 1149 URC

Overview at 10 μ m

Gauss (1.2x1.2)





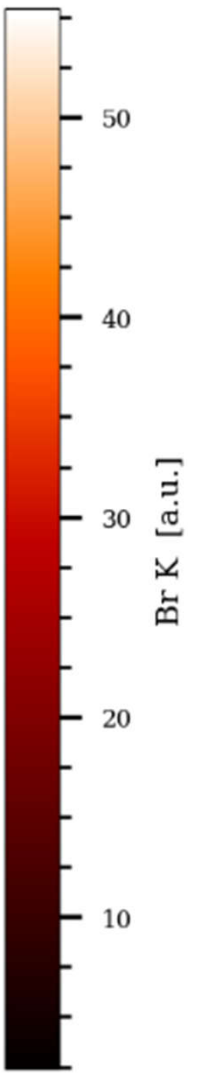
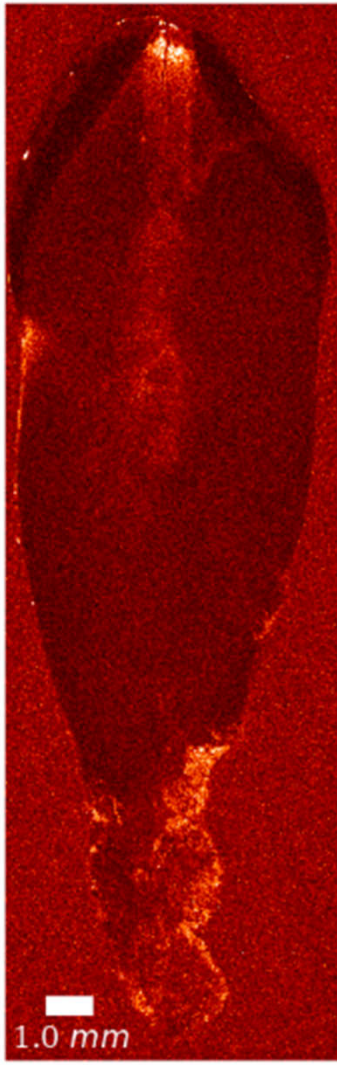
Odense 1149 URC

Overview at 10 μm

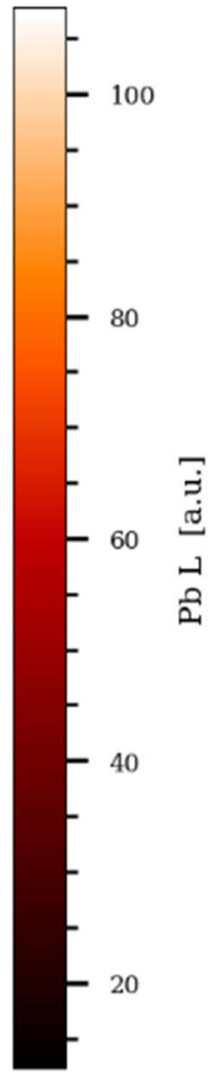
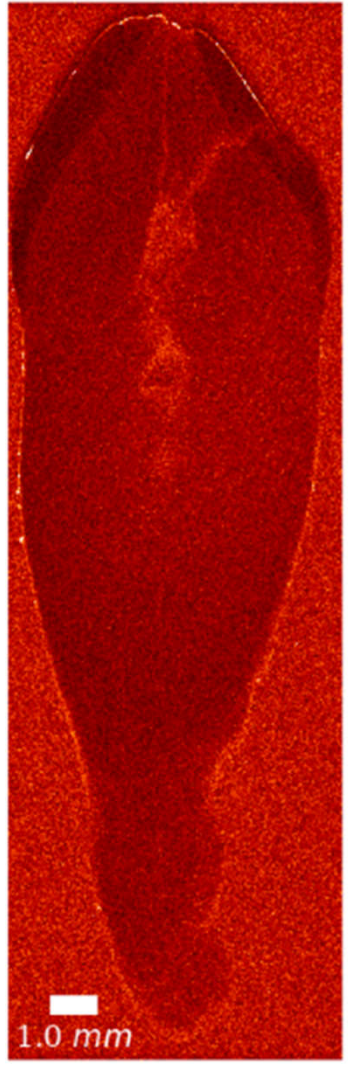
Uncalibrated data
(arbitrary units)

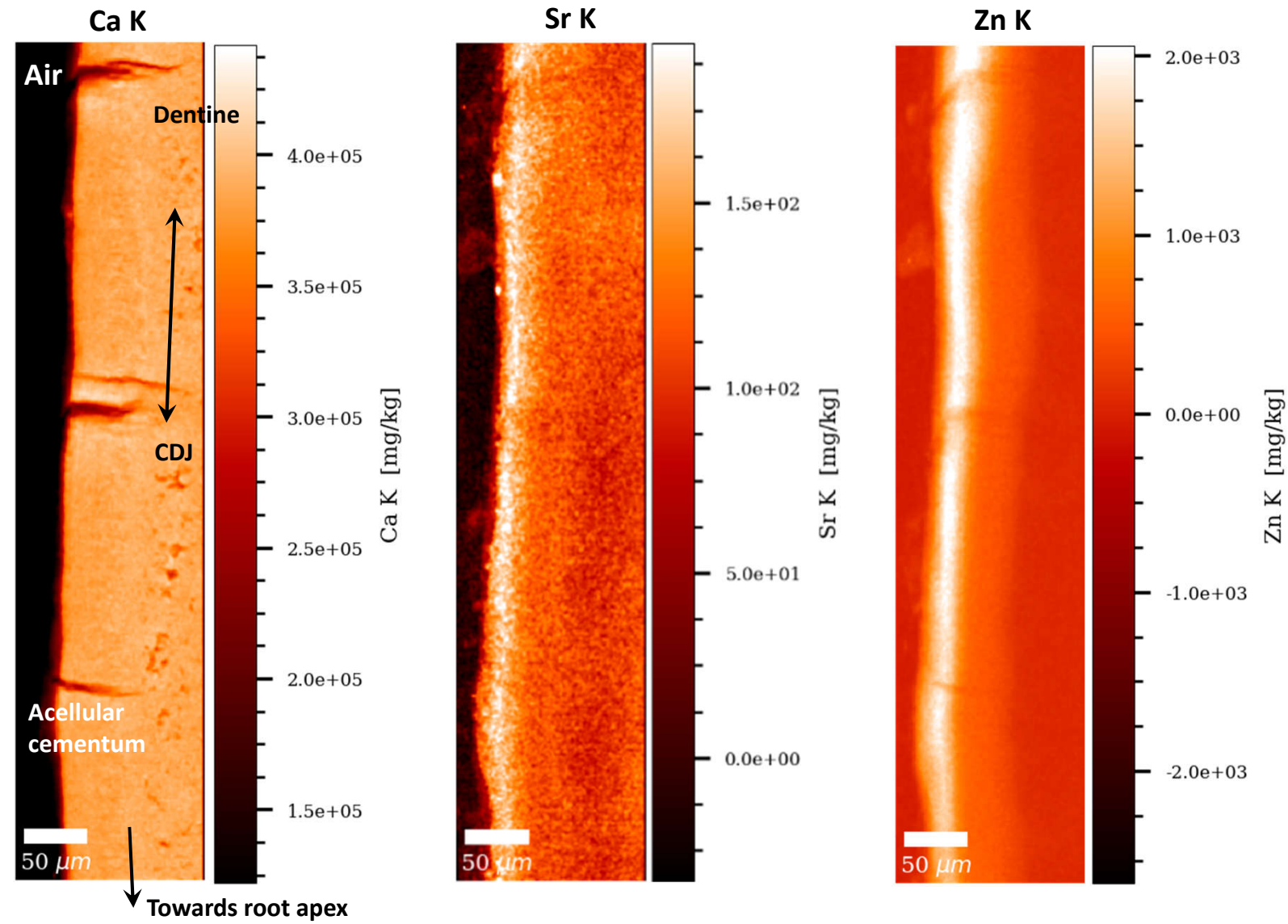
Gauss (1.2x1.2)

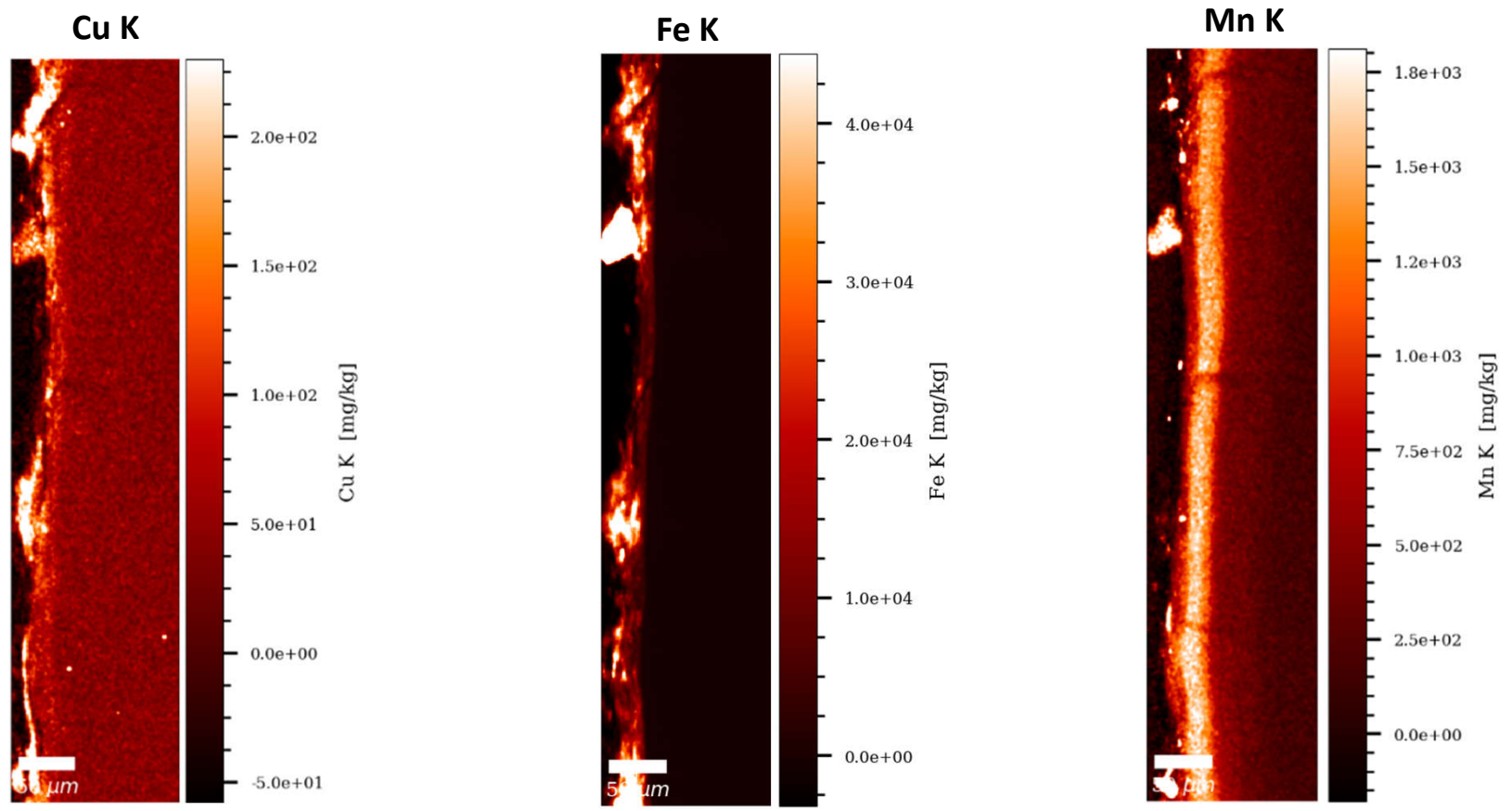
Br K



Pb L



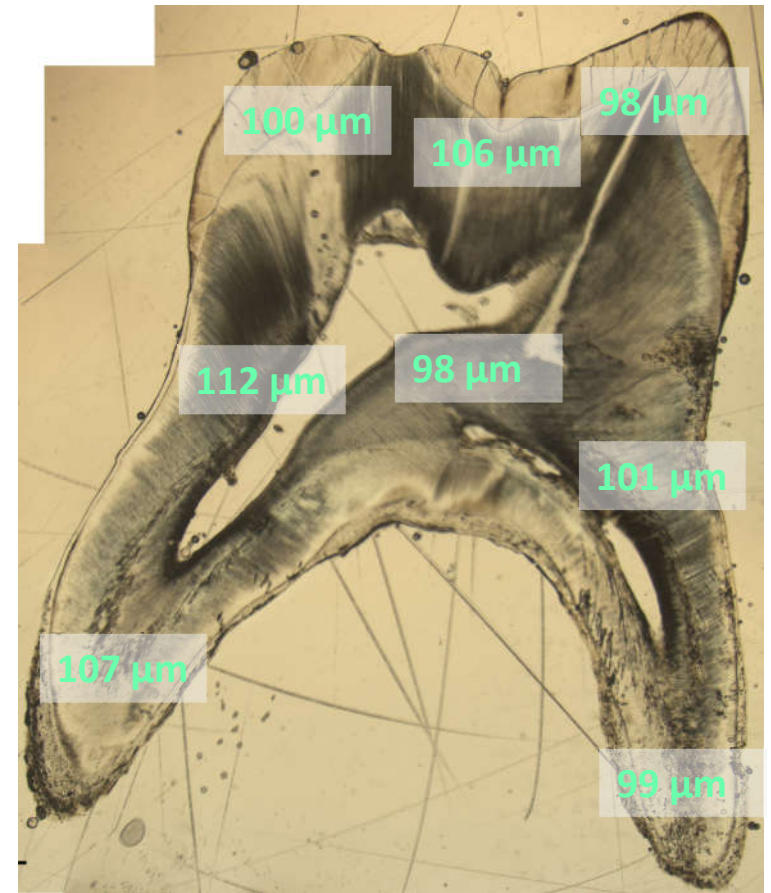
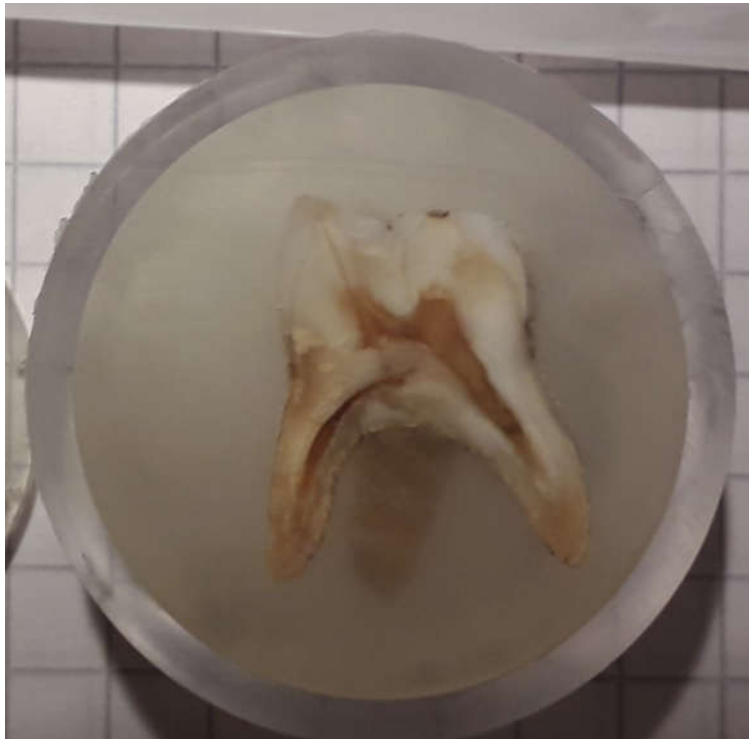




Odense – 1149 ULM1

♀ 20-30 yrs. 1301 – 1415 cal. CE

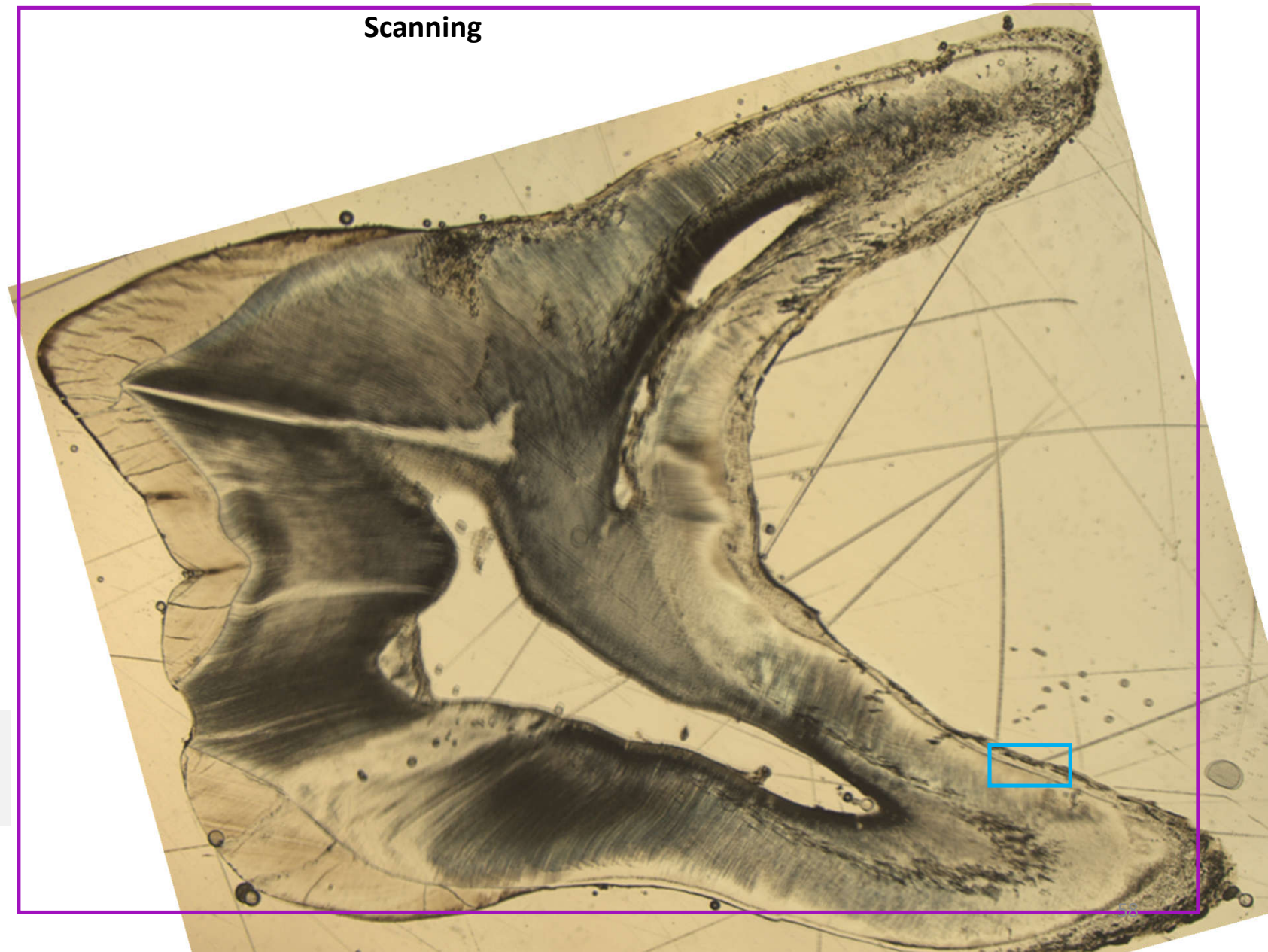
Average tooth section thickness
(μm): 103.5



Odense 1149 ULM1

Overview at 10 μm
*Problem of offset when
centering sample*

Scanning



**High resolution at 1 μm in
mixed cellular and acellular
cementum**

Odense 1149 ULM1

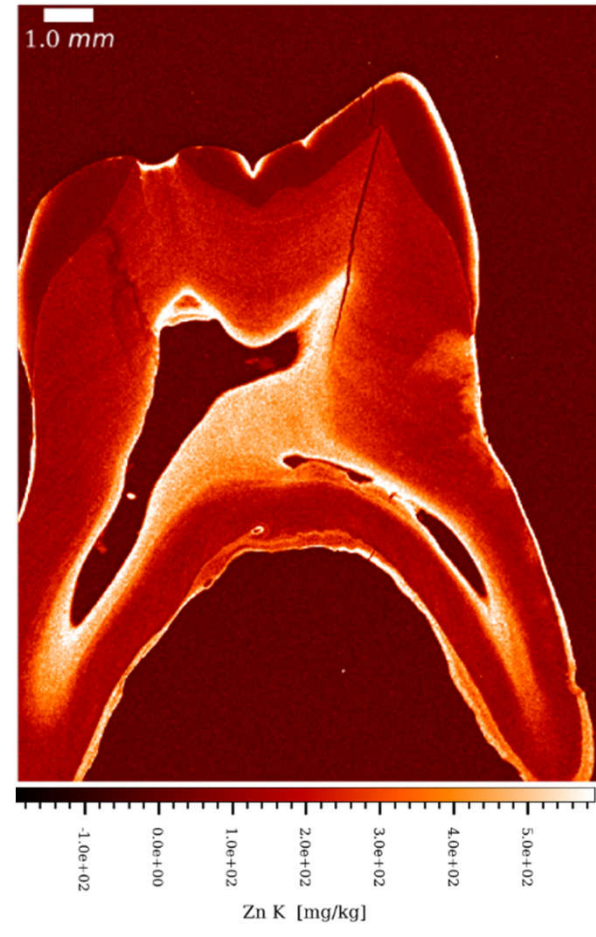
Overview at 10 μ m

Gauss (1x1)

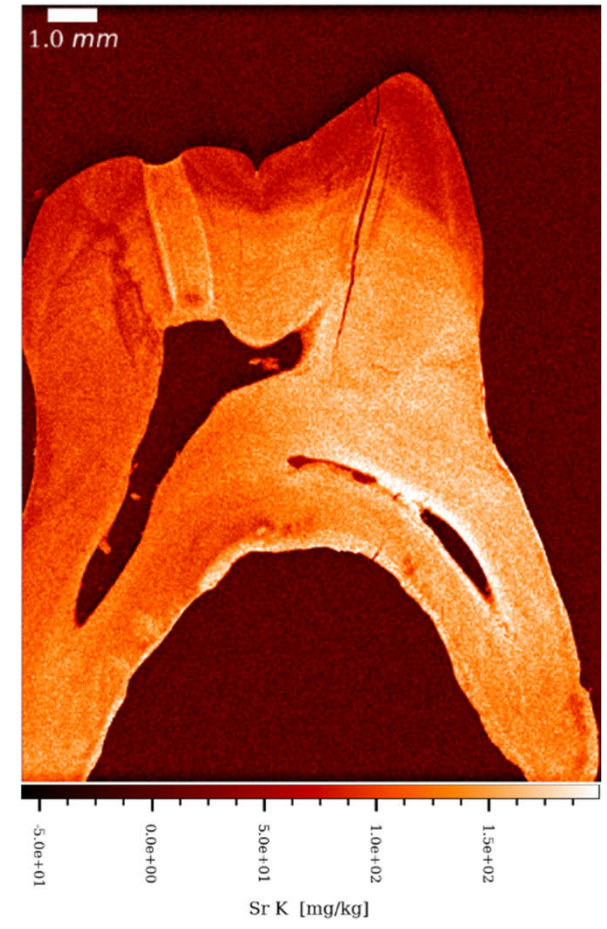
Ca K



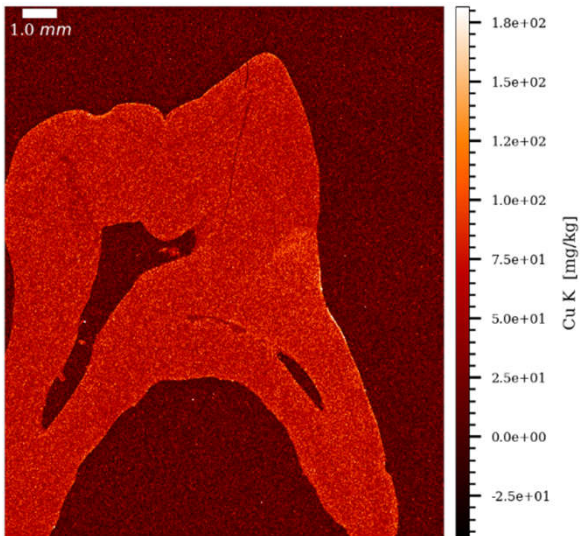
Sr K



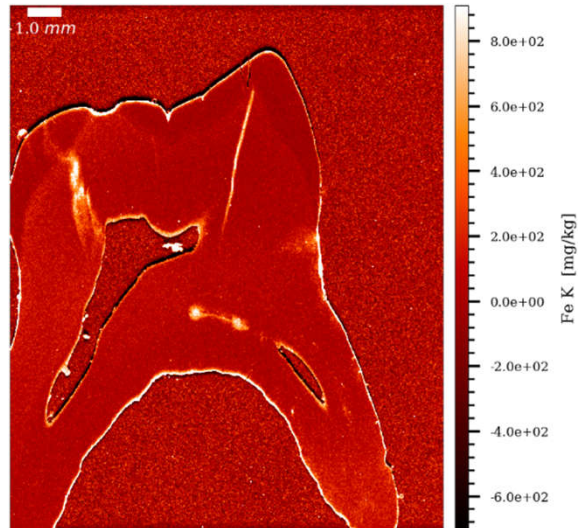
Zn K



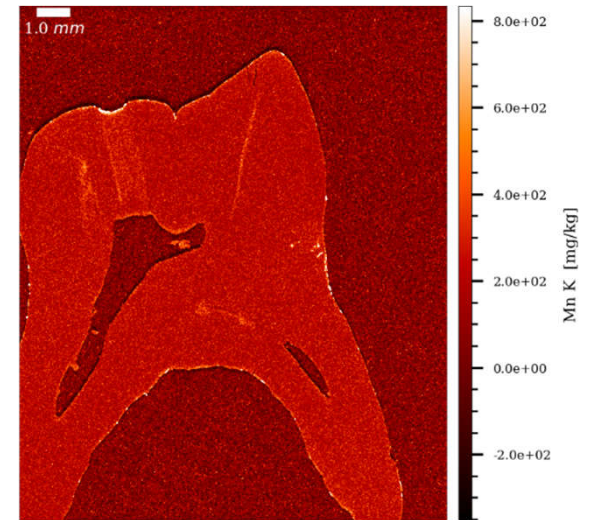
Cu K



Fe K



Mn K



Odense 1149 ULM1

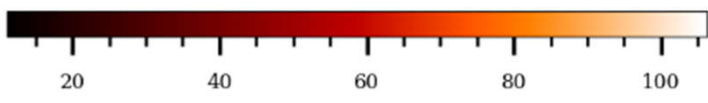
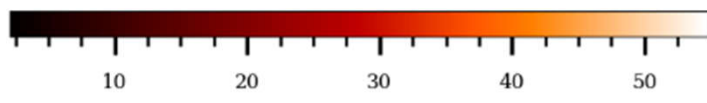
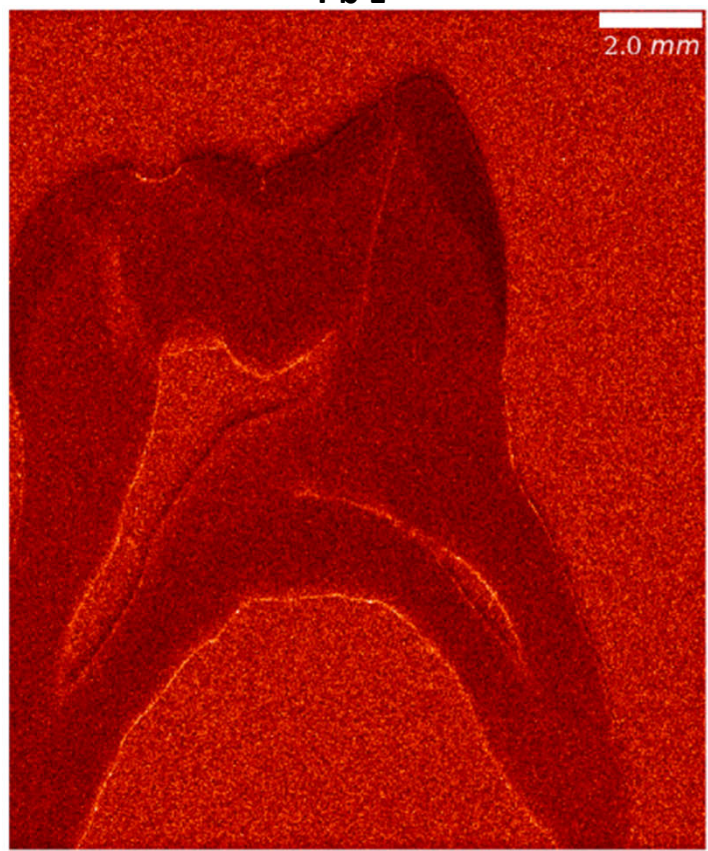
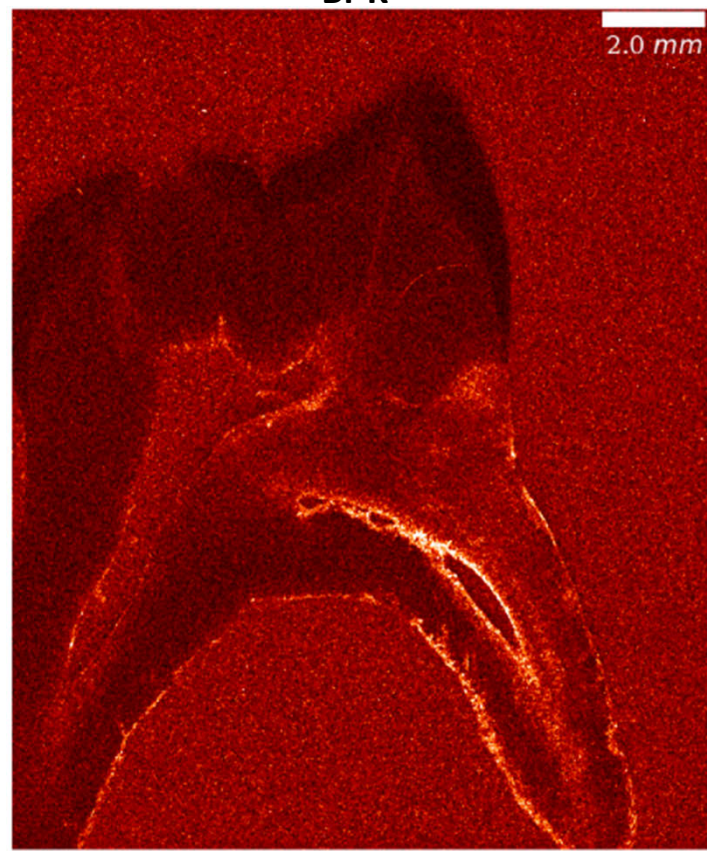
Overview at 10 μ m

Uncalibrated data
(arbitrary units)

Gauss (1x1)

Br K

Pb L



Br K [a.u.]

Pb L [a.u.]

Odense 1149 ULM1

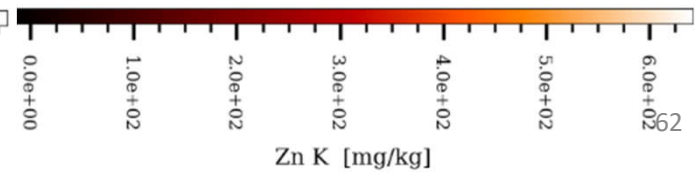
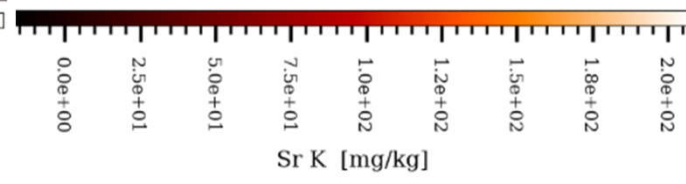
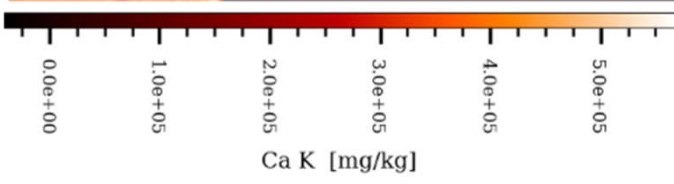
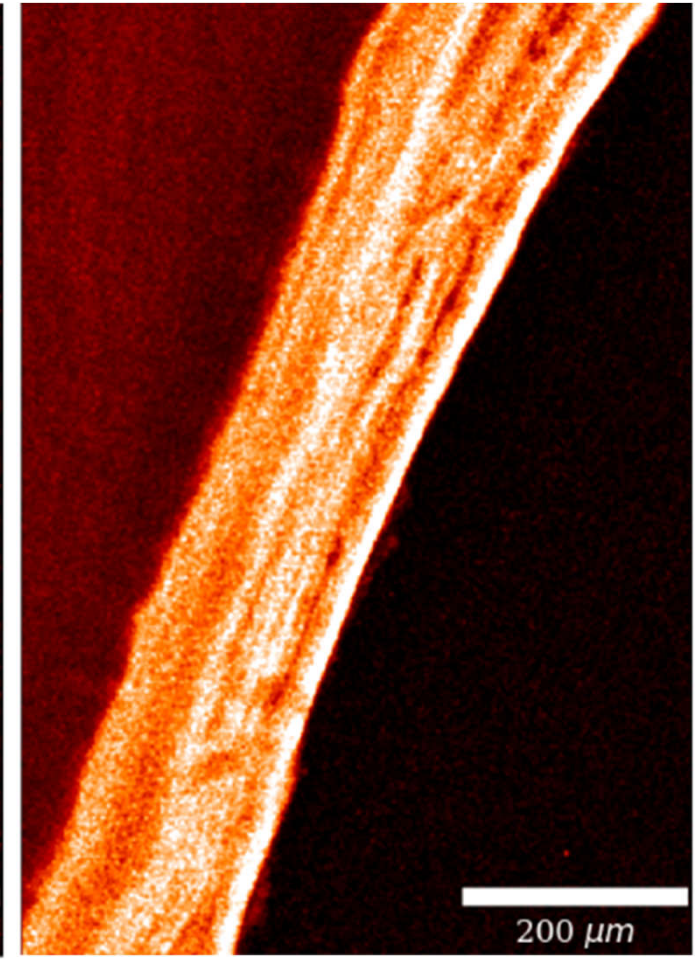
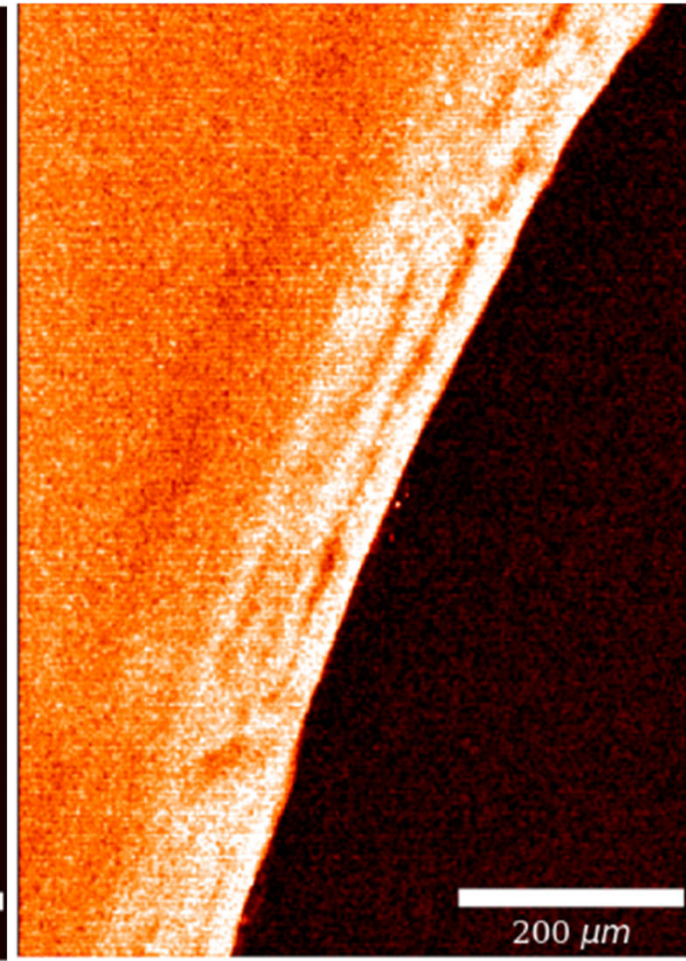
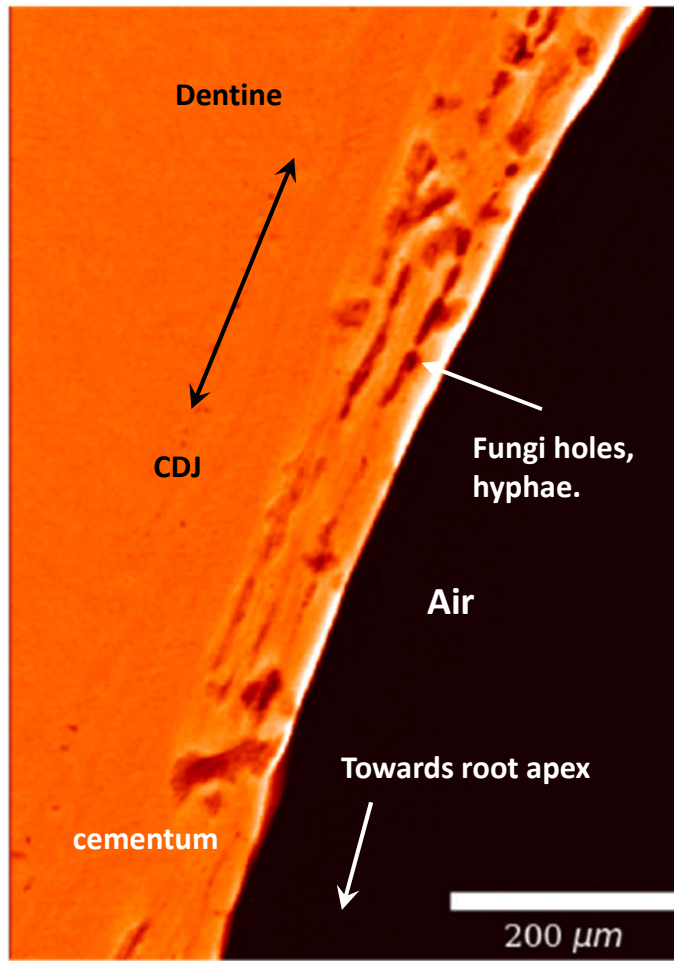
High resolution at 1 μm

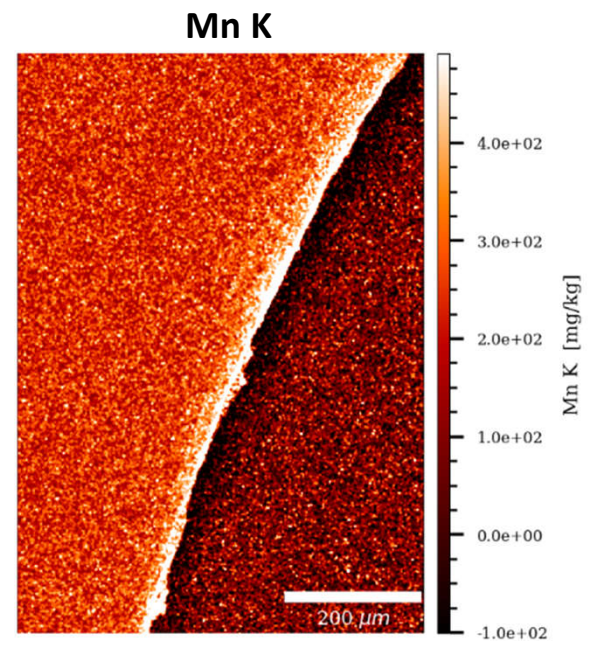
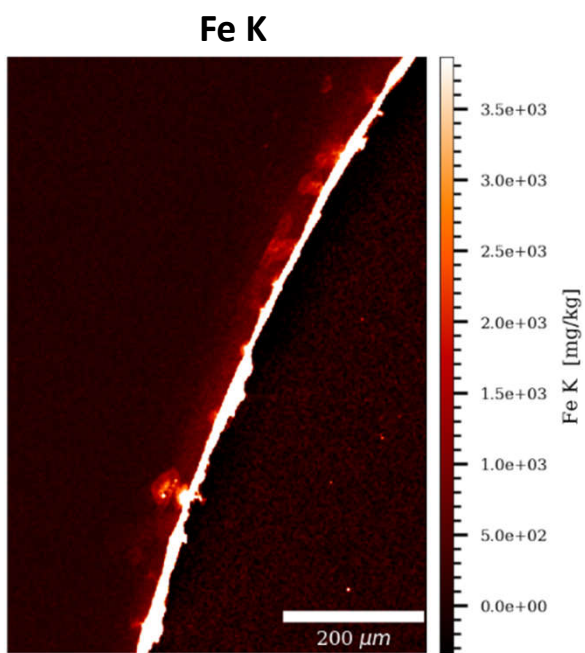
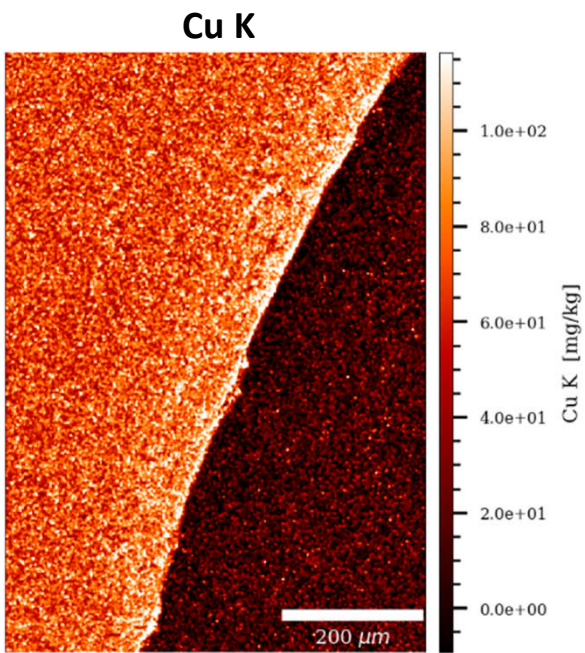
Gauss (1.2x1.2)

Ca K

Sr K

Zn K

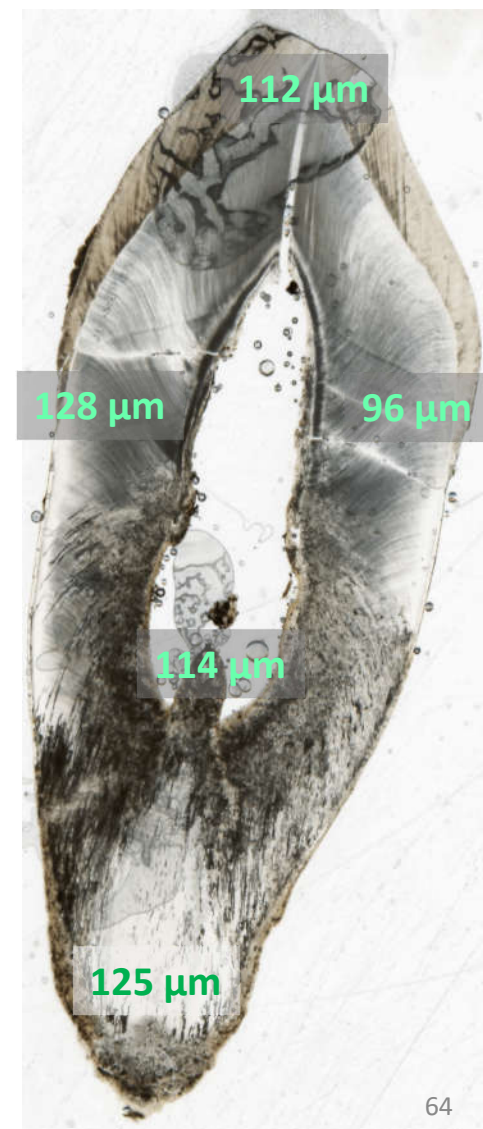




Næstved – 6 ULC



~20 yrs. mid-13th – mid-16th c. CE



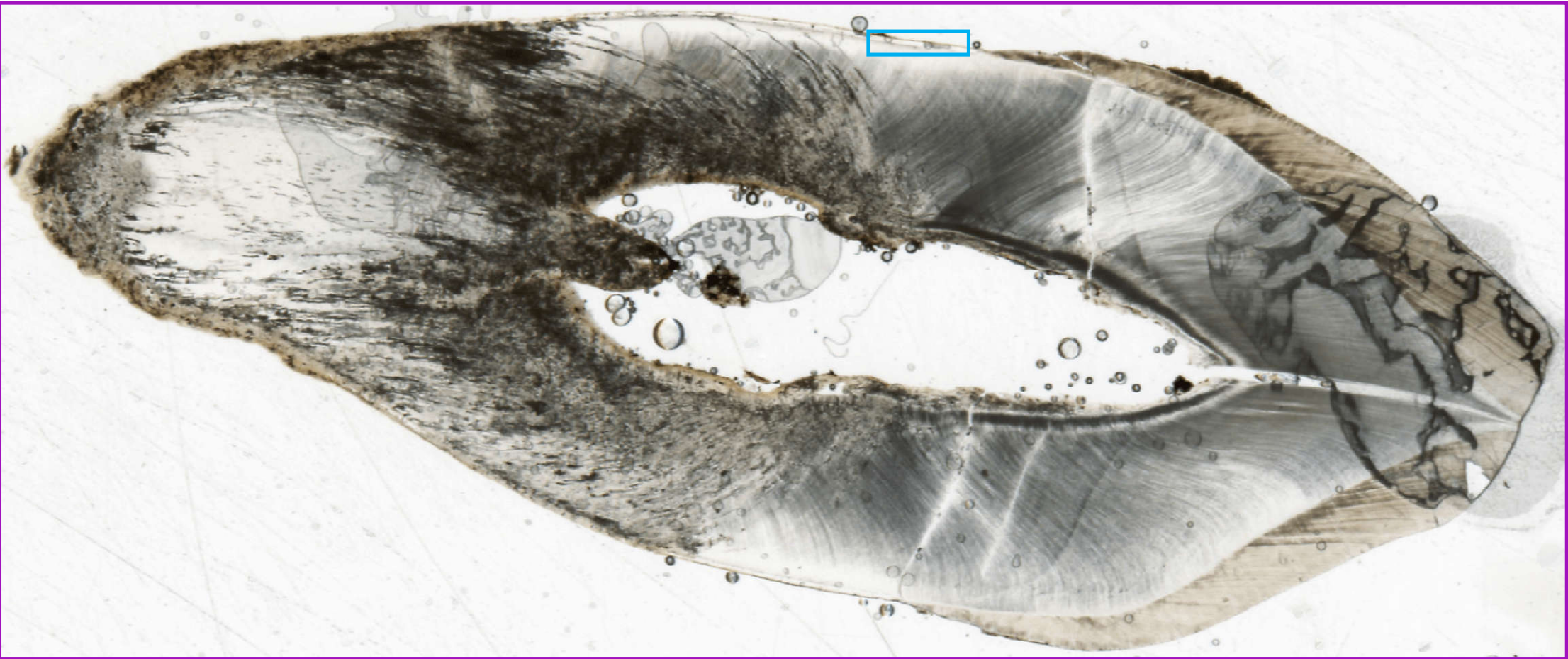
Average tooth section
thickness (µm): 115.0

Næstved 6 ULC

Scanning

Overview at 10 μm

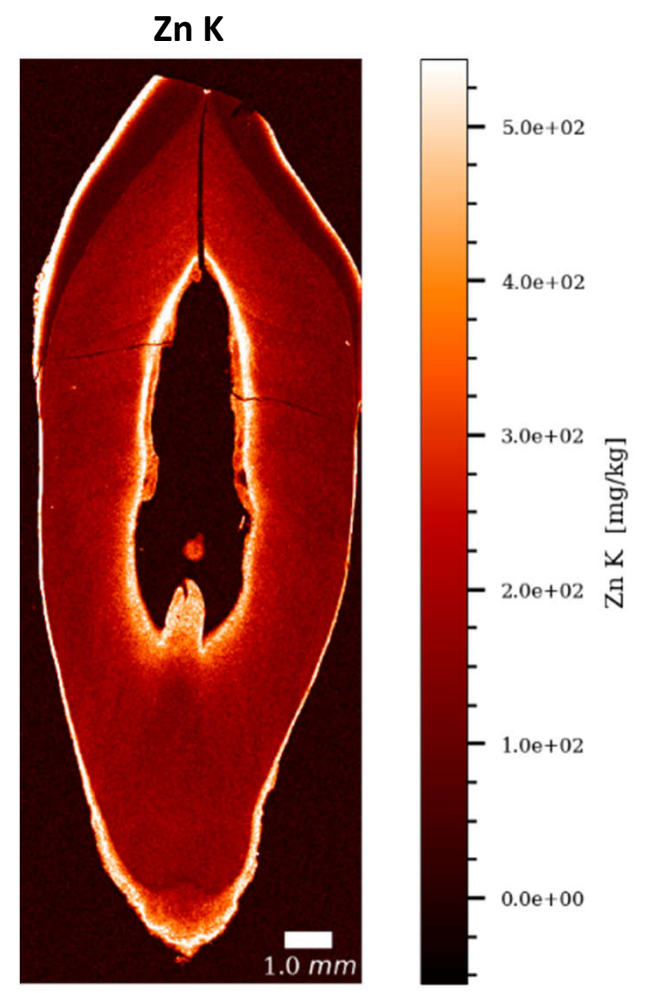
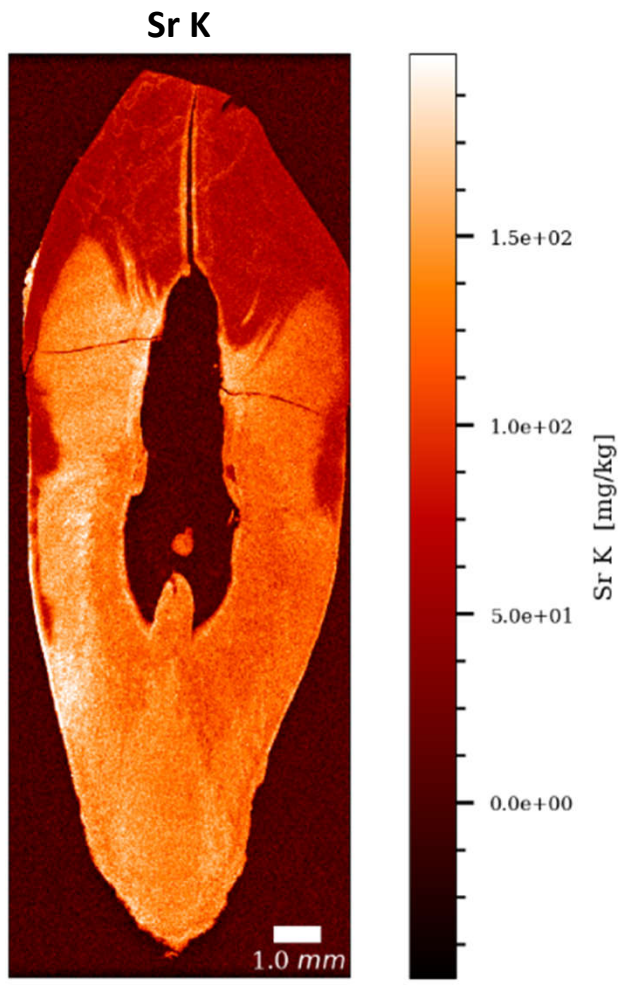
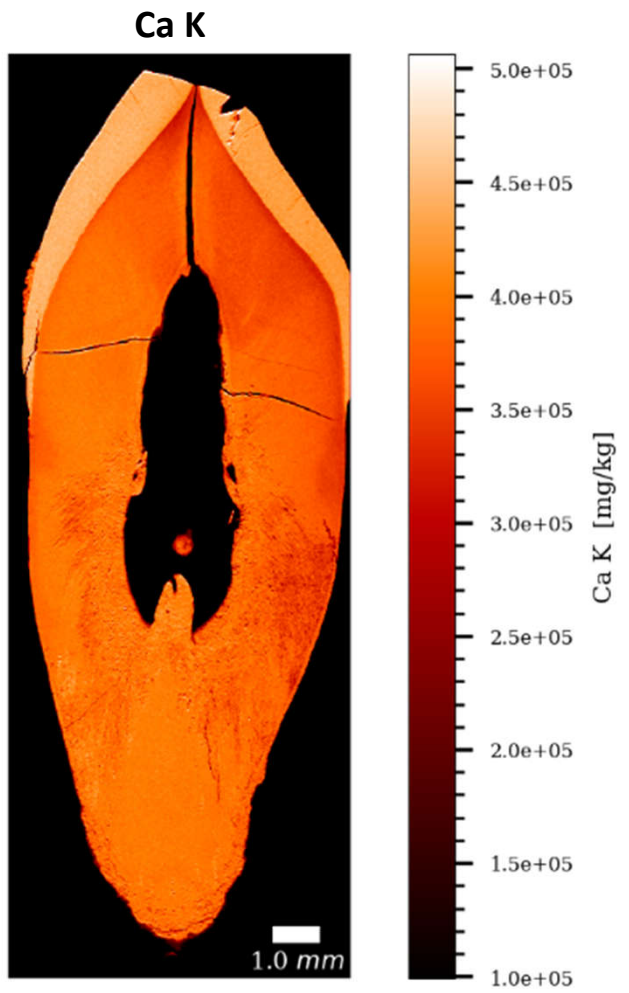
High resolution at 1 μm in acellular cementum

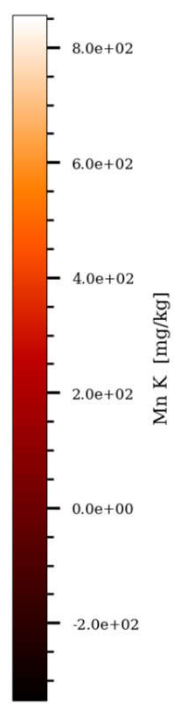
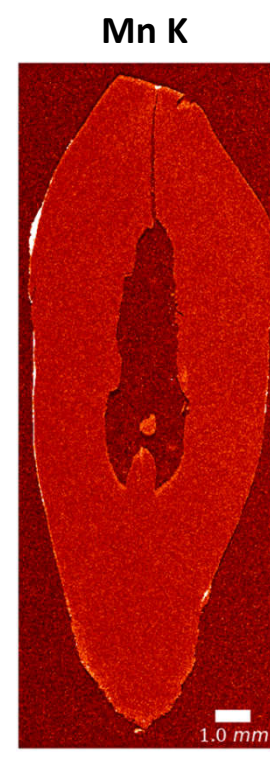
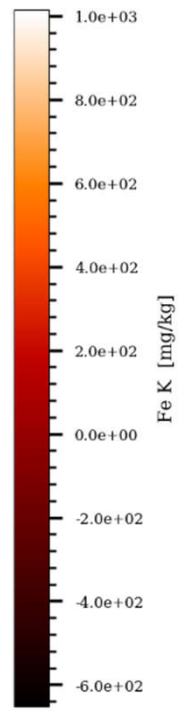
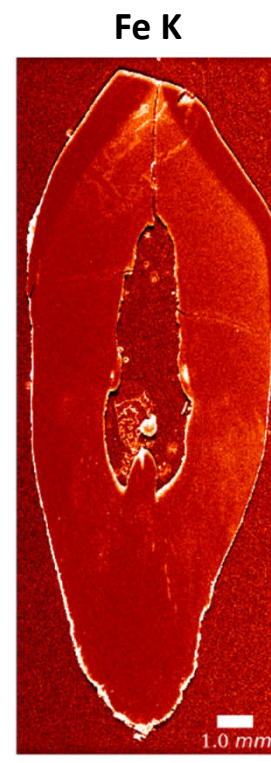
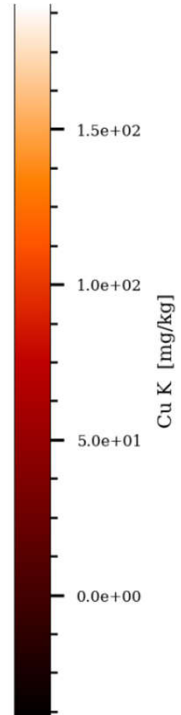
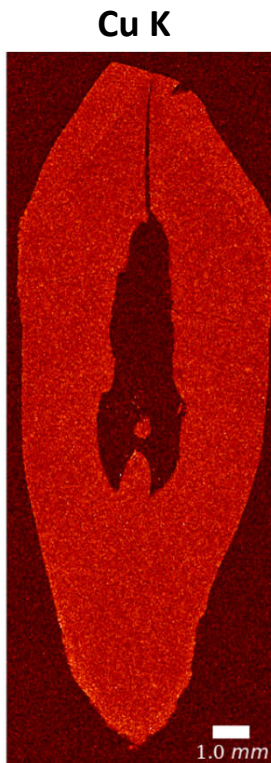


Næstved 6 ULC

Overview at 10 μ m

Gauss (1x1)



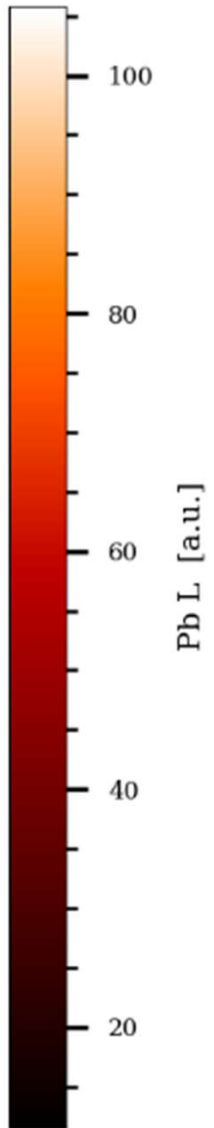
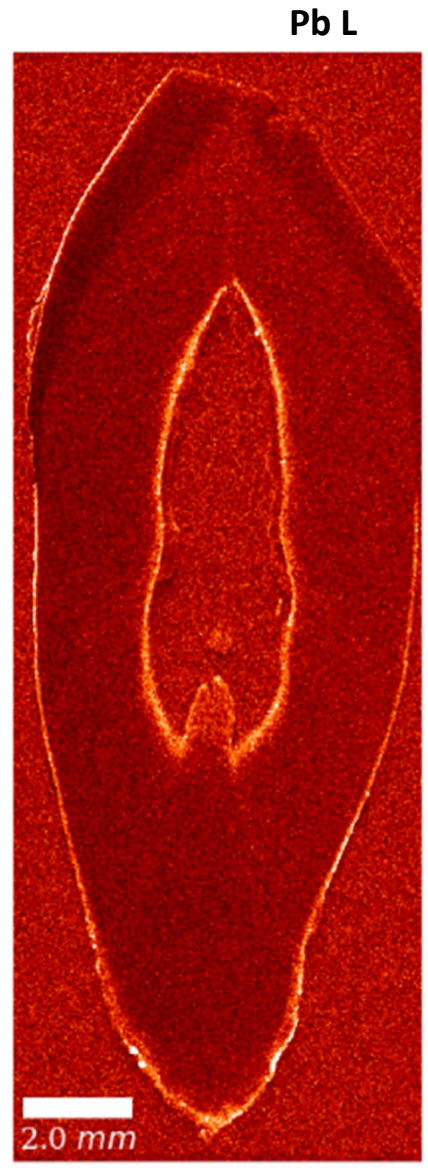
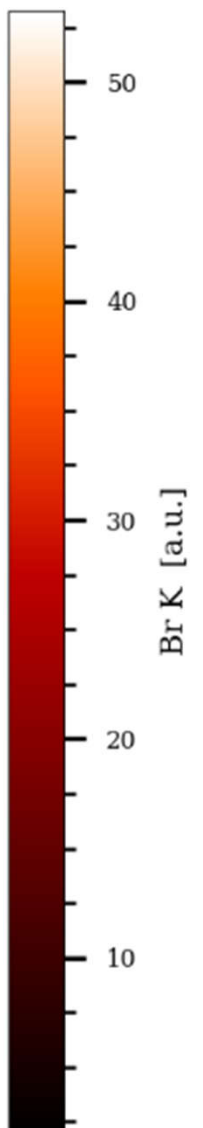
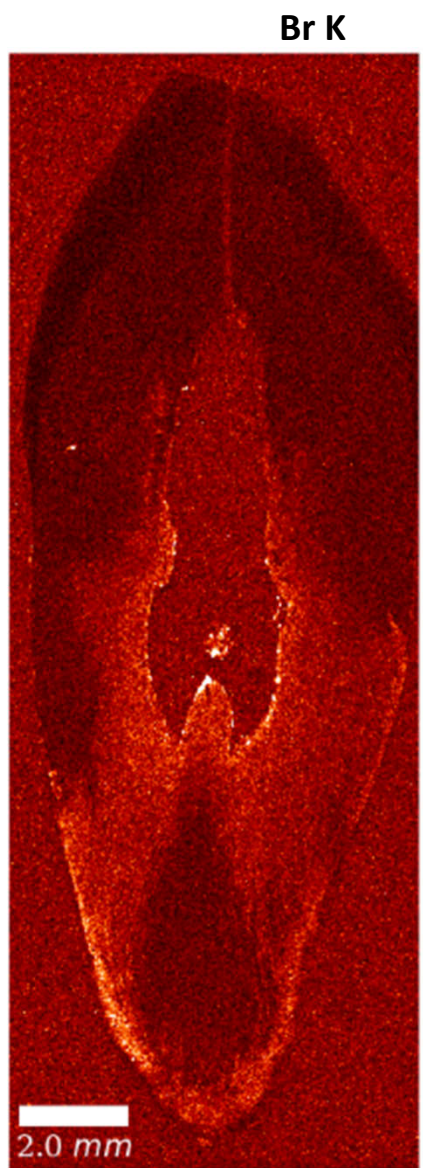


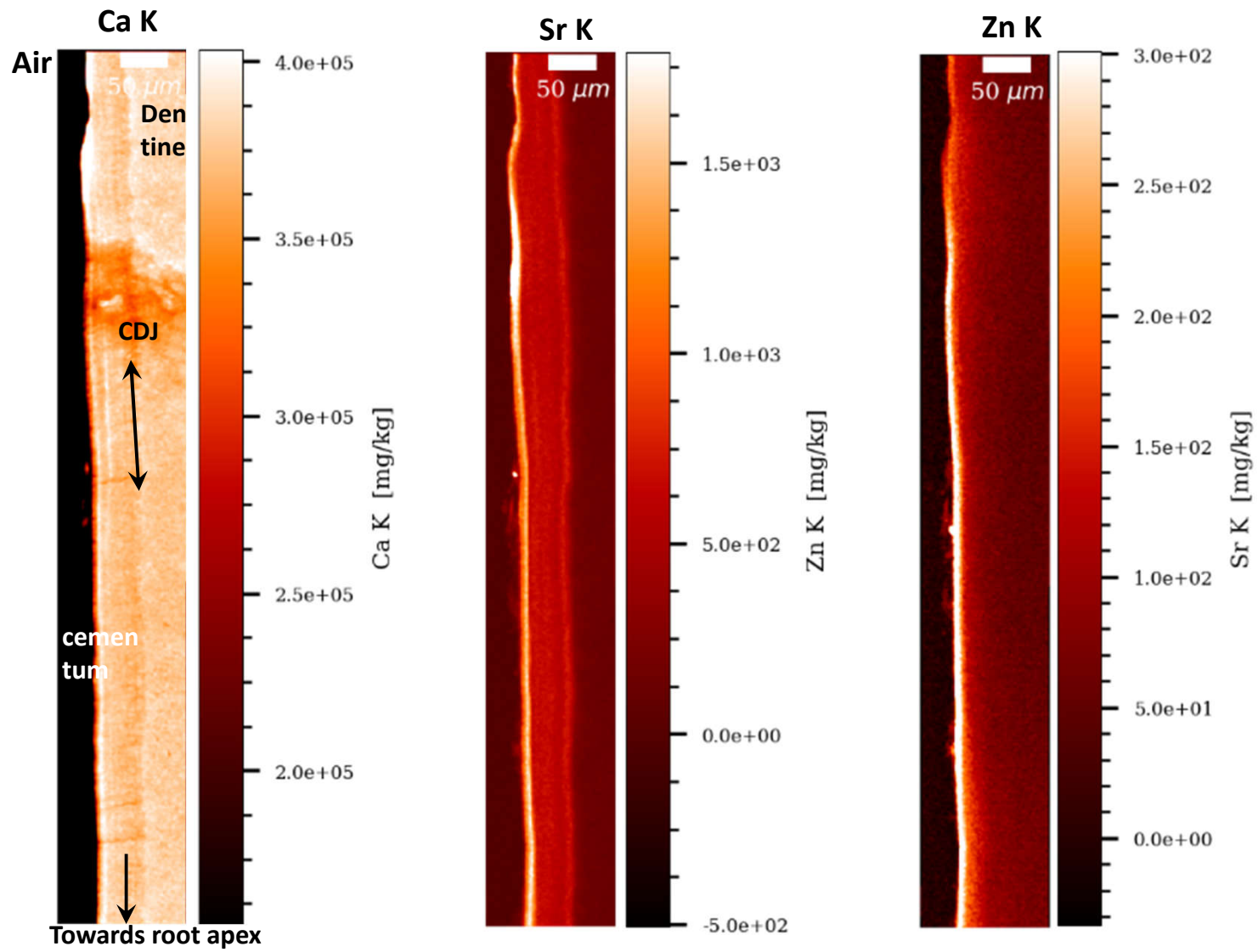
Næstved 6 ULC

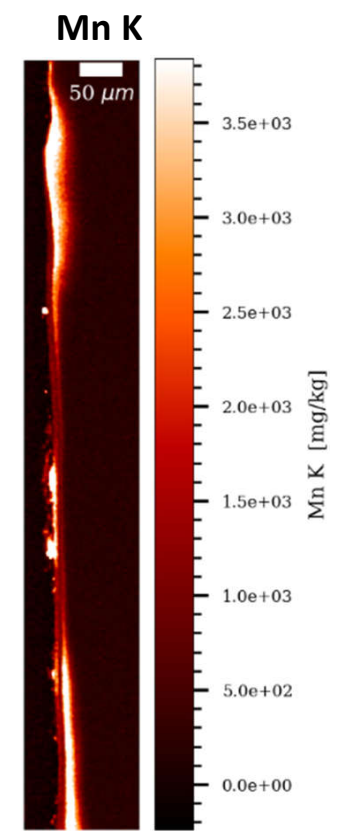
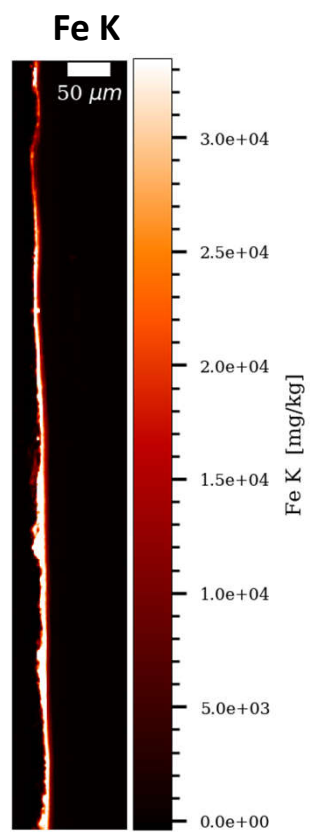
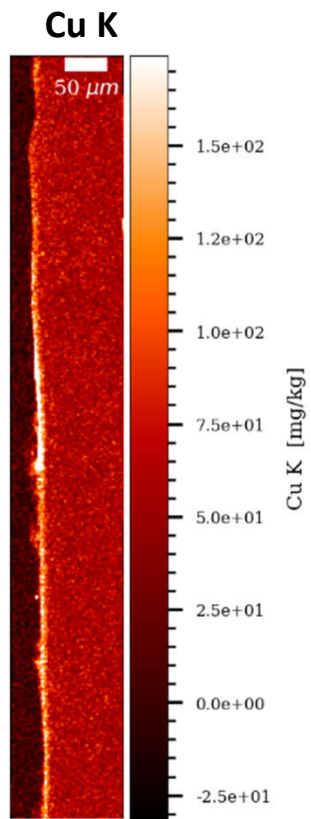
Overview at 10 μm

Uncalibrated data
(arbitrary units)

Gauss (1x1)



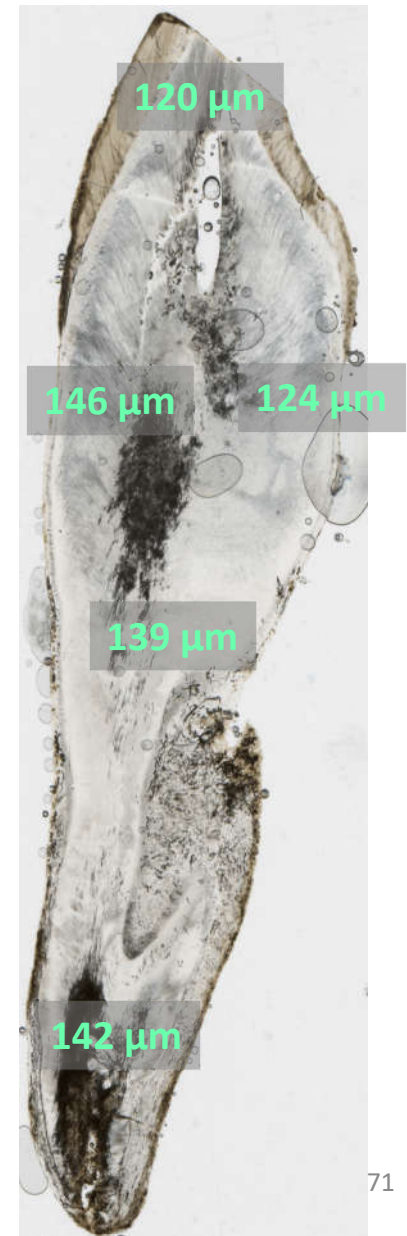




Næstved – 211 URC



40-45 yrs. 1184 – 1266 cal. CE



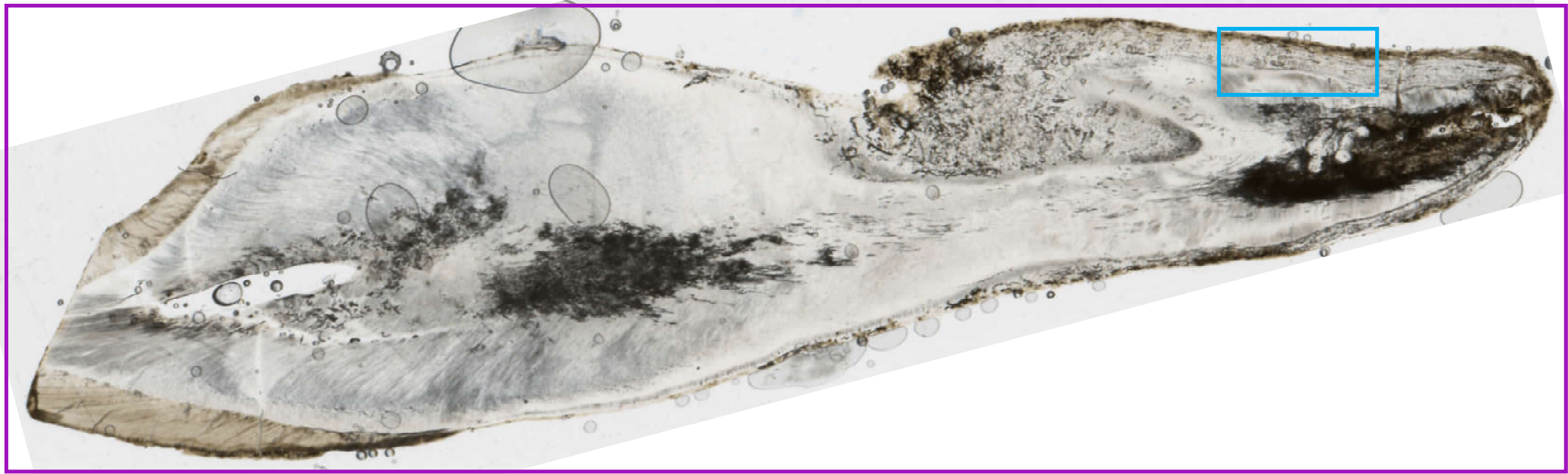
Average tooth section thickness (μm): 134.2

Næstved 211 URC

Scanning

Overview at 10 μ m

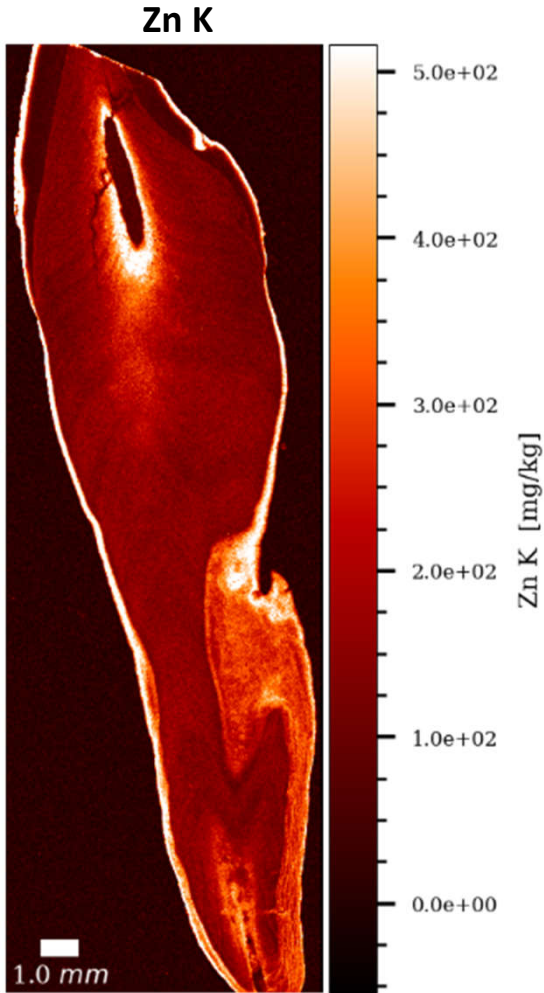
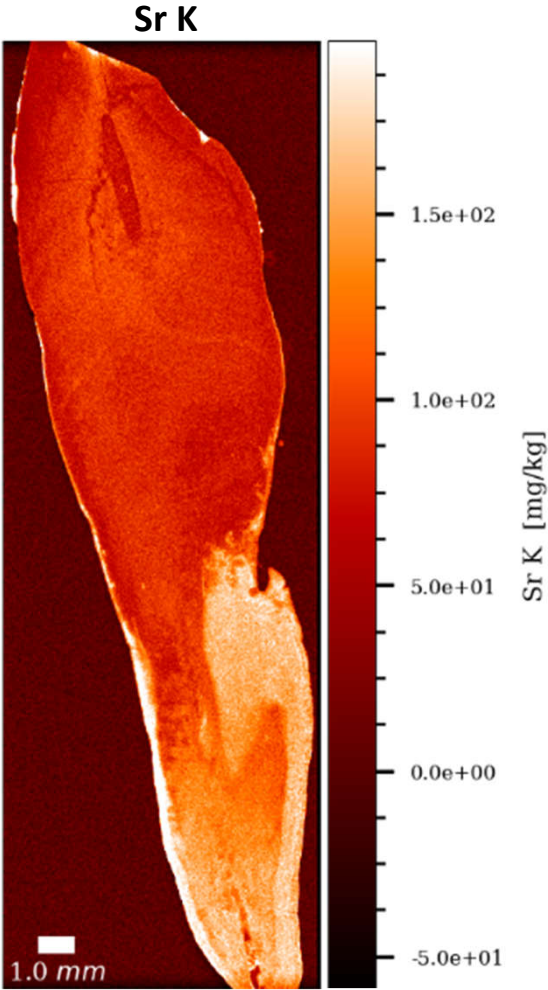
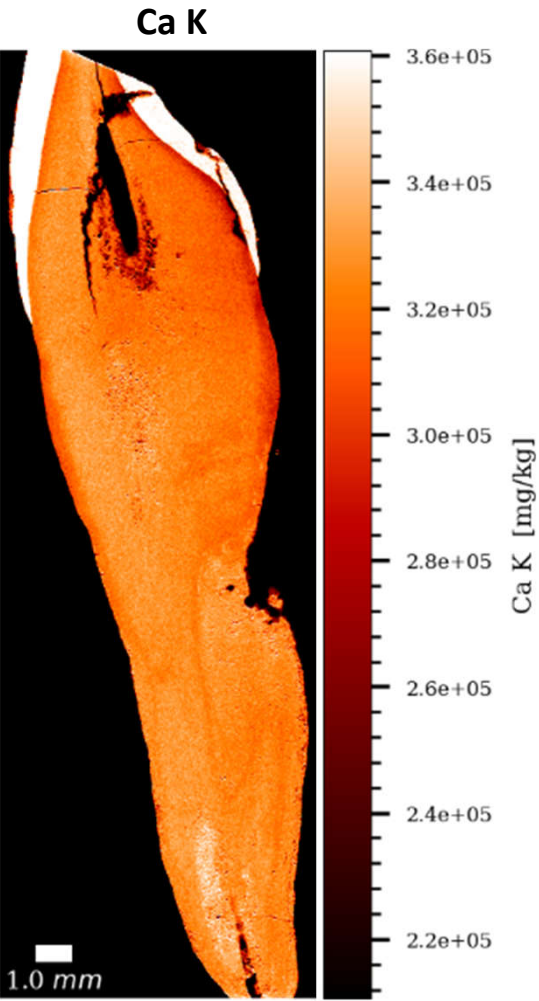
High resolution at 1 μ m

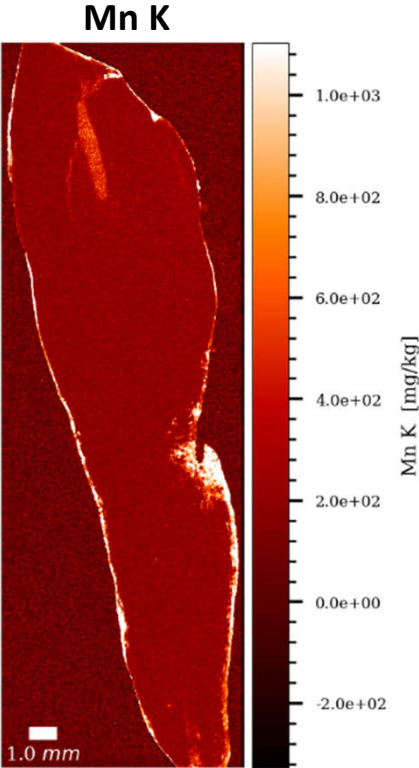
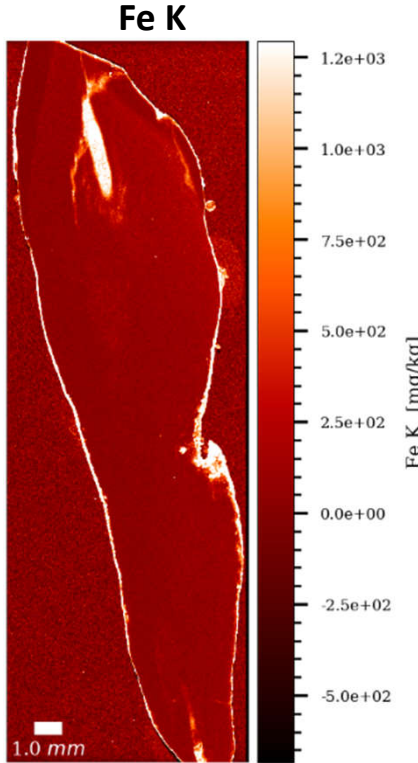
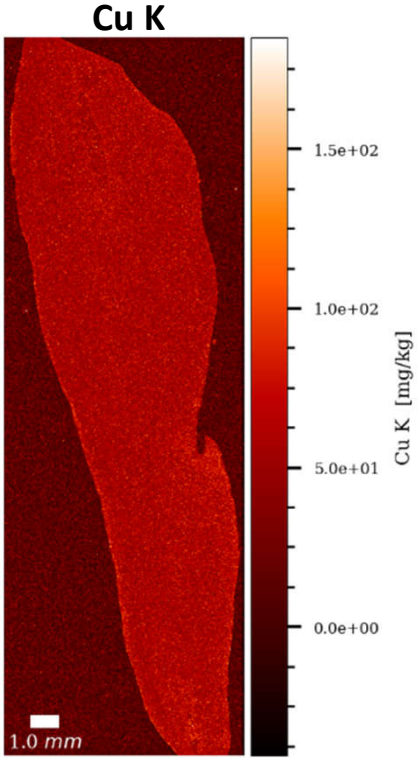


Næstved 211 URC

Overview at 10 μ m

Gauss (1.2x1.2)





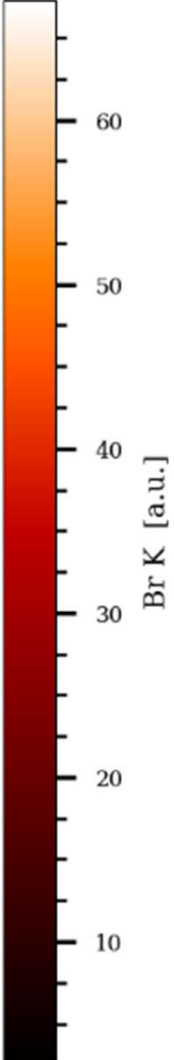
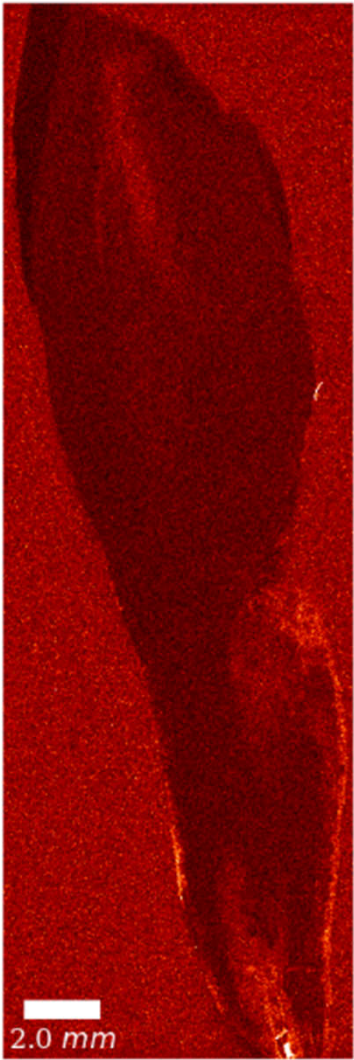
Næstved 211 URC

Overview at 10 μm

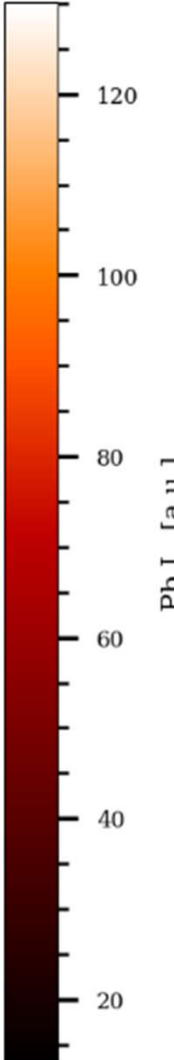
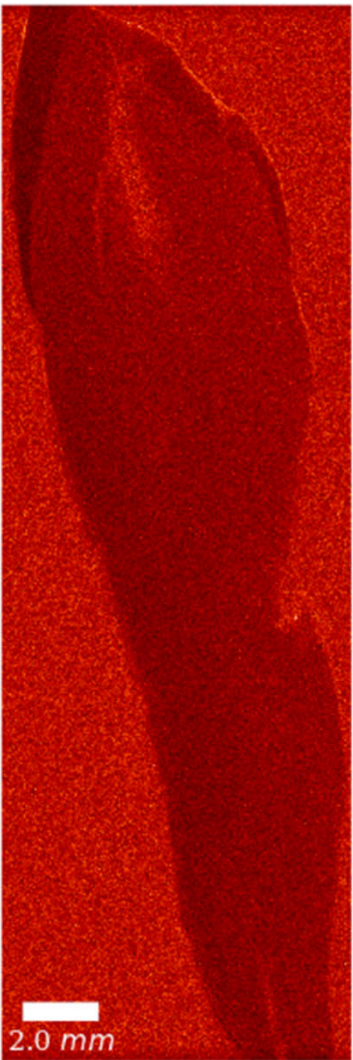
Uncalibrated data
(arbitrary units)

Gauss (1.2x1.2)

Br K



Pb L



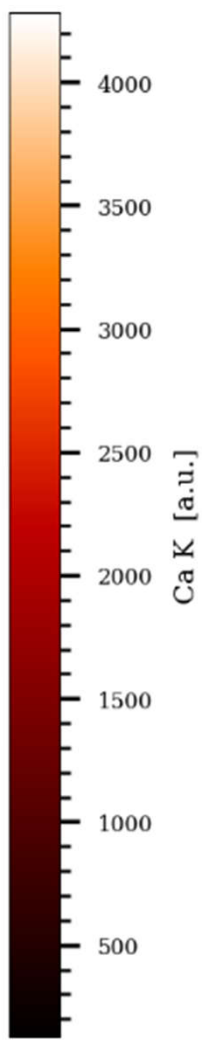
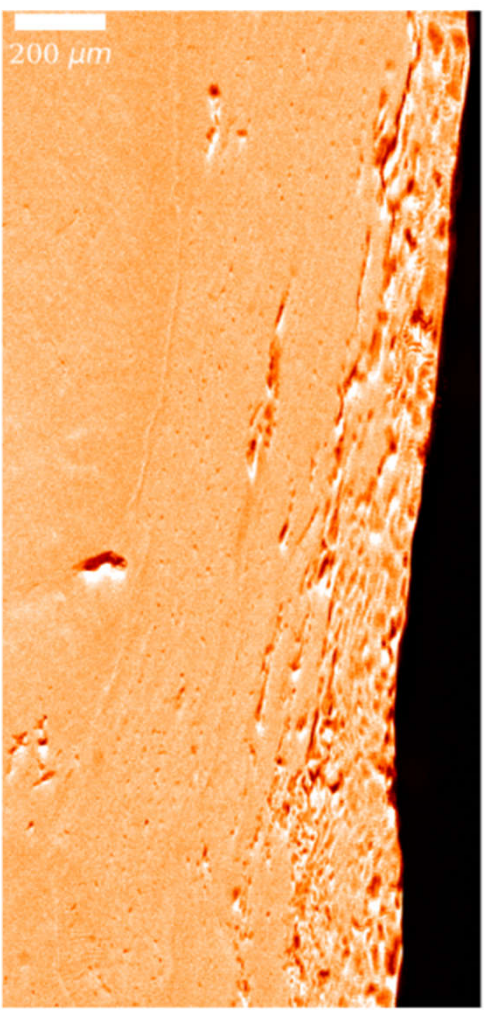
Næstved 211 URC

High resolution at 1 μm

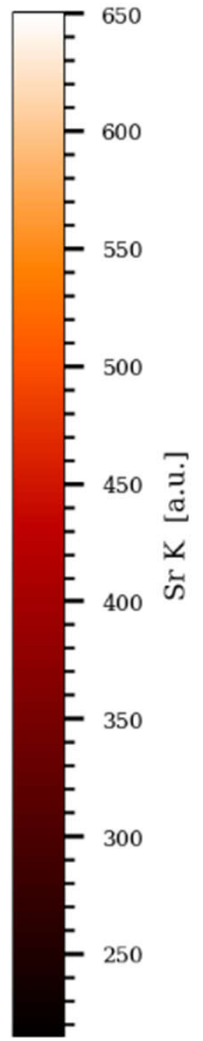
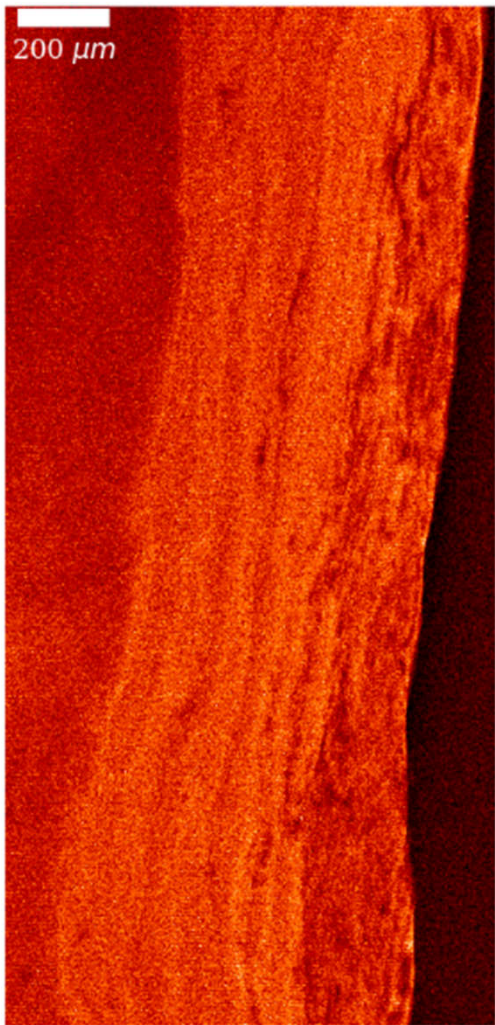
Uncalibrated data
(arbitrary units)

Gauss (1x1)

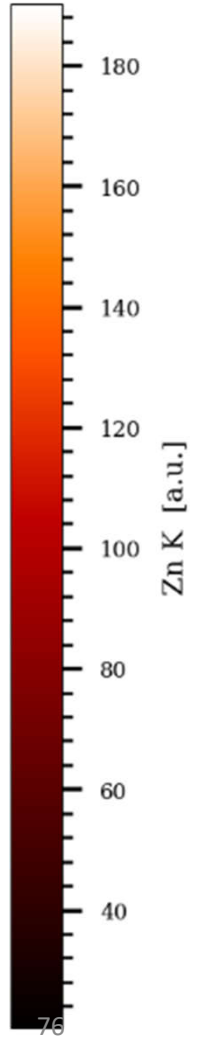
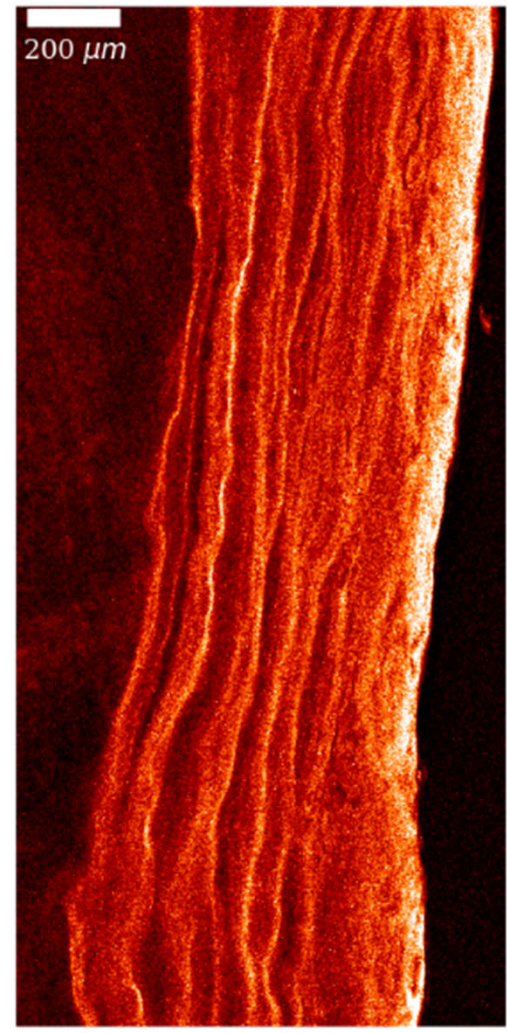
Ca K

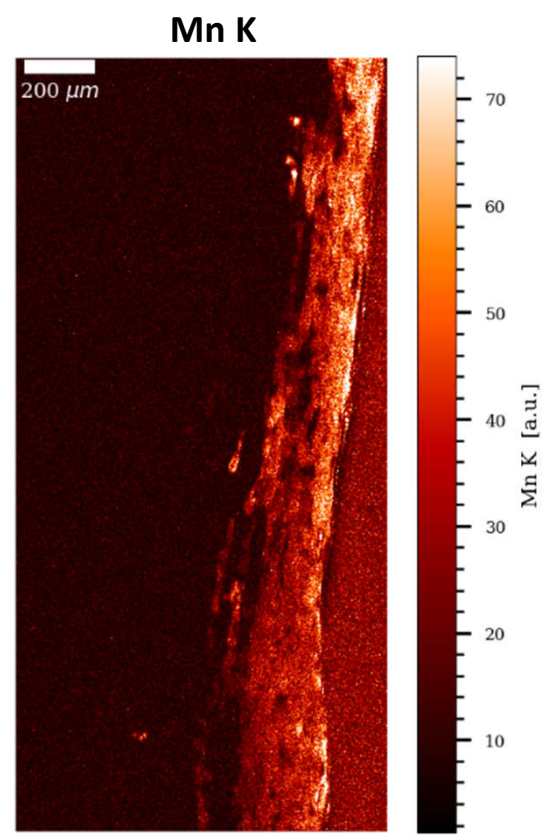
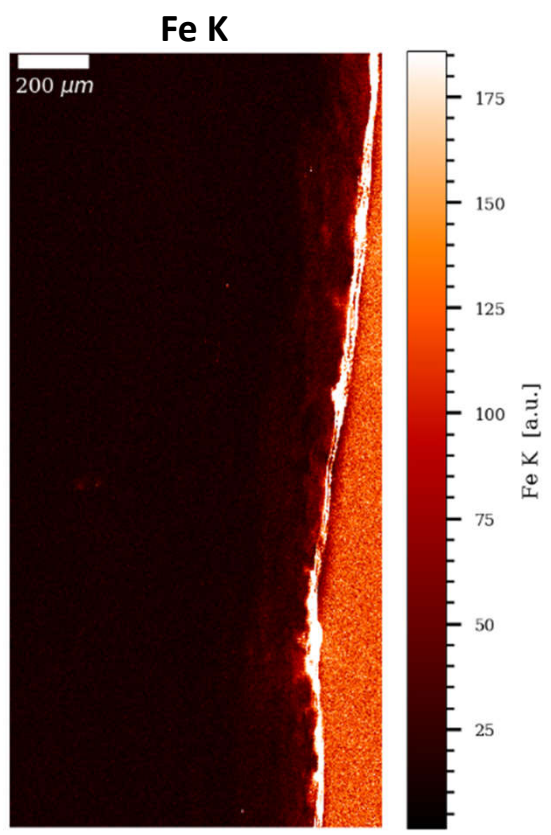
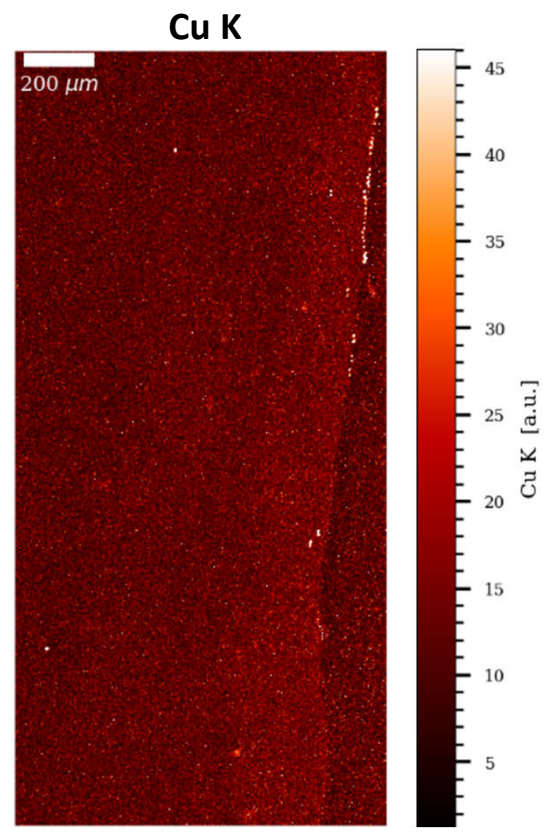


Sr K



Zn K





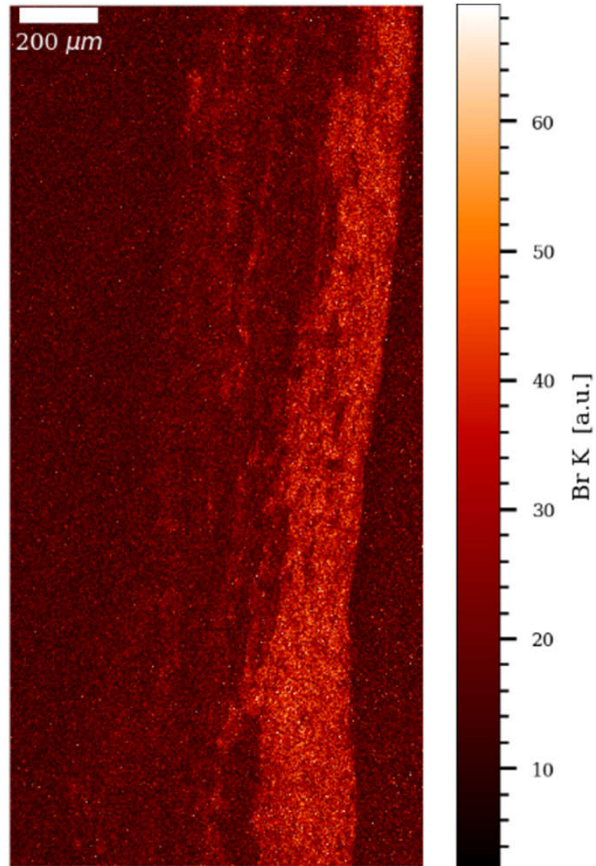
Næstved 211 URC

High resolution at 1 μm

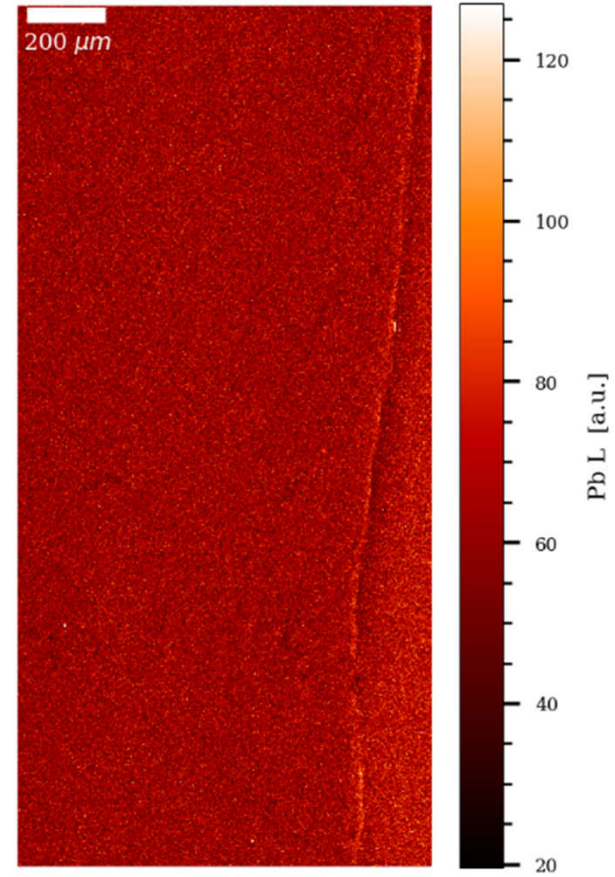
Uncalibrated data
(arbitrary units)

Gauss (1x1)

Br K

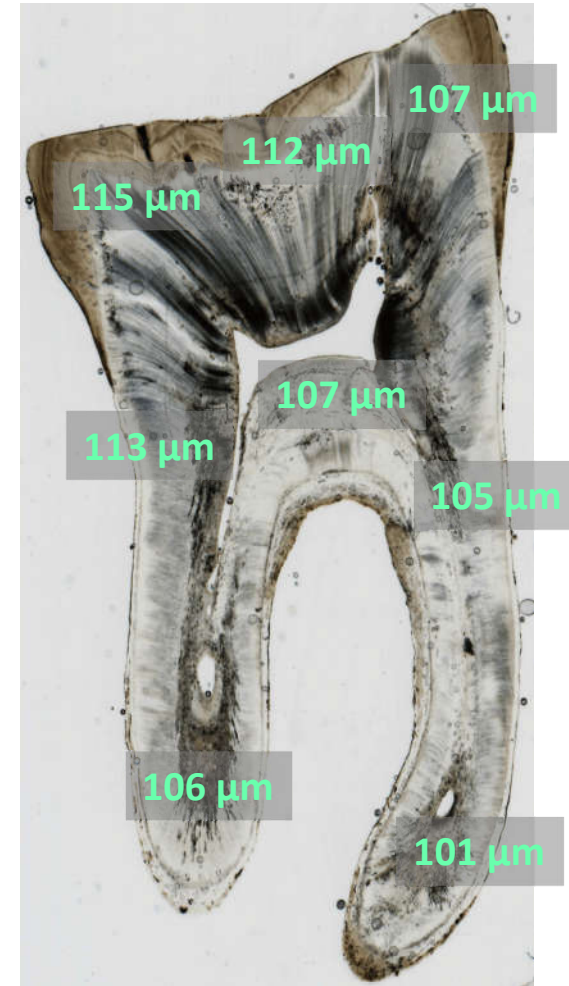
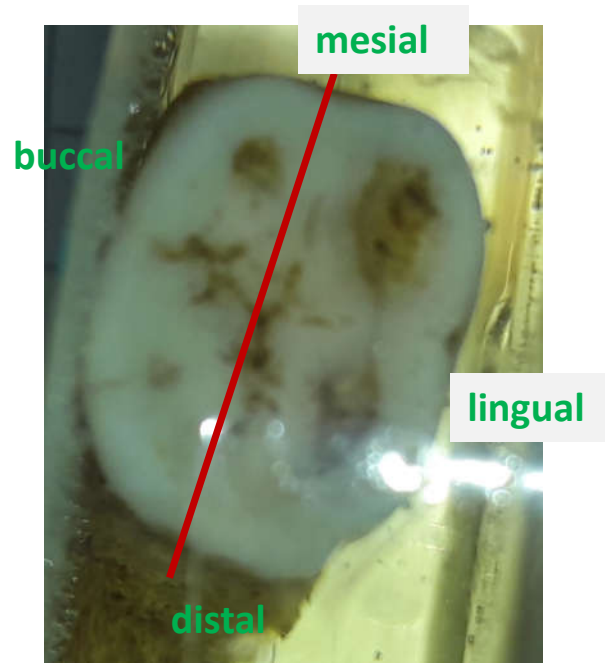


Pb L



Næstved – 211 LRM1

♀ 40-45 yrs. 1184 – 1266 cal. CE



Average tooth section thickness (µm): 108.3

Overview at 10 μm

High resolution at 1.5 μm in
acellular cementum



Næstved 211 LRM1

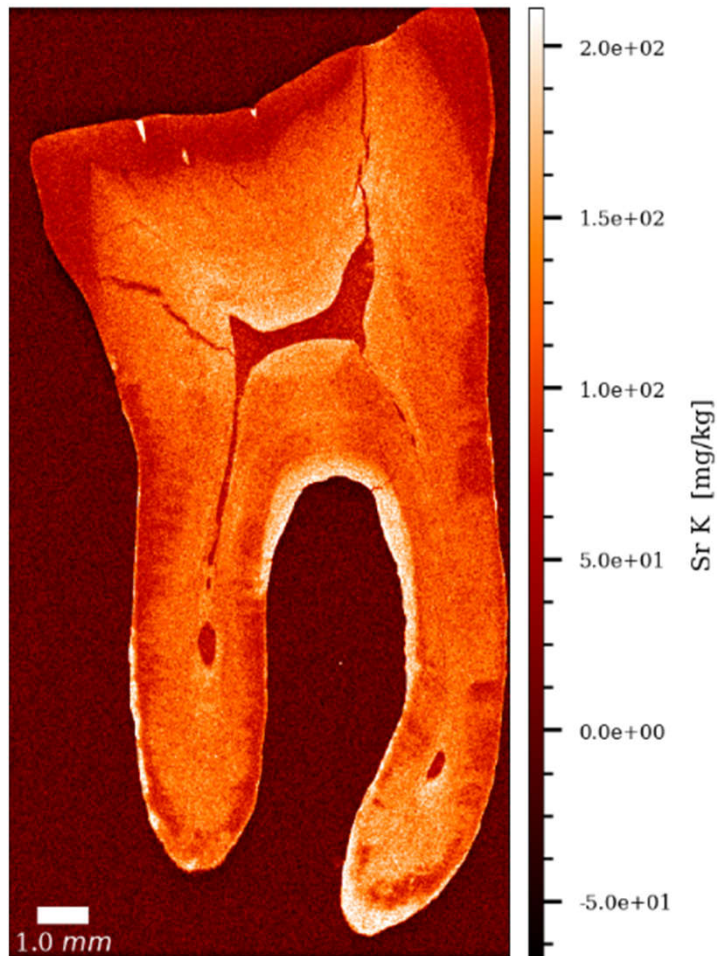
Overview at 10 μ m

Gauss (1x1)

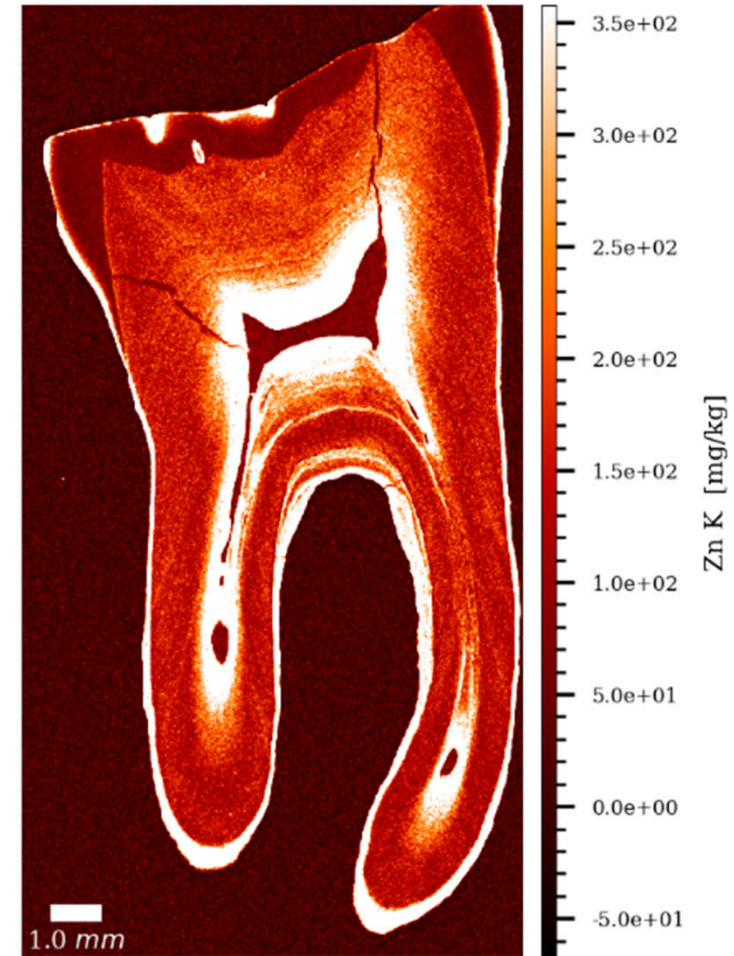
Ca K

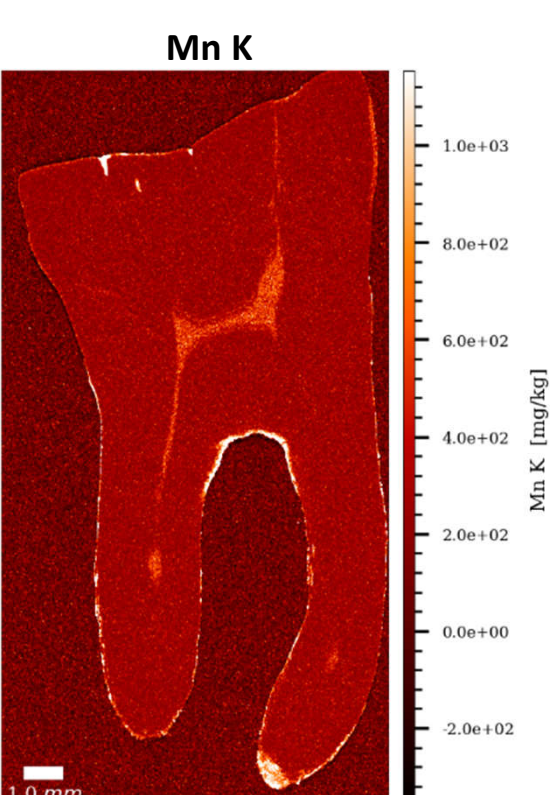
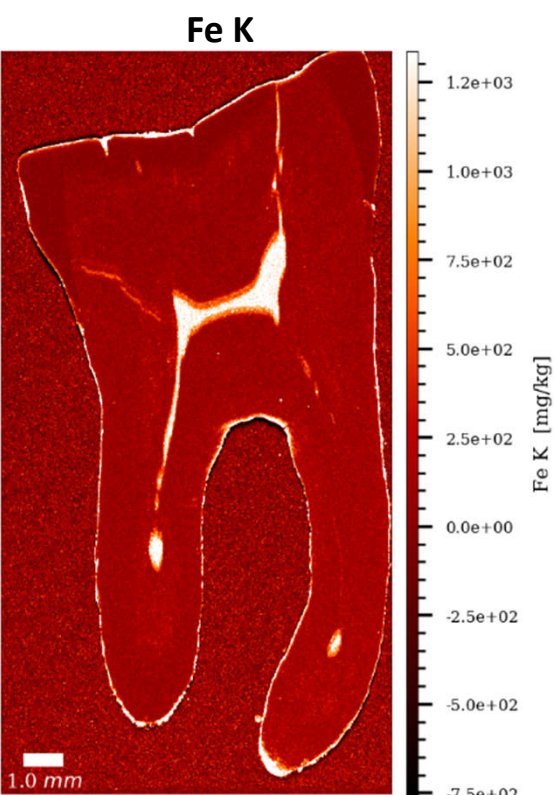
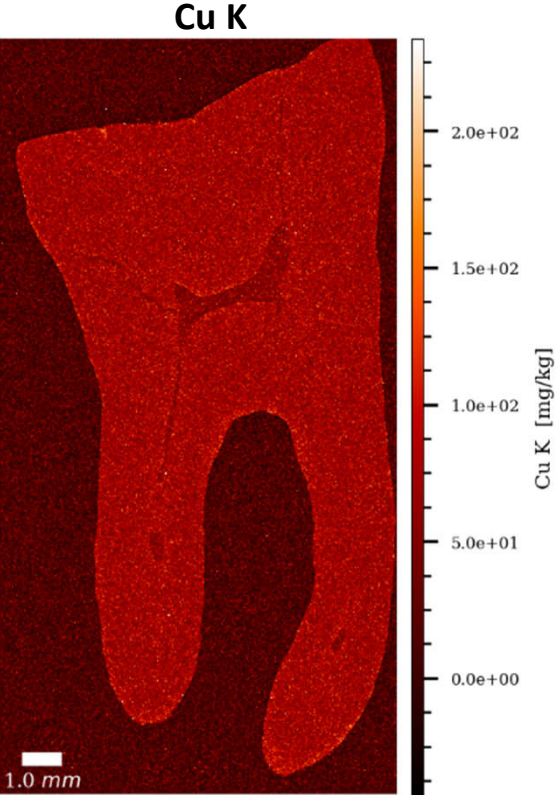


Sr K



Zn K





Næstved 211 LRM1

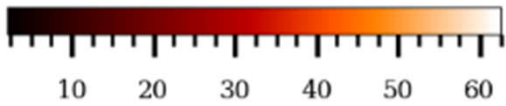
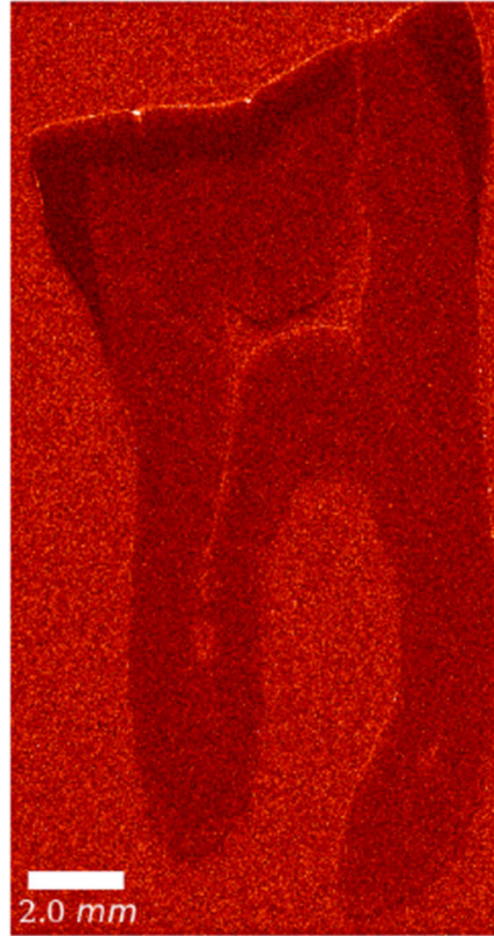
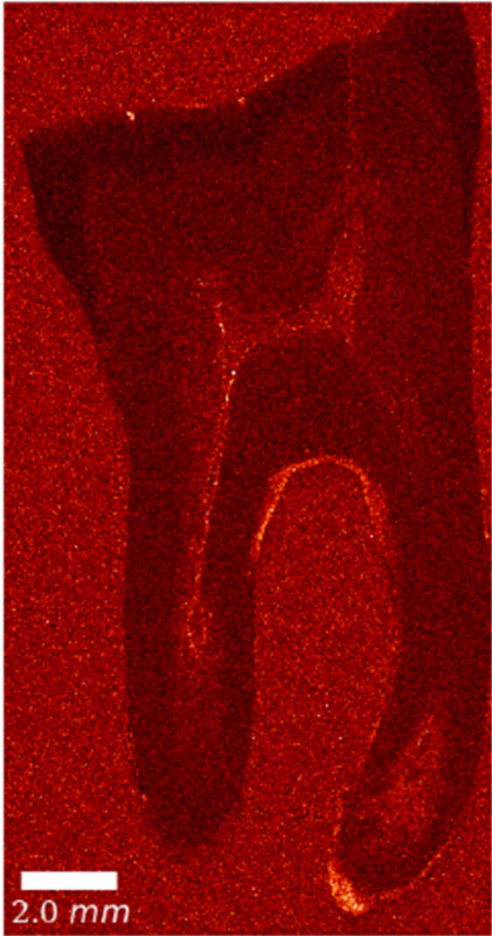
Overview at 10 μm

Uncalibrated data
(arbitrary units)

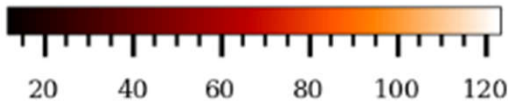
Gauss (1x1)

Br K

Pb L



Br K [a.u.]

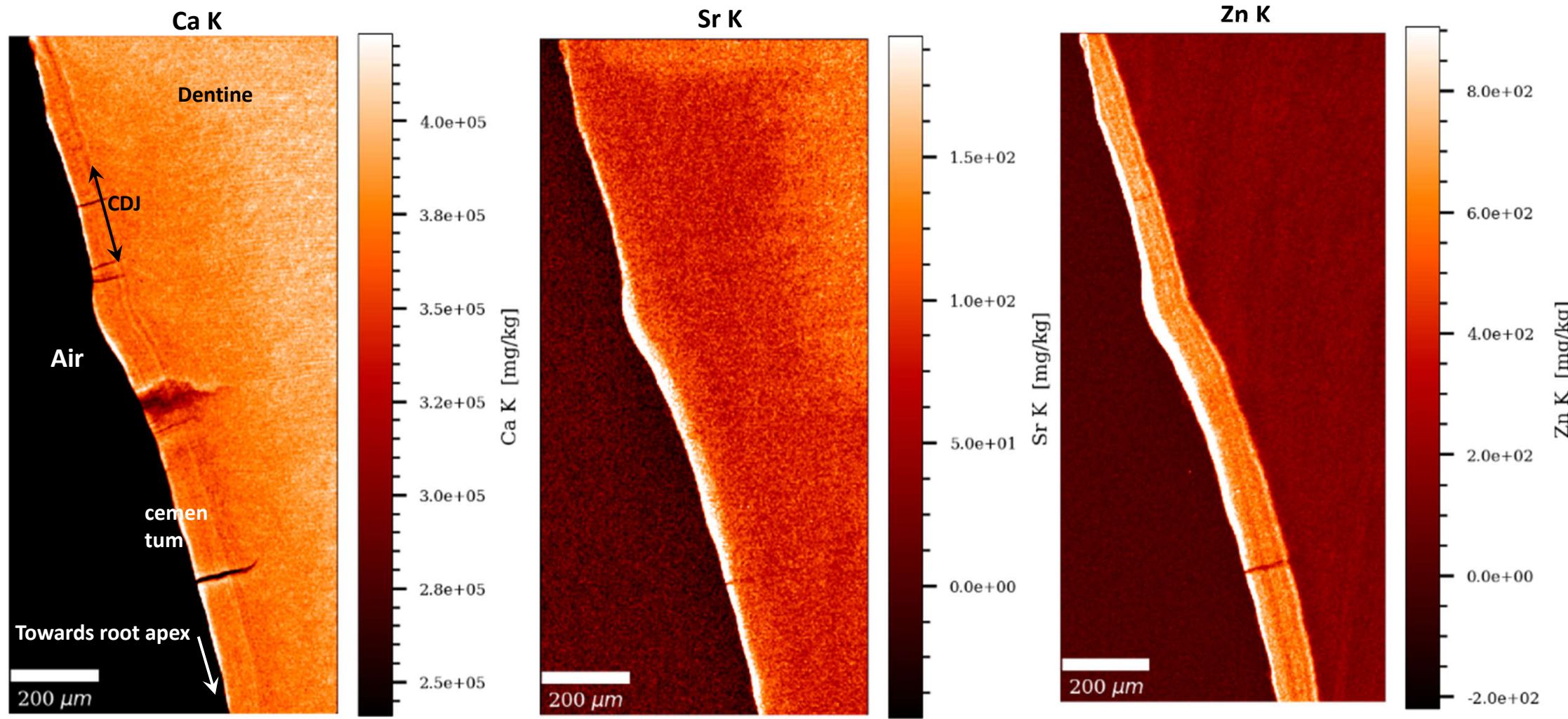


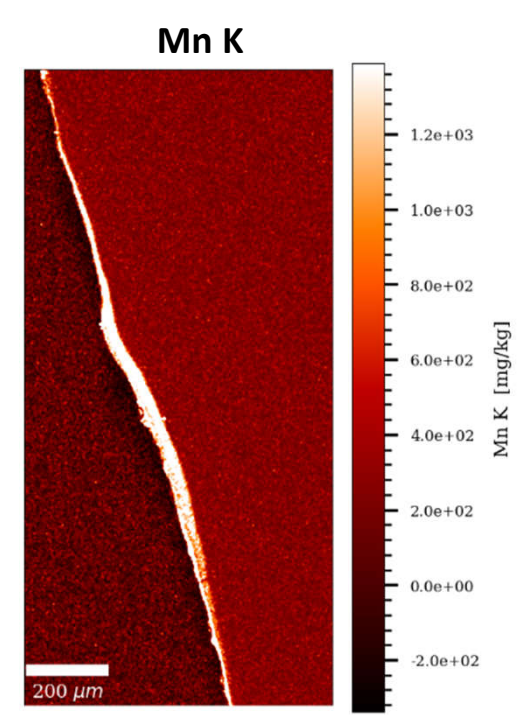
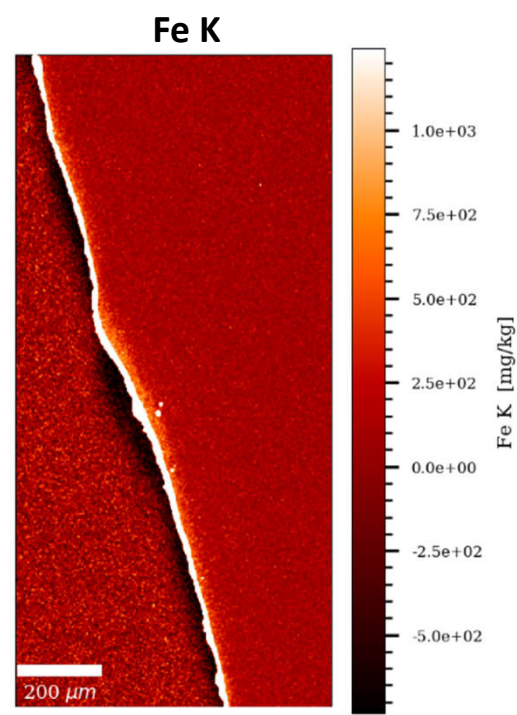
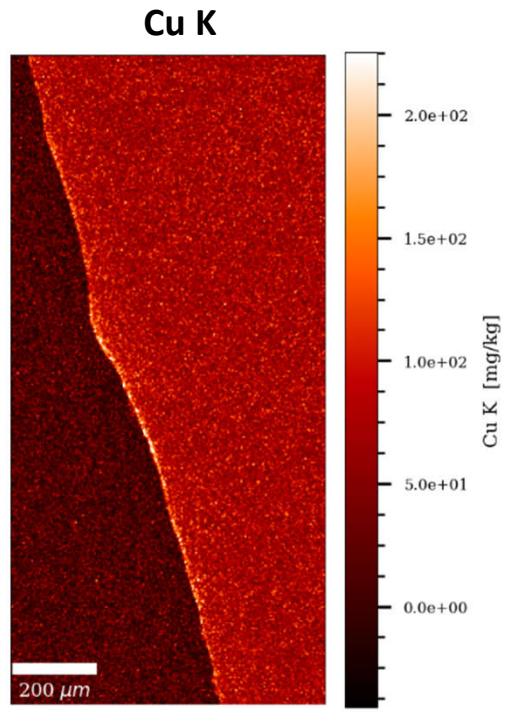
Pb L [a.u.]

Næstved 211 LRM1

High resolution at 1.5 μ m

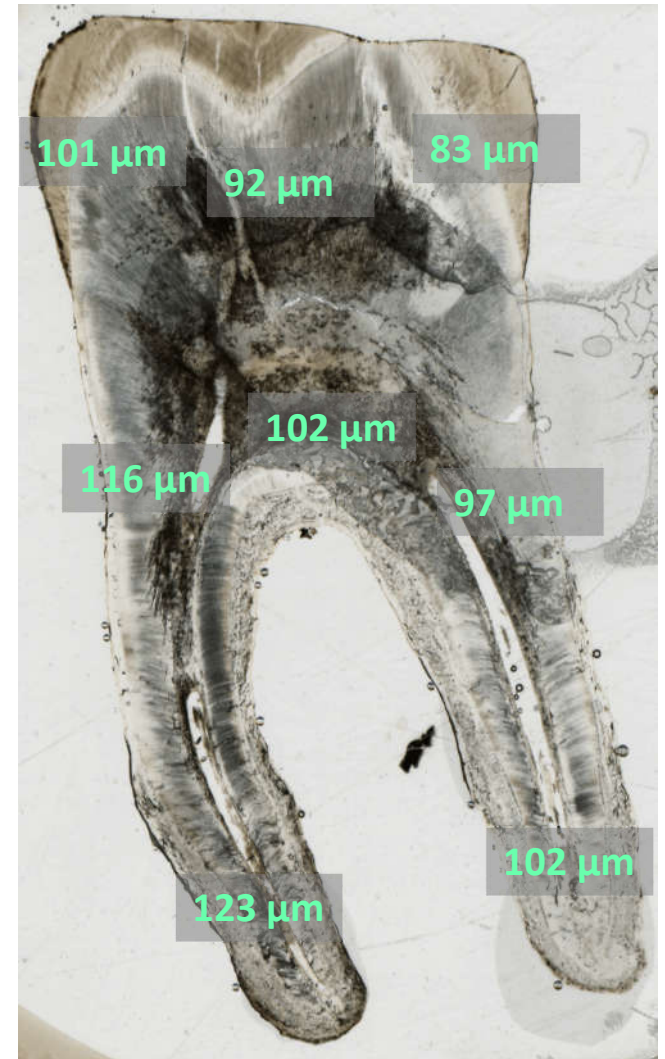
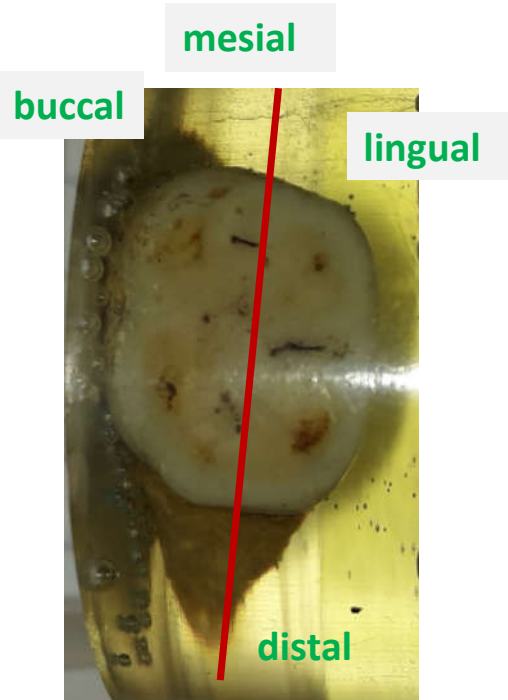
Gauss (1x1)





Næstved – 268 LLM1

♂ 30-40 yrs. 1441 – 1522 cal. CE



Average tooth section thickness (μm): 102.0⁸⁶

Næstved 268 LLM1

Scanning

Overview at 10 μm

High resolution at 1.5 μm in cellular cementum

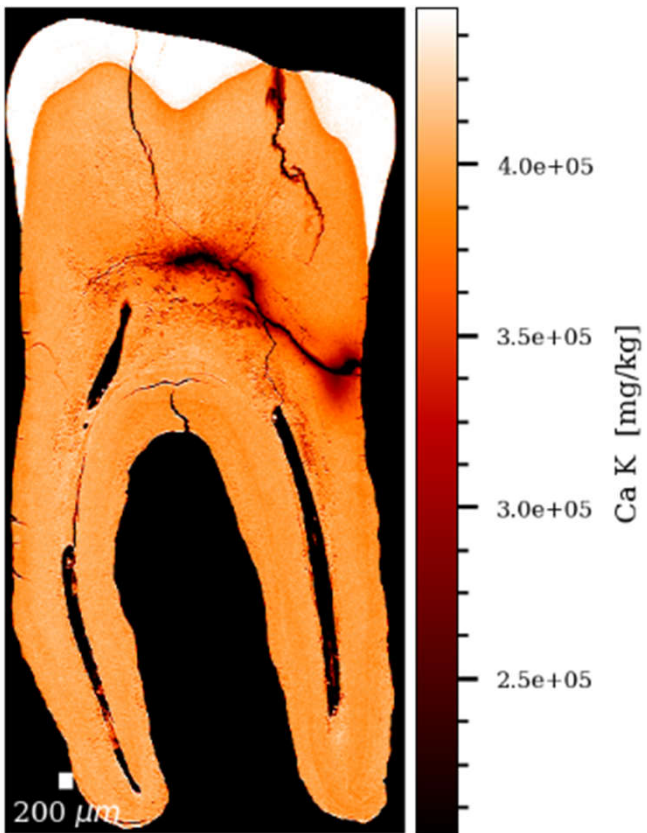


Næstved 268 LLM1

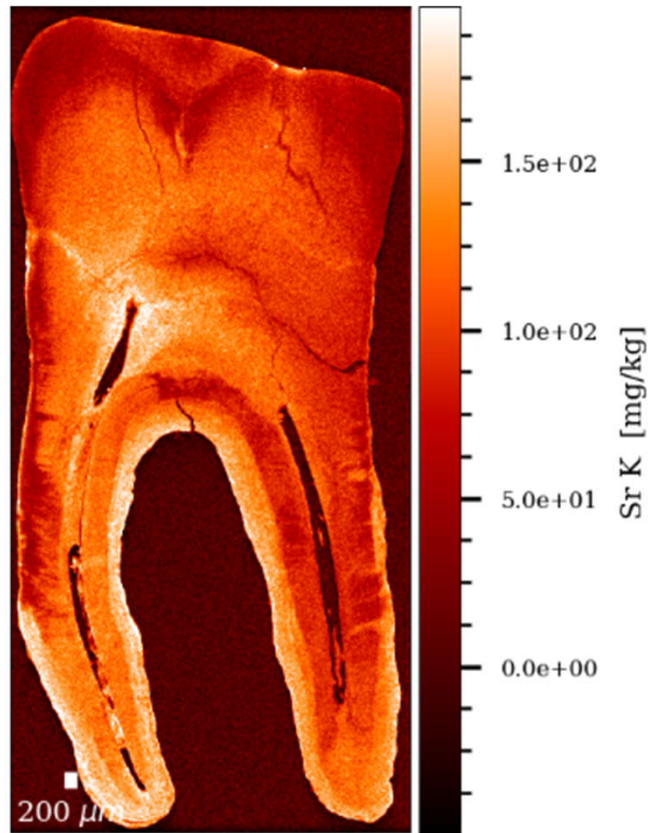
Overview at 10 μm

Gauss (1.2x1.2)

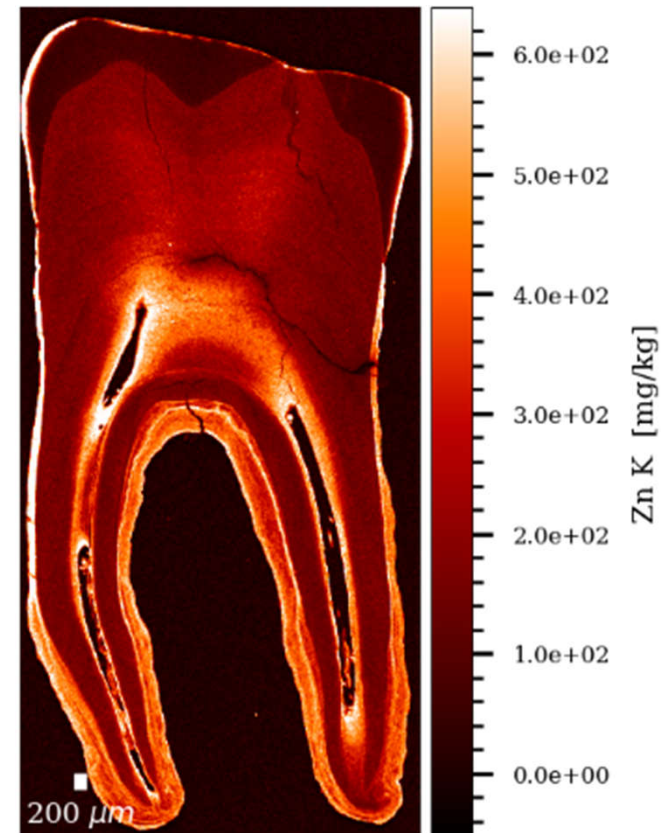
Ca K

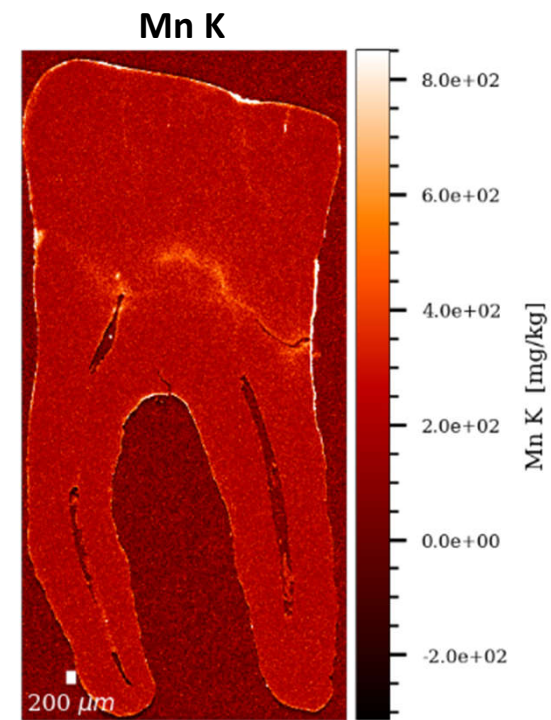
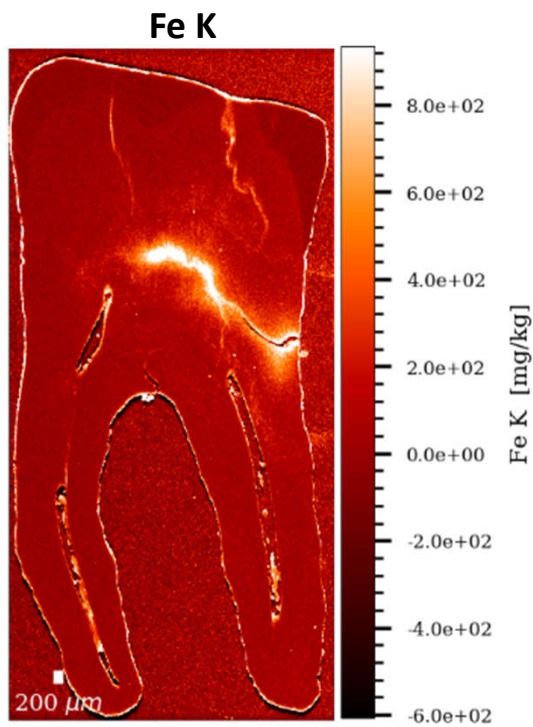
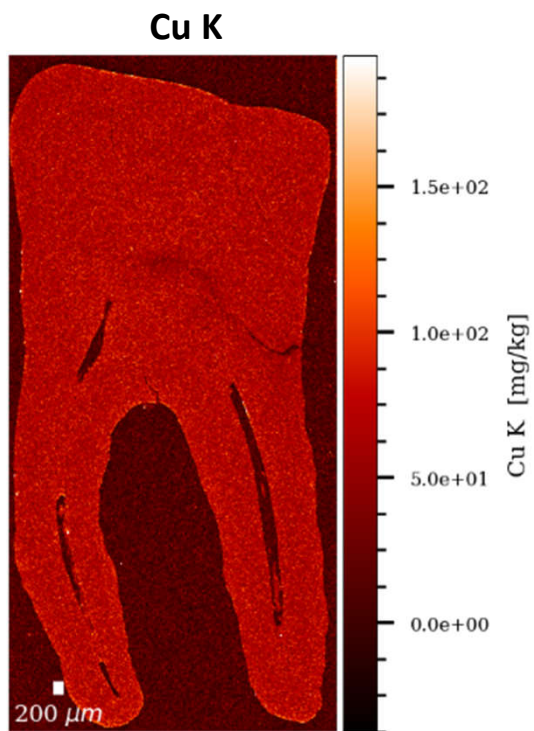


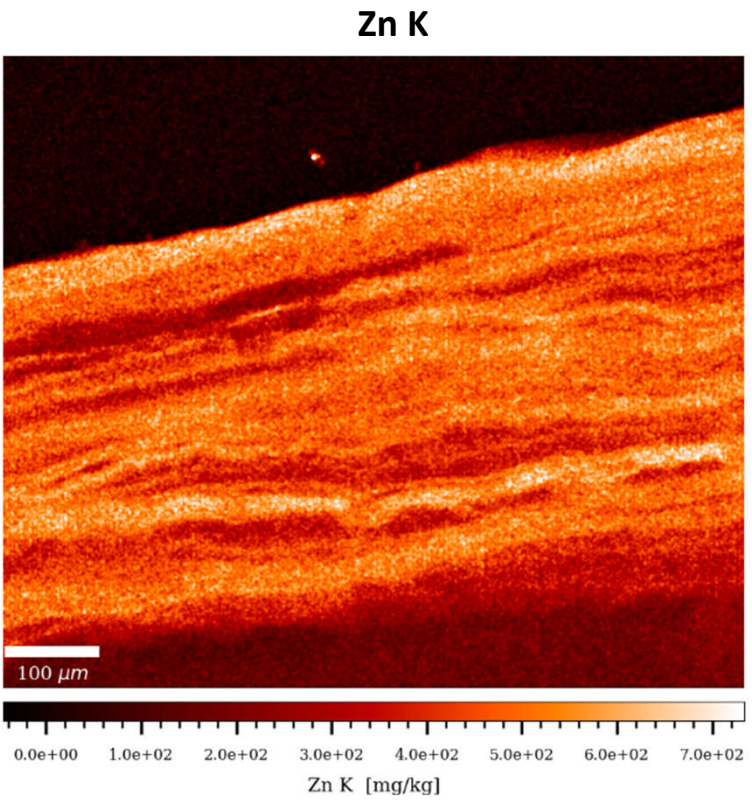
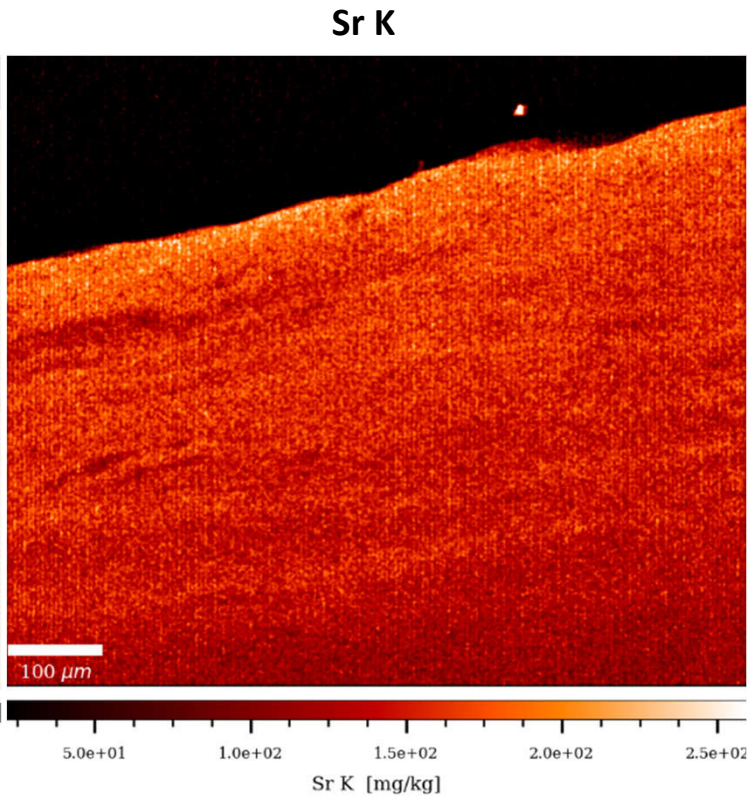
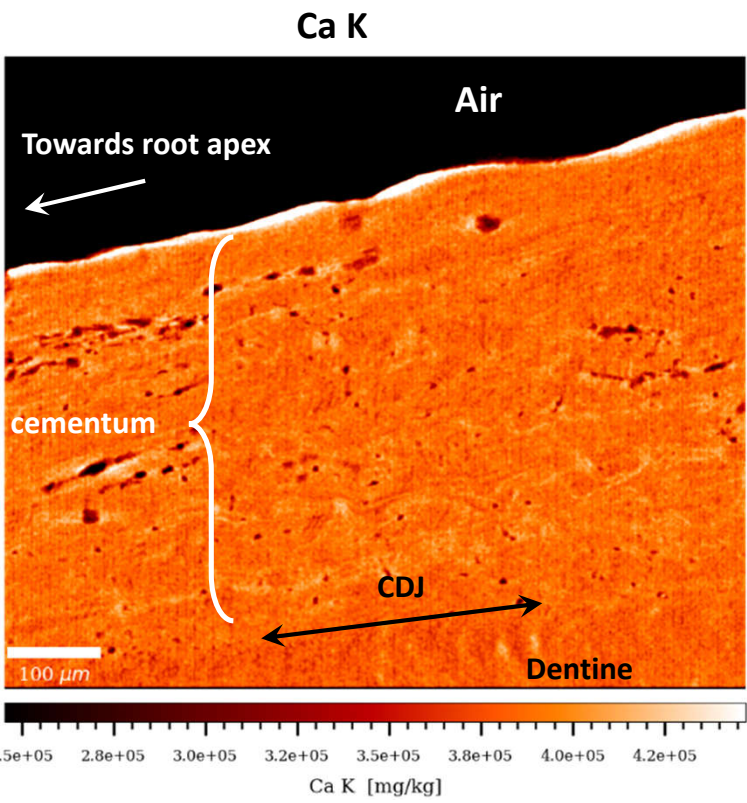
Sr K



Zn K





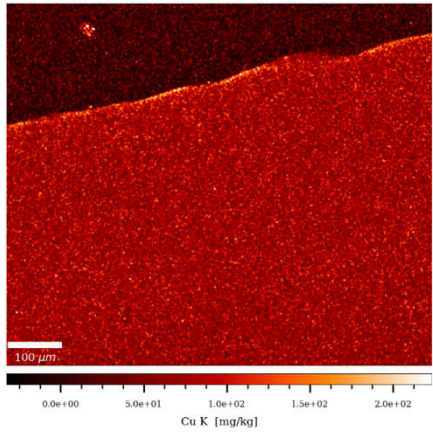


Næstved 268 LLM1

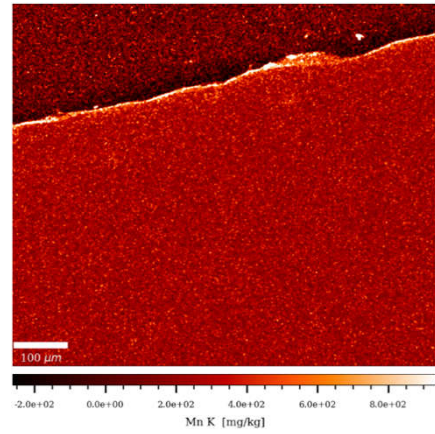
High resolution at 1 μm

Gauss (1x1)

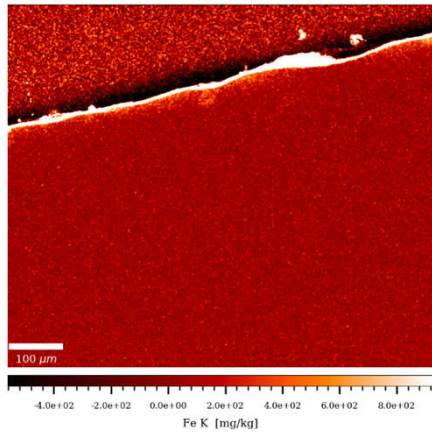
Cu K



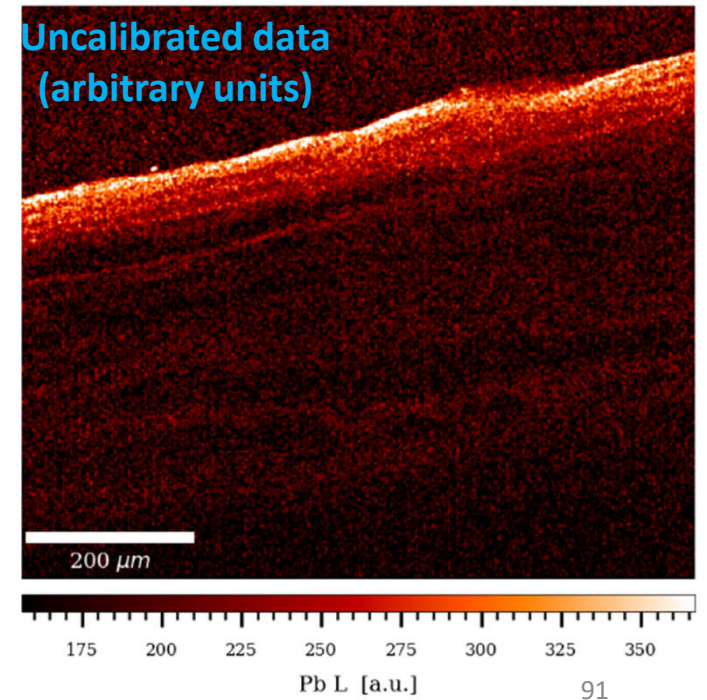
Mn K



Fe K



Pb L



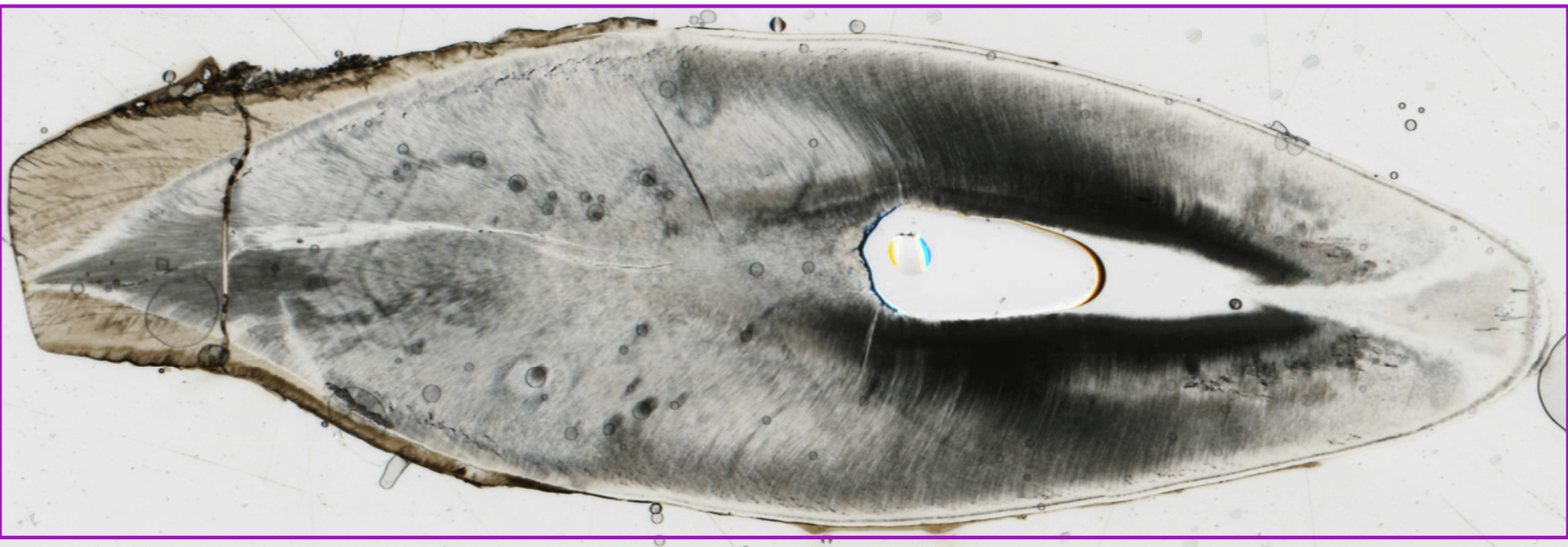
Næstved – 305 LLC

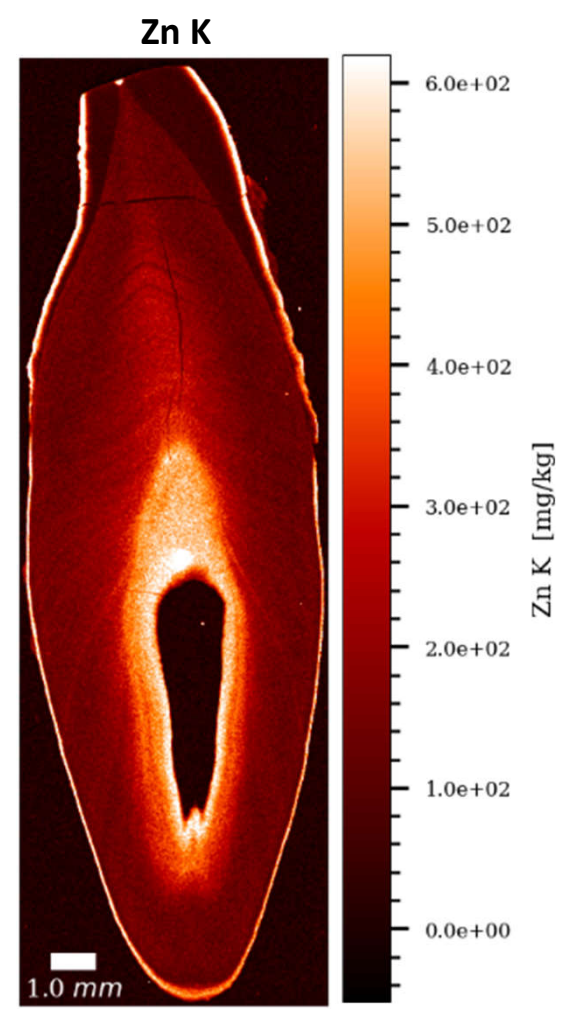
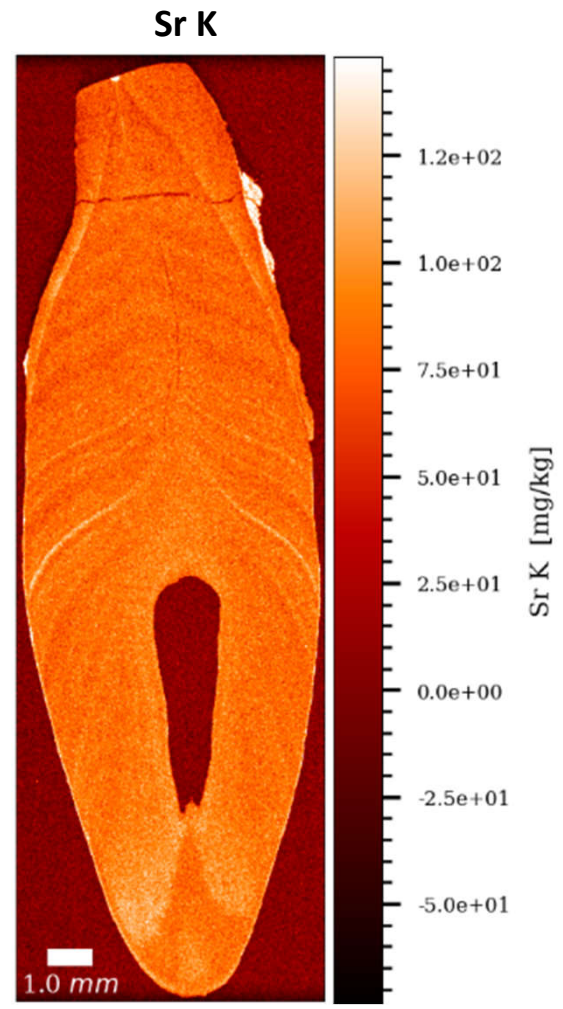
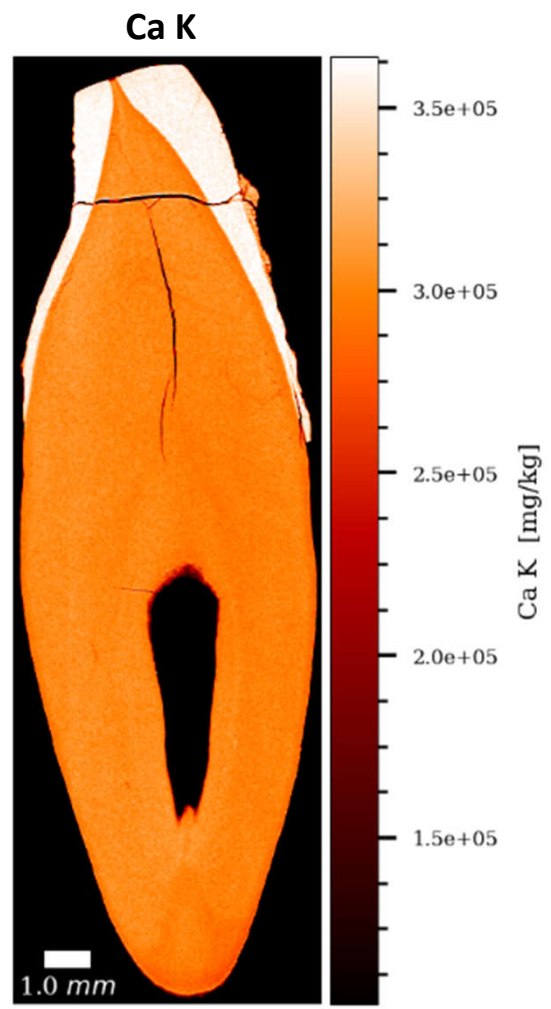
♂ 30-35 yrs. mid-13th – mid-16th c. CE

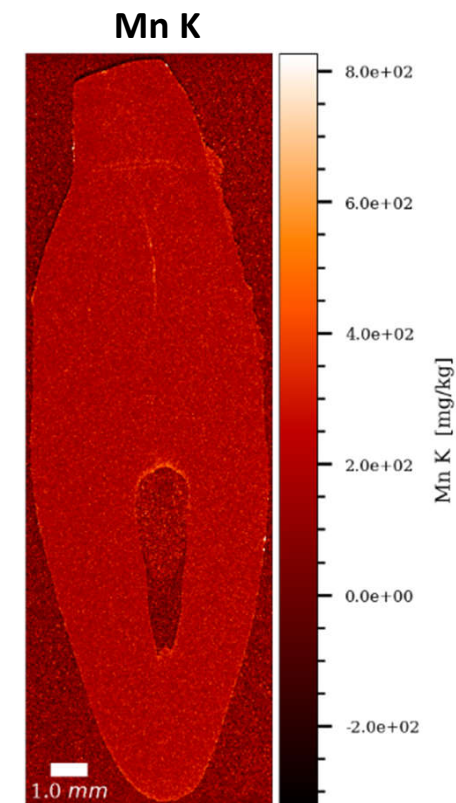
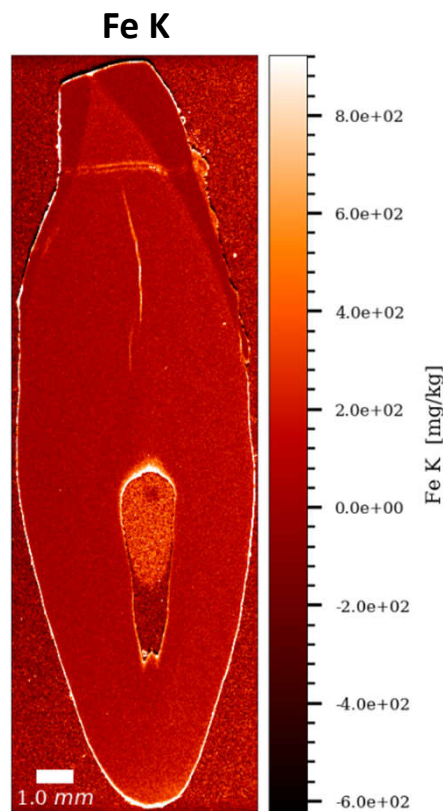
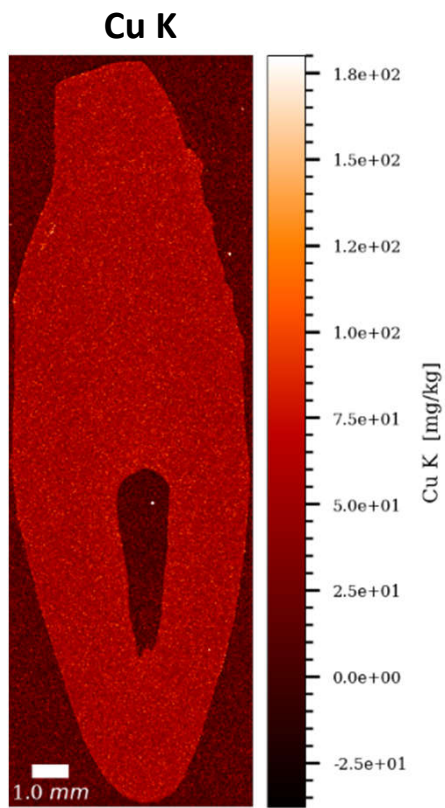


Average tooth section thickness (µm): 119.0

Overview at 10 μm





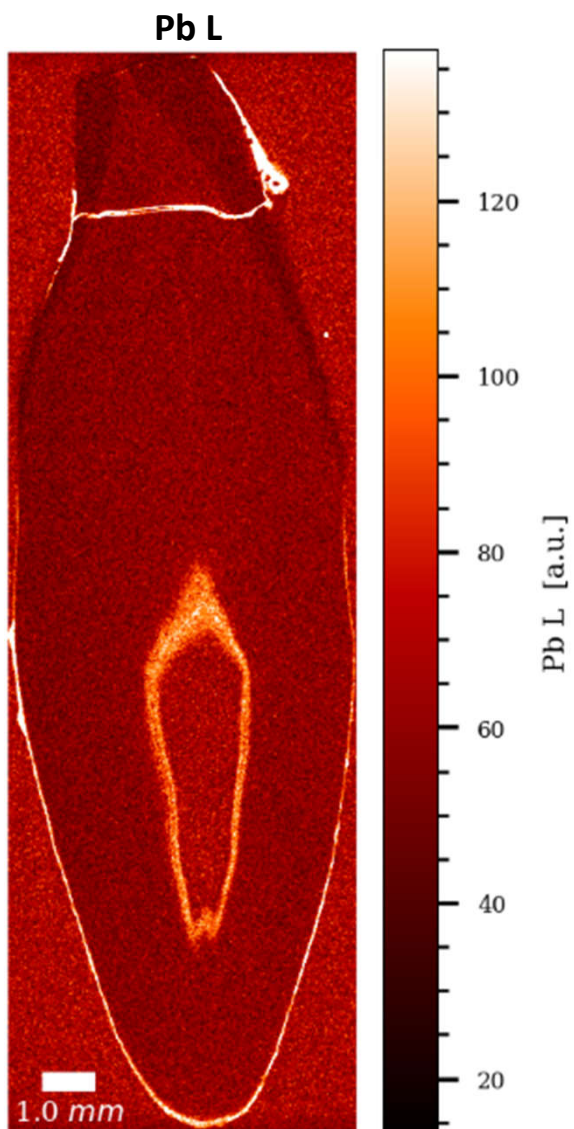
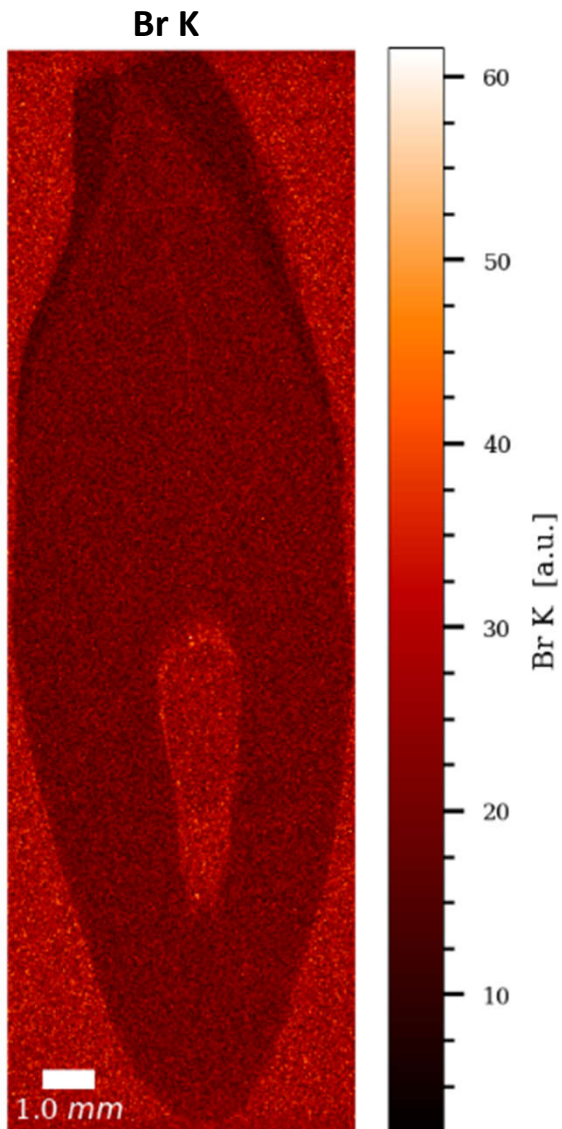


Næstved 305 LLC

Overview at 10 μm

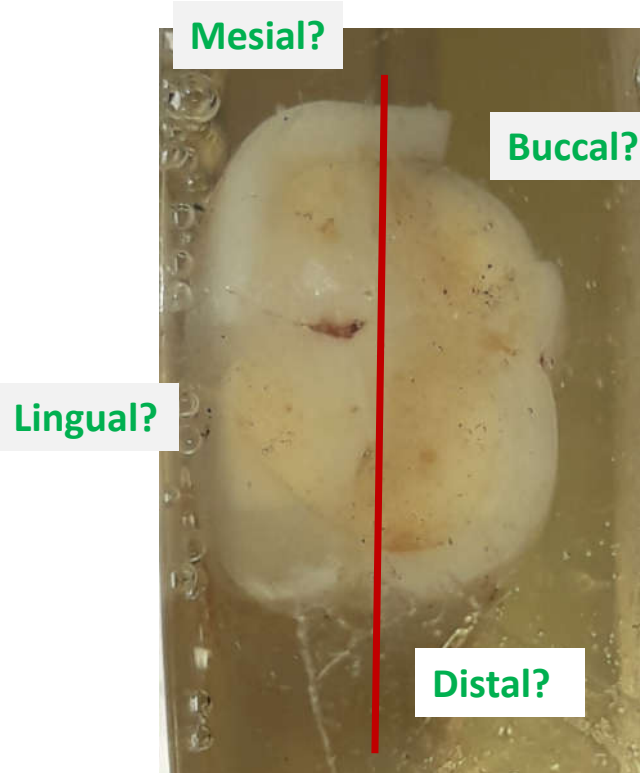
Uncalibrated data
(arbitrary units)

Gauss (1.2x1.2)

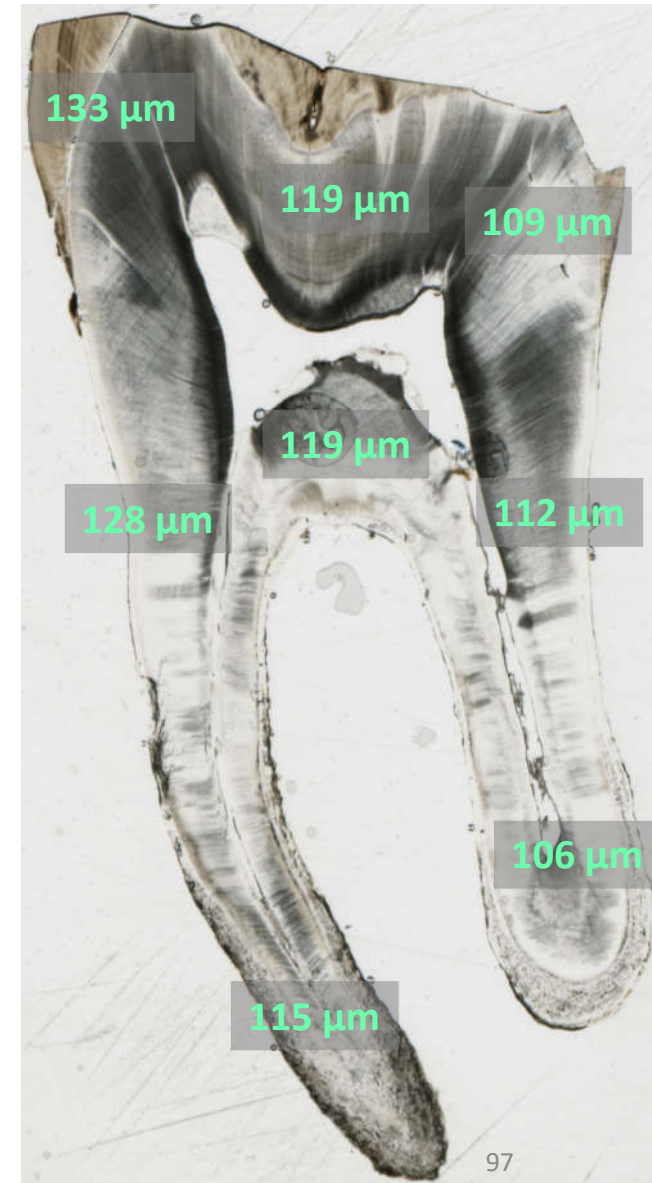


Næstved – 305 LRM1

♂ 30-35 yrs. mid-13th – mid-16th c. CE



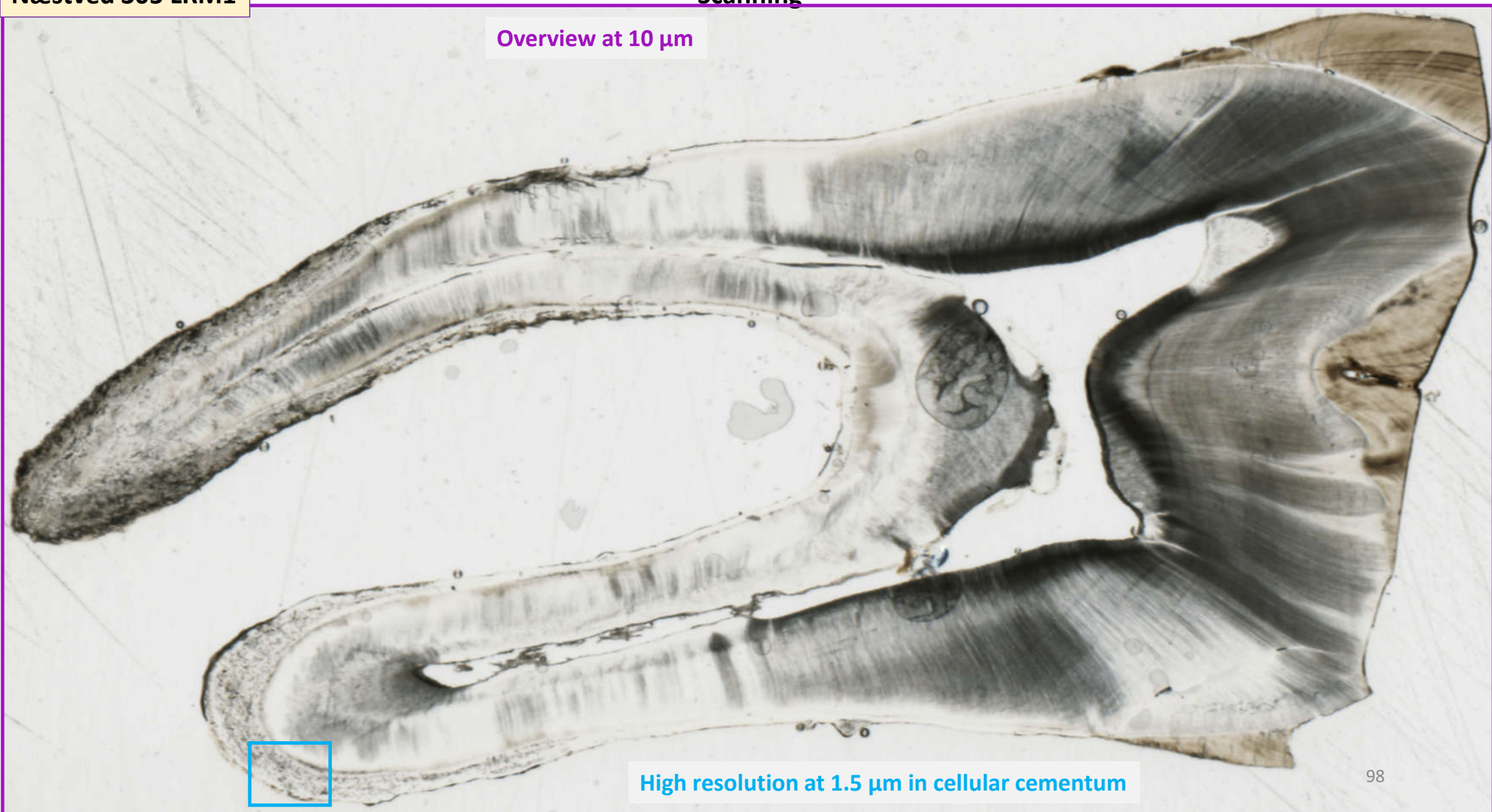
Average tooth section thickness (μm): 117.6



Næstved 305 LRM1

Scanning

Overview at 10 μ m



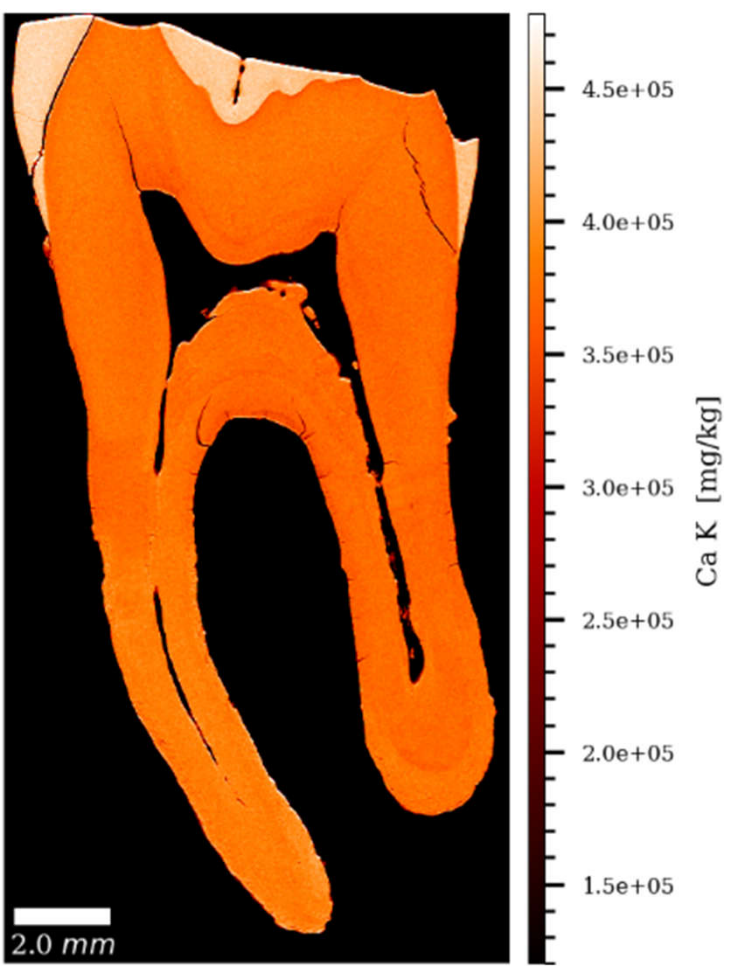
High resolution at 1.5 μ m in cellular cementum

Næstved 305 LRM1

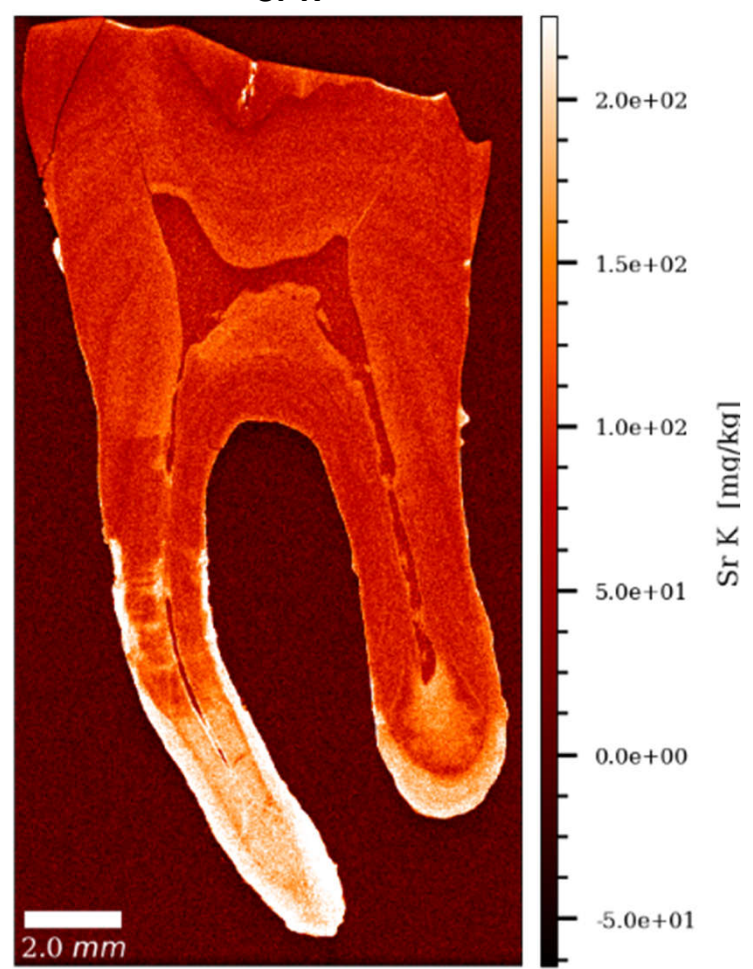
Overview at 10 μm

Gauss (1x1)

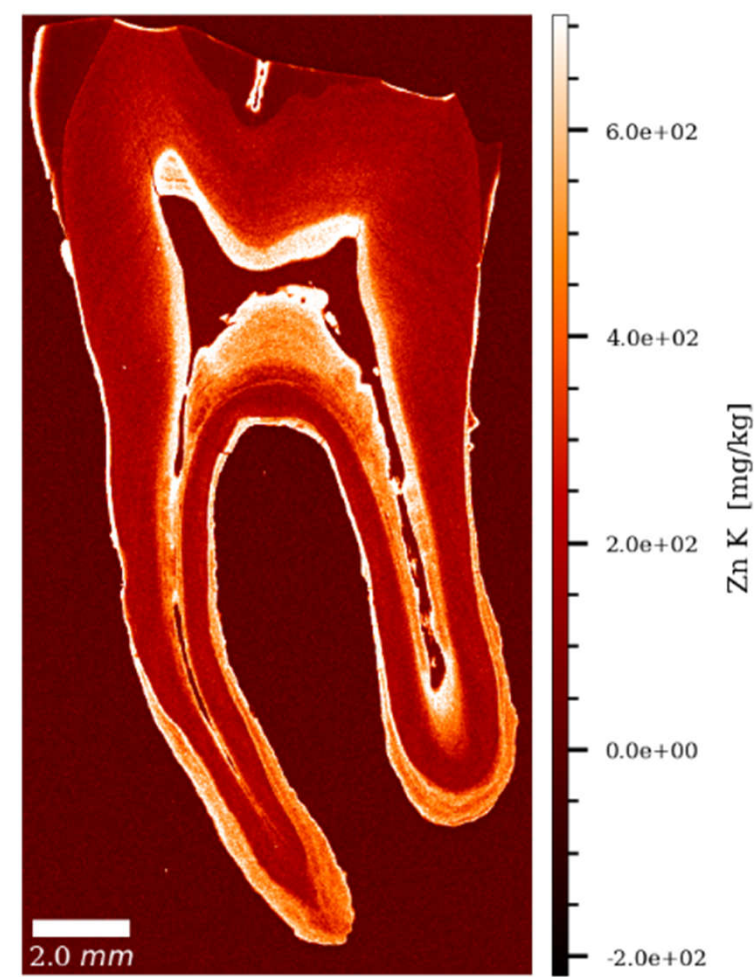
Ca K

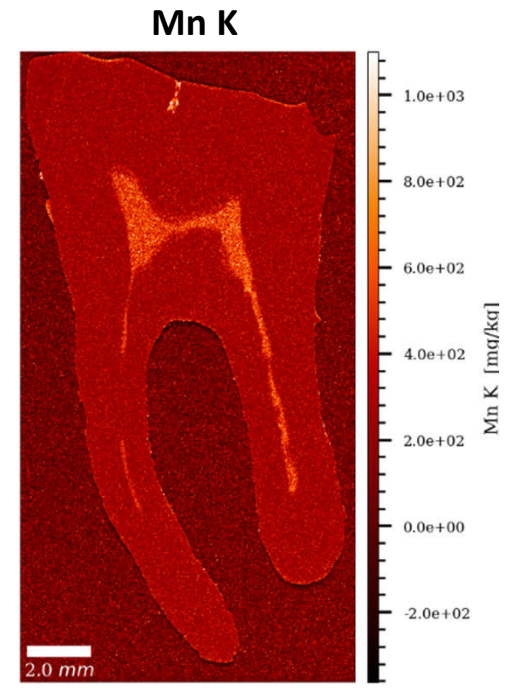
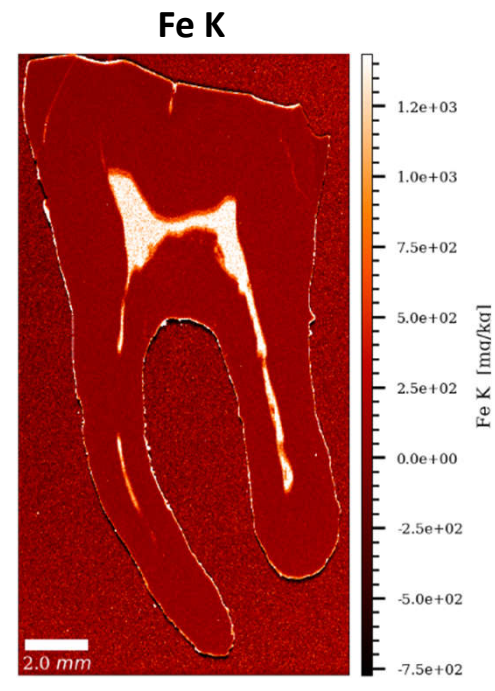
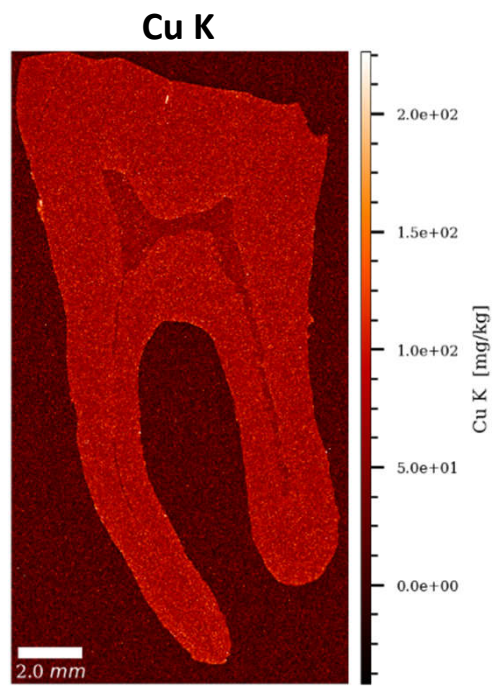


Sr K



Zn K





Næstved 305 LRM1

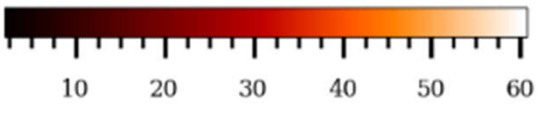
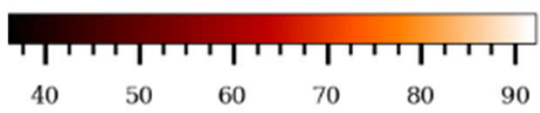
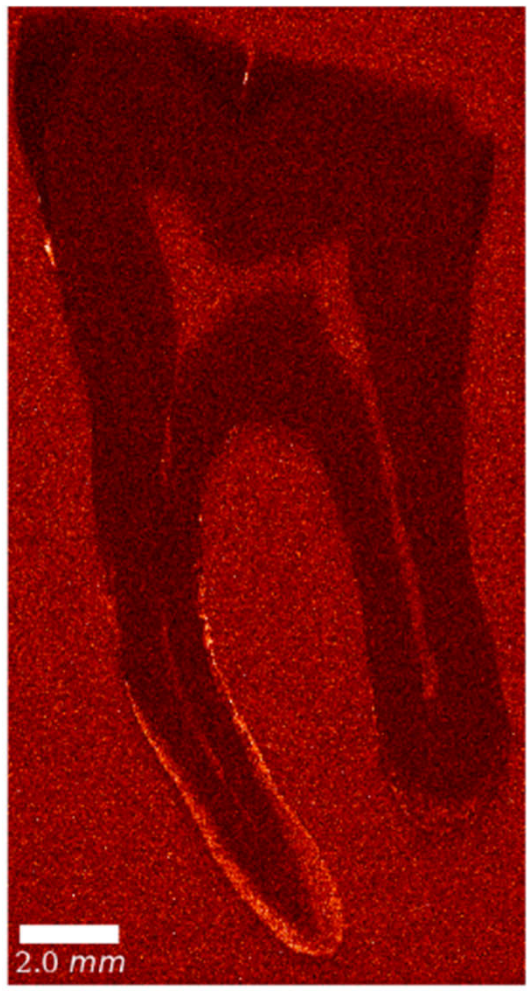
Overview at 10 μm

Uncalibrated data
(arbitrary units)

Gauss (1x1)

Pb L

Br K



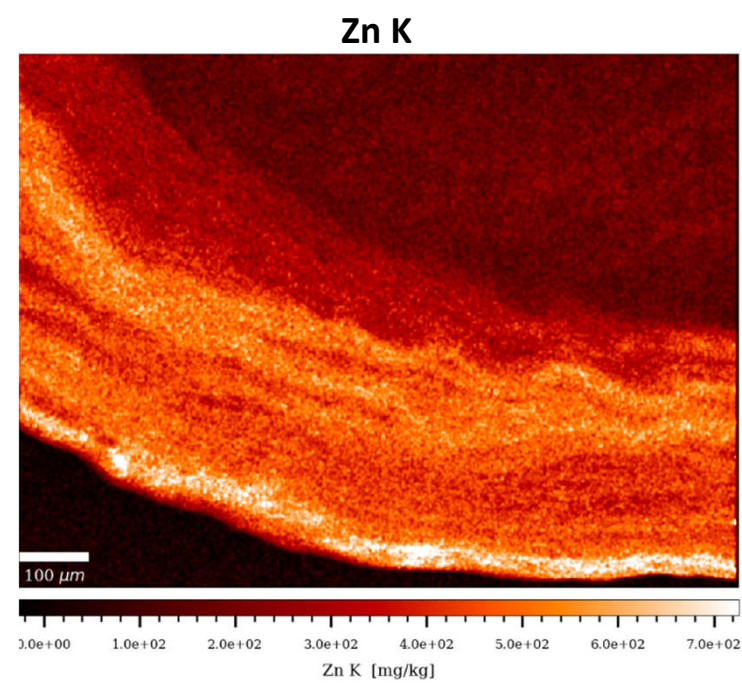
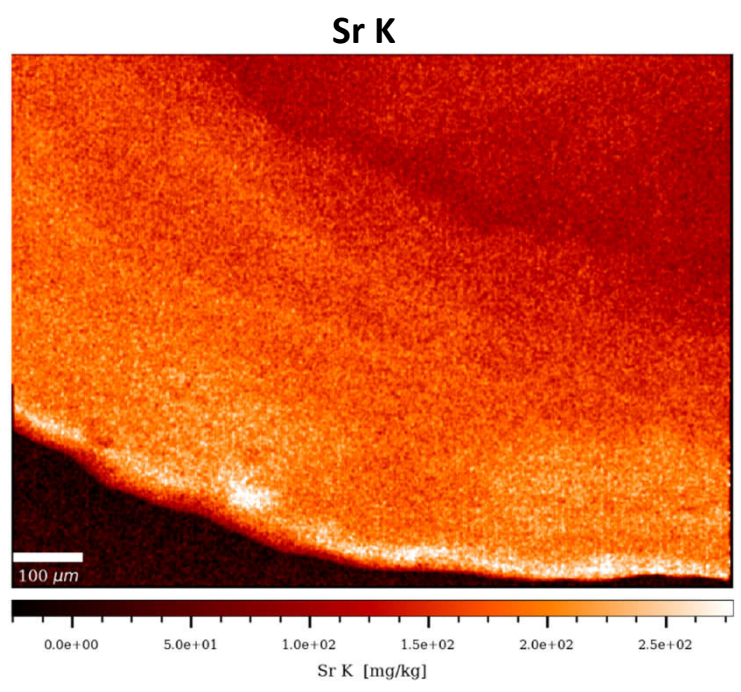
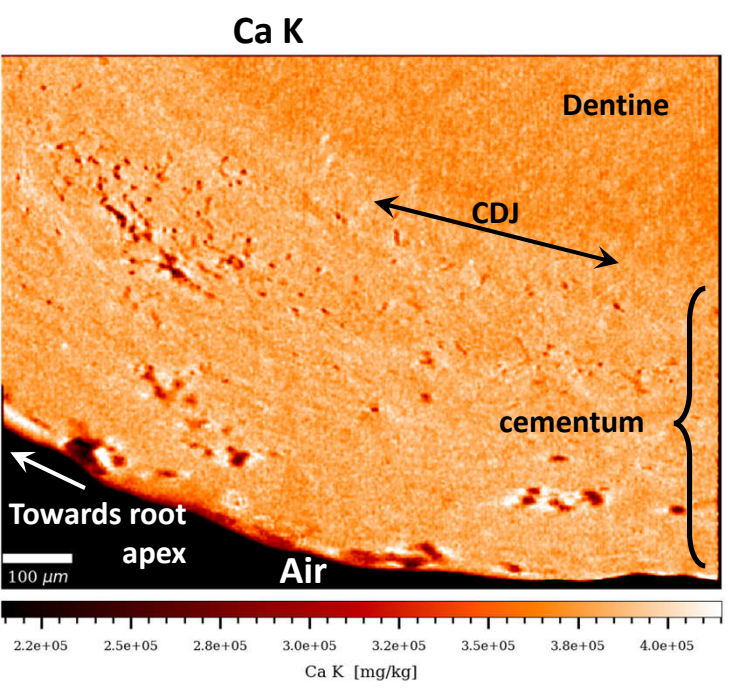
Pb L [a.u.]

Br K [a.u.]

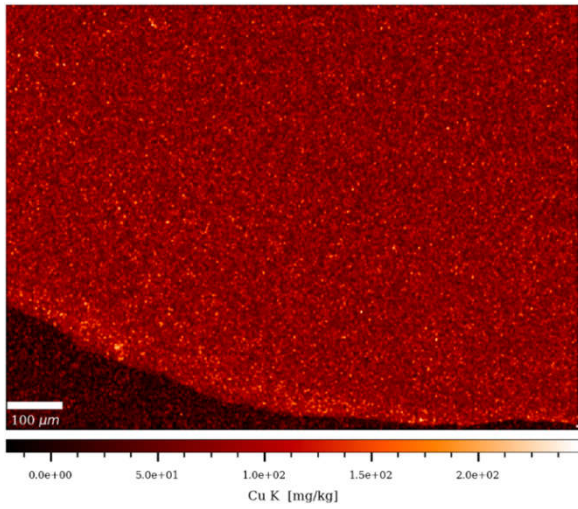
Næstved 305 LRM1

High resolution at 1.5 μm

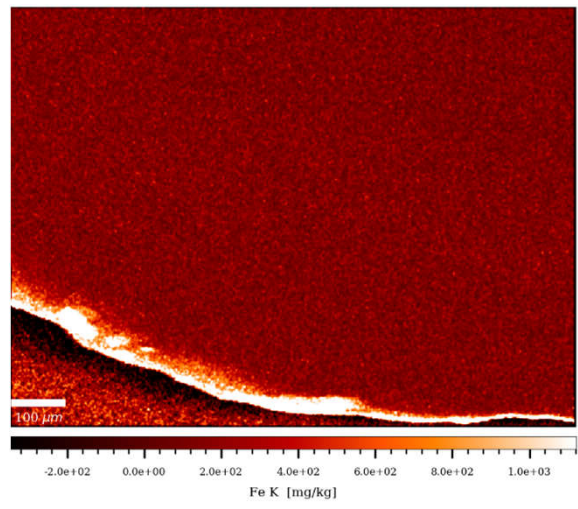
Gauss (1x1)



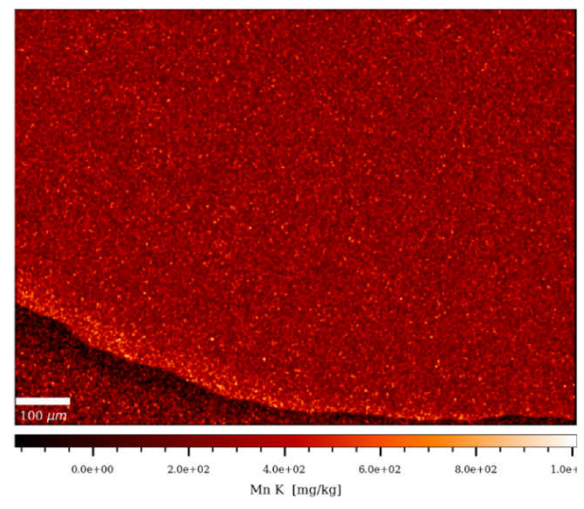
Cu K



Fe K



Mn K



File S3

Laser Ablation (LA-ICP-TOFMS) results

Using SXRF and LA-ICP-TOFMS to explore evidence of treatment and physiological responses to leprosy in medieval Denmark

Biology

Anastasia Brozou, Marcello A. Mannino, Stijn J.M. Van Malderen, Jan Garrevoet, Eric Pubert, Benjamin T. Fuller, M. Christopher Dean, Thomas Colard, Frédéric Santos, Niels Lynnerup, Jesper L. Boldsen, Marie Louise Jørkov, Andrei Dorian Soficaru, Laszlo Vincze, Adeline Le Cabec

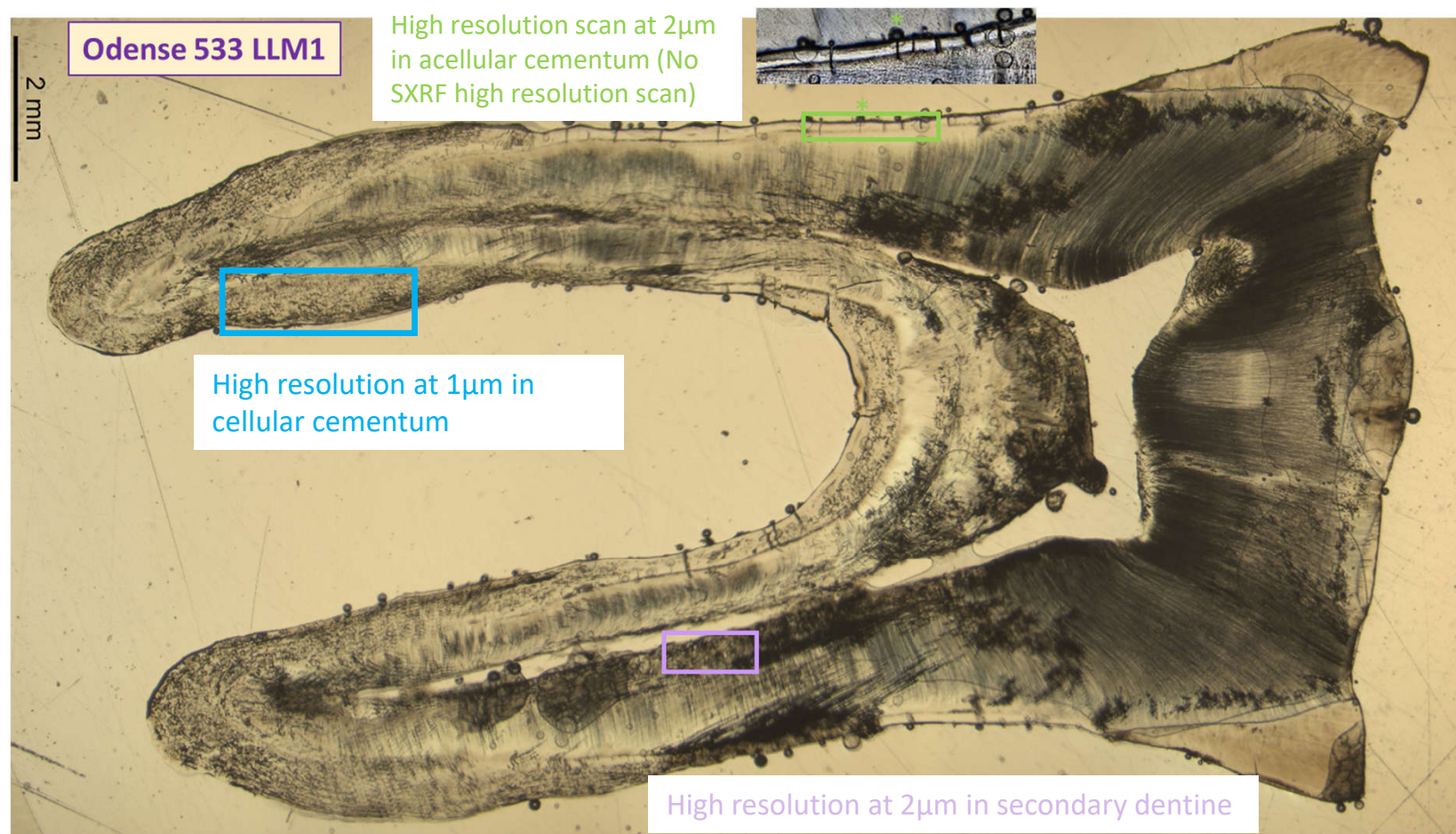
Corresponding author:

Adeline Le Cabec

E-mail: adeline.le-cabec@u-bordeaux.fr

Teeth with the best SXRF signal in cellular cementum.

Odense 533 LLM1:
The cellular cementum and the secondary dentine are also imaged with SXRF. The acellular cementum is scanned here for comparison.



Naestved 211 URC – Cellular Cementum

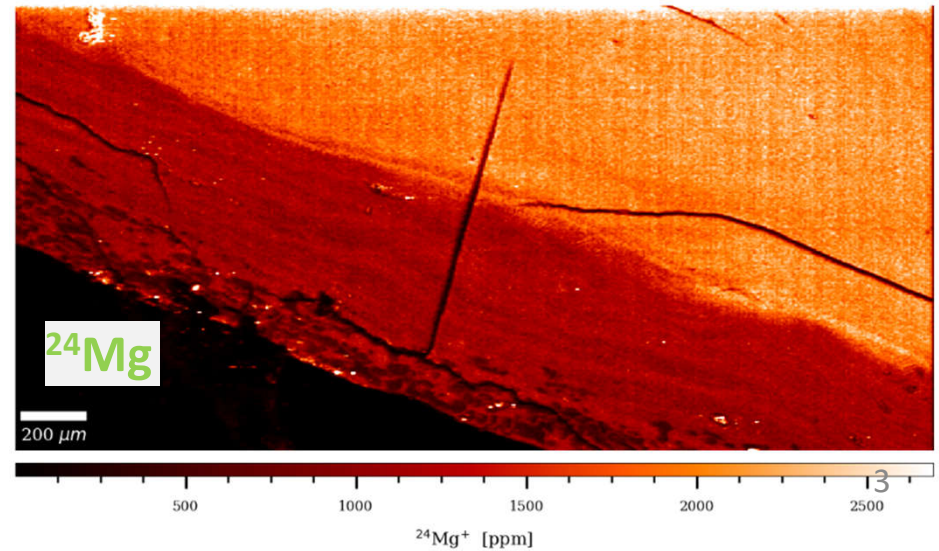
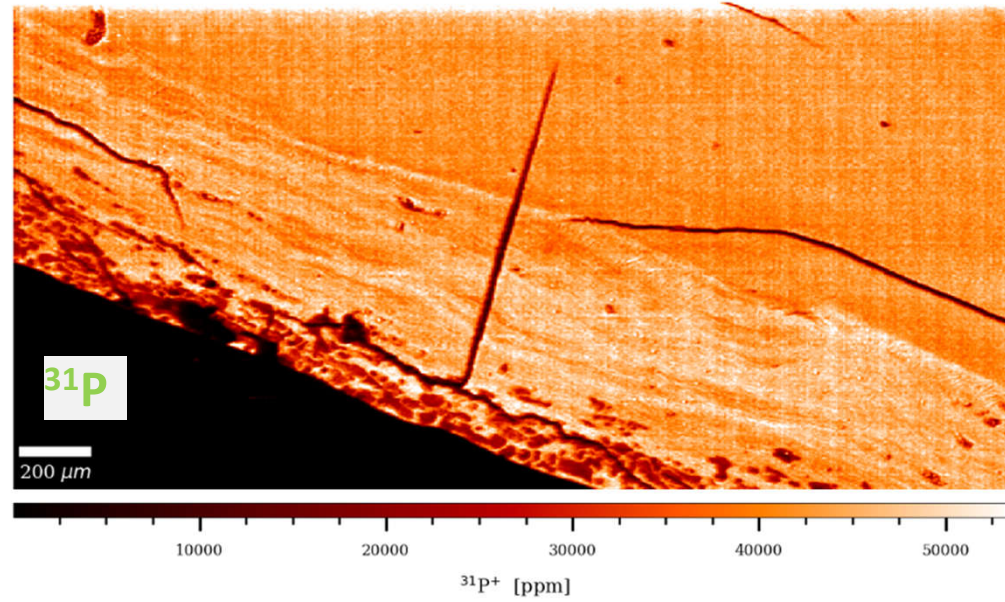
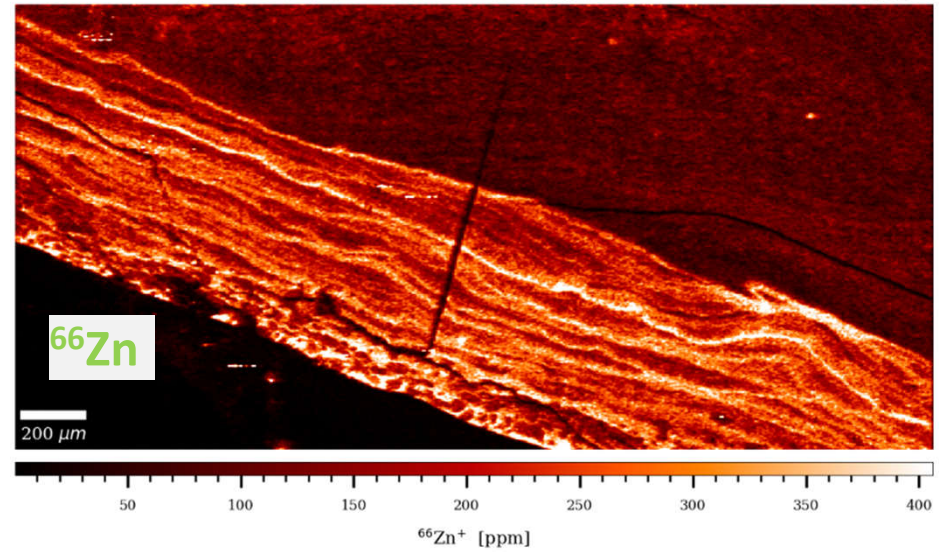
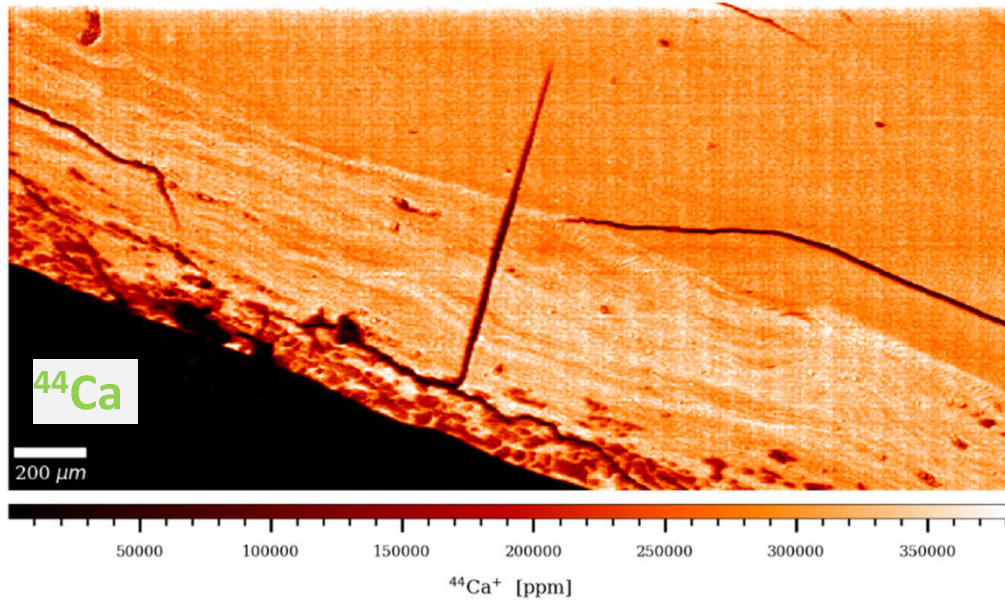
Cellular cementum

Primary dentine

Air

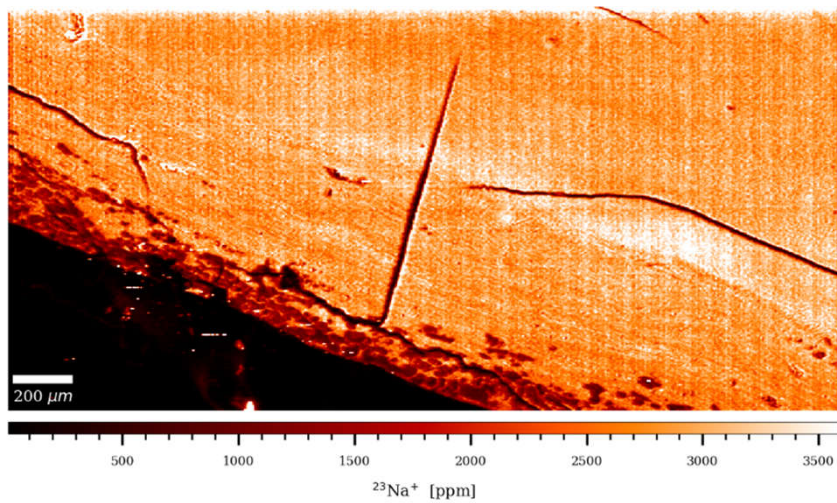
Root surface

Gauss 0.8 x 0.8

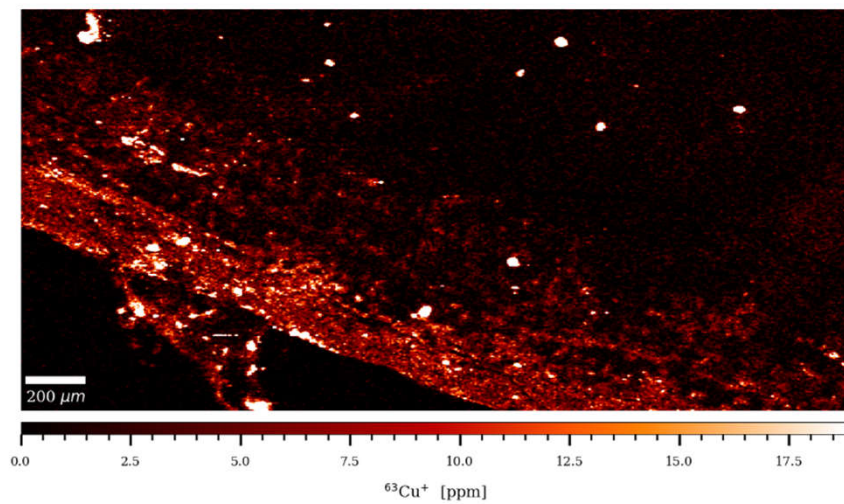


Næstved 211C – Cellular Cementum

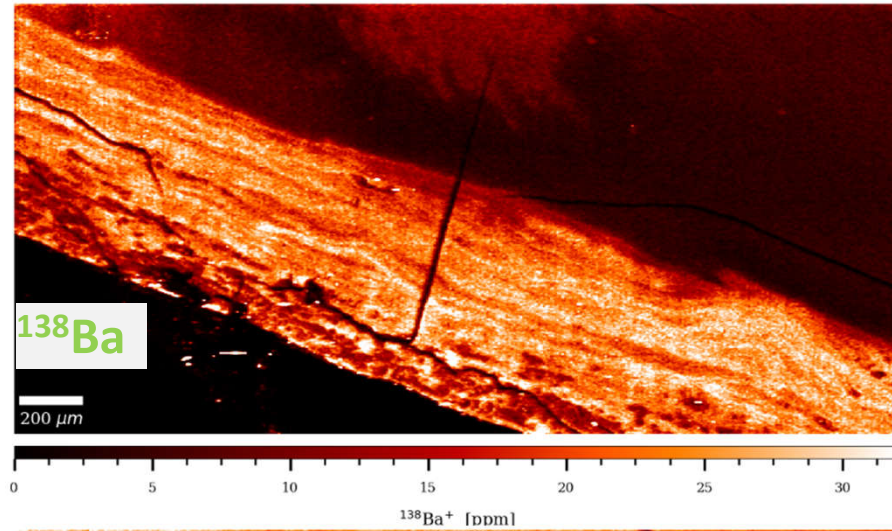
^{23}Na



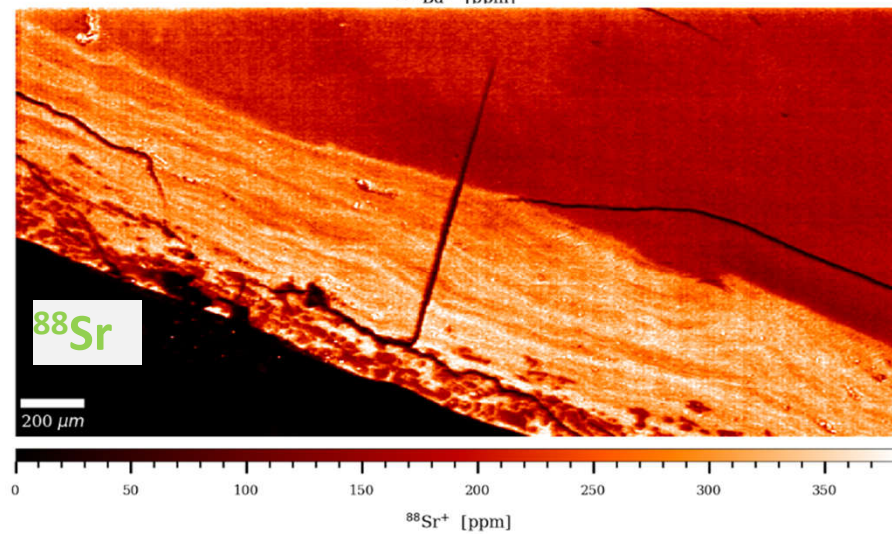
^{63}Cu



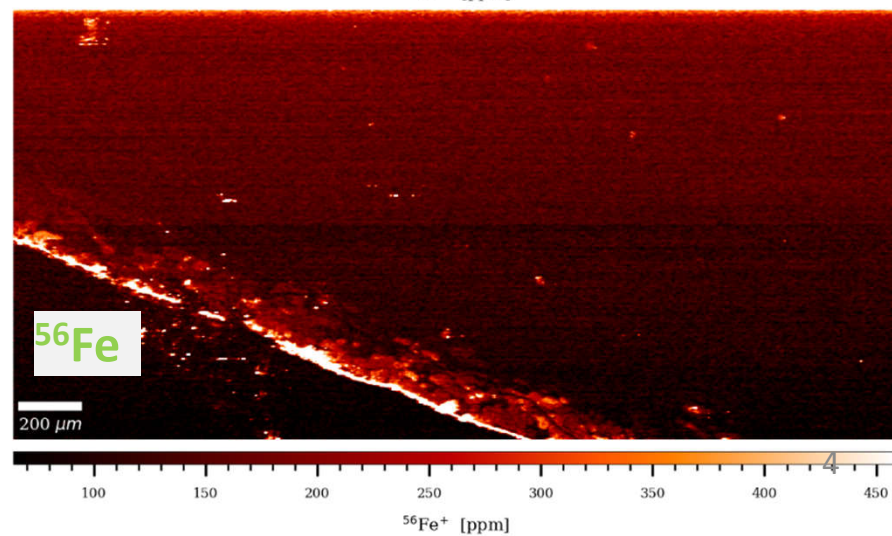
^{138}Ba



^{88}Sr

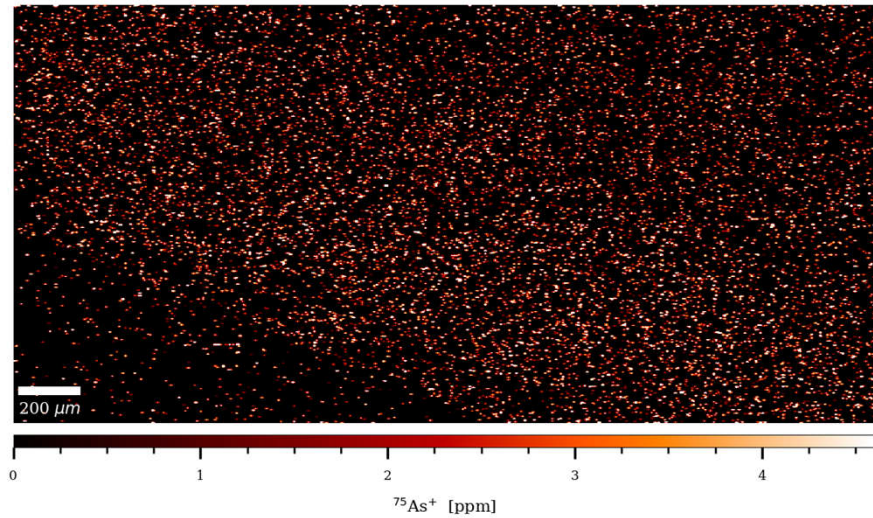


^{56}Fe

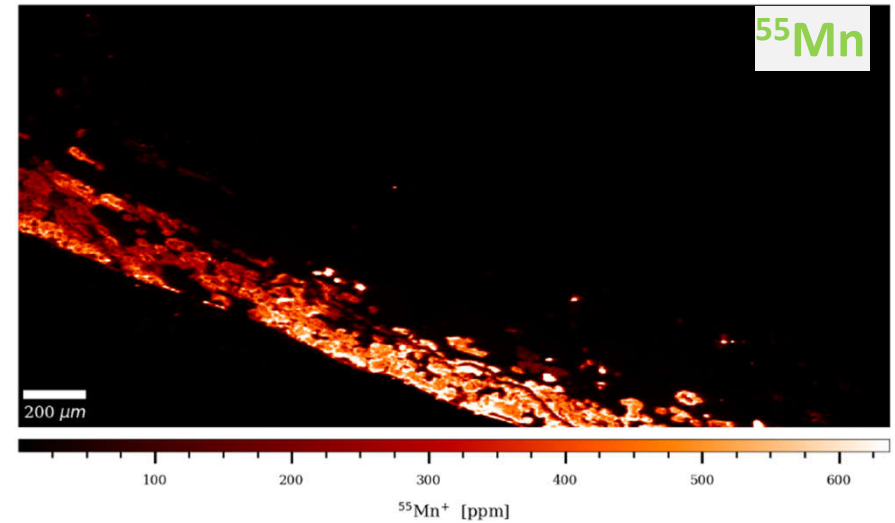


Næstved 211C – Cellular Cementum

^{75}As

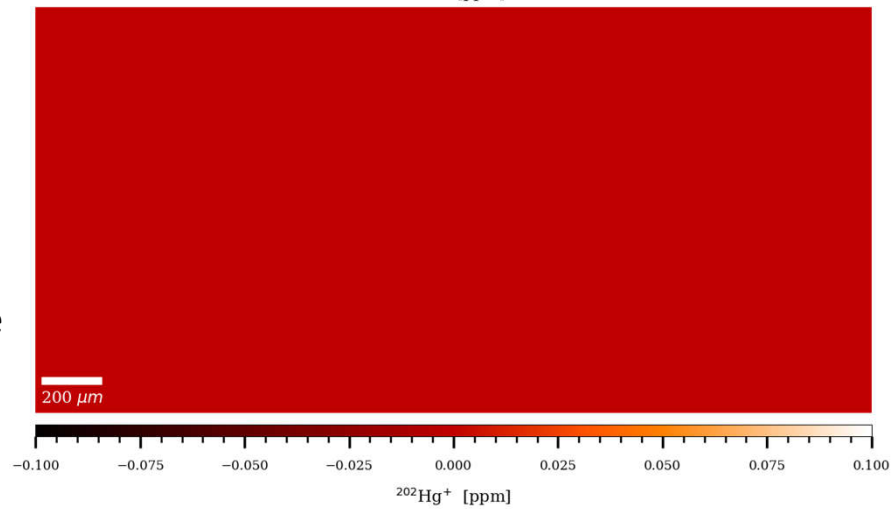


^{55}Mn

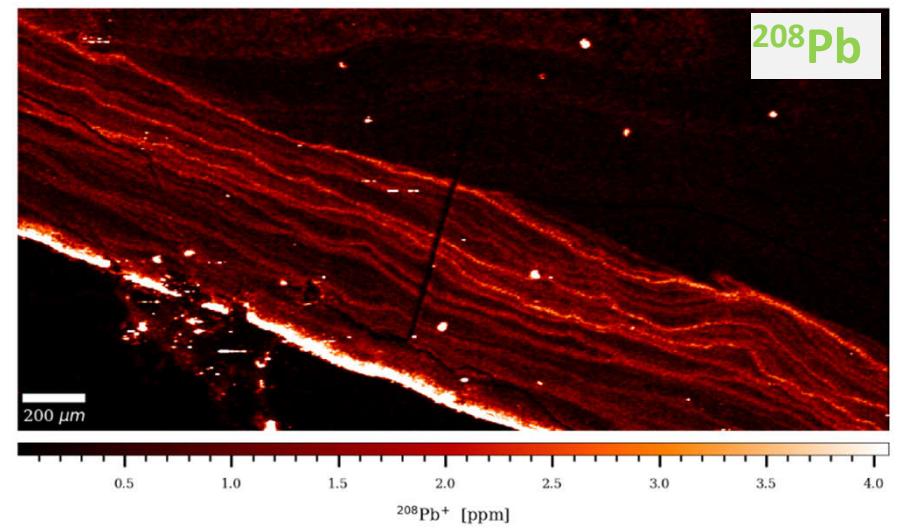


^{202}Hg

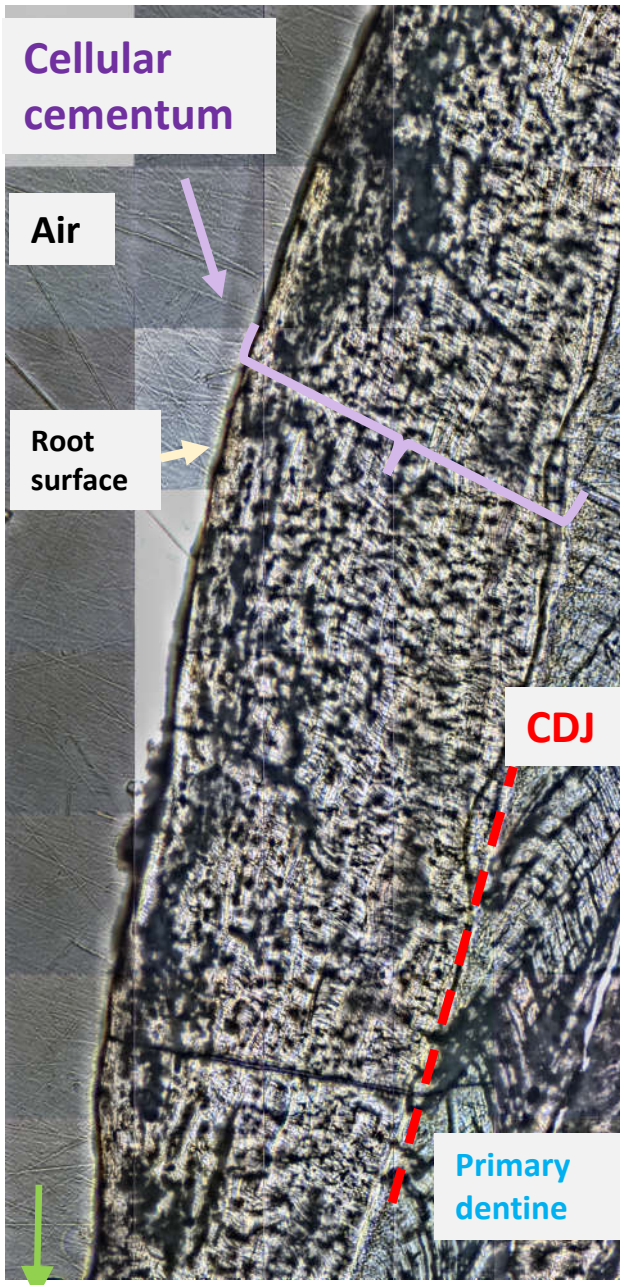
No detectable mercury



^{208}Pb

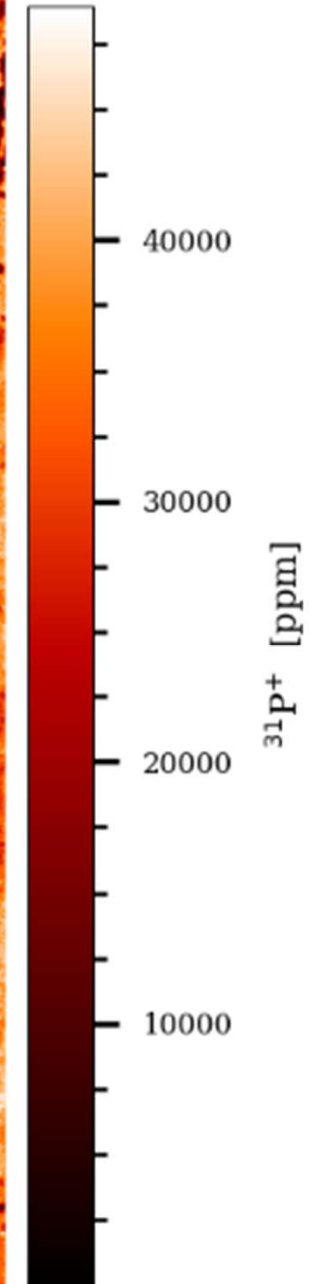
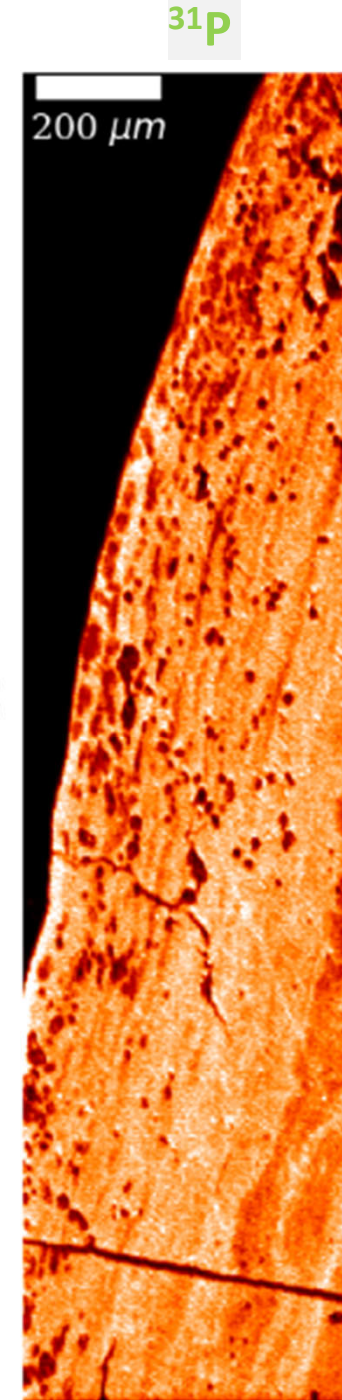
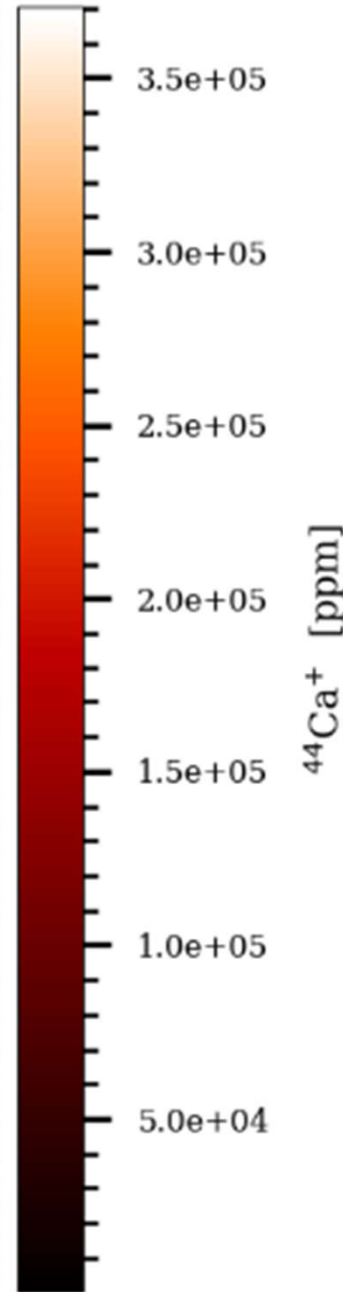
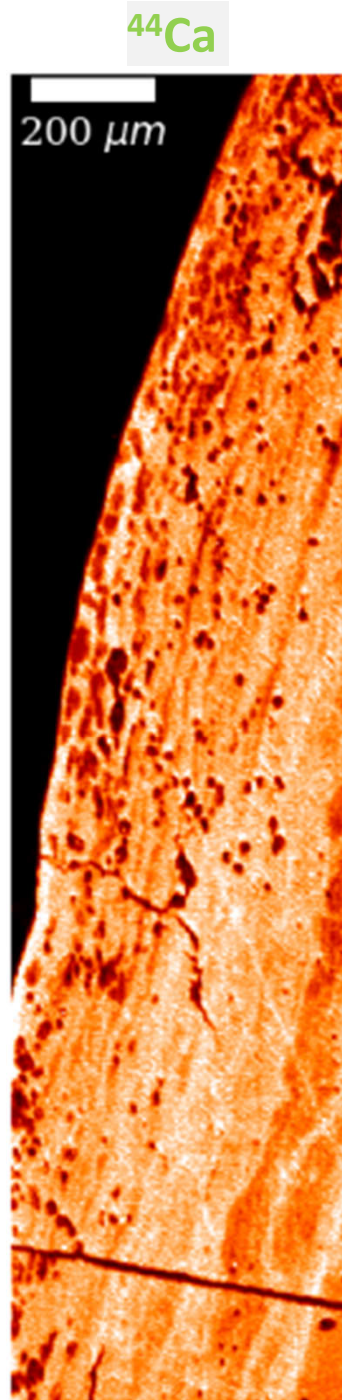


Odense 533 LLM1 – Cellular Cementum



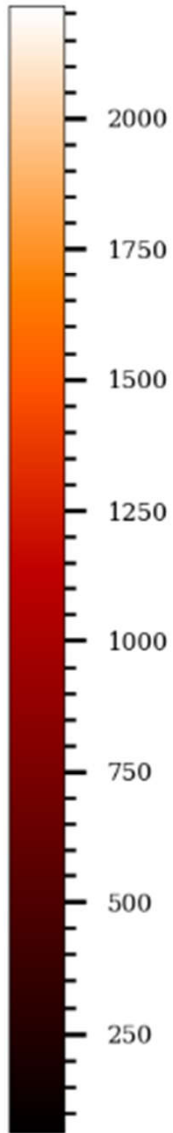
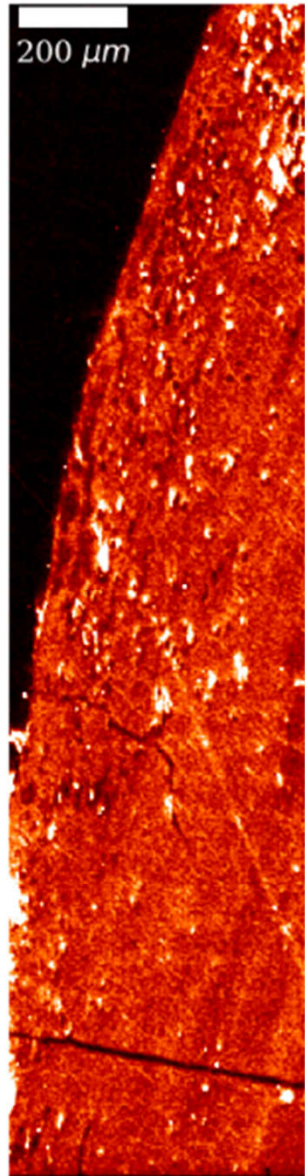
Towards root apex

Gauss 0.9 x 0.9

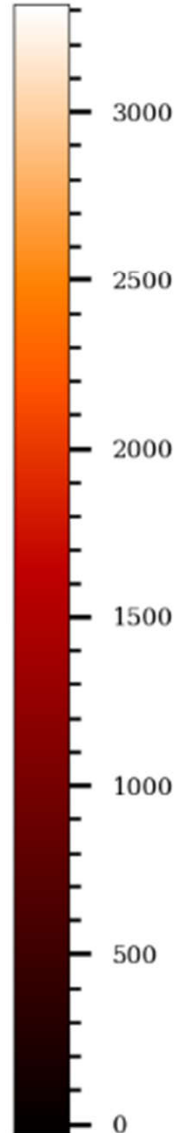
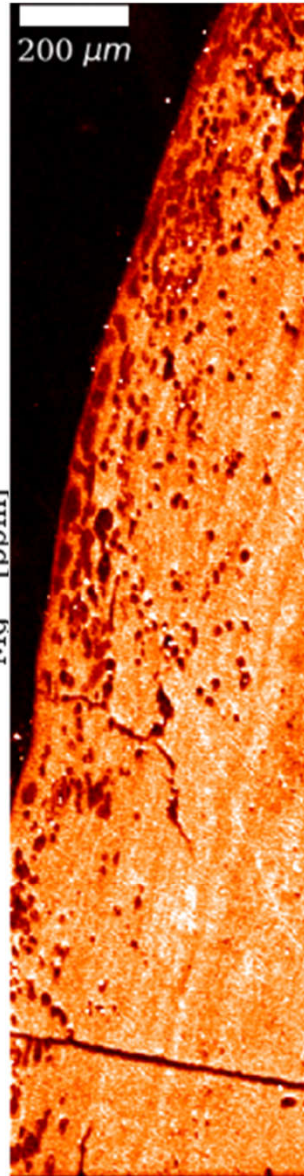


Odense 533M – Cellular Cementum

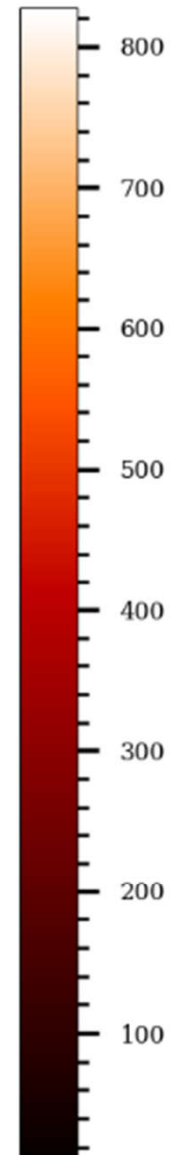
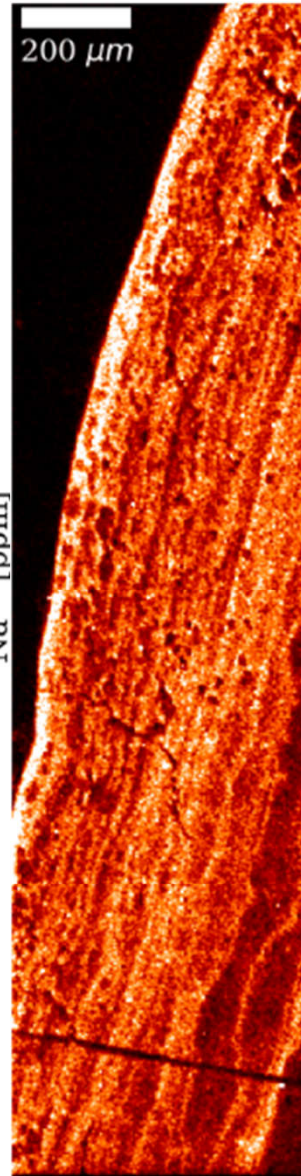
^{24}Mg



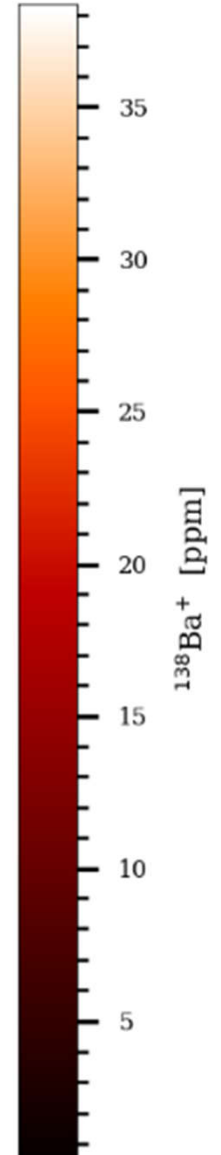
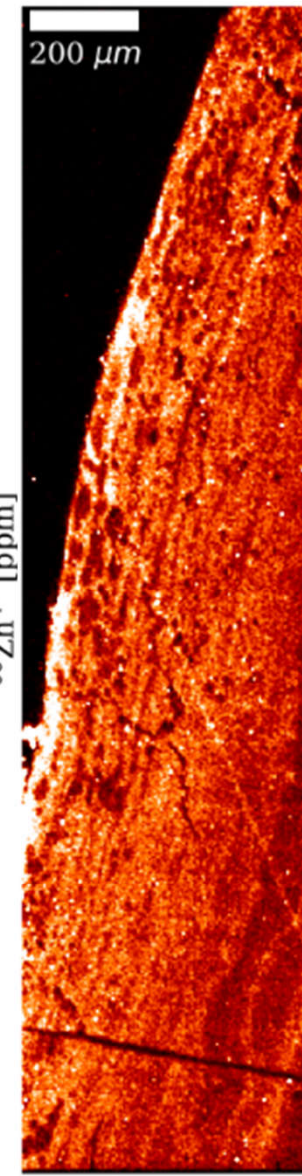
^{23}Na



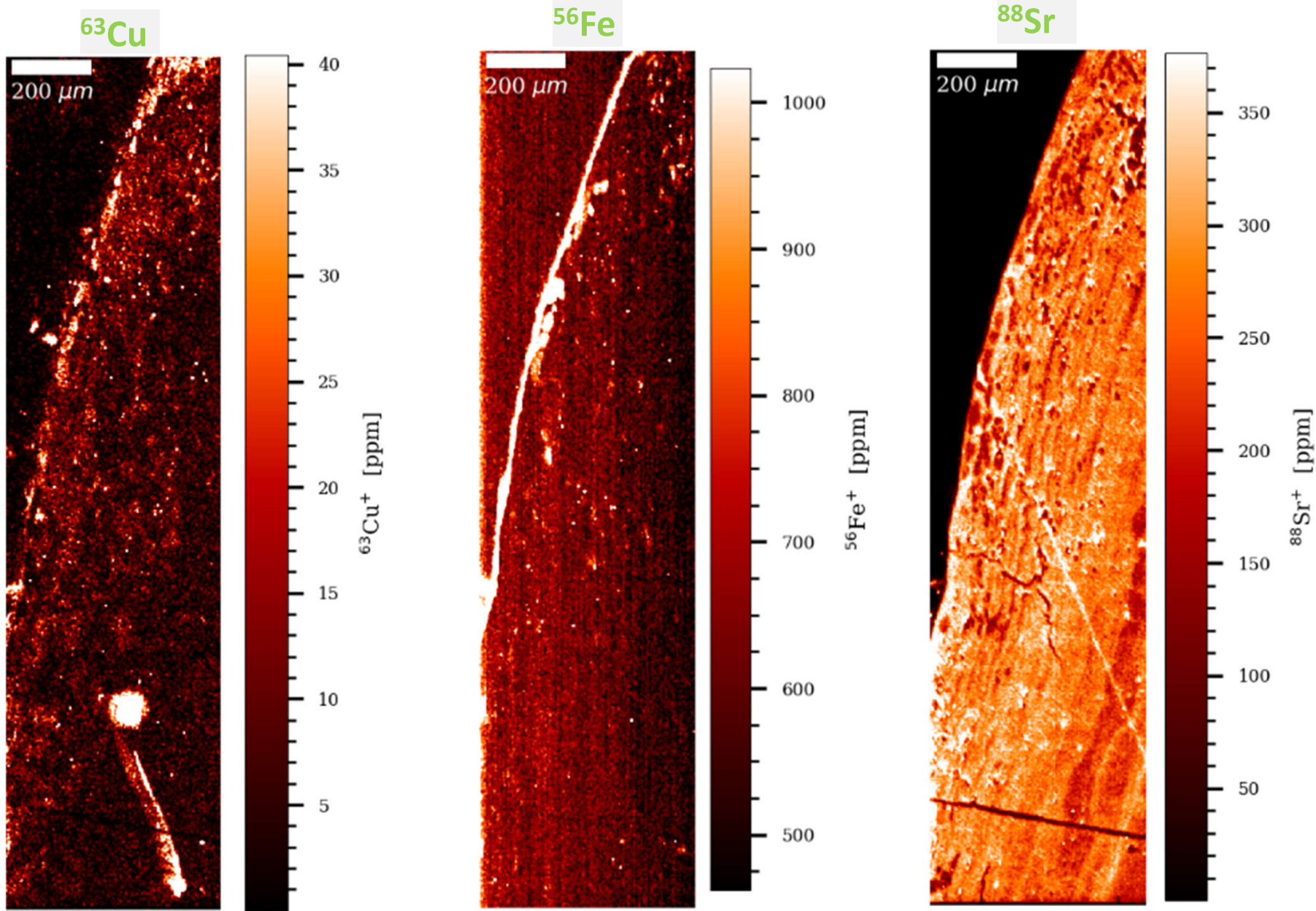
^{66}Zn



^{138}Ba

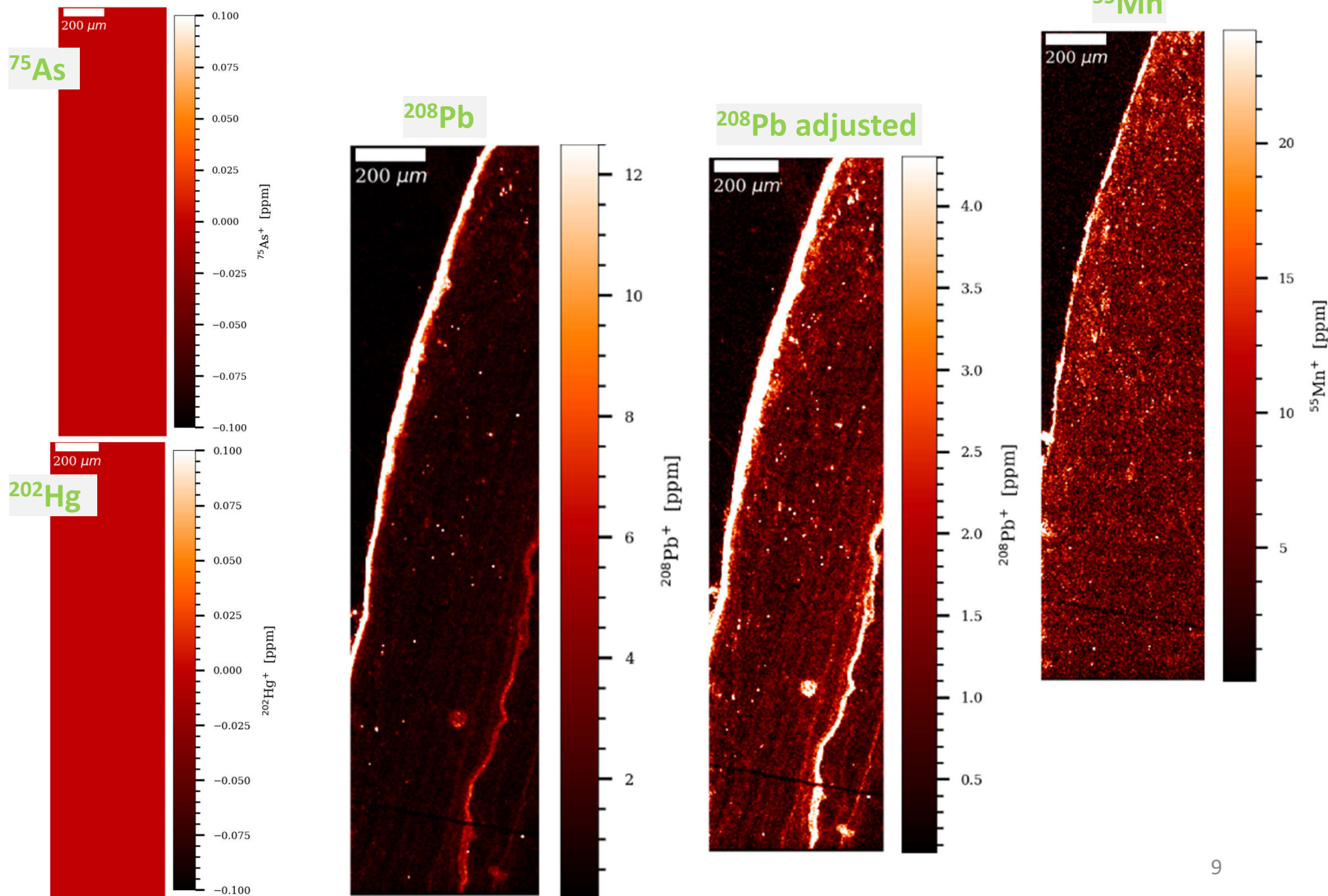


Odense 533M – Cellular Cementum



Odense 533M – Cellular Cementum

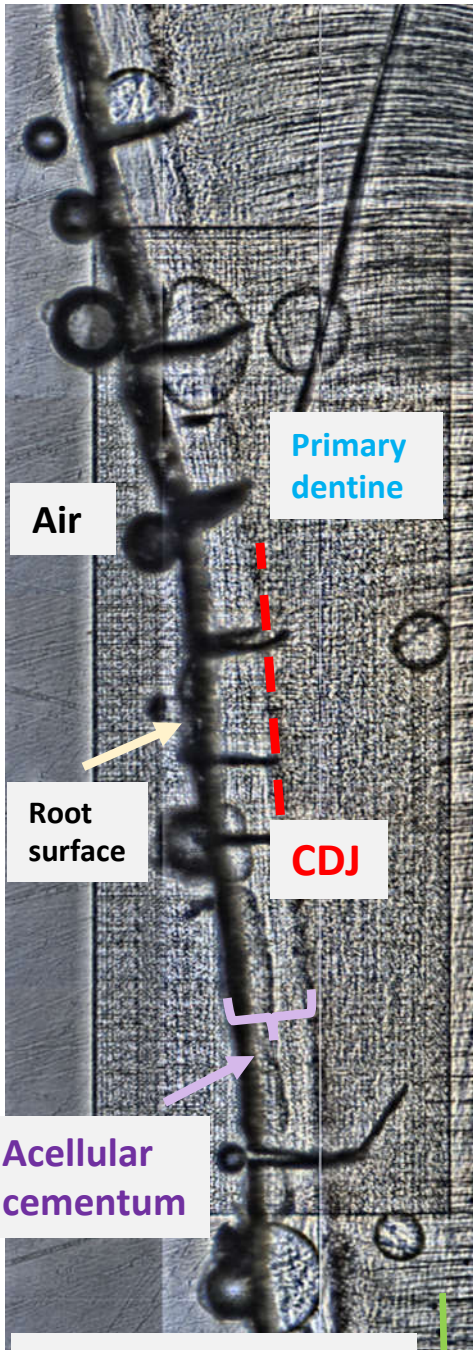
No detectable mercury or arsenic



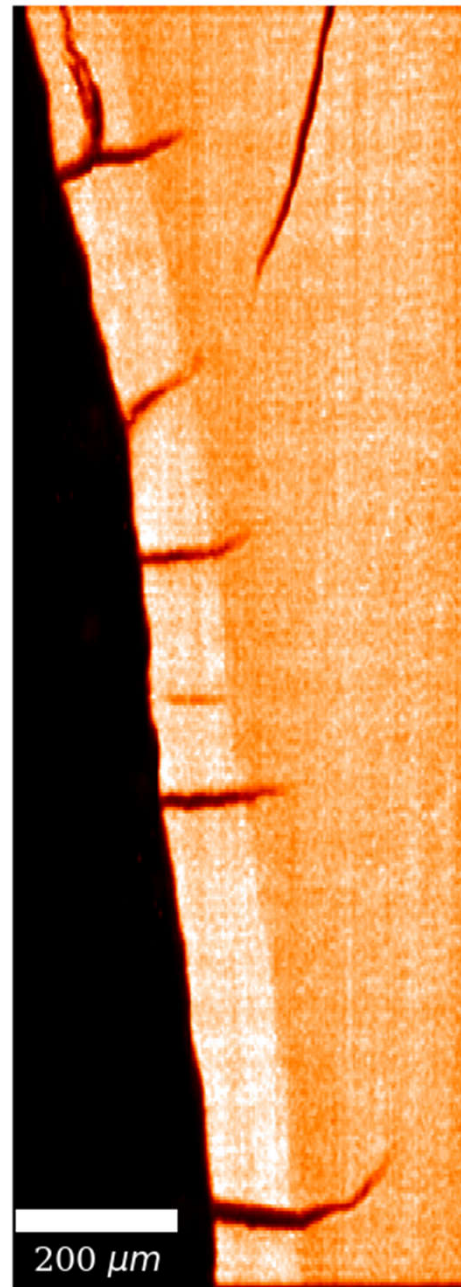
Odense 533 LLM1 –

Gauss 0.8 x 0.8

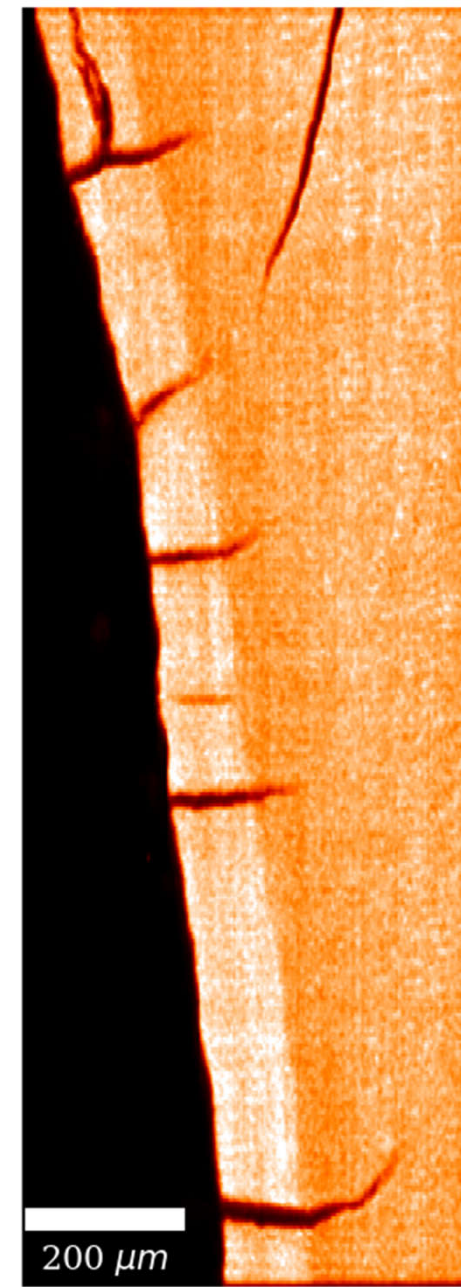
Acellular Cementum



⁴⁴Ca



³¹P



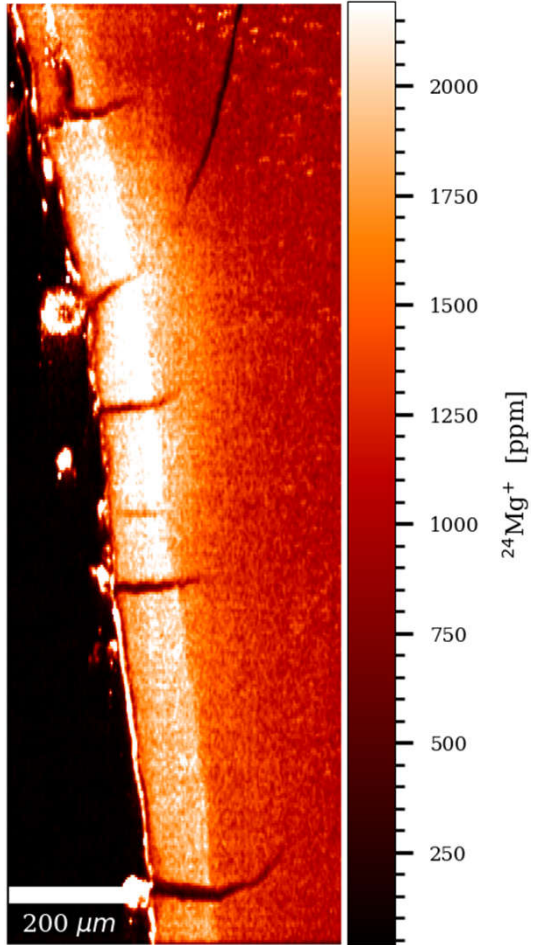
⁴⁴Ca+ [ppm]

³¹P+ [ppm]

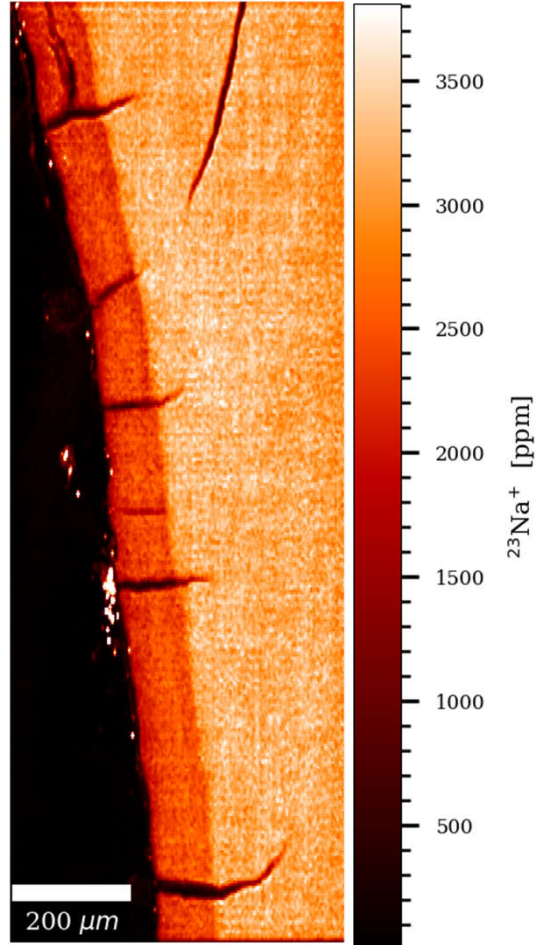
Towards root apex

Odense 533M – Acellular Cementum

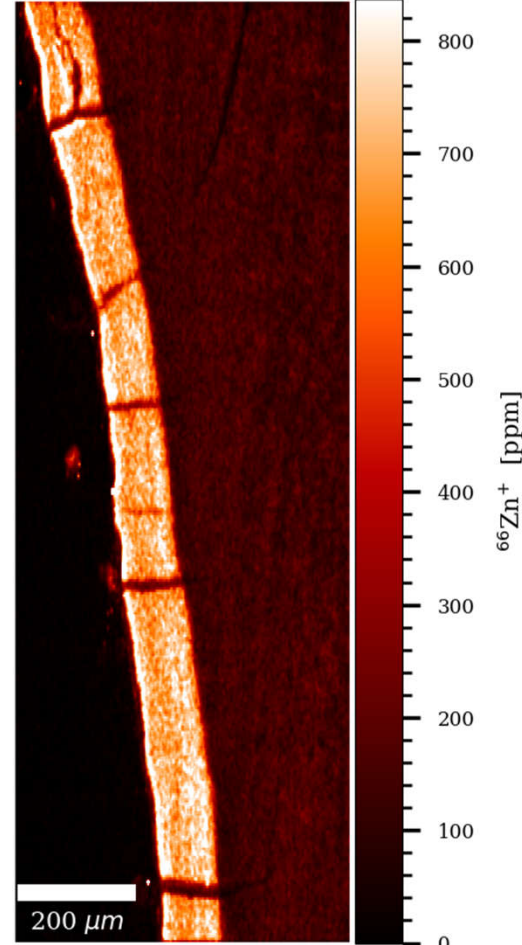
^{24}Mg



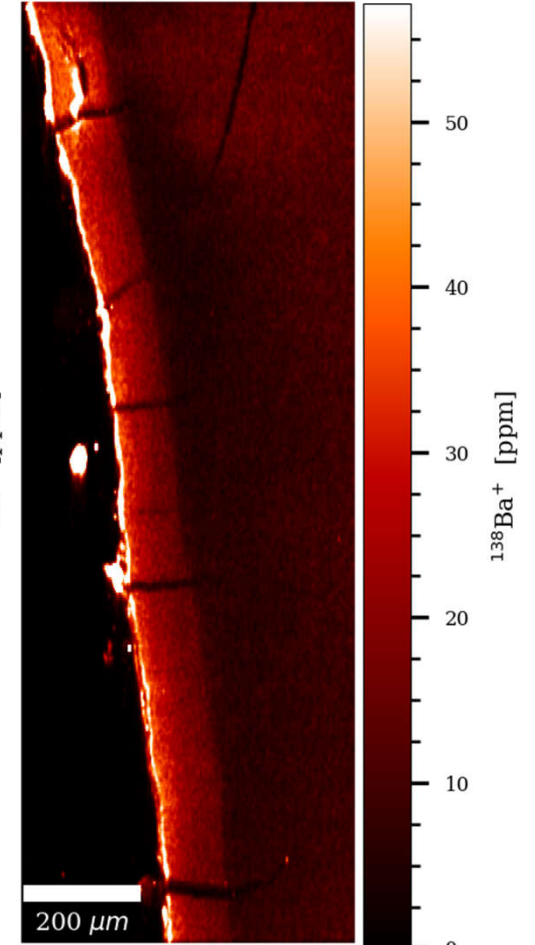
^{23}Na



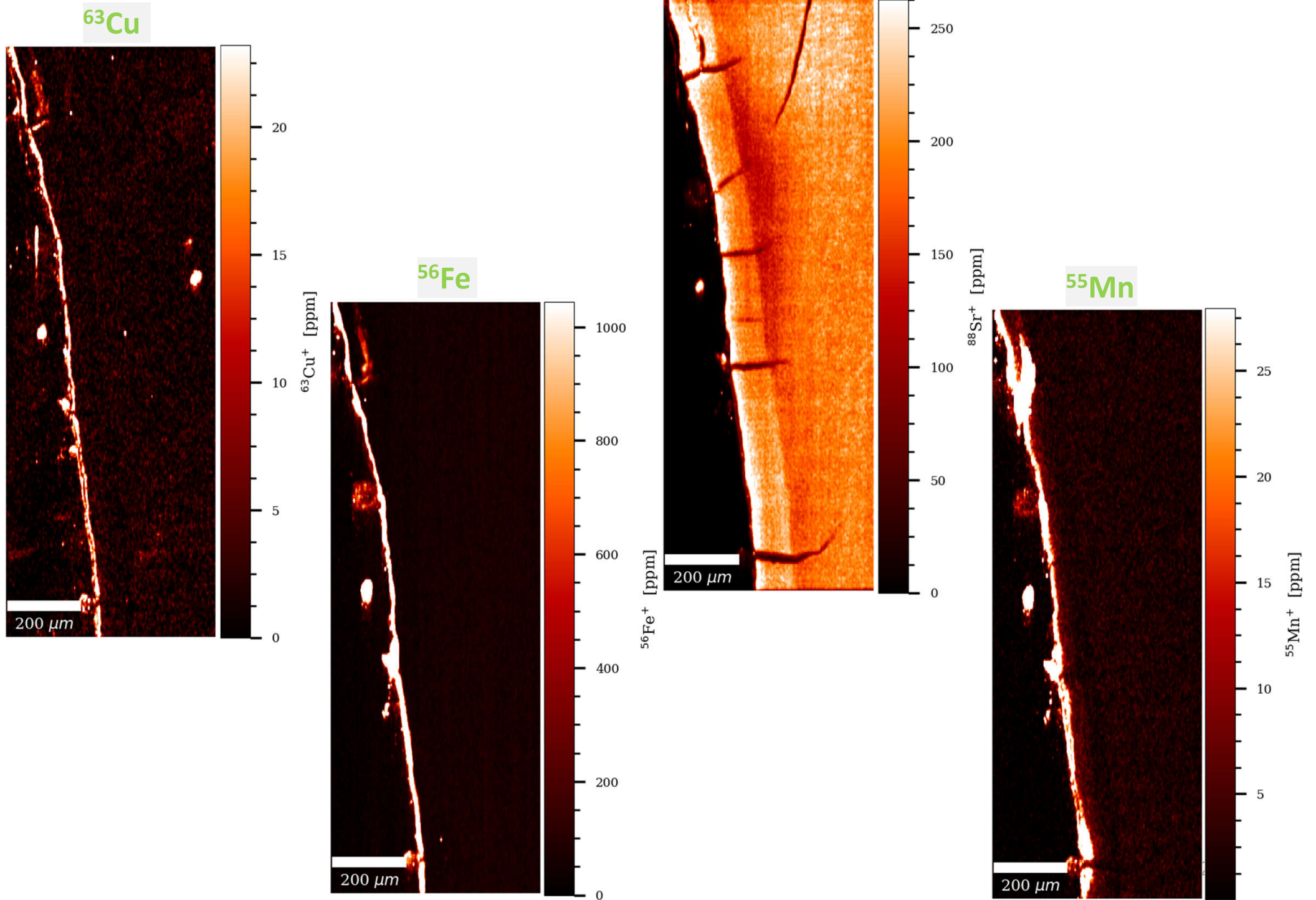
^{66}Zn



^{138}Ba

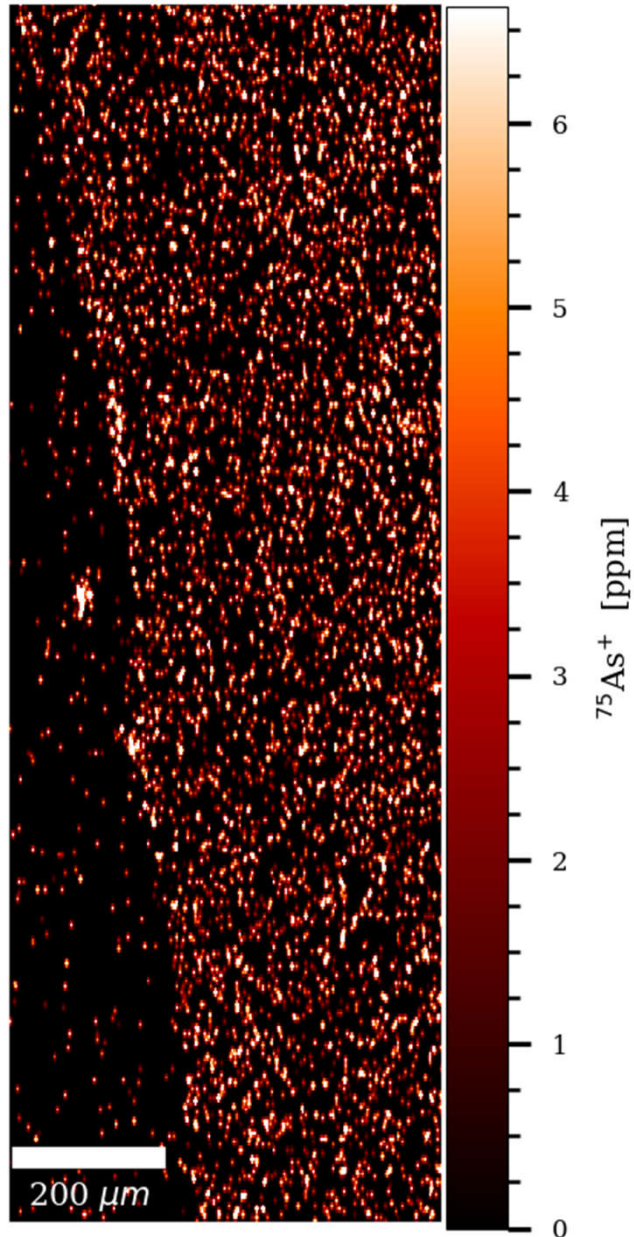


Odense 533M – Acellular Cementum

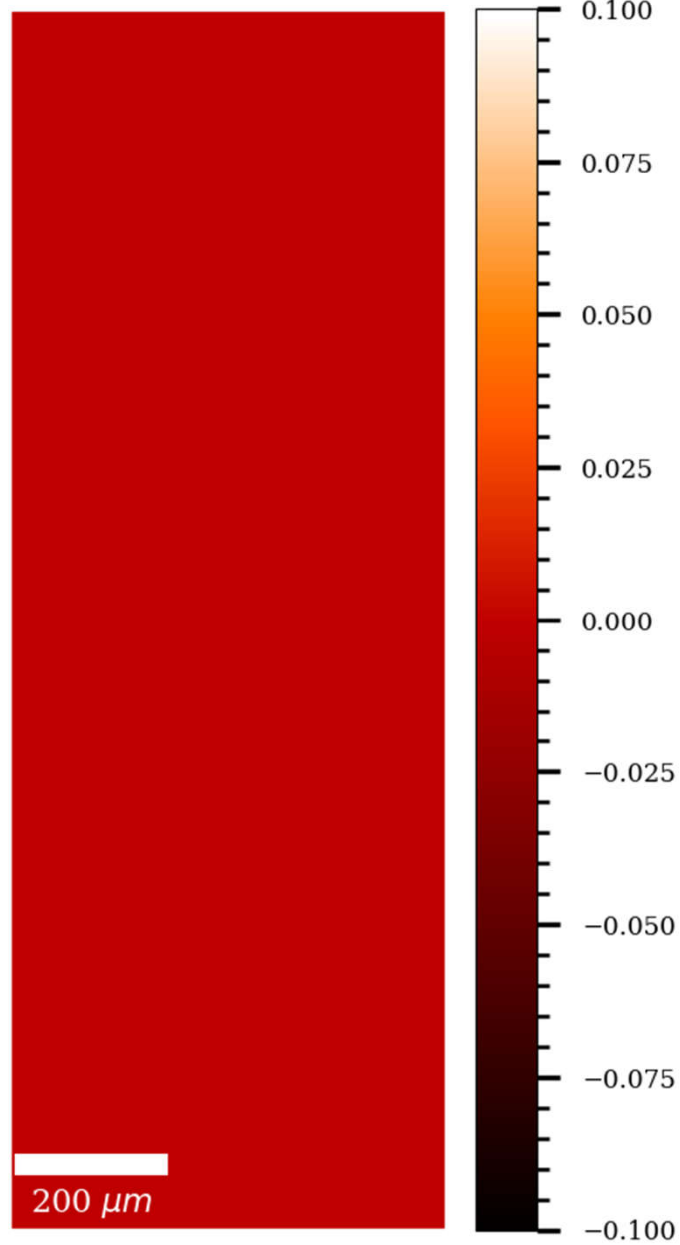


Odense 533M – Acellular Cementum

^{75}As

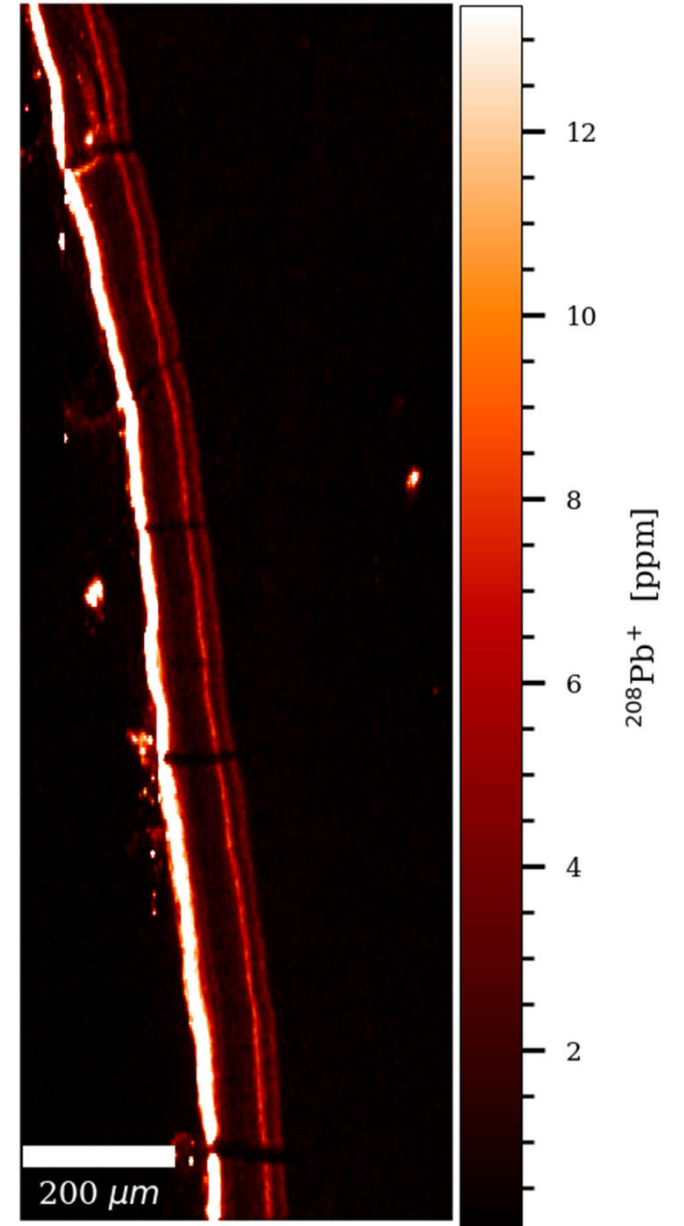


^{202}Hg

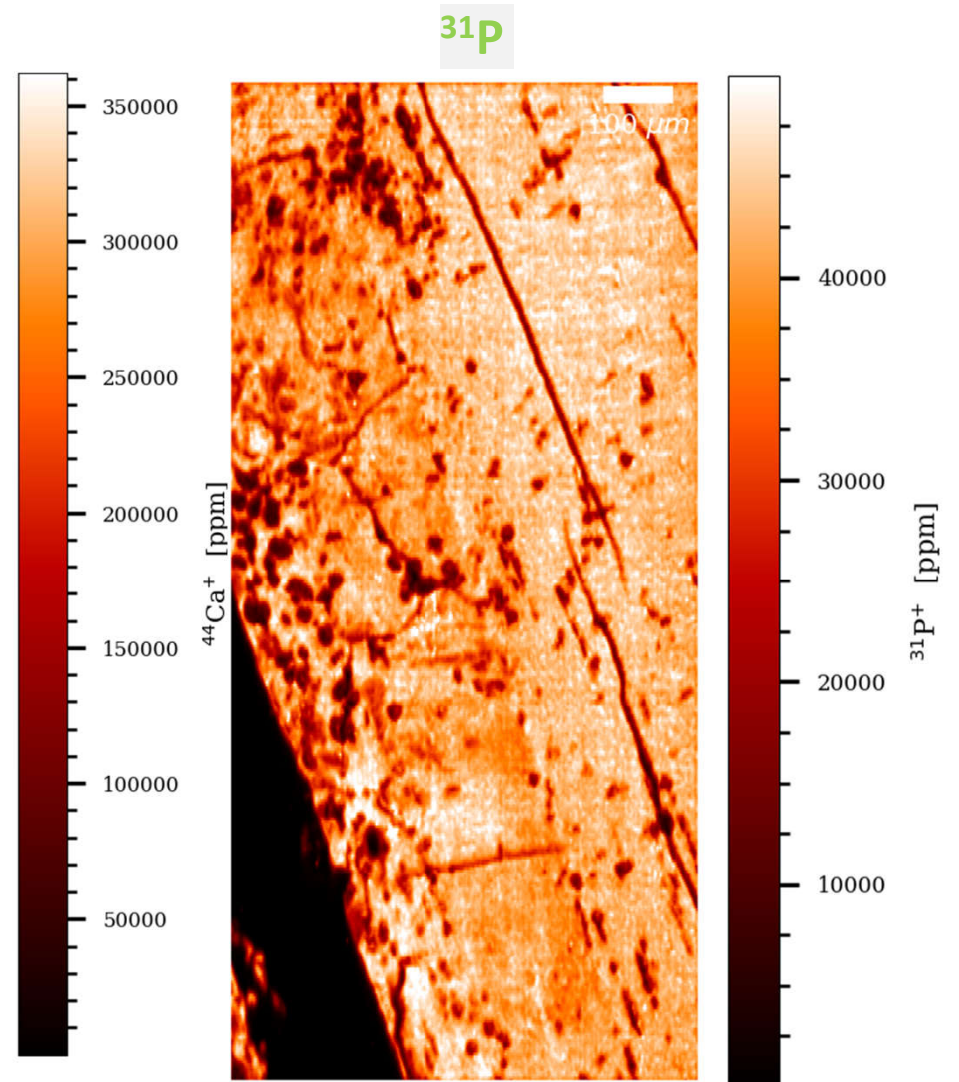
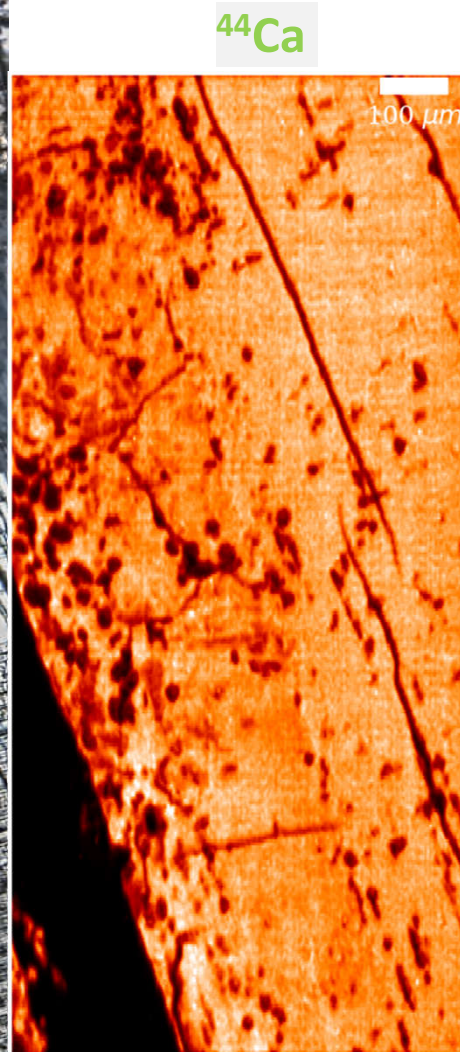
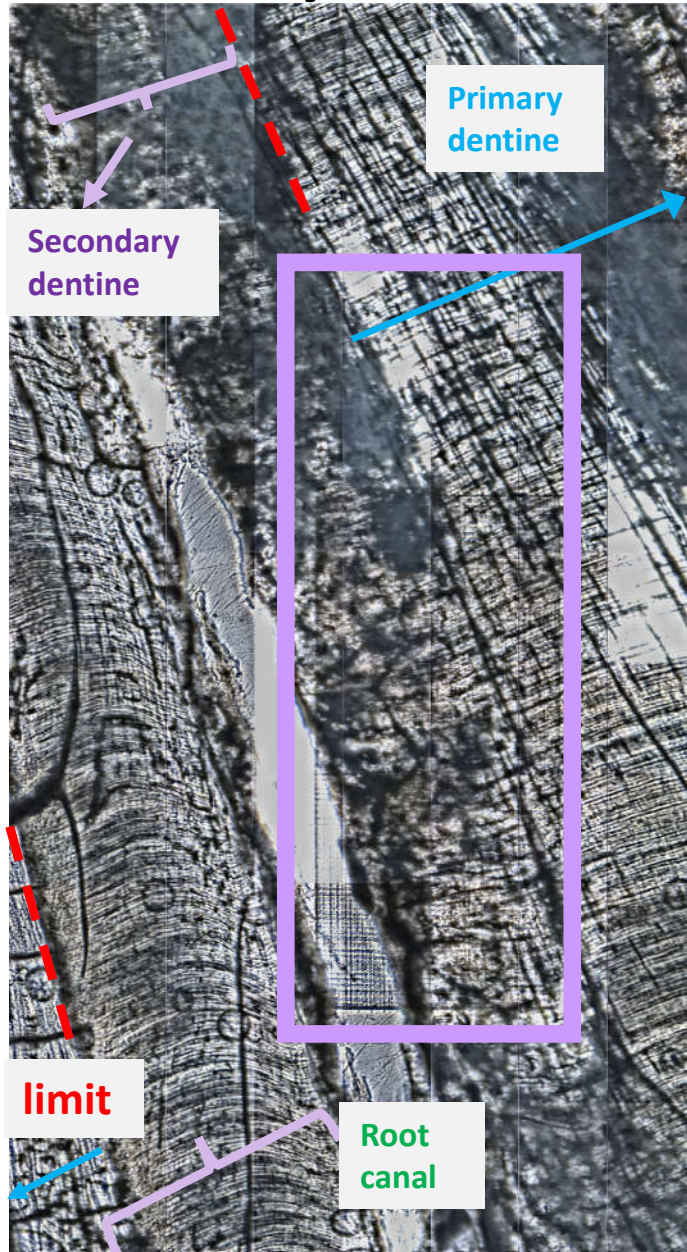


No detectable mercury

^{208}Pb



Secondary Dentine



Towards root apex

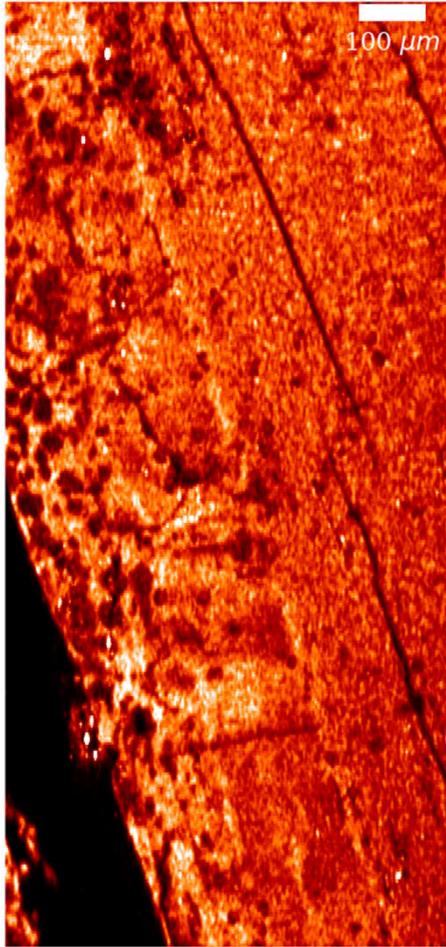
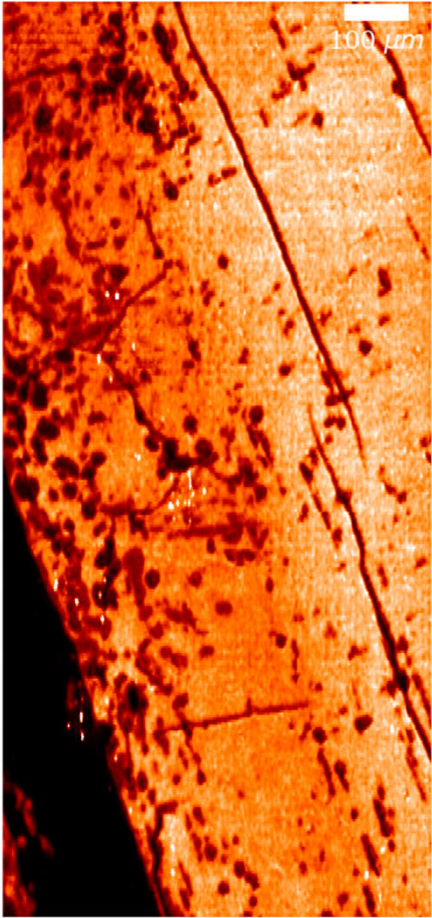
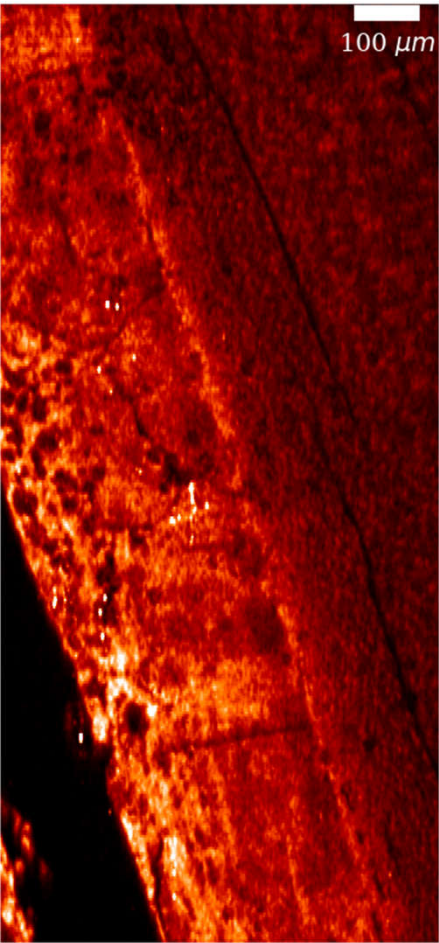


Odense 533M – Secondary Dentine

⁶⁶Zn

²³Na

¹³⁸Ba

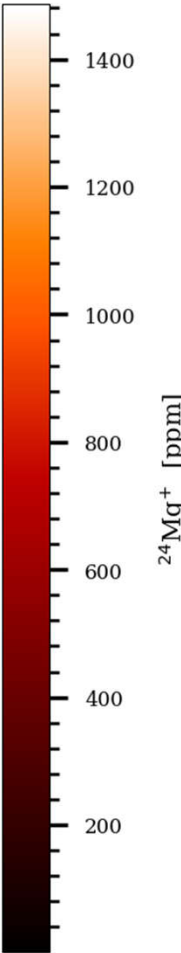
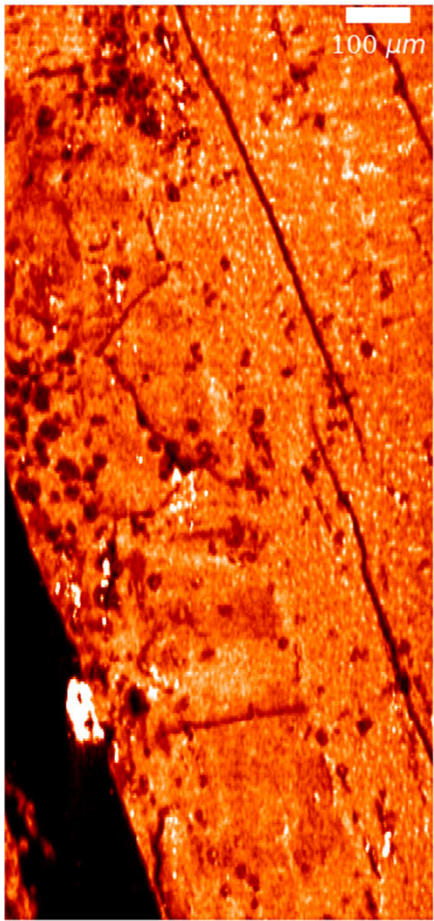
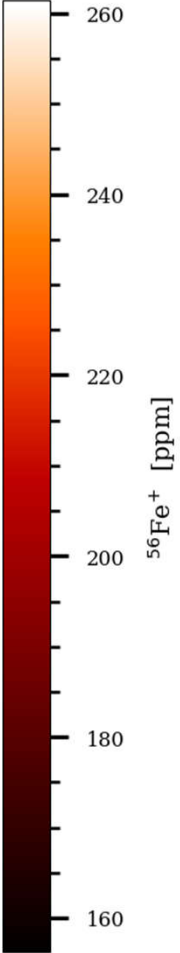
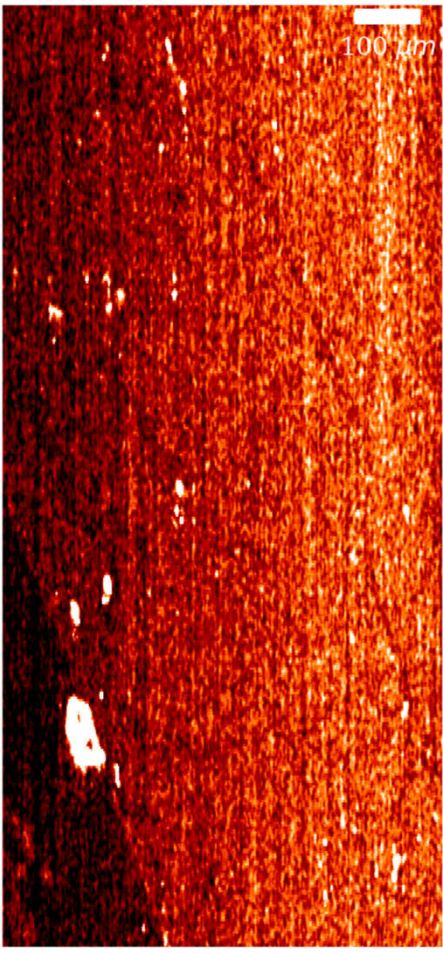
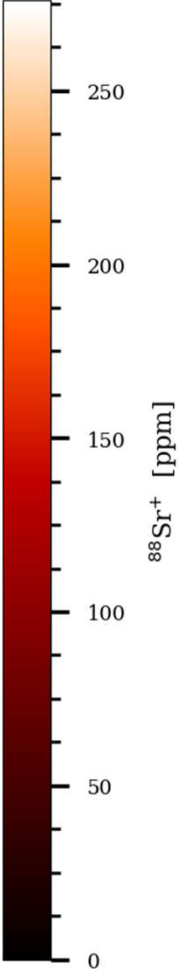
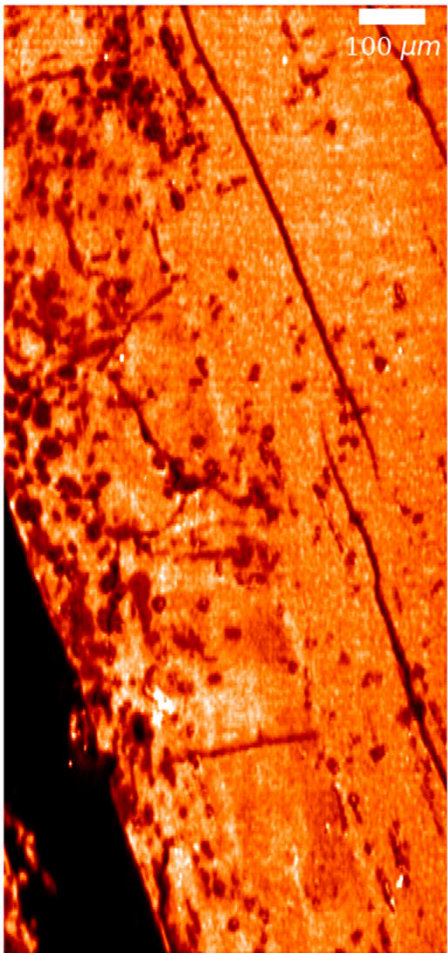


Odense 533M – Secondary Dentine

^{88}Sr

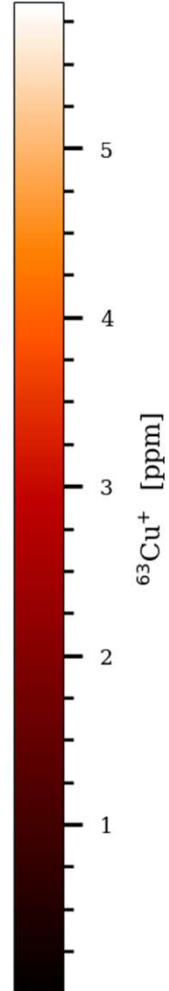
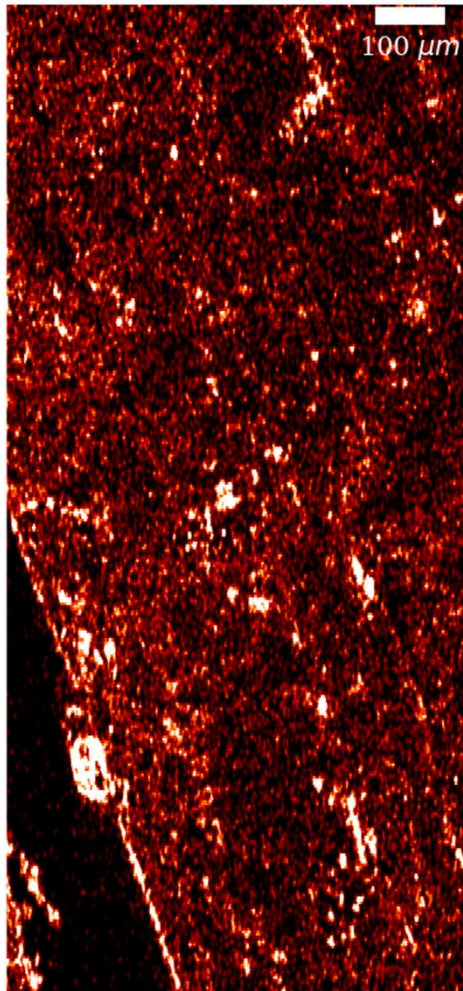
^{56}Fe

^{24}Mg

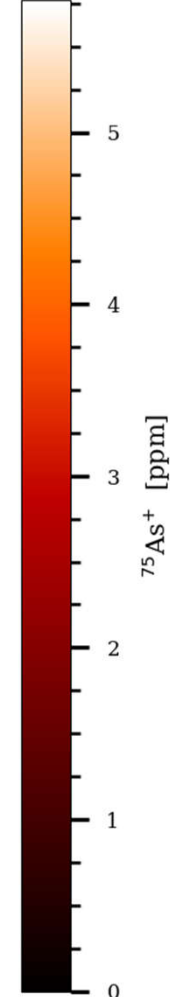
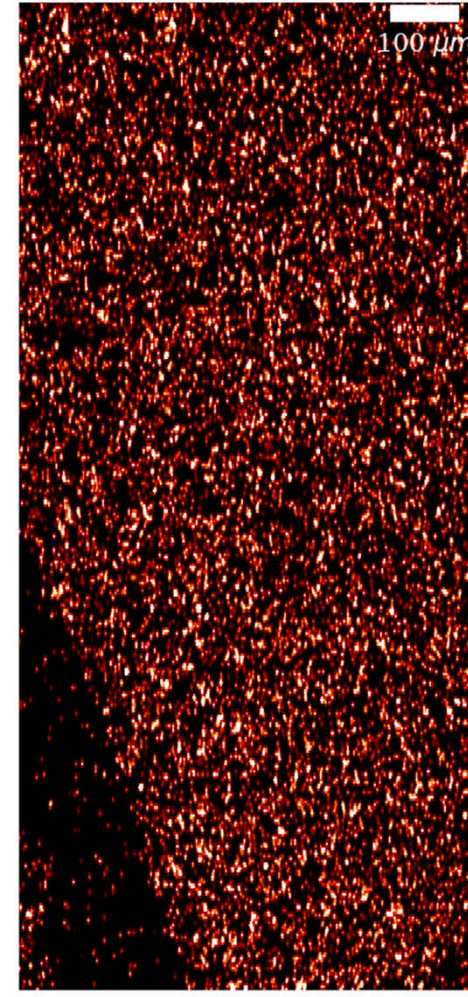


Odense 533M – Secondary Dentine

^{63}Cu

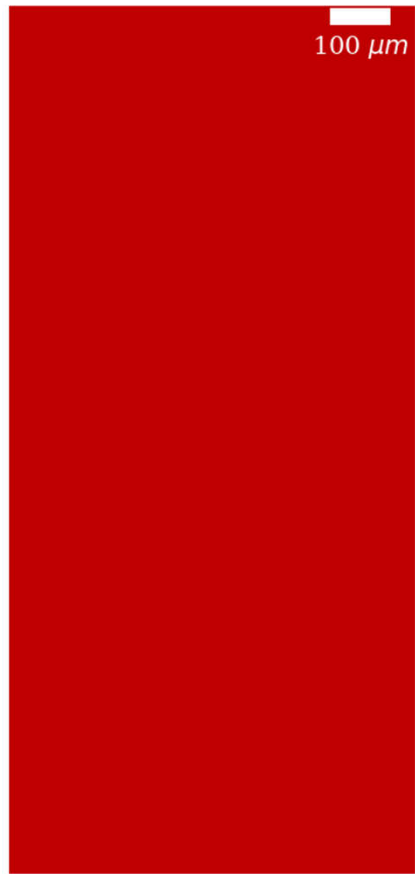


^{75}As

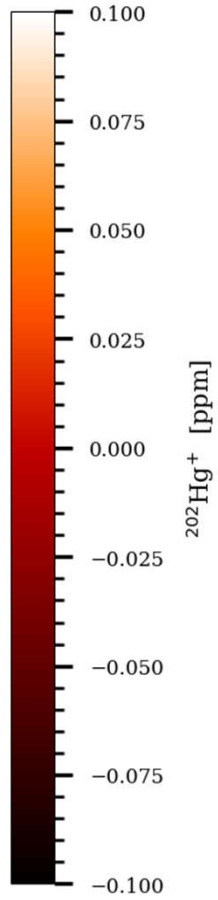


Odense 533M – Secondary Dentine

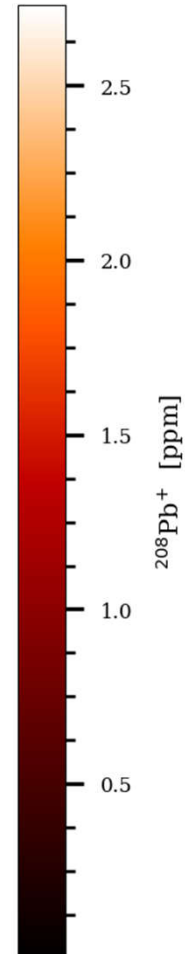
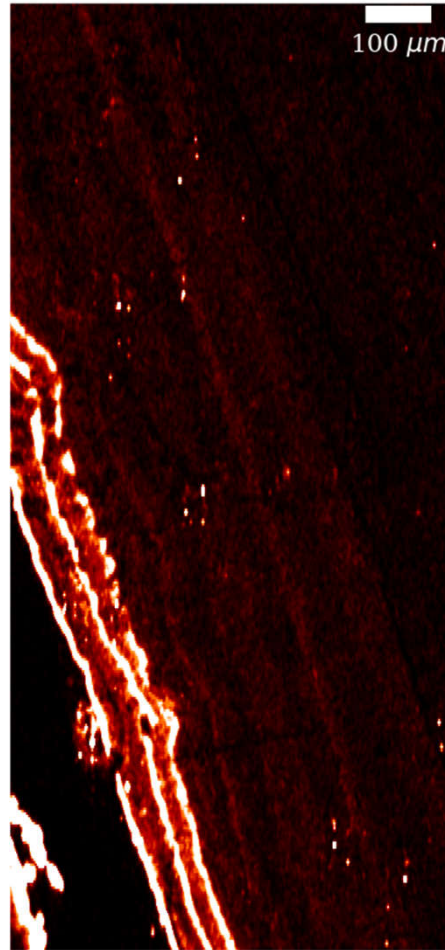
^{202}Hg



No detectable mercury



^{208}Pb



^{55}Mn

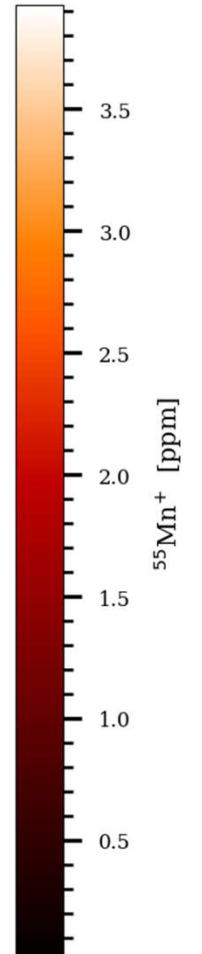
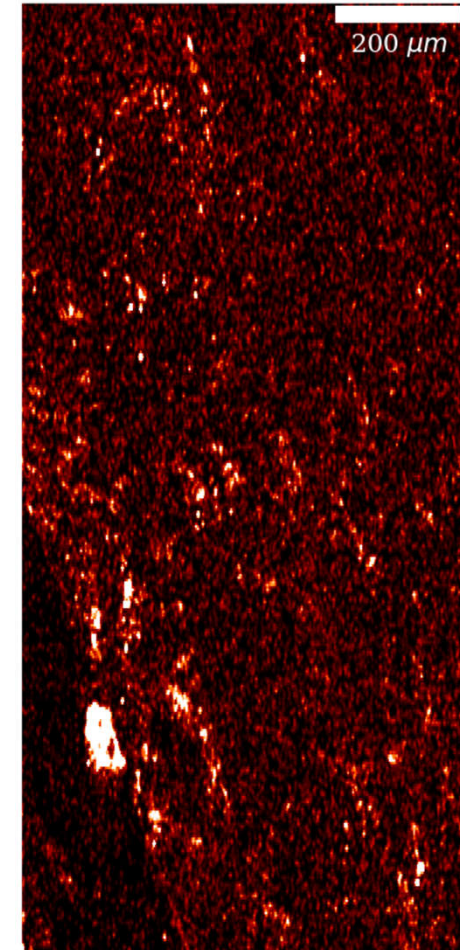


Table S1. List of individuals and teeth included in the study from the two medieval Danish leprosy sites (Odense and Næstved).

Site	Gr. Nr.	Teeth	Rounding of the edge of nasal aperture right	Rounding of the edge of nasal aperture left	Atrophy of the anterior nasal spine	Recession of the alveolar process of the premaxilla right	Recession of the alveolar process of the premaxilla left	Porosity / perforation of the palate right	Porosity / perforation of the palate left	Bones of hands	Lower legs	Bones of feet
Odense	265	LRC, ULM1	0	0	0	0	0	1	1	volar groove in two proximal phalanges	no indication	no indication at present elements
Odense	533	LLC, LLM1	1	1	1	1	1	1	1	no indication at present elements	tibiae: lamellar bone at areas of all shaft; fibulae: dense lamellar bone at medial distal shaft	no indication at present elements
Odense	896	LLC, LLM1	1	1	1	1	1	-	-	no indication at present elements	not present	no indication at present elements
Odense	914	LRC, ULM1	1	1	1	0	0	0	0	no indication at present elements	not present	not present
Odense	936	LLC, ULM1	1	0	1	1	1	1	1	volar groove in three proximal phalanges	not present	not present
Odense	1149	URC, ULM1	1	1	1	0	0	1	1	volar groove in two proximal phalanges	no indication	no indication at present elements
Næstved	6	ULC, URM1	1	1	0	0	0	1	1	non observable	slight porosity at the shaft of tibiae	no indication at present elements
Næstved	110	URC, LRM1	-	-	-	-	-	1	1	no indication at present elements	fibulae: porosity and lamellar bone at mid shaft and woven bone at distal shaft (laterally); left tibia: woven and lamellar bone at mid shaft and woven at ends of diaphysis	diaphyseal remodelling of one metatarsal, bone destruction at one tarsal fragment (calcaneus?)
Næstved	206	URC, ULM1	0	0	1	0	0	1	1	no indication at present elements	tibiae and fibulae: dense lamellar bone at all shaft; fibulae: bony outgrowths at the shaft	woven and lamellar bone at some metatarsals and phalanges (among others: 1 st metatarsals and proximal and distal 1 st phalanges)
Næstved	211	URC, LRM1	0	1	2	0	0	1	1	no indication at present elements	tibiae and femora: lamellar bone at all shaft	5 th left metatarsal: woven at inferior mid shaft
Næstved	268	LRC, LLM1	0	0	0	0	0	1	1	proximal phalanx: pointed distal end (?) (post mortem damage in the area, but medullary cavity seems reduced)	left tibia: lamellar bone at all sides of shaft (more dense at the proximal inferior and at the mid and distal lateral sides); right tibia: woven bone at all sides of shaft (at the medial side mixed with lamellar bone, at the proximal inferior very dense); right fibula: dense lamellar at the inferior and medial shaft; left fibula: all shaft dense lamellar bone (shaft seems swollen, no cloaca)	right calcaneus: bone remodelling (also postmortem damage); left calcaneus: bone remodelling (mix woven and lamellar bone) at all sides of mid and distal parts; 2 nd right metatarsal: dense woven at the inferior shaft and thinner layer at the superior shaft
Næstved	305	LLC, LRM1	1	1	2	0	0	1	1	right: bone remodelling on shaft of metacarpals (mainly 5 th) and phalanges; left: remodelling on shaft of metacarpals (mainly 4 th)	right tibia and fibula: mix of woven and lamellar bone at all shaft; left tibia and fibula: non observable	non observable

The scoring system for changes on facial bones is provided by Boldsen and Freund (2006, *Scandinavian Journal of Forensic Sciences*, 2:67-72) and Boldsen (2007, *Leprosy in Medieval Denmark – A comprehensive analysis*) (Scores: -: No information due to poor preservation of the relevant bone area, 0: Unaffected, 1: Slightly affected, 2: Severely affected).

Abbreviations for teeth are designated as follows: 'L' or 'U' for 'lower' or 'upper'; 'L' or 'R' for 'left' or 'right'; 'C' or 'M' for 'canine' or 'molar'; and finally the tooth position in Arabic numerals. For instance, 'LLM1' represents 'lower left first molar'.

Table S2. Age and sex determination and ¹⁴C dates of the individuals of interest for SXRF and LA-ICP-TOFMS scanning.

Site	Gr. Nr.	Sex	Age	Calibrated age CE (modelled) (2σ; 95.4%)	SXRF scans	LA-ICP-TOFMS scans
Næstved	6	female	~20	-	x	
Næstved	305	male	30-35	-	x	
Odense	896	male	35-45	1183 – 1265 [95.4%]	x	
Næstved	211	female	40-45	1184 – 1266 [95.4%]	x	x
Odense	533	female	25-35	1191 – 1269 [95.4%]	x	x
Odense	1149	female	20-30	1301 – 1415 [95.4%]	x	
Næstved	268	male	30-40	1441 – 1522 [95.4%]	x	
Odense	914	female	25-35	1459 – 1566 [95.4%]	x	

¹⁴C dates from Brozou et al. 2021, American Journal of Physical Anthropology, doi: 10.1002/ajpa.24339

Table S3. Limits of detection (LOD) and of quantitation (LOQ) of the calibrated LA-ICP-TOFMS data.

	LOD [ppm]	LOQ [ppm]	
[23Na]+	240	780	
[24Mg]+	320	1070	
[31P]+	900	2950	
[44Ca]+	-	-	no Ca in the reference, so values cannot be calculated.
[55Mn]+	50	180	
[56Fe]+	50	170	
[63Cu]+	110	360	
[66Zn]+	330	1110	
[75As]+	380	1250	
[81Br]+	180	610	
[88Sr]+	30	90	
[138Ba]+	-	-	no Ba in the reference, so values cannot be calculated.
[202Hg]+	-	-	no Hg in the reference, so values cannot be calculated.
[208Pb]+	5	16	

Values are rounded to the nearest ten. LOQ values are shaded in blue as these are the values used to assess the significance of concentrations observed in the data.

674.32	2 931.76	53.06	1 697.25	31.85	40 637.73	581.07	299 805.88	3 247.55	0.48	0.08	148.80	5.76	1.44	0.31	236.65	6.24	0.00	0.00	7.02	0.61	250.58	4.81	12.47	0.32	0.00	0.00	1.98	0.08
676.44	2 878.09	65.96	1 683.82	23.33	40 971.47	669.36	296 499.25	3 609.96	0.63	0.14	150.15	4.84	1.76	0.32	231.39	5.52	0.00	0.00	6.49	0.55	251.34	4.91	11.96	0.38	0.00	0.00	1.82	0.11
678.57	2 846.99	73.21	1 645.88	22.95	41 131.68	575.78	295 319.65	2 699.49	0.51	0.12	143.71	2.88	1.68	0.37	218.01	4.88	0.00	0.00	6.19	0.45	251.39	3.07	11.42	0.22	0.00	0.00	1.56	0.10
680.70	2 851.77	56.07	1 617.65	24.60	41 262.11	459.13	297 607.44	3 057.71	0.30	0.08	136.61	2.06	1.46	0.35	207.37	2.58	0.00	0.00	7.82	0.58	253.01	4.32	11.36	0.14	0.00	0.00	1.39	0.06
682.82	2 891.25	50.63	1 650.86	32.68	42 230.16	455.13	303 432.57	3 193.86	0.38	0.11	135.51	2.64	1.34	0.20	211.71	5.02	0.01	0.01	9.77	1.03	259.48	4.73	11.94	0.30	0.00	0.00	1.29	0.05
684.95	2 903.99	70.72	1 715.01	39.76	43 161.38	529.37	308 497.88	3 689.81	0.52	0.15	136.39	2.52	0.95	0.14	226.65	6.30	0.11	0.08	9.94	1.62	265.71	4.32	12.55	0.31	0.00	0.00	1.20	0.05
687.08	2 912.98	70.38	1 772.32	35.34	43 513.25	675.93	312 222.61	4 930.83	0.51	0.16	133.36	2.81	0.49	0.11	237.45	5.82	0.36	0.22	7.92	1.12	268.45	4.41	12.81	0.35	0.00	0.00	1.10	0.07
689.21	2 941.25	67.83	1 788.14	28.67	43 194.99	681.89	312 859.07	4 369.03	0.35	0.09	129.84	2.16	0.26	0.11	239.02	5.27	0.40	0.21	7.59	1.14	267.79	4.37	12.77	0.24	0.00	0.00	1.05	0.07
691.33	2 930.23	72.15	1 795.24	32.40	42 720.13	745.74	311 480.52	4 022.55	0.23	0.04	129.23	1.88	0.27	0.18	244.01	3.84	0.15	0.07	9.42	1.35	266.79	5.32	12.63	0.22	0.00	0.00	1.07	0.06
693.46	2 887.93	69.49	1 842.12	39.97	43 110.32	807.92	312 344.55	4 303.03	0.17	0.02	138.13	2.15	0.29	0.15	260.02	4.01	0.02	0.01	8.74	0.52	267.10	5.73	12.77	0.28	0.00	0.00	1.18	0.06
695.59	2 757.78	72.73	1 807.74	40.63	42 702.27	709.13	304 916.18	4 479.92	0.17	0.03	143.32	1.98	0.33	0.11	262.06	4.42	0.00	0.00	7.34	0.83	260.47	3.78	12.86	0.32	0.00	0.00	1.32	0.07
697.72	2 570.87	72.23	1 661.85	31.42	40 939.54	759.54	287 990.10	5 591.92	0.16	0.04	137.26	3.46	0.37	0.08	241.70	8.05	0.00	0.00	6.72	1.06	247.23	2.67	12.03	0.32	0.00	0.00	1.36	0.08
699.84	2 366.92	114.47	1 507.90	51.02	38 268.45	1 346.73	267 241.71	10 147.69	0.10	0.02	130.71	3.01	0.27	0.09	222.02	12.38	0.00	0.00	6.03	0.54	229.92	6.50	10.96	0.56	0.00	0.00	1.29	0.06
701.97	2 169.12	135.98	1 386.74	66.96	35 229.23	1 719.81	246 390.13	12 836.94	0.10	0.02	133.66	2.17	0.10	0.04	217.12	9.46	0.01	0.01	6.73	0.59	209.65	10.02	10.04	0.76	0.00	0.00	1.15	0.02
704.10	2 014.45	134.60	1 317.43	68.96	32 760.99	1 861.10	230 925.53	13 953.03	0.17	0.06	142.24	3.30	0.04	0.01	213.43	7.08	0.08	0.07	8.67	0.91	192.77	11.75	9.30	0.63	0.00	0.00	0.99	0.03
706.22	1 887.37	141.33	1 257.65	84.50	30 549.64	2 069.61	217 051.91	15 512.11	0.14	0.05	143.07	3.91	0.16	0.04	191.95	10.44	0.22	0.16	9.79	0.84	180.88	13.64	8.55	0.52	0.00	0.00	0.89	0.07
708.35	1 887.32	123.20	1 227.78	95.45	29 563.73	2 088.22	209 275.48	15 335.79	0.06	0.02	136.27	3.99	0.34	0.11	174.23	12.56	0.21	0.13	9.58	0.68	175.91	13.41	8.26	0.66	0.00	0.00	0.88	0.10
710.48	2 020.40	154.76	1 271.44	128.02	30 728.39	2 697.76	216 676.46	20 017.89	0.09	0.02	132.20	5.86	0.28	0.11	184.73	16.47	0.07	0.04	8.22	0.32	182.95	16.08	8.69	0.87	0.00	0.00	0.90	0.13
712.61	2 179.18	176.19	1 368.17	140.37	33 518.35	2 968.28	236 652.91	21 898.65	0.30	0.06	134.91	5.02	0.20	0.06	214.23	18.70	0.11	0.07	7.00	0.53	201.84	17.43	9.32	0.87	0.00	0.00	0.86	0.12
714.73	2 381.68	143.93	1 549.51	115.98	37 880.65	2 437.63	266 985.59	17 606.85	0.47	0.08	143.32	3.40	0.37	0.16	252.00	17.19	0.59	0.23	7.69	0.98	230.87	13.81	10.25	0.67	0.00	0.00	0.82	0.07
716.86	2 601.60	113.31	1 725.41	77.51	41 675.24	1 649.05	293 186.03	12 174.70	0.46	0.06	147.20	3.12	0.42	0.18	276.21	14.69	1.41	0.36	9.08	1.72	253.54	9.09	10.92	0.46	0.00	0.00	0.82	0.05
718.99	2835.94	105.79	1801.21	53.08	43431.47	1201.97	305807.11	9087.12	0.47	0.10	143.68	3.31	0.26	0.06	284.62	13.38	1.73	0.48	8.80	1.84	259.79	6.47	10.88	0.53	0.00	0.00	0.82	0.04
721.11	3015.38	84.08	1827.79	47.38	44122.76	1152.58	310591.39	8065.33	0.40	0.10	140.86	3.94	0.31	0.08	273.66	10.89	1.29	0.30	8.89	0.98	256.14	6.66	10.48	0.66	0.00	0.00	0.76	0.04

383.40	2 863.03	3.77	1 141.98	13.79	43 935.24	264.10	300 284.73	1 291.03	0.62	0.15	229.15	1.40	1.04	0.15	239.56	10.30	0.39	0.22	4.47	0.67	203.12	1.33	9.06	0.46	0.00	0.00	0.24	0.02
385.49	2 935.73	19.57	1 073.50	6.46	42 250.43	251.25	294 728.67	2 245.33	0.65	0.20	220.23	1.05	0.39	0.04	212.36	9.81	0.44	0.22	6.04	0.94	194.65	0.46	8.00	0.36	0.00	0.00	0.19	0.02
387.59	2 962.13	27.92	1 035.35	7.09	41 505.41	169.55	293 534.06	3 279.68	0.58	0.22	214.49	1.31	0.15	0.08	200.30	6.35	0.58	0.12	7.45	1.24	192.95	1.48	7.55	0.16	0.00	0.00	0.17	0.02
389.68	2 915.61	29.91	1 040.06	6.71	41 727.04	175.24	294 424.43	3 565.34	0.52	0.19	218.48	1.46	0.37	0.22	200.55	2.86	1.07	0.34	7.07	0.98	198.23	1.85	7.92	0.14	0.00	0.00	0.20	0.02
391.78	2 856.57	32.90	1 068.80	21.22	42 001.02	111.48	292 175.47	2 429.20	0.44	0.13	228.98	1.04	1.08	0.32	202.52	3.92	1.43	0.39	5.68	0.61	201.45	1.96	8.33	0.05	0.00	0.00	0.20	0.00
393.87	2 834.26	29.95	1 115.36	17.70	42 433.30	132.68	290 349.91	978.09	0.49	0.08	236.92	5.18	2.00	0.15	196.70	1.46	1.49	0.46	5.52	0.42	206.52	0.98	8.58	0.24	0.00	0.00	0.18	0.02
395.97	2 849.68	8.10	1 130.76	19.83	42 915.38	268.10	292 503.09	1 420.74	0.57	0.09	237.49	-6.61	2.24	0.18	192.83	5.34	1.32	0.47	7.25	0.84	208.90	2.55	8.68	0.25	0.00	0.00	0.16	0.03